NOVEL ADHESIVE ANCHORING SYSTEM THROUGH ENGINEERED INTERFACE

by

Hua Liu

A Dissertation Submitted in

Partial Fulfillment of the

Requirements for the Degree of

Doctor of Philosophy

in Engineering

at

The University of Wisconsin-Milwaukee

August 2020

ABSTRACT

NOVEL ADHESIVE ANCHORING SYSTEM THROUGH ENGINEERED INTERFACE

by

Hua Liu

The University of Wisconsin-Milwaukee, 2020
Under the Supervision of Professor Jian Zhao

An adhesive anchoring system usually consists of a threaded rod inserted into a drilled hole in concrete with adhesives such as epoxy acting as the bonding agent. The behavior of traditional adhesive anchors can be inconsistent because the bond on adhesive-concrete interface can be affected by many factors. It is known through laboratory tests and field studies that the bond strength of adhesive anchors can be adversely impacted by installation conditions, service conditions, and factors related to the adhesive material. While some factors are considered in the capacity equations in building codes and design guidelines, many other factors, especially those related to installation such as hole cleaning, must be addressed adequately in practice.

This study focused on an innovation for adhesive anchors that improves the robustness of adhesive-concrete interface such that the consistence of adhesive anchors can be improved. The innovation is about creating threads/grooves in drilled holes in concrete before the holes are filled with adhesive and anchors are installed. The hardened adhesive in the grooves fundamentally change the load carrying mechanism of the adhesive-concrete interface bond from shear adhesion to mechanical interlock. The new adhesive anchor system is expected to ensure robust connections with a reasonable increase in construction cost.

The new adhesive anchoring system was verified in this study using both unconfined and confined pullout tests in uncracked concrete. The tests were divided into to two groups, one on

traditional adhesive anchors and the other on the new adhesive anchors, considering two anchor sizes and three hole-cleaning conditions that represent typical practices. The test results documented in this dissertation showed that the new adhesive anchors greatly improved the capacity and consistence of adhesive anchors. Finite element (FE) analyses using ABAQUS were also conducted to simulate the behavior of the adhesive anchors under the tensile load. The nonlinear analyses incorporating surface-to-surface contact, concrete damaged plasticity and nonlinear spring models were found suitable to capture the global and local behavior of the adhesive anchors with pullout bond failure.

While further studies are needed to verify the new adhesive anchoring systems under a variety of other conditions, this study indicated that the new adhesive anchors will help engineers to design/construct safe connections for a variety of connections. The application of the innovative anchoring system is expected to improve the capacity of adhesive anchors, to simplify construction procedures, to provide reliable anchoring systems and to improve public safety.

To

my parents,

Zenglong Liu and Zhifang Li,

my brother,

Min Liu;

and my sisters,

Rong Liu and Yun Liu

TABLE OF CONTENTS

LIST OF FIGURES

LIST OF TABLES

LIST OF NOMENCLATURE

A_{fg} = the gross area of the tension flange, in.^{2} [mm^2]

A_{fn} = the net tension flange area after the holes are subtracted, in.^{2} [mm^2]

A_{Nc} = projected concrete failure area of single anchor or group of anchors for calculation of strength in tension, in.^{2} [mm^2]

A_{Nco}= projected concrete failure area of single anchor for calculation of strength in tension if not limited by edge distance or spacing, in.^{2} [mm^2]

A_p = the cross-section area of the axis compression member, in.^{2} [mm^2]

A_{st} = the required area of steel reinforcement, in.^{2} [mm^2]

A_{se} = effective cross-sectional area of anchor, in.^{2} [mm^2]

b_w = web width or diameter of circular section, in. [mm]

c_{cr} = edge distance where strength of anchor is not influenced by free edge, in. [mm]

d = outside diameter of anchor, in. [mm]

d_a = anchor diameter, in. [mm]

d_s = anchor diameter, in. [mm]

d_0 = hole diameter, in. [mm]

d_t is distance from extreme compression fiber to centroid of longitudinal tension reinforcement, in.[mm]

E_s = the young modulus of steel, ksi [MPa]

F_u = the ultimate strength of the steel, ksi [MPa]

F_y = the yield strength of the steel, ksi [MPa]

f_y = specified minimum yield strength of reinforcement, ksi [MPa]

f_{uta} = specified minimum tensile strength of anchor steel, ksi [MPa]

f_r = modulus of rupture of concrete, ksi [MPa]

h_{nom} = the length between end of the screw anchor and the concrete surface, in. [mm]

h_{nom} = the embedment depth/setting depth of the screw anchor in concrete, in. [mm]

h = the distance between the threads, in. [mm]

h_s = the distance between the tip of the screw anchor and fist thread, in. [mm]

h_t = the distance of the thread, in. [mm]

I = the moment of inertia, in^4 [mm^4]

I_g = moment of inertia of gross concrete section about centroidal axis, neglecting reinforcement, in^4 [mm^4]

M = the flexural strength of the member, lb-in [kN-m]

M_n = the nominal flexural strength of the member, lb-in [kN-m]

M_{cr} = cracking moment, lb-in [kN-m]

N_{no} = concrete cone failure load of one anchor unaffected by edge or overlapping stress cones, lb [N]

N_u= ultimate predicted strength of the anchor, lb [N]

$\overline{N_b}$ = mean basic concrete breakout strength in tension of single anchor in uncracked concrete, lb [N]

N_{cb} = the concrete breakout capacity, lb [N]

$\overline{N_{cb}}$ = mean concrete breakout strength in tension of single anchor at edge or of group of anchors in uncracked concrete, lb [N]

$\overline{N_T}$ = mean bond pullout strength in tension of single adhesive anchor at edge or of group

of adhesive anchors in uncracked concrete, lb [N]

$\overline{N_\tau}$ = mean bond pullout strength in tension of single adhesive anchor in uncracked concrete, lb [N]

$\alpha\beta\gamma\delta$ = variables used in regression analysis of database

COV = coefficient of variation

$\sqrt{f_c'}$ = concrete compression strength measured on 6 by 12-in. cylinders, psi [MPa]

f_c = compressive strength of concrete, psi [MPa]

f_{ac} = maximum compressive strength of the prism (1:2), psi [MPa]

f_{acp} = the predict of compressive strength, psi [MPa]

h_{ef} = the effective embedment depth, in. [mm]

l = the length of the member, in. [mm]

τ = bond stress, psi [MPa]

$\bar{\tau}$ = mean uniform bond strength at steel/mortar interface, psi [MPa]

τ_v = the shear stress, psi [MPa]

P = the ultimate load of loading rod, lb [N]

Q = the first moment of area, in^3 [mm^3]

t = the thickness of the member, in [mm]

V = the transverse shear force based on the ultimate load of loading rod, lb [N]

V_c = the nominal shear strength provided by concrete, lb [N]

s_{cr} = edge distance where strength of anchor is not influenced by free edge, in. [mm]

S = the section modulus of the member, in^3 [mm^3]

y_t = distance from centroidal axis of gross section, neglecting reinforcement, to tension face, in.[mm]

δ = the deflection of the member

λ = a modification factor to reflect the reduced mechanical properties of light weight concrete relative to normal weight concrete of the same compressive strength

$\Psi_{ed,N}$ = factor used to modify tensile strength of anchors based on proximity to edges of concrete member

$\Psi_{g,N}$ = factor used to modify tensile strength of adhesive anchors based on number and spacing of anchors in group and mean bond strength

$\Psi_{g,No}$ = factor used with $\Psi_{g,N}$ to modify tensile strength of adhesive anchors based on number of anchors in group and mean bond strength

α_n = reduction factor for the uniform bond strength

$\emptyset$ = reduction factor

σ = axis compression strength of the member, psi [MPa]

ε = the strain corresponding to compressive strength

ε_0 = the strain corresponding to maximum compressive strength

ACKNOWLEDGEMENTS

This project was helped by many individuals, firms, and organizations, to whom I appreciate for their helps.

First, I would like to thank my advisor Dr. Jian Zhao for his patience and guidance, like a family member and a friend in the past four and half years. Words cannot express my feelings, nor my thanks for all your help.

I wish to thank my committee: Dr. Benjamin C Church, Dr. Todd Davis, Dr. Habib Tabatabai and Dr. Konstantin Sobolev. Their comments improved the quality of my dissertation and helped me to be an engineer.

The project was funded by the Catalyst Grant in UWM foundation and Department of Civil & Environmental Engineering at UWM. Additional funding for the author was provided by the University of Wisconsin-Milwaukee Chancellor's Graduate Student Award and Teaching Assistant. Mr. Brian Thompson, President, UWM Research Foundation Director, helped the project. Mr. Kyle Jansson, UWM Prototyping Center Director, helped to make a tapping bit for the project.

Dr. Steven Hardcastle in Advanced Analysis Facility provided guidance and helped in the adhesive tests including a laser confocal microscope, nanoindentation and Energy Dispersive X-Ray Spectroscopy.

Dr. Al Ghorbanpoor allowed me using structural lab and Mr. Rahim Reshadi, the Manager of Structures Lab, helped to make the concrete specimens for anchor pullout tests and other material tests. Mr. Avie Judes, the Lab Manager of Mechanical Engineering, shared many tools and materials to assist in testing adhesive anchors. Student Machine Shop in UWM personnel assisted

in the various fabrication of the testing frame, namely: Mike Brown, John Condon, Robert Breske and Michael Powley.

Mr. Phongsavanh assisted in the fabrication of the testing connections. The concrete ready-mix supplier OZINGO, Milwaukee, provided contractor discount of concrete for test specimens. Mr. Jerry King in Precast Engineering Company provided fabrication of rebars and donated the rebars for this project. Ms. Siobhán Sawyer, Mr. Jack Olson and Mr. Bret Turley in DeWalt and Simpson Strong-Tie Company were very generous in donating many materials and provided information for this project. Ms. Yan Liu, Chongqing Vocational Institute of Engineering, helped to conduct preliminary unconfined tests. Dr. Yin Lin, Ningbo University of Technology, helped to collect data of fracture energy for the finite element analyses. Dr. Da Luo and Dr. Qian Lin assisted the author in developing and testing adhesive anchors. Several graduate students and undergraduate students assisted the author to fabricate concrete specimens namely: Farzaneh Elyasigorji, Cui Fu, Roy E Wittenberg II, Marina Ivanovna Kozhukhova, Mark Nosonovsky, Mohammad Omar Al-Barqawi and Behrouz Farahi.

DISCLAIMERS

Authors' disclaimer: The contents of this report reflect the views of the author, who is responsible for the facts and the accuracy of the data presented herein. This report does not constitute a standard, specification, or regulation.

Patent disclaimer: There was one invention or discovery conceived or first actually reduced to practice in the course of or under this contract, which is patentable under the patent laws of the United States of America or any foreign country. U.S. Patent Application 16/362,282 filed by UWM Research Foundation on behalf of Dr. Jian Zhao on 3/4/19.

CHAPTER 1 INTRODUCTION

1.1 Introduction of Adhesive Anchoring Systems

Drilled-in, adhesive anchors are widely used in buildings and bridges, for example, to fix ceiling panels or pipelines to concrete floor slabs. An adhesive anchor consists of a threaded rod inserted into a drilled hole with adhesive materials acting as the bonding agent, as illustrated by the yellow layer in Figure 1.1. The structural adhesive materials are defined by ACI 355.4-11 as polymers used in adhesives can include, but are not limited to, epoxies, polyurethanes, polyesters, and vinyl esters; or inorganic polymers. The behavior of anchors has been discussed at length in CEB (1994), Klingner et al. (1998), and Cook et al. (2001). Heavy loads on these anchors are transferred to concrete through bond on the epoxy-concrete interfaces (Figure 1.2). Adhesive anchors are likely to fail in a variety of failure modes in laboratories, including at the adhesive-concrete interface, as summarized in Figure 1.3 by Cook et al. (1998). This study focuses on the load transfer in an anchoring system in tension, which starts with the steel-adhesive interface, through the adhesive, and ends with the adhesive-concrete interface.

The tensile capacity of adhesive anchors can be impacted by many factors as demonstrated by Cook et al. (1994), Cook et al. (1996), and Cook and Konz (2001). Davis (2012) summarized these factors as shown below.

1.1.1 Factors related to installation conditions

1. Hole Orientation: downward, horizontal, upward;
2. Hole Drilling: rotary hammer, core drill, or drilled in accordance with manufacturer's instructions;

3. Hole Cleaning: uncleaned, partially cleaned, or cleaned in accordance with the manufacturer's instructions;
4. Moisture in Installation: dry, damp, water-filled, submerged, or installed in holes with moisture limitation conditions in accordance with manufacturer's instructions;
5. Installation Temperature: concrete at low temperature, adhesive at low temperature or preheated;
6. Depth of Hole (embedment depth);
7. Anchor Diameter;
8. Type of Concrete: Portland cement only, Portland cement with blast furnace slag, fly ash, or other additives;
9. Concrete Strength: low compressive strength, high compressive strength;
10. Type of Coarse Aggregate: mineralogy, absorption, and hardness; and
11. Concrete Age: installed and/or loaded at early age.

1.1.2 Factors related to service conditions

1. Elevated Temperature: temperature variations during the life of the structure, and effects of sustained elevated temperature;
2. Cracked or Uncracked Concrete: the presence of cracks can reduce the bond strength significantly;
3. Reduced Temperature: brittleness associated with reduced temperature;
4. Moisture in Service: adhesive anchor subjected to dry, damp, or immersed conditions during the life of the anchor;
5. Freeze Thaw: magnitude and frequency of freeze thaw cycles;

6. Seismic load: assess the anchor performance in cracked concrete conditions under cyclic loading;
7. Sustained loading (creep): evaluate the performance of anchors under sustained load at standard temperature and maximum long-term temperature;
8. Torque load: evaluate the maximum level of torque that can be applied to the installed anchor without inducing tension yield of the anchor element or damaging the adhesive bond;
9. Fatigue load: evaluate the performance of anchors under a fatigue program that specifies the loading method, load levels, frequency, and number of cycles; and
10. Shock load: withstand a certain shock load or maximum shock load, an anchor system can withstand without failure.

1.1.3 Factors related to the adhesive material

1. Type of Adhesive: for example: epoxy -mercaptan, epoxy -amine, vinylester, polyester, or hybrid;
2. Mixing Effort: how well the constituent parts are mixed prior to installation;
3. Adhesive Curing Time When First Loaded: 24 hours, 7 days, 28 days, or longer;
4. Bond Line Thickness: how much space is there between the anchor and the sides of the hole;
5. Fiber Content of Adhesive: type and proportion of fillers in the adhesive; and
6. Chemical Resistance: alkalinity, sulfur dioxide, and other compounds;

Many of these factors have been considered in design codes and guidelines, such as ACI 318 (2014), ACI 355.4 (2011) and EOTA (2002). Specifically, Factors 1.1.1.6~1.1.1.9, 1.1.2.2, 1.1.2.6, and 1.1.2.7 are considered in the capacity equations in ACI 318-14. In addition, Factors

1.1.1.2~1.1.1.5, 1.1.10, 1.1.2.1~1.1.2.5, and 1.1.3 mainly affect the bond of adhesive-concrete interfaces and are considered in this study.

1.2 Bond of Adhesive-Concrete Interface in Adhesive Anchors

Adhesive anchors are able to fully develop the capacities of threaded rods and deformed bars similar to cast-in place anchors; however, practices have indicated that bonding between the epoxy and concrete may not be reliable. As summarized in Cook et al. (2001), "*Products installed into holes that were damp, wet, or uncleaned generally showed reductions in bond strength with increased variation*." Bond failure with unexpected low capacities have been observed in practices if dust is left in the drilled hole due to construction errors, as indicated by the local contractor/installer. Other factors include high temperature/humidity, freeze/thaw cycles in the concrete, and sustained loading. For example, bond failure, shown in Figure 1.4 by the yellow color on the steel rod being pulled out, may be responsible to the failure of the anchors that support concrete ceiling panels in the Central Artery/Tunnel in Boston. On July 10, 2006, a 26-ton concrete ceiling panel fell on a car traveling in the tunnel, killing a passenger and injuring the driver (NTSB). During this influential accident, twenty adhesive anchors attaching a ceiling support beam to a concrete tunnel roof were pulled out and the ceiling panel fell onto the roadway. The national transportation safety board (NTSB) investigation concluded that the creep of the adhesive materials is the major reason for the failure. The analysis indicated that the maximum loads on the anchors was 2,823 pounds while the investigative tests of a total of 188 anchors from the same tunnel indicated that the actual capacities varied widely, from a low of 1,121 pounds to a high of 24,242 pounds, which is close to the reported capacity from laboratory results.

Failed epoxy anchors have also caused a larger-scale tunnel ceiling collapse in Tokyo-bound Sasago Tunnel on the Chuo Expressway in on December 2, 2012 near Tokyo, Japan. An

investigation and examination committee formed by the Ministry of Land, Infrastructure, Transport and Tourism (MLIT) of Japan for the ceiling panel collapse concluded that hydrolytic degradation of adhesive is one of main factors developed voids that cause the reduction of tensile capacity of adhesive anchors (Figure 1.5). In addition, cracks on adhesive-concrete interface was also a critical factor to reduce the bond strength. It is recommended that design of adhesive anchors must recognize that most of structural members are working in cracking state.

It is important to understand the nature of adhesive-concrete bond. Two-component adhesives start curing when the liquid-state resin component and hardener component are mixed together. The viscosity of the mixed adhesive increases and the adhesive hardens as time goes by due to the formation of cross-links within the material. The adhesive-concrete bond thus has three components: chemical bond, physical adhesion, and micro-mechanical interlock. The chemical bond is created through weak hydrogen bond between Magnesium, Calcium and Sodium in cement and the hardener of two-part adhesives. Physical adhesion is generated when liquid resin/hardener flow into capillary pores in cement paste. These two bond mechanisms can be significantly reduced/damaged with a tiny separation along the adhesive-concrete interface, caused by either concrete dust and moisture in drilled holes, or a crack in concrete passing the interface. The majority (around 65 percent according to Tatar et al. (2013)) of the bond capacity comes from mechanical interlock, as illustrated in Figure 1.6. Carbide-tipped hammer-drill bits and proper hole cleaning produce rough-sided holes such that hardened adhesive forms deformations that fit the concrete profile. Pullout failure occurs when these miniature deformations get crushed by the harder concrete, as shown by the traces of white power in Figure 1.6.

1.3 Engineered Adhesive-Concrete Interface for Adhesive Anchors

An invention has been formulated to change the adhesive-concrete interface and the safety of adhesive anchors. The invention is to create grooves in the drilled holes, as illustrated in Figure 1.7 before the holes are filled with adhesive. The hardened adhesive in the grooves will fundamentally change the load carrying mechanism of the epoxy-concrete interface from shear friction to mechanical interlock, making the interface reliable and robust. The goal of this study was to experimentally prove the idea that with grooves, the capacity and reliability of adhesive anchors can be greatly improved.

The threads should be created using a special concrete tapping bit, which is documented in the patent application (US Patent application No. 16/362,282 filed by UWM Research Foundation on behalf of Dr. Jian Zhao). However, the design and fabrication of the concrete tapping bit was beyond the scope of this study. Therefore, in the laboratory tests described below, screw anchors were used to cut threads in drilled holes. For example, for the ½-in [13 mm] adhesive anchors in the tests, the holes were drilled with a 9/16-in [14 mm]. hammer drill bit and a 5/8-in. [16 mm] screw anchor from Powers was used to cut threads. Female threads with a height of 0.12 in. [3 mm] were created by screw anchors and matching male threads with the same thread height were created after the adhesive anchor is installed.

Pullout tests were conducted in this study to examine the tensile capacities of the new adhesive anchors. The main factors considered in the tests included anchor diameters, hole cleanness, and pullout test setups among other factors such as moisture and concrete strength.

1.4 Organization of Dissertation

The proposed study is described below following a brief literature review in Chapter 2. Advanced surface analyses were conducted to better understand the adhesive-concrete interface (Chapter 3). Laboratory tests are presented in Chapter 4 and the results are analyzed in Chapter 5. A mixed pullout and concrete breakout failure mode was common, especially when the holes were thoroughly cleaned. Finite element (FE) analyses were presented in Chapter 6. The study is summarized in Chapter 7, which also includes a list of suggested future research topics. A total of ten appendices are included to document all the details of the study.

CHAPTER 2 LITERATURE REVIEW

2.1 Typical Behavior of Adhesive Anchors

The failure of adhesive anchors in tension can be controlled by anchor fracture, concrete breakout and anchor pullout. Cook and Klingner (1989) investigated the behavior of anchor connections governed by the strength of the anchor steel (anchor fracture) and strength of concrete (concrete breakout). It was observed that when the strength of the steel governs anchor ultimate strength, an anchor connection is ductile. When the strength of the embedment governs anchor ultimate strength, an anchor connection is non-ductile. Eligehausen et al. (2006b) summarized that failure modes of adhesive anchors include concrete cone failure, adhesive-concrete failure, threaded rod-adhesive failure, combination failure, steel failure in uncracked concrete. As Figure 2.1a shown, adhesive anchors with good adhesion has elastic performance up to their peak loads. Post-peak performance, that is after interface bond failure, is marked by gradual load drops with an increase in the pullout displacement because the frictional resistance is only a part of the adhesive-concrete adhesion. As Figure 2.1b shown, bonded anchors with low adhesion have short elastic performance up to the peak load and the hardened adhesive would experience the rough surface of the drilled hole when the anchor is pulled out. The large displacement is associated with the ultimate load because the adhesion strength is lower than the frictional resistance produced by the non-uniform surface of the drilled hole. The ultimate load of anchors that rely on the frictional resistance has large scatter. Specifically, anchors with poor bond strength would fail quickly after the peak load (Figure 2.1c). As Figure 2.1d shown, adhesive anchors with a relatively weaker adhesive-steel (A-S) interface (compared with the adhesive-concrete (A-C) interface) has elastic performance up to peak load and the post-peak part of the curve drops quickly as displacements increase because in

this case, the adhesive between the anchor threads is sheared off to cause relatively small frictional resistance between the adhesive and the anchor rod.

2.2 Capacity Prediction of Adhesive Anchors

2.2.1 Anchors controlled by pullout failure

Cook et al. (1992) compared the load-displacement behavior of retrofit (post-installed) anchors, including adhesive anchors, with cast-in (headed) anchors under monotonic tensile loading. The authors pointed out that "*for adhesive anchors, the load is transferred through the adhesive to the concrete along the entire embedded portion of the anchor. This load transfer depends on the strength of the adhesive-steel bond and the adhesive-concrete bond, and also on the extent to which the adhesive impregnates the concrete surrounding the drilled hole*." Bond failure was observed at both A-C interfaces (relatively ductile failure) and A-S interfaces (brittle failure). According to Cook et al. (1992), with increasing embedment depth, the shear stress is more uniform on the interface between the concrete and adhesive.

Cook et al. (1998) investigated different capacity models of single adhesive anchors with sufficient edge distances against a database consisting of nearly 3000 tests from European, Japanese, and American research reports. The collected tests had ranges of parameters, including the anchor diameter, concrete strength, and embedment depth, as listed in Table 2.1. A regression analysis was first attempted with an empirical equation shown below to gain insights on the critical factors for the tensile capacity of adhesive anchors.

$$N_u = \alpha d^{\beta} h_{ef}^{\gamma} f_c^{\delta} \tag{1}$$

The regression analysis indicated that "*it appears that the influence of hole diameter (β) and embedment depth (γ) can be approximated with sufficient accuracy by influence exponents $\beta = \gamma = 1.0$. The influence of concrete strength, on the other hand, varies significantly between data sets (products)*." The authors derived that the concrete strength may impact bond strength of adhesives. Cook et al. (1998) considered five different bond models to explain the test results both in terms of the measured ultimate capacity and the observed anchor failure modes (as shown in Figure 2.2). Specifically, a shallow concrete cone is likely form when adhesive anchors fail due to bond failure, on A-C interface, A-S interface, or partial of both interfaces. These models included

- Bond models: models that are dependent on the bond strength of the product, the diameter, and the embedment length;
- Bond models neglecting the shallow concrete cone: Similar to bond models except that the embedment length is reduced to account for the shallow concrete cone;
- Cone models with bond models: Models that use concrete cone formulas for shallow embedment and bond stress formulas for deeper embedment;
- Combined cone/bond model: Models that use concrete cone formulas for shallow embedment and combined cone/bond models for deeper embedment; and
- Two interface bond model: A bond model that is based on distinguishing between bond failure modes at the steel/ adhesive interface and adhesive/concrete interface.

Cook et al. (1998) concluded that "Uniform bond stress models provide a good fit to the database and are based on a simple physical model" though a combined cone models with bond models may provide a better fit to the data.

The equation of uniform bond stress is shown in Equation (2),

$$N_u = \tau\pi d_a h_{ef} \quad (2)$$

where h_{ef} is embedment depth; d_a is anchor diameter; and τ is the bond strength. The equation is valid for $4 \leq h_{ef}/d_a \leq 20$, $d_a \leq 2$ in. [50 mm], and a bond area $\pi d_a h_{ef} \leq 90$ in.^{2} [58,000 mm^2]. (Eligehausen et al. 2006a)

Due to a direct shear test cannot properly predict the bond strength between the concrete and the adhesive, confined or unconfined tests have been used to evaluate the bond strength. Eligehausen et al. (2004) found that the bond stress is distributed nonlinearly along the embedment length at the ultimate load, with lower bond stresses at the concrete surface and higher bond stresses at the end of the anchor based on the experimental results.

Cook et al. (1996) found that with proper installation, the mean bond strength of individual adhesive products could vary from 2.3 MPa [334 psi] to 19.5 MPa [2828 psi] and the bond strengths are specific to adhesive products. The conclusion was based on about 1300 confined pullout tests (the test setup is shown in Figure. 2.3) of 20 adhesive products from 12 manufacturers. In addition, the authors indicated that the bond strengths from confined pullout tests cannot be directly used for design purposes because the anchors in the extensive tests did not represent those in the field, including both the stress field and adverse installation/in-service conditions.

Zamora et al. (2003) conducted unconfined pullout tests of concrete anchors, including 129 adhesive anchors. The test setup is shown in Figure 2.4. The tests indicated an average bond strength of 18.4 MPa [2669 psi] as shown in Figure 2.5. Note that 92 percent of the tests were controlled by bond failure at the A-S interface. This may have been caused by minor anchor adjustment during installation as revealed in Appendix V. In addition, typical failed anchors

included a concrete breakout cone (Figure 2.6) that cannot be categorized as shallow cone as assumed in the earlier study by Cook et al. (1998).

Eligehausen et al. (2006a) summarized that a behavioral model Equation (3a) to estimate the ultimate tension capacity of adhesive anchors. This behavioral model offers design provisions of adhesive anchorage systems for building codes and standards and is based on widespread numerical and experimental results. The nominal bond strength of adhesive bonded anchors is product specific and relied on the mean bond strength of anchors installed based on the manufacture's guidelines. The final bond strength must be corrected by the scatter of the test results and the sensitivity to installation and in-service conditions.

$$\overline{N_T} = \frac{A_{Nc}}{A_{Nco}} \Psi_{ed,N} \Psi_{g,N} \overline{N_\tau} \leq \overline{N_{cb}} \ (lb \ or \ N) \tag{3a}$$

$$\overline{N_{cb}} = \frac{A_{Nc}}{A_{Nco}} \Psi_{ed,N} \ \overline{N_b} \ (lb \ or \ N) \tag{3b}$$

$$\overline{N_b} = 35\sqrt{f_c} h_{ef}^{1.5} \ (lb), \overline{N_b} = 14.7\sqrt{f_c} h_{ef}^{1.5} \ (N), \tag{3c}$$

$$\Psi_{ed,N} = 0.7 + 0.3 \frac{c_{a1}}{c_{cr}} \ if \ c_{a1} < c_{cr} \tag{3d}$$

$$\Psi_{g,No} = \Psi_{g,No} - \frac{s}{s_{cr}} (\Psi_{g,No} - 1), s = 0 \ where \ \Psi_{g,N} = \Psi_{g,No}; s_{cr} = where \ \Psi_{g,N} = 1.0 \tag{3f}$$

$$\overline{N_\tau} = \bar{\tau} \pi d_a h_{ef} \ (lb \ or \ N) \tag{3e}$$

Where A_{Nc} and A_{Nco} are determined according to Figure 2.7; $\bar{\tau}$ is $\bar{\tau}$ = mean uniform bond strength at steel/mortar interface, psi [MPa]; d_a is anchor diameter in. [mm]; c_{cr} is edge distance where strength of anchor is not influenced by free edge, $1.5h_{ef}$, in. [mm]; s_{cr} is edge distance where strength of anchor is not influenced by free edge, $0.3h_{ef}$, in. [mm]; h_{ef} is embedment depth in. [mm]; f_c = compressive strength of concrete, psi [MPa]; $\overline{N_\tau}$ is the uniform bond stress for adhesive

anchors; $\overline{N_{cb}}$ is mean concrete breakout strength in tension of single anchor at edge or of group of anchors in uncracked concrete, lb [N]; $\overline{N_b}$ is mean basic concrete breakout strength in tension of single anchor in uncracked concrete, lb [N]; $\overline{N_T}$ is mean bond pullout strength in tension of single adhesive anchor at edge or of group of adhesive anchors in uncracked concrete, lb [N]; $\overline{N_\tau}$ = mean bond pullout strength in tension of single adhesive anchor in uncracked concrete, lb [N]; $\Psi_{ed,N}$ is factor used to modify tensile strength of anchors based on proximity to edges of concrete member; $\Psi_{g,N}$ is factor used to modify tensile strength of adhesive anchors based on number and spacing of anchors in group and mean bond strength; $\Psi_{g,No}$ = factor used with $\Psi_{g,N}$ to modify tensile strength of adhesive anchors based on number of anchors in group and mean bond strength.

2.2.2 Anchors controlled by concrete breakout failure

Concrete breakout failure is not the focus of this study; hence, the literature review is very brief. Fuchs et al. (1995) developed the concrete capacity design (CCD) approach to predict the concrete failure load of anchors in uncracked concrete under monotonic loading. The searchers compared ACI 349-85 method and CCD method with a database including about 1200 European and American tests. The single anchor far from and near the edge, anchor group, tension loading, and shear loading were considered as variations. An inclination between the failure surface and surface of the concrete specimen is assumed about 35 degree. The concrete cone failure load of a single anchor in uncracked concrete without edge influence or overlap cones of neighboring anchors is defined by the equation (4).

$$N_{no} = k_{nc}\sqrt{f_c'}h_{ef}^{1.5}, \quad (4)$$

where k_{nc} is 35 for post-installed mechanical anchors; $\sqrt{f_c'}$ is concrete compression strength measured on 6 by 12-in. cylinders in psi; and h_{ef} is the effective embedment depth. Eligehausen

et al., (2006a) later extended the applicability of this equation and k_{nc} factor of 35 to adhesive anchors.

Shirvani et al. (2004) investigated four methods to estimate the concrete breakout capacity of single anchors under static tension loading in both uncracked concrete and cracked concrete. The methods included 45-degree cone method, concrete capacity design method (CCD method), a theoretical method, and a variation of the CCD method. The 45-degree cone method is that assume a constant tensile stress of $4\sqrt{f_c'}$ acts on the projected area of a 45-degree cone radiating towards the free surface from the bearing edge of the anchor. The CC method combined extensive test results and some extent on fracture mechanics (Fuchs et al. 1995). The theoretical method is based on linear elastic fracture mechanics, in which the failure criterion is expressed in terms of the energy consumed per unit crack length increment and includes the size effect (Bazant 1984; Eligehausen and Ozbolt 1992). The comparison with a worldwide database of 1566 tests confirmed the applicability of CCD method proposed by Fuchs et al. (1995).

2.3 Factors Impacting Bond Strength of Adhesive Anchors

Lee et al. (1980) found that the cleanliness of the drilled hole impacts the bond strength between the adhesive-concrete interface. Mark et al. (1988) indicated that the bond development of chemical anchors transfers the load to the hole wall of the concrete and through by the mechanical interlock formed by the rough wall. Two component systems, an active component and a reactant, mixed together to generate bonding are for all forms of chemical adhesives. The performance of anchors is greatly impacted by the cracks occurred in concrete. The anchor behaviors in uncracked concrete are significantly different from ones in cracked concrete such as load-displacement behavior and ultimate strengths.

Eligehasuen and Meszaros (1996) compared load-displacement curves of bond anchors M12 under cleaned holes using a stiff brush and blowing with hand pump to under uncleaned holes. The results show that the bond strength of injection anchors, the adhesive premixes in the nozzle, can be reduced by up to 50% under inadequate hole cleaning. Meszaros and Eligehausen (1998) conducted influence of intensity of hole cleaning on the bond strength of injection anchor M12 in dry concrete and considered that it is critical to clean drilled holes by using a proper stiff brush and blowing clean. Using compressed air only cannot remove adequately the dust on the inside wall of drilled holes. Cook, Kunz, Fuchs, Konz (1998) concluded that for most adhesive products, the bond strength in higher compressive concrete can be reduced due to increasing hole smoothness.

Spieth and Eligehausen (2002) investigated bond stress-displacement curves of injection type bonded anchors with a diameter d_s = 20 mm anchored in holes made by hammer drilling. The results show that the bond strength from a hammer-drilled hole is higher than one from a core drilled hole. The load-bearing behavior of bonded anchor system is greatly impacted by a diamond drill, as shown in Figure. 2.8.

Cook and Konz (2001) studied many factors that may impact the performance of adhesive anchors. The authors conducted 765 confined pullout tests of adhesive anchors using 20 adhesive products from 12 manufactures to investigate potential influence of bond strength impacted various factors. The intent of using confined pullout tests was to focus on comparisons of bond strength under different conditions instead of determining a design bond strength.

It was found that the cleanliness of the hole greatly influences the bond strength due to dusts left in drilled holes likely during construction. Uncleaned holes were defined such that the loose concrete particles leave on the inside surface of the hole and trap in the pores created by the drilling

process. To simulate the uncleaned holes, the researchers drilled holes a little deeper to provide spaces for the settlement of concrete particles without impacting the due embedment depths and no any material was removed from the drilled holes. This is similar to 0% cleaning as defined in this study shown in Appendix V. The bond strength of anchors in uncleaned holes decreased and the variation of test results increased. The average bond strength from the uncleaned holes was 71% of that from the reference specimens with anchors installed in properly cleaned holes. The average coefficient of variation (COV) was 20% while the observed COV was only 10% in the reference tests.

The moisture is another factor to impact the bond strength and it happens anywhere. In a damp hole, the adhesive material cannot penetrate the pores that were filled water and were created by drilling and cleaning. The bond strength of adhesive anchors was reduced because the mechanical interlock of the interface between the adhesive and the concrete was interfered. The chemical reaction between resin and hardener was also blocked. To model the field moisture condition, for damp holes, drilled holes were filled with water after cleaning and kept the water 1 in. height above the holes for 7 days. Before the installation, the standing water in and around the holes was removed by compressed air. Compared with the value of a dry installation, the bond strength decreased, and the test variation increased. The average bond strength from the damp holes was 77% compared with reference holes. The average coefficient of variation was 23%. The average bond strength from the wet holes was 43% compared with reference holes. And the average coefficient of variation was 27%. There is no reason that the bond strength of product R from the wet hole increases 64% over the dry hole. Therefore, it was concluded that moisture can interfere the interactions between the adhesive and the concrete.

Lefebvre et al. (2000) used two model compounds to verify the influence of water molecular on interactions between hydroxyls and other hydrogen bonding sites in the epoxy under the critical humidity condition. One simulated the epoxy network, and another is that hydrogen atoms replace all the hydroxyl groups. Lefebvre used molecular simulation software to simulate these model compounds and found that the hydrogen bond network in the epoxy was replaced by the water molecular at high water concentration.

Matsuzaki et al. (2010) studied effect of the embedment length and the edge distance on tensile resistance. Matsuzaki claimed that bonded anchors rely on the schemed surface of the anchor rod or the roughened surface of the inside drilled hole and shear resistance of the bonding agent hardened. From the Figure 2.9, the adhesive filled the gap between the surface of the anchor rod and holes on the concrete surface. Figure 2.10 shows different effective embedment lengths cause different types of cone failure. The effective embedment length is less than 10 d_a (anchor diameter) while the cone failure zone is large. When the embedment length is more than 10 d_a, the cone failure zone is smaller, and the chance of bond failure mode is obviously increasing. The embedment length for strength calculation is that the effective embedment length subtracts two times anchor diameter because the small-scale cone failure caused by tensile force is near to the concrete surface, insufficient adhesive is filled near the concrete surface, and lose adhesion caused by the bearing pressure of the concrete under shear forces. The secure an edge distance is 10 d_a or more and anchor spacing of 20 d_a or more. If the edge distance or the anchor spacing cannot meet this requirement, the average bond strength is determined by multiplying the basic average bond strength by α_n shown in Figure 2.11.

Davis (2012) studied the sustained load performance of adhesive anchors in concrete under various installation and in-service conditions. The sensitivity of three ICC-ES 308 approved adhesive

anchor systems was measured by using a stress versus time-to-failure approach. Results shown that only elevated in-service temperature and manufacture's cure time on sustained loads have more adverse effects compared to those in short-term tests with fully cured adhesive during a reasonable structure lifetime of 75 years.

2.4 Adhesive Anchors in Cracked Concrete

The bond strength of adhesive anchors can be impacted greatly in cracked concrete. Eligehausen and Balogh (1995) considered that the bond anchor is more sensitivity in cracked concrete compared with uncracked concrete. The authors studied the behavior of fasteners loaded in tension in cracked reinforced concrete because most of reinforced concrete members are assumed that the concrete is cracked during service status. The concrete slabs with a depth of 9.8 in. [248.9 mm] reinforced with wire mesh. Load applied on the fasteners was 1.3 times the admissible load. The slab was loaded gradually up to the admissible service load to generate the hairline cracks. The average crack width was 0.008 in. [0.2 mm] and the anchorage zone of all anchors was passed through directly by cracks under the allowable service load. The post-installed anchors were closed to hairline cracks produced without loading on the member. To obtain the desired width, loading the specimen was used to expand the cracks and a load- or deformation-controlled method was used to load the anchor till failure while the crack was keeping open. A line crack with closely constant width along the member depth was running in one direction and was in the anchors. The bond stress between the anchor and adhesive and inside surfaces of the drilled hole was used to resist a tension load. Due to the concrete strength is normally less than adhesive strength, the crack will pass through the anchor and the adhesion around concrete and adhesive will be weaken. The friction along the rough adhesive surface in the drilled hole might be happened to increase the resistance when the bond strength is over. The researchers found that the cracks will develop

around the anchor holes in the concrete and the cracks will reduce adhesion on the adhesive-concrete interface. The authors concluded that the reduction of bond strengths in cracked concrete for chemical anchors can be around 33% compared to the value in uncracked concrete and a crack width was 0.012 in. [0.3 mm].

Meszaros (1999) conducted putout tension tests of injection anchors in cracked concrete. The anchors were installed in hairline cracks and then the desired crack width was enlarged. The anchors were pulled out up to failure with keeping the crack width desired. The results were scattered due to the abnormal crack paths. For example, cracks partly pass through the plane of the anchor axis. The anchor capacities that a crack width varied from 0.012 in. [0.3 mm] to 0.016 in. [0.4 mm] in cracked concrete are approximately 25% to 80% of the value in uncracked concrete.

Eligehausen et al. (2004) introduced the method to form and open cracks in the concrete for testing anchors due to ACI 355.2 does not have these details. Anchors are applied static tension loading in static cracks (width = 0.012 in. [0.3 mm] and 0.02 in. [0.5 mm]). The crack width must be kept the same roughly over the depth of the test member and the crack must keep roughly perpendicular to the surface of the concrete member to make sure that the axis of the anchor is in the plane of the crack. To ensure enough reinforcement percentage for opening cracks in concrete members, the reinforcement ratio is at least 1% of the cross-sectional area of the concrete member that is parallel to the crack plane. To ensure closely uniform crack width through the concrete member, the symmetrical reinforcement should be setup close to the top and bottom surfaces of the concrete member. Thin strips of sheet metal are normally used as crack inducers to generate the cracks within a small band. The thin strips that is cast into the concrete member weaken the cross section of concrete at the required location. The reinforcement between the thin strips and the concrete is applied the oil and grease to reduce the bond. The crack inducers should be placed at the mean

crack spacing in the concrete member. A central external tensile loading is applied on the reinforcing bars to form the crack and to control the crack width. The average crack opening width for a test series shall be more than the crack width required. Individual crack opening widths shall be less than 15% of the crack width required. A square support of the hydraulic ram is used to avoid a non-uniform crack width over the depth of the concrete member. The depth of the concrete member is more than twice of the effective embedment depth of the anchor.

Eligehausen et al. (2006b) claimed that fasteners rely on mechanical interlock, friction, chemical bond or some combination of these mechanisms to transfer external loads. In addition, the failure modes of bonded anchors are pullout, anchor rupture, and combination failure in cracked concrete. Pullout failure normally occurs bond losses between adhesive and concrete or between adhesive and anchor rod. Concrete cone failures scarcely happen during tests in cracked concrete. As Figure 2.12 shown, the ultimate load in cracked concrete is lower than the load in uncracked concrete. After losing adhesion between adhesive and drilled hole, the anchor rod is pulled out while increasing the load with large displacements due to the friction between adhesive and rough surfaces in drilled holes. The load-displacement behavior of bonded anchors after losing initial bond cannot be expected in cracked concrete because the condition of hole surfaces highly impacts the friction resistance. The further reduction of the ultimate load is also influenced by improper hole cleaning in cracked concrete. The reduction caused by unclean drilled hole is up to 60% for injection-type anchors.

Elighausen et al. (2006b) claimed that the crack path redirects around the anchor along adhesive-concrete interface caused by reopening the crack after anchor installation that use the tensile strength of the polymer adhesives. The reason of this is that the high tensile strength of the polymer adhesives was used in the anchor system. Moreover, as Figure 2.13 shown, the redirection of the

crack path leads to the eccentricity between the resultant of the bond resistance and tensile load. This causes tensile stresses perpendicular to bond interface to reduce the bond capacity.

Anton et al. (2008) investigated the behavior of various types of post-installed anchors (M12 existing European Technical Approval) in cracked concrete under simulated seismic loading using a MDOF shake table. The purpose of this paper is that the resistance of the fastening between existing buildings and retrofitted members can be calculated by the testing results of the anchors under seismic conditions. The hammering in steel wedges with sleeves in the tube was used to generated fine hair cracks. Then, the anchors were placed in the cracks and the steel weights (300 kg per anchor) and the prescribed torque for the prestress were applied on the anchors. The half torque was remained after 10 minutes and the crack width of 0.06 in. [1.5 mm] was widened.

The failure mode of the bonded anchor was totally pullout at 800% of the design peak ground acceleration. The Figure 1 shows the plastic deformation of the different anchor types in axial and vertical direction are plotted as a function of the seismic level. The axil and vertical displacements of the bonded anchor are the highest at each seismic level. The bonded anchor shows a higher reliability with 0.06 in. [1.5 mm] wide cracks compared to expansion and undercut anchor systems. The author also found one undercut anchor did not suffered damages during the entire tests due to the crack was branched at the anchor position that the crack width is only approximately 0.02 in. [0.5 mm]. It means that the degree of damage of the concrete significantly impacts anchor performance under seismic loading.

2.5 Behavior of Screw Anchors

Screw anchors cut threads on the surface in the drilled hole and the mechanical interlock transfers the tensile load into the concrete. The screw anchors are driven by using an electric screw-gun and a torque wrench. The over torque of the screw anchor can damage the thread cut into the surface

in the drilled hole so that the failure load is greatly reduced. Using a larger embedment depth can prevent from the damage of the threads cut into the surface in the drilled hole.

Küenzlen and Sippel (2001) conducted pull-out tension tests of screw anchors in uncracked concrete and found that the concrete cone breakout contributed to the failure without over-torqued during installation. The failure stats from the first thread at the tip of the screw anchor under the small embedment depth. The concrete breakout is near the surface and the rest of the screw is pulled out while the embedment depth is increasing. This failure mode is same as that of bonded anchors. The steel failure occurs when the embedment depth is larger.

Eligehausen and Küenzlen (2002) investigated the failure loads of screw anchors in uncracked concrete that are a thread over the entire embedment depth from different manufactures and different diameters. The equation (5) of the average failure load is

$$N_u = 10.5\sqrt{f_{cc200}}\, h_{ef}^{1.5} \tag{5}$$

Where the embedded depth h_{ef} is h_{nom} -0.5 h-h_s, in which h_{nom} is the length between end of the screw anchor and the concrete surface, h is the distance between the threads, $h_s$is the distance between the tip of the screw anchor and fist thread, and f_{cc200}= 30 N/mm^2 by assuming a square root function.

Olsen et al. (2012) conducted an empirical model based on several types of metric screw anchors tested in Europe. The design model was evaluated by using the existing database (Table 2.2) of tension tests on metric screw anchors including many tests on inch-sized screw anchors in cracked and uncracked concrete. The equation (6) for tension loads is

$$N_{cb} = k_c\sqrt{f_c'}\, h_{ef}^{1.5}, \tag{6}$$

where h_{ef} is the calculated effective embedment depth of the concrete screw, $0.85(h_{nom} - 0.5\ h_t - h_s)$, in which, h_{nom} = the embedment depth/setting depth of the screw anchor in concrete; h_t = the distance of the thread; h_s = the length of the tip of the concrete screw; N_{cb} = the concrete breakout capacity; k_c =35 for uncracked concrete to calculate average ultimate loads, and 24.5 for cracked concrete to calculate average ultimate load; and f_c' = the concrete compressive strength.

2.6 Summary

From the literature review above, one may conclude that the tensile capacities of adhesive anchors are greatly impacted by dusts, moisture and cracks in the drilled hole. The adhesive-concrete interface is very important because most reductions of the bond strength occur at the interface between the adhesive and the concrete. The proposed new adhesive anchors in this study is not about engineering new adhesives, but the load transfer through the adhesives.

CHAPTER 3 UNDERSTANDING OF ADHESIVE-CONCRETE INTERFACE

3.1 Introduction

The bond between adhesive and concrete consists of mechanical and chemical bond as revealed by Tatar et al. (2013) in a study of bond between fiber reinforced polymer (FRP) strips and cement mortar. The authors developed a direct shear test to measure the fracture energy between epoxy and mortar cubes considering a Mode II fracture process, as illustrated in Figure 3.1. Concrete surface roughness, which mainly controls the mechanical bond (i.e., the static friction), was controlled through various surface treatments such as sandblasting and polishing. Polished mortar surfaces, with a much lower surface profile shown in Figure 3.2a were deemed smooth surfaces, on which the adhesive-mortar bond was assumed mainly through chemical bond. On the other hand, both the mechanical bond and chemical bond were assumed on sandblasted surfaces with rougher surface profiles (Figure 3.2b). The authors used calculated fracture energy, instead of measured peak loads, to quantify that chemical bond contributed about 35 percent of the total bond strength while mechanical bond contributed 65 percent. The profile heights across a 1/4 in. distance shown in Figure 3.2b indicate that the sandblasted surface had multiple valleys with a depth around 0.8 microinchs and opening about 1/50 in. Equipment at the UWM Advanced Analysis Facility (AAF) was used to examine surface of holes drilled in concrete using a rotary hammer drill bit.

3.2 Observation of surface of Drilled Hole using a Laser Confocal Microscope

To observe the profile of the surface of a drilled hole in concrete, a small piece (Figure 3.3) was peeled from inside wall of the drilled hole. The observed area (1.3×1.3 mm [0.05×0.05 in.]) is located near a black aggregate particle as indicated by the arrow in Figure 3.3. With a

magnification of 200 times, Figure 3.4a shows the picture of the observed area and Figure 3.4b shows the pane view of the observed area with colored profile heights (the color scale is from the lowest point within the observed area). These two plots were viewed in 3D in Figures 3.4c and 3.4d. Section views of the observed area are shown in Figure 3.5 for five sections perpendicular to the X-axis and Figure 3.6 for sections perpendicular to the Y-axis. These section views described a profile valley within the observed area, with a diameter of roughly 1 mm [0.04 in.] and a depth of 0.3 mm [0.012 in.]. In addition, the valley has a much larger opening at the surface compared with that at the bottom, which contradicts the conceived profile by Matsuzaki et al. (2010), as shown in Figure 2.10. It is reasonable to assume that the black aggregate particle in Figure 3.3 represents the wall surface of the drilled hole, and the valley represents the rough surface created by a proper cleaning process. The observation confirmed the profilometer measurements by Tatar et al. (2013). Adhesive flow into such profile valleys would form spikes as shown in Figure 1.6 after hardening, and the adhesive spikes provide mechanical bond as explained in Section 1.2 and by Tartar et al. (2013).

The microscope lens was moved away before some dust from hole drilling was randomly blown to the observed area shown in Figure 3.7, and the sample was observed again. This observation sequence was selected in order to maintain the same observation area (1.3×1.3 mm [0.05×0.05 in.]) near a black aggregate particle) though randomly placed dust may not represent the surface of an uncleaned hole. The dust filled most of the profile valley though one must be cautious about the newly formed dust peak. It is envisioned that valleys filled with dust or loose concrete particles will prevent adhesive from forming spikes, leading to greatly reduced mechanical bond. Concrete dust left in drilled holes also reduces chemical bond between adhesive and concrete. This is

examined using a scanning electronic microscope (SEM) and an energy dispersive x-ray spectroscope.

3.3 Observation of Adhesive-Concrete Interface using SEM and EDS

Chemical bond between adhesive and concrete is generally created through weak hydrogen bond between Magnesium, Calcium and Sodium in concrete and the hardener of a two-part adhesive. In studying the epoxy coating on Portland cement concrete, Djouani et al. (2011) studied the wettability of the cementitious substrate by polymer, through observing the penetration of adhesive into the cement substrate using a fluorescent dye incorporated into the epoxy adhesive. The authors stated that "*observations by optical microscopy under ultraviolet (UV) light illumination showed that the epoxy adhesive can penetrate the porous structure of the cementitious substrates up to depths of 100–200 micrometer, depending both on the porosity and the degree of water saturation of the cementitious substrate, and on the viscosity of the resin*." The observed cement paste–epoxy interface is shown in Figure 3.8.

An adhesive sample was peeled from a tested anchor (Figure 3.9), on which a small piece of concrete was attached. The cross section of the adhesive-concrete interface was studied. To make an observable specimen, the adhesive sample was temporarily fixed, and mounting epoxy made by Electron Microscopy Sciences was used to keep the sample in place. The sample was then grounded down to expose the adhesive-concrete interface, polished, and adding with a metal coating (Au) as shown in Figure 3.10.

To identify the location of adhesive-concrete interface, an element analysis was conducted. At the location marked by "spectrum2" in Figure 3.11, elements of CaCO3 and SiO2 were 36.6 and 11.24 percent of the total weight and 75.91 and 17.5 percent of the total atomic weight, respectively. This indicates that specturm2 is on the adhesive side. At the location marked by "spectrum3" in

Figure 3.12, the analysis indicates that elements of CaCO3, SiO2 and MgO were 12.17, 27.59, and 11.44 percent of the total weight and 29.33, 49.89, and 13.61 percent of the total atomic weight, respectively. Note that the element of MgO is one of concrete ingredients, indicating that spectrum3 is on the concrete side. Before the specimen is observed under EDS, an additional point, spectrum4 shown in Figure 3.16, was analyzed near the apparent interface zone. The analysis shows that elements of CaCO3, SiO2, MgO were 15.3, 13.44, and 4.3 percent of the total weight and 46.32, 30.55, and 6.43 percent of the total atomic weight, respectively. The element of MgO at a lower concentration confirms the interface passing Point spectrum4.

The sample was selected randomly, and the magnification is 10 times higher than the images obtained using the laser confocal microscope; hence there is no way to link the adhesive-concrete interfaces in Figures 3.11 through 3.13 with the profiles revealed in Figure 3.10. Nevertheless, the apparent adhesive-concrete interface in Figures 3.11 through 3.13 did bend near the top center region of the figures, which may reflect the curvy concrete surfaces. At a magnification about 2000 times, the images show that adhesive impregnated pore structures in the cement paste. In addition, both adhesive on the left side and cement past on the right side have a denser microstructure than the adhesive-concrete interface, indicating that the interface itself may be weak, and it is the micro-level interlock that provides mechanical bond-frictional resistance against relative motion on the interface.

The adhesive-concrete interface of the sample was observed along a scan line using an Energy Dispersive X-Ray Spectroscope. Figure 3.14 shows the variation of the intensity of several elements including, calcium, magnesium, Silicon, aluminum, oxygen, and carbon. The calcium and magnesium intensity along the scan line across the adhesive-concrete (cement paste) are shown in Figure 3.15. There is a local element peak between 5 and 10 micrometers, indicating that

calcium and magnesium, two elements belong to cement paste, are drawn towards adhesive. This may confirm Djouani's conclusion that chemical reaction may have occurred at the interface: the chemical bond was caused by the electronic attraction between the hardener and concrete. Specifically, the N-H bond from the hardener carries positive charge and O-H bond from C-S-H (hydrated cement) carries negative charge during the interaction. In the electron donor-acceptor interaction, calcium and magnesium may have crosslinked with OH bond. More importantly, the reaction seems have occurred with a distance around 5μm as shown in Figure 3.16.

This one EDS analysis may not be sufficient to draw any firm conclusion, However, it may reveal that dust left in drilled holes, as shown in Figure 3.7, would completely damage the needed chemical bond on the adhesive-concrete interface, thus reducing the capacity of adhesive anchors. The impact of dust on adhesive-concrete interface was studied using nano-indentation because EDS analyses for adhesive-dust-concrete interface would show similar results except that the chemical reaction would have been between adhesive and dust, which has the same chemical elements as concrete.

3.4 Observation of Adhesive-Concrete Interface using Nano-Indentation

The mechanical properties of the adhesive-dust-concrete interface was tested using a Model G200 nano indenter G200 by Agilent Technologies. An adhesive sample with dusts was peeled from a tested anchor. The indent area was shown in Figure 3.17a. The magnification of the interface is 150 times by using optical microscope as Figure 3.17b. The interface was blocked by a layer dust with about 100 μm of the thickness. This also shows that the chemical bond on the adhesive-concrete interface would damage by dusts. The test parameters required input were shown as follows: the surface approach velocity was 10 nm/s; Depth limit was 2000 nm; Strain rate target was 0.05 per second; Harmonic was 2 nm; Frequency was 45 Hz; Surface approach distance was

1000 nm and poisons ratio were 0.2. As Figure 3.18 shown, three indented points were around the interface and another 3 points far away from the interface for comparations. As Table 3.19 shown, those properties are very closed, but it cannot say that the dust does not interact with epoxy. This analysis was not successful largely because the specimen was not properly polished such that the indentation could not reach comparable depth consistently.

3.5 Summary

It is envisioned that a tiny separation along the adhesive-concrete interface, caused by either concrete dust and moisture in drilled holes, or a crack in concrete passing the interface, may cause significant damage to the bond strength, both the chemical bond and mechanical bond. Concrete dust/moisture and cracks do exist in practices. For example, a recent field study was conducted on the field installation of adhesive anchor systems at construction sites in California, Florida, Illinois, New York, and Pennsylvania in 2011 (Grosser et al. 2011). Out of 26 applications monitored, the drilled holes in only a small number of installations were cleaned following a general Manufacturer's Printed Installation Instruction (MPII). In addition, Black (2017) conducted proof tests of adhesive anchors used in fixing metal railing to bridges. Out of 48 bridges studied, the adhesive anchors in 35 bridges had bond issues that some adhesives that were not appropriate for the application. Author attribute the weak bond to installation deficiencies including improper cleaning of drilled holes, insufficient mixing of adhesive, shallow holes, inadequate amounts of adhesive injected into holes prior to anchorage placement, injection and anchorage placement procedures which resulted in air pockets in the adhesive, saturated or wet conditions in the holes prior to anchor placement, and improper leveling and placement of anchorages which resulted in shallow embedment (Black 2017).

CHAPTER 4 EXPERIMENTAL RESEARCH

4.1 Introduction

It is envisioned that the new adhesive anchoring system with threads in drilled holes can provide more robust behavior even with many adverse factors identified in Chapter 1. The literature review on Chapter 2 identified that the tensile capacities of adhesive anchors are greatly impacted by dusts, moisture and cracks in the drilled hole. In this study, moisture was not chosen as a parameter because our preliminary tests (Appendix IX) showed that the vinylester adhesive we used is not sensitive to this condition. Test of anchors installed in cracked concrete could not be finished due to limitations in the project funding and time. Hence, this chapter documents the tests of adhesive anchors in uncracked concrete to provide behavioral data for the new adhesive anchoring system.

4.2 Experimental program

The purpose of tension tests is to measure the tension capacity of two types of adhesive anchors likely dominated by bond strength. The comparison of new adhesive anchors with traditional anchors considered the following parameters:

1. Anchor diameters: ½ in. [13 mm] and 5/8 in. [16 mm];
2. Hole cleaning conditions: unclean; partially clean; and fully clean;
3. Reinforcement in concrete: no reinforcement and code-conforming anchor reinforcement; and
4. Test setup: confined pullout tests and unconfined pullout tests.

Reinforcement was used only for anchors in fully cleaned holes and one group of partially cleaned threaded holes; hence, a total of fourteen tests were planned as shown in Table 4.1. Each test was repeated four times for result consistency. Specimens in the test matrix were named as follows: unconfined test of anchors in a smooth hole (UC), anchors in a unclean smooth hole (UC0%),

anchors in a partially cleaned smooth hole (UC50%), unconfined test of anchors in a threaded hole (UCT), anchors in a unclean threaded hole (UCT0%), anchors in a partially cleaned threaded hole (UCT50%), anchors in a clean threaded hole drilled in concrete with code-conforming anchor reinforcement (UCT#R) and anchors in a partially clean threaded hole drilled in concrete with code-conforming anchor reinforcement (UCT#R50%). Again, the use of code-conforming anchor reinforcement does not implicate any practical purpose because post-installed anchors are not usually installed in concrete with proper anchor reinforcement.

4.2 Design of Unconfined Test Specimens

4.2.1 Embedded depth of anchors

Traditional adhesive anchors were expected to develop bond failure at A-C interface for the purposed of this study. Hence, the embedded depth of the test anchors must be properly chosen. Adhesive anchors in tension may fail in anchor fracture, concrete breakout, and pullout as shown in Figure 1.2. The capacities of the selected anchors (made of ½-in. [13-mm] or 5/18 in. [16-mm] ASTM A193 Grade B7 threaded rods) are compared in Figures 4.1 and 4.2 for a range of embedded depths.

The concrete breakout capacities were calculated assuming a compressive strength of 6000 psi [41.4 MPa]. Two groups of preliminary tests were conducted as briefly documented in Appendix IX, in which the first group of tests were conducted with a concrete strength around 5000 psi [34.5 MPa] and the second group on 8000 psi [55.2 MPa] concrete; hence a more commonly seen concrete strength was chosen. The actual compressive strength of the concrete was about 6200 psi [42.8 MPa] over the entire test period as shown in Appendix I. The concrete capacity design (CCD) method (Equation (4) in Chapter 2) was used with a constant (k_{nc}) of 35. Note that this constant

is different from that (k_{nc} =24) stipulated in ACI 318-14 for design capacity calculation, and represents observations documented in the literature (Eligehausen et al., 2006b).

The capacities corresponding to steel fracture were calculated assuming an ultimate tensile strength (f_{uta}) of 125 ksi [862.5 MPa], which is the minimum required tensile strength in ASTM A193 (2000). This was slightly below the strength of similar materials used in previous studies (Zhao 2014), 131 ksi [903.9 MPa]. The actual ultimate tensile strength of the threaded rods in this study was measured using both standard coupon specimens and threaded rod specimens, as documented in Appendix II.

The capacities corresponding to pullout failure were calculated using the well-recognized uniform bond stress model (Equation (2) in Chapter 2). Note that a shallow breakout cone is expected to develop in anchors failed by pullout, as illustrated in Figure 1.2. In addition, Cook et al. (1998) suggested that a mixed concrete breakout with uniform bond model may provide more accurate prediction of anchor capacities. However, the depth of such breakout cones is difficult to predict from research presentations in ACI Committee 355. Therefore, the uniform bond model with a bond strength (τ) of 2000 psi [13.8 MPa] was used for ½-in. [13-mm] diameter anchors. This bond strength was obtained from our preliminary tests (Appendix IX) using the same adhesive. In addition, the bond strengths for anchors with larger diameters are expected to decrease. The product brochure of the adhesive product also recommended a lower calculated bond strength for 5/8-in. [16-mm] diameter anchors. Therefore, a bond strength (τ) of 1800 psi [12.4 MPa] was used for the 5/8-in. [16-mm] diameters anchors.

The new adhesive anchors with hardened adhesive threads interacting with surrounding concrete may resemble that of screw anchors, especially when the threads in this study were created using screw anchors. Hence, the breakout capacities of screw anchors were included in the analyses. The

capacities corresponding to concrete breakout failure were calculated using the screw anchor model (Equation (6) in Chapter 2). We simplified the calculation that the effective embedment length was 0.85 of the embedment due to the actual thread dimension was not measured. As Figure 4.2 and Figure 4.3 shown, the screw anchor line (k_c=35) is slightly above the concrete breakout (k_{nc} = 24) which is from code.

The tensile capacities of ½-in. [13-mm] anchors corresponding to four failure modes are shown in Figure 4.2. A 4-in. [102-mm] embedded depth was chosen for the ½-in. [13-mm] diameter anchors. It was expected that the anchors in smooth hole in all three cleaning conditions would be controlled by pullout failure at about 12.6 kips [56.1 kN] (in general, anchors in partially cleaned and uncleaned holes would be pulled out at lower loads based on the literature and also the preliminary tests in Appendix IX). The anchors in threaded holes were expected develop higher tensile capacity such that the failure may be controlled by concrete breakout at 14.9 kips [66.3 kN] as an adhesive anchor. In addition, the threads formed by hardened adhesive indicates that may further increase to 17 kips [75.7 kN] corresponding to concrete breakout as a screw anchor. In order to examine the potential of the new adhesive anchors, test group UCT#R was designed with code-conforming anchor reinforcement such that concrete breakout failure may be delayed such that the new adhesive anchors may be able to achieve the full steel capacity at 17.7 kips [78.8 kN]. Note that code-conforming anchor reinforcement (details are shown in Section 4.2.3) is not usually available in practice for post-installed anchors, hence this group of specimens are for academic exploration purpose only.

The tensile capacities of 5/8.-in. [16-mm] anchors are shown in Figure 4.3. A 5-in. [127-mm] embedded depth was chosen for the 5/8-in. [16-mm] diameter anchors. It was expected that the anchors in smooth hole in all three cleaning conditions would be controlled by pullout failure at

about 17.7 kips [78.8 kN] (in general, anchors in partially cleaned and uncleaned holes would be pulled out at lower loads based on the literature and also the preliminary tests in Appendix IX). The anchors in threaded holes were expected develop higher tensile capacity such that the failure may be controlled by concrete breakout at 23.8 kips [105.9 kN] as a screw anchor. In order to examine the potential of the new adhesive anchors, Test group UCT#R was designed with code conforming anchor reinforcement such that concrete breakout failure may be delayed such that the new adhesive anchors may be able to achieve fill steel capacity at 28 kips [124.6 kN]. Again, this group of specimens are for academic exploration purpose only.

4.2.2 Dimensions for concrete blocks

The block length was determined based on the requirements of typical unconfined tension tests in ACI 355.4 (2011). Specifically, the reaction supports need to be placed $2h_{ef}$ away from the test anchors, where h_{ef} is the embedded depth. This requirement is for the anchor to permit unrestricted development of a conical concrete fracture surface (ACI 355.4.11, 4.7.3.1) plus an extra 4 in. [102 mm] for both supports. The block length is 24 in. [610 mm] for ½-in. [13 mm] anchors and 28 in. [711 mm] for 5/8-in. [16 mm] anchors. Test of anchors in Group UCT50% and UCT (the anchors in partially cleaned and cleaned holes) were conducted on blocks with a larger dimension due to unexpected severe damage caused to their blocks. The same reaction spacing of $2h_{ef}$ was maintained for all the tests.

The block widths were determined based on the minimum edge distance required for unconfined pullout tests in ACI 355.4 (2011). Also, anchors were installed on four side edges; hence the block widths were also determined based on the minimum depth of concrete specimens in ACI 355.4. Specifically, Section 10.7.1 requires that the specimen thickness shall not be less than

$$h_{min} = h_{ef} + \Delta h \geq 2\ in., \tag{7}$$

where $\Delta h \geq 2d_0 \geq 1.25$ in. applies to all anchor types without restriction and $\Delta h \geq 2d_0 \geq 0.6$ in. applies to all where the remote face of the concrete member can be inspected; h_{ef} is the effective embedment depth of anchor, in.; Δh is the concrete thickness beyond h_{ef}.

The width/thickness of block was also controlled by the fact that the specimen should not crack under the maximum possible tensile loads to be developed in the test anchors. The equation (8) and (9) of cracking moment is shown as follow (ACI318-14, 24.2.3.5b) (ACI318-14, 22.5.5.1). Based on calculations, no need longitudinal reinforcement and stirrups for all blocks but we determined the all sections using 2#4's on bottom and 2#4's on top. 1#3 stirrup for each end of the block.

$$M_{cr} = \frac{f_r I_g}{y_t} \tag{8}$$

$$V_c = 2\lambda\sqrt{f_c'}\, b_w d_t \tag{9}$$

where M_{cr} is cracking moment, in.-lb; f_r is modulus of rupture of concrete, ksi; I_g is moment of inertia of gross concrete section about centroidal axis, neglecting reinforcement, in.^{4}; y_t is distance from centroidal axis of gross section, neglecting reinforcement, to tension face, in. (ACI318-14, 24.2.3.5b); V_c is the nominal shear strength provided by concrete, lb; λ is a modification factor to reflect the reduced mechanical properties of light weight concrete relative to normal weight concrete of the same compressive strength; f_c' is specified compressive strength of concrete, psi; b_w is web width or diameter of circular section, in., d_t is distance from extreme compression fiber to centroid of longitudinal tension reinforcement, in. (ACI318-14, 22.5.5.1).

As shown in Figure 4.3, the dimension was 12×12×24 in. [305×305×610 mm] for ½-in. [13-mm] anchors and 15×15×28 in. [381×381×711 mm] for 5/8-in. [16-mm] anchors. The fabrication of the specimens is shown in Appendix VIII.

4.2.3 Anchor reinforcement

The anchor reinforcement was used in Group UCT and UCT50% to explore the potential of the new adhesive anchors. It was expected to delay concrete breakout such that other failure modes, preferably anchor fracture in tensile, can control the tensile behavior of the new anchoring system. The anchor reinforcement for cast-in anchors in tension in ACI 318 (2014) consists of U-shaped hairpins with legs parallel to the anchors located within $0.5d_a$ from the anchors. Petersen et al. (2018) indicated that anchor reinforcement can be closed stirrups, two next to the anchors and others spaced in 2 to 3 in. [50.8 to 76.3 mm]. Equation (10) shown below can be used to determine the required anchor reinforcement for cast-in anchors to achieve their full tensile capacity,

$$A_{st} \geq \frac{A_{se} f_{uta}}{f_y} \tag{10}$$

where A_{st} is the required area of steel reinforcement, in.^{2}; A_{se} is effective cross-sectional area of anchor, in.^{2}; f_{uta} is specified minimum tensile strength of anchor steel, ksi; f_y is specified minimum yield strength of reinforcement, ksi.

The anchor reinforcement (Figure 4.4) was calculated as 4 No. 3's for ½-in. [13-mm] anchors based on its ultimate load (18 kips) [78.8 kN] and 2 No. 3's plus 2 No. 4's for 5/8-in. [16-mm] anchors based on its ultimate load (28 kips) [124.6 kN]. These reinforcing bars cannot be placed next to the test anchors because the anchors were installed after concrete was placed. In addition, U-shaped hairpins as recommended by ACI 318-14 were not used because anchors were to be installed on all four faces; hence two pairs of C-shaped hooks (tied together to form two closed

stirrups) were used for anchors installed on two opposite faces, as shown in Figures 4.5. The center-on-center spacing of the closed stirrups was 3 in. [76 mm] in one direction and 3.5 [89 mm] in the perpendicular direction. On average the stirrup legs that serve as anchor reinforcement were expected to be roughly $0.5h_{ef}$ away from the test anchor.

In addition to the legs parallel to the anchors serving as anchor reinforcement, Petersen et al. (2018) requires sufficient corner reinforcement on all concrete faces to control splitting cracks. Design equations were provided to determine the crack-controlling reinforcement. In the block width direction, two No. 3 closed stirrups were used not only to fix the anchor reinforcement but also to delay splitting cracks in the longitudinal direction. In the block length direction, the short legs of the C-shaped hooks were tied together to delay splitting cracks in the transverse direction. The details of the anchor reinforcement are shown in Appendix VIII.

4.3 Materials

4.3.1 Concrete

Concrete used in this study was ordered from a local ready-mix batching plant. The concrete blocks were covered with plastic sheet to maintain wet and cylinders kept in their plastic molds under an indoor condition with temperatures between 60-80 degrees Fahrenheit [15.6-26.7 Celsius] for 7 days. The specified concrete strength was 4520 psi. Considering the past experience with the concrete provided by the batching plant, a slump of 5 in. [127 mm] was also specified. The concrete had a measured slump of 7.25 in. [184 mm].

The 3-day strength of cylinders from tests of three (4×8 in.) [101.6 × 203.2 mm] cylinders, made according to ASTM C31 was 3270 psi [22.6 MPa]. The 7-day strength of cylinders from tests of three (4×8 in.) [101.6 × 203.2 mm] cylinders was 4520 psi [31.2 MPa]. The formwork of the

concrete blocks was thus removed at this age and the cylinders were demolded. Both the concrete blocks and the concrete were kept at the same indoor condition (roughly with a consistent temperature of 70 degrees Fahrenheit [21.1 °C]) till the tests began at 28 days.

The detailed concrete material tests are documented in Appendix I. The average compressive strength was 6200 psi [42.7 MPa] at 28 days from the tests of standard 4 inch by 8-inch [101.6 x 203.2 mm] cylinders. This strength (very close to the assumed concrete in Section 4.2) was deemed constant because the tests at 90 days indicated that the concrete strength was 6280 psi [43.3 MPa].

4.3.2 Steel

The ASTM A193 Grade B7 threaded rods for the tests in this study were purchased from Grainger Industrial Supply. Tensile tests were conducted for both standard coupons and threaded rods. The details of the tests are documented in Appendix II. The results show different properties of the threaded rods from the same batch. The results of standard coupons show that the yield strength of 112 ksi [772.2 MPa] and a tensile strength of 129 ksi [889.4 MPa] were specified for this grade. The test details are shown in Appendix II.

4.3.3 Adhesive

The adhesive used in this study was a two-component vinylester adhesive. The working time is 6 minute and full curing time is 45 minutes when the temperature of based material is 68 Fahrenheit (20 Celsius). For the cleaning procedure of drilled holes, use a vacuum with a nozzle to remove the dust and concrete debris left at the bottom of holes. Then, insert and spin a brush into to the drilled hole for four times. Final, insert a nozzle of a hand pump into drilled holes to blow dusts for four times. The properties of the adhesive material (1:2 prism) are shown as follows. The modulus of Elasticity (E_a) was 315.4 ksi [2.17 GPa]. The Poisson's ratio was between 0.375 and

0.4. The maximum compressive strength (f_{ac}) 11 ksi [75.8 MPa] at the corresponding strain 0.0668. The tensile properties of the adhesive material are shown as follow. The modulus of elasticity is 316.7 ksi [2.18 GPa]. The maximum tensile strength 2.31 ksi [15.9 MPa] at the corresponding strain 0.0213. The detail information is shown in Appendix III.

The results of these tests indicate that the adhesive material is brittle similar to concrete. Equation (11), established for concrete is used to model the compressive behavior as revealed by the stress-strain curve of the prism with an aspect ratio of 2:1,

$$f_{acp} = \frac{f_{ac}\,\beta x^{\alpha}}{\beta - \alpha + \alpha x^{\beta}}, \tag{11}$$

Where $x = \frac{\varepsilon}{\varepsilon_0}$, f_{ac} is maximum compressive strength of the prism with an aspect ratio of 2:1, psi; f_{acp} is compressive stress, psi; ε is the compressive strain; ε_0 is the strain corresponding to peak compressive strength. As shown in Figure 4.6, the model curve with β = 20; α = 0.65 fits well the measured stress-strain curve of the adhesive in compression. The ascending portion controlled by the parameter α and the descending portion controlled by parameter β need more tests of the adhesive to be determined.

4.4 Confined Pullout Tests

All confined pullout tests were conducted on the same blocks as the confined tension tests. Tests were performed only for ½-in. [13-mm] anchors. The embedment depths of confined tests were 2 in. [50.8 mm] and 3 in. [76.2 mm] according to Section 4.7.2.1.2 of ACI 355.4 (2011). A total of four groups of four tests were performed including anchors in clean smooth holes (C) and anchors in clean threaded holes (CT), as listed in Table 4.2. Additional tests were performed for partially cleaned holes. No tests were performed for uncleaned holes because the dust accumulated at the

bottom of the hole can significantly impact the embedded depths. The hole conditions are defined in the standard installation procedure in Appendix VII.

4.5 Test setup and Instrumentation

4.5.1 Setup for unconfined pullout tests

The test setup for the unconfined tension tests is schematically shown in Figure 4.7 and a picture of the test setup in Figure 4.8. The entire test setup is a self-balanced system. The loading beam was used to transfer the load from the loading rod to the concrete surface. The ultimate strength of the tested anchor was less than the yield strength of the loading rod. The diameter of the loading rod was ¾ in. [19 mm] for both ½ in. [13 mm] and 5/8 in. [16 mm] diameter anchors. The tested anchor was connected with the loading rod using a high-strength transition nut. Two types of high-strength coupler were used for the entire project including 1/2 in. [13 mm] to ¾ in. [19 mm] and 5/8 in. [16 mm] to ¾ in. [19 mm]. A 2 in. [51 mm] diameter hole was cut in the center of the loading beam to allow the loading rod to go through during pullout tests. The HSS shapes (6×4×3/8 in. and 4×4×¼ in.) of steel were used as the loading beam and post. The loading post stood on the base plate (11 × 4 × 3/8 in. [279 × 102 × 9.5 mm] to distribute the even load to the concrete surface. Note that the beam cannot deform during pullout tests. The maximum load was based on the ultimate load of the loading rod. The equations (12) (13) (14) of the loading beam is shown as follows (AISC 2005). The equation (15) of the loading post is shown as follows (AISC 2005).

$$\emptyset M_n = \frac{F_u A_{fn}}{A_{fg}} S \quad < M = \frac{Pl}{4} \tag{12}$$

$$\tau_v = \frac{VQ}{I2t} < \emptyset F_y \tag{13}$$

$$\delta = \frac{pl^3}{E_s I} < l/360 \quad (14)$$

$$\sigma = \frac{P}{A_p} < F_y \quad (15)$$

M_n is the nominal flexural strength of the member, kips-in; M is the flexural strength of the member, kips-in; A_{fg} is the gross area of the tension flange; A_{fn} is the net tension flange area after the holes are subtracted. F_u is the ultimate strength of the steel, ksi; F_y is the yield strength of the steel, ksi; S is the section modulus of the member, in^3; τ_v is the shear stress, ksi; V is the transverse shear force based on the ultimate load of loading rod, kips; Q is the first moment of area, in^3; I is the moment of inertia, in^4; t is the thickness of the member, in; δ is the deflection of the member less than l/360 (ACI 318.14, Table 24.2.2); l is the length of the member, in; P is the ultimate load of loading rod, kips; E_s is the young modulus of steel, ksi; $\emptyset$ is the reduction factor 0.9 for the nominal flexural and 0.6 for the shear stress. σ is axis compression strength of the member, ksi; A_p is the cross-section area of the axis compression member;

The test anchors had a length of 3 in. [76 mm] above the concrete surface as the operation length. This allows to verify the embedment depth of adhesive anchors during the installation because the post level had the same height. The operation length also allows the LVDTs to be mounted properly. The metal LVDT holder was made by steel plate (1/2 × 20 × 1/4 in. [13 × 508 × 6 mm] for 4 in. [102 mm]) of embedment depth and (1/2 × 24 × 1/4 in. [13 × 610 × 6 mm]) for 5 in. [127 mm] of embedment depth. The LVDT hole was 1 ½ in. [38 mm] from each end of the plate so that the distance between LVDT probe and anchor center is larger than the twice embedment depth (8 in. [203 mm] and (10 in. [254 mm]. This reduces the influence of LVDT reading from the concrete breakout during pullout tests.

The transition nut was on the top of the LVDT holder and the position of tested anchor in the nut was watched by witness holes on the nut. To reduce installation skew to impact the loading, screwed the loading rod into the nut and adjusted the position of the loading beam to avoid the friction between the loading rod and loading beam with 2 in. [51 mm] diameter of loading hole. Adjustable wrenches were used to tighten the transition coupler and retaining nut below the LVDT holder at the same time to avoid extra torque applied on the tested anchors. Then, the hollow hydraulic jack was positioned on the loading beam and adjusted position to avoid friction between the loading rod and inner wall of the jack. The inner diameter of the jack was larger than the diameter of loading rod and the capacity of the jack was larger than the ultimate load of the loading rod. An extension pipe for the pump handle may be used to reduce hand force when the jack reached the larger load. A load cell (Model THD-50K-Y) with 1 in. [25.4 mm] diameter of center hole was used for entire project due to the maximum loading rod was ¾ in. [19 mm]. The loading cylinder above the loading surface of the load cell was faced the loading tube of the hydraulic jack. Two steel plates with 3/8 in. [9.5 mm] thickness and with ¾ in. [19 mm] diameter hole were used at both top and bottom of the load cell so that the uniform load was transferred to the load cell.

4.5.2 Setup for confined pullout tests

Instead of two supports far away from the test anchors, the reaction force in confined tension tests was directly applied to concrete though a steel plate, as illustrated in Figure 4.9. The plate has a dimension of 5×5 in. [127×127 mm]. The hole in the plate is 1 in. [25.4 mm] and the thickness of the plate is 0.5 in. [13 mm] for the ½-in. [13-mm] diameter anchor as required by Section 4.7.3.2 of ACI 355.4 (2011). To minimize the friction between the plate and concrete, a 1/8-in. (3.2-mm) thick plastic sheet with the same dimension of the plate was placed between the reaction plate and the concrete. Trial tests were first conducted with Teflon plates to reduce friction, because without

the friction reduction plates, the bond failure was mostly on adhesive-steel (A-S) interface. It was later decided that plastic sheets were needed not to reduce friction because there was no apparent relative motion between concrete and the reaction plate. Rather the plastic sheets between the steel reaction plate and concrete allowed lateral deformation of concrete surface during the pullout tests. A sheet of Teflon was cut in the same size as the confining plate to reduce friction between confining plate and concrete surface to achieve adhesive-concrete interface failure mode. Hence, harden plastic sheets instead of Teflon sheets were used throughout the entire test program. The plastic sheet with was cut in 4 pieces to further minimize the confining effects of the reaction plate, as illustrated in Figure 4.11 in confined tension tests. The plastic sheet was cut in the same size of the base plate for unconfined tension tests.

For the confined test setup shown in Figure 4.9 and 4.10, the loading frame with one base plate stranded on a test member with a friction reducing sheet and tension load transferred by a coupling rod connected with an anchor was measured by a load cell (Model THD-50K-Y) that was on top of a hydraulic jack. Note that confined tension tests are usually conducted to measure the tension resistance of the adhesive anchor dominated by bond strength. Hence, axial displacement of an anchor was not measured. Started the collection data more than 10 seconds before the actually loading. These data were dealt by using a MATLAB program and discussed in Section 4.5.4.

4.5.3 Instrumentation plan

Test anchor was measured by a load cell (Model THD-50K-Y) that was on top of a hydraulic jack. Two Model 0345 linear variable differential transformers (LVDTs) were fixed at each end of a steel flat bar locked between a hex nut and a coupling nut to directly measure axial displacement of an anchor. The calibration of these sensors is documented in Appendix II.

An IO Tech DaqBook 2000 was used to collect data from the LVDTs and the load cell with a sampling rate of 10 Hz. A preload was applied about 200 lb [0.89 kN]. A wrench was used to tighten the retaining nut on the top plate until the reading of the load cell was about 0.04 volts from the data acquisition. Started the collection data more than 10 seconds before the actually loading. These data were dealt by using a MATLAB program and discussed in Section 4.5.4.

4.5.4 Data processing

The raw data collected by the data acquisition system is DC voltages. With the conversion factors listed in Appendix II, data in engineering units were converted and processed using an in-house MATLAB program (Datamining.m). With a sampling rate of 10 Hz, the converted data contained noise signals that may affect the determination of peak loads and the corresponding displacements. Hence, the collected data first went through a 2^{nd} order lowpass digital Butterworth filter with a cutoff frequency of 0.1 Hz to reduce noise levels. The filtering process is triggered by any input next to the cutoff frequency in the graphic user interface shown in Figure 4.12. Sensors may also have initial readings that must be removed before proper load-displacement curves are generated. Meanwhile, the low pass filter sometimes may cause unexpected spikes at the beginning of the signals; hence, the initial readings are determined as the average of the data between the "lead time" and the "start time" specified on the graphic user interface. Finally, the data after the specimen failure can be excluded by specifying an "end time," as shown in Figure 4.13.

CHAPTER 5 TEST RESULTS

Behavior of traditional adhesive anchors and the new anchors had been compared in our preliminary tests, which are summarized in Appendix IX. The results of the confined tension tests and unconfined tension tests, planned in Chapter 4, are discussed in this chapter. A total of 14 groups of unconfined pullout tests and four groups of confined pullout tests are summarized in Tables 5.1 and 5.2 while the details of the individual test are documented in Appendices VI and VII. These tests support the hypothesis that with threads generated in drilled holes in concrete, adhesive anchors can have more reliable behavior and often higher pullout capacities compared with traditional anchors with the same adhesive material.

5.1 Behavior of anchors in fully clean holes

5.1.1 Behavior of ½-in. anchors in fully clean holes

Three out of four ½-in. anchors in clean smooth holes (Specimens UC-0.5-4.0#1, #2, #3) were pulled out with bond failure at the adhesive-concrete interfaces as expected. The average bond strength of these three anchors was 1977 psi [13.6 MPa], with a coefficient of variation of 9.6%. The depths of the concrete cones varied from 0.44 to 2 in. [11.2 to 50.8 mm] though the ultimate capacities did not show any apparent trends with the cone depths. It is hypothesized that the cone depth was mainly controlled by hardened adhesive in few large pockets in drilled holes, randomly generated during the drilling and cleaning process, as shown in Appendix V (Figure V.7b). As a proof, the fourth anchor (UC-0.5-4.0#4) in this group was controlled by concrete breakout/splitting failure as shown in Figure VI.4c. A close look at the hardened adhesive (Figure VI.4d) indicates that several large-size, deep adhesive lumps near a depth about 3 in. [76.2 mm], which may have disabled the pullout failure. The measured capacity was 11.27 kips [50.2 kN], which is very close

to a predicted capacity assuming a 3-in. [76.2 mm] deep breakout simultaneously with a 1-in. [25.4 mm] deep bond failure (12.84 kips) [57.1 kN]. Note that this anchor was installed on the side face of Block BR7, on which the anchors on the top and bottom faces were provided with anchor reinforcement, made with two C-shaped hooks. As a result, two stirrups legs pass the potential breakout cone, as shown in Figure VI.4c appeared that the reinforcing bars were bypassed by the breakout/splitting failure and did not provide any benefit to the ultimate capacity of the anchors.

Compared with the anchors in clean smooth holes, all four anchors in clean threaded holes (Specimens UCT-0.5-4.0#1, #2, #3, #4) were controlled by concrete breakout failure. This proved our hypothesis that the threads created using screw anchors in drilled holes acted similarly to the random large-size pockets in that hardened adhesive in the threads provided mechanical interlock to the load resisting mechanism and disabled the bond-failure at adhesive-concrete interfaces. The average capacity of this group of anchors was 12 kips [53.4 kN] with a coefficient of variation of 6%. As shown in Figures VI.7d and VI.8c, the adhesive threads clearly integrate the anchor with the drilled holes. This observation repeated those observed in the preliminary tests as documented in Appendix IX. The expected concrete breakout capacity was not achieved mainly due to a reduced breakout cone depth: the threads at the bottom of these holes were not in full depth because the cutting tip of screw anchors, which were used instead of a special concrete tapping bit, may have worn out as illustrated in Appendix IV. Therefore, the breakout cones were about 3 in. deep with the last 1 in. controlled by bond failure. The concrete breakout capacities for Specimens #3 and #4 may have also been negatively affected by the splitting cracks developed on the side faces of the blocks during the tests of other anchors. This is an encouraging evidence leading to the need for special concrete tapping bits that will generate desired threads (all to be studied in the future).

The anchor reinforcement provided to another group of anchors in clean threaded holes did improve the tensile capacity of the anchors; however, the expected steel fracture was not achieved. The average bond strength (UCT#R-0.5-4.0) of anchors was 14 kips [62.3 kN] with a coefficient of variation of 16%. The large COV is mainly because of the high capacity of Specimen UCT#R-0.5-4.0#2, for which, the ultimate load (16.81 kips) [74.8 kN] was only 5% lower than the anchor failure load (17.7 kips) [78.8 kN]. The inability of anchor reinforcement may be attributed to the following observations:

1) With hardened adhesive in threads, concrete breakout cone might form at any depth along the embedment; hence, the observed breakout cone in this group of specimens all started a bit below the (Figure VI.10d) top leg of C-shaped hooks, and the breakout crack bypassed the vertical legs that were designed as anchor reinforcement as shown in Figures VI.9d, VI.10d and VI.12d.

2) The embedded depth of these anchors was not sufficient as required by Petersen et al. (2018); therefore, even with interaction between the C-shaped hook and corner reinforcement, the anchor reinforcement would not be developed in a shallow breakout cone. This is the major difference between a cast-in anchor and an adhesive anchor. Code-conforming anchor reinforcement may not behave as expected for adhesive anchors.

3) The tied short legs were not able to restrain splitting cracks, a very important function of anchor reinforcement as pointed out by Petersen et al. (2018). As shown in Figures VI.9d, a splitting crack passed through the reinforcement (shown by the marks of the reinforcing bar in the figure). In addition, the depth of anchor reinforcement varied much due to fabrication uncertainties. Specifically, in this specimen, the splitting crack started above the reinforcing bars and the tied short legs were not surrounded by concrete. However, the concrete below the anchor reinforcement

was better confined such that the bond failure was forced to adhesive-steel interface, which was expected and observed in confined tension tests documented in Section 5.3.

5.1.2 Behavior of 5/8-in. anchors in fully clean holes

The threads helped 5/8-in. anchors much more than ½.-in. [13 mm] anchors. The anchor (UC-0.625-5.0#1, #2) in this group were controlled by concrete breakout/splitting failure as not expected. The measured capacities were 16.57 kips [73.7 kN] and 18.46 kips [82.1 kN], which are lower than the expected concrete breakout capacity 20.8 kips [92.6 kN]. However, the measured capacities are very close to a predicted capacity assuming a 2.87-in. [72.9 mm] and 4.09-in. [103.76 mm] deep breakout simultaneously with a 2-in. [50.8 mm] and 0.75 -in. [19.05 mm] deep bond failure (16.25 kips) [72.33 kN] and (18.25 kips) [81.22 kN]. This assumed that the cone depth was mainly controlled by hardened adhesive in few large pockets in drilled holes, randomly generated during the drilling and cleaning process. As shown in Figure 5.1, the anchor is applied a tension load on the top of the anchor. This load causes the fracture energy of the concrete at the crack 1. The part b of the anchor does not slip due to the load is smaller than the bond strength at part b. Then, the load with increasing gradually causes the fracture energy of the concrete at the crack 2 and 3. The part b of the anchor slips under the load that causes the fracture energy of the concrete at the crack 4 and is larger than the bond strength at part b. Finally, the concrete cone is formed at crack 4 and the anchor is pulled out. This was proved by the result (UC-0.5-4.0#4) observed in unconfined tension tests documented in Section 5.1.1. The ultimate load of adhesive anchors is that the concrete breakout of part a plus bond failure at part b. These two tests had incomplete concrete breakout.

Two out of four 5/8-in. [16 mm] anchors in clean smooth holes (Specimens UC-0.625-5.0#3, #4) were pulled out with bond failure at the adhesive-concrete interfaces as expected. The average

bond strength of these two anchors was 1277 psi [8.8 MPa], with a coefficient of variation of 14.5%. The depths of the concrete cones varied from 0.9 to 1 in. [22.86 to 25.4 mm] though the ultimate capacities did not show any apparent trends with the cone depths. However, the crack represented splitting in the transverse direction about 0.5 to 1 in [12.7 to 25.4 mm] close to the anchor. The measured capacity was 12.76 kips [56.4 kN] and 10.63 kips [47.3 kN], which are lower than a predicted capacity in cracked concrete measuring a 4-in. [101.6 mm] deep breakout simultaneously with a 1-in. [25.4 mm] deep bond failure (15.5 kips) [69 kN]. This may cause by the large hole is difficult to be cleaned, as shown in Figure V.7c.

Compared with the anchors in clean smooth holes, all three anchors in clean threaded holes (Specimens UCT-0.625-5.0#1, #2, #3) were controlled by concrete breakout failure. This proved our hypothesis that the threads created using screw anchors in drilled holes acted similarly to the random large-size pockets in that hardened adhesive in the threads provided mechanical interlock to the load resisting mechanism and disabled the bond-failure at adhesive-concrete interfaces. The average capacity of this group of anchors was 21 kips [93.5 kN] with a coefficient of variation of 3.8%. The expected concrete breakout capacity (20.8 kips) [92.6 kN] was achieved. As shown in Figures VI.37d, VI.38c and VI.39d, the adhesive threads were sheared off mainly due to the concrete breakout was restraint by the stirrup. Note that these anchors were installed on Block BR22 and BR18, on which the anchors were installed 2.5 in. [63.5 mm] (Figure VI.37c) away from the stirrup. As a result, one stirrup leg passes the potential breakout cone, as shown in Figure VI.39c and VI.40b. One side of the breakout cone was restraint and the other was not. The specimen (UCT-0.625-5.0#4) were not controlled by concrete breakout and the bond strength was 19.95 kips [88.8 kN], which is close to the expected concrete breakout capacity (20.8 kips) [92.6 kN] mainly due to a reduced breakout cone depth: the threads at the bottom of these holes were

not in full depth because the cutting tip of screw anchors, which were used instead of a special concrete tapping bit.

The anchor reinforcement provided to another group of anchors in clean threaded holes did improve the tensile capacity of the anchors; however, the expected steel fracture was not achieved. The average bond strength (UCT#R-0.625-5.0) of anchors was 23 kips [102.4 kN] with a coefficient of variation of 1.9%. The inability of anchor reinforcement may be attributed to the following observations same as mentioned in Section 5.1.1.

5.2 Behavior of adhesive anchors in partially cleaned holes and uncleaned holes

5.2.1 Behavior of ½-in. anchors in partially cleaned holes and uncleaned holes

The threads helped greatly the anchors in partially cleaned holes and uncleaned holes. The uncleaned hole represents that the work in the field does not clean the hole. All 1/2-in. [13 mm] anchors in unclean smooth holes (Specimens UC0%-0.5-4.0#1, #2, #3, #4) were pulled out with bond failure at the adhesive-concrete interfaces as expected. The average bond strength of these three anchors was 443 psi [3.1 MPa], with a coefficient of variation of 35%. The large COV is mainly due to the profile of inner wall of drilled holes is not uniform and the thickness of dusts is randomly distributed on the inner wall. This also proved in Chapter 3. As shown in Figure VI.13c, VI.14c, VI.15c and VI.16c, the adhesive-concrete interface was covered by the dusts acted as the lubricant and bond breaker on inner wall in drilled holes.

Compared with the anchors in unclean smooth holes, all four anchors in unclean threaded holes (Specimens UCT0%-0.5-4.0#1, #2, #3, #4) were pulled out with bond failure at the adhesive-concrete interfaces as not expected concrete breakout failure. The average bond strength of these three anchors was 1077 psi [7.4 MPa], with a coefficient of variation of 12.7%. As shown in Figure

VI.21c, VI.22c, VI.23c and VI.24c, the threads were not well formed due to the dust blocked the adhesive penetrated the grooves generated by the screw blot. The incomplete threads caused the mechanical interlock on the adhesive-concrete interface to improve the tensile capacities, which is 143% higher than traditional adhesive anchors under the same condition. This shows that the current thread profile may not work well, and this is an encouraging evidence leading to the need for special concrete tapping bits that will generate desired threads (all to be studied in the future). The partially clean hole represents that the work in the field blows the hole but does not brush the hole. All 1/2-in. [13 mm] anchors in partially clean smooth holes (Specimens UC50%-0.5-4.0#1, #2, #3, #4) were pulled out with bond failure at the adhesive-concrete interfaces as expected. The average bond strength of these four anchors was 1084 psi [7.5 MPa], with a coefficient of variation of 10.7%.

All 1/2-in. [13mm] anchors in partially clean threaded holes (Specimens UCT50%-0.5-4.0#1, #2, #3, #4) were pulled out with bond failure at the adhesive-concrete interfaces as not expected concrete breakout failure. The average bond strength of these four anchors was 2083 psi [143.7 MPa], with a coefficient of variation of 5.8%. The small COV shows that anchors installed in threaded holes can have more reliable behavior and often higher pullout capacities compared with traditional anchors with the same adhesive material. The incomplete threads caused the mechanical interlock on the adhesive-concrete interface to improve the tensile capacities, which is 92% higher than traditional adhesive anchors under the same condition.

All 1/2-in. [13 mm] anchors in partially clean threaded holes with anchor enforcement (Specimens UCT#R50%-0.5-4.0#1, #2, #3, #4) were pulled out with bond failure at the adhesive-concrete interfaces as not expected concrete breakout failure. The average bond strength of these four anchors was 1968 psi [135.8 MPa], with a coefficient of variation of 6.3%. As shown in Figure

VI.29c, VI.30c, VI.31c and VI.32c, the threads were not well formed due to the dust blocked the adhesive penetrated the grooves generated by the screw blot. The inability of anchor reinforcement may be attributed to the reason that current screw anchors cannot work in dust condition well.

5.2.2 Behavior of 5/8-in. anchors in partially cleaned holes and unclean holes

The threads helped greatly the anchors in partially cleaned holes and unclean hoes. All 5/8-in. [16 mm] anchors in unclean smooth holes (Specimens UC0%-0.625-5.0#1, #2, #3, #4) were pulled out with bond failure at the adhesive-concrete interfaces as expected. The average bond strength of these three anchors was 500 psi [3.45 MPa], with a coefficient of variation of 13.6%. As shown in Figure VI.45c, VI.46c, VI.47c and VI.48c, the adhesive-concrete interface was covered by the dusts acted as the lubricant and bond breaker on inner wall in drilled holes.

The partially clean hole represents that the work in the field blows the hole but does not brush the hole. All 5/8-in. [16mm] anchors in partially clean smooth holes (Specimens UC50%-0.625-5.0#1, #2, #3, #4) were pulled out with bond failure at the adhesive-concrete interfaces as expected. The average bond strength of these four anchors was 1030 psi [7.1 MPa], with a coefficient of variation of 12.8%.

Compared with the anchors in partially unclean smooth holes, all four anchors in partially threaded holes (Specimens UCT50%-0.625-5.0#1, #2, #3, #4) were pulled out with bond failure at the adhesive-concrete interfaces as not expected concrete breakout failure. The average bond strength of these four anchors was 1591 psi [11 MPa], with a coefficient of variation of 11%. As shown in Figure VI.53c, VI.54c, VI.55c and VI.56c, the threads were not well formed due to the dust blocked the adhesive penetrated the grooves generated by the screw blot. The incomplete threads caused the mechanical interlock on the adhesive-concrete interface to improve the tensile capacities, which is 54% higher than traditional adhesive anchors under the same condition. This

shows that the current thread profile may not work well, and this is an encouraging evidence leading to the need for special concrete tapping bits that will generate desired threads (all to be studied in the future).

5.3 Behavior of adhesive anchors in confined pullout

The threads forced A-S failure which can be more reliable with higher capacity, but maybe with a cap by the material strength. Note that confined tension tests are usually conducted to measure the tension resistance of the adhesive anchor dominated by bond strength. To minimize the friction between the plate and concrete, a 1/8-in. (3.2-mm) thick plastic sheet with the same dimension of the plate was placed between the reaction plate and the concrete. Trial tests were first conducted with Teflon plates to reduce friction, because without the friction reduction plates, the bond failure was mostly on adhesive-steel (A-S) interface. It was later decided that plastic sheets were needed not to reduce friction because there was no apparent relative motion between concrete and the reaction plate. Rather the plastic sheets between the steel reaction plate and concrete allowed lateral deformation of concrete surface during the pullout tests. A sheet of Teflon was cut in the same size as the confining plate to reduce friction between confining plate and concrete surface to achieve adhesive-concrete interface failure mode. To assess the influence of cutting line of the harden plastic sheets, the cutting line was in two direction on the concrete surface. As shown in Figure 5.2, the cutting line was in the longitudinal direction. The results are shown in Figure VII.1 and VII.2, the anchors (trail confined test C-3.0-#1,#2) were pulled out with bond failure at the adhesive-steel interfaces (A-S). After passing the ultimate load, the load was dropped sharply and the adhesive on anchor was sheared off due to the lateral deformation of concrete surface was restraint. The turning point at 0.125 in and 1.5 in. of displacement represented the adhesive sheared off. As shown in Figure 5.3, the cutting line was in the transvers direction. The result is shown in

Figure VII.3, the anchor (trail confined test C-3.0-#3) was pulled out with bond failure at the adhesive-concrete interfaces (A-C). After passing the ultimate load, the load dropped gradually with increasing displacement. The result is shown in Figure VII.4, the anchor (trail confined test C-3.0-#4) was pulled out with bond failure at the adhesive-concrete interfaces (A-C). After passing the ultimate load, the load dropped slowly with increasing displacement. And then the load dropped sharply at 0.45 in. of displacement due to the adhesive at the tip of the anchor was sheared off. The ultimate load of adhesive anchors with the plastic sheet cutting line in transverse direction was 25 percent lower than the one in longitudinal direction. This is verified by FE analyses in Chapter 6. This also indicates that the bond strength in A-S failure mode is higher than the one in A-C failure mode. Hence, harden plastic sheets instead of Teflon sheets were used throughout the entire test program. The plastic sheet with was cut in 4 pieces to further minimize the confining effects of the reaction plate, as illustrated in Figure 4.11 in confined tension tests.

Adhesive-steel failure mode is caused by the minor adjustment because the adhesive used is high viscosity. The adhesive is like the slit. When anchors are moved by the minor adjustment in the adhesive, the adhesive around the anchor is hard to move with the anchor and this causes the gap between the anchor and adhesive and weaken the adhesion between them. Based on trial tests, most failure modes were adhesive-steel interface due to the operator applied the minor adjustment after anchors reached the desired embedment depth.

As shown in Table 5.2, The bond strength in threaded hole is higher than one in smooth hole. The failure modes in threaded holes were adhesive-steel (AS) or adhesive-concrete/adhesive-steel (AC+AS) interface failure. All Figures of confined tests are shown in Appendix VII. The failure modes in smooth holes were adhesive-concrete interface failure. As shown in Figure 5.4 and 5.5, The bond strengths in clean threaded holes are 12% to 17% higher than ones in smooth holes. In

addition, as shown in Figure 5.6 and 5.7, the bond strengths in partially clean threaded holes are 109% to 126% higher than ones in partially clean smooth holes. The large COV is mainly due to the profile of inner wall of drilled holes is not uniform and the thickness of dusts is randomly distributed on the inner wall. This also proved in Chapter 3. The results show that adhesive anchors in threaded holes can have more reliable behavior and often higher pullout capacities compared with traditional anchors with the same adhesive material. This also indicates that the bond strength in A-S failure mode is higher than the one in A-C failure mode and that is proved by the trail tests. The ultimate tensile strength was 2.31 ksi [15.9 MPa] mentioned in Appendix III and the limitation of bond strength may be controlled by the material strength. Hence, this condition needs to be considered for special concrete tapping bits that will generate desired threads.

5.4 Summary

In this study, these tests support the hypothesis that with threads generated in drilled holes in concrete, adhesive anchors can have more reliable behavior and often higher pullout capacities compared with traditional anchors with the same adhesive material. The expected results were not achieved due to threads were not formed well on the concrete interface. A summary of the results of this research is shown as follows.

- The average bond strength (UCT -0.5-4.0) of anchors was 1885 psi [13 MPa] with a coefficient of variation of 6%. The average bond strength is 3% lower than traditional anchors (UC).
- The average bond strength (UCT#R-0.5-4.0) of anchors was 2222 [15.3 MPa] with a coefficient of variation of 17.1%. The average bond strength is 14.5% higher than traditional anchors (UC).
- The average bond strength (UCT0%-0.5-4.0) of anchors was 1077 [7.4 MPa] with a coefficient of variation of 12.7%. The average bond strength is 143% higher than traditional anchors (UC0%).
- The average bond strength (UCT50%-0.5-4.0) of anchors was 2083 [14.4 MPa] with a coefficient of variation of 5.7%. The average bond strength is 92% higher than traditional anchors (UC50%).
- The average bond strength (UCT#R50%-0.5-4.0) of anchors was 1968 [13.6 MPa] with a coefficient of variation of 6.3%. The average bond strength is 81% higher than traditional anchors (UC50%).

- The average bond strength (UCT -0.625-5.0) of anchors was 2250 psi [15.5 MPa] with a coefficient of variation of 7.5%. The average bond strength is 47% higher than traditional anchors (UC).
- The average bond strength (UCT#R-0.625-5.0) of anchors was 2396 psi [16.5 MPa] with a coefficient of variation of 2.3%. The average bond strength is 56% higher than traditional anchors (UC).
- The average bond strength (UCT50%-0.625-5.0) of anchors was 1591 psi [11 MPa] with a coefficient of variation of 11%. The average bond strength is 54% higher than traditional anchors (UC50%).
- The average bond strength (CT-0.5-2.0) is 12% higher than traditional anchors (C-0.5-2.0).
- The average bond strength (CT-0.5-3.0) is 17% higher than traditional anchors (C-0.5-3.0).
- The average bond strength (CT50%-0.5-2.0) is 109% higher than traditional anchors (C50%-0.5-2.0).
- The average bond strength (CT50%-0.5-3.0) is 126% higher than traditional anchors (C50%-0.5-3.0).

CHAPTER 6 FINITE ELEMENT ANALYSES

6.1 Introduction

Finite element (FE) analyses were conducted in this study to model the performance of adhesive anchors in concrete. Specimens in Chapter 5 were modeled in three-dimensional elements with a damage plasticity model for modelling concrete behavior, surface-to-surface contact for adhesive-concrete interface, and nonlinear springs to simulate the interaction on adhesive-concrete interface with bond slip relationship.

6.2 Literature review

Nilforoush (2017) used an FE program MASA to simulate the behavior of single headed anchors loaded in tension. MASA program is able to model bond-slip behavior of reinforcement in concrete with a bond element, which is a bond-slip relationship of a one-dimensional nonlinear spring based on the discrete bond-slip model from Lettow (2007), which originated from bond model proposed by Eligehause et al. (1983). The author considered that the individual nonlinear springs can be used to simulate the contact interaction between different materials.

Delhomme and Brun (2018) conducted numerical study to investigate the mechanical performance of bonded anchors in ultra-high performance fiber reinforce concrete (UHPFRC) and proposed a 3D model to simulate pullout behavior by using a nonlinear incremental static analysis. The model used 4-node, bilinear, axisymmetric, quadrilateral elements (CAX4R) for both the concrete and the anchor. The element sizes were 4×4 mm (coarse mesh) at the edges and 2×2 mm (refined mesh) around the anchor based on a mesh sensitivity analysis. The geometric and boundary conditions are shown in Figure 6.1. The author used damage plastic model (CDP) to simulate the concrete as a homogeneous material and the concrete constitutive laws is shown in Figure 6.2. A surface-based

cohesive behavior model was used for the anchor-concrete interface without considering the thickness of the adhesive. The model assumed a linear elastic traction-separation law before damage and progressive degradation of the cohesive stiffness for the determination of the failure of the cohesive bond. Other parameters are shown in Table 6.1. As shown in Figure 6.3, the bond stays up to the ultimate load and the sliding behavior matches the experimental test. However, From the Figure 6.3, the mesh of concrete element is moved with the anchor during pulling out. There is no relative displacement on the interface between the anchor and concrete. This may not match the experimental observation in Chapter 5 that the anchor is separated with the concrete and the adhesive is worn down during pulling out.

The brief literature review indicates that a surface-based cohesive behavior may not be used for the anchor-concrete interface without considering the thickness of the glue. Nonlinear springs may be used to simulate the contact interaction along the adhesive-concrete (A-C) interface. FE models were created for the unconfined pullout tests documented in Chapter 5 for single ½-in. diameter anchors.

6.3 Finite Element Models of Experimental Tests

6.3.1 Model geometry and boundary conditions

The unconfined pullout tests have two symmetric planes; hence, only quarter of the specimen was modeled in ABAQUS. The modeled concrete block for Specimen UC-0.5-4.0, as shown in Figure 6.4, is 305 mm [12 in.] wide, 610 mm [24 in.] long, and by 305 mm [12 in.] deep. The concrete block is divided into two parts in the height direction: the top 102 mm [4 in.] part has an unstructured mesh to accommodate the drilled hole while the bottom 204 mm [8 in.] part has a structured mesh to reduce the total number of elements. The 13 mm [0. 5 in.] diameter anchor is

made from an ASTM A193 Grade B7 threaded rod, 102 mm [4 in.] embedded in concrete and 51 mm [2 in.] above the concrete surface. The hole in concrete has a diameter of 16 mm [0.625 in.]. The bond failure along A-S interface was not considered in this study, hence the adhesive anchor part consists of a solid steel rod with an equivalent area of 91.3 mm^2 [0.1415 $in.^2$] at the center and a ring of mixed steel-adhesive material with an inside diameter of 10.8 mm [0.4244 in.] and an outside diameter of 16 mm [0.625 in.]. A 102×152×6 mm [4×6×0.25 in.] plate was placed at the ends of concrete block to simulate the reaction when tensile loads are applied to the anchor. Finally, longitudinal crack-controlling bars and stirrups were modeled using 3D wires located at the center of the bars, as shown in Figure. 6.5.

The interface between the top and bottom block was modeled using a tied constraint. The interface the reaction plate and the top block was also modeled using a tied constraint; however, the Young's modulus the reaction plates varied to approximate the effect of the plastic/Teflon sheets placed below the steel reaction plates as illustrated in Figure 6.4. The interface between concrete block and the adhesive anchor is critical to the FE analyses because bond failure along the A-C interface was the focus of this study. Pullout failure is only possible when relative displacement is allowed at the A-C interface; hence, the interface was modeling separately in two directions: normal to the interface, frictionless, hard contact was used, and the elements were prevented from separation; parallel to the interface along the anchor, a total of eight layers of three nonlinear springs were used to model the A-C interface bond. Rotational motion along the interface was prevented by the applied displacement at the top of the anchor: only Z-direction motion was allowed such that the rigid-body rotation was prevented. This combined interface model was shown to be critical to the FE analyses because using discrete springs to model interface bond created unreasonable concentrated tensile forces on the nodes of related concrete elements with a damage plasticity

material model, which could cause significant convergence issues. The inseparable hard contact constraint between complex concrete elements and elastic adhesive elements effectively released the impact of the concentrated forces.

General purpose brick elements (Type C3D8R) were used for all parts in the model. The element size was roughly controlled with a smallest edge length of 6 mm [0.25 in.] near the anchor and 51 mm [2 in.] away from the anchor. Along the perimeter eight elements were used for the concrete block and sixteen elements were used for the concrete anchors, leading to eight coincident points along the perimeter, where nonlinear springs were specified. A total of eight layers of solid elements were used for the concrete and anchor within the embedded length; hence, eight layers of springs (with three springs each layer due to symmetry) were used as illustrated in Figure. 6.6. The number of element layers was from the number of threads created in drilled holes using screw anchors as shown in Chapter 5. A total of twenty-four nonlinear springs are used in the quarter model to simulate the interaction on adhesive-concrete interface. Note that when nonlinear springs are used, ABAQUS CAE cannot be used to perform the complete pre-processing, and the analysis must be started from an input file. The input file for a model from this study is shown in Appendix X.

6.3.2. Material properties

A damage plasticity model (Lubliner et al. 1989 and Lee and Fenves. 1998) was used for concrete elements similar to the study in the literature (Delhomme and Brun 2018). The Young's modulus was 30945.05 MPa [4488.2 ksi] based on the 6200 psi of concrete strength. The Poisson' s ratio was 0.17 as suggested by (McCormac and Brown 2014).

Equation (6.1), established base on measured stress-strain curves of concrete in the literature, was used to model the compressive behavior of concrete,

$$f_c = \frac{f_{cp}\,\beta x^{\alpha}}{\beta - \alpha + \alpha x^{\beta}}, \tag{16}$$

where, $\varepsilon_0 = 0.00208\,(\frac{f_{cp}}{1000\times4})^{0.25}$ is the peak strain, α is the ascending power index, $\alpha = 1 - \frac{0.25}{1+\frac{55}{(f_{cp}/1000)^{2.5}}}$, and β is the descending power index, $\beta = 0.452e^{(\frac{f_{cp}}{1000\times4})} + 0.8$, $x = \frac{\varepsilon}{\varepsilon_0}$, f_c is compressive strength of the concrete, psi; f_{cp} is compressive stress predicted, psi; ε is the compressive strain; ε_0 is the strain corresponding to compressive stress predicted. To generate the inputs for the damage plasticity model, a spreadsheet was created for concrete stresses at a total strain interval of 0.0001. The needed plastic strains were then calculated by subtracting the elastic strains (the stress divided by the Young's modulus) from the total strains.

A bilinear curve was used to model the tensile behavior of concrete. The tensile strength was taken as $0.1f_c'$. The descending part of the concrete model in tension was not considered in this study because the focus of this study was on the pullout failure of adhesive anchors controlled by the bond on A-C interfaces. The use of nonlinear springs caused unreasonable tensile stress concentration on concrete and including the post-peak behavior caused convergence problems.

The parameters of Concrete Damaged Plasticity are shown as follows ((Delhomme and Brun 2018).

- *"Dilation angle ψ is a measurement of how much volume of how much volume increase occurs when the material is sheared. For a Mohr-Coulomb material, dilation is an angle that generally varies between zero (non-associated flow rule) and the friction angle (associate flow rule). A default value of 38°was considered (Henriques et al. 2013 and Molina et al. 2015)."*
- *"Flow potential eccentricity ε is a small positive number that defines the rate at which the hyperbolic flow potential approaches its asymptote. A default value of 0.1 was considered.*

The plastic-damage model assumes non associated potential flow (Drucker-Prager hyperbolic function)."

- *"σ_{b0}/σ_{c0} is the ratio of initial equibiaxial compressive yield stress to initial uniaxial compressive yield stress with a default value of 1.16."*
- *"K_c is the ratio of the second stress invariant on the tensile meridian to the compressive meridian with a default value of 2/3."*
- *"Viscosity parameter μ is used for the visco-plastic regularization of the concrete constitutive equations. Szczecina and Winnicki. (2015) recommend a maximal value of 0.0001 to avoid convergence difficulties in implicit analysis with material models exhibiting severe degradations."* A value of 5e-05 was considered in this study.

The adhesive was modeled as an elastic behavior again because the focus of this study was on the pullout failure of adhesive anchors controlled by the bond on A-C interfaces. The modulus of Elasticity (E_a) was 315.4 ksi [2.17 GPa] and the Poisson's ratio was 0.38 from Appendix III.

The Young's modulus of anchor was 29000 ksi [199.9 GPa]. The Poisson' s ratio was 0.25. The yield strength was 112 ksi [772.2 MPa] and the ultimate stress was 129 ksi [889.4 MPa] at a plastic strain of 0.054 in./in. from Appendix II.

6.3.3 Nonlinear spring properties

For the simulation of the bond failure of adhesive anchors, surface-to-surface frictionless, hard contact was used normal to the adhesive-concrete interface. Nonlinear springs were used to simulate the bond behavior on adhesive-concrete interface. Nonlinear spring with a predefined bond-slip law have been used to model the interaction between concrete and reinforcement (Molina et al. 2015). Hence, this was deemed suitable for modeling bond failure of adhesive

anchors during pullout tests. As mentioned in Chapter 3, adhesive flow into the profile valleys on concrete surfaces would form spikes and the adhesive spikes provide mechanical interlock after hardening. Pullout failure starts when these hardened adhesive spikes are sheared off. Subsequently, the bond strength is maintained through friction on the adhesive-concrete interface. This procedure is similar to the pullout of a deformed bars from concrete; hence, a bond-slip relationship similar to that proposed by Eligehausen et al. (1983) was chosen to simulate the bond failure adhesive anchors.

Figure 6.7 shows the proposed bond-slip relationship: The ascending branch was assumed linear up to a maximum bond stress (τ_{max}) at a slip of s_1. The τ_{max} is [2000 psi] obtained from the average bond stress of unconfined pullout tests used in specimen design in Chapter 5. Note that bond strengths are often measured using confined pullout tests, in which case a proper conversion factor must be used to estimate the bond strength in unconfined tension tests. The maximum bond stress is maintained till the slip reaches at s_2, beyond which, the bond stress reduces to a bond stress mainly from friction τ_3. The lowest bond stress is the friction in the proposed model. τ_3 was taken as 1000 psi, which is the average bond stress from unconfined pullout tests of anchors in partly clean holes. As shown in Appendix V, partly cleaned holes are the holes that were not brushed such that adhesive is not able to form spikes, and the bond strength would be provided only by the friction between adhesive and concrete wall in drilled holes.

The characteristic slips s_1 and s_2 were estimated from the observation of hardened adhesive spikes: s_1 being the minimum spike width and s_2 the maximum width, respectively. Six spikes shown in red arrows were randomly selected on the Figure 6.8 and the observation indicates that s_1=0.02 in. [0.5 mm] and s_2=0.08 in. [2 mm]. The slope of descending part of the bond slip is controlled by s_3 as shown in Figure 6.7. This characteristic slip, s_3 was randomly selected as 0.5 in. [12.7 mm].

This slip value coincides with the element size in Z-direction, as mentioned in Section 6.3.1, eight elements of the concrete are meshed along the embedment depth of adhesive anchors. In the case of anchors in threaded holes, all hardened adhesive threads would have been damaged after a slip of 0.5 in.

The bond-slip model must be converted into a load-displacement for the nonlinear springs illustrated in Figure.6.7. The displacement was automatically calculated as the difference of displacement of the nodes that define the springs in Z-direction (DOF 3 in the input file in Appendix X); hence the displacement is simply the slip. The spring forces are calculated from the total bond force with a ½-in. height. For example, corresponding to the peak bond stress (at a slip of 0.02 in. [0.5 mm]), the spring force should be $(\pi \times 0.625" \times 0.5") \times 2000psi/12 = 0.16kips$.

6.4 Results of FE analyses

An analysis was first conducted for a case similar to Specimen UC-0.5-4.0, and the obtained load-displacement behavior is compared with the test in Figure 6.9. Three unconfined tests from fully cleaned holes with bond failure are selected for the comparison. The simulated anchor behavior was controlled by bond failure at the A-C interface as indicated by the elongated springs in Figure. 6.6. With the assumed peak bond strength, the analysis was able to capture the peak load of the anchor. The displacements were measured relative to concrete during the test while the displacement in Figure 6.9. was total displacement, which includes contribution from plastic concrete deformation. Note that the damage plasticity model for concrete is not developed for quasi-brittle behavior of concrete in tension; hence, the deformation of concrete in Z-direction is localized while in many of the pullout tests, a shallow breakout cone may have formed. The spring forces in Figure 6.10 at the peak load are not uniform along the embedment, which confirms the statement by Eligehausen et al. (2004). The three layers of springs with large deformation reach

the defined peak forces based on the spring color. However, one must note that the primitive spring model cannot consider many factors that are critical to the bond stresses at adhesive-concrete interfaces, including the splitting of concrete at the top.

Another analysis was conducted for Specimen UC50%-0.5-4.0. In this case, in which the drilled hole was not brushed, the bond-slip model was simplified as a bilinear model as shown in Fig. 6.11. Four unconfined tests from partially cleaned holes with bond failure are selected for the comparison. As shown in Figure 6.12, the experimental results, again controlled by bond failure, are well captured by the analysis. At a smaller applied tension, the plastic deformation of concrete is smaller, and the spring forces, representing the bond stresses, are more evenly distributed.

To further verify the FE models, a separate analysis was conducted for an earlier specimen, which was not documented in Appendix IX. The specimen has the same configuration as Specimen UCT-0.5-4.0 except that the concrete compressive strength was about 8400 psi. Strain gages were installed on this specimen, as shown in Figure 6.13 and Figure 6.14 to measure the strains on concrete surface during tension tests. Specifically, Gage 4 and Gage 5 were in the transverse direction of the concrete block and Gages 6 and 7 the longitudinal direction. The spacing between gauges and anchor center is 0.5 in. The measured strains were compared with those obtained from the FE analysis. Strains read from one node in the FE analysis may not represent the average strains measured from 90-mm [3.5-in.] long gages. As shown in Figure 6.15, strains taken from Node 64, Node 62, Node 63 and Node 13 (all are about 1.2 in. away from the center of the anchor and within the gage length) in the FE analysis were plotted against the measured strains from Gage 7 in the longitudinal direction. Strains measured from Node 52, Node 51, Node 71, Node 60 and Node 15 (all about 0.6 in. from the center of the anchor) are plotted against the measurements from Gage 6 the longitudinal direction. Strains measured from Node 30, Node 42, Node 52 and Node 64 were

compared with readings from Gage 4 in the transverse direction, and strains measured from Node 28, Node 50, Node 71 and Node 63 were compared with readings from Gage 5 in the transverse direction.

As shown in Figure 6.16, 6.17, 6.18 and 6.19, the solid line with the triangle sign in plots represents strains measured from the gages. Strains measured from gage 6 are larger than ones measured from Gage 7 because the Gage 6 is close to the anchor in the longitudinal direction of concrete block. The strains from Node 15 and Node 60 are slightly larger than the strains measured from gage 6, but average strains from Node 15, Node 60, Node 71, Node 51 and Node 52 may be close to the strains measured from Gage 6. The strains from Node 13 and Node 63 are slightly larger than the strains measured from Gage 7, but average strains from Node 13, Node 63, Node 62 and Node 54 may be close to the strains measured from Gage 7. Similarly, strains measured from Gage 5 are larger than ones measured from Gage 4 because the Gage 5 is close to the anchor in the transverse direction of concrete block. The strains from Node 30 and Node 42 are slightly larger than the strains measured from Gage 4, but average strains from Node 30, Node 42, Node 52 and Node 64 may be close to the strains measured from Gage 4. The strains from Node 28 and Node 50 are slightly larger than the strains measured from Gage 5, but average strains from Node 28, Node 50, Node 71 and Node 63 may be close to the strains measured from Gage 5.

Further finite element analyses were not documented in this thesis on the behavior of adhesive anchors. Instead, Fe analyses were conducted to explore the impact of decisions made for the experimental tests. For example, to investigate the effect of the confining effects of the reaction plates and evaluate the impact of plastic sheets used beneath the reaction plates, the elastic modules of the reaction plate at the end of the concrete block in Fig. 6.4 were varied: 200 GPa [29000 ksi] was used to simulate the confining effect while 138 MPa [20 ksi] to represent the effect of using

plastic sheets below the reaction plate as shown in Fig. 6.20. With plastic sheets, the horizontal reaction from the reaction plates is about 83 percent smaller than that without the plastic sheets. This indicates that the plastic sheets should be used in tests to minimize the confining effects of the base plate though the simple nonlinear springs cannot reflect the impact on A-C interface bond properties and the tensile behavior of adhesive anchors.

In addition, FE analyses were attempted to investigate the behavior of the anchor in holes. In this case, the spring forces were increased from the total bond force for anchors in smooth holes to consider the impact of hardened adhesive threads. Assume that the width of each thread is 3 mm [1/8 in.] wide and the threads are sheared off during anchor pulled out. The compressive stress of the adhesive is 11 ksi shown in Appendix III. The spring force should be $(\pi \times 0.625"\times 0.5" \times 2\ ksi + \pi \times 0.625" \times 1/8" \times 11\ ksi \times 0.6)/12 = 0.3\ kips$. As shown in Figure 6.21, the anchor installed in a threaded hole indicates a steel failure because the anchor stress reaches the ultimate load (129 ksi [889.4 MPa]) measured from Appendix II and the anchor installed in a smooth hole is pullout failure shown in Figure 6.22.

Finally, FE analyses were also conducted to investigate the effect of the stirrups placed near test anchors in some specimens. The stirrups and the longitudinal crack controlling reinforcement were modeled using truss elements embedded in concrete as shown in Figure 6.23. The stirrup is 38 mm [1.5 in.] from the center of the anchor. As shown in Figure 6.24, the stirrups did not change the behavior of adhesive anchors significantly. Specifically, for an anchor installed in threaded hole with stirrups, the displacement corresponding to peak load is slightly larger than the one without stirrups. For an anchor installed in smooth hole with stirrups, the descending portion of the curve is slightly lower than the one without stirrups.

6.5 Summary of finite element analyses

The finite element modelling using ABAQUS allows to simulate the behavior of the adhesive anchors under the tensile loads. The surface-to-surface contact, the concrete damaged plasticity model and the nonlinear spring model in this study are suitable to predict the global and local behavior of the adhesive anchors with pullout bond failure. The plastic sheet below the base plate is critical to reduce the confining effects of the base plate. Finally, the anchors installed between two stirrups do not impact the test results.

CHAPTER 7 SUMMARY AND CONCLUSION

7.1 Summary

Adhesive anchors are widely used in construction connecting steel members to hardened concrete. The behavior of traditional adhesive anchoring systems can be inconsistent because the adhesive-concrete interface can be affected by many factors. The literature review in Chapter 2 indicates that the tensile capacities of traditional adhesive anchors can be negatively impacted by dusts, moisture and cracks in the drilled hole. The adhesive-concrete interface is very important because most reductions of the bond strength occur at the interface between the adhesive and the concrete. The impact of these adverse factors has been confirmed by laboratory tests and the inconsistent behavior of adhesive anchors was also found in the field.

The equipment at the UWM Advanced Analysis Facility (AAF) was used to examine surface of holes drilled in concrete using a rotary hammer drill bit and the results confirmed that bond along adhesive-concrete interface is mainly attributed to micro interlock formed by hardened adhesive within micro indents on the wall of fully cleaned holes. It is thus established that hole cleaning process can have significant impact on the quality of adhesive-concrete bond. Tests were also conducted to examine the impact of installation procedure as published as manufacturers printed installation instructions (MPII).

An invention was formulated to improve the adhesive-concrete interface. Specifically, threads were introduced in drilled holes such that the adhesive-concrete bond is guaranteed by macro-level interlocks between hardened adhesive in the threads. Unconfined and confined pullout tests were conducted in this study to examine the tensile capacities of the new adhesive anchors. The main factors considered in the tests included ½ in. [13mm] and 5/8 in. [16mm] diameter anchor, cleaned

holes, uncleaned holes, and partially cleaned holes. The embedment depth 4 in. [102mm] and 5 in. [127mm] were based on bond failure of two anchor sizes, respectively. It was expected that the anchors in traditional smooth holes would be controlled by pullout failure while anchors in threaded holes would force the failure to concrete breakout under increased loads. In addition, the hole cleaning condition would have negligent effect on anchors in threaded holes. Finally, anchor reinforcement was used in some specimens to further explore the potential capacity of anchors in threaded holes because with anchor reinforcement, concrete breakout failure was expected to be delayed such that the new adhesive anchors may be able to achieve their full steel capacity.

These testing parameters result in a total of 14 groups of unconfined pullout tests and 4 groups of confined pullout tests. To minimize the friction between the plate and concrete, a 1/8-in. [3.2-mm] thick plastic sheet with the same dimension of the plate was placed between the reaction plate and the concrete. The need to minimize the confining effect of reaction plates was verified using nonlinear finite element (FE) analyses. Specimens used in unconfined tension tests were modeled in three-dimensional elements with a damage plasticity model for modelling concrete behavior, surface-to-surface contact for adhesive-concrete interface, and nonlinear springs to simulate the interaction on adhesive-concrete interface with the proposed bond slip relationships.

7.2 Conclusion

The concept of the new adhesive anchoring system was verified for the conditions considered in this study. Specifically, the confined tension tests indicated that adhesive anchors in thread holes achieved much higher bond strength than traditional adhesive anchors. The failure was forced on more consistent adhesive-steel interface, and the maximum bond strength could be only limited by the tensile strength of the adhesive material. The unconfined tension tests indicated that all anchors in threaded holes were able to carry loads above the code stipulated capacity, even in uncleaned

holes though the measured tensile capacity in uncleaned and partially cleaned threaded holes were not as high as those in cleaned holes. This indicates greatly improved tensile behavior of adhesive anchors.

These test results support the hypothesis that with threads generated in drilled holes in concrete, adhesive anchors can have more reliable behavior and often higher pullout capacities compared with traditional anchors with the same adhesive material. While further studies are needed to verify the new adhesive anchoring systems under a variety of other conditions, this study indicated that the new adhesive anchors will help engineers to design/construct safe connections for a variety of connections. The application of the innovative anchoring system is expected to improve the capacity of adhesive anchors, to simplify construction procedures, to provide reliable anchoring systems and to improve public safety.

7.3 Future work

The study is limited in scope. The new adhesive anchors must be further studied before being used for practice. Specifically,

1. A special concrete tapping bit is needed with a tough cutting tip and an optimized cutting tip geometry. As mentioned in Appendix IV, the wedge bolts were used only twice in this study to create threaded holes, but the cutting tip of screw anchors may wear down at the first time use due to the quality issue. The test results show that the threads at the bottom of these holes were not in full depth because the cutting tip of screw anchors and this may cause concrete breakout capacity is not achieved. The thread profile is needed with a special design so that the threads are well formed, and the dust does not block the adhesive to penetrate the grooves generated by the bit.

2. Test of anchors installed in cracked concrete is recommended because cracks can greatly reduce adhesive-concrete bond strength and the tensile capacity of traditional adhesive anchors. On the other hand, the new adhesive anchors are expected to be less sensitive to cracks under service loading.
3. Elevated temperature is known to reduce the tensile capacity of traditional adhesive anchors. Similarly, elevated temperature may impact of the performance of new adhesive anchors.
4. Evaluating the performance of anchors under sustained load at standard temperature and maximum long-term temperature is also recommended.
5. Assessment of the performance of the new adhesive anchors in cracked concrete under cyclic loading is recommended.

REFERENCES

1. ACI 318-14 (2014). Building Code Requirements for Structural Concrete, *American Concrete Institute*, Farmington Hills, MI.
2. ACI 355.4 (2011). Qualification of Post-Installed Adhesive Anchors, *American Concrete Institute*, Farmington Hills, MI.
3. ACI Committee 355, "State-of-the-Art Report on Anchorage to Concrete," *American Concrete Institute*, Detroit, unpublished.
4. Afendi, M. (2011). Study on Effect of Bond Thickness upon Adhesive Strength and Fracture Characteristics of Brittle Epoxy Adhesively Bonded Dissimilar Joint. Graduate School of Systems and Information Engineering, University of Tsukuba.
5. American Institute of Steel Construction (2005), Manual of Steel Construction, 13th Edition. Chicago.
6. Anton Rieder, Παναγιώτης ΣΠΥΡΙΔΗΣ, Konrad Bergmeister (2008): Seismic behavior of post-installed anchors in concrete –A case study.
7. ASTM A193 (2003). Standard Specification for Alloy-Steel and Stainless Steel Bolting for High Temperature or High Pressure Service and Other Special Purpose Applications. *American Society for Testing and Materials*, West Conshohocken, PA. United States.
8. ASTM A370 (2018). Standard Test Methods and Definitions for Mechanical Testing of Steel Products, *ASTM International*, West Conshohocken, PA.
9. ASTM C1231 / C1231M (2000). Standard Practice for Use of Unbonded Caps in Determination of Compressive Strength of Hardened Cylindrical Concrete Specimens, *ASTM International*, West Conshohocken, PA.

10. ASTM C143 / C143M (2015). Standard Test Method for Slump of Hydraulic-Cement Concrete, *ASTM International*, West Conshohocken, PA.
11. ASTM C31 / C31M (2003). Standard Practice for Making and Curing Concrete Test Specimens in the Field, *ASTM International*, West Conshohocken, PA.
12. ASTM C39 (2005). Standard Test Method for Compressive Strength of Cylindrical Concrete Specimens, *American Society for Testing and Materials*, West. Conshohocken, PA.
13. ASTM D638 (2002a). Standard Test Method for Tensile Properties of Plastics, *ASTM International*, West Conshohocken, PA.
14. ASTM D695 (2002a). Standard Test Method for Compressive Properties of Rigid Plastics, *ASTM International*, West Conshohocken, PA.
15. ASTM E8 / E8M (2013a). Standard Test Methods for Tension Testing of Metallic Materials, *ASTM International*, West Conshohocken, PA.
16. Bazant, Z. P., (1984), Size Effect in Blunt Fracture: Concrete, Rock, Metal, *Journal of Engineering Mechanics*, ASCE, V. 110, No. 4, pp. 518-535.
17. Black, J. (2017). Adhesive Anchorages. Minnesota: Department of Transportation. Retrieved from https://www.dot.state.mn.us/bridge/pdf/lrfdmanual/workshop/06-adhesive-anchorages.pdf
18. BNP. (2020, 3 31). The MBC-16B1 Manual Rebar Bender/Cutter. Retrieved from http://www.bnproducts.com//assets/pdf/MBC-16B1_4-Pager-2020.pdf
19. Comité Euro-International du Béton (CEB) (1994): Fastenings to Concrete and Masonry Structures: State-of-the-art report. BulletinD' Information No. 216, Lausanne, published by Thomas Telford Services Ltd, London,1994.

20. Cook, R. A.; Klingner, R. E. (1989): Behavior and design of ductile multiple anchor steel to concrete connections. Report No. CTR1126–3. University of Texas at Austin.
21. Cook, R.A. and Konz, R.C. (2001). Factors Influencing Bond Strength of Adhesive Anchors. ACI Structural Journal, 98 (1), pp. 76 -86.
22. Cook, R.A., Bishop, M.C., Hagedoorn, H.S., Sikes, D.E., Richardson, D.S., Adams, T.L., and DeZee, C.T. (1994). Adhesive-Bonded Anchors: Bond Properties and Effects of in -Service and Installation Conditions. University of Florida, Gainesville, FL.: Structures and Materials Research Report No. 94-2.
23. Cook, R.A., Konz, R.C., and Richardson, D.S. (1996). Specifications for Adhesive-Bonded Anchors and Dowels. University of Florida, Gainesville, FL.: Structures and Materials Research Report No. 96-3.
24. Cook, R.A., Kunz, J., Fuchs, W., and Konz, R.C. (1998). Behavior and Design of Single Adhesive Anchors Under Tensile Load in Uncracked Concrete. *ACI Structural*, 95 (1), pp. 9 -26.
25. Cook. R. A., Collins, D. M., Klingner, R. E., and Polyzoi, D. (1992). Load-deflection behaviour of cast-in-place and retrofit concrete anchors. *ACI Struct. J*., 89(6). 639-649.
26. Davis, T. M. (2012). Sustained Load Performance of Adhesive Anchor Systems in Concrete. Thesis.
27. Delhomme, F. & Brun, M. (2018). Pullout simulation of post installed chemically bonded anchors in UHPFRC. MATEC Web of Conferences. 199. 11007. 10.1051/matecconf/201819911007.
28. Djouani, F., Connan, C., Delamar, M., Chehimi, M. M., Benzarti, K. (2011). Cement paste-epoxy adhesive interactions. *Constr. Build. Mater*, 25 (2), pp. 411 -423.

29. Eligehausen, R. and Balogh, T. (1995). Behavior of Fas teners Loaded in Tension in Cracked Reinforced Concrete. *ACI Structural Journal*, 92(3), pp. 365 -379.
30. Eligehausen, R., and Ozbolt, J., (1992), Influence of Crack Width on the Concrete Cone Failure Load, Fracture Mechanics of Concrete Structures, Z. P. Bazant, ed., Elsevier Applied Science, pp. 876-881.
31. Eligehausen, R., Appl, J. J., Lehr, B., Meszaros, J., and Fuchs, W. (2004): Tragverhalten und Bemessung von Befestigungen mit Verbunddübeln unter Zugbeanspruchung, Part 1: Einzeldübel mit großem Achs- und Randabstand (Load-bearing Behavior and Design of Fastenings with Adhesive Anchors under Tension Loading – Part 1: Single Anchors with Large Axial and Edge Spacing), Beton und Stahlbetonbau 99, No. 7, pp. 561–571.
32. Eligehausen, R., Cook, R.A., and Appl, J. (2006a). Behavior and Design of AdhesiveBonded Anchors, *ACI Structural Journal*, 103(6), pp. 822 -31.
33. Eligehausen, R., Mallee, R., and Silva, J.F. (2006b). Anchorage in Concrete, *Construction*, Ernst & Sohn, Berlin, Germany.
34. Eligehausen, R., Popov, E.P. & Bertero, V.V. (1983). Local bond stress-slip relationships of deformed bars under generalized excitations, Report No. UCB/EERC-83/23. Berkeley: University of California.
35. Eligehausen, R.; Küenzlen, J. H. R. (2002): Tragverhalten von Befestigungen mit Schraubdübeln (Load-bearing behaviour of screw anchors). Beton- und Stahlbetonbau 97, 2002, No. 2, pp. 61–68 (in German).
36. Eligehausen, R.; Meszaros, J. (1996): Influence of Installation Inaccuracies on the Behaviour of Bonded Anchors, Evaluation of the Test Results. Report No. 1/80-96/11. Institut für Werkstoffe im Bauwesen, Universität Stuttgart, 1996, not published.

37. EOTA. (2002). Bonded Anchors. ETAG 001 Guideline for European Technical Approval of Metal Anchors for Use in Concrete, Part 5, European Organization for Technical Approvals, Brussels.
38. Fuchs, W.; Eligehausen, R.; and Breen, J. E., (1995). "Concrete Capacity Design (CCD) Approach for Fastening to Concrete," *ACI Structural Journal*, V. 92, No. 1, Jan.-Feb., pp. 73-94.
39. How to Calculate the Cutting Length of Rectangular Stirrup. (HCCLRS) (2017, 10 23). Retrieved from Civil Click.com: https://www.civilclick.com/calculate-cutting-length-rectangular-stirrup
40. J. Henriques, L. Simões da Silva, I.B. Valente, (2013). Numerical modeling of composite beam to reinforced concrete wall joints: Part I: Calibration of joint components. *Eng. Struct*. 52, 747–761.
41. J. Lubliner, J. Oliver, S. Oller and E. Oñate, (1989). A plastic-damage model for concrete, *Int. J. Solids and Structures*. Vol. 25 (3), pp. 299-326
42. J. Tatar, C. Weston, P. Blackburn, H.R. Hamilton. (2013). Direct shear adhesive bond test. In: Proceedings of the 11th International Symposium of Fiber Reinforced Polymer for Reinforced Concrete Structures (FRPRCS -11). Guimaraes, Portugal.
43. Jack C. McCormac, Russell H. Brown. (2014). Design of Reinforced Concrete NINTH EDITION. John Wiley & Sons, Inc.
44. Jacob Olsen, Thilo Pregartner, and Anthony J. Lamanna. (2012). Basis for Design of Screw Anchors in Concrete. *ACI Structural Journal*, V. 109, No. 4.

45. Klingner, R. E.; Hallowell, J. M.; Lotze, D.; Park, H.-G.; Rodriguez, M.; Zhang, Y.-G.(1998): Anchor Bolt Behaviour and Strength During Earthquakes. Report No. NUREC/CR-5434. The University of Texas at Austin, August 1998.
46. Küenzlen, J. H. R.; Sippel, T. M. (2001): Behaviour and design of fastenings with concrete screws. In: RILEM Proceedings PRO 21 Symposium on Connections between Steel and Concrete. Cachan Cedex, 2001, pp. 919–929.
47. L. Molina, F. Javier, F. Ruiz, M. Alejandro, E.H. Montes, A. Alonso, M. Cruz, (2015). Bond strength of galvanized steel: experimental and numerical study based on pull-out tests. Conference: Third International Conference on Mechanical Models in Structural Engineering At: University of Seville (Spain)Volume: pp. 143-158. ISBN: 978-84-606-9356-7.
48. Lee J. and Fenves G.L. (1998). Plastic-damage model for cyclic loading of concrete structure. *ASCE J*. Eng. Mech.124 892-900
49. Lee, N.K., Mayfield, B., and Snell, C., (1980). "Resin Anchors in Concrete," *Civil Engineering*, London, April 1980, pp. 35-41; June 1980, pp.47-53.
50. Lefebvre, D. R., Elliker, P. R., Takahashi, K. M., Raju, V. R., Kaplan, M. L. (2000). The critical humidity effect in the adhesion of epoxy to glass: role of hydrogen bonding. *J. Adhes. Sci. Technol*, 14 (7), 925-937.
51. Lettow, S. (2007). “Ein Verbundelement für nichtlineare Finite Elemente Analysen – Anwendungauf Übergreifungsstöße” Dissertation, IWB Universität Stuttgart, Germany (in German).
52. M. Szczecina, A. Winnicki, (2015) "Calibration of the CDP model parameters in ABAQUS" Proceedings of the 2015 World Congress on Advances in Structural Engineering and Mechanics (ASEM15), Incheon, Korea, pp 25-29.

53. Mark K. Johnson, H. S. Lew, Long T. Phan. (1988). Literature Review of Post-Installed Anchorage in Concrete. U.S. DEPARTMENT OF COMMERCE.

54. Mereco (2019). why-is-the-sky-blue. Retrieved from www.mereco.com: http://www.mereco.com/resources/ask-the-doctor/why-is-the-sky-blue

55. Meszaros, J. (1999): Tragverhalten von Verbunddübeln im ungerissenen und gerissenen Beton (Load-bearing behaviour of bonded anchors in non-cracked and cracked concrete). Doctor thesis, Universität Stuttgart, 1999 (in German).

56. Meszaros, J.; Eligehausen, R. (1998): Einfluß der Bohrlochreinigung und von feuchtem Beton auf das Tragverhalten von Injektionsdübeln (Influence of hole cleaning and of humid concrete on the load-bearing behaviour of injection anchors). Report No. 98/2-2/2, Institut für Werkstoffe im Bauwesen, Universität Stuttgart, 1998, not published (in German).

57. National Transportation Safety Board (NTSB), Highway Accident Report, Ceiling Collapse in the Interstate 90 Connector Tunnel, Boston, Massachusetts, July 10, 2006, NTSB/HAR-07/02. The Epoxy Adhesive, Numerous Anchor Bolts, [Online images], http://www.ntsb.gov/publictn/2007/HAR0702.pdf.

58. Nilforoush, R. (2017). Anchorage in Concrete Structures: Numerical and Experimental Evaluations of Load-Carrying Capacity of Cast-in-Place Headed Anchors and Post-Installed Adhesive Anchors. Luleå, Sweden: Luleå University of Technology.

59. Petersen, D., Lin, Z., & Zhao, J. (2018). Design of anchor reinforcement for seismic tension loads. *Engineering Structures*, 164, 109-11.

60. Philipp Grosser, Werner Fuchs, Rolf Eligehausen. (2011). A Field Study of Adhesive Anchor Installations. *Concrete international*.

61. PNSPCC. (2019, 8 29). Properties of normal strength Portland cement concrete. Retrieved from civilengineeringbible.com: https://civilengineeringbible.com/article.php?i=14

62. Shirvani, M. & Klingner, R.E. & III, H.L.. (2004). Breakout capacity of anchors in concrete - Part 1: Tension. *ACI Structural Journal*. 101. 812-820.

63. Dickey, B., Faller, R., Rosenbaugh, S., Bielenberg, R., Lechtenberg, K., and Sicking, D., (2012) Development of a Design Procedure for Concrete Traffic Barrier Attachments to Bridge Decks Utilizing Epoxy Concrete Anchors, Final Report to the Wisconsin Department of Transportation, Transportation Research Report No. TRP 03-264-12.

64. Spieth, H. A.; Eligehausen, R. (2002): Bewehrungsanschlüsse mit nachträglich eingemörtelten Bewehrungsstäben (Starter bars with post-installed rebars). Beton- und Stahlbetonbau 97, No. 9, pp. 445–459, Berlin, 2002 (in German).

65. Suozzo, M.J., & Dewoolkar, M.M. (2014). Evaluation of Strength and Hydraulic Testing Methods of Pervious Concrete.

66. The Investigation and Examination Committee. (IEC) (2013). Outline of the Report on the Tunnel Ceiling Panel Collapse. Retrieved from Ministry of Land, Infrastructure, Transport and Tourism of Japan: http://www.mlit.go.jp/road/road_e/02topics/release/release_201307_1. html

67. Yasuhiro Matsuzaki, Tomoaki Akiyama and Katsuhiko Nakano (2010). Outline of Japanese guideline of post-installed bonded anchors effect of the embedment length and the edge distance on tensile resistance.

68. Zamora, N.A. & Cook, Ronald & Konz, R.C. & Consolazio, Gary. (2003). Behavior and design of single, headed and unheaded, grouted anchors under tensile load. *ACI Structural Journal*. 100. 222-230.

69. Zhao J. (2014). Seismic behavior of single anchors in plastic hinge zones of RC columns. Proceedings of the 10th National Conference in Earthquake Engineering, Earthquake Engineering Research Institute, Anchorage, AK.

Figure 1.1. Schematics of an adhesive anchor in concrete.

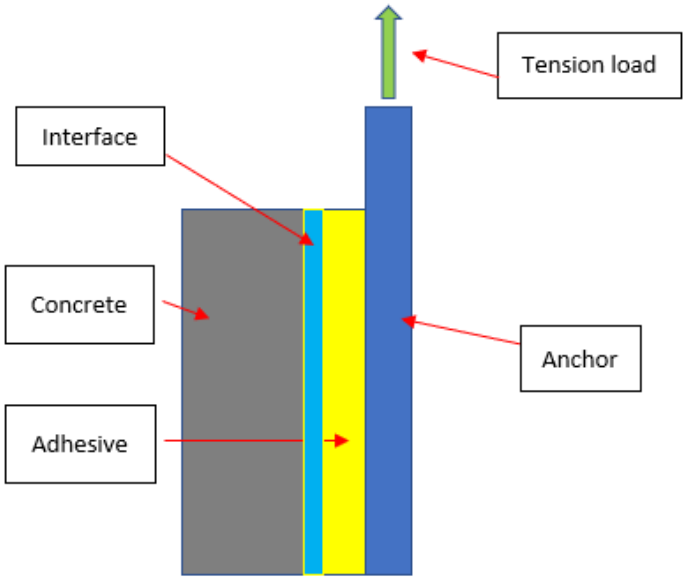

Figure 1.2. Schematics of the load transfer of adhesive anchor in concrete.

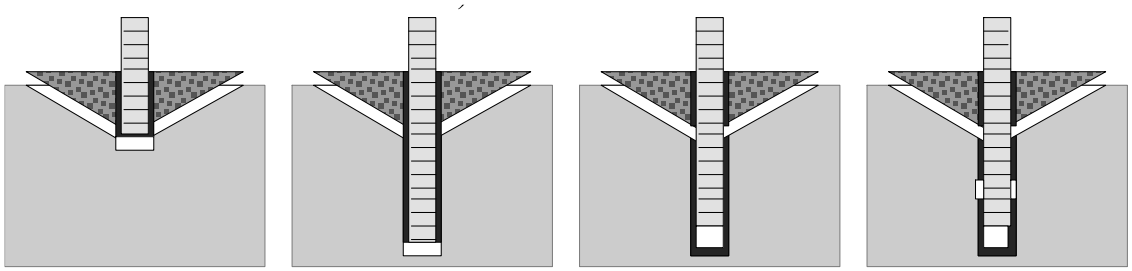

Figure 1.3. Adhesive anchor failure observed in laboratory.

Figure 1.4. Adhesive anchors failure in a Boston Tunnel.

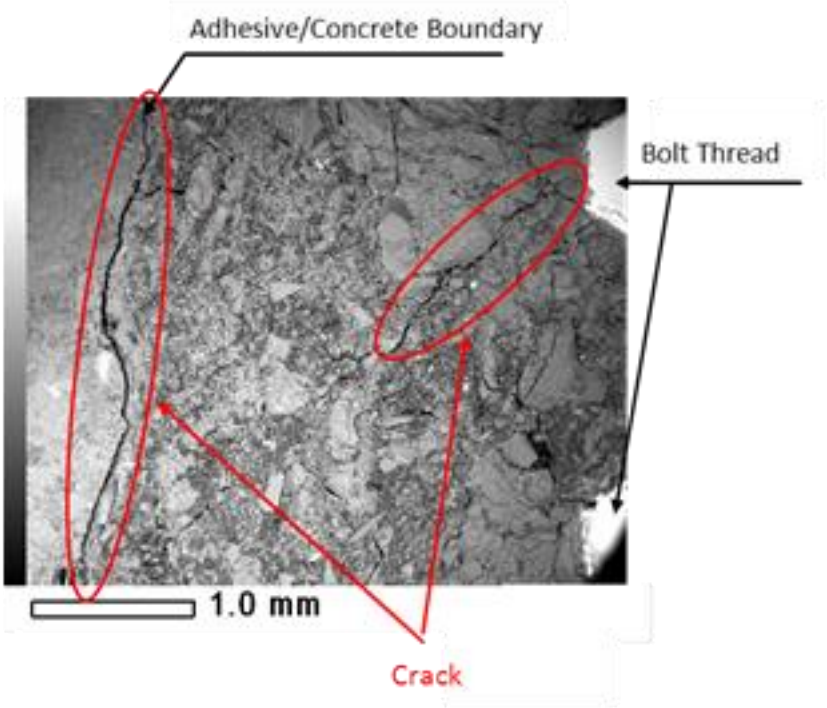

Figure 1.5. Deterioration of adhesive material and adhesive-concrete interface in anchors of Sasago Tunnel near Toyoko, Japan (IEC 2013)

(a) adhesive from this study (b) adhesive from Dickey et al. (2012)

Figure 1.6. Adhesive-concrete interface showing micro-level adhesive deformation

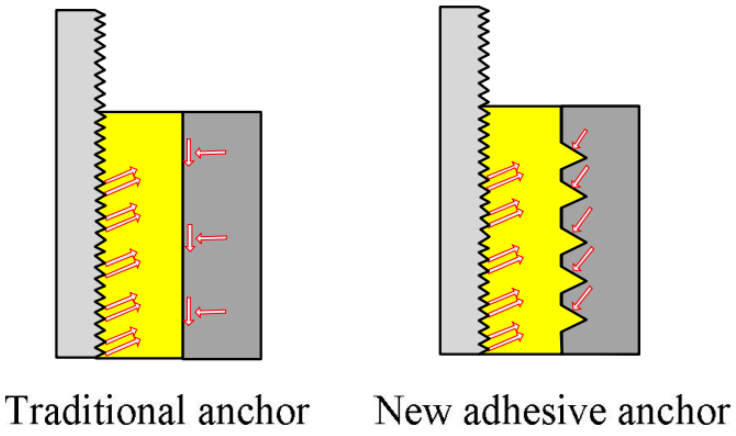

Figure 1.7. New Engineered adhesive-concrete interface design

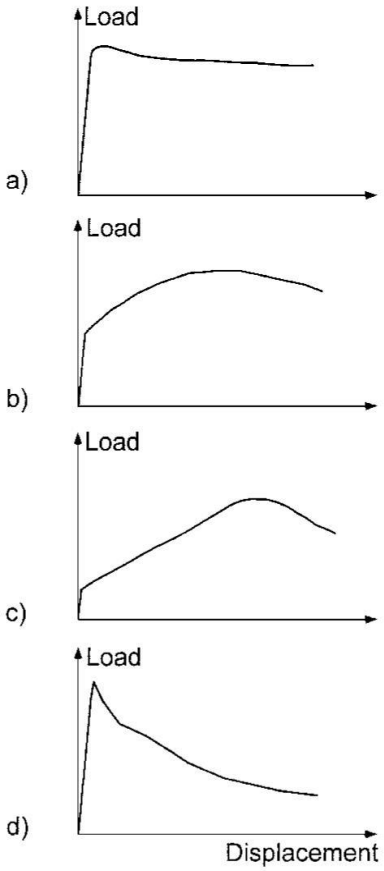

Fig. 6.5 Load-displacement curves of single bonded anchors (schematic) (*Meszaros* (1999))
a) Failure between mortar and wall of drilled hole (bond force between mortar and concrete higher than friction force)
b) Failure between mortar and wall of drilled hole (bond force between mortar and concrete lower than friction force)
c) Failure between mortar and wall of drilled hole (bond force between mortar and concrete significantly lower than friction force)
d) Failure between mortar and rod

a) A-C failure (high bond strength); b) A-C failure (low bond strength);
c) A-C failure (poor bond strength); d) A-S failure

Figure 2.1. Schematic load-displacement curves of single adhesive anchors (Eligehausen et al. 2006b)

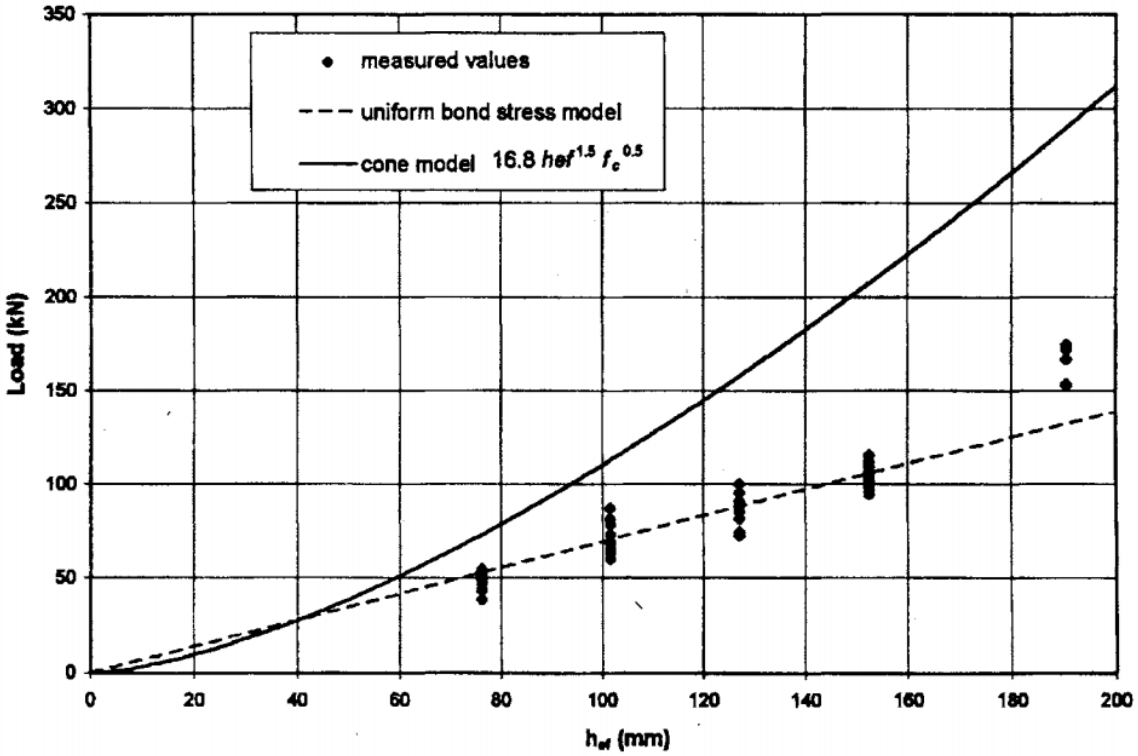

Fig. 12—Comparison of cone model Eq. (3) with uniform bond model Eq. (5) for data sets 7 and 8

Figure 2.2. Comparison of cone model with uniform bond model (Cook et al. 1998)

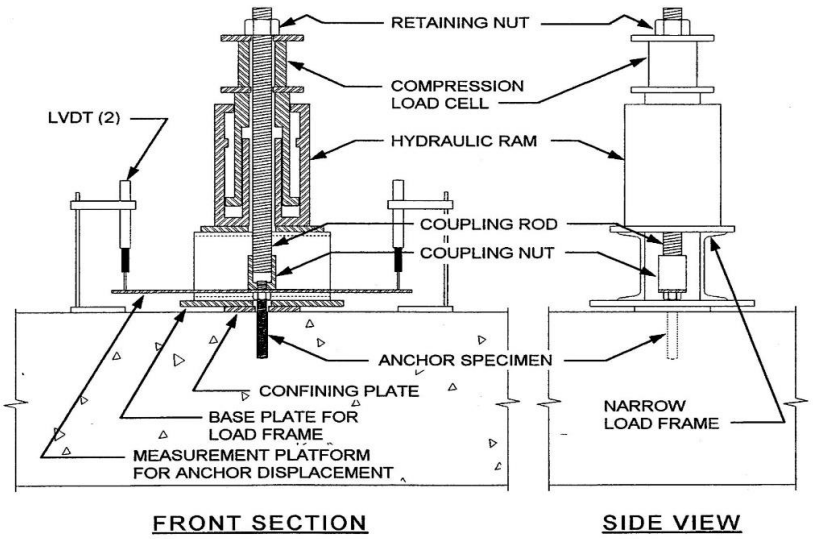

Figure 1. Testing Apparatus for Confined Specimens

Figure 2.3. Schematic of confined pullout tests (Cook et al. 1996)

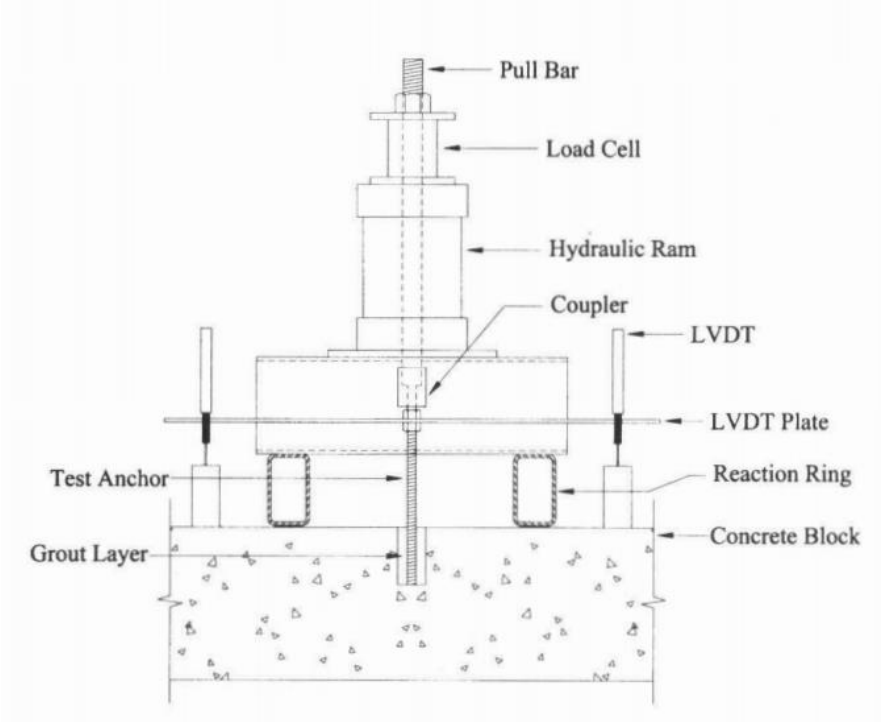

Figure 2.4. Schematic of unconfined pullout tests (Zamora et al. (2003))

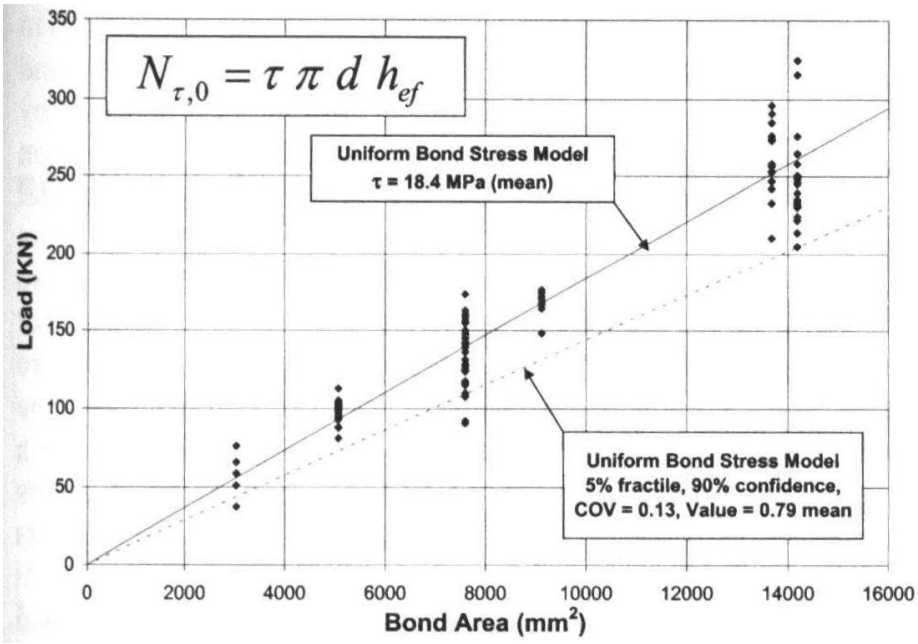

Figure 2.5. Comparison of test results of unheaded anchors that developed steel/grout bond failure to uniform bond stress model (Zamora et al. (2003))

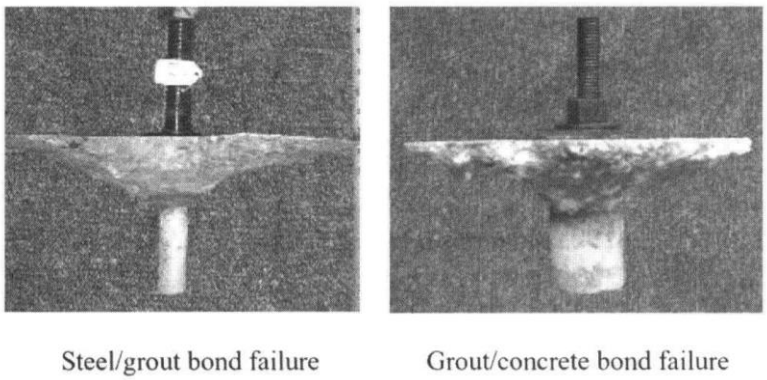

Figure 2.6. Bond failure of adhesive anchors with significant cone depth in Zamora et al. (2003)

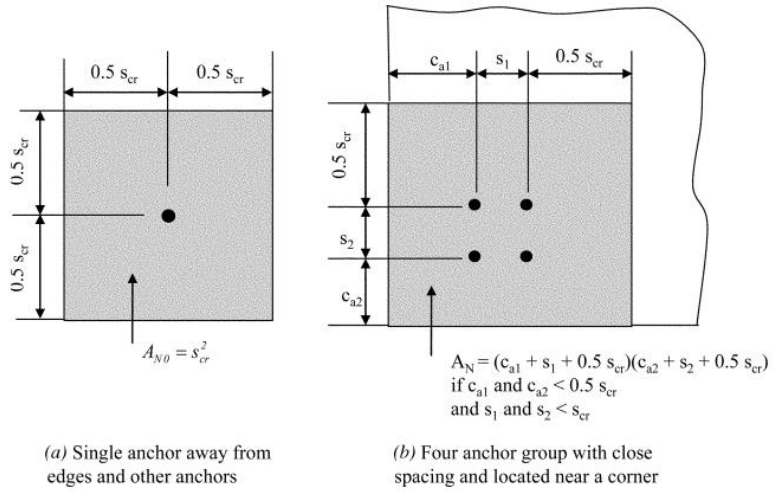

Figure 2.7. Determine of effective areas (Eligehausen et al. 2006a)

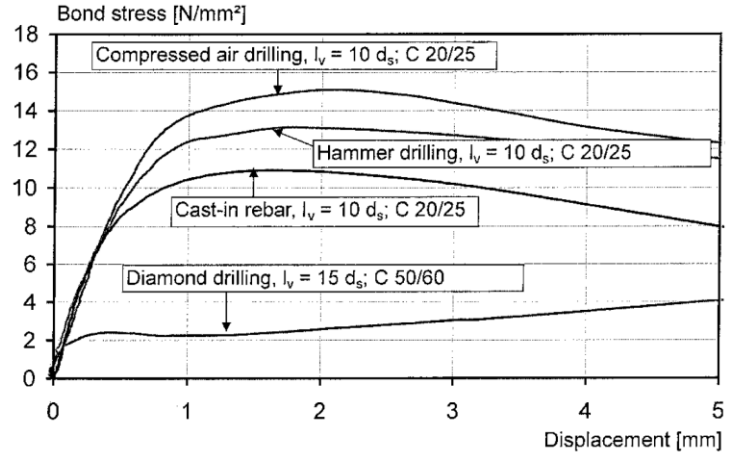

Figure 2.8. Bond stress-displacement curves of injection type boned anchors with anchor diameter d_s= 20mm anchored in holes made by hammer and diamond drilling (Eligehausen et al. (2006b))

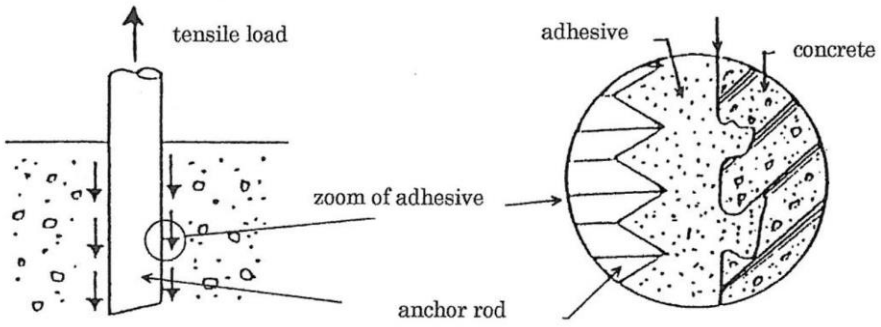

Figure 1.1 Tensile resistance transfer mechanism Figure 1.2 Zoom of adhesive

Figure 2.9. The adhesive filled the gap (Matsuzaki et al. (2010))

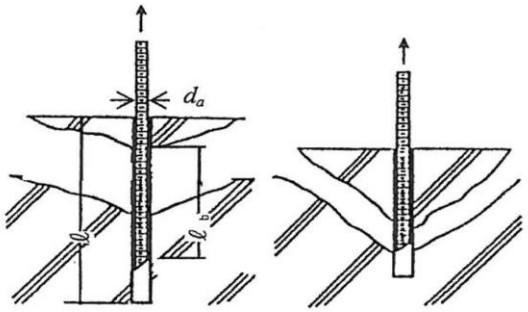

l : embedment length, l_b: bond failure length
(1) Long embedment length (2) Short embedment length

Figure 1.4 Different types of cone failure result from different effective embedment lengths (l_e)

Figure 2.10. Cone failure with different effective embedment lengths (Matsuzaki et al. (2010))

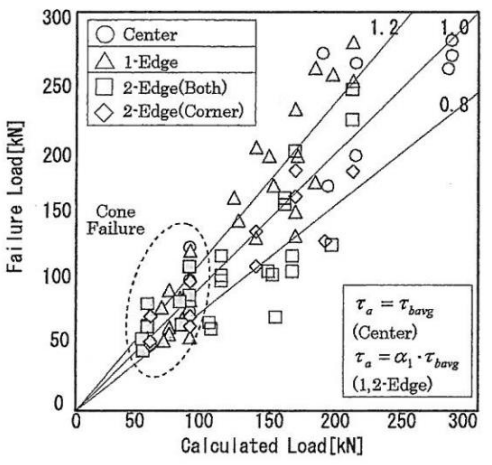

Figure 1.12 Calculation compared with test (case2: $\alpha_1 \cdot \tau_a = \tau_{bavg}$)

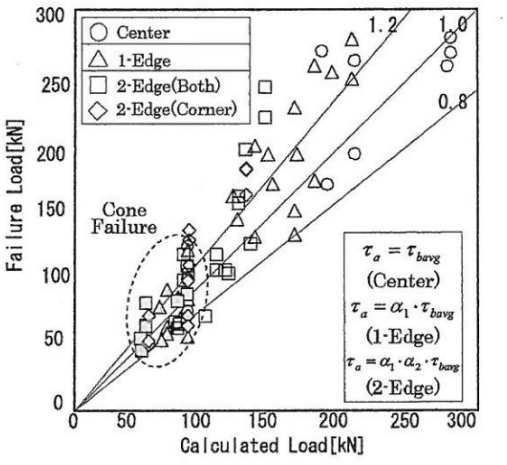

Figure 1.13 Calculation compared with test (case3: $\alpha_1 \cdot \alpha_2 \cdot \tau_a = \tau_{bavg}$)

Figure 2.11. The average bond strength multiplied by reduction factor"α_n"(Matsuzaki et al. (2010))

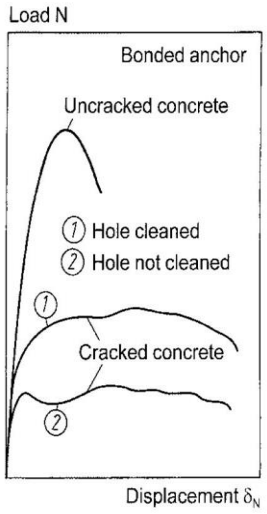

Fig. 6.39 Load-displacement curves of bonded anchors in non-cracked and cracked concrete (schematic) (*Eligehausen, Mallée, Rehm* (1997))

Figure 2.12. Schematic of adhesive in cracked and uncracked concrete (Eligehausen et al. (2006b)

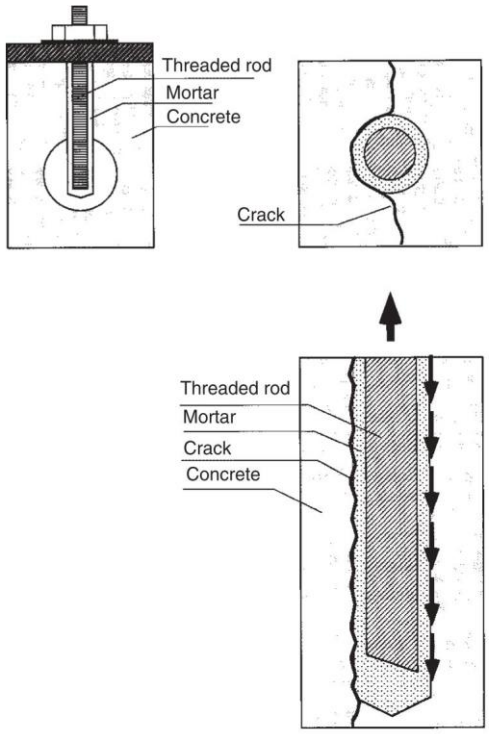

Fig. 6.43 Disturbance of bond between mortar and concrete by a crack

Figure 2.13. Schematic of adhesive in cracked and uncracked concrete (Elighausen et al. (2006b))

Table 2.1. Test parameters of adhesive anchors (Cook et al. 1998)

Table 1—Main parameters of tests used for model development

Data set no.	Number of tests	d, mm			h_{ef}, mm			d_o / d			h_{ef} / d			f_c, MPa		
		min.	max.	avg.	min.	max.	avg.	min.	max.	avg.	min.	max.	avg.	min.	max.	avg.
1	205	8.0	24.0	14.9	80	300	147	1.10	1.83	1.26	7.8	15.0	9.9	21.3	68.0	29.0
2	141	9.5	32.3	18.2	89	457	187	1.13	1.38	1.28	6.9	18.7	10.4	13.4	39.7	24.8
3	296	8.0	25.0	13.6	44	254	118	1.04	1.33	1.12	4.5	14.0	8.8	21.3	47.6	29.6
4	120	9.5	50.8	19.0	84	482	179	1.13	1.25	1.18	6.5	12.7	8.0	13.5	43.0	26.1
5	23	12.7	32.3	18.6	114	254	151	1.17	1.25	1.23	6.3	10.0	8.5	27.6	37.0	28.5
6	56	12.7	25.4	18.0	95	321	184	1.13	1.29	1.20	5.9	18.0	8.7	13.0	31.6	22.9
7	27	15.9	15.9	15.9	76	191	127	1.20	1.20	1.20	4.8	12.0	8.0	43.7	44.6	44.0
8	20	15.9	15.9	15.9	76	152	114	1.20	1.20	1.20	4.8	9.6	7.2	42.1	42.1	42.1
All	888	8.0	50.8	15.9	44	482	149	1.04	1.83	1.20	4.5	18.7	9.5	13.0	68.0	28.0

Table 2.2. The existing database of screw anchor (Olsen et al. (2012))

Table 1—Summary of screw anchor database

Data source	Unique thread profiles	Diameter range, mm	Embedment range, mm	Number of tests		
				Single anchor, uncracked	Single anchor, cracked	Group of two or four anchors
Original data (Kuenzlen[6])	9	8.00 to 18.00	30 to 110	268	126	106
New data (from independent testing)	8	6.35 to 19.05	25.4 to 127	194	122	37
Total	17	6.35 to 19.05	25.4 to 127	462	248	143

Note: 1 mm = 0.0394 in.

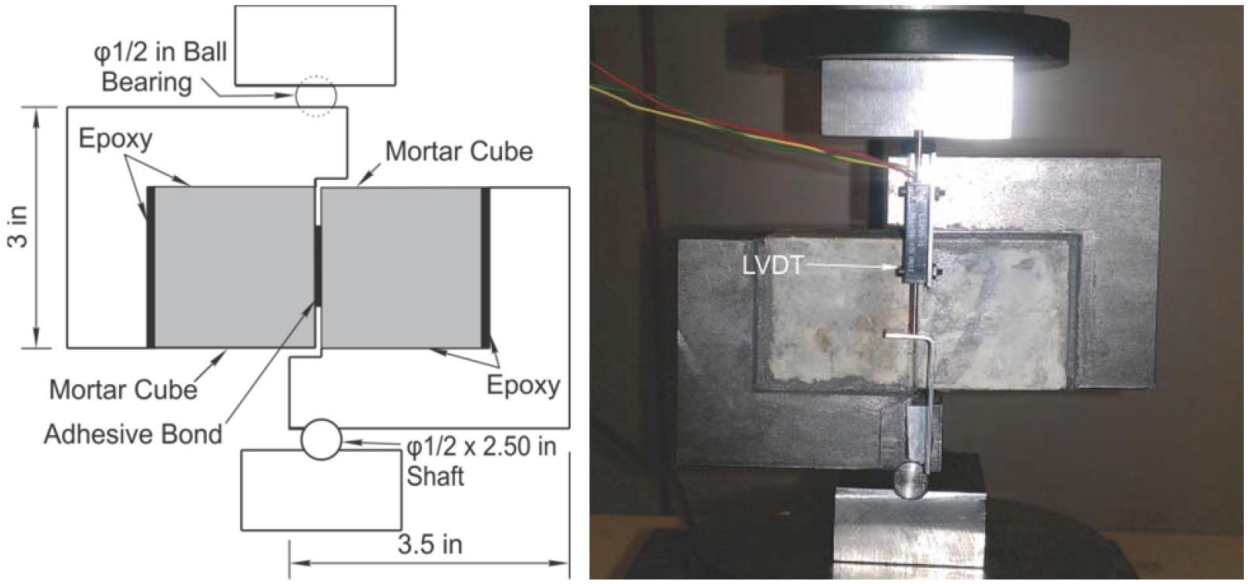

Figure 3.1 Direct shear test specimen and set up by Tartar et al. (2013)

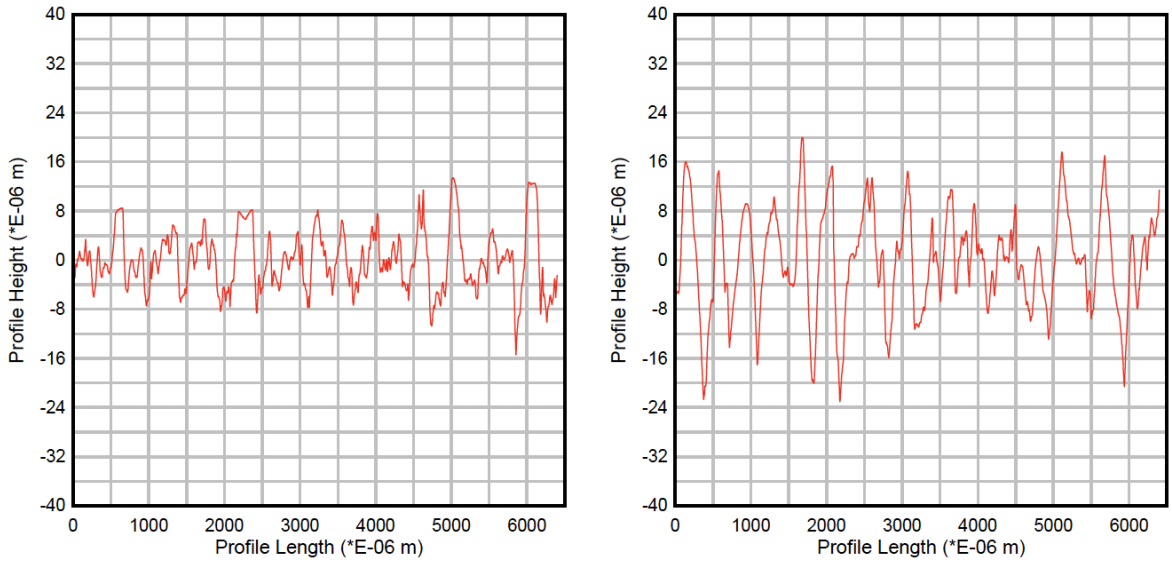

Figure 3.2. Roughness profile using a Mitutoyo SJ-400 Diamond profilometer for a) polished mortar cube and b) sandblasted/roughened mortar cube in the bond study by Tartar et al. (2013)

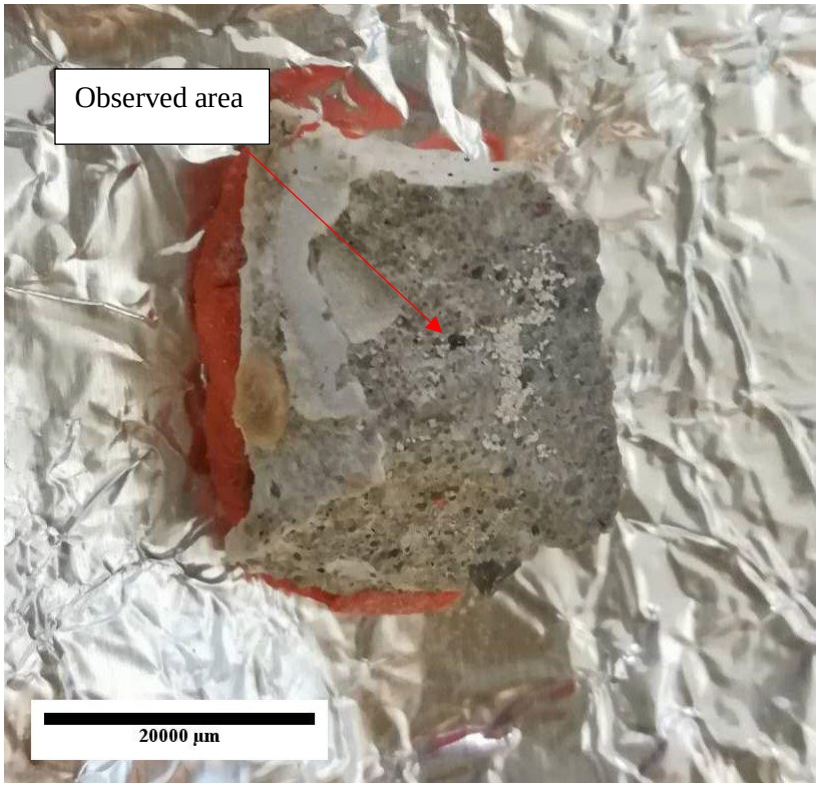

Figure 3.3. Observed area of a concrete piece peeled from a drilled hole

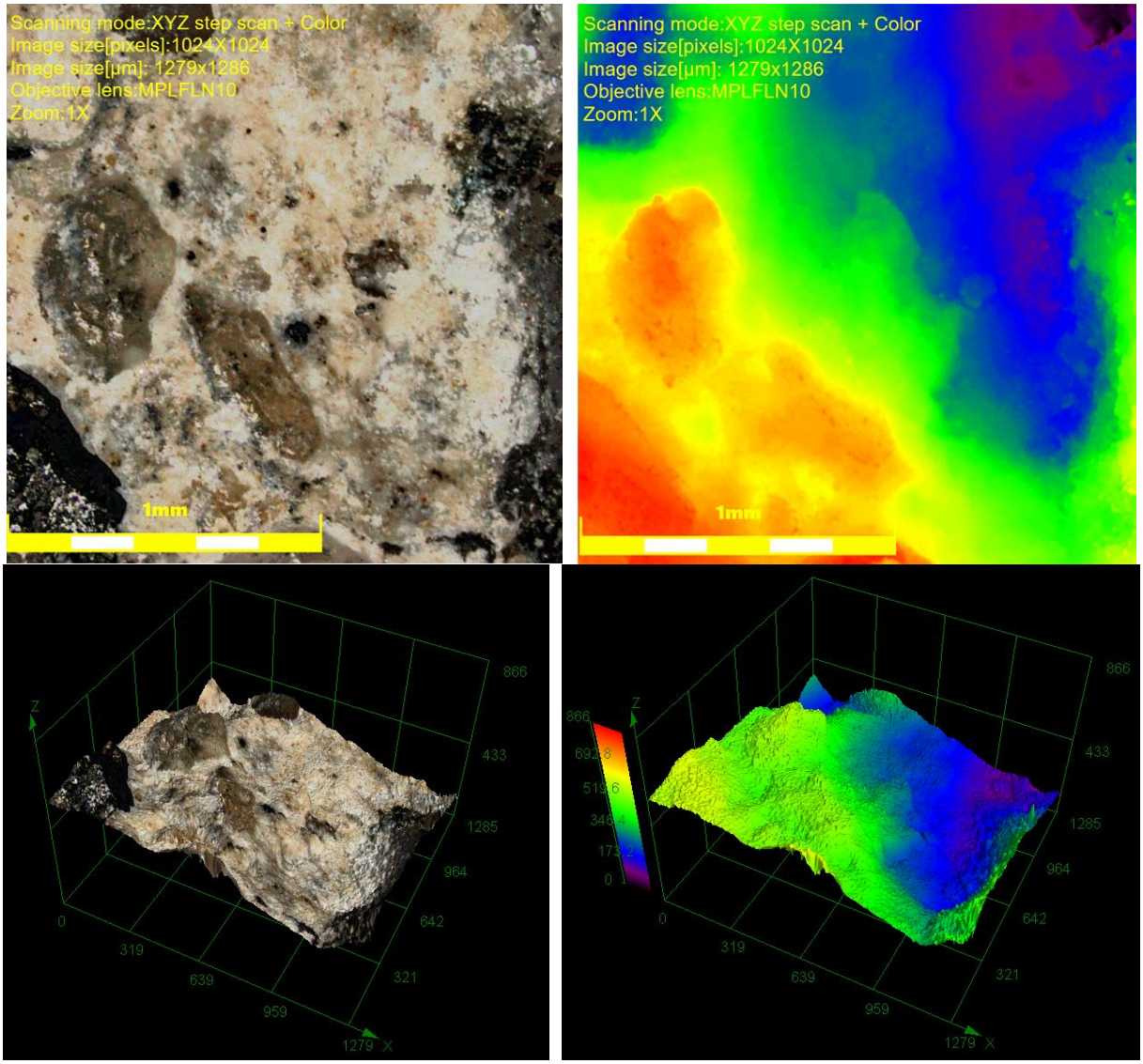

(a) plane view of the observed area; (b) pane view of the observed area with colored profile heights; (c) 3D view of the observed area; (d) 3D view of the observed area with profile heights

Figure 3.4. Observed area of the concrete piece under laser confocal microscope

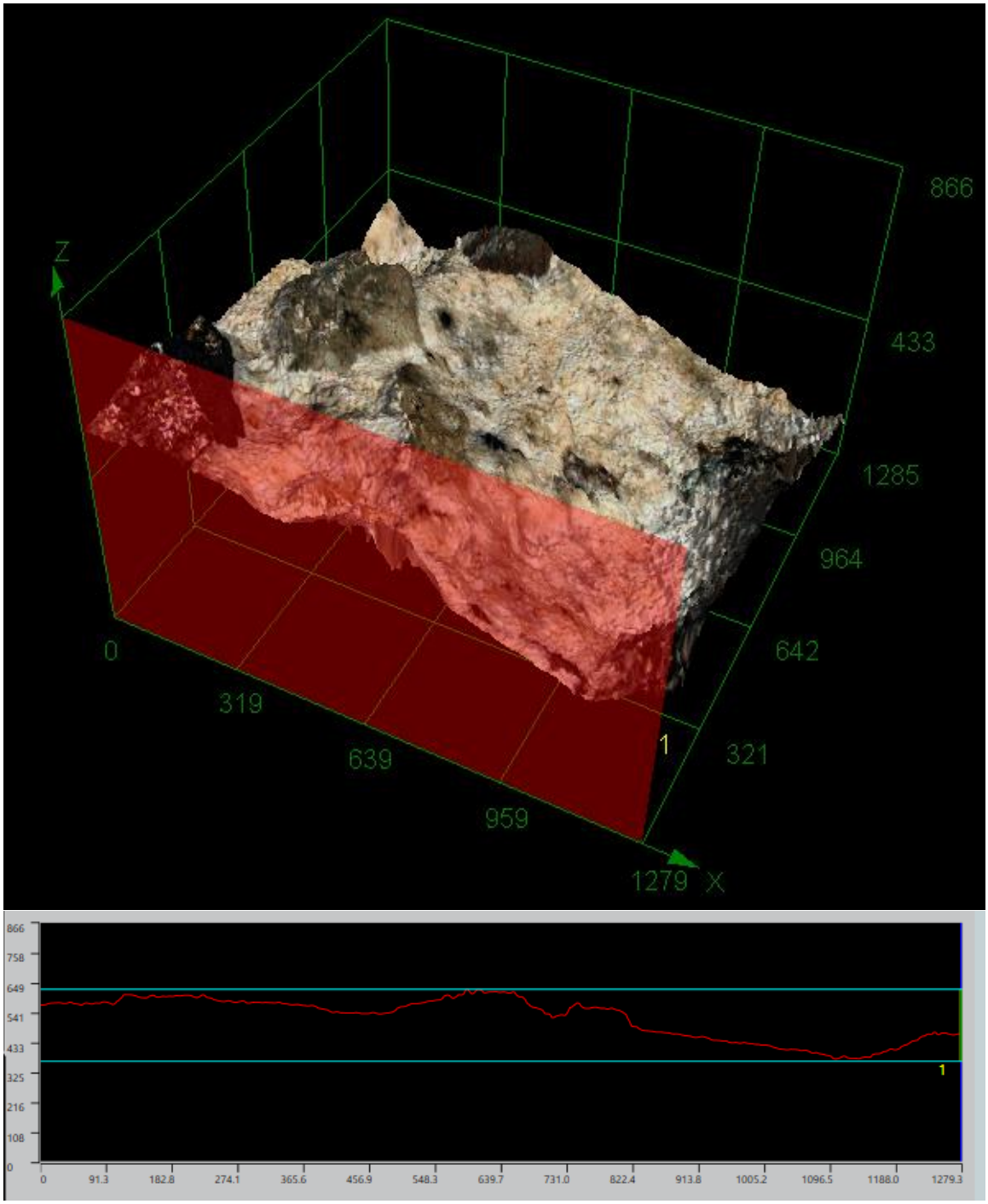
Z
866
433
1285
964
642
0
319
639
959
1
321
1279
X
866
758
649
541
433
325
216
108
0
1
0
91.3
182.8
274.1
365.6
456.9
548.3
639.7
731.0
822.4
913.8
1005.2
1096.5
1188.0
1279.3

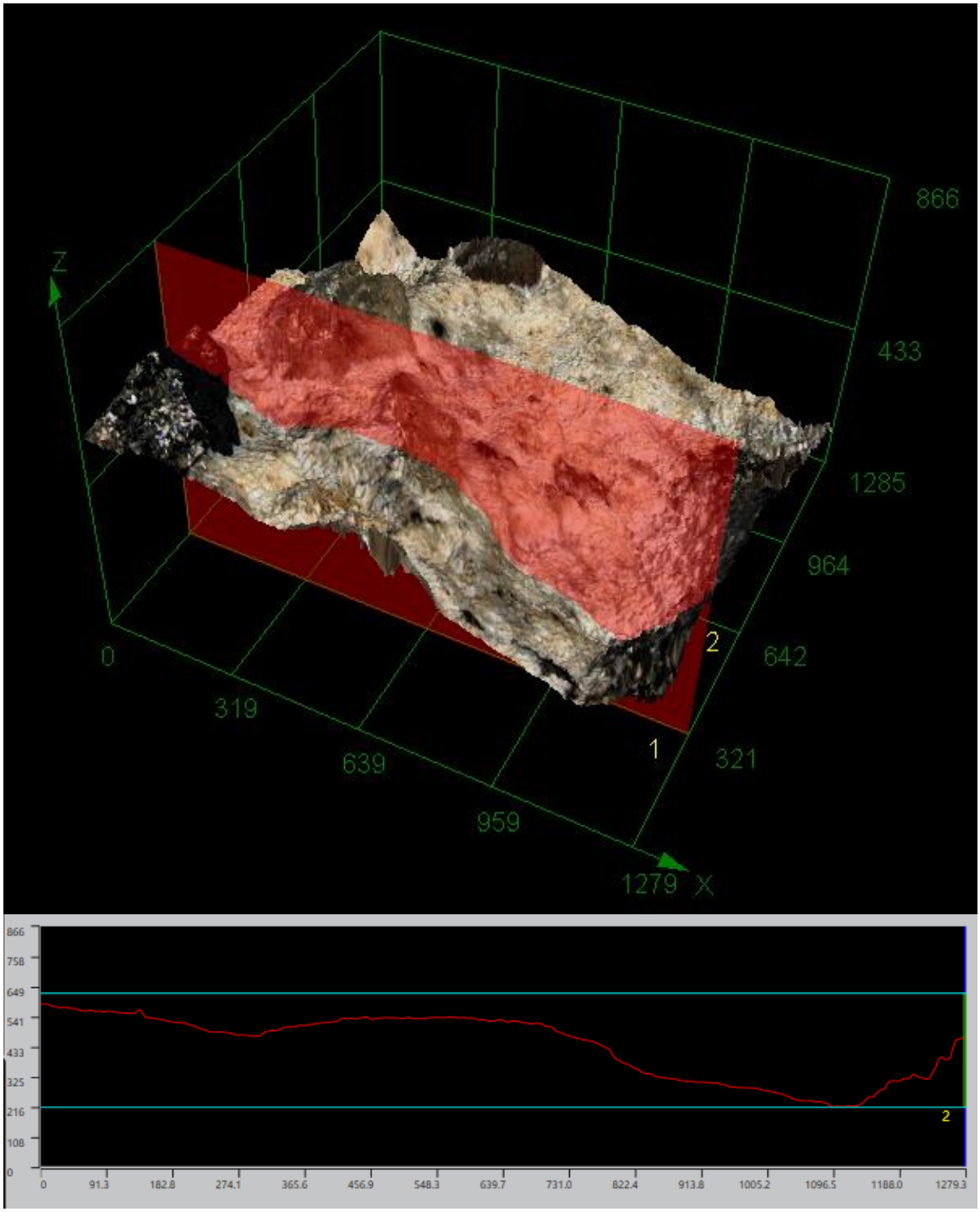
Z
866
433
1285
964
642
321
0
319
639
959
1279
X
1
2
866
758
649
541
433
325
216
108
0
0
91.3
182.8
274.1
365.6
456.9
548.3
639.7
731.0
822.4
913.8
1005.2
1096.5
1188.0
1279.3
2

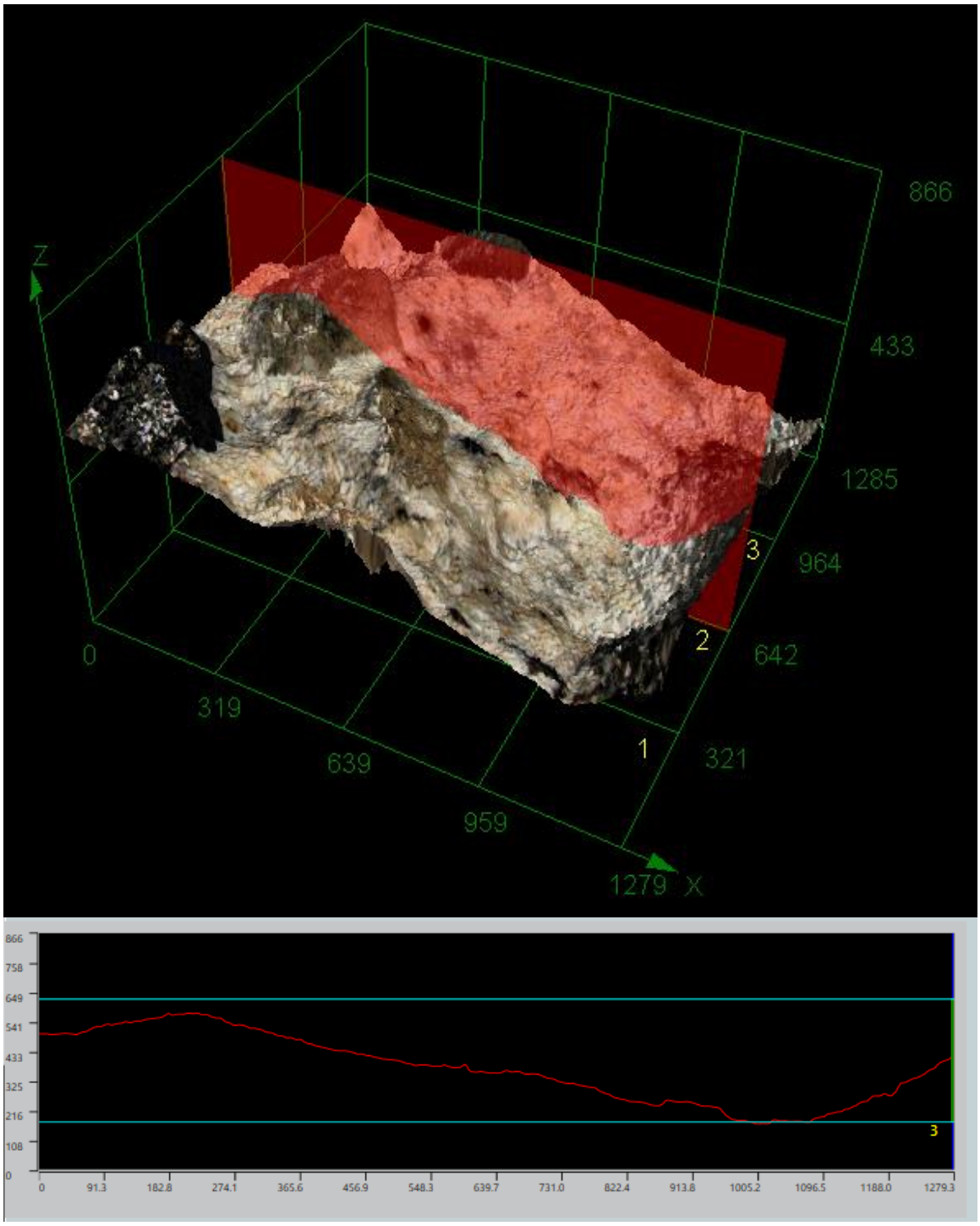
Z
866
433
1285
964
642
321
0
319
639
959
1279
X
1
2
3
866
758
649
541
433
325
216
108
0
0
91.3
182.8
274.1
365.6
456.9
548.3
639.7
731.0
822.4
913.8
1005.2
1096.5
1188.0
1279.3
3

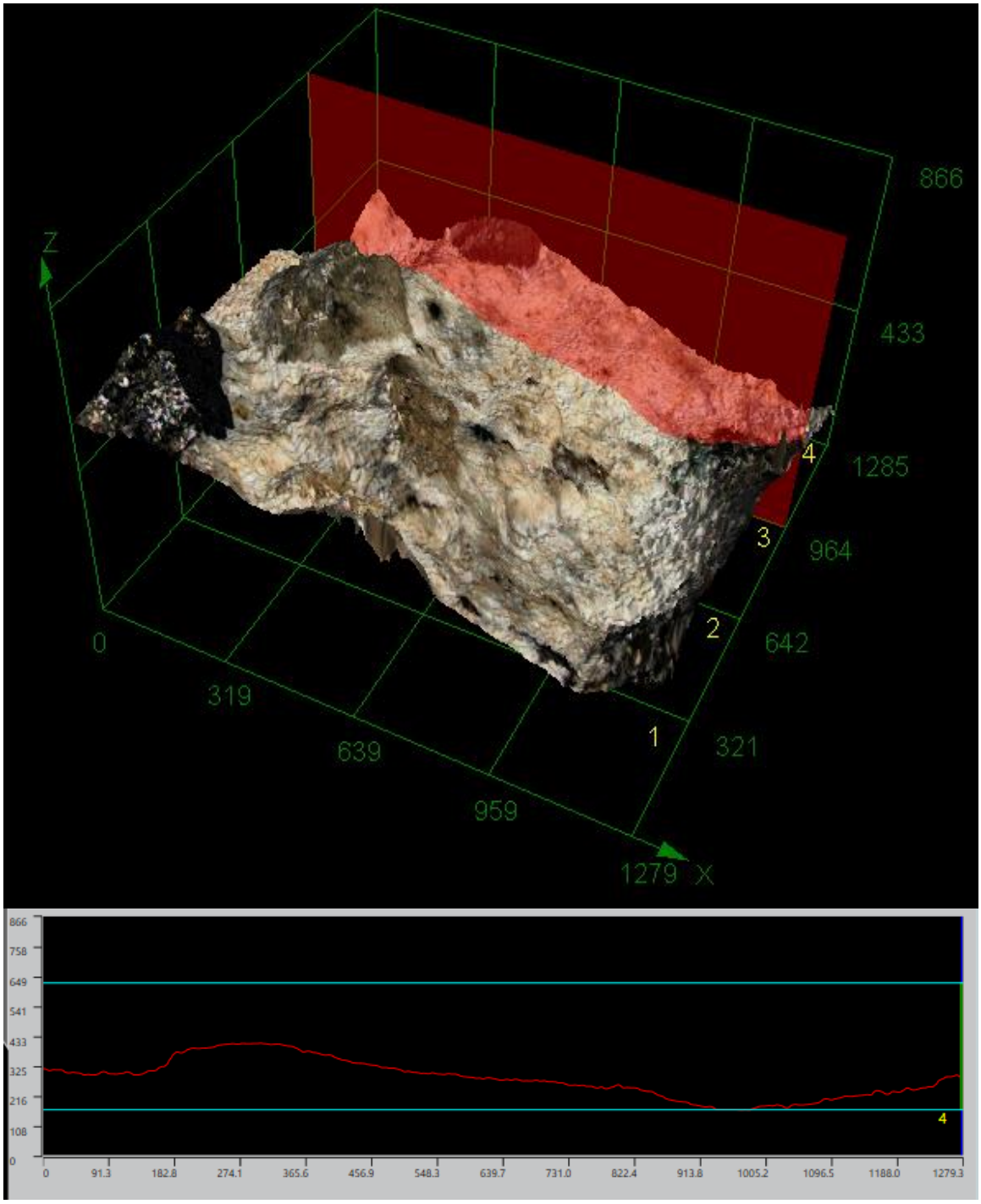
Z
866
433
1285
964
642
321
0
319
639
959
1279
X
1
2
3
4
866
758
649
541
433
325
216
108
0
0
91.3
182.8
274.1
365.6
456.9
548.3
639.7
731.0
822.4
913.8
1005.2
1096.5
1188.0
1279.3
4

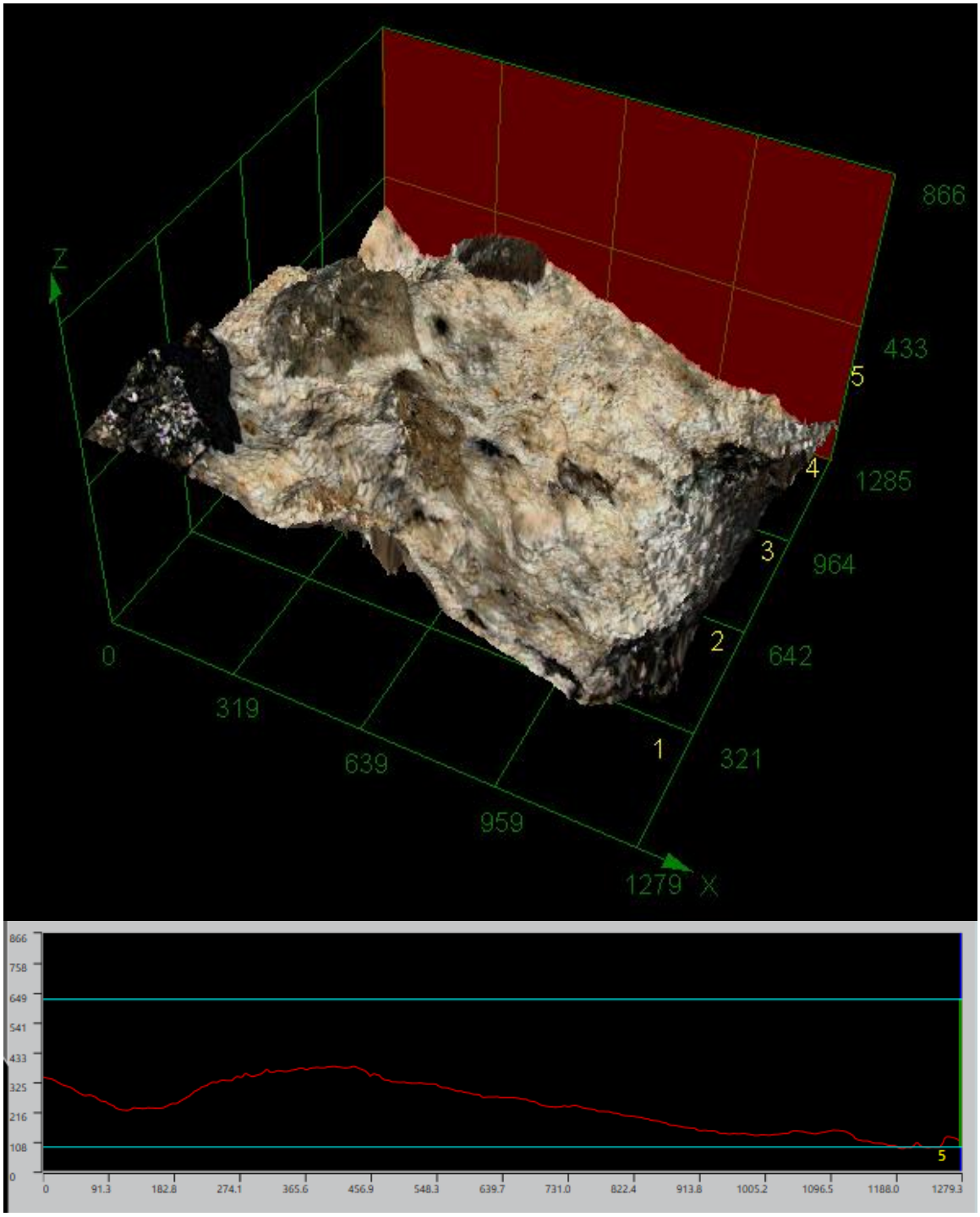

Figure 3.5. Section views of the observed area for five sections parallel to the X-axis

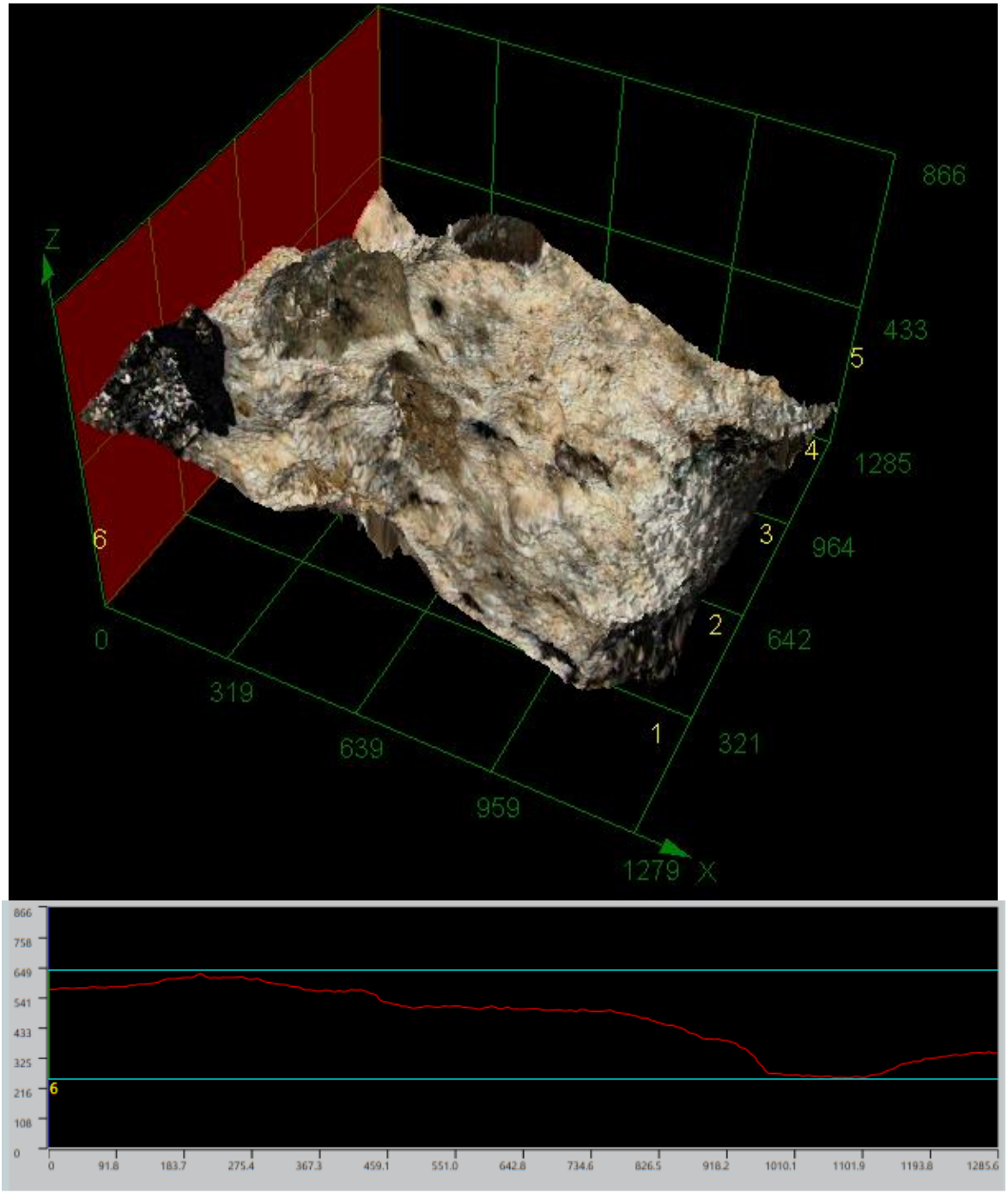
Z
866
433
5
4
1285
3
964
6
0
2
642
319
1
321
639
959
1279
X

866
758
649
541
433
325
216
108
0
6
0
91.8
183.7
275.4
367.3
459.1
551.0
642.8
734.6
826.5
918.2
1010.1
1101.9
1193.8
1285.6

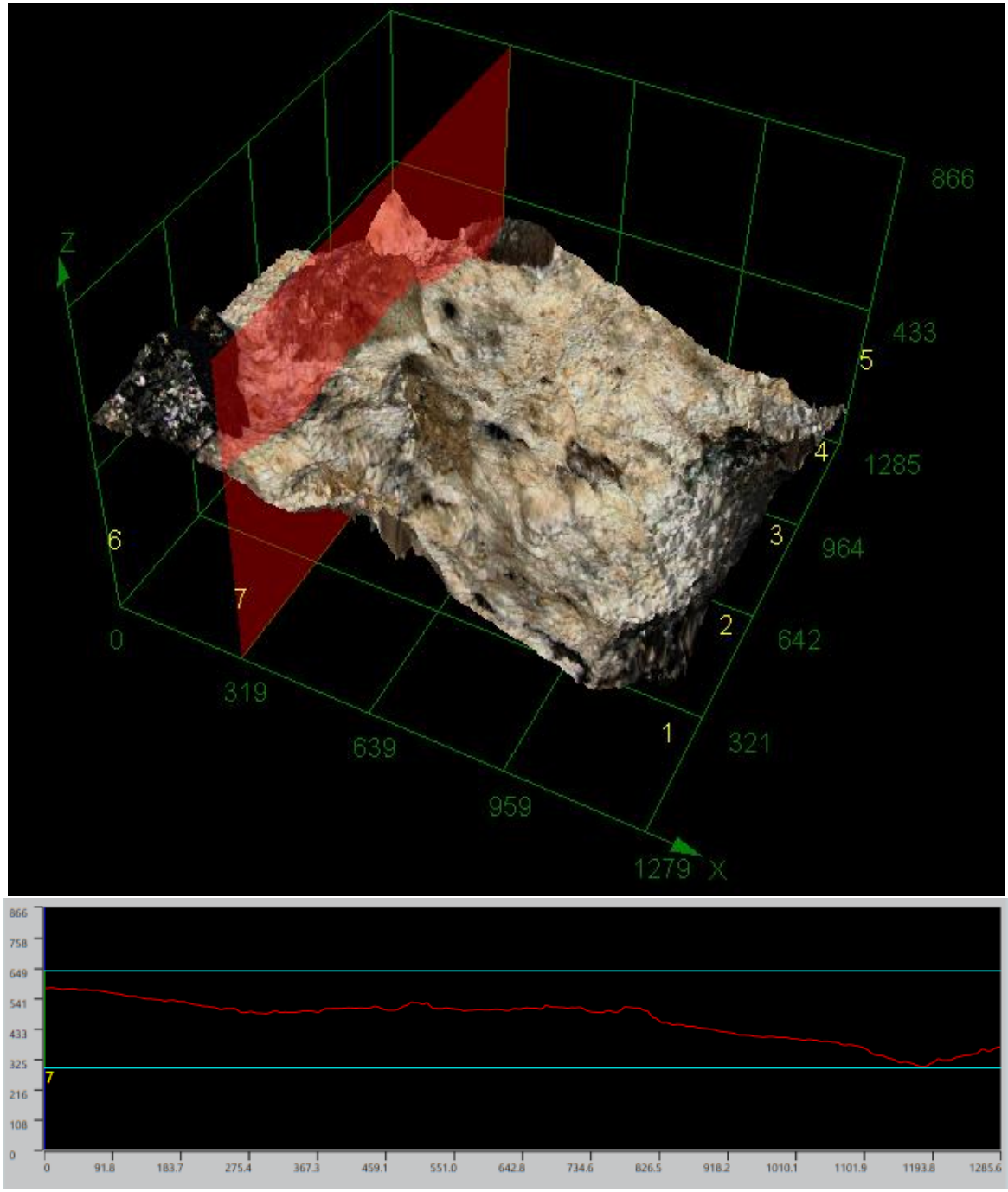
Z
866
433
1285
964
642
321
0
319
639
959
1279
X
0
1
2
3
4
5
6
7

866
758
649
541
433
325
216
108
0
7
0
91.8
183.7
275.4
367.3
459.1
551.0
642.8
734.6
826.5
918.2
1010.1
1101.9
1193.8
1285.6

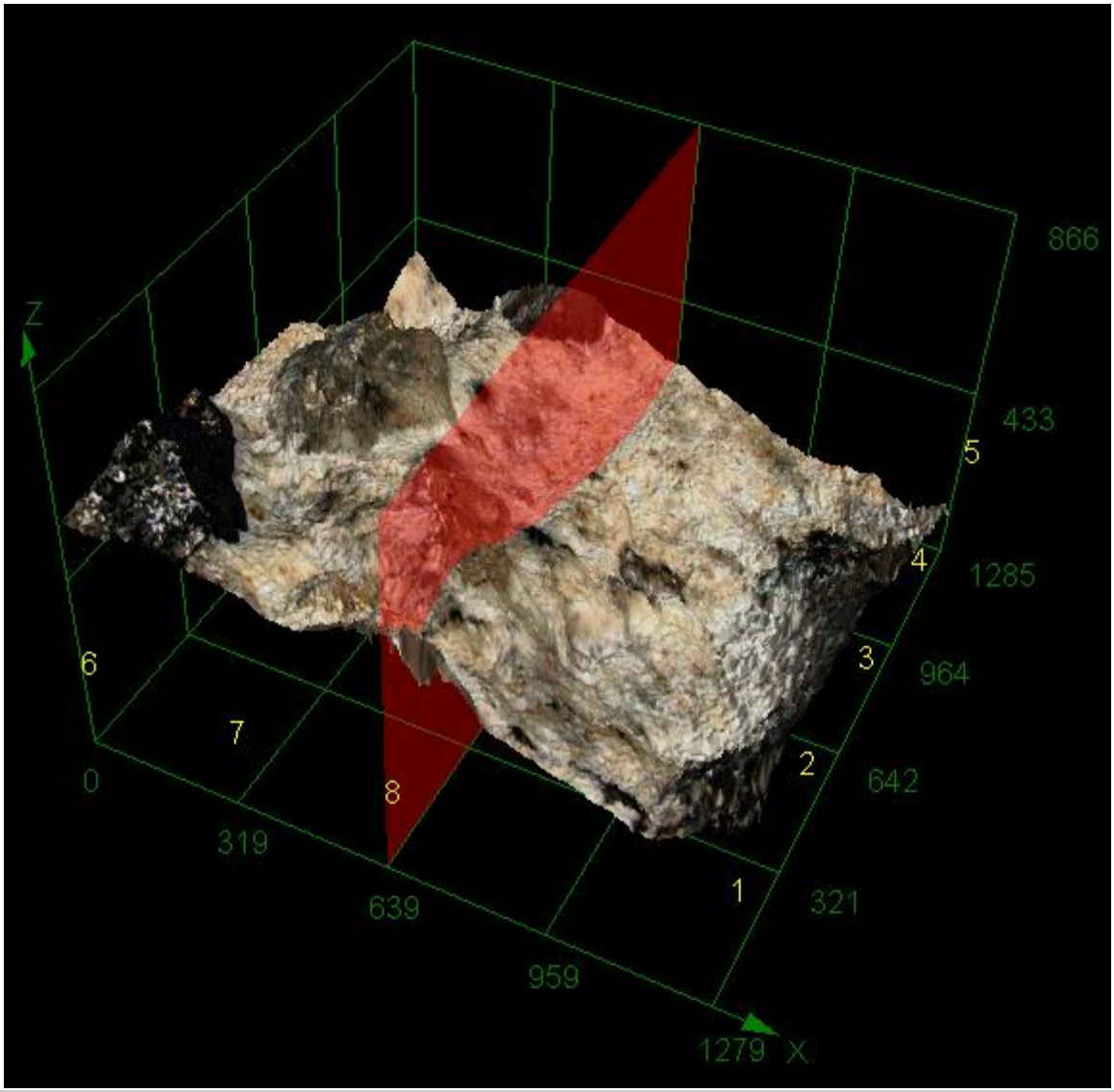
Z
866
433
1285
964
642
321
0
319
639
959
1279
X
6
7
8
5
4
3
2
1

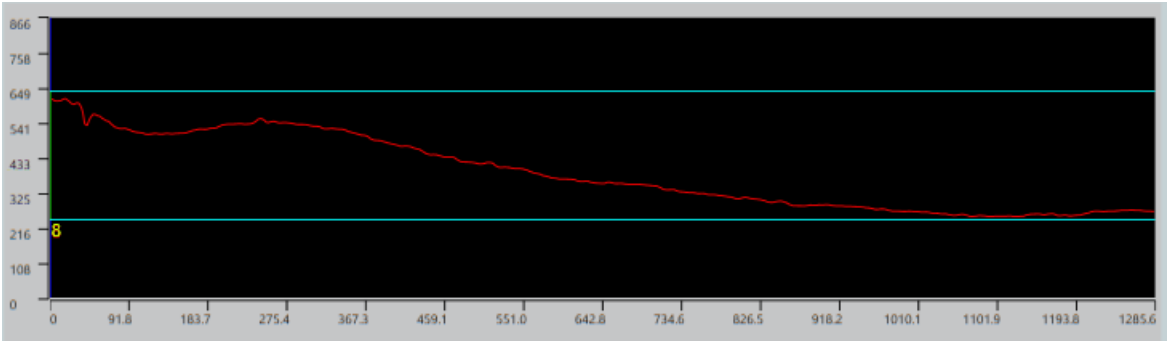
866
758
649
541
433
325
216
108
0
8
0
91.8
183.7
275.4
367.3
459.1
551.0
642.8
734.6
826.5
918.2
1010.1
1101.9
1193.8
1285.6

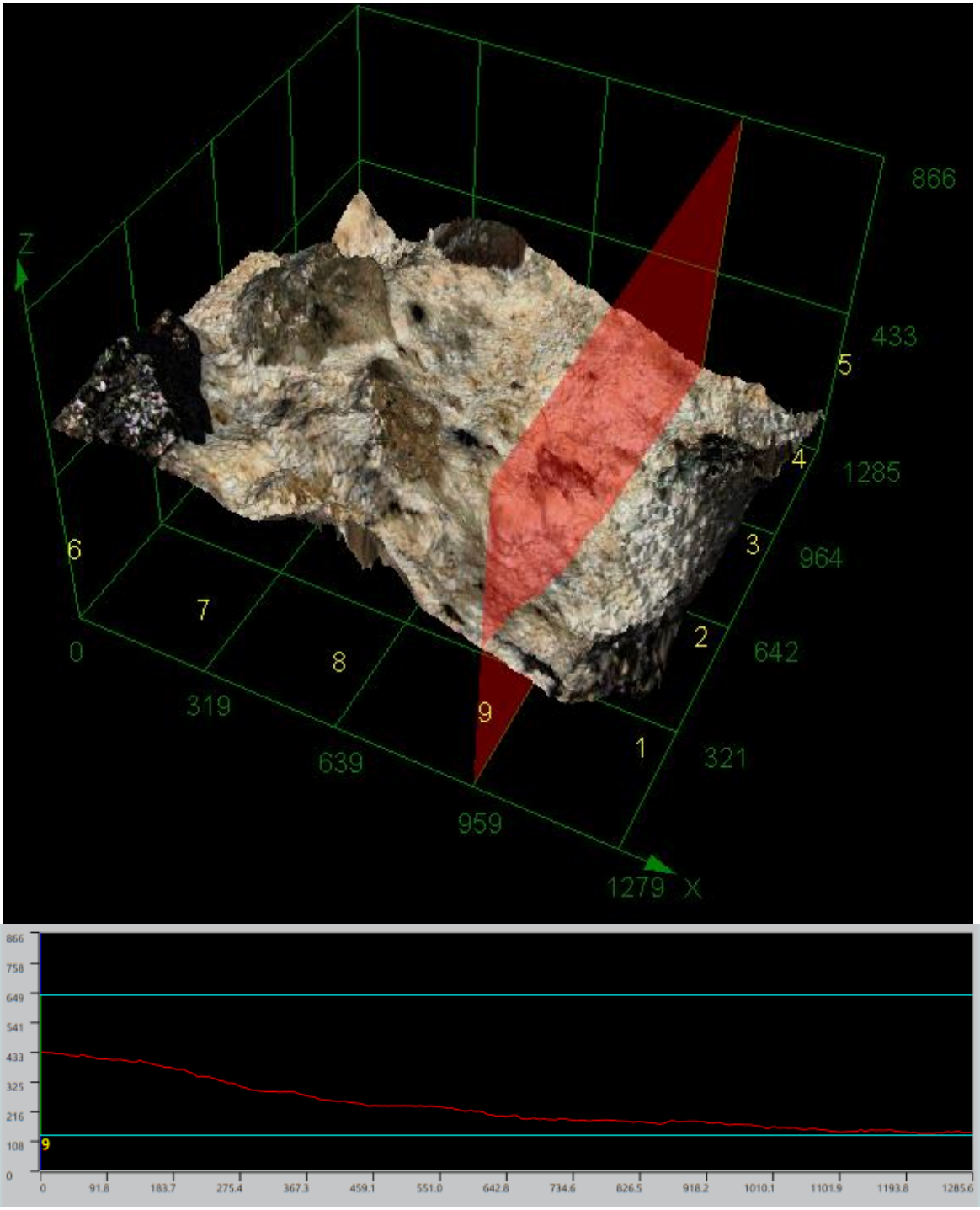
Z
866
433
5
1285
4
964
3
642
2
321
1
1279
X
959
639
319
0
6
7
8
9

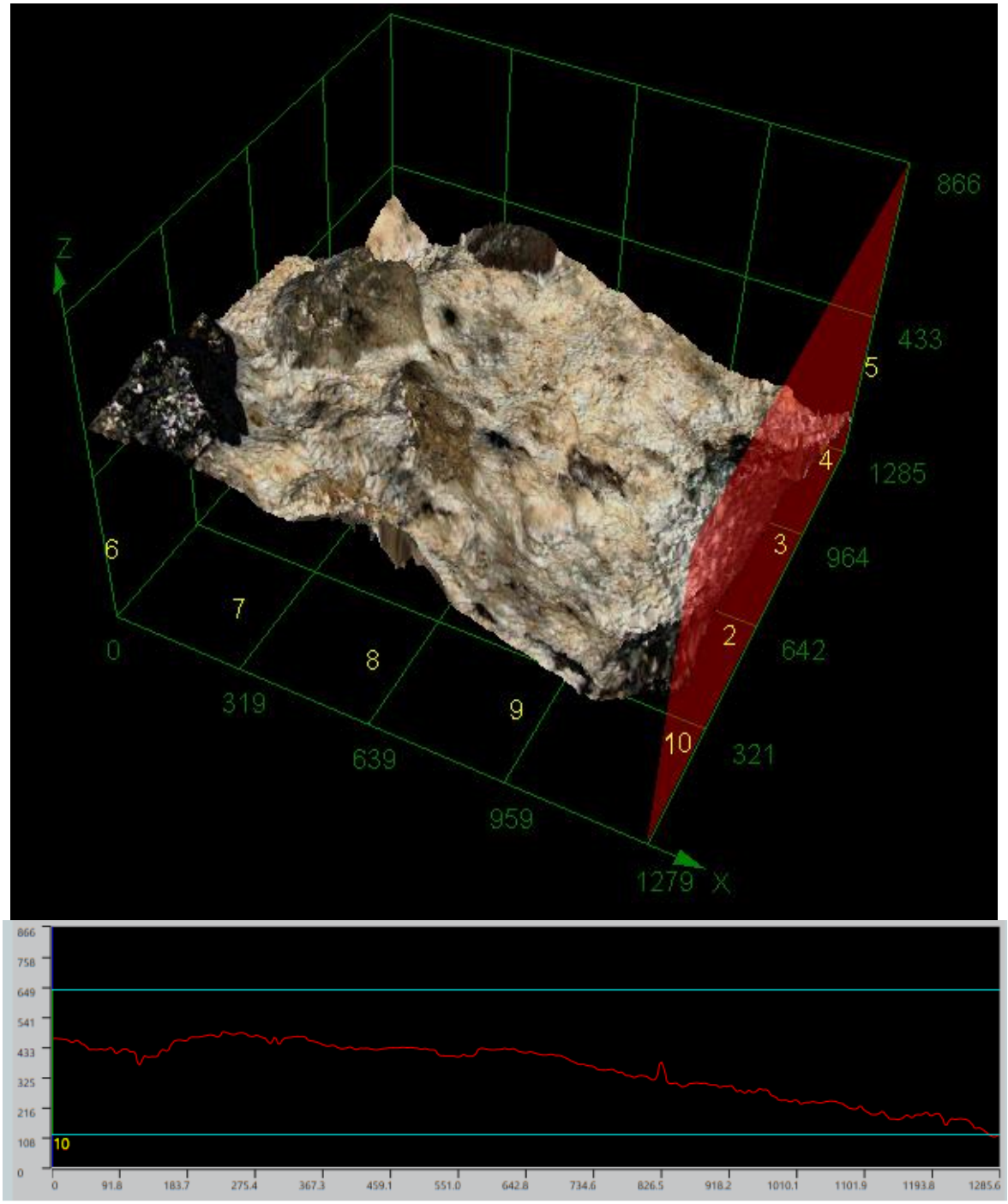

Figure 3.6. Section views of the observed area for five sections parallel to the Y-axis

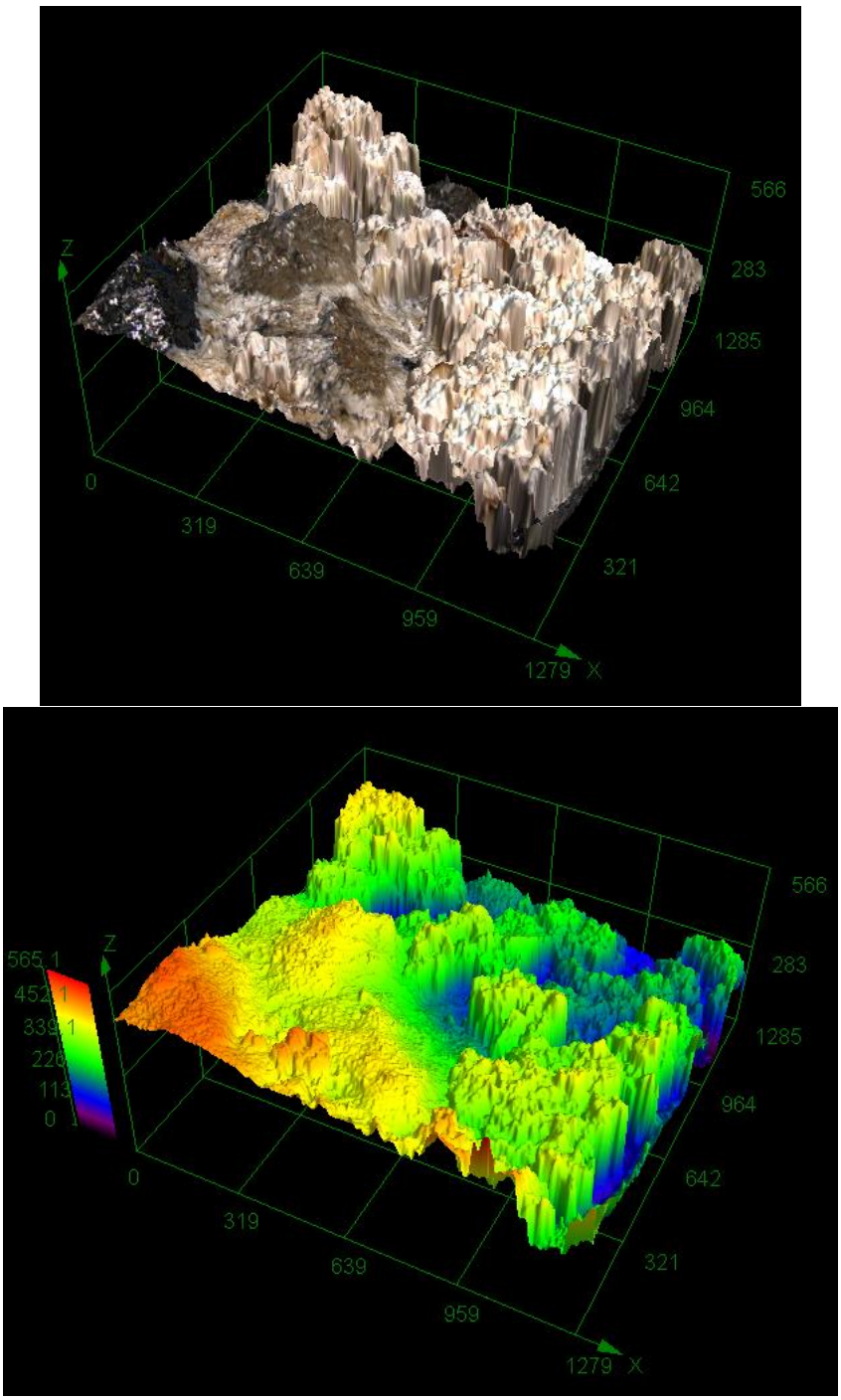

Figure 3.7. 3D views of the observed area with randomly placed dusts

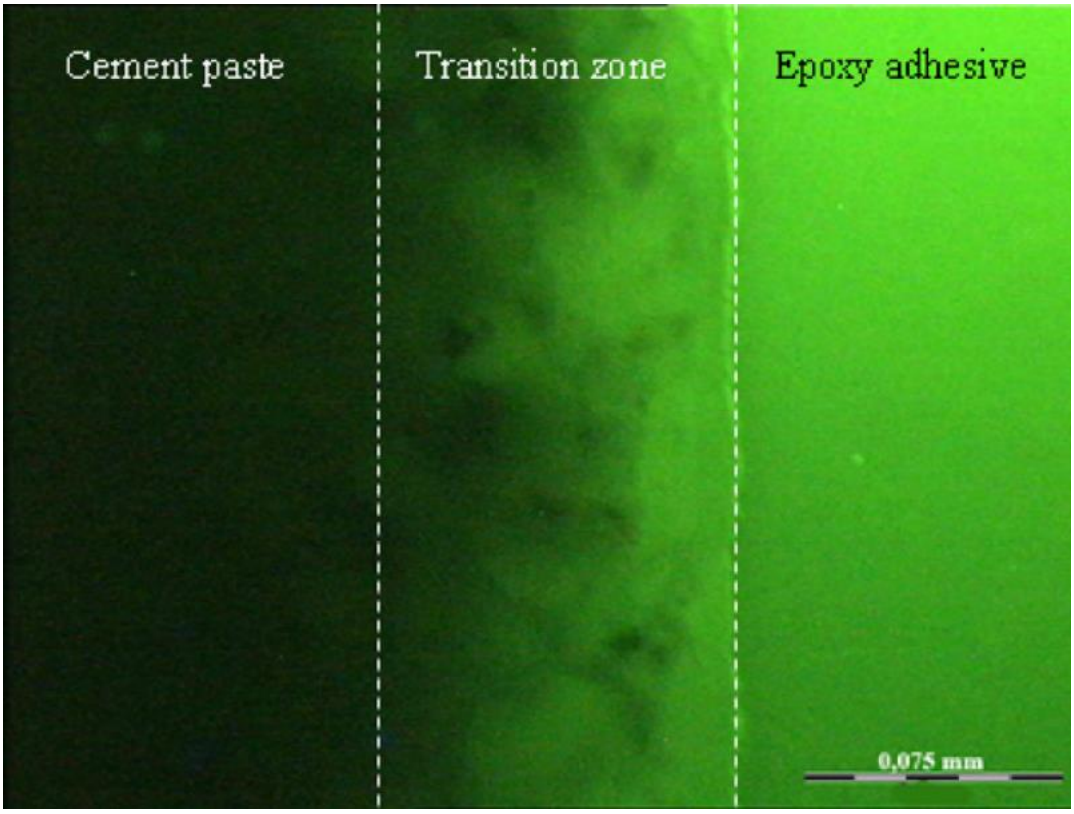

Figure 3.8. Hardened cement paste–epoxy adhesive interface image obtained by optical microscopy under UV light illumination by Djouani et al. (2011)

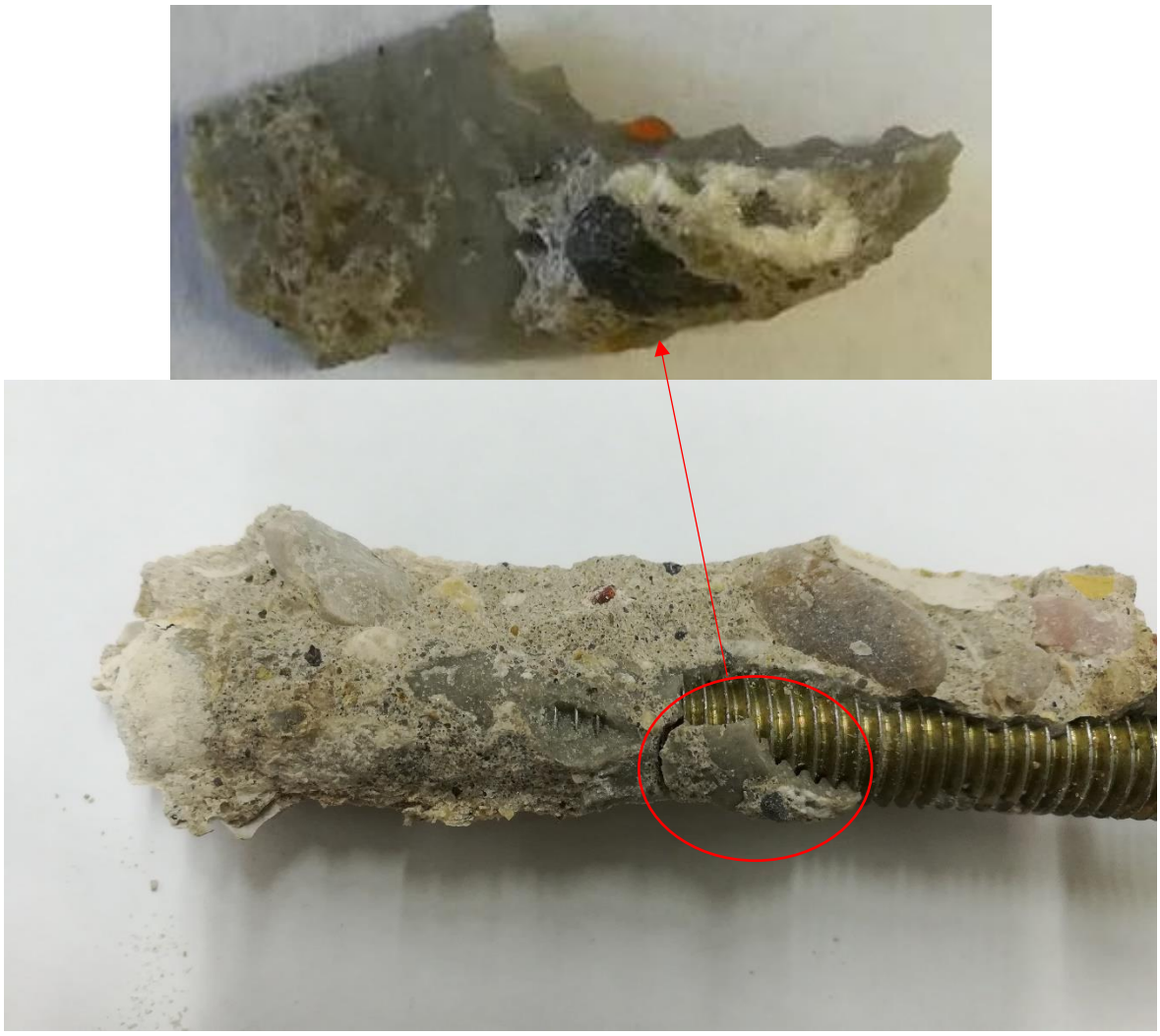

Figure 3.9. A sample of adhesive-concrete interface.

Figure 3.10. A sample of adhesive-concrete interface before coating for EDS

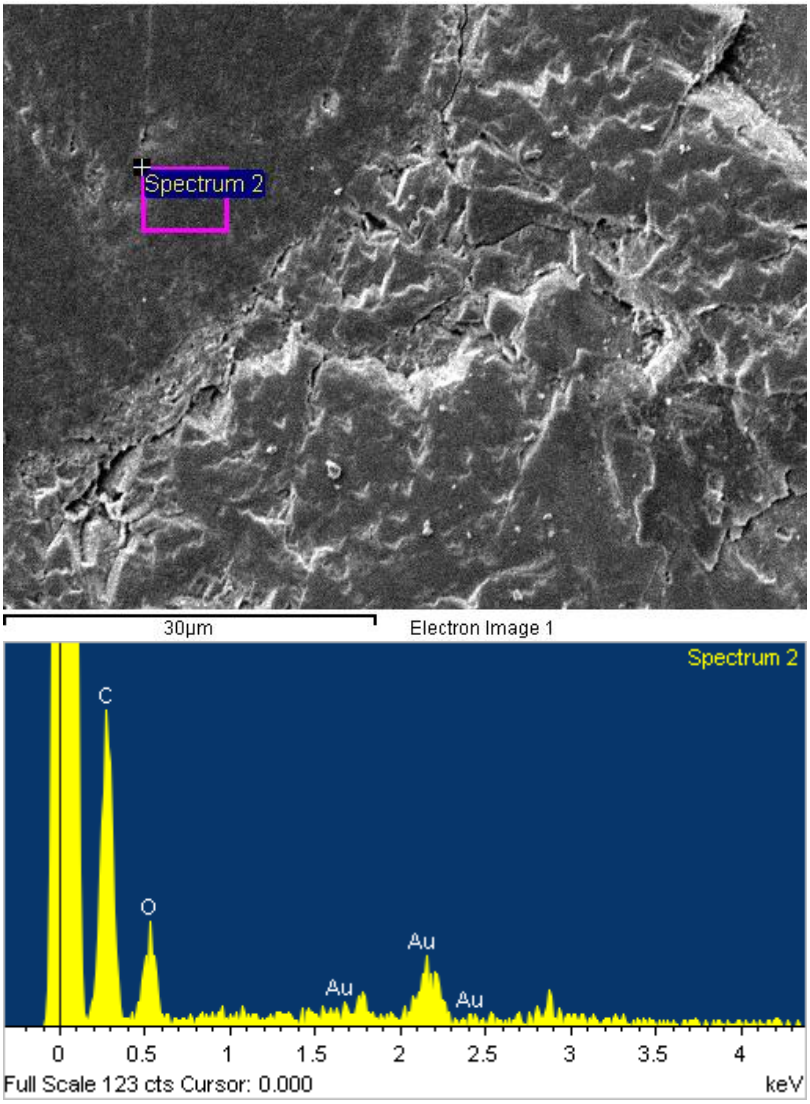

Figure 3.11. Spectrum analysis of elements near Point 2 representing adhesive

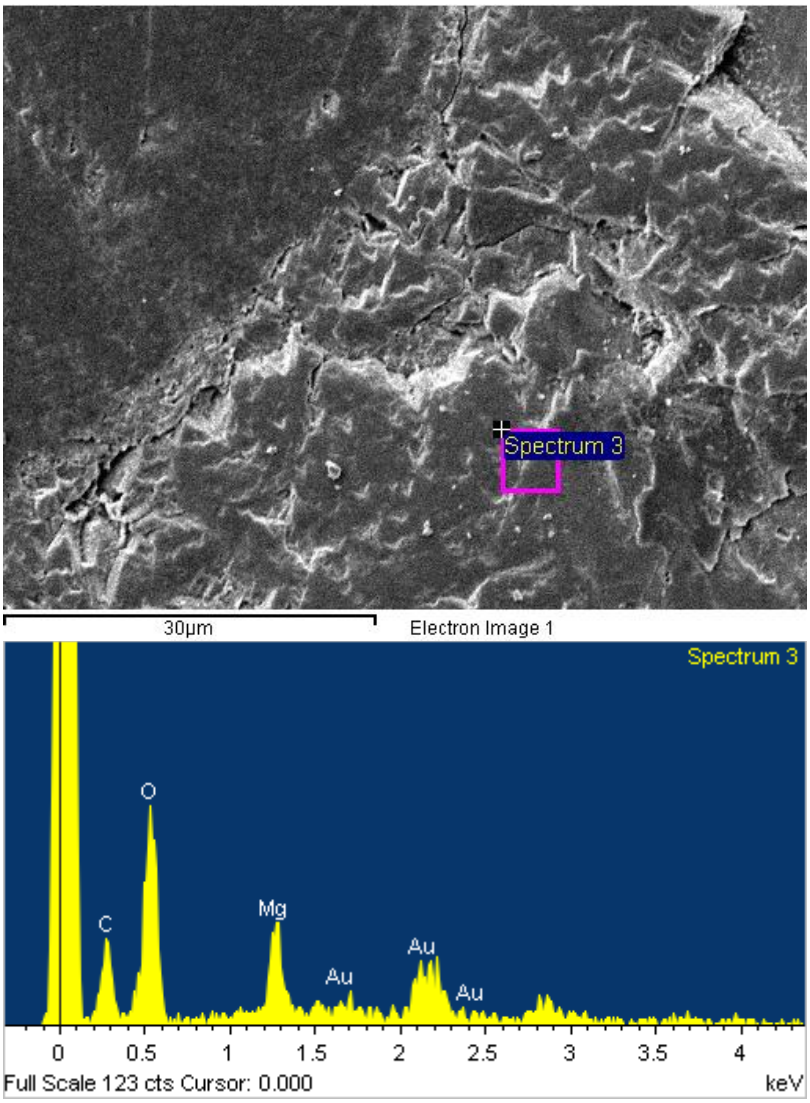

Figure 3.12. Spectrum analysis of elements near Point 3 representing concrete

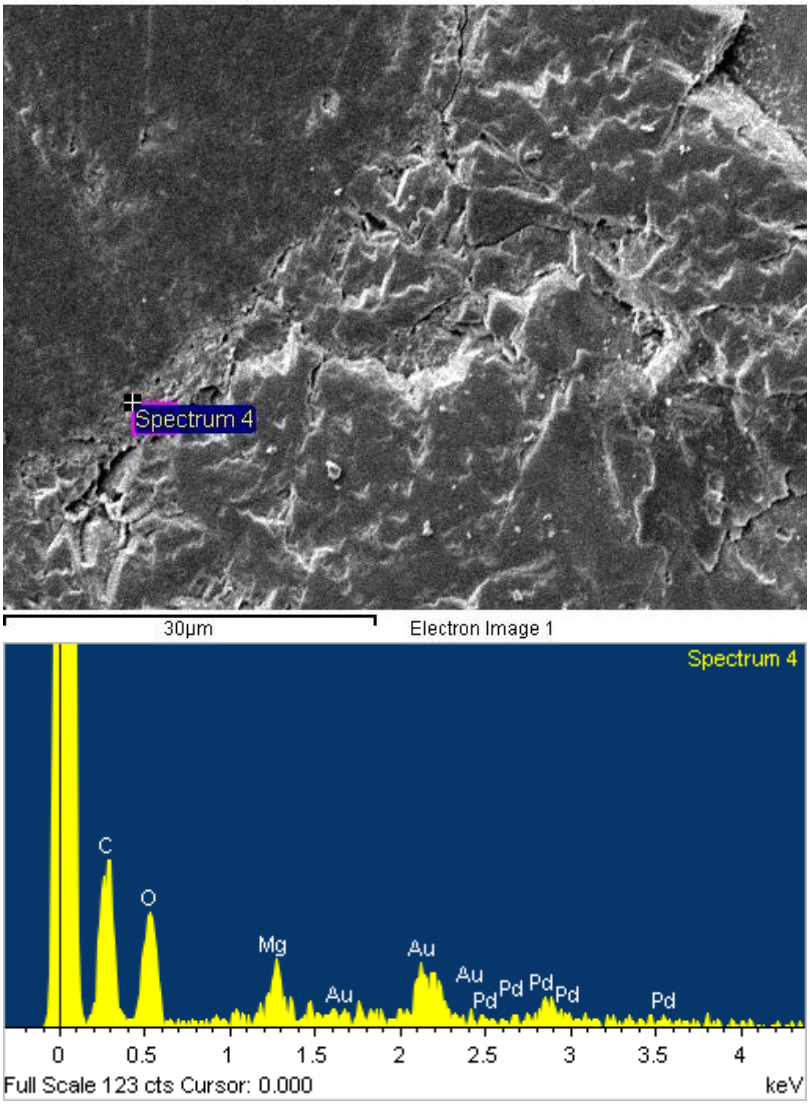

Figure 3.13 Spectrum analysis of elements near Point 4 representing adhesive-concrete interface

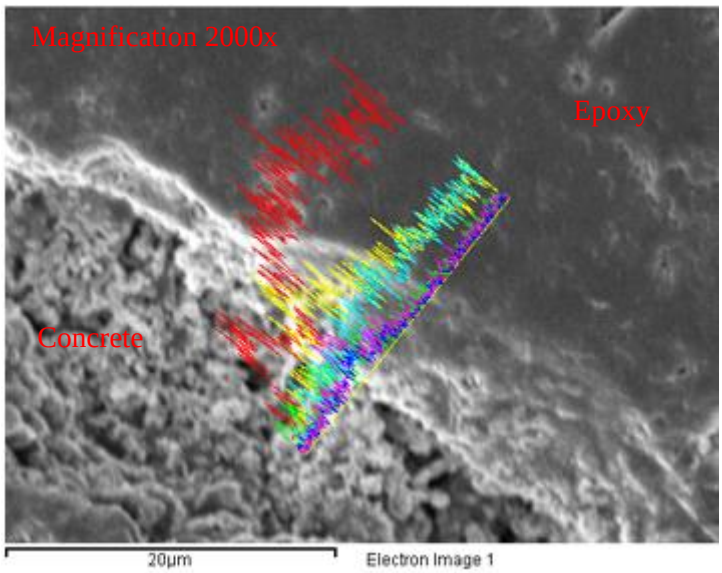

Figure 3.14. A scan line across adhesive-concrete interface.

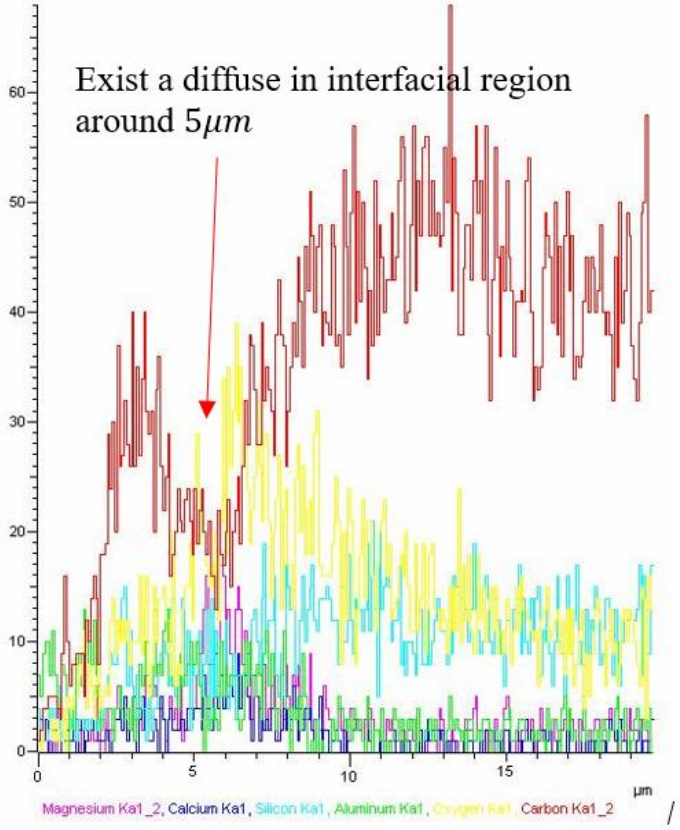

Figure 3.15. Detected element along the scan line.

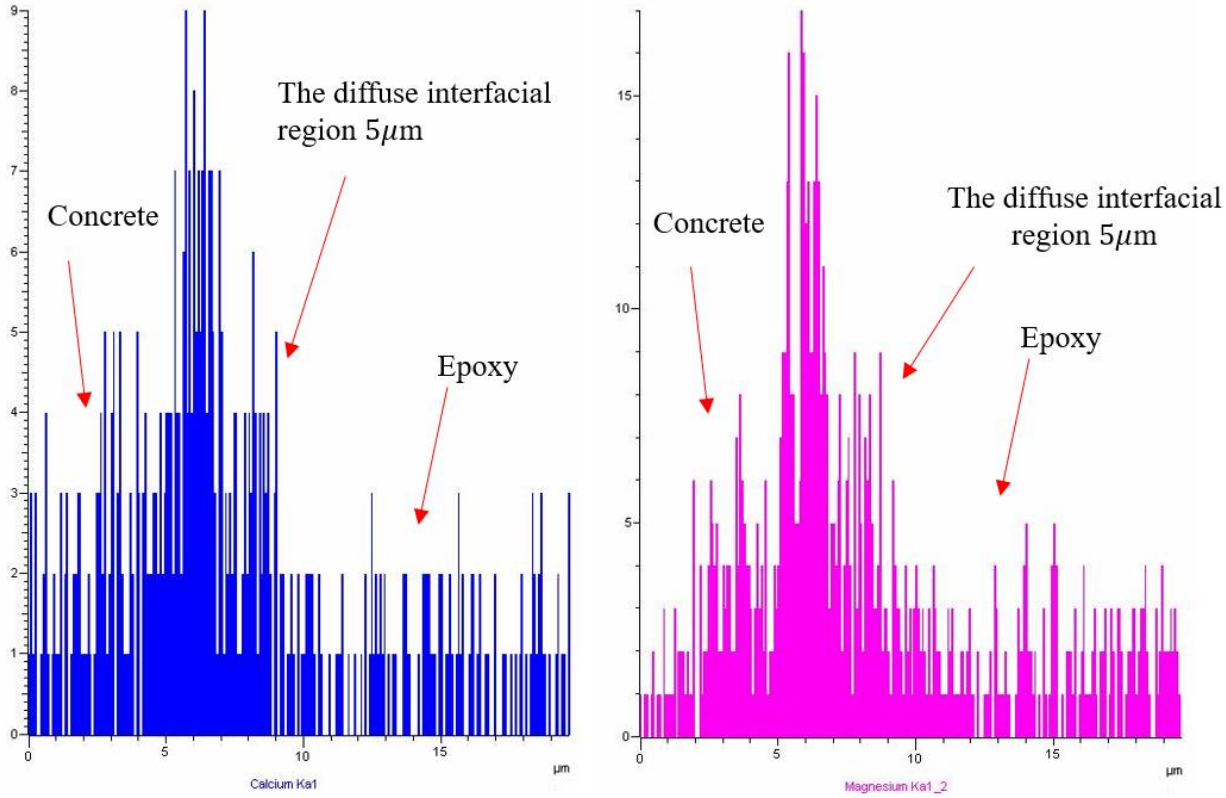

Figure 3.16. Local concentration of calcium and magnesium elements indicating chemical interaction at adhesive-concrete interface.

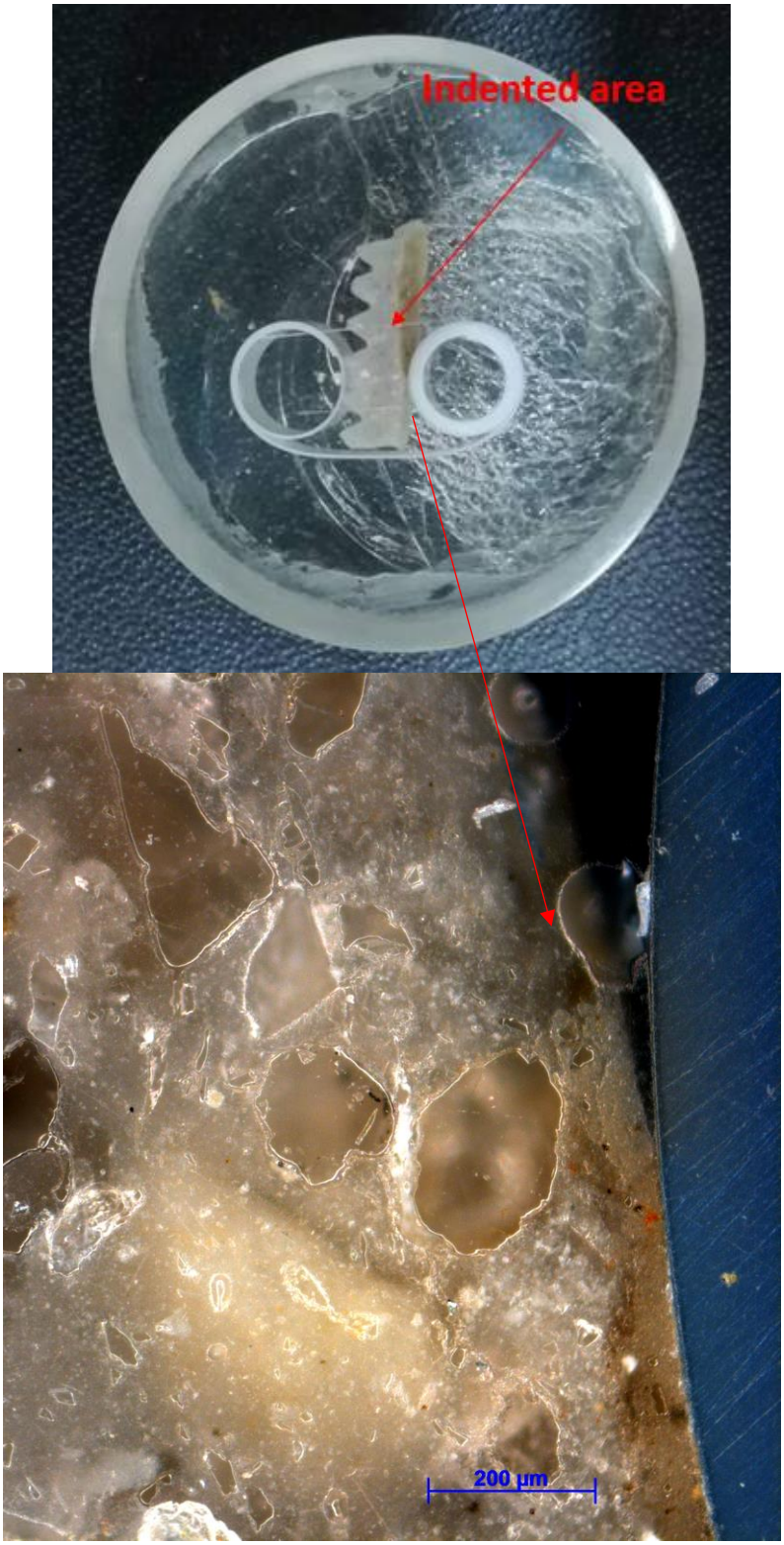

Figure 3.17. (a) Adhesive-concrete interface sample without cleaning after polishing; (b) The interface observed by using optical microscope (magnification 150x)

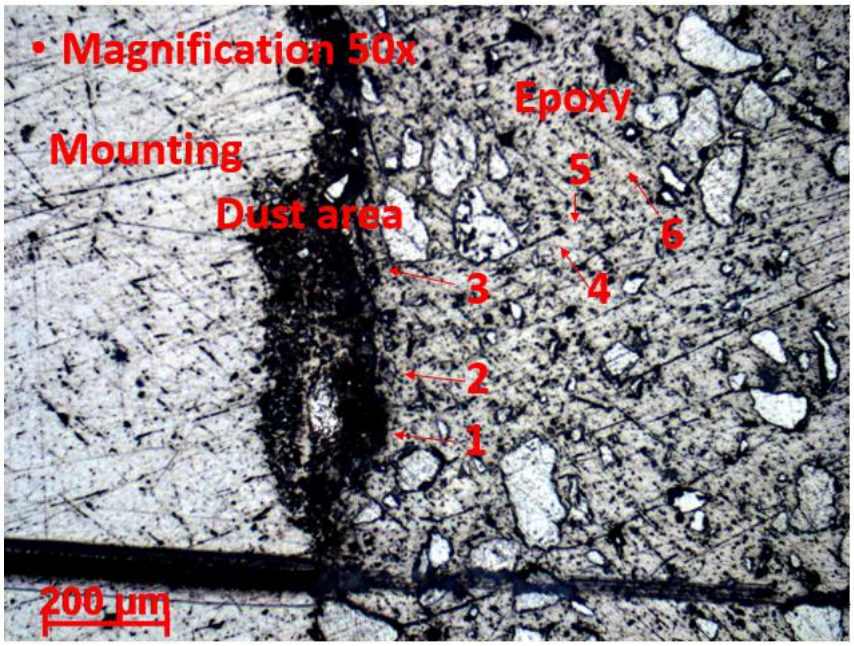

Figure 3.18. Indented spots on the sample (Epoxy-Dust).

Table 3.19 Summaries of the nanoindentation

Sample names	Ave Modulus (GPa)	Avg Hardness (Gpa)
Near Interface Epoxy_Dust 1	6	0.34
Near Interface Epoxy_Dust 3	5.1	0.3
Epoxy far from Dust interface 4	5	0.27
Epoxy far from Dust interface 5	5.3	0.31
Pure Epoxy 7-1 (vinylester adhesive)	5.7	0.35
Mounting Epoxy	3.4	0.18

Note: nanoindentation did not generate results from Points 2 and 6.

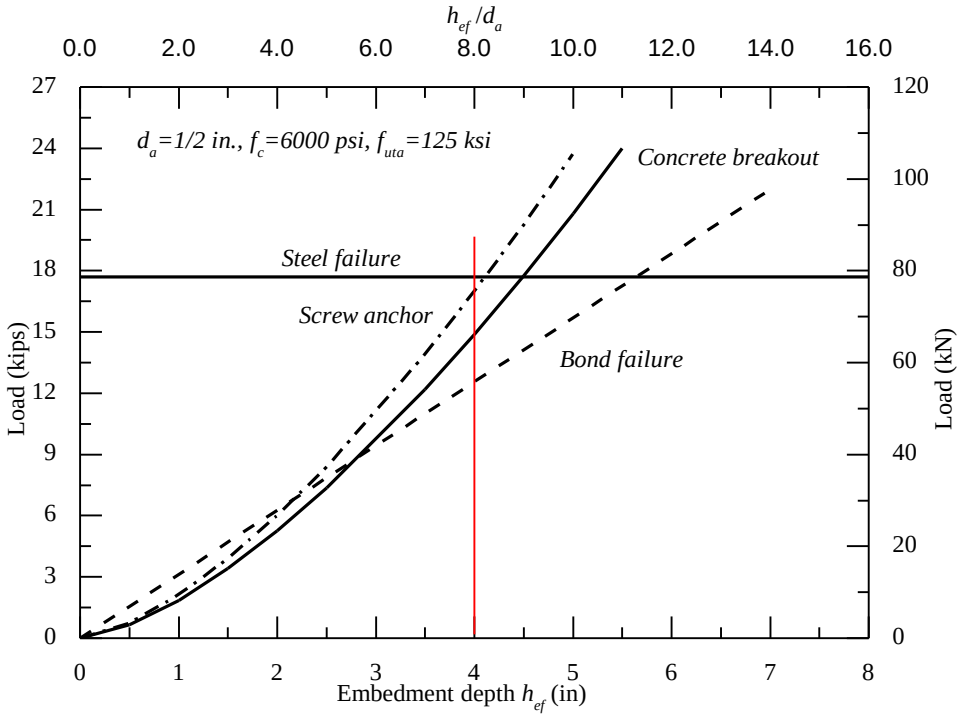

Figure 4.1. Comparison of capacities controlled by potential failure modes for ½-in. anchors

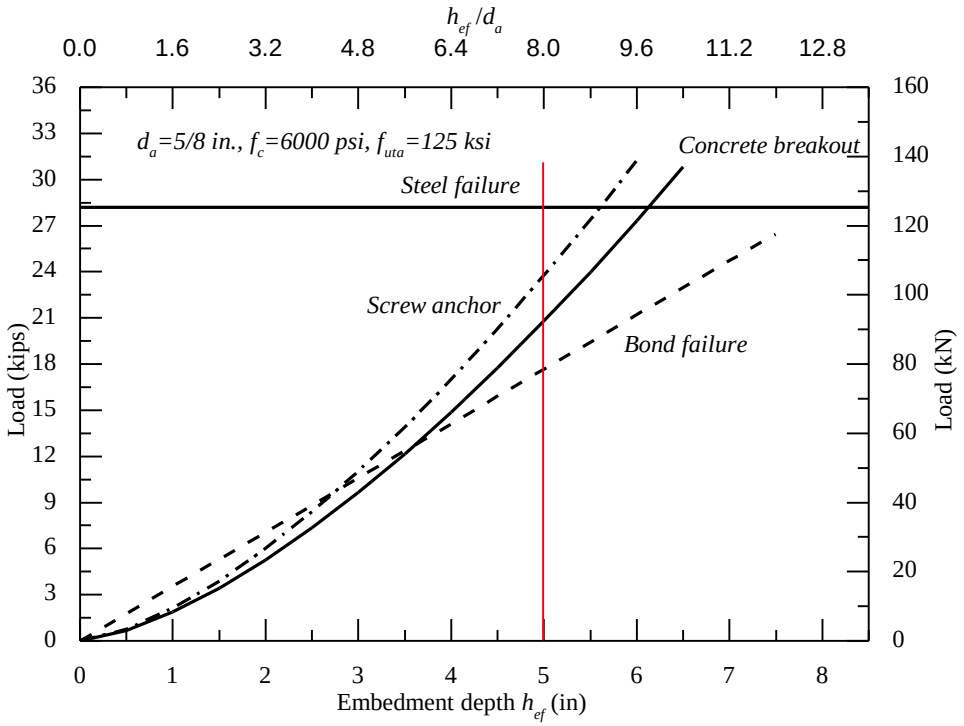

Figure 4.2. Comparison of capacities controlled by potential failure modes of 5/8-in. anchor

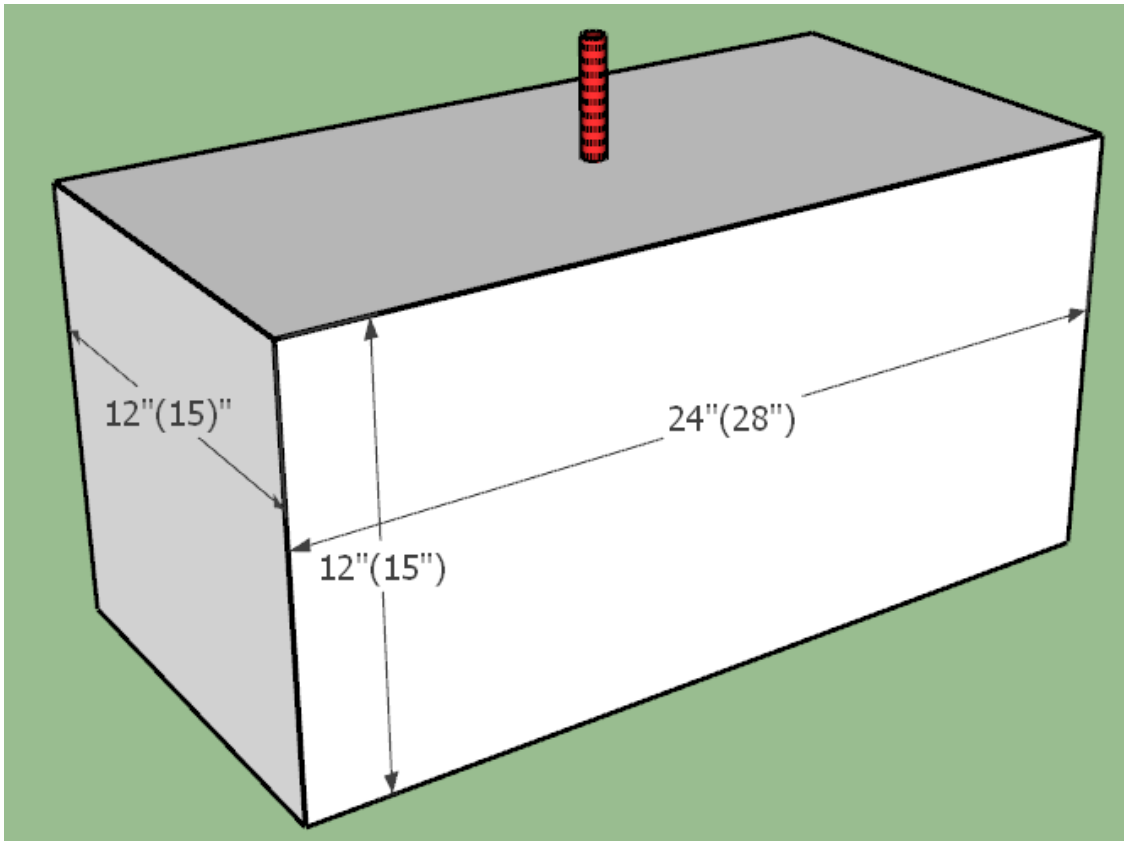

Figure 4.3. Specimen dimensions for unconfined pullout tests

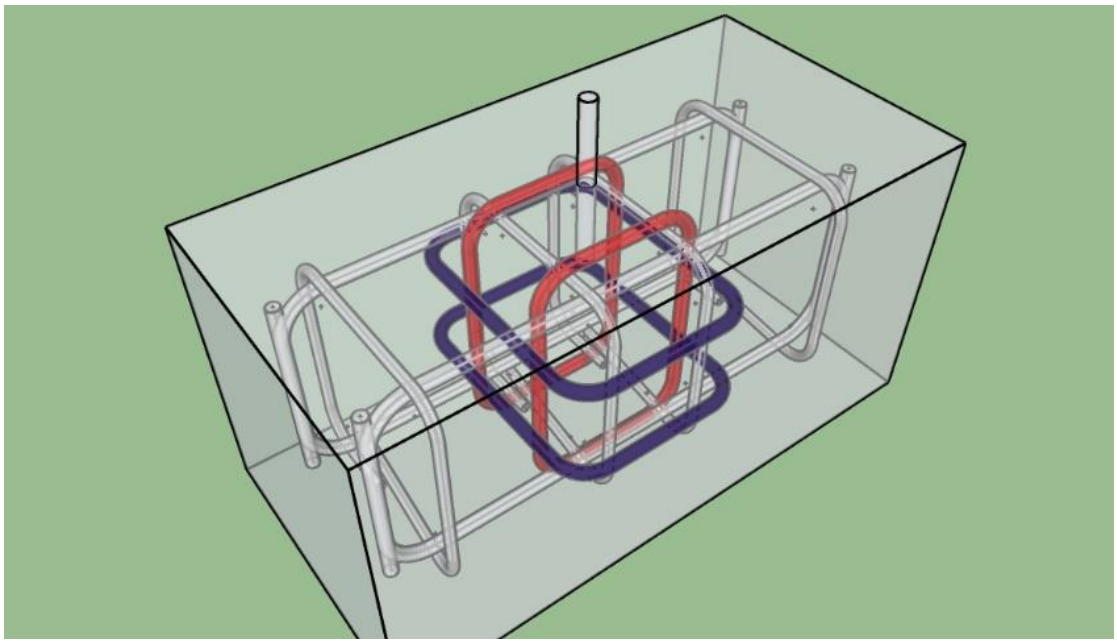

Figure 4.4. Schematics of anchor reinforcement for unconfined pullout tests

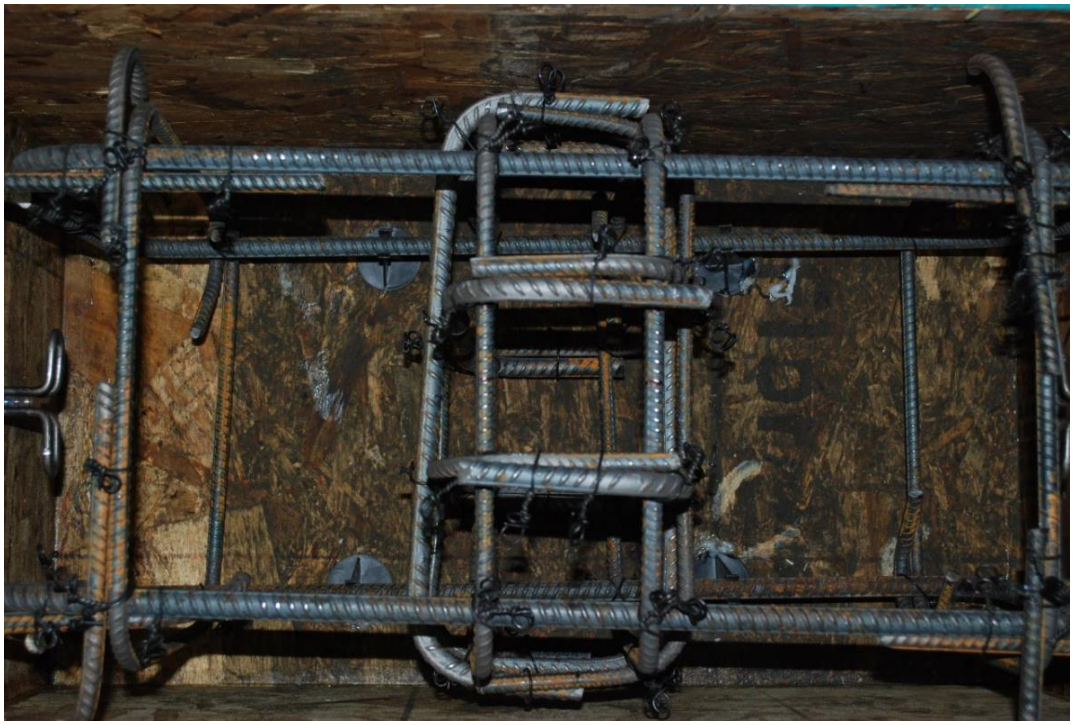

Figure 4.5. Pictures of anchor reinforcement for unconfined pullout tests

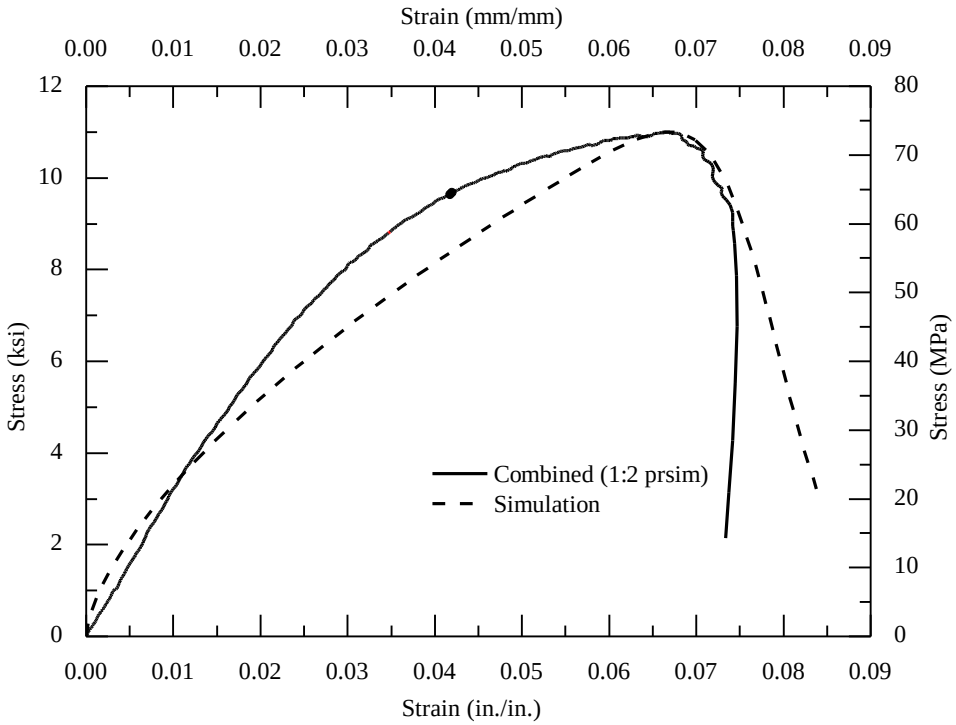

Figure 4.6. Simulation curve of the prism (1:2).

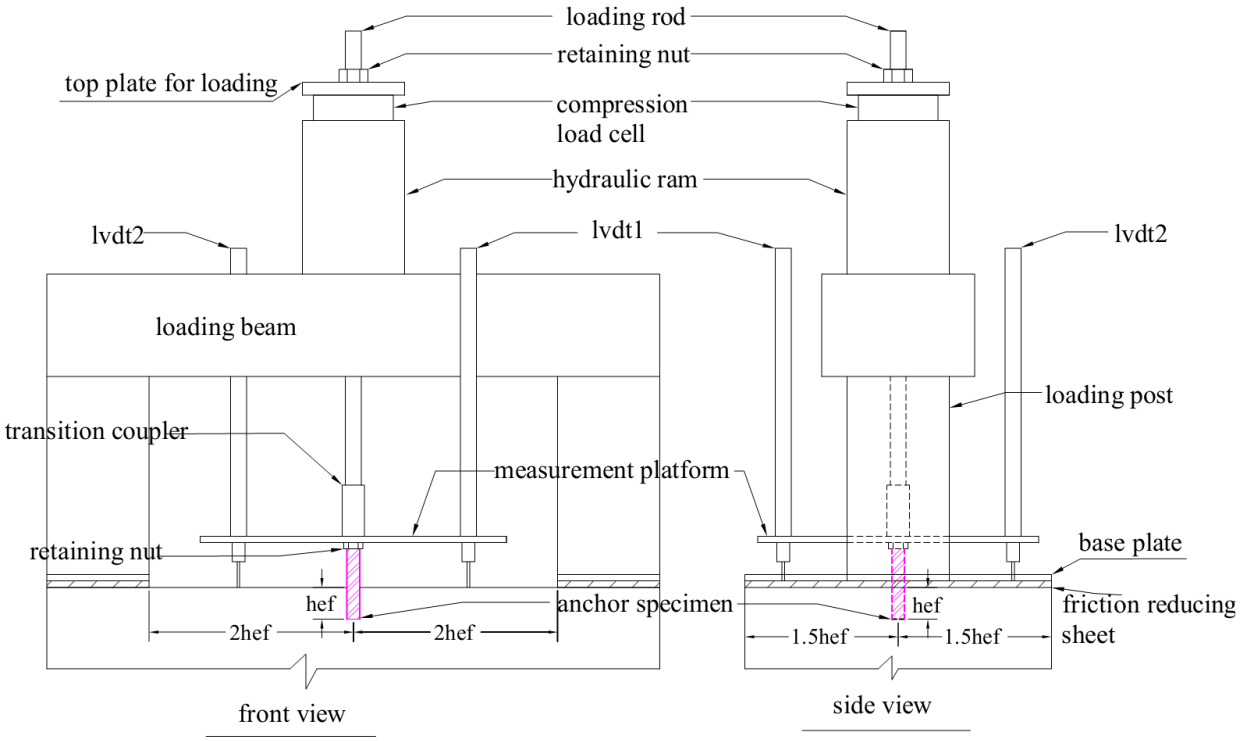

Figure 4.7. Schematics of test setup (unconfined)

Figure 4.8. Picture of test setup (unconfined)

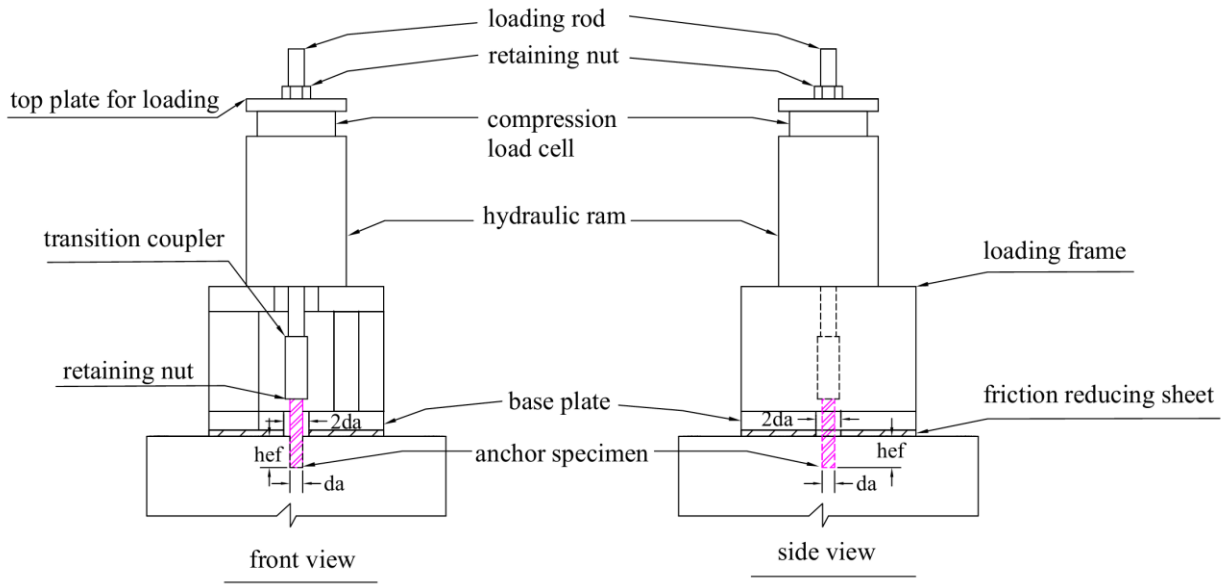

Figure 4.9. Schematics of test setup (confined)

Figure 4.10. Picture of test setup (confined)

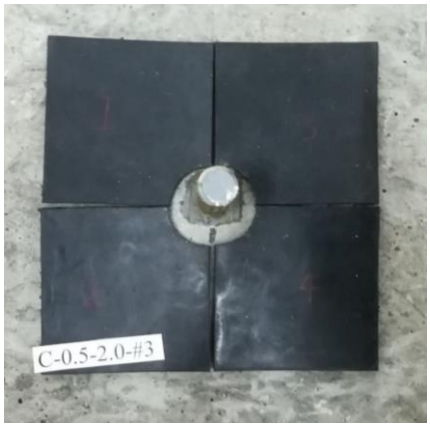

Figure 4.11. Picture of plastic sheet (confined)

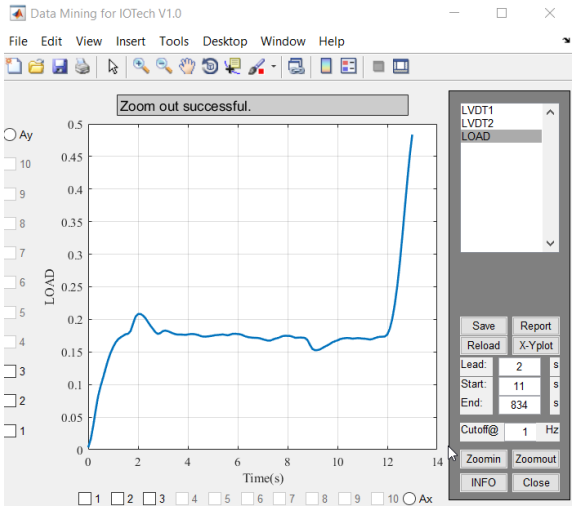

Figure. 4.12. The cutoff frequency in the graphic.

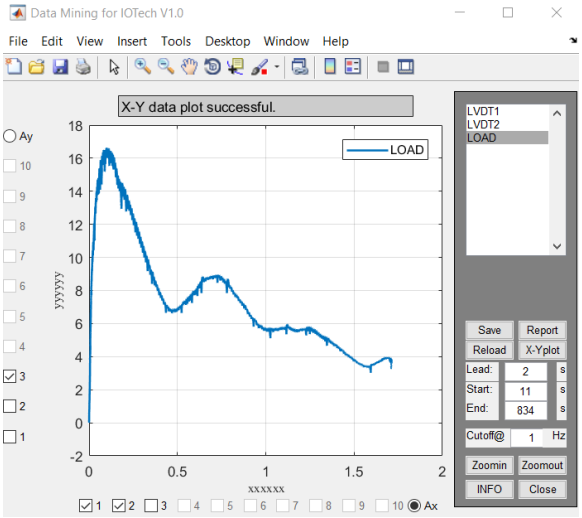

Figure. 4.13. The data after processing

Table 4.1. Test matrix (unconfined)

Numbers	Name	d_a (in.)	h_{ef} (in.)	Block (in3)	Test frequency
1	UC	1/2	4.0	12 × 12 × 24	4
2	UCT	1/2	4.0	12 × 12 × 24	4
3	UCT#R	1/2	4.0	12 × 12 × 24	4
4	UC0%	1/2	4.0	12 × 12 × 24	4
5	UCT0%	1/2	4.0	12 × 12 × 24	4
6	UC50%	1/2	4.0	12 × 12 × 24	4
7	UCT50%	1/2	4.0	12 × 12 × 24	4
8	UCT#R50%	1/2	4.0	12 × 12 × 24	4
9	UC	5/8	5.0	15 × 15 × 28	4
10	UCT	5/8	5.0	15 × 15 × 28	4
11	UCT#R	5/8	5.0	15 × 15 × 28	4
12	UC0%	5/8	5.0	15 × 15 × 28	4
13	UC50%	5/8	5.0	15 × 15 × 28	4
14	UCT50%	5/8	5.0	15 × 15 × 28	4

Table 4.2. Test matrix (confined)

Numbers	Name	d_a (in.)	h_{ef} (in.)	Test frequency
1	C-0.5-2.0	1/2	2	4
2	C-0.5-3.0	1/2	3	4
3	CT-0.5-2.0	1/2	2	4
4	CT-0.5-3.0	1/2	3	4
5	C50%-0.5-2.0	1/2	2	3
6	C50%-0.5-3.0	1/2	3	3
7	CT50%-0.5-2.0	1/2	2	3
8	CT50%-0.5-3.0	1/2	3	3

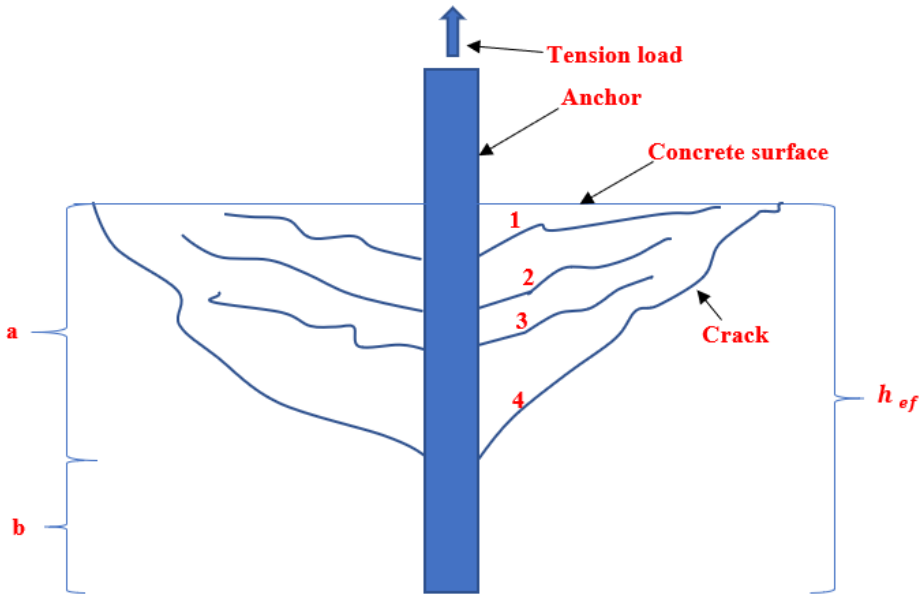

Figure 5.1. Schematics of the sequence of load transfer (unconfined)

Figure 5.2. The cutting line in the longitudinal direction (confined)

Figure 5.3. The cutting line in the transverse direction (confined)

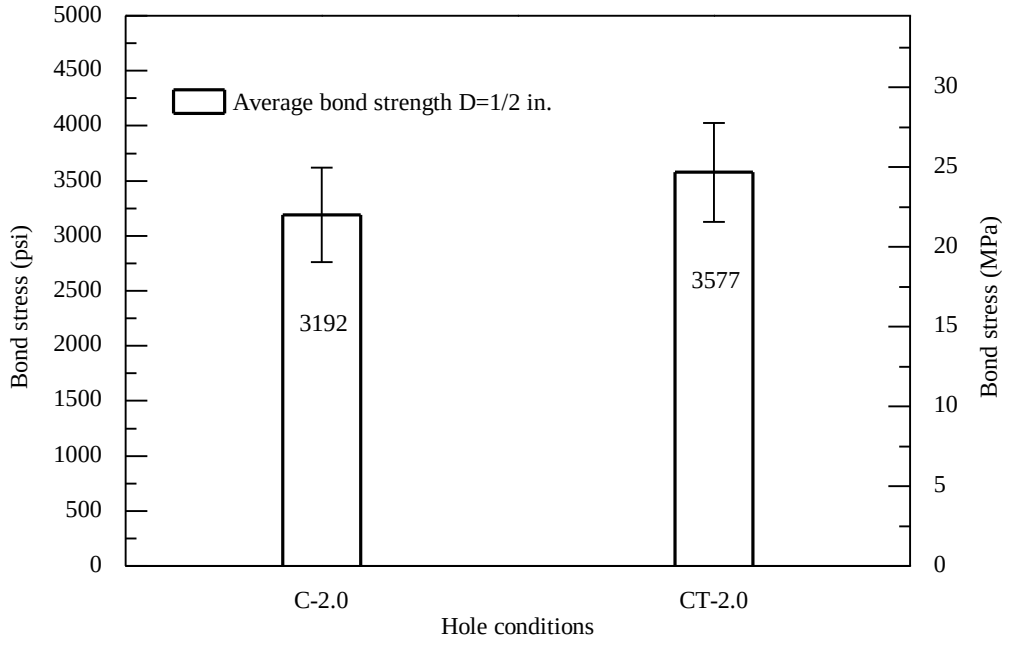

Figure 5.4. Comparisons of confined smooth holes and threaded holes (h_{ef} =2.0 in.)

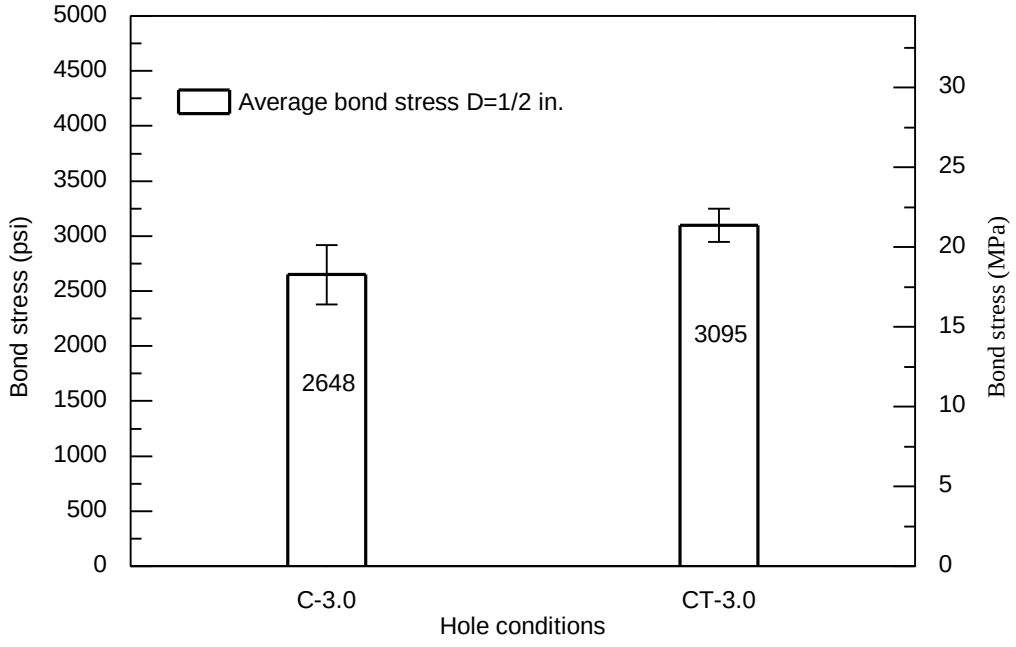

Figure 5.5. Comparisons of confined smooth holes and threaded holes (h_{ef} =3.0 in.)

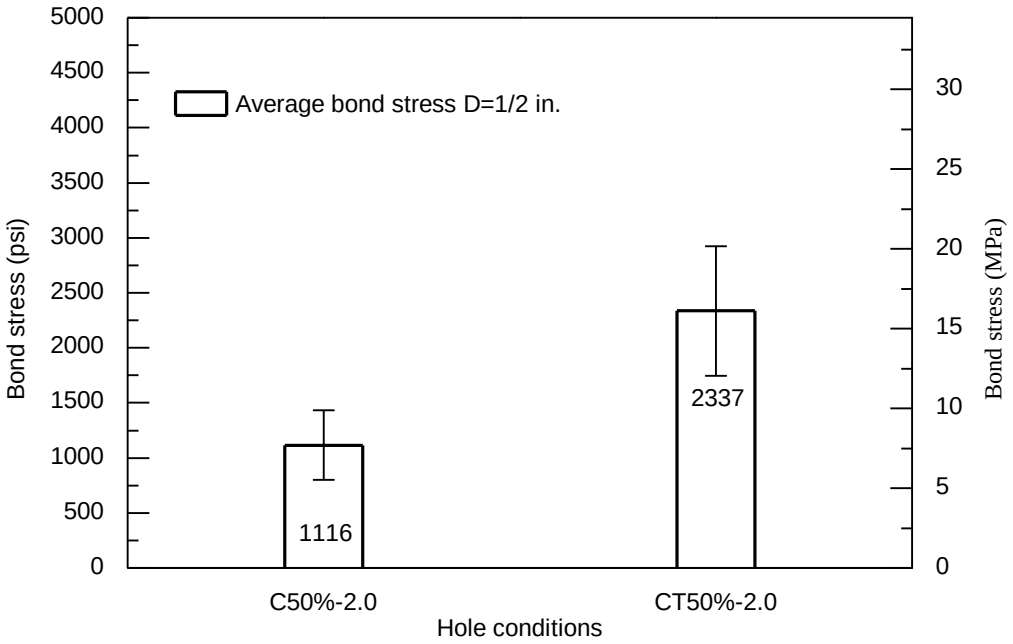

Figure 5.6. Comparisons of confined partially cleaned smooth holes and threaded holes (h_{ef} =2.0 in.)

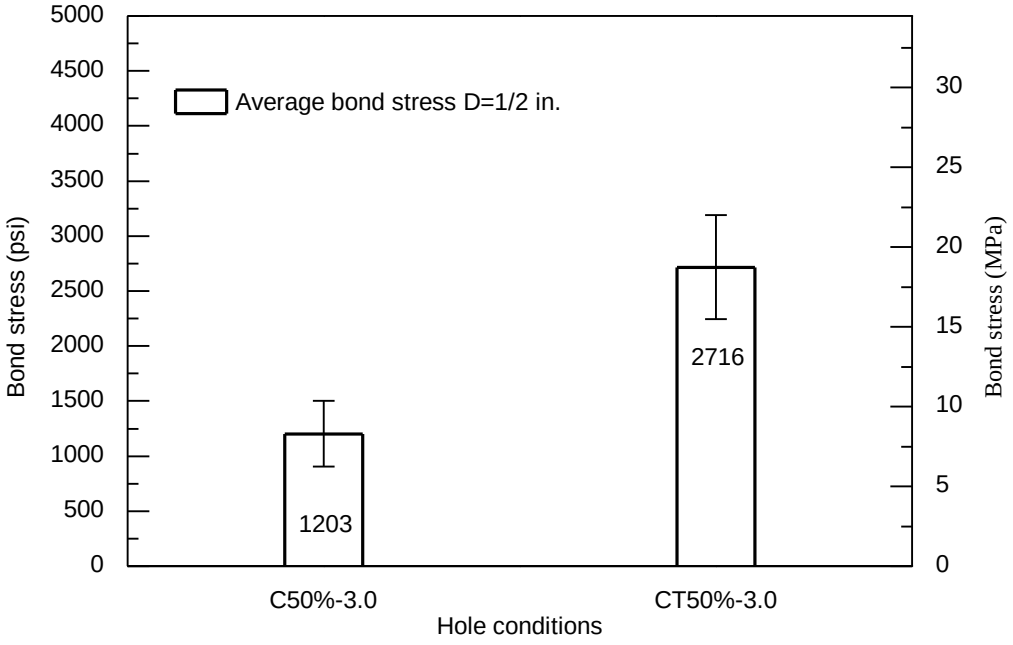

Figure 5.7. Comparisons of confined partially cleaned smooth holes and threaded holes (h_{ef} =3.0 in.)

Table 5.1. Summaries of unconfined tests under various conditions.

NO	Specimens	d_a (in.)	h_{ef} (in.)	Mean bond strength (psi)	Standard deviation	COV (%)	5% fractile (psi)
1	UC	1/2	4.0	1941	171	9	1659
2	UCT	1/2	4.0	1885	111	6	1702
3	UCT#R	1/2	4.0	2222	380	17	1597
4	UC0%	1/2	4.0	443	155	35	188
5	UCT0%	1/2	4.0	1077	137	13	851
6	UC50%	1/2	4.0	1084	116	11	893
7	UCT50%	1/2	4.0	2083	120	6	1886
8	UCT#R50%	1/2	4.0	1968	123	6	1765
9	UC	5/8	5.0	1533	378	25	911
10	UCT	5/8	5.0	2250	169	8	1971
11	UCT#R	5/8	5.0	2396	56	2	2304
12	UC0%	5/8	5.0	500	68	14	388
13	UC50%	5/8	5.0	1030	132	13	813
14	UCT50%	5/8	5.0	1591	176	11	1303

Table 5.2. Summaries of confined tests under clean hole condition.

NO	Specimens	d_a (in.)	h_{ef} (in.)	Mean bond strength (psi)	Standard deviation	COV (%)	5% fractile (psi)
1	C-0.5-2.0	0.5	2	3192	429	13	2486
2	C-0.5-3.0	0.5	3	2648	268	10	2207
3	CT-0.5-2.0	0.5	2	3577	450	13	2838
4	CT-0.5-3.0	0.5	3	3095	151	5	2847
5	C50%-0.5-2.0	0.5	2	1116	317	28	595
6	C50%-0.5-3.0	0.5	3	1203	297	25	714
7	CT50%-0.5-2.0	0.5	2	2337	589	25	1368
8	CT50%-0.5-3.0	0.5	3	2716	472	17	1939

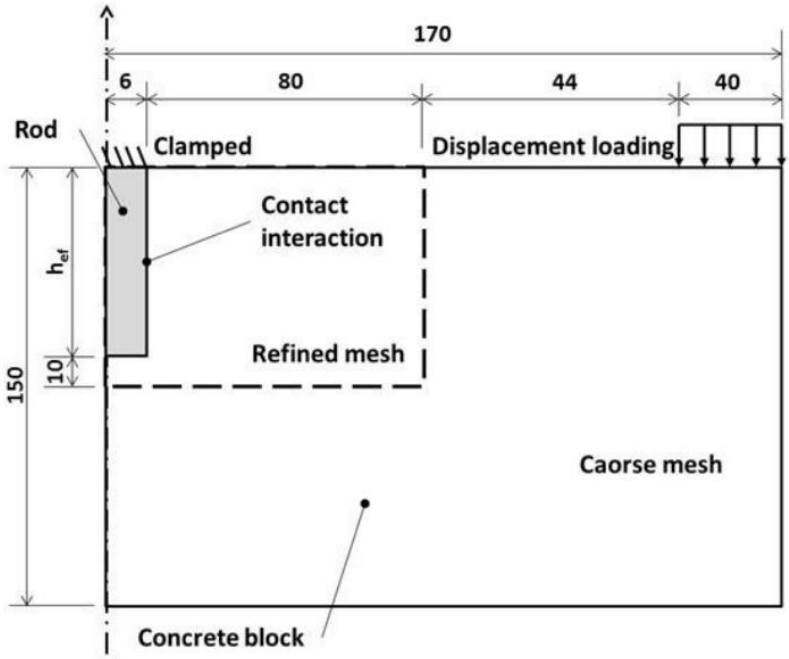

Fig. 3. Geometric and boundary conditions of the model (dimensions in mm).

Figure 6.1. The geometric and boundary conditions. (Delhomme and Brun 2018)

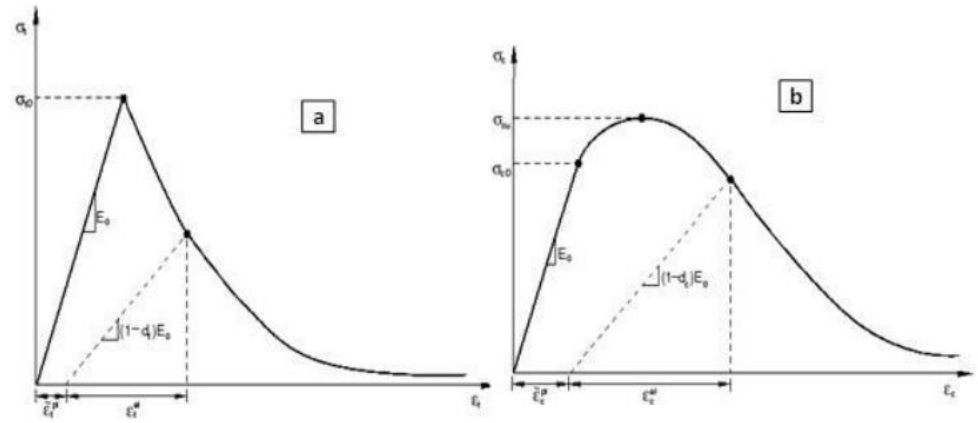

Fig. 4. Uniaxial stress–strain curve with damage (a) in tension and (b) compression [16].

Figure 6.2. The concrete constitutive laws. (Delhomme and Brun 2018)

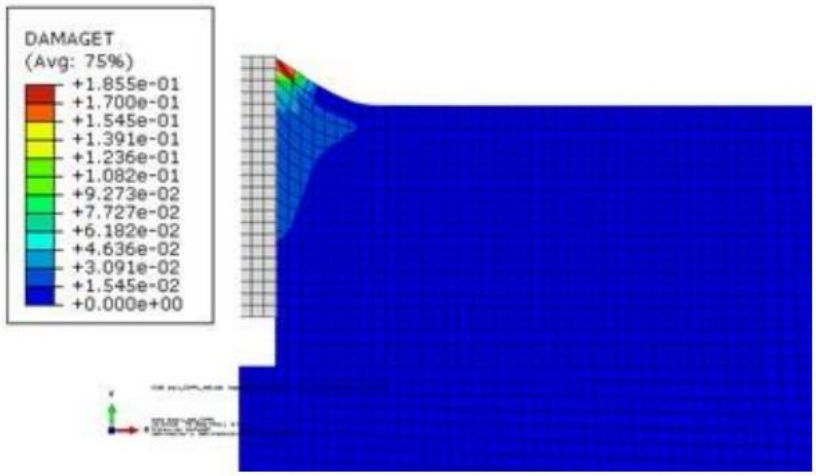

Figure 6.3. The sliding of the anchor under the tensile load applied. (Delhomme and Brun 2018)

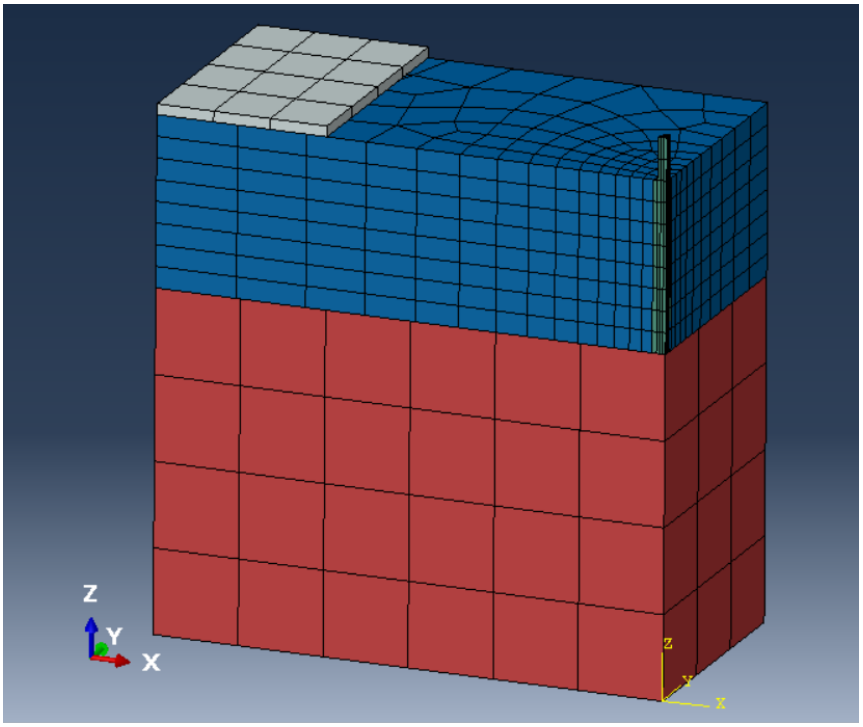

Figure 6.4. The model of an adhesive anchor in concrete block

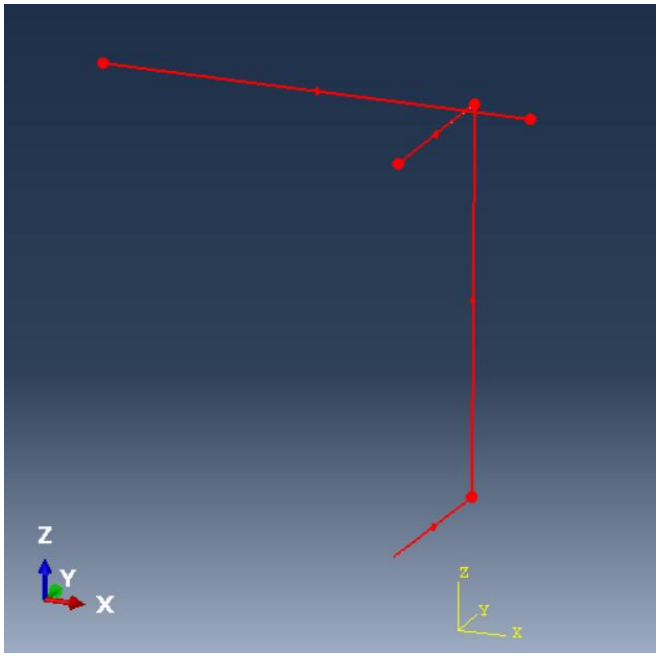

Figure 6.5. The longitudinal bars and stirrups in concrete block

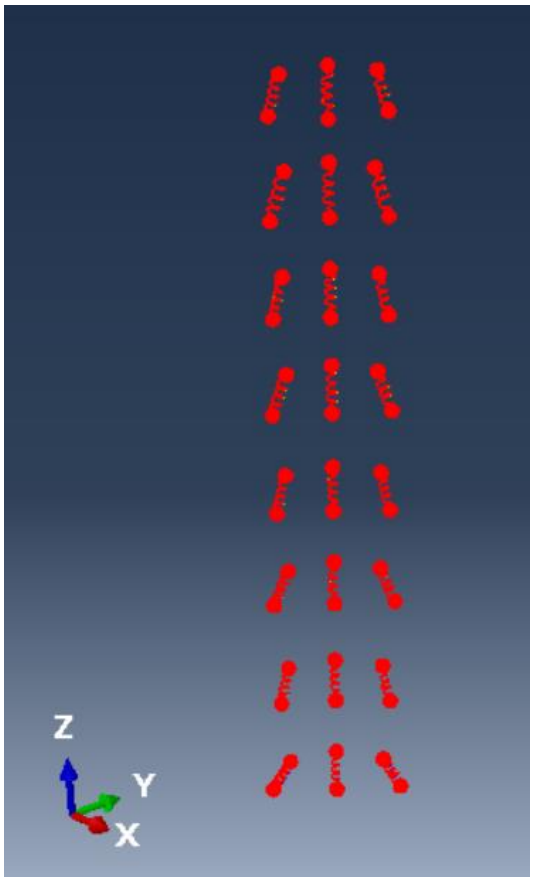

Figure 6.6. The nonlinear springs in Z direction

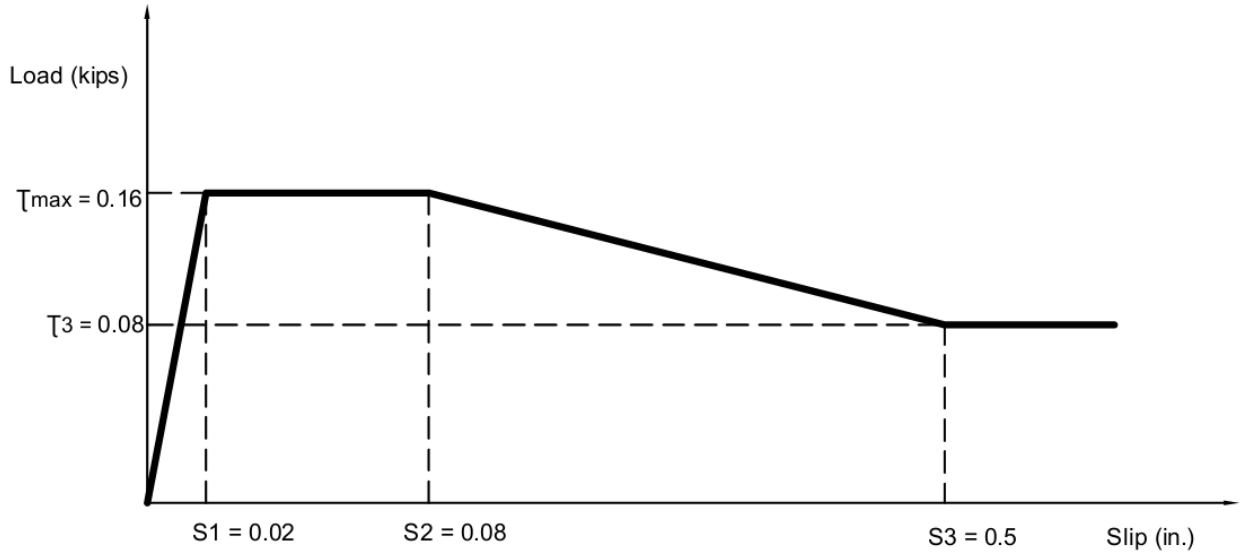

Figure 6.7. The bond slip relationship of nonlinear springs for fully cleaned holes.

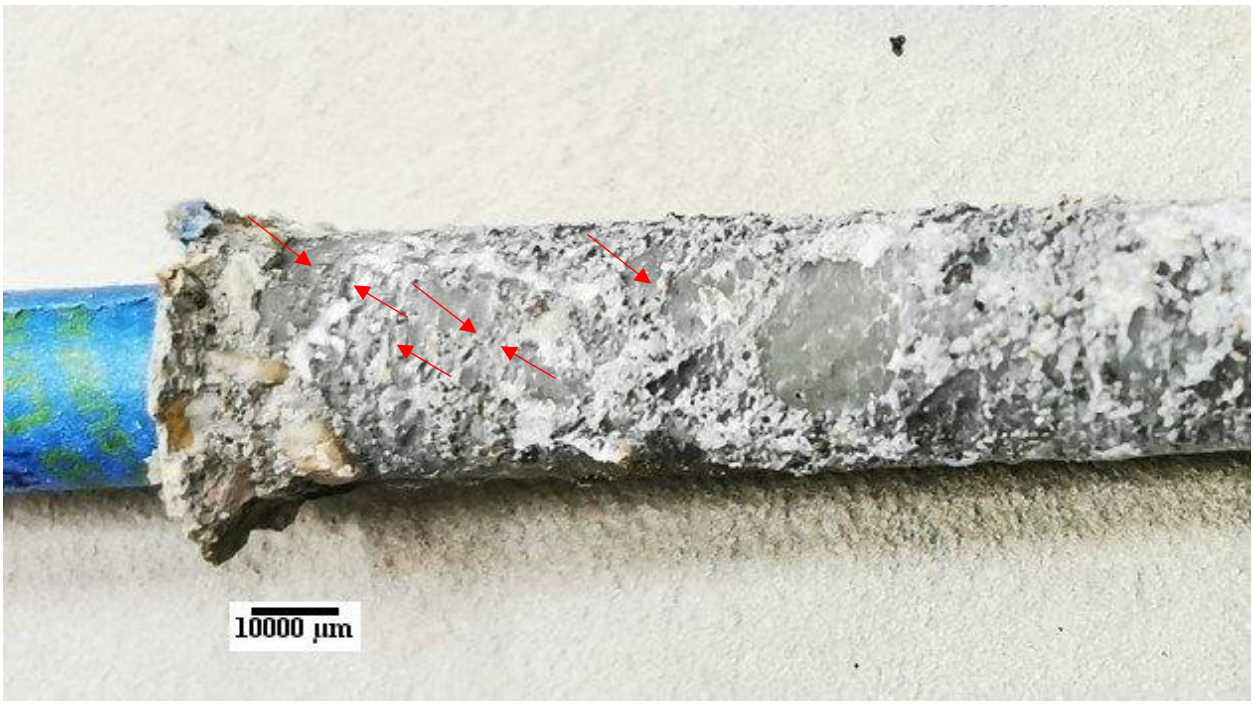

Figure 6.8. Randomly selected six spikes.

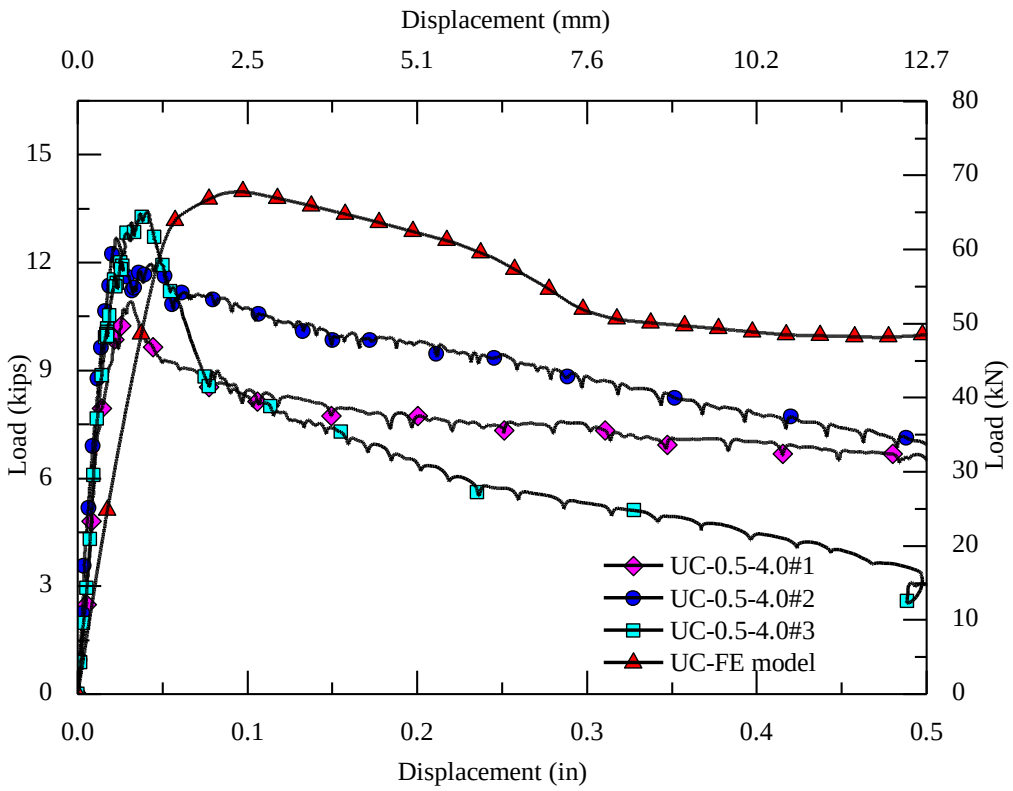

Figure 6.9. Comparison between experimental and numerical results for fully cleaned holes.

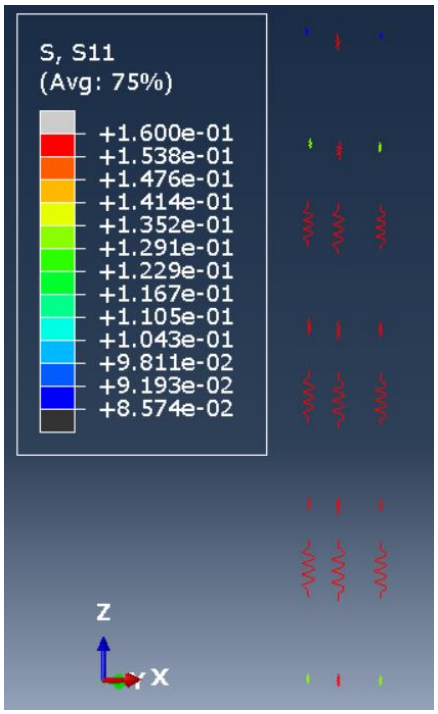

Figure 6.10. The spring forces at the peak load.

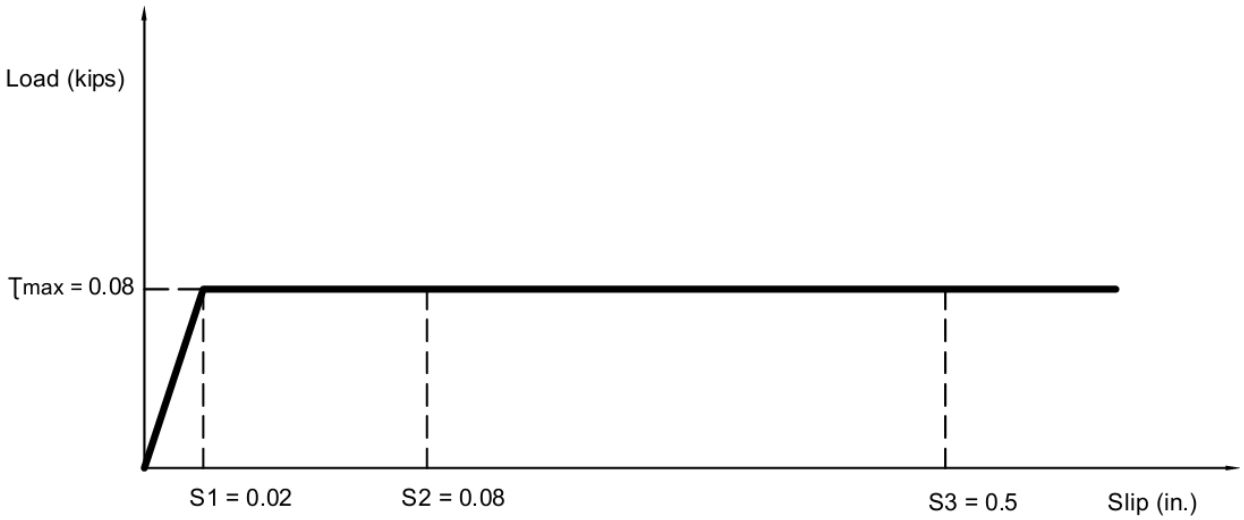

Figure 6.11. The bond slip relationship of nonlinear springs for partially cleaned holes.

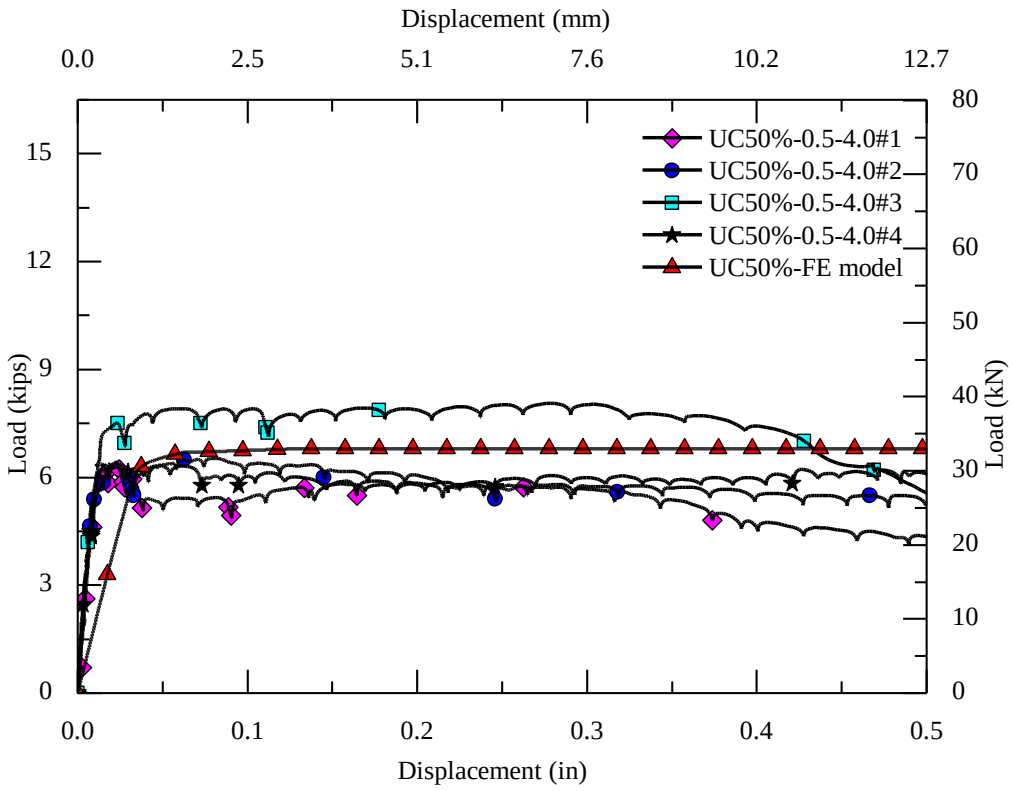

Figure 6.12. Comparison between experimental and numerical results for partially cleaned holes.

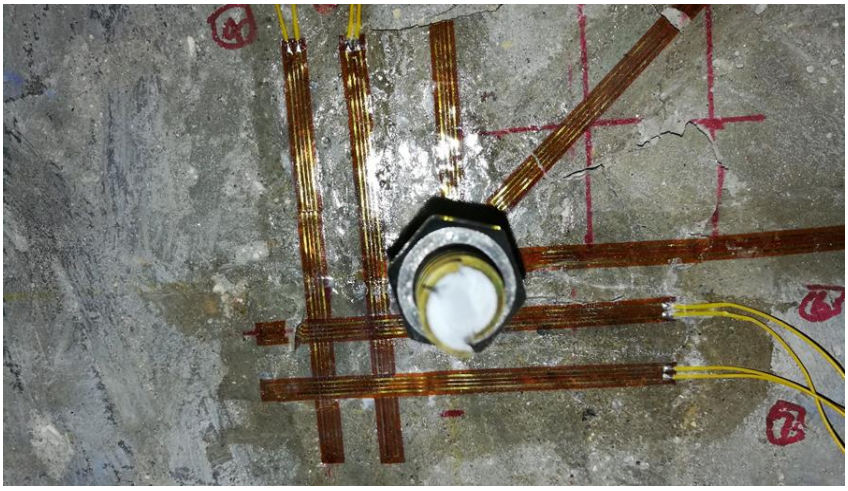

Figure 6.13. Strain gages installed on concrete surface.

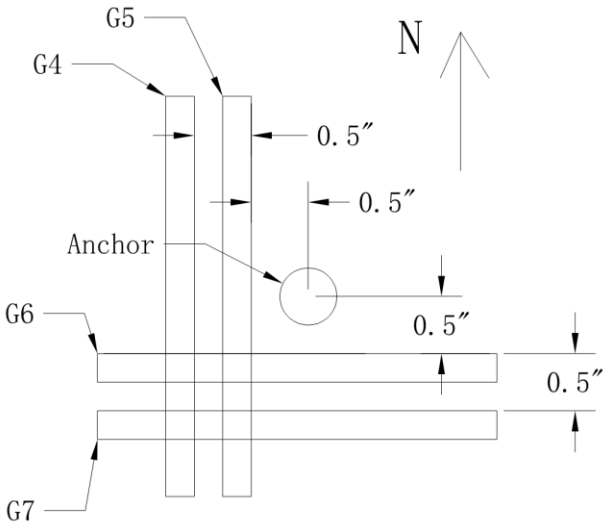

Figure 6.14. Schematics of strains gages on concrete surface.

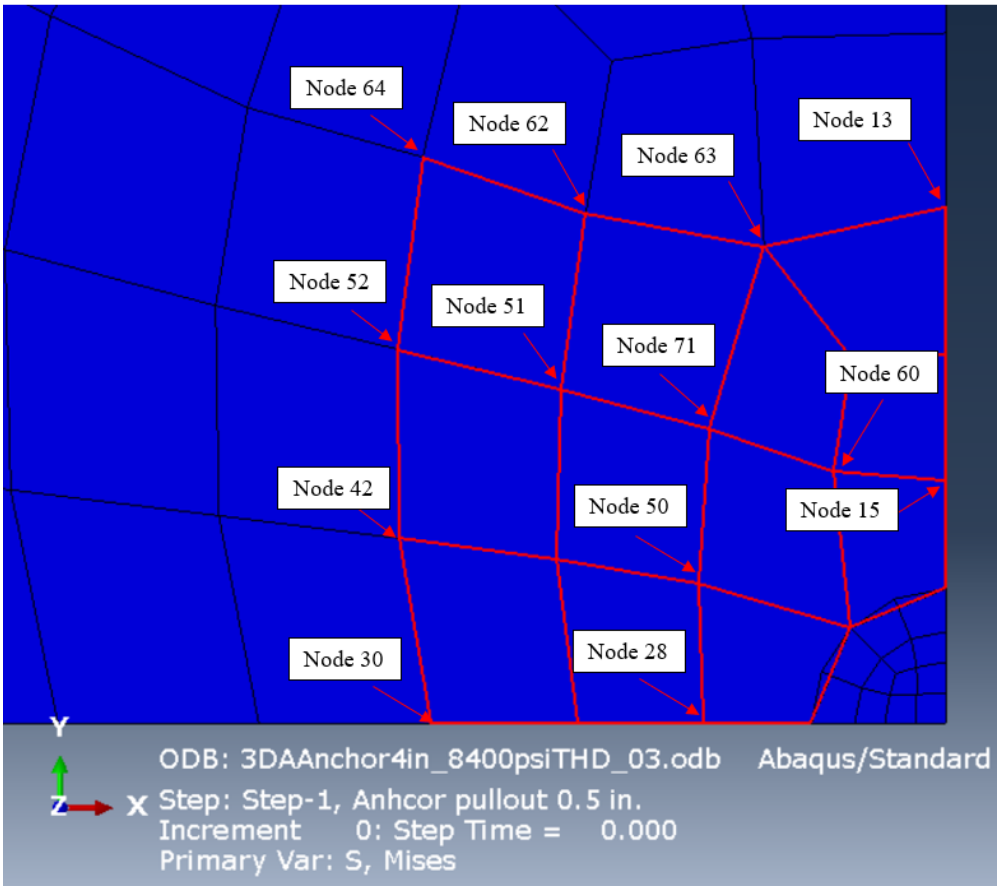

Figure 6.15. The strains measured from nodes on the model.

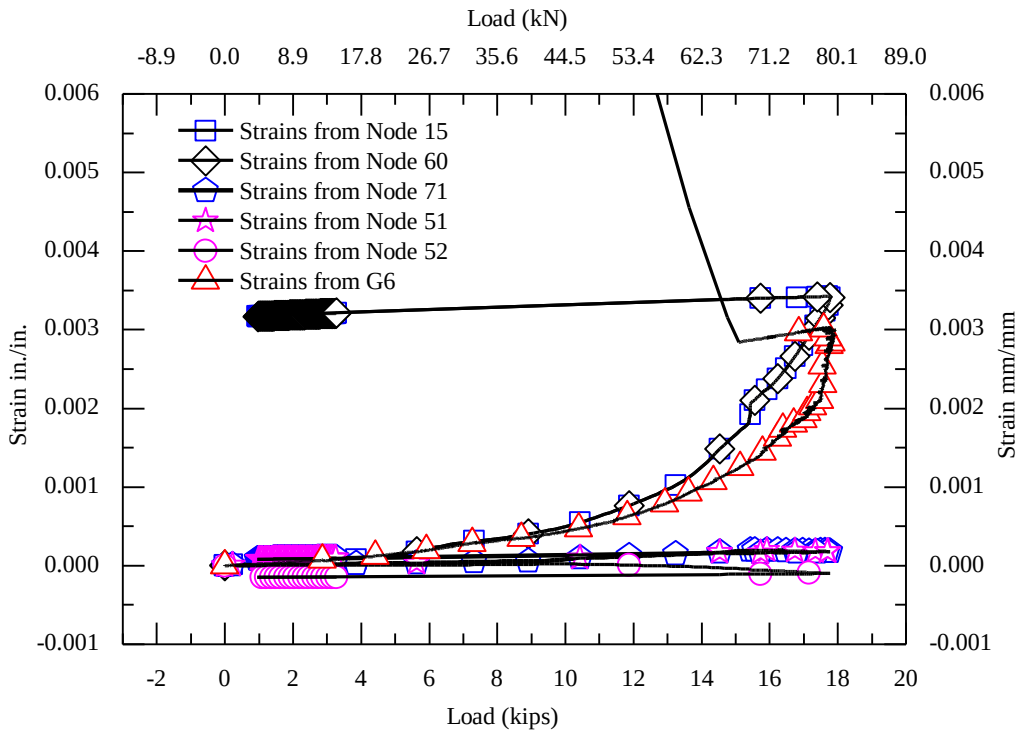

Figure 6.16. Measured strains in the longitudinal direction.

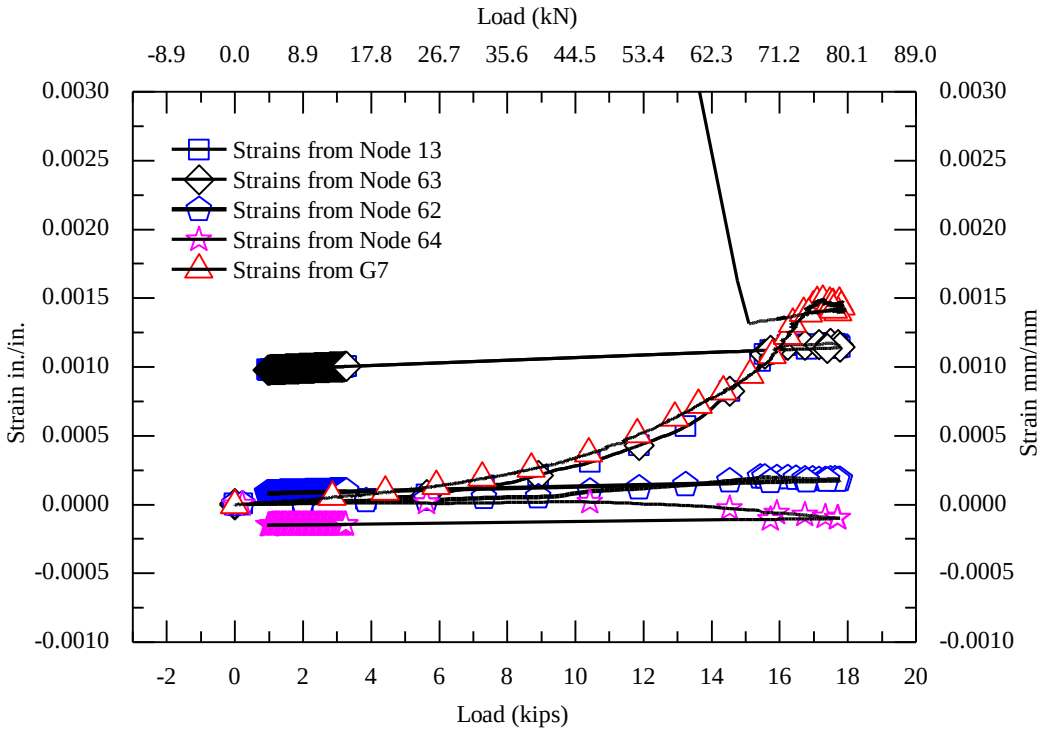

Figure 6.17. Measured strains in the longitudinal direction.

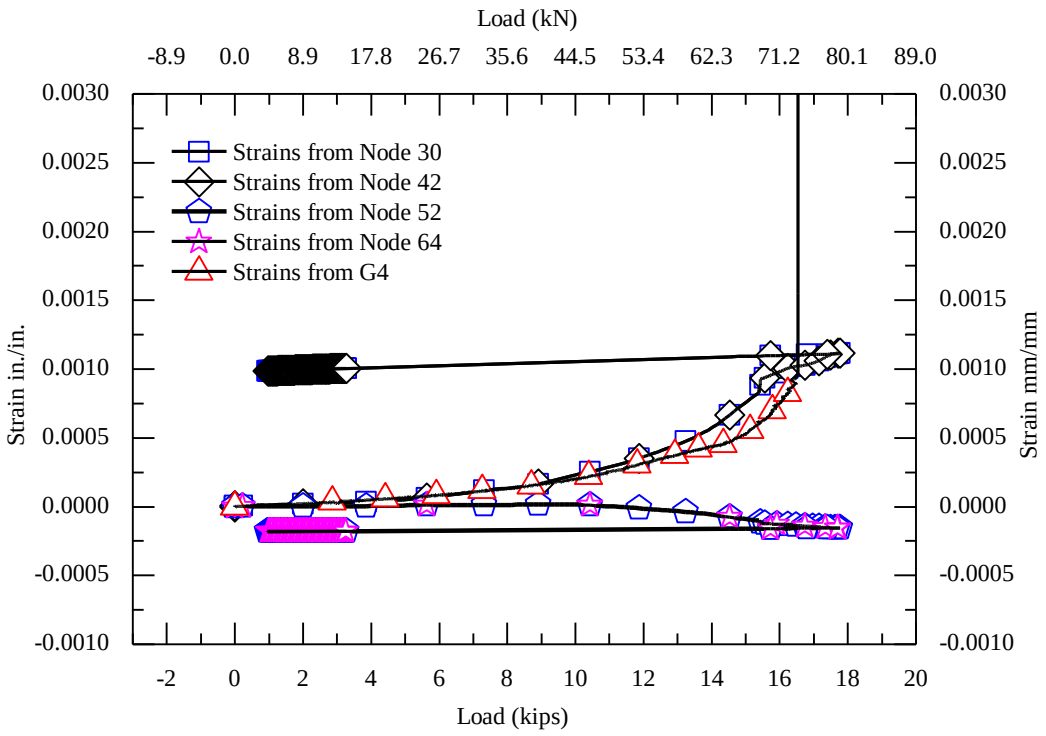

Figure 6.18. Measured strains in the transverse direction.

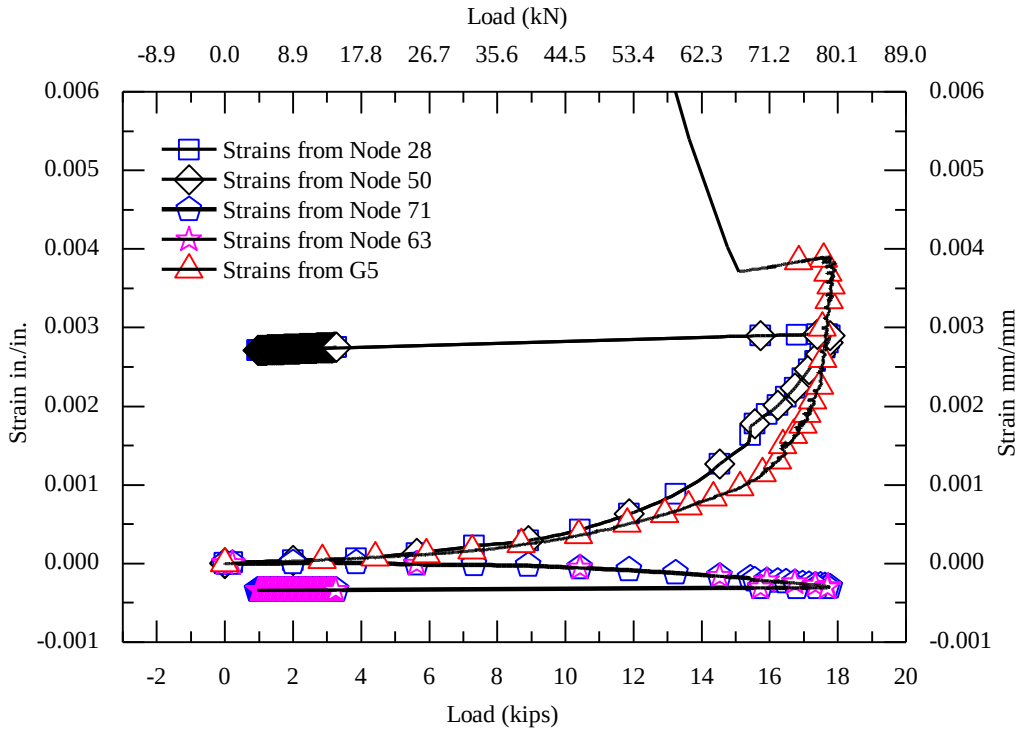

Figure 6.19. Measured strains in the transverse direction.

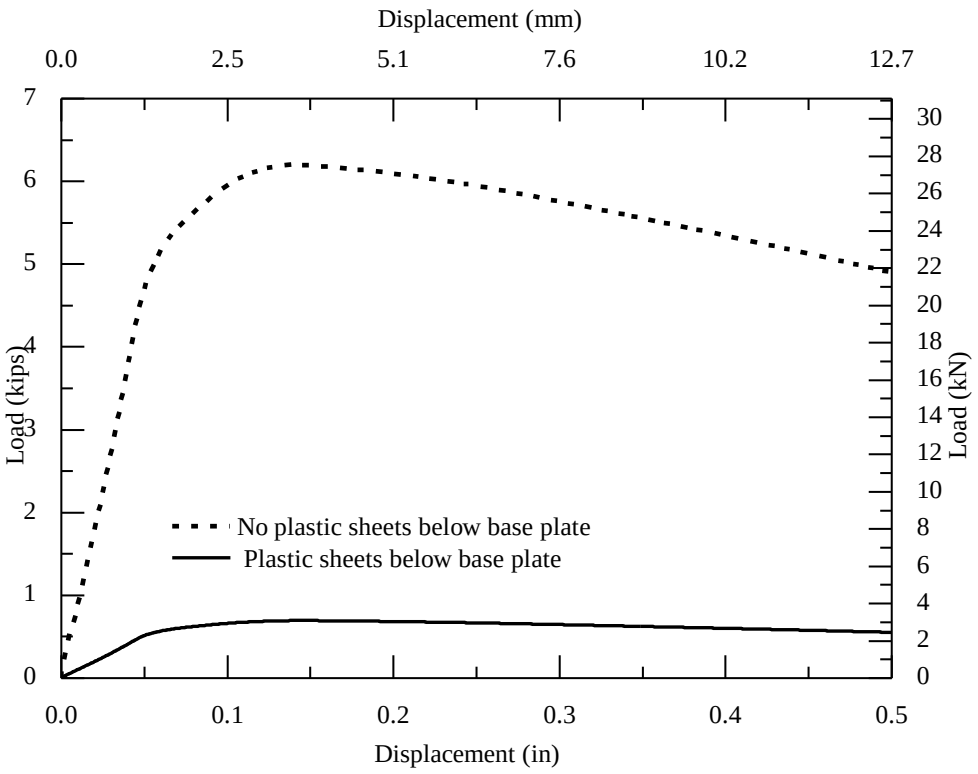

Figure 6.20. Horizontal reaction between the base plate and the concrete surface.

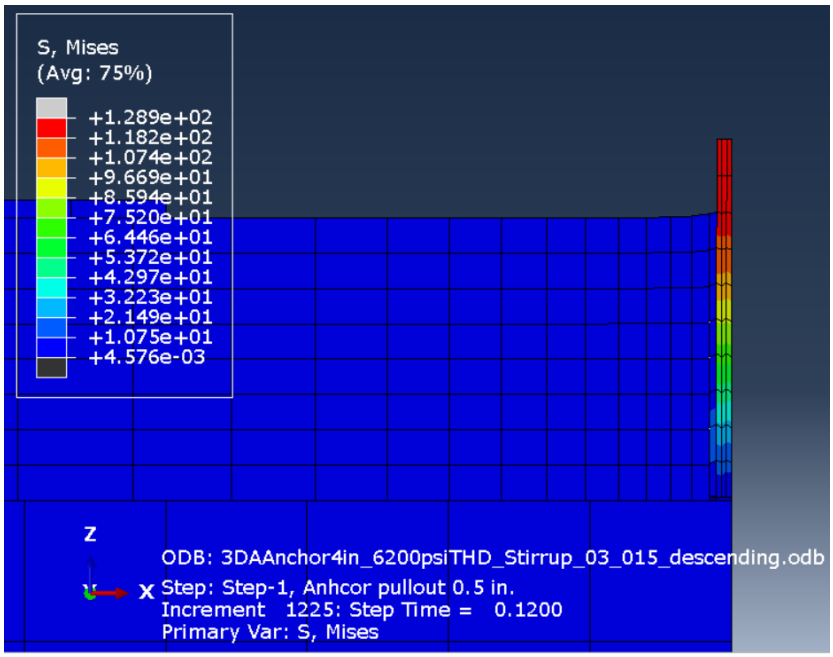

Figure 6.21. The anchor installed threaded hole and steel failure.

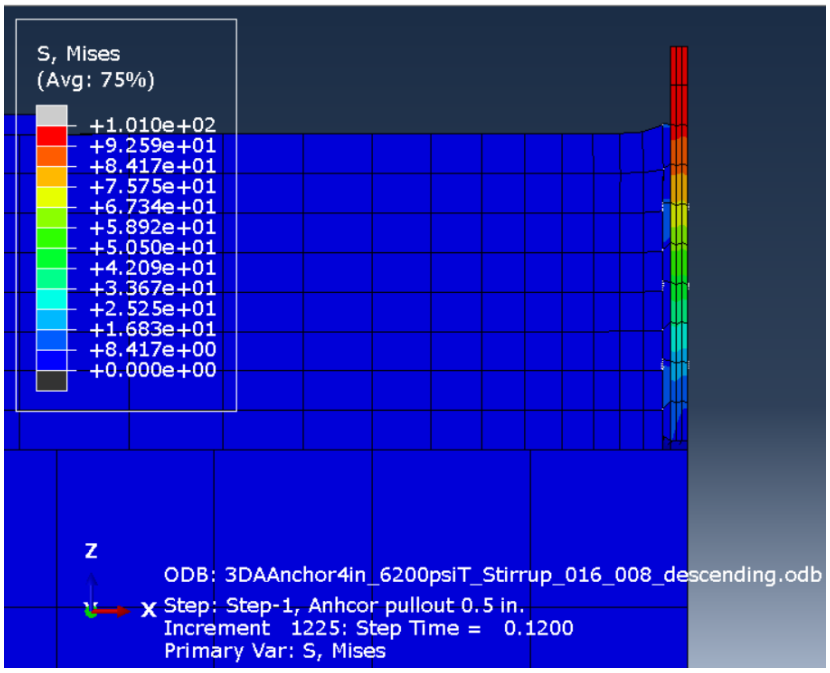

Figure 6.22. The anchor installed smooth hole and bond failure.

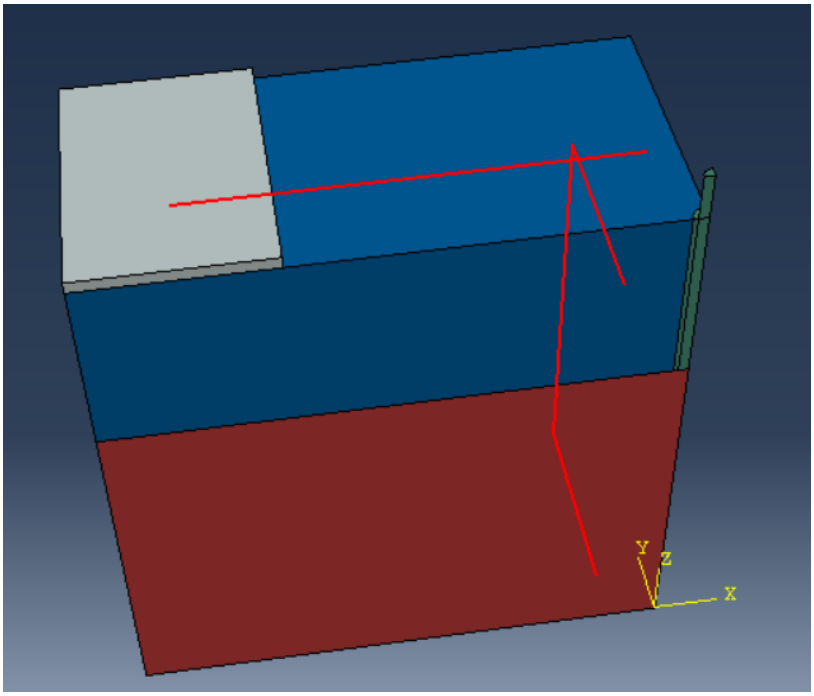

Figure 6.23. The stirrup beside the anchor in concrete block.

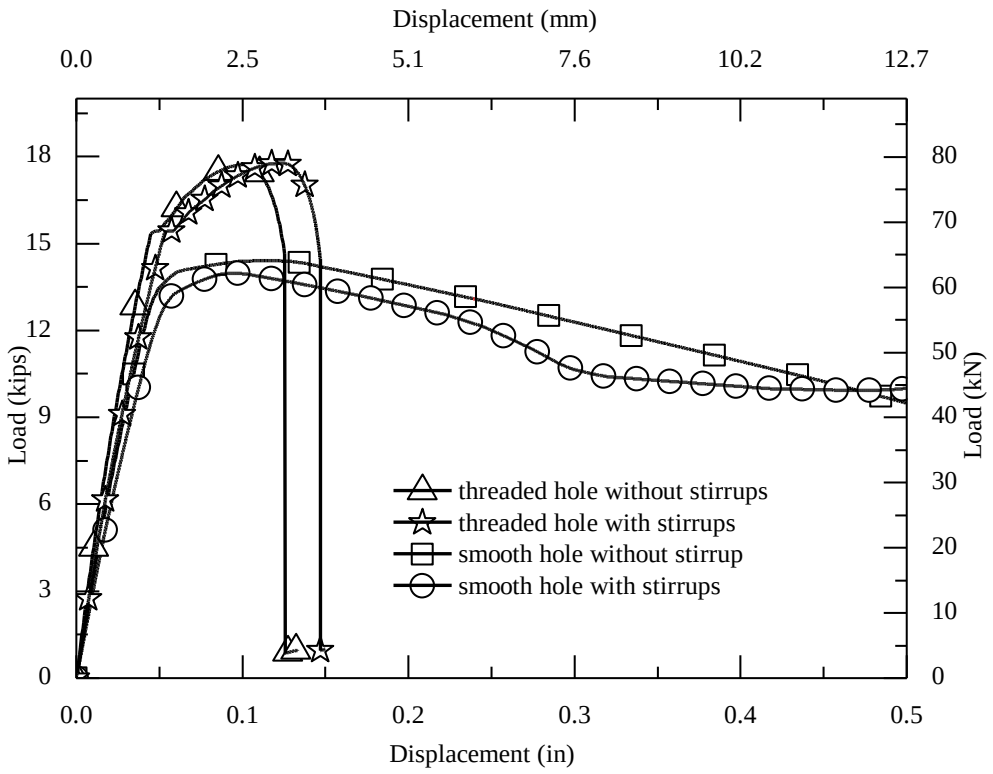

Figure 6.24. Anchor installed in threaded hole and smooth hole w/ without stirrups.

Table 6.1. The Parameters of the CDP and the cohesive element. (Delhomme and Brun 2018)

Table 4. Parameters of the CDP model and the cohesive element.

ψ (°)	ε	σ_{b0}/σ_{c0}	K	μ	t_s^0 (MPa)	δ_s^t (mm)	k_{ss} ($N.m^{-2}$)	k_{nn} ($N.m^{-2}$)
38	0.1	1.16	2/3	0.0001	37	6.8	45.5	45500

Appendix I: Concrete Materials

Concrete used in this study was ordered from a local ready-mix batching plant. Table I.1 shows the concrete mixture design provided by the plant. Considering the reduced concrete cover in some specimens, where anchor reinforcement was installed in two perpendicular directions outside transverse reinforcement (Figure 4.3), a maximum aggregate size of 3/8 in. [9.53mm] and a slump of 5 in.[127mm] were specified. This is reasonable according to ACI 355.4 (2011) Section 4.3.2: Use a maximum coarse aggregate size of either 3/4 in.[19mm] or 1 in.[25.4mm].

The reported water-cementitious material ratio (W/C) was 0.315. The measured slump following ASTM C143 was 7¼ inches [184.2mm]. Concrete cylinders (4×8 in.) [102 × 203mm] were made according to ASTM C31, some with tamping rods while others were later made using a vibration table. The cylinders were kept in their plastic molds under an indoor condition with temperatures between 60 - 80 degrees Fahrenheit [15.6 – 26.7 C°] till the specimens were demolded at 7 days. Instead of the standard curing condition as specified in ASTM C31, the concrete specimens and cylinders were kept to the same indoor environment (roughly with a consistent temperature of 70 degrees Fahrenheit [21.1 C°]).

Suozzo and Dewoolkar (2014) claimed that the compressive strength measurement between elastomeric pad and sulfur-capped specimens were not significant distinction in statistics. They recommended elastomeric pad capping because it is simple for preparation. Hence, compression tests were conducted using an ELE INTERNATIONAL compression machine (450 kips) following ASTM C1231 as shown in Figure I.1. High-alloy steel retaining caps with elastomeric pads (ASTM C1231) were used during the tests to provide uniform load at cylinder ends. The compressive loading was applied at a rate about 540 lb/sec [2.4 kN/sec]. Three cylinders were

tested at 3, 7, 14, 21, 28, 56, and 90 days. The test results are listed in Table I.2. Note that the diameters of the randomly selected cylinders were not measured before their tests; however the diameters of the remaining 32 cylinders (out of 50 made in total) were checked, and the measurements indicated that the cylinder diameters were 4 in. on average with a standard deviation of 0.008; Hence, the nominal cylinder diameter (4 in.) was used in the strength calculation in Table I.2.

The cylinder tests indicate that the 28-day strength of the concrete was 6200 psi [42.7 MPa] and the same strength was maintained throughout the anchor tests. The details of the cylinder tests are documented below:

Figure I.2 shows the fracture pattern of Cylinders 1 and 2 are well-formed cone on one end, vertical cracks running through caps, no well-defined cone on other end, which is Type 2 defined by ASTM C39. The fracture pattern of Cylinder 3 is columnar vertical cracking through both ends, no well-formed cones, which is Type 3 defined by ASTM C39. Figure I.3 shows the fracture pattern of Cylinders 4, 5 and 6 are well-formed cone on one end, vertical cracks running through caps, no well-defined cone on other end, which is Type 2 defined by ASTM C39. Figure I.4 shows the fracture pattern of Cylinders 7, 8 and 9 are well-formed cone on one end, vertical cracks running through caps, no well-defined cone on other end, which is Type 2 defined by ASTM C39. Figure I.5 shows the fracture pattern of Cylinders 10, 11 and 12 are well-formed cone on one end, vertical cracks running through caps, no well-defined cone on other end, which is Type 2 defined by ASTM C39. Figure I.6 shows the fracture pattern of Cylinders 13, 14 and 15 are well-formed cone on one end, vertical cracks running through caps, no well-defined cone on other end, which is Type 2 defined by ASTM C39. Figure I.7 shows the fracture pattern of Cylinders 16, 17 and 18 are well-

formed cone on one end, vertical cracks running through caps, no well-defined cone on other end, which is Type 2 defined by ASTM C39.

The observed strength development of the concrete is well within the suggested range established by the batching plant based on its own tests as indicated in Figure I.8. Specifically, the compressive strength at 72 hours is expected between 3000 to 3500 psi [20.7 to 24.1 MPa] while the observed average strength at 3 days was 3270 psi [22.5 MPa]. The compressive strength at 168 hours is expected around 4500 psi [31 MPa] while the observed strength at 7 days was 4520 psi [31.2 MPa]. The compressive strength at 336 hours is expected around 5800 psi [40 MPa] while the observed strength at 14 days was 5980 psi [41.2 MPa]. The compressive strength at 504 hours is expected around 6000 psi [41.4 MPa] while the observed strength at 21 days was 6200 psi [42.7 MPa]. The compressive strength at 672 hours is expected around 6500 psi [44.8 MPa]. The observed strength at 28 days was 6200 psi [42.7 MPa]. In addition, the measured strength at 90 days was 6280 psi [43.3 MPa], which is only 1.3% higher than the 28-day strength.

The concrete strength is also compared with typical concrete strength development as shown in Figure I.9. Specifically, the compressive strength at 3 day, 7 days, 14 days, 21 days, 28 days and 90 days are expected around 40%, 65%, 90%, 97%, 99%, and 100% of the 28-day strength for normal strength Portland cement concrete. The measured strength closely followed the typical strength development except near the 7 days, when the measured strength was lower. This was attributed to the fact that the cylinder molds were removed at the age of 7 days and the cylinders were stored near the specimens, which did affect the strength development. The concrete strengths after 28 days, during which the tests in this study were conducted, were not affected. Therefore, it is concluded that the compressive strength was 6200 psi [42.7 MPa] for the concrete in this study.

Table I.1 Mixture design of concrete in this study

Material	Description	Design Qty/yd3	Required for 3 yd3	Batched in 3 yd3	% Var	% Moisture	Actual water
CA-PGR-LFC	ASTM C33 #8	1684 lb	5052 lb	5080 lb	0.55%		
SND-NS-GNC	ASTM C33 SAND	1540 lb	4800 lb	4780 lb	-0.42%	3.75% M	21 gl
FLY-LAFOC	FLYASH LAFARG	159 lb	477 lb	485 lb	1.68%		
CEM-BUZF	CEM TYPE I	476 lb	1428 lb	1420 lb	-0.56%		
WATER1	WATER	24 gl	49.5 gl	50 gl	0.93%		50 gl
MR-MBP1020	POLY 1020 BASF	6 /C	114 oz	116 oz	1.49%		

Table I.2 Concrete cylinder test results

Age: 3 Days	A	12.56 in2	fc	3270 psi		
No	P	fc	Average fc	Deviation	ASTM C39 Acceptable Range	
	lbs	psi	psi			
C-01	39160	3118	3270	-0.047	<	0.106
C-02	41740	3323		0.016	<	
C-03	42310	3369		0.030	<	

Age: 7 Days	A	12.56 in2	fc	4520 psi		
No	P	fc	Average fc	Deviation	ASTM C39 Acceptable Range	
	lbs	psi	psi			
C-04	54590	4346	4523	-0.039	<	0.106
C-05	57360	4567		0.010	<	
C-06	58470	4655		0.029	<	

Age: 14 Days	A	12.56 in2	fc	5980 psi		
No	P	fc	Average fc	Deviation	ASTM C39 Acceptable Range	
	lbs	psi	psi			
C-07	75720	6029	5975	0.009	<	0.106
C-08	72690	5787		-0.031	<	
C-09	76730	6109		0.022	<	

Age: 21 Days	A	12.56 in2	fc	6200 psi		
No	P	fc	Average fc	Deviation	ASTM C39 Acceptable Range	
	lbs	psi	psi			
C-10	79090	6297	6200	0.016	<	0.106
C-11	75270	5993		-0.033	<	
C-12	79270	6311		0.018	<	
Age: 28 Days	A	12.56 in2	fc	6200 psi		
No	P	fc	Average fc	Deviation	ASTM C39 Acceptable Range	
	lbs	psi	psi			
C-13	81560	6494	6204	0.047	<	0.106
C-14	75830	6037		-0.027	<	
C-15	76390	6082		-0.020	<	
Age: 90 Days	A	12.56 in2	fc	6280 psi		
No	P	fc	Average fc	Deviation	ASTM C39 Acceptable Range	
	lbs	psi	psi			
C-16	77100	6139	6278	-0.022	<	0.106
C-17	81250	6469		0.030	<	
C-18	78200	6226		-0.008	<	

Figure I.1. Illustration of compressive tests of concrete cylinders

Figure I.2. Failure pattern of Cylinders 1, 2, 3 at 3 days

Figure I.3. Failure pattern of Cylinders 4, 5, 6 at 7 days

Figure I.4. Failure pattern of Cylinders 7, 8, 9 at 14 days

Figure I.5. Failure pattern of Cylinders 10, 11, 12 at 21 days

Figure I.6. Failure pattern of Cylinders 13, 14, 15 at 28 days

Figure I.7. Failure pattern of Cylinders 16, 17, 18 at 90 days

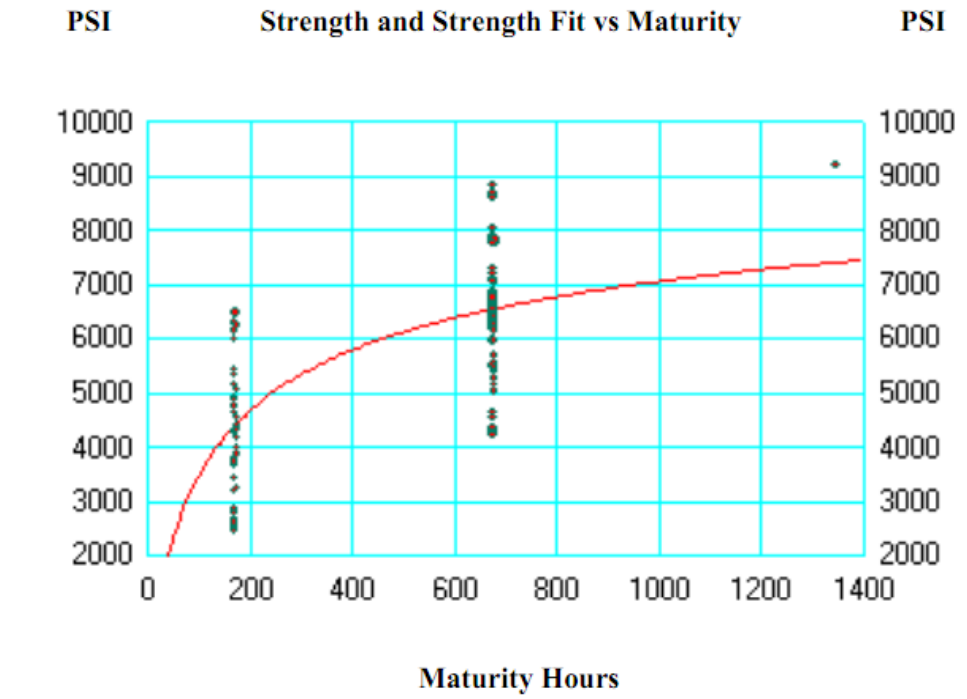

Figure I.8. Concrete strength vs time relationship provided by the batching plant.

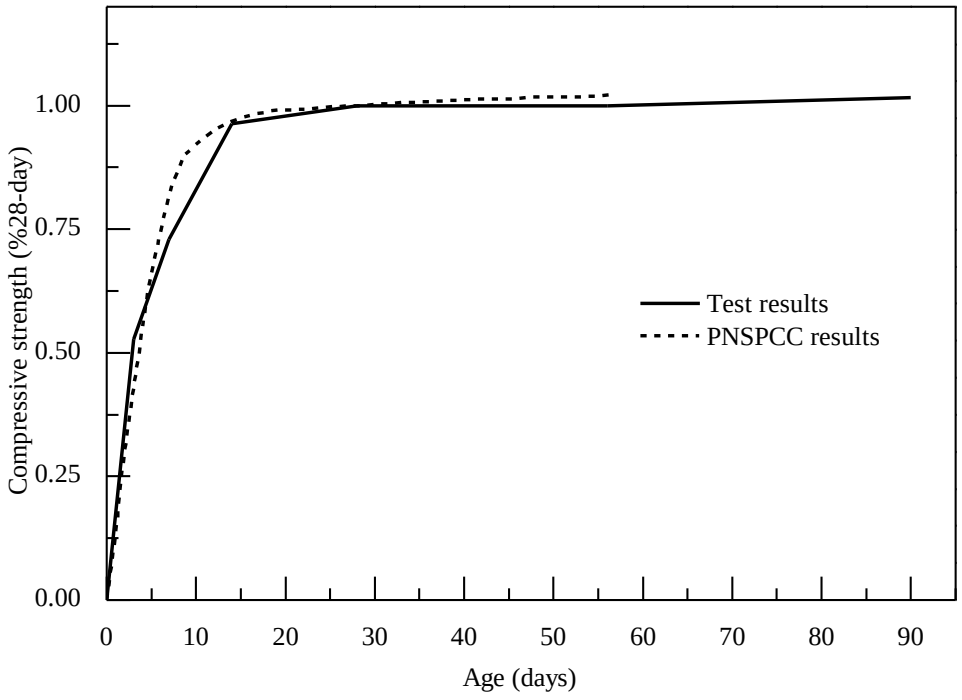

Figure I.9. Comparison with typical compressive strength development of concrete (PNSPCC 2019)

Appendix II: Steel Anchor Materials

The ASTM A193 Grade B7 threaded rods for the tests in this study were purchased from Grainger Industrial Supply. Tensile tests were conducted for both standard coupons and threaded rods. This is required by ACI 355.4, Section R10.5, "*Where the strength of the anchor element is addressed by other standards, for example, all-thread rods by ASTM, separate tension tests to determine the tension strength of the rod/nut assembly are not required*."

The tensile tests of anchor steel were conducted with the same sensors used in the pullout tests. These sensors were calibrated before the tests as shown below.

Calibration of load cell and LVDTs

Series 350 general purpose linear variable differential transformers (LVDTs) from Trans-Tek were used for measuring the displacement of anchor bolts. The sensitivity is 0.8431 VDC/inch/Volt Input. The working range is ±1 inch. [± 25.4 mm]. Before the pullout tests, the LVDT's were calibrated using a digital scriber made by STANDARD GAGE. The setup for the calibration is shown in Figure II.1. The calibration was conducted by taking readings from the data acquisition system at each 0.1 in. [2.5 mm] stop. The specification of Model 0345-0000 LVDT's from Trans-Tek is shown in Figure II.2, and the color codes for the lead wires are shown in Figure. II.3. The LVDT's can take a DC power supply from 6 to 28 volts. The LVDTs were tested with a 12-volt power supply such that at the maximum displacement, the voltage outputs are about 10 volts, which is the maximum voltage allowed by the data acquisition system.

The measured data against the displacement is shown in Figure II.4. Linear regressions of the measured voltages vs. displacements, with an intersection set at the origin, indicate that both LVDTs have a conversion factor of 0.1 in./volt [2.5 mm /volt] by inverting the slopes.

A Model THD-50K-Y load cell from Transducer Techniques® was used for measuring the load capacity of anchor bolts. The excitation voltage is 10 VDC. The load cell connects with load cell amplifier signal conditioner (Modules LCA-RTC) and the color codes for the lead wires are shown in Figure. II.5. Wires on left side are output signal (black pins) and power supply (green pins) and wires on right side are input signal from the load cell. Before testing the load cell, the amplifier and load cell should be calibrated together. First, setup a digital multimeter to DV model to measure the output signal on the amplifier and use a screwdriver to turn a screw called “zero” on the amplifier until the meter reading is zero. Second, press shunt bottom on the amplifier and turn a screw called “span” until the meter reading is 5 volts. The load cell was also tested by using an Instron 3369 compression testing machine. The calibration was conducted by taking measurement from the data acquisition system at every 1.0 kip [4.45 kN] that the Instron applied compression load on the load cell. Total load of 9 kips [40.1 kN] was reached due to the limitation of maximum capacity of the machine. The measured two data against the load is shown in Figure. II.6. Linear regressions of the measured voltage vs. load, with an intersection at the origin, indicates that the load cell has conversion factor of 5.35 kips/volt [23.8 kN/volt] by inverting the slopes.

Tests of full-size threaded rods

According to ASTM A370-18, "Test specimens shall be (1) the full cross section of material, or (2) machined to the form and dimensions shown in Figs. 3-6. The selection of size and type of specimen is prescribed by the applicable product specification. Full cross section specimens shall be tested in 8-in. (200-mm) gauge length unless otherwise specified in the product specification (ASTM A370-18)."

The tests were conducted under monotonic load control using a TINIUS OLSEN testing machine. A high-strength coupler nut was used at each end of the test specimen such that the ½ in. [13 mm] diameter rod was extended by two pieces of ¾-in. [19-mm] diameter rods to fit in the testing machine, as shown in Figure. II.7. The length of the threaded grip is 0.5 in. [13 mm] for each end such that the gauge length for the testing rod is 8 in. [203 mm] ($16d_a$, where d_a is the diameter of the rod). The small plates on the extension rods were used to prevent broken rods from flying away. The elongation of the specimen was measured using two Model 0345 LVDTs by Trans-Tek® while the corresponding load was measured using a Model THD-50K-Y load cell from Transducer Techniques® mounted on the top, as shown in Figure. II.7. The data acquisition system (DaqBook2000) captures the displacement and the corresponding loads with a sampling rate of 10 Hz. The tests were conducted using an open-loop load control with a loading rate of around 3000 lb/min [13.4 kN/min] (ASTM A370-18). A pretension about 160 lb [0.71 kN] was applied to the specimens before the test to remove the slack from the load string. The stresses were calculated from the measured load divided by the cross-sectional areas calculated from measured section dimensions (average of three measurements along the specimens). The LVDT measurements were deemed the same as the deformation of the specimen, from which the axial strains were calculated

by dividing the displacement by the measured gauge length between the transition nuts (8 in.) [203 mm].

All data obtained from the data acquisition were processed using an in-house MATLAB program and details are shown in Chapter 4. The Young's modulus was calculated by the linear regressions of the stress-strain curve between an intersection before yield stress and the origin due to there is no specific requirement from AST A370. The yield strength was obtained using the standard 0.2% offset method (ASTM A370): draw a line connecting two points on the stress-strain graph: one at (0.002, 0) and the other on at ($0.002+f_u/E$, f_u); and the yield strength is read from the stress-strain curve at the intersection point.

Tests of threaded rods were conducted for ½-in. [13 mm] diameter rods only. Two rods were randomly selected from the ordered stock, and one 9-in. [228.6 mm] specimen was cut from an end of each selected rod. The measured stress-strain curves are shown in Figures II.8. The yield strength is 99 ksi [682.1 MPa] and 114 ksi [785.5 MPa], which are 5.7% smaller and 8.6% larger than the minimum specified strength 105 ksi [723.5 MPa] based on the ASTM report (ASTM A193, 2012). The ultimate strengths are 112 ksi [771.7 MPa] and 131 ksi [902.6 MPa] for ½ in [13 mm] diameter rod and 10.4% smaller and 4.8% larger than the minimum specified strength 125 ksi [861.3 MPa] based on the ASTM report (ASTM A193, 2012).

Although the rods were ordered from the same vendor, two different types of tensile behavior were observed: As shown in Figure. II.9, the ultimate loads of the TF-0.5-G8-9-19-2019 and TF-0.5-G8-9-24-2019 are 15.9 kips [70.8 kN] and 18.53 kips [82.5 kN] and 1.8 % and 3.85% smaller than the loads obtained from the testing machine.

Coupon tests of threaded rods

Two standard 0.35-in [8.9-mm] diameter coupons of ASTM A193 Grade B7, as shown in Figure. II.10, were fabricated based on Test Methods and Definitions ASTM E8-13a to create the constitutive relationship of the steel material. Sample rods were randomly selected from the ordered stock, and one 3 1/2-in. [88.9 mm] specimen was cut from an end of each selected rod. A crosshead was used at each end of the test specimen such that the ½ in. [13 mm] diameter rod to fit in the testing machine as shown in Figure. II.11. The length of the threaded grip is 0.5 in. [13mm] for each end such that the gauge length for the testing rod is 2 in. [50.8 mm] ($4d_a$, where d_a is the diameter of the rod).

The elongation of the specimen was measured using one linear variable differential transformers (LVDTs) and two strain gauges, as shown in Figure. II.11. The data acquisition system (HP 34970A) captures the displacement and the corresponding loads from the machine. The tests were conducted using an open-loop load control using a TINIUS OLSEN testing machine with a loading rate of around 3000 lb/min [13.4 kN/min] (ASTM A370-18). A pretension about 200 lb [0.89 kN] was applied to the specimens before the test to remove the slack from the load string.

The stresses were calculated from the measured load divided by the cross-sectional areas calculated from measured section dimensions (average of three measurements along the specimens). The LVDT measurements were deemed the same as the deformation of the specimen, from which the axial strains were calculated by dividing the displacement by the gauge length (2.186 in.) [55.5 mm] and (2.234 in.) [56.7 mm]. Two strain gauges (Gage 1 and Gage 2), mounted at the mid-height along the specimen, were used to measure the tension strain of the specimens.

All data obtained from the data acquisition were processed using an Excel program. The Young's modulus was calculated by the linear regressions of the stress-strain curve between an intersection

before yield stress and the origin due to there is no specific requirement from AST A370. The yield strength was obtained using the standard 0.2% offset method (ASTM A370): draw a line connecting two points on the stress-strain graph: one at (0.002, 0) and the other on at ($0.002+f_{uta}/E_s$, f_{uta}); and the yield strength is read from the stress-strain curve at the intersection point.

The measured stress-strain curves are shown in Figures II.12 and II.15 for the coupon tests respectively. The readings from Gages 1 and 2 are compared in Figures II.14 and II.17, and the average strains are shown in dotted lines in the stress-strain curves. Strains from Gage 2 and Gage 1 are similar for the coupon test 1, indicating that the specimen may not be subjected to uneven loading. Strains from Gage 2 are higher than those from Gage 1 for the coupon test 2, indicating that the specimen may be subjected to uneven loading. The strains captured by Gages 1 and 2 approached the values of yield point for all two tests. Beyond the yield point, the strains of the presented stress-stain curves were calculated from the LVDT reading, shown in dashed lines in Figures II.12 and II.15.

The stress-strain relationships are compared in Figure II.18 and their failure modes in Figure II.19. All two specimens exhibited the local necking and the cup-cone tensile fracture surfaces, which is typical for ductile metals. The elastic moduli for these two specimens are similar to each other: 26912 ksi [185.5 GPa] from the coupon test 1, 23375 ksi [161.2 GPa], from the coupon test 2. The elastic moduli from the coupon test 1 is closed to the elastic moduli (29000 ksi) [199.9 GPa].

It is thus recommended to use the coupon test 1 at stipulated in ASTM A370 for tension tests of threaded rod. For the threaded rod used in this study, the measured tension strength (f_{uta}) was 129 ksi [888.8 MPa] and modulus of Elasticity (E_s) was 26912 ksi [185.5 GPa].

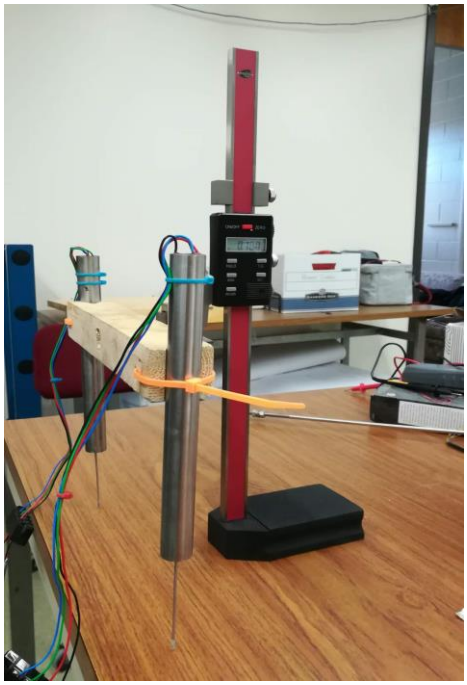

Figure II.1 Calibration equipment setup

Figure II.2. Specifications of the LVDTs Model 0345

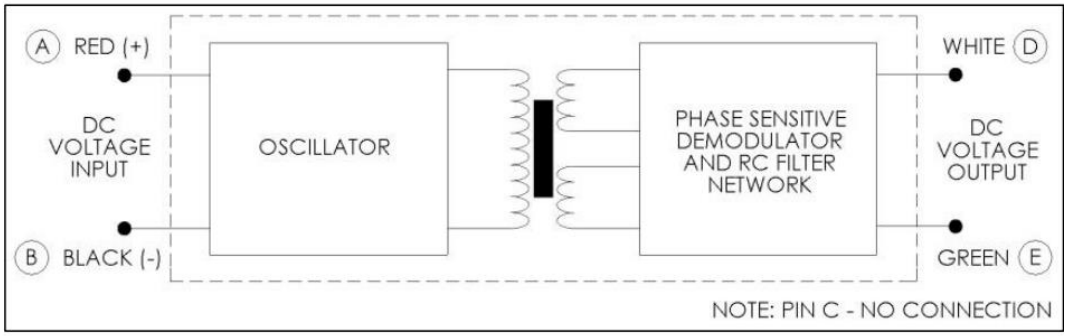

Figure. II.3. Color codes of the wires

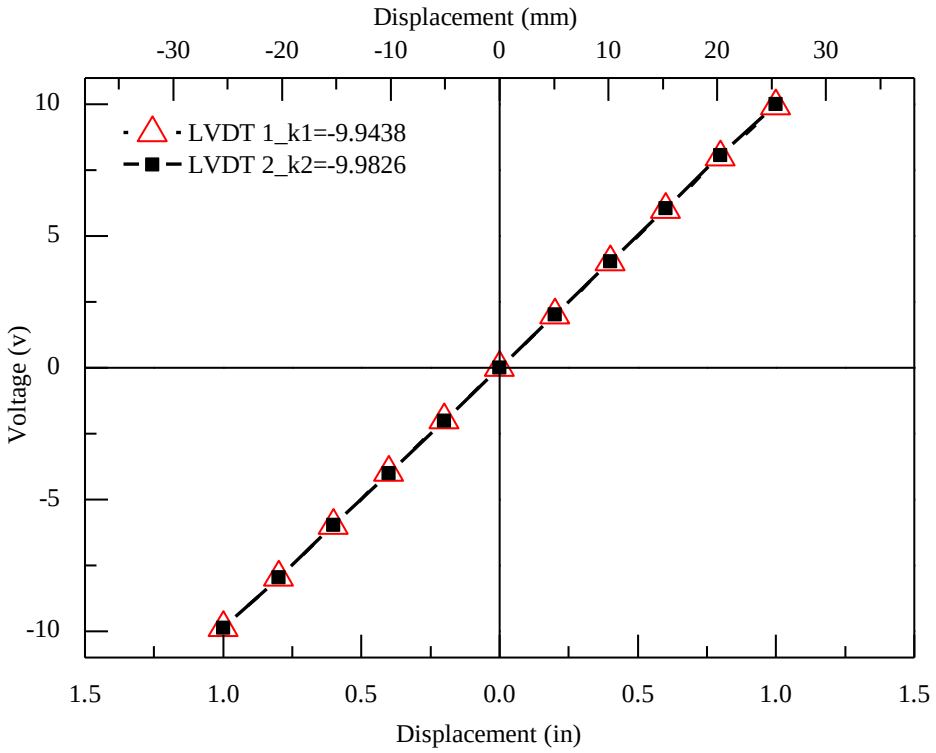

Figure II.4 Voltage vs. Displacement

Figure. II.5. Color codes of the wires for a load cell amplifier

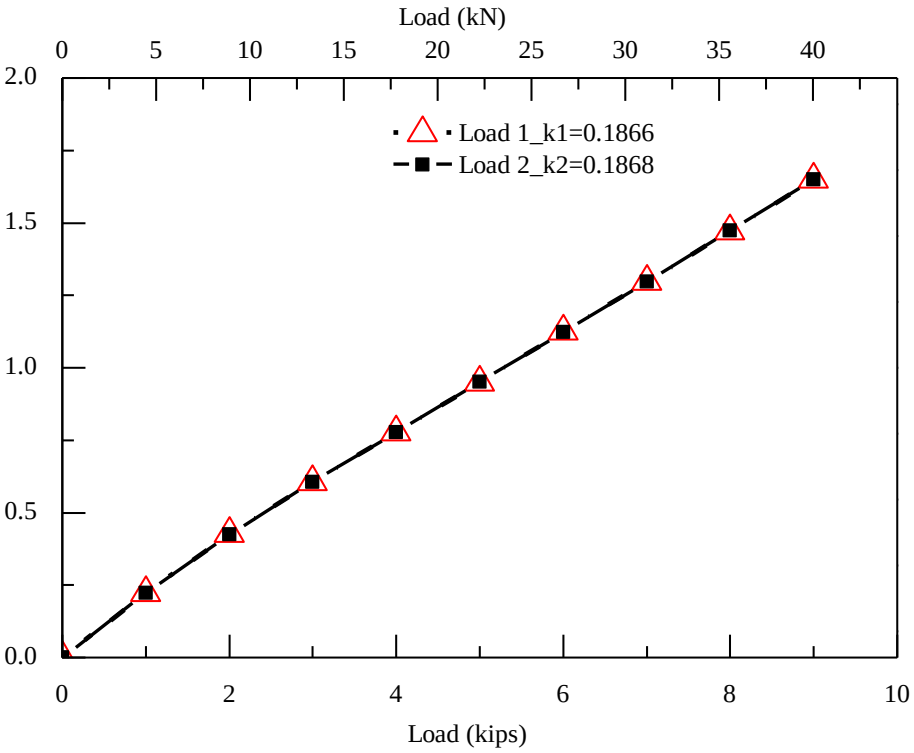

Figure. II.6 Voltage vs. Load

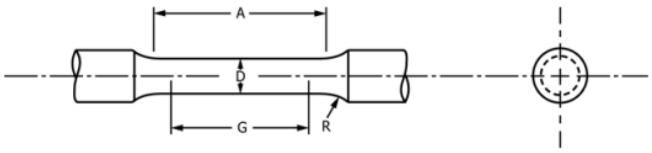

DIMENSIONS

Nominal Diameter	Standard Specimen		Small-Size Specimens Proportional to Standard							
	in.	mm	in.	mm	in.	mm	in.	mm	in.	mm
	0.500	12.5	0.350	8.75	0.250	6.25	0.160	4.00	0.113	2.50
G—Gauge length	2.00± 0.005	50.0 ± 0.10	1.400± 0.005	35.0 ± 0.10	1.000± 0.005	25.0 ± 0.10	0.640± 0.005	16.0 ± 0.10	0.450± 0.005	10.0 ± 0.10
D—Diameter (Note 1)	0.500± 0.010	12.5± 0.25	0.350± 0.007	8.75 ± 0.18	0.250± 0.005	6.25 ± 0.12	0.160± 0.003	4.00 ± 0.08	0.113± 0.002	2.50 ± 0.05
R—Radius of fillet, min	3/8	10	1/4	6	3/16	5	5/32	4	3/32	2
A—Length of reduced section, min (Note 2)	2 1/4	60	1 3/4	45	1 1/4	32	3/4	20	5/8	16

Figs. 3-6 Specimen dimensions

Figure. II.7. Test setup for tensile tests of anchor rods

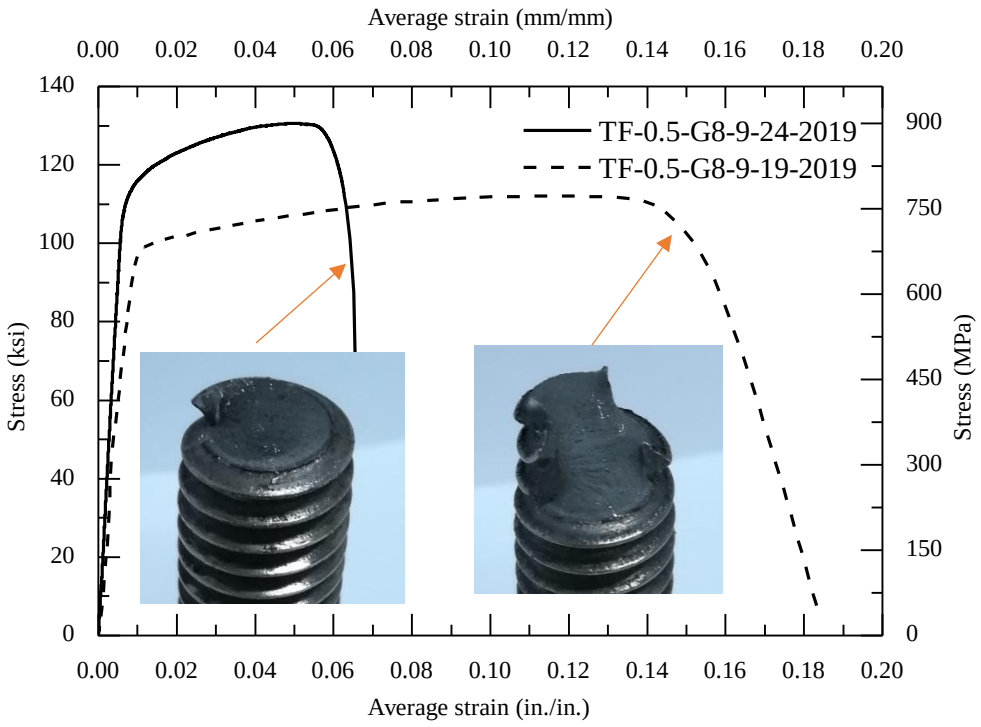

Figure. II.8. The stress-strain curves of threaded rods.

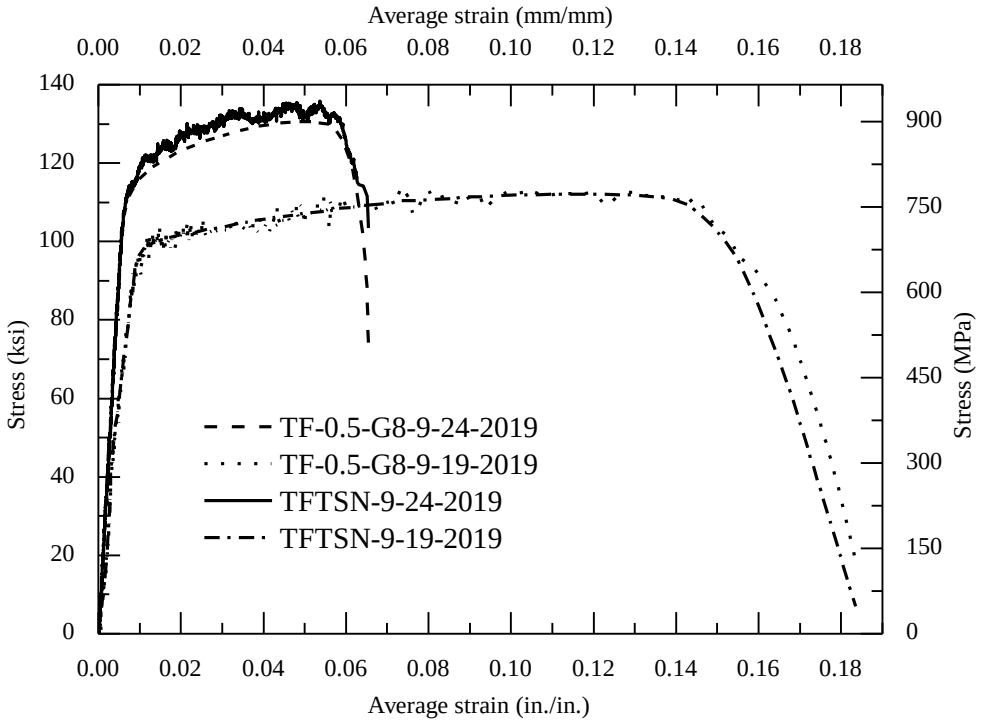

Figure. II.9. Compression load cell vs testing machine.

Figure. II.10. Standard 0.35-in (8.9-mm) diameter coupon of A193 anchor rods

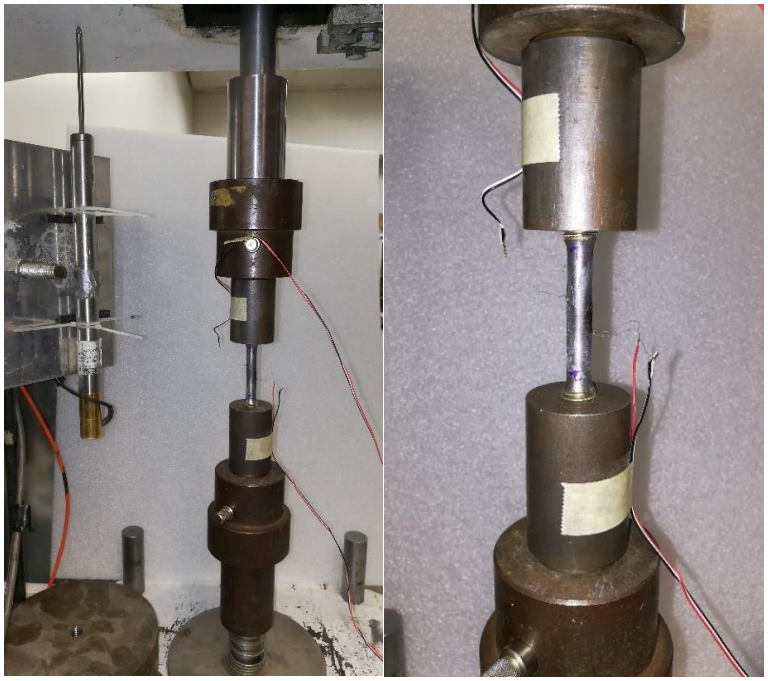

Figure. II.11. Coupon test in Tinius Olsen machine

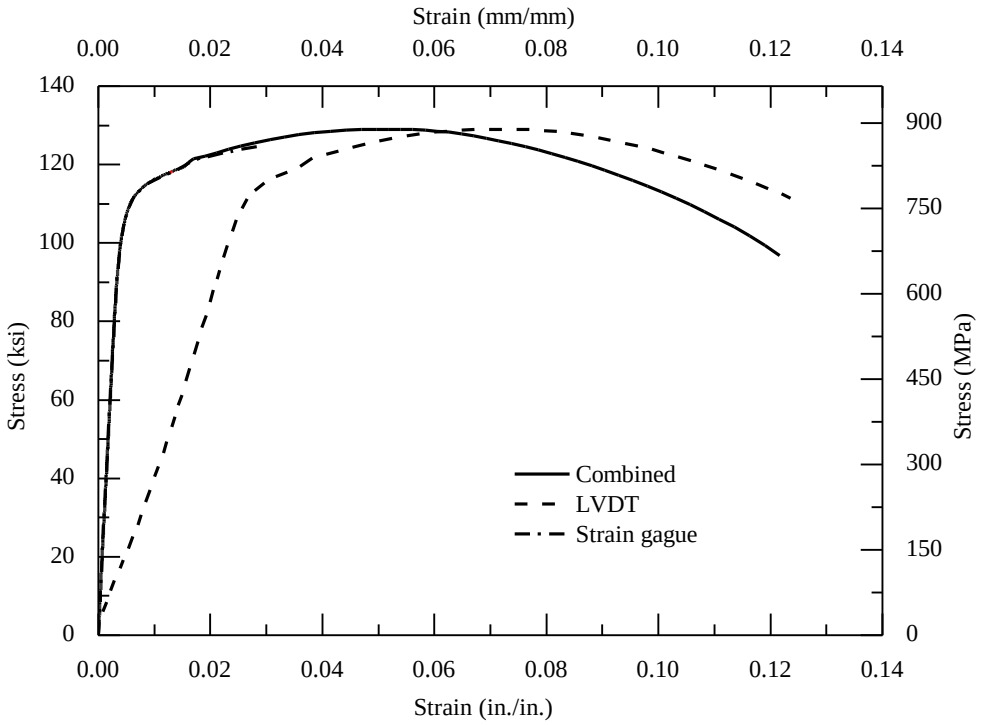

Figure. II.12 The stress-strain curves of the coupon test (1).

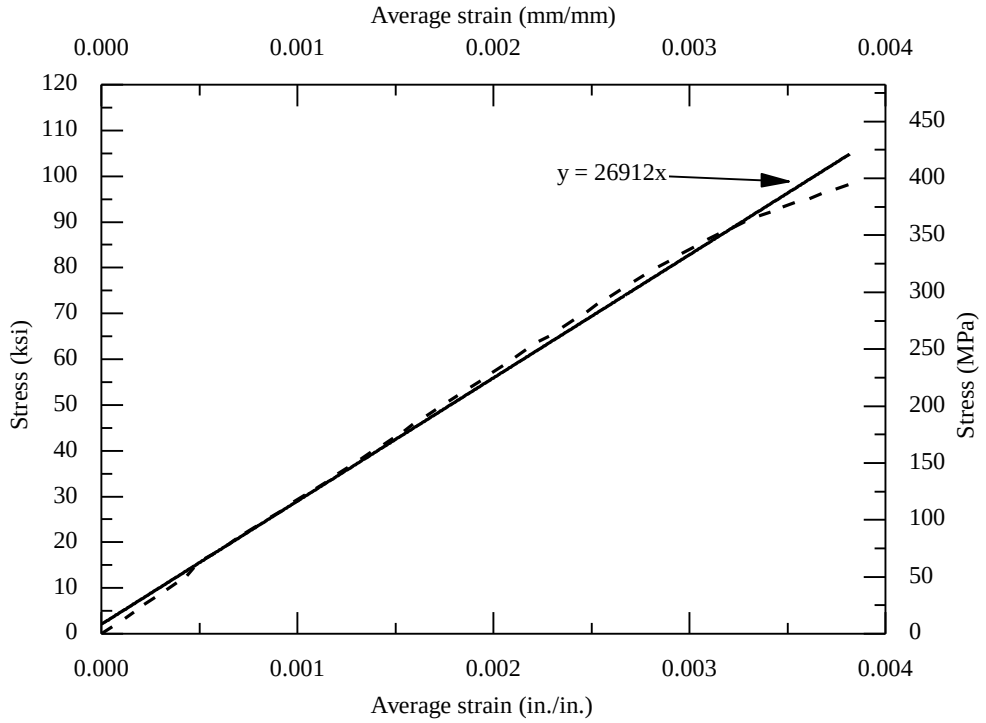

Figure II. 13. Stress vs strain curve (before yield strength) of the coupon test (1).

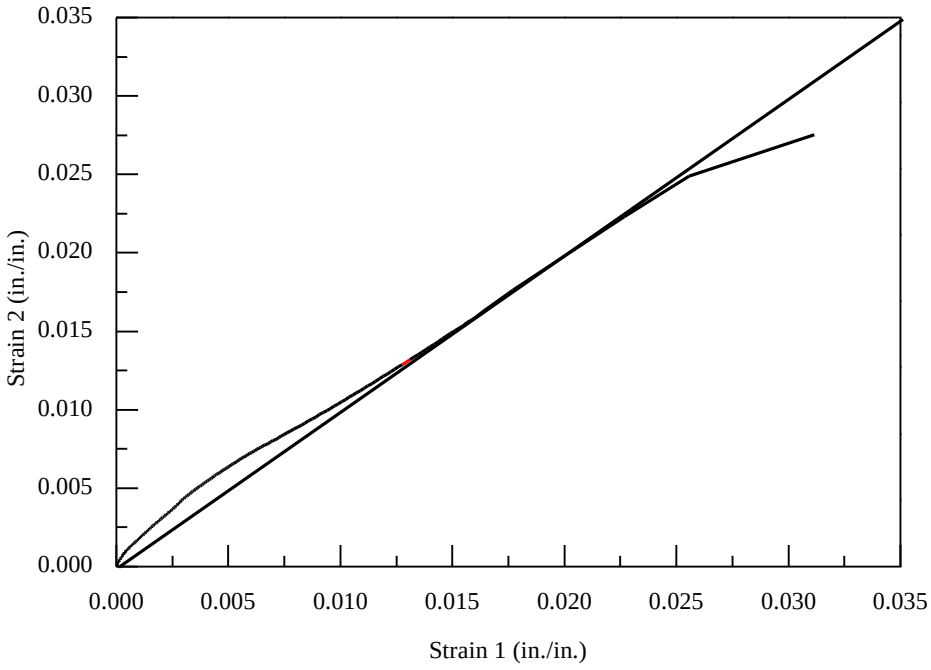

Figure II. 14. Strain 2 vs strain 1 of the coupon test (1).

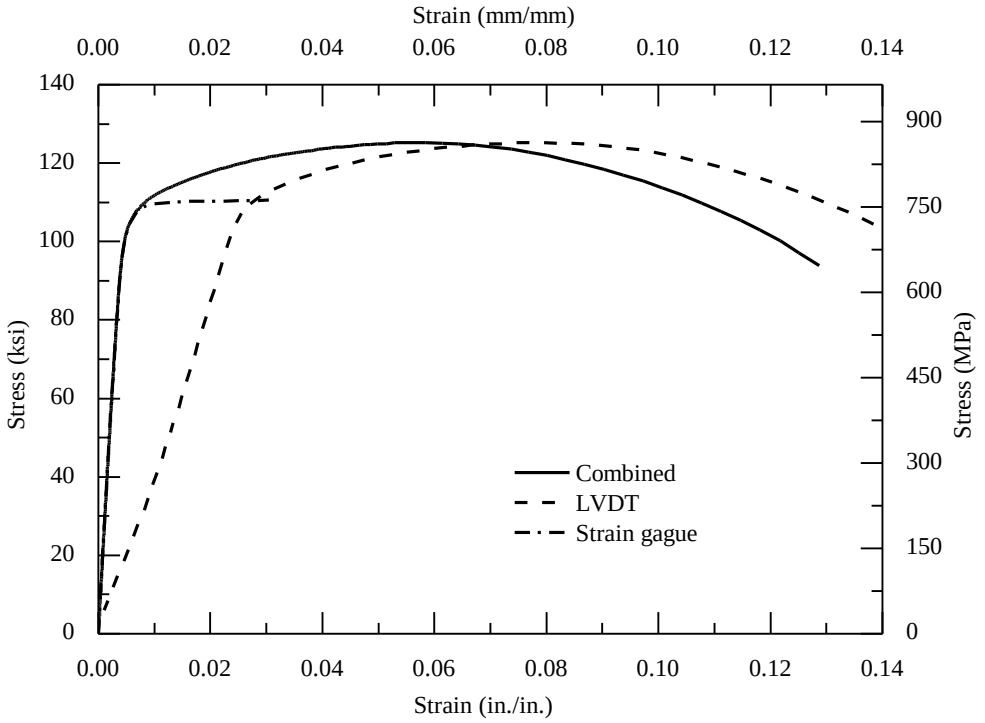

Figure. II.15 The stress-strain curves of the coupon test (2).

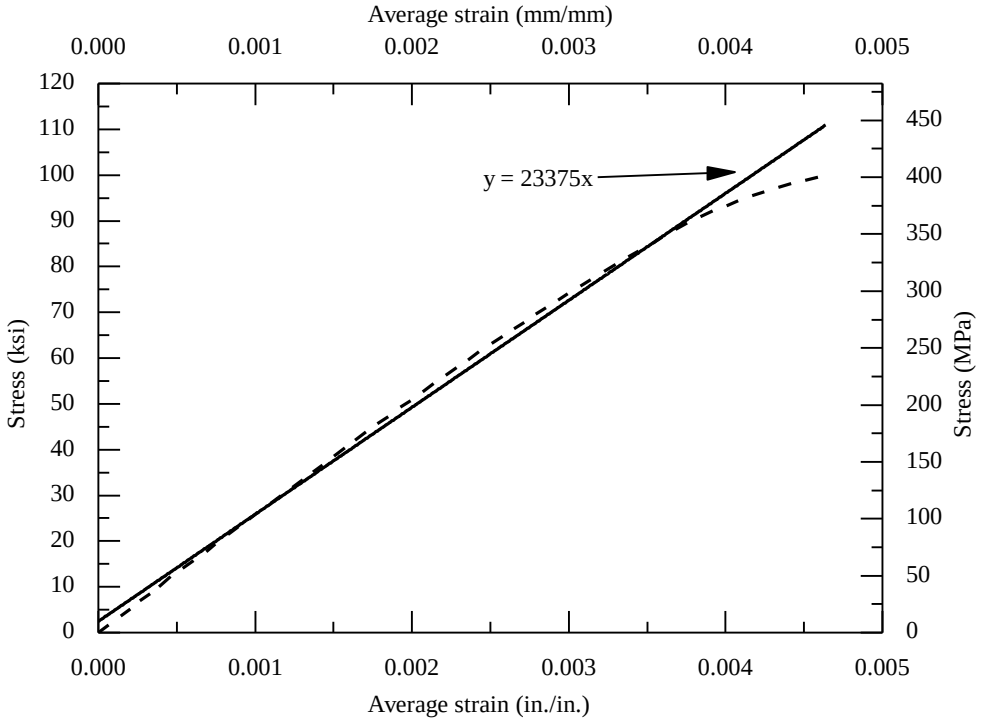

Figure II. 16. Stress vs strain curve (before yield strength) of the coupon test (2).

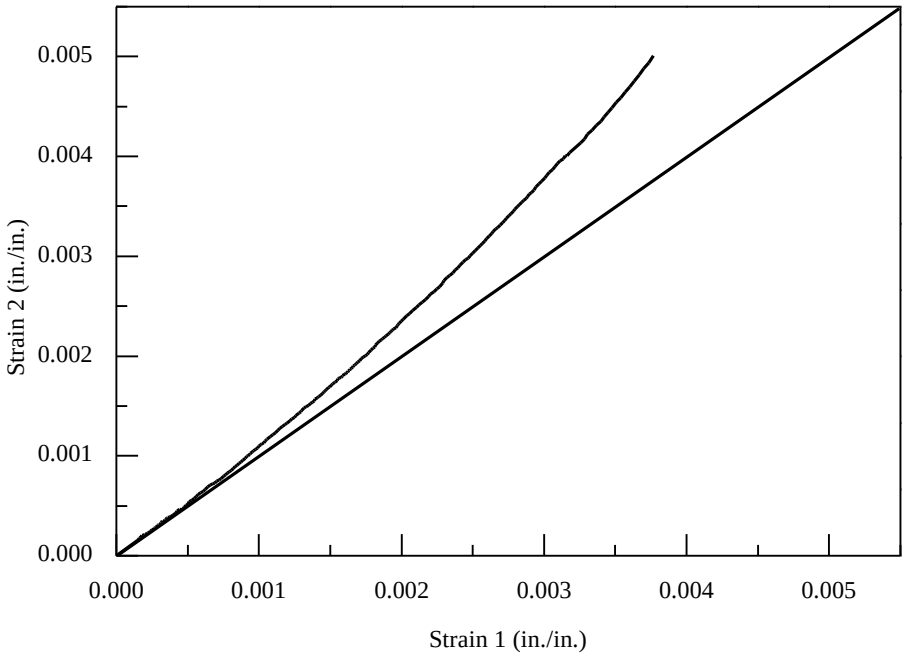

Figure II. 17. Strain 2 vs strain 1 of the coupon test (2).

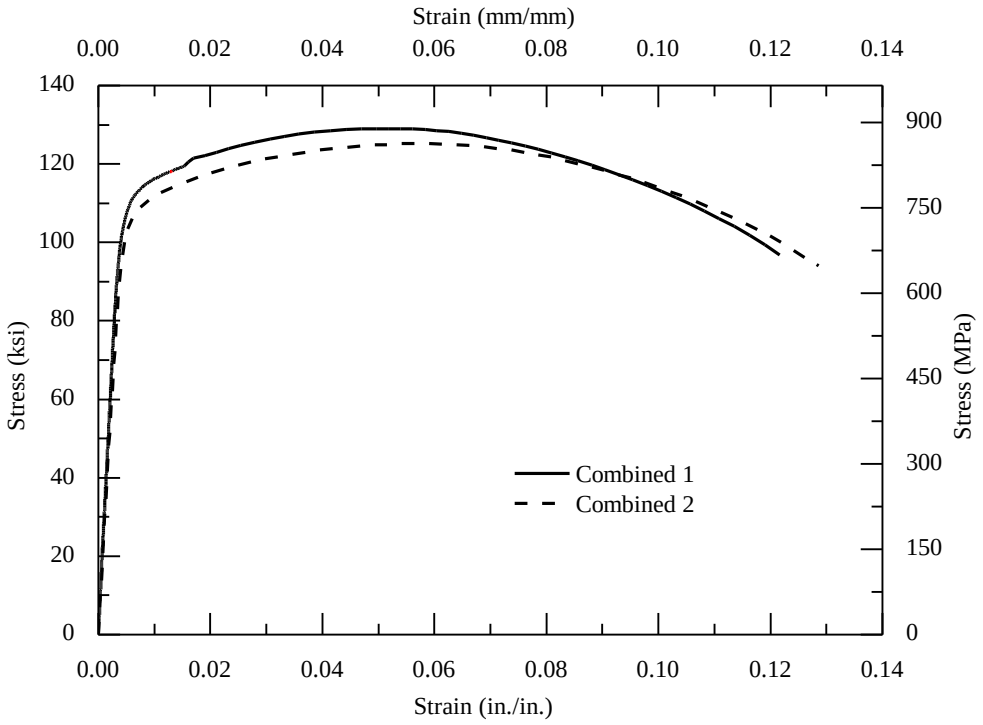

Figure. II.18. Compared stress vs strain curves.

Figure II.19. Tensile fracture surface of A193 anchor rod

Appendix III: Adhesive Materials

The adhesive for the tests in this study was a two-component vinylester adhesive. Tests were conducted for the adhesive material in both compression (ASTM D695-02a) and tension (D638-2a). The standard compression test calls for prism specimens with a dimension of 0.5×0.5×2 in [12.7×12.7×50.8 mm]. Considering the fact the hardened adhesive in adhesive anchors has a much smaller aspect ratio, additional prism samples were tested with a dimension of 0.5×0.5×1 in [12.7×12.7×25.4 mm] and 0.5×0.5×0.5 in [12.7×12.7×12.7 mm], cut from the standard specimen. Tensile specimens with a dimension of 0.25×0.75×4.5 in [6×19×115 mm] were fabricated based on Type IV coupons in ASTM D638-02a.

III.1 Specimen Preparation

The procedures of making the specimens were shown below before the description of the test results.

a. **Prepare aluminum prism mold**. Assembly the molds as shown in Figures III.1. Clean the molds and spray adhesive release agent (Type UNI-SOLVE from Smith and Nephew) on all faces of the molds.
b. **Dispense adhesive for prisms**. Start placing adhesive from the far end of the prism mold, as illustrated in Figure III.1. Move the injection nozzle backwards slowly while dispensing adhesive till the mold is full. This resembles the adhesive dispense process in a drilled hole. Use a putty knife (covered with the adhesive release agent) to press adhesive on the mold and remove the excessive adhesive, as shown in Figure III.2. Start from the far end of the prism; keep an acute angle between the knife and the prism surface; and minimize the number of passes. The working time for this step should be within 5 minutes under indoor

room temperature in this study. Remove the screws underneath the mold and the steel bars separating the prisms after 24 hours.

c. **Prepare plastic coupon mold.** Assembly the molds as shown in Figures III.3. Clean the molds and spray adhesive release agent (Type UNI-SOLVE from Smith and Nephew) on all faces of the molds. It is fairly difficult to create defect-free adhesive coupons; hence, the coupon mold has space for six coupons.

d. **Dispense adhesive for coupons**. Start injecting adhesive between grips of the coupon mold, as illustrated in Figure III.4a. The adhesive injection was same as that in making prism specimens. Alternatively, start depositing adhesive from the near end of the gage length and move the nozzle forward while dispensing adhesive. This may minimize gaps and air bubbles in adhesive within the gage length, which can be detrimental to the tensile tests. When adhesive reaches the other end of the gage length, fill adhesive on both ends of the mold (the grip regions). Use a Putty knife to press adhesive on the mold and remove excessive adhesive on the mold, as shown in Figure III.4b. minimize the passes, and observe the 5-min working time under indoor room temperature from the moment adhesive leaves the mixing nozzle to the end of this step. After 24 hours, remove the aluminum base. Use a heat gun to soften the plastic mold and separate the coupons carefully from the mold.

III.2 Compression tests

The adhesive prisms with three aspect ratios are shown in Figure III.5. The tests were conducted using an Instron Model 3369 loading frame, and the loading was applied under open-loop displacement control with a loading rate of 1.3mm/min [0.05in./min]. In addition to the built-in sensors, the displacement of the crosshead was measured using a Trans-Tek (Model 0345-0000)

linear variable differential transformer (LVDT), as shown in Figure III.6. A small precompression about 30 lbs [0.13 kN] was applied to the specimens before the test; hence, the LVDT measurements were deemed the same as the deformation of the prism specimens, from which the axial strains were calculated by dividing the displacement by the measured specimen heights. Two strain gauges (Gage 1 and Gage 2), mounted at the mid-height along the prisms, were used to measure the compressive strain of the specimens. An additional strain gage (Gage 3) was placed on top of Gage 2 to capture the dilation of the specimens, from which Poison's ratios were calculated. The applied compressive loads were captured using a Model THD-50K-Y load cell placed below the prism specimens, as shown in Figure III.6. The stresses were calculated from the measured load divided by the cross-sectional areas calculated from measured section dimensions (average of three measurements along the specimens). An IOtech data acquisition system was used to collect data from the LVDT, strain gages and the load cell with a sampling rate of 10 Hz.

The measured stress-strain curves are shown in Figures III.7, III.11, and III.15 for the prism specimens with an aspect ratio of 4:1, 2:1, and 1:1, respectively. The readings from Gages 1 and 2 are compared in Figures III.10, III.14, and III.18, and the average strains are shown in dotted lines in the stress-strain curves. Strains from Gage 2 are lower than those from Gage 1, especially for 1:2 and 1:1 prisms, indicating that slicing process may have produced a skewed face such that the prisms may be subjected to uneven loading. The uneven loading may have also come from unparallel loading plates, located both on top and bottom of the prism specimens as shown in Figure III.6. Due to the limitation of the strain gages and the adhesive used for attaching the gages, measurements of strains higher than 2% were deemed unreliable; hence, only the beginning portions of the presented stress-strain curves (in solid lines) are from strain gage readings up to a point corresponding to 45 percent of the measured peak stresses. This point was selected because

1) the stress and strain data up to this point was used to determine the elastic modulus of the materials as shown in Figures III.8, III.12, and III.16; 2) the stress-strain curves indicate that the two-part vinylester adhesive with quartz fillers is a brittle material, similar to typical concrete; hence, the use of 45 percent of the peak stress as the proportional limit is justified; and 3) the strains captured by Gages 1 and 2 approached the maximum useable value, especially for the 1:2 prism. Beyond the proportional limit, the strains of the presented stress-stain curves were calculated from the LVDT reading, shown in dashed lines in Figures III.7, III.11, and III.15.

The stress-strain relationships are compared in Figure III.19 and their failure modes in Figure III.20. All three specimens had a brittle failure. The failure of 1:4 prism was preceded by splitting (III.20a) while the 1:2 prism failed by shear failure a roughly 45-degree angle (III.20b), similar to concrete cylinders in Appendix I. The elastic moduli for these two specimens are similar to each other: 299.1 ksi [2060.8 MPa] from the 1:4 prism and 315.4 ksi [2173.1 MPa] from the 1:2 prism, which are close to the reported elastic moduli. The behavior of the 1:1 prism was affected the confinement from the steel loading plates: the specimen almost crushed (Figure III.20c) and the elastic modulus was 488 ksi [3362.3 MPa] (Figure III. 16).

It is thus recommended to use prisms with an aspect ratio of 1:2 instead of 1:4 at stipulated in ASTM D695-02a for compressive tests of adhesive with quartz fillers because the resulting material is a brittle material similar to concrete. For the adhesive material used in this study, the measured compressive strength (f_{ac}) was 11 ksi [75.8 MPa] and the modulus of Elasticity (E_a) was 315.4 ksi [2173 MPa]. The Poisson's ratio was between 0.375 and 0.4 from Figure III.13. This estimation is similar to that obtained from the test of 1:4 prism within the initial proportional limit, beyond which, the inelastic Poisson's ratio increases with an increase of the average compressive strain (Figure III.9). The results from the 1:1 prism is shown inn Figure III.17: with unknown

influence from the loading plate, the calculated Poisson's ratio grew past 0.5, which is not clear to the author.

III.3 Tension tests

The adhesive coupon is shown in Figure III.21. The tests were conducted using an Instron Model 3369 loading frame (Figure III.22), and the loading was applied under open-loop displacement control with a loading rate of 1.3mm/min [0.05in./min]. In addition to the built-in sensors, the displacement of the crosshead was measured using a Trans-Tek (Model 0345-0000) linear variable differential transformer (LVDT), as shown in Figure III.22. A small pretension about 10 lbs was applied to the specimens before the test; hence, the LVDT measurements were deemed the same as the deformation of the prism specimens, from which the axial strains were calculated by dividing the displacement by the gage length (114.3 mm [4.5 in.]). Two strain gauges (Gage 1 and Gage 2), mounted at a visually identified weak section instead of the mid-height, were used to measure the axial strain of the specimen. The applied tensile loads were captured using a Model THD-50K-Y load cell placed above the crosshead, as shown in Figure III.22. The stresses were calculated from the measured load divided by the smallest cross-sectional areas calculated from measured section dimensions (among three measurements along the specimens). An IOtech data acquisition system was used to collect data from the LVDT, strain gages and the load cell with a sampling rate of 10 Hz.

The measured stress-strain curve is shown in Figure III.23. The strains were average strains from Gage 1 and Gage 2, the readings from which are compared in Figures III.24. Again, strains from Gage 2 are lower than those from Gage 1, indicating potential uneven loading or unknown systematic error. The measured ultimate strength (f_{at}) was 2.31 ksi [15.9 MPa]. It should be noted that that total applied load 0.0836 kips [0.37 kN] was very small compared with the 50-kip [222.4-

kN] measurement range of the load cell; hence the load measurements may have been influenced by measurement noises.

The tensile behavior of the adhesive material can be characterized as elastic till fracture. As Figure III.25 shown, the modulus of elasticity is 316.7 ksi [2183.6 MPa], calculated from the peak stress and the corresponding strain. This is similar to the result of a. linear regression analysis as shown in Figure III.12. The adhesive material contains the quartz sand, which certainly cause discontinuity and stress concentrations. In addition, the air bubbles trapped in the material during the coupon making process may have worsened the situation.

Figure III.1. Inject adhesive into prism molds

Figure III.2. Remove excessive adhesive from prism mold

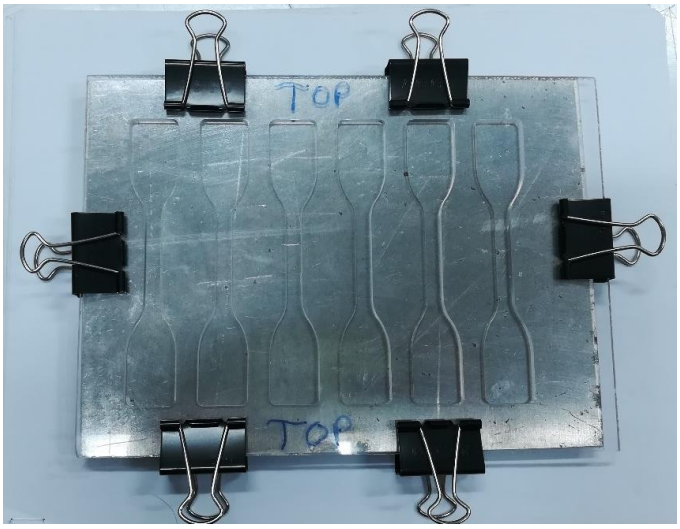

Figure III.3. Plastic coupon mold with aluminum base

a) dispense adhesive in coupon mold; b) compact adhesive and remove excessive adhesive

Figure III.4. Inject adhesive and remove excessive adhesive from coupon mold

Figure III.5. Adhesive prism specimens with three aspect ratios

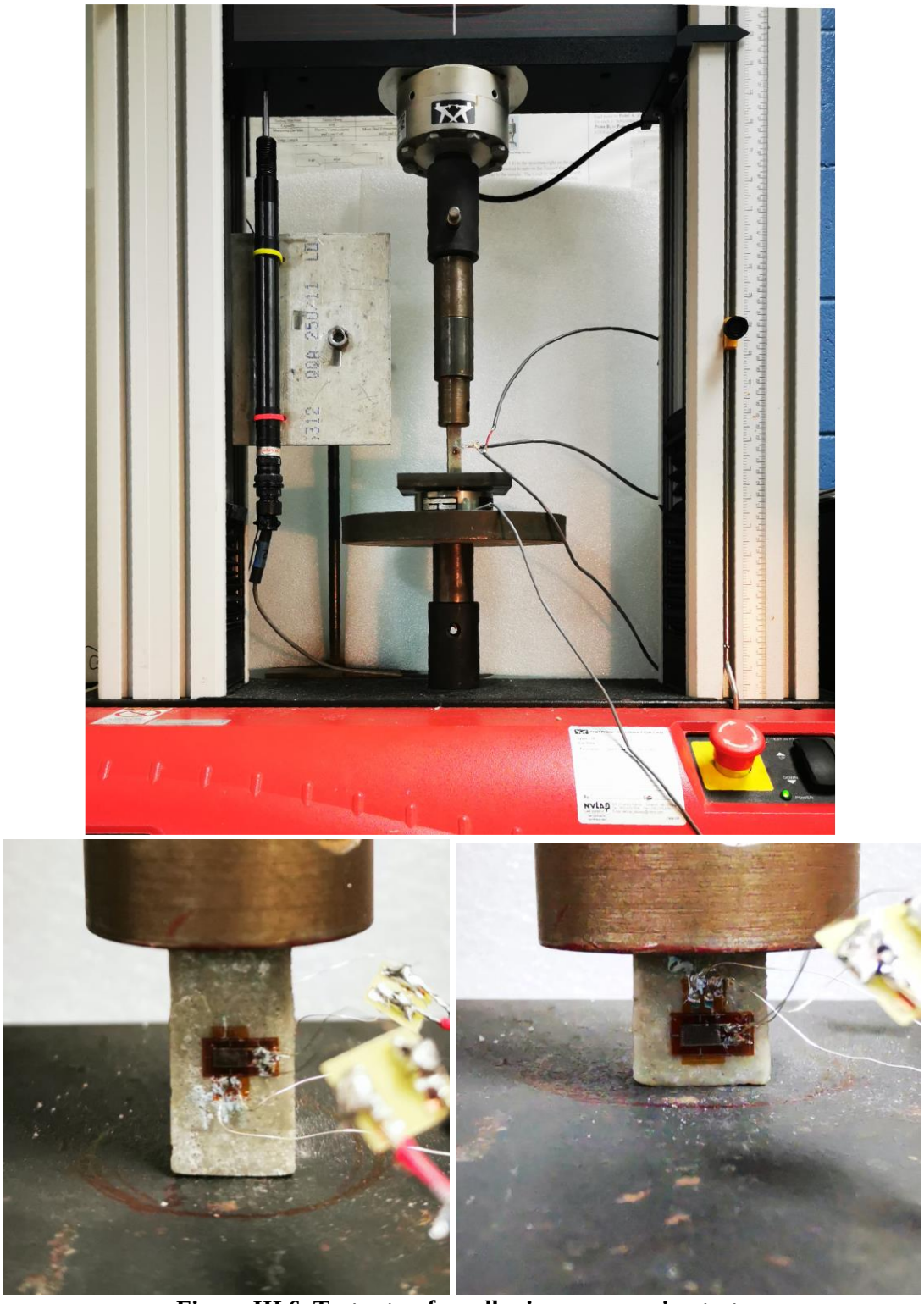

Figure III.6. Test setup for adhesive compression tests

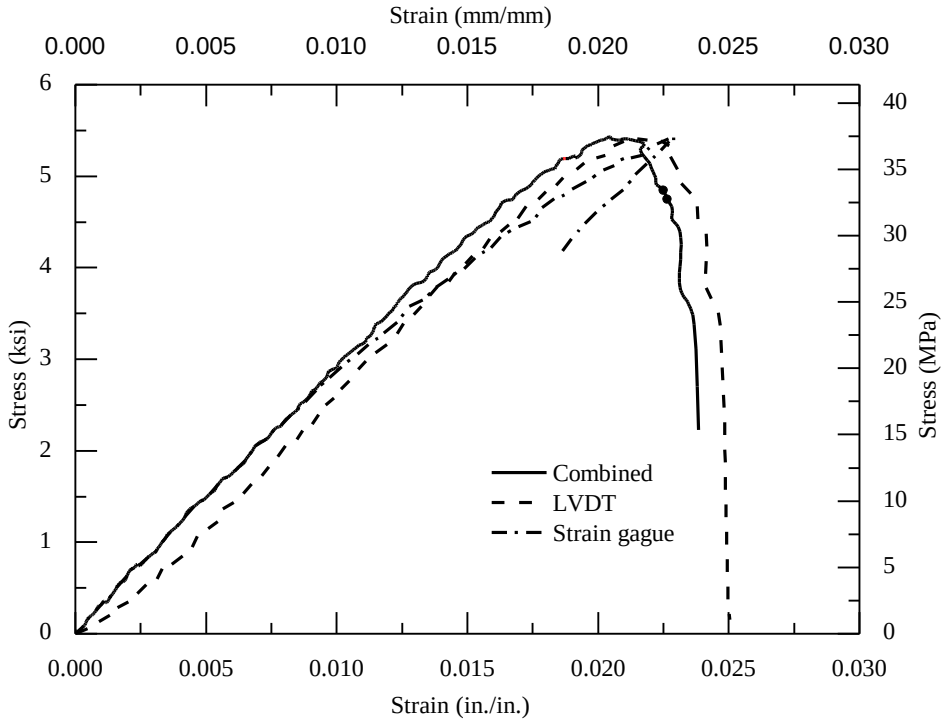

Figure III. 7. Stress vs strain curve of the prism (1:4).

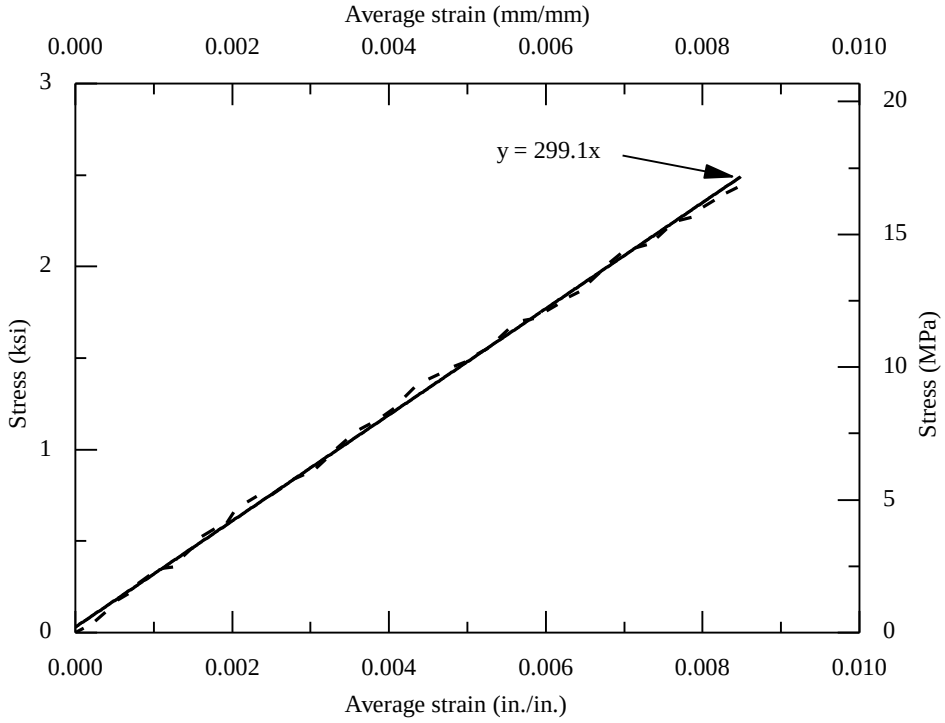

Figure III. 8. Stress vs strain curve (0 ~ 45%) of the prism (1:4).

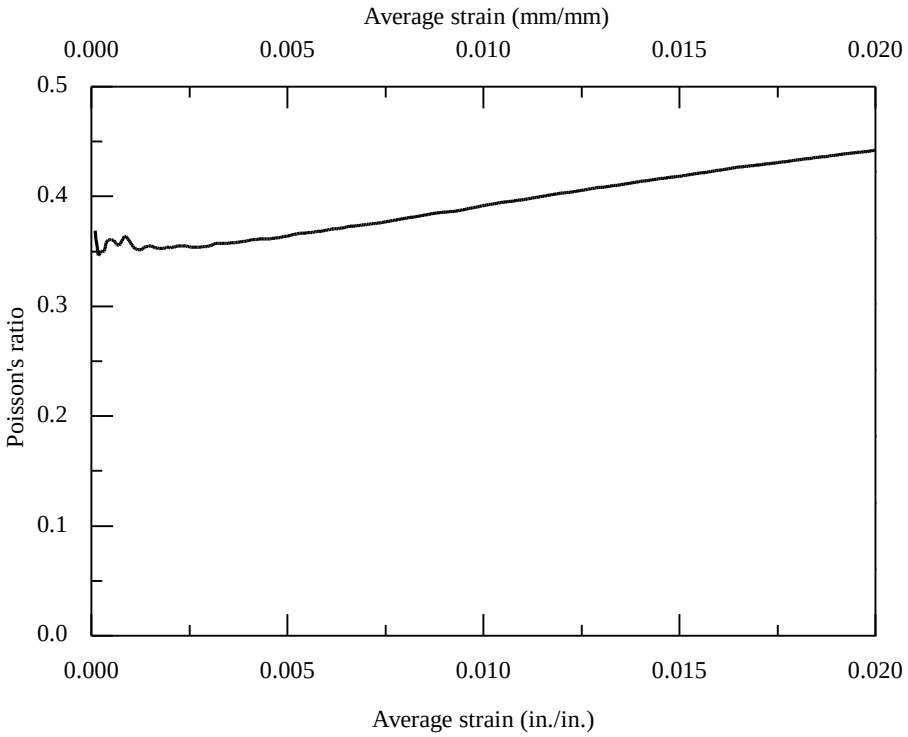

Figure III. 9. Poisson's ratio of the prism (1:4).

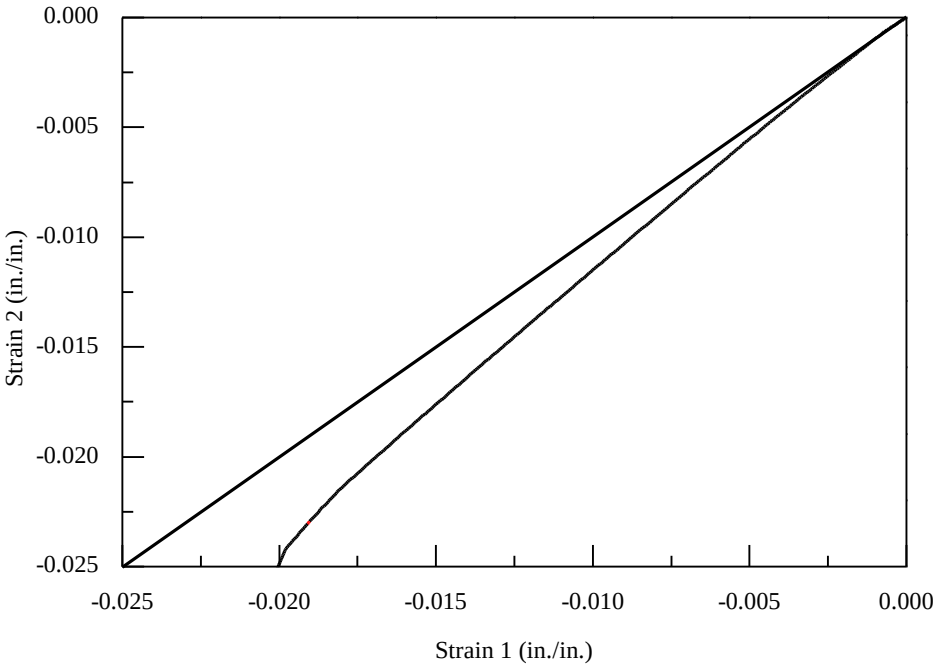

Figure III. 10. Strain 2 vs strain 1 of the prism (1:4).

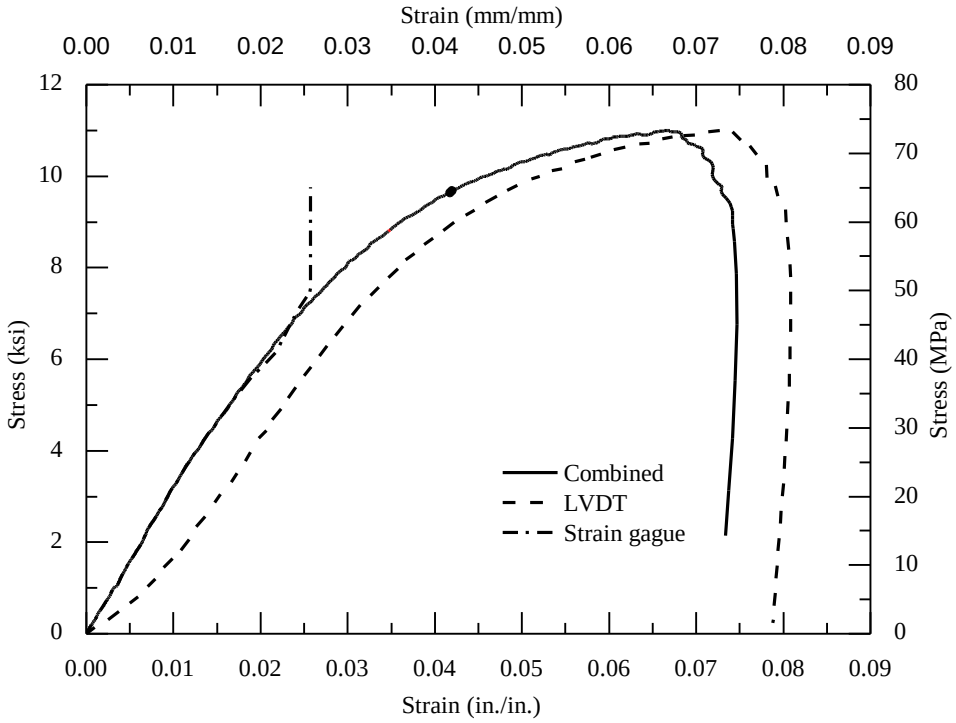

Figure III. 11. Stress vs strain curve of the prism (1:2).

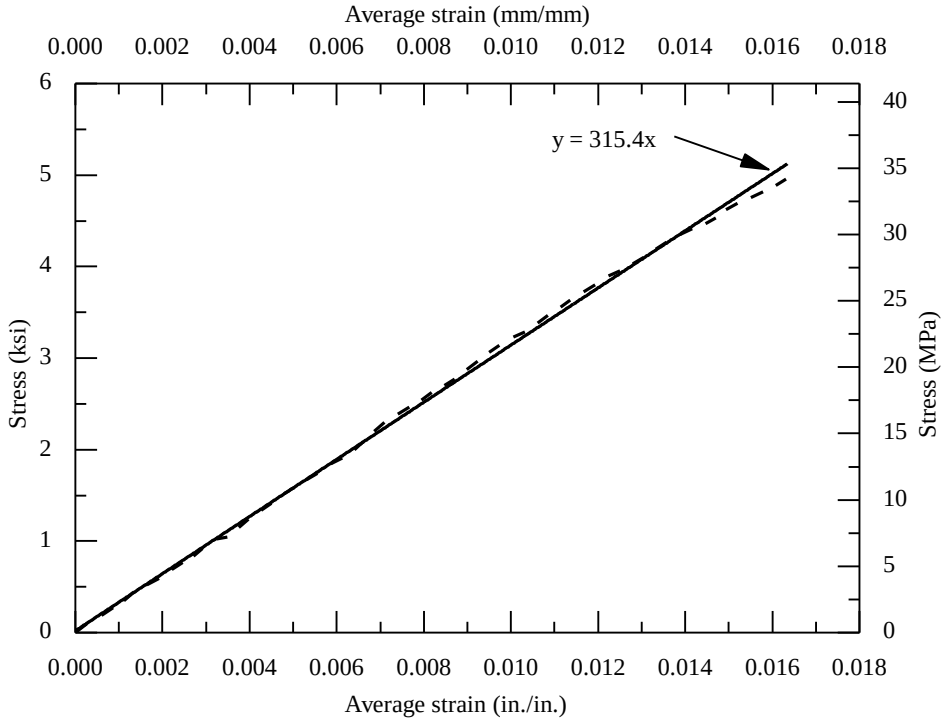

Figure III. 12. Stress vs strain curve (0 ~ 45%) of the prism (1:2).

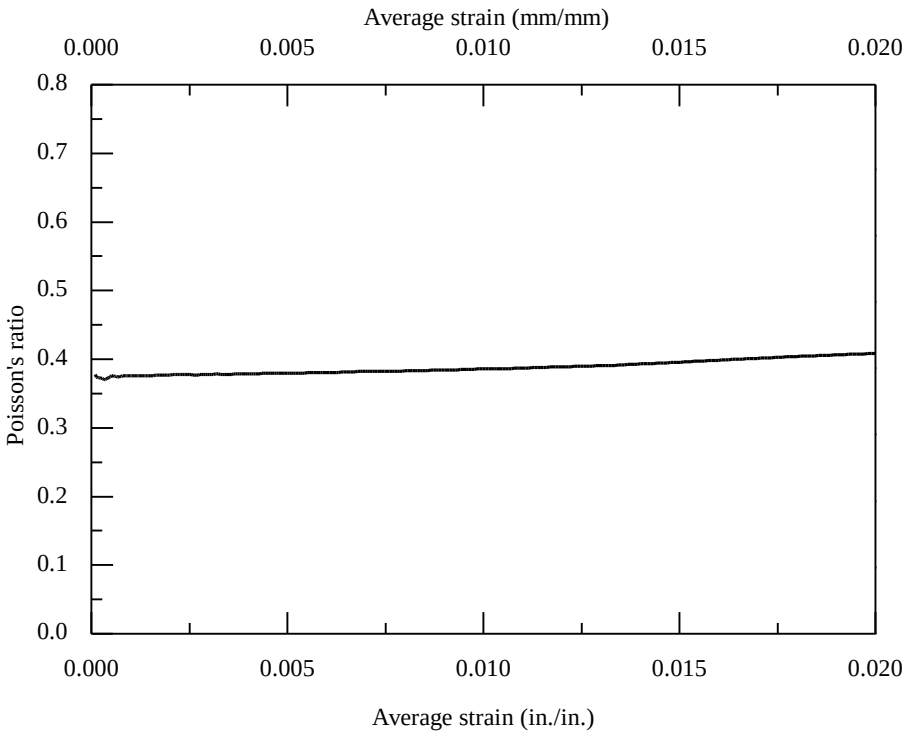

Figure III. 13. Poisson's ratio of the prism (1:2).

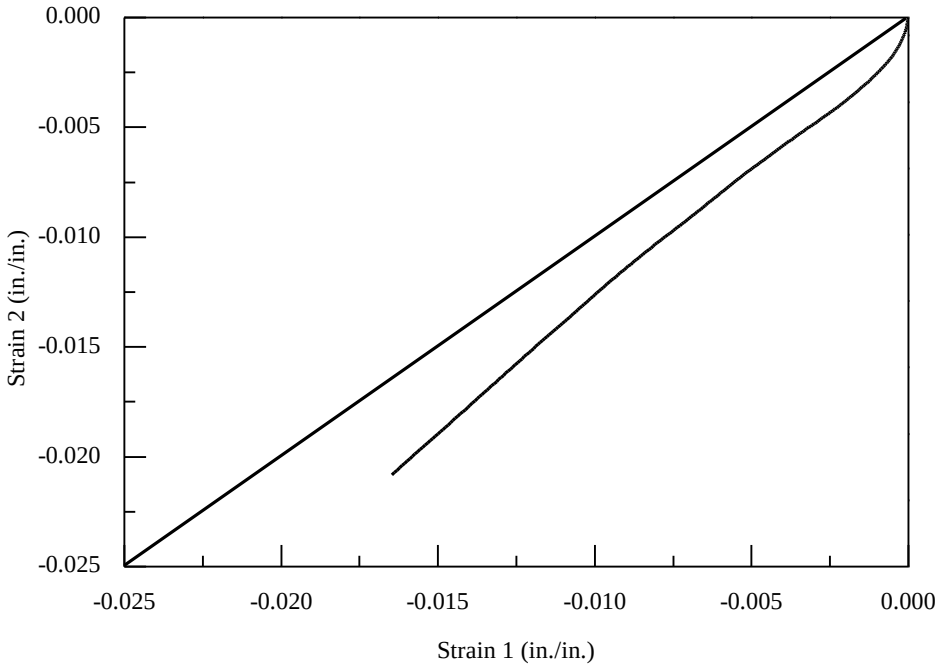

Figure III. 14. Strain 2 vs strain 1 of the prism (1:2).

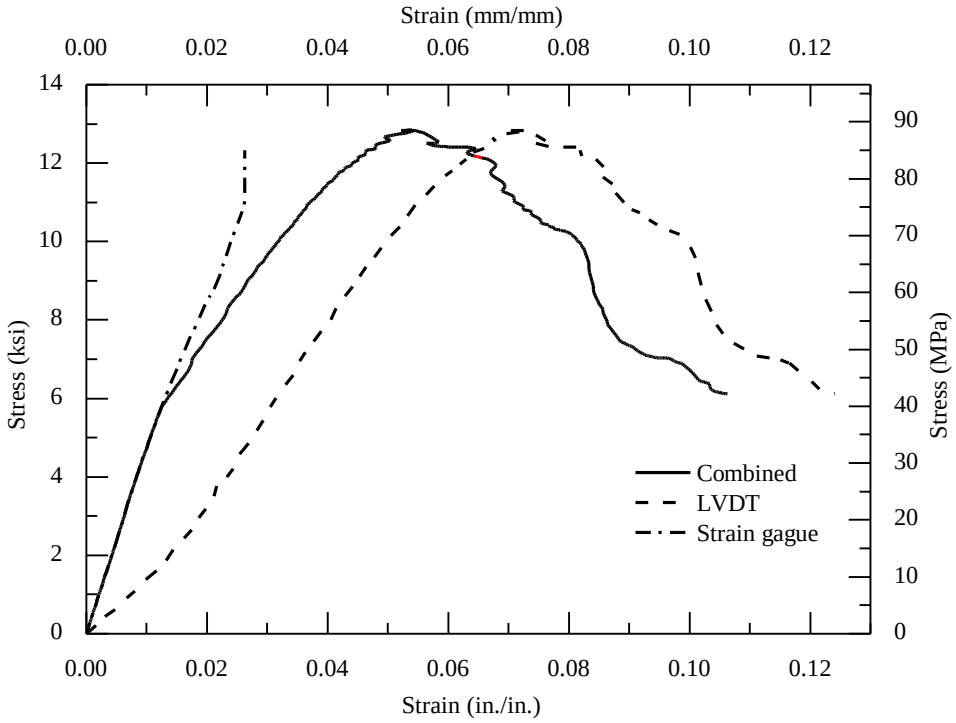

Figure III. 15. Stress vs strain curves of the prism (1:1).

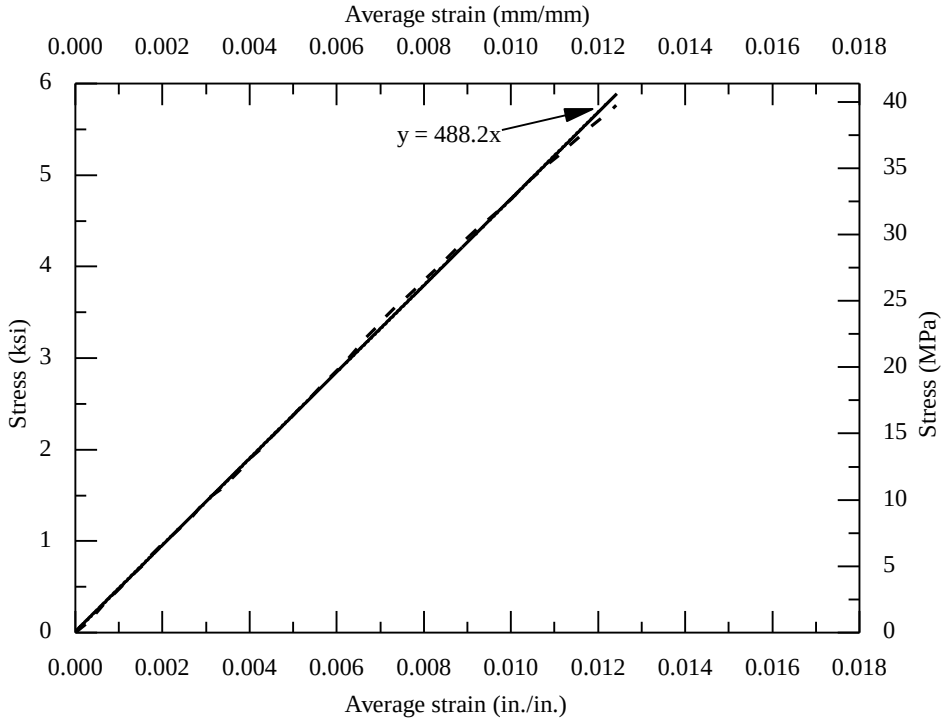

Figure III. 16. Stress vs strain curve (0 ~ 45%) of the prism (1:1).

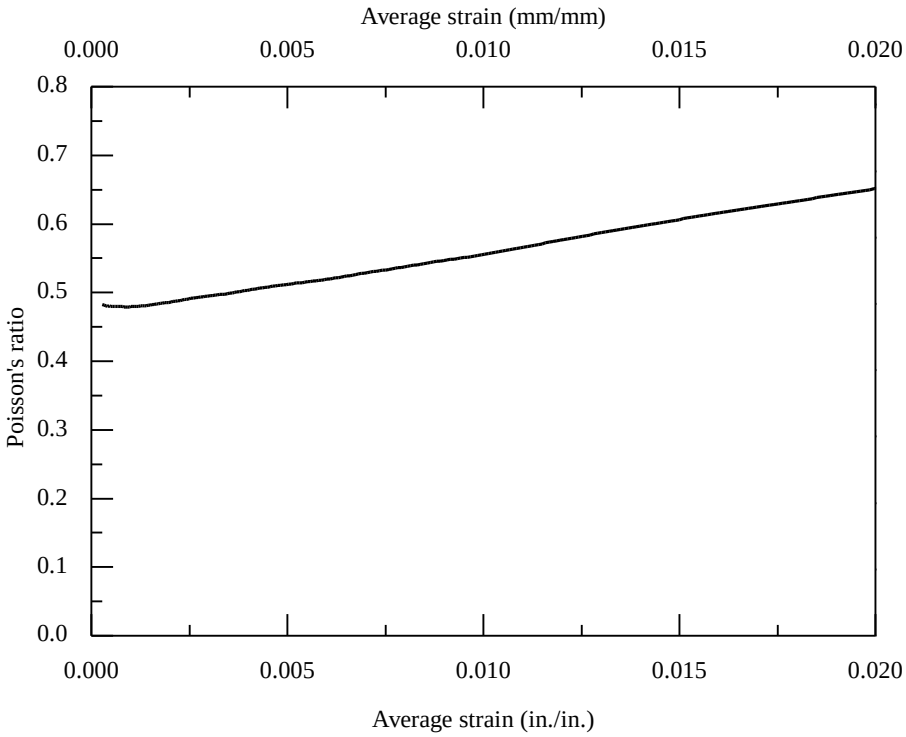

Figure III. 17. Poisson's ratio of the prism (1:1).

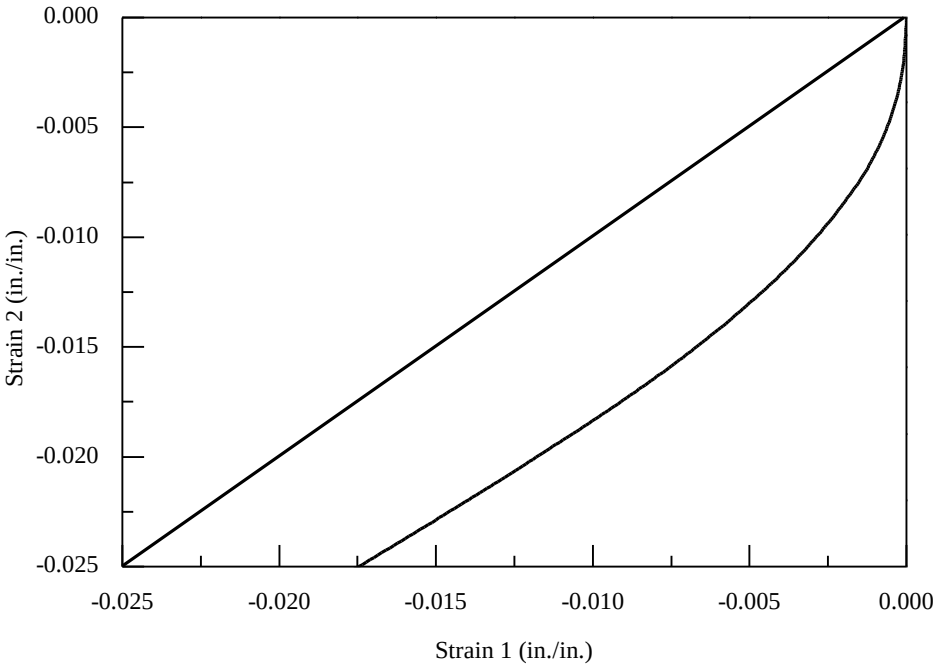

Figure III. 18. Strain 2 vs strain 1 of the prism (1:1).

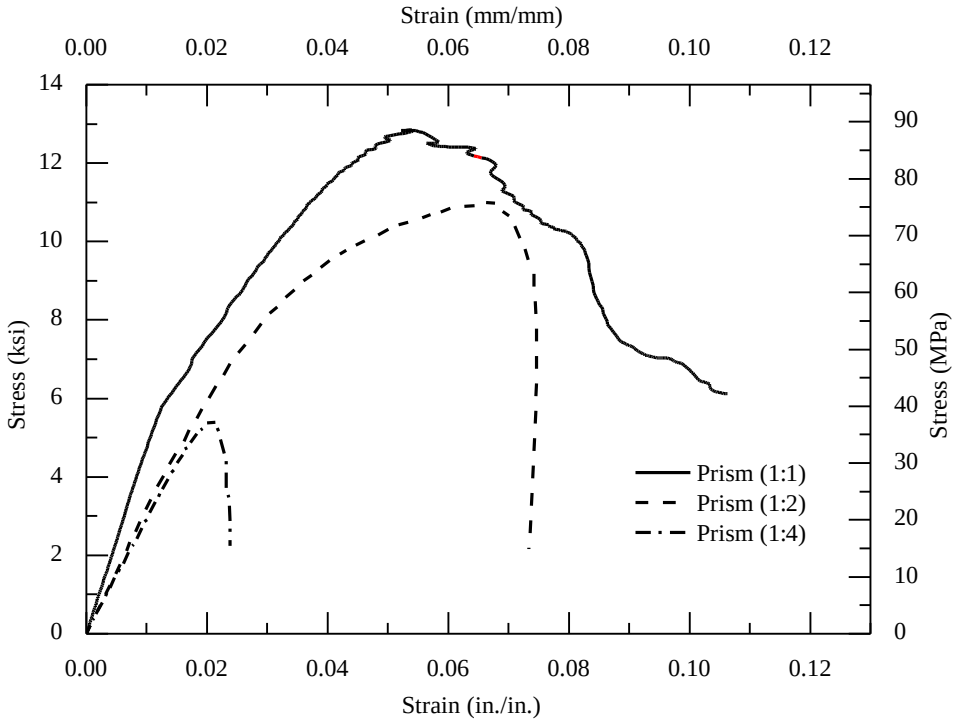

Figure III. 19. Compared stress vs strain curves.

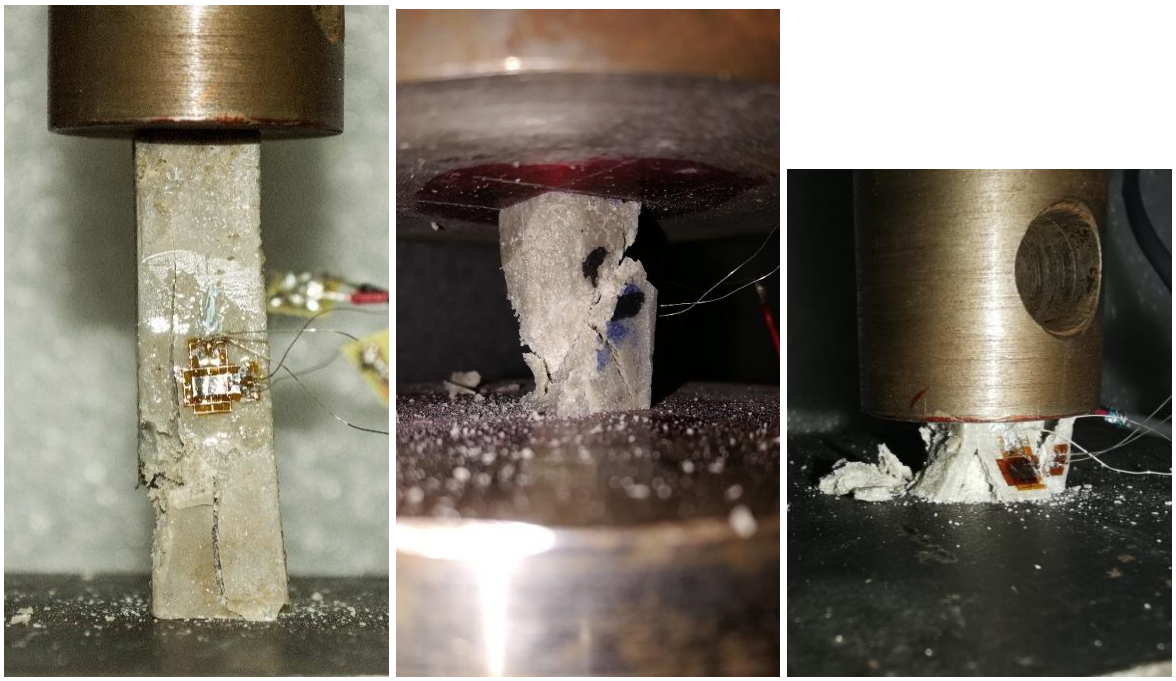

a) specimen with 1:4 ratio; b) specimen with 1:2 ratio; c) specimen with 1:1 ratio;

Figure III.20. Failure of adhesive prisms with different aspect ratios.

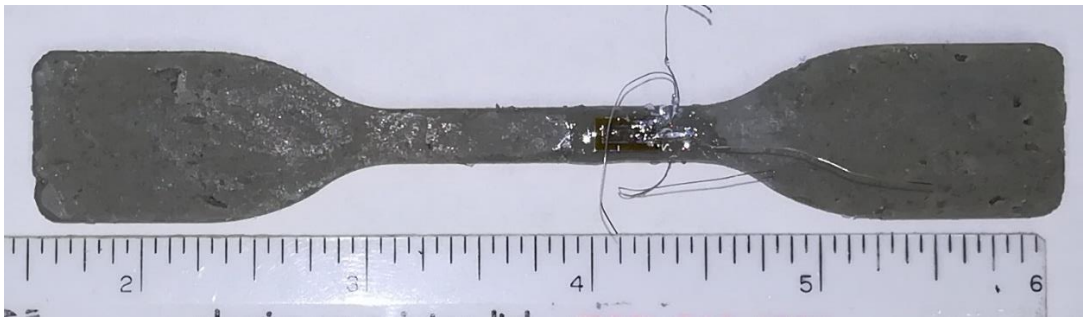

Figure III.21. Adhesive coupon specimen for tensile test.

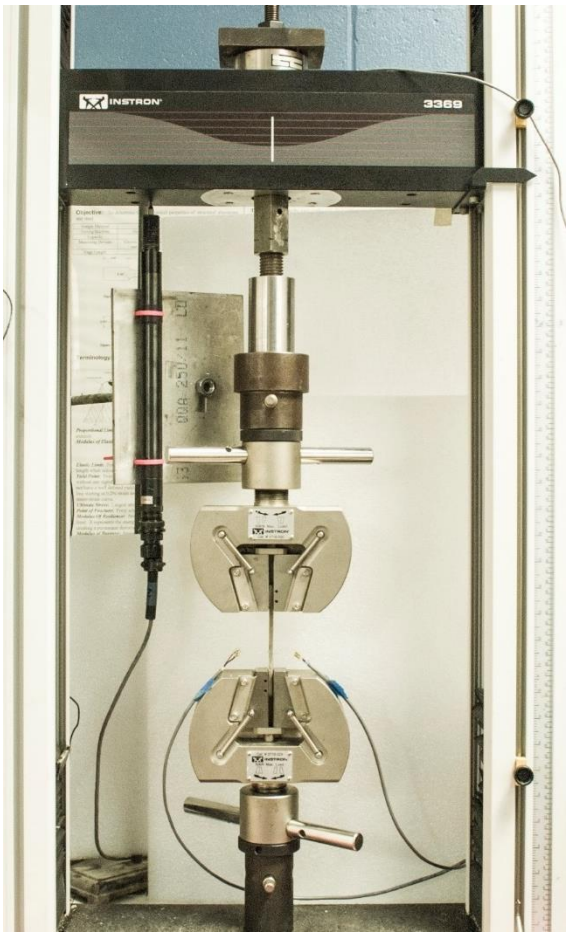

Figure III.22. Test setup for adhesive tension tests.

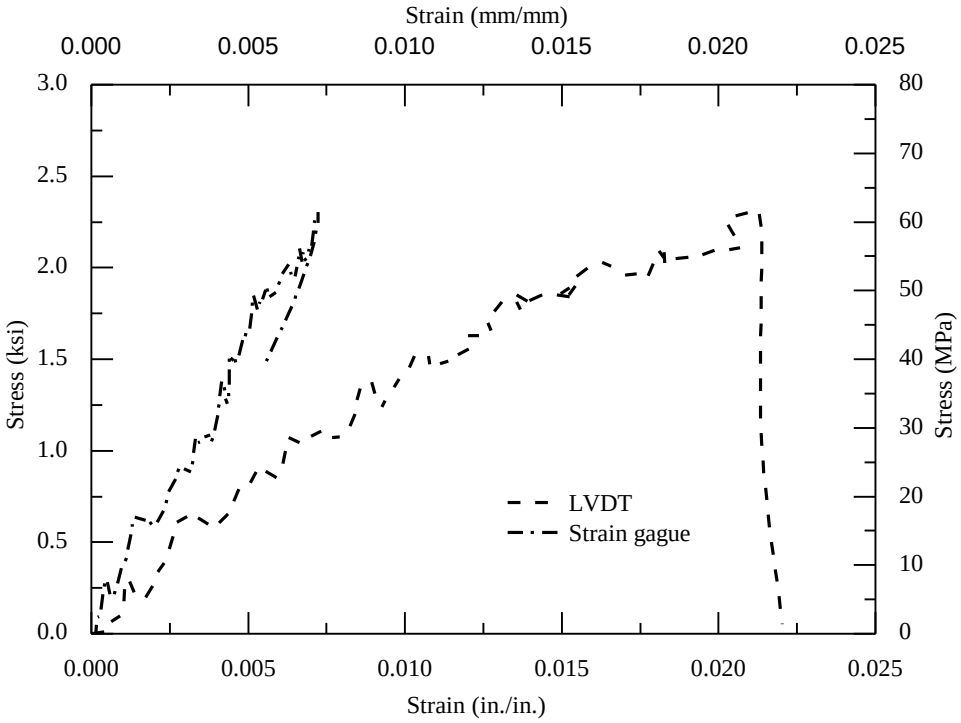

Figure III. 23. Stress vs strain curves of the coupon.

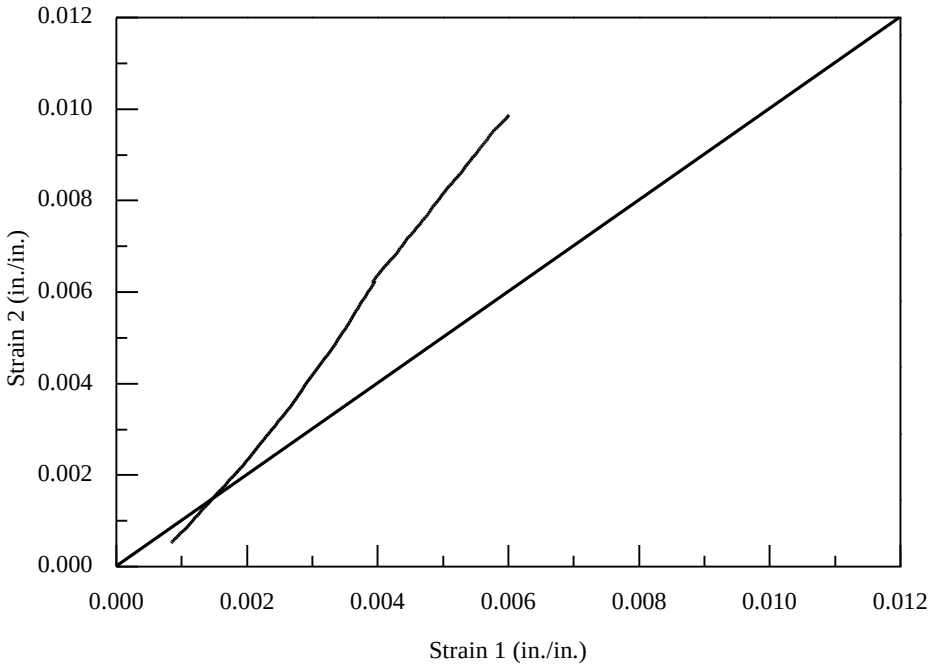

Figure III. 24. Strain 2 vs strain 1 of the coupon.

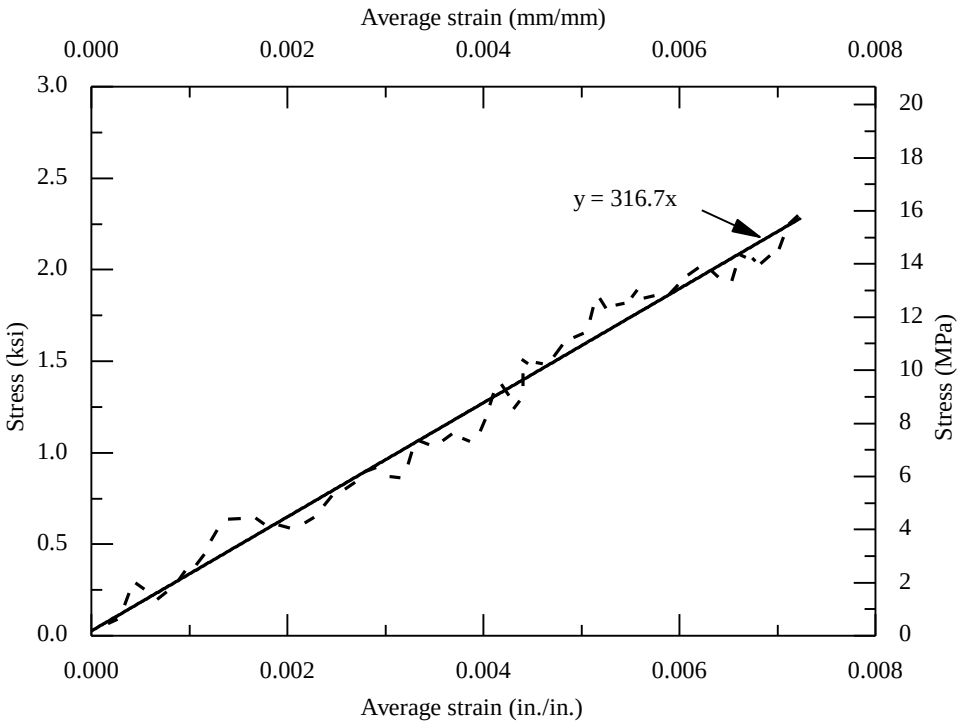

Figure III. 25. Stress vs strain curve (0 ~ 45%) of the coupon.

Appendix IV: Thread Abrasion of Screw Anchors

Blue tip screw anchors were used in this study to create threads in drilled holes. All screw anchors used in this study were purchased from a local Lincoln Contractors store. Because the single-use screw anchors were expected to function multiple times, a thread abrasion test was conducted for a 5/8-in. diameter screw anchor, as shown in Figure IV.1, randomly selected from the ordered stock.

Thread height measurements were recorded using a Kodak Contour Projector (Model No. 14-5) with NEWALL DP700-3 Axis Digital Readout shown in Figure IV.2. The measurement was from the thread crest to the bolt body. The screw anchor was placed on a metal holder and its location fixed by a steel block to prevent movement during the measurements, as shown in Figure IV.3. A total of four thread height measurements were made. The first measurement was taken for the unused bolt, and before each subsequent measurement, the screw anchor was driven into a 5-in. deep drilled hole in a concrete block using an impact wrench (See Appendix V) and was removed by using a hand wrench. The bolt location is marked on the hex head to ensure the subsequent measurements are at the same spot.

The heights of the first thread and the second thread from the blue tip were measured four times, as shown in Figure IV.4. The height of the first thread within the blue tip, (in hardened steel, known as the cutting tip) was reduced by 4.2 percent after the first use. An additional 2 percent reduction was observed after the second use. The cutting thread in a new screw anchor is sharp; however, the thread became blunt after the first use such that the thread abrasion after the second use was less prominent. Meanwhile, the thread of the cutting tip lost 20.8 percent of the original height. This is confirmed by the magnified image of the cutting thread inn Figure IV.5. With a worn

cutting tip, the screw anchor was difficult to be driven into the drilled hole during the third use. Hence, the screw anchors were used only twice in this study to create threaded holes. The abrasion of the second thread is negligible, as shown in Figure IV.4; however, this thread is not hardened for cutting threads. Hence, once the first thread was damaged, the bolt cannot be used anymore. A concrete tapping bit is needed with a tough cutting tip and an optimized cutting tip geometry.

Figure IV.1. A 5/8-in. diameter, 5-in. long screw anchor

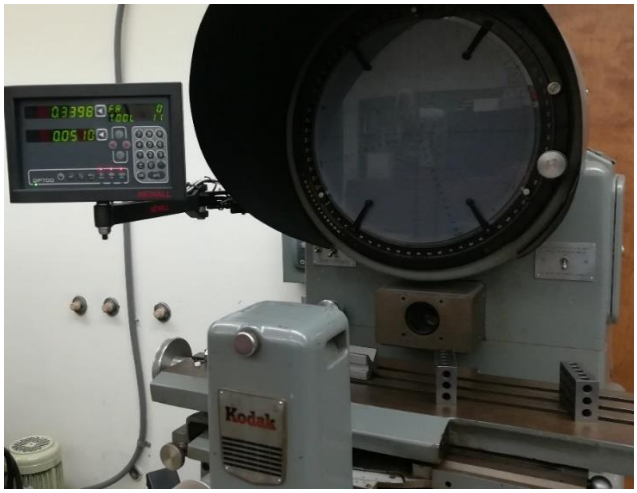

Figure IV.2. Kodak Contour Projector for thread height measurement

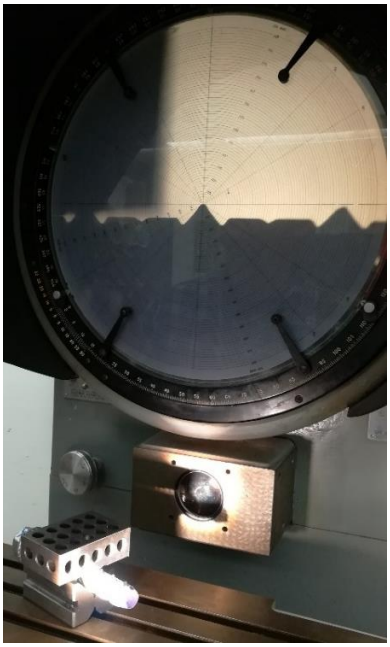

Figure IV.3. Measurement setup for thread heights (unused screw anchor)

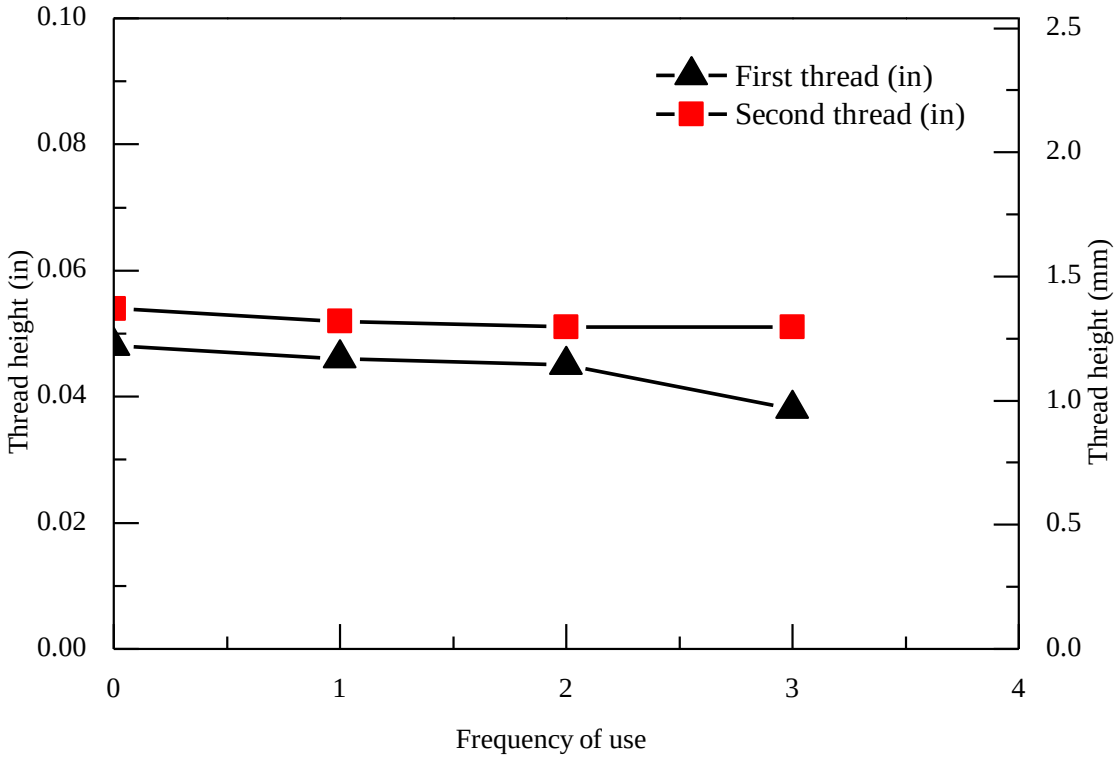

Figure IV.4. Thread abrasion measurements for a screw anchor

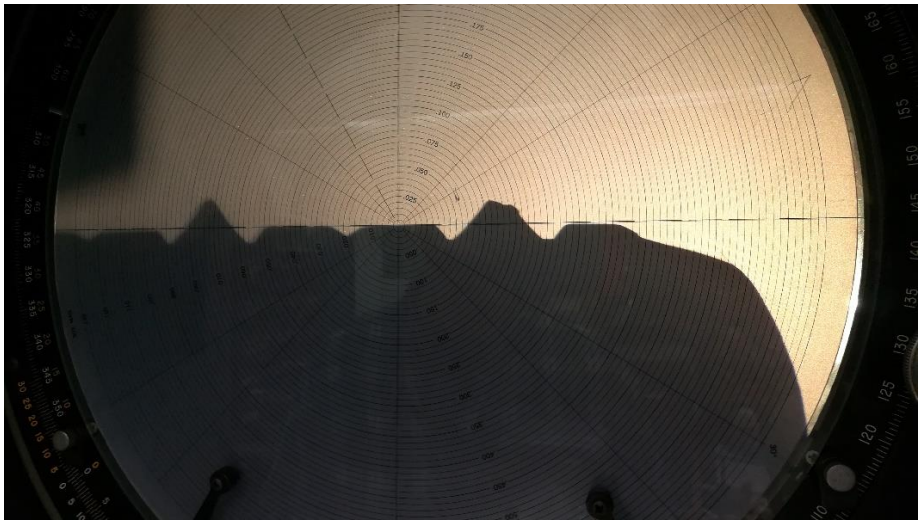

Figure IV.5. Thread profile of the screw anchor after the third use

Appendix V: Standard Installation Procedure of Adhesive Anchors

The following installation procedure is based on the Manufacturer's Printed Installation Instructions (MPII) for vinylester adhesive. The procedure can be divided into four major steps: 1) material preparation/handling; 2) hole drilling and cleaning; 3) adhesive placement; and 4) anchor installation and post-installation care.

1. **Select proper tools**. Proper drill bits and hole-cleaning brushes must be used following the requirements in the MPII. The tools are listed in Table V.1 for the anchors used in this study. The diameter of holes may impact the pullout capacity of adhesive anchors and the likely the failure surfaces, that is adhesive-steel anchor (AS) interface and/or adhesive-concrete (AC) interface. Although the impact has not been fully quantified in the literature nor in this study for adhesive anchors, tensile tests on adhesive lap joints has shown that the bond strength reduces with an increase in the bond line thickness (Afendi 2011).
2. **Use proper brushes listed in Table V.1 to clean the holes drilled in Step 3**. Note that brushes with relatively soft wires may not clean the hole thoroughly while those with hard wires may smooth the surface texture of drill holes, thus reducing the bond strength. Experiences have shown that brushes listed in Table V.1 for ½-in. holes are more effective in removing dusts than those for larger size holes. This may have been related to the relative rigidity of the steel wires as all brushes listed in Table V.1 are made from wires of the same size.
3. **Store adhesive cartridges according to the product instruction**. Storing adhesive in the refrigerator is not allowed. Opened adhesive cartridges should be capped and stored properly. In this case, it is reasonable to assume that the unfinished cartridges may have a similar shelf life as unopened ones.

4. **Prepare threaded rods**. The length of anchor specimens should be at least the required embedment depth plus 3 in. as the operation length. Saw-cutting may leave bent threads, as shown in Figure V.1, which may cause stress concentration at anchor-adhesive interface; hence bent threads at the end of anchor or along the embedded depth should be removed using a file tool and/or an angle grinder tool. Debris and dusts should be removed from the anchor rods using a metal wire brush. Use a paper/fabric towel to remove dust, oil, grease, or water if needed.
5. **Drill holes in concrete**. The anchors must be perpendicular to the concrete surface; hence the impact hammer drill is fixed to a drill jig as shown in Figure V.2. The drill jig has two steel pipe poles with a threaded end connecting to a steel base plate, and the hammer drill is fixed to a frame that moves along the poles. The desired drilling depth is measured from the base plate and marked on the drill bit using a masking tape, as shown in Figure V.2. The hole location is pre-marked on the concrete surface and dented using a metal center spot punch. Before placing the drill jig, remove debris on the concrete surface and the bottom of the drill jig plate to ensure the concrete surface is flat and the base plate does not have a gap from the concrete surface. The base plate must maintain full and stable contact with concrete during drilling. Adjust the base plate such that the drilled hole is perpendicular to the concrete surface local to the hole position. This is particularly important for anchors in confined pullout tests. After the bit is placed at the location, the operator shall stand on the base plate of the drill jig such that the drilling is straight downward. The impact of a slightly tilted hole to the behavior and pullout capacity of an anchor was not studied in details in this study though skew of less than 3 degrees can be negligible.

6. **Dust will pile up by the hole during drilling**. Start the hammer drill after putting pressure (e.g., from partial body weight) downwards and keep drilling without stop-and-check until the masking tape that marks the drill depth swipes the dusts off the base plate. Intermittent stops during drilling may create slightly curved vertical hole profile instead of a desired straight hole. The curvy hole profile may delay adhesive-concrete bond failure, which was critical to this study, as illustrated by Figure V.3 because the adhesive trapped in areas marked by arrows is likely subjected to compression during testing. Trial tests have shown that this may force the desired AC bond failure into AS bond failure. Stop the hammer drill and retract the bit with the hammer drill off. This step may also be important to this study because leaving the hammer drill on during bit retraction may create extra dents on the hole wall, which in turn may delay the desired adhesive-concrete bond failure. Drill holes shown in Figure V.7a are designated as holes with uncleaning in this study.
7. **Tap holes if needed.** This study includes some tests of anchors in threaded holes with a purpose to improve the reliability of adhesive-concrete bond behavior. This procedure starts after Step 5a. A concrete tapping bit is yet to be developed; hence, screw anchors were used to create threads in drilled holes in this study. The size of the screw anchors used in this study is listed in Table V.1. When using an impact wrench to drive a screw anchor into the drilled hole, put pressure using the operator's body weight in the beginning to start the threads. Keep tapping without stop-and-check till the screw anchor touches the bottom of the hole. Stop the impact wrench and remove the screw bolt manually. Use a hand wrench if needed. The resulting thread pattern is shown in Figure V.4. Note that the hardened tip of screw anchors gets worn off after tapping two 4-in. deep holes, as documented in Appendix IV.

8. **Clean drilled holes.** Drilled holes must be cleaned for adhesive to form bond with based concrete. The hole cleaning included blowing dusts followed by brushing and additional blowing (the industry blow-brush-blow procedure). MPII allows the use of compressed air from either an air compressor with a minimum pressure of 90 psi or a hand pump to blow dusts left in drilled holes. The anchors are less than or equal to ¾ inches in this study; hence a hand pump is allowed and a 25 fl. oz. hand pump from Powers fasteners was used, as shown in Figure V.5. Note that this study considers uncleaned and partially cleaned situations to study the sensitivity of anchors to hole cleaning according to ACI 355.4 (2011). The cleaning process used in this study is shown below:

    a) Use a vacuum with a nozzle (e.g., the same nozzle for adhesive dispense) to remove the dust and concrete debris left at the bottom of holes. This step replaces the first dust-blowing step documented in MPII because air blowing cannot completely remove dust left at the bottom of holes during the drilling process (Figure V.6), which may impact the final anchor embedment depths. In addition, dust in air may contain high levels of crystalline silica, which can be hazardous to installers. A threaded rod with the desired embedment can be used to verify the hole depth. The holes after this step are designated as partially cleaned, as shown in Figure V.7b.

    b) Use proper brushes listed in Table V.1 to clean the holes as shown in Figure V.5. Install the brush to a power drill, insert a brush briefly into to the drilled hole, and start the drill with full high-speed rotation. Push the brush to the back of the hole and pull it out right away. Repeat the brushing process four times according to the MPII. Note that alternating rotating directions during this brushing process may result in better results, however brushes rotating counterclockwise has shown to bring dusts up, which in turn

fills the clockwise threads created in Step 4; hence brushes shall be kept rotating clockwise in this step. Note that the wire brush may wear off; hence check the outside diameter of the brush periodically. Replace the brush when the wires are significantly bent, and the brush diameter is less than the values in Table1. Note that the brushing process may create vastly various hole conditions, as indicated in Figure V.7c. The brush wire stiffness was found critical to the cleaning results.

c) Extended the nozzle of a hand pump all the way to the back of a drilled hole and blow dusts (from Step 5b) out by pulling the piston all the way out and pushing it in quickly. Repeat this step four times according to the MPII. Compressed air can also be used in this step provided that the air nozzle is extended to the back of a drilled hole. The holes cleaned after this step are designated as fully cleaned. Cover cleaned holes with a masking tape till Step 6. Smooth holes and threaded holes are shown in Figure V.8. Note that smooth holes drilled with hammer drills may have accidental “defects,” as indicated by arrows in the figure (left side). Hardened adhesive within these large dents will create macro mechanical interlock, leading to increased AC interface bond. Sometimes they may impact failure modes of adhesive anchors. On the other hand, the threaded holes on the right side of Figure V.8 create systematic macro mechanical interlock.

d) The cleaning process is same as above for anchors in threaded holes. Insert a rod with the desired embedment to detect large debris generated from tapping the holes and/or brushing the tapped holes. Step 5a can be used one additional time at last if the hand pump or compressed air cannot remove the large debris.

9. **Inject adhesive into drilled holes**. This study uses a two-component vinylester adhesive anchoring system. Two-component adhesives start curing when the resin component and the hardener component are mixed together. The viscosity of the mixed system increases as time goes by while cross-links form within the material. Working with two-component adhesives needs attention on the following three time-constants:

    a) Gel time: Gel time is defined as the time it takes for a mixed resin system become so highly viscous that it can no longer be considered workable. The gel time is also the time for the polymer formation from starting of cross-linking to the point that if the polymer gel state is disturbed then the final polymer will not have well-established properties, such as adequate bonding strength or adhesion. The adhesive in vinylester adhesive has a gel time of 6 minutes in room temperature as shown in Table V.2.

    b) Curing time: The adhesive continues its cure from a gel to a solid state after the gel time. It is usually customary to specify a time when the adhesive reaches sufficient strength to be put into light operation such as fixture installation. The corresponding strength is often called working strength, which may be 60 percent of its final bond strength. The technical document for vinylester adhesive reports a “full curing time” of 45 minutes in room temperature in Table V.2. This time is viewed as the curing time in this study.

    c) Full cure time: The time the adhesive takes to build up to its full, final strength. According to ACI 355.4 (2011), tests are conducted on anchors allowed to cure for the curing time specified in the MPII plus an additional 24 hours.

Note that the cross-links form at a much faster speed in adhesive towards the end of the gel time. Hence, the working time for both anchor installation (from adhesive injection in Step 6b though

anchor placement in Step 7c) and the use of mixing nozzle is set at 5 minutes under indoor room temperature in this study. This is one minute less than the gel time reported by Powers fasteners (Table V.2) following online recommendations on general adhesive handling (Mereco, 2019). Note that the installed anchors shall not be disturbed, moved, handled after this working time. The adhesive injection process is shown below:

a) Put masking tape on the surface of concrete such that excessive adhesive can be easily cleaned later. The assisting lines are created from the center of the drill holes with a theoretical offset of a half anchor diameter, as illustrated in Figure V.9. To create the assisting lines, the right-angle corner of an Empire Polycast post level cut to 3 in. height was placed against a threaded rod inserted and centered in a hole. Mark the position of the level along two sides while a centered threaded rod rest on the corner of the level.

b) Prior to injecting adhesive into a drilled hole for the first time through a new mixing nozzle, dispense at least THREE strokes of adhesive through the mixing nozzle till the adhesive is in consistent gray color. Start the clock immediately for the 5-minute working time. The color difference of the gel in this initial dispense is illustrated in Figure V.10, where the darker and consistent color indicates gel is fully mixed. In addition, observations have shown that the two components mix gradually in the mixing tube as shown in Figure V.11. The adhesive further into the mixing tube is more completely mixed and the curing process progresses through Step 7. This part of adhesive thus should be discarded for new anchor installation to ensure consistent adhesive quality among all anchor specimens. Therefore, when working in between anchors, discard at least ONE stroke of adhesive through the mixing nozzle prior to injecting adhesive into a second drilled hole, after which, restart the clock for the next 5-minute working time.

c) Fill the hole half to two-thirds full (see Table V.3 for the number of full strokes needed for the anchors used in this study). The mixing nozzle must start at the bottom of the drilled hole. Slowly withdraw the mixing nozzle during injection. The withdrawing speed can be estimated based on the number of full stroked needed shown in Table V.3. Although all installation in this study is downward, operator still must avoid creating air pockets or voids during injection. Perform Step 7 immediately. Shortening the time for Steps 6 and 7 may reduce the uncertainties, leading to repeatable test results.

d) Filling the threads consistently is not easy due to the high viscosity of vinylester adhesive. In addition to the requirement that the mixing nozzle must start at the bottom of the drilled hole, a small counter-clockwise circling motion must be applied to the tip of the mixing nozzle to deposit additional adhesive in threaded holes, especially for 5/8-in. diameter and larger anchors. Slowly withdraw the mixing nozzle while keeping the circling motion during injection because the threads in drilled holes are clockwise.

10. **Install threaded rods**. The anchor placement process is shown below:

    a) Place the assisting post level in Step 6a at the location marked on the masking tape and use the left hand to hold the post level as shown in Figure V.12. Drop the rod in the hole against the right-angle corner of the post level using the left hand. Use the right hand to push the rod in while turning it clockwise to assist with adhesive distribution in threads. Twist the anchor continually into the hole until the cross-section of the anchor is the same height of the post level, which is 3 in. Adhesive must completely fill the annular gap at the concrete surface. Some adhesive should flow out of the hole and ALL around the anchor. The actual embedment depth can be determined based on the total length of the anchor minuses the remain of anchor above the concrete surface. Do NOT pull out an inserted anchor and replace it in any case.

    b) The assisting post level in Step 7a is to ensure proper anchor placement and to minimize skew. Do NOT perform minor adjustment of the anchor rod once it is in pace. The viscosity of vinylester adhesive is high, especially with the quartz fillers; hence the adhesive does not flow with anchor adjustments once it is in position. As a result, any adjustment may cause a gap between the anchor rod and the adhesive, thus weakening the AS interface, which was detrimental to the tests in this study.

    c) Briefly wipe most of the excessive adhesive on the concrete surface around the anchor rod. No need to completely clean the rod as this will be done before testing by peeling off the masking tape installed on the anchor rod in Step 2 and the concrete surface in Step 6a.

    d) Repeat Steps 6 and 7 for the next anchor. Observe the 5-minute working time, which is measured from the beginning of Step 6b to the end of Step 7c. Work fast because the shorter

the actual working time, the less disturbance to the cross-link formation within the adhesive, and the better chance to get consistent adhesive materials and bond properties.

11. **Cure adhesive**. For all installations the anchor element must be fully restrained from movement throughout the specified full cure time, where necessary through the use of temporary wedges, external supports, or other methods. Do not touch the anchor after the gel time. ACI 355.4 stipulates a minimum of 24 hours curing after the installation. The anchors in this study are allowed a minimum of 24 hours indoor curing before the fixture for testing was installed.
12. **Handle specimens**. Move concrete specimens with care. The anchor shall not be hit by tools and/or components during the installation of test equipment. To lock the aluminum beam that holds two LVDT's on to the test anchors, as shown in Figure V.13, use two wrenches to tighten the nut with a transition coupler. A transition coupler must be firmly attached to the testing anchor such that a loading rod can be used to apply tensile force to the anchor through a hydraulic jack. In addition, a small pre-load (arbitrarily 200 lbs in this study) can be applied before testing to minimize the initial slag in the testing system. The hut on the top of the plate washer is tightened for this purpose. Observe the maximum torque that can be applied to the anchor as listed in Table V.4 during the process. Use a torque wrench when possible. In order to apply 200-lb preload for a ½-in. anchor, the nut can be given an additional 1/6 turn from the snug tight position.

Table V.1: Equipment selection for the adhesive anchors in this study

Anchor dia. (da) (in.)	Drill bit type and size (in.)	Steel wire brush (cat. #)	Min. brush diameter (in.)
1/2	9/16	08285	0.60
1/2 *	5/8 WB	08275	0.67
5/8	3/4	08278	0.79
5/8*	3/4 WB	08278	0.79
3/4	7/8	08287	0.92

*: Anchors installed in threaded holes.

Table V.2: Recommended time constants for vinylester adhesive

Temperature of Base Material		Gel Time	Curing Time	Full cure time
◦F	◦C			
32	0	45 minutes	7 hours	24 hours
41	5	25 minutes	2 hours	
50	10	15 minutes	90 minutes	
68	20	6 minutes	45 minutes	
86	30	4 minutes	25 minutes	
95	35	2 minutes	20 minutes	
104	40	1.5 minutes	15 minutes	

Table V.3: Recommended number of full strokes to fill the anchor holes ½ to 2/3 full

Anchor dia. (in.)	Depth of holes (2 in.)	Depth of holes (3 in.)	Depth of holes (4 in.)	Depth of holes (5 in.)	Depth of holes (6 in.)
1/2	1	1	1.5	2	2
1/2*	1	1.5	2	2.5	3
5/8	1.5	1.5	2	2.5	3
5/8*	1.5	2	3	3.5	4
3/4	2	2.5	3.5	4	5

*: anchors installed in threaded hole.

Table V.4: Maximum torque on adhesive anchors

Threaded rod diameter (in.):		1/2	5/8	3/4	7/8	1
Maximum torque (only possible after full cure time of adhesive) (ft-lbs.)	A36 or F1554 carbon steel rod	25	50	90	125	165
	ASTM A193, Grade B7; B8/B8M2 Class 2B	33	60	105	125	165
	ASTM A 193 Grade B8/B8M Class 1	20	40	60	100	165

Figure V.1. Bent threads on an anchor rod.

Figure V.2. A drill jig to control drilling direction

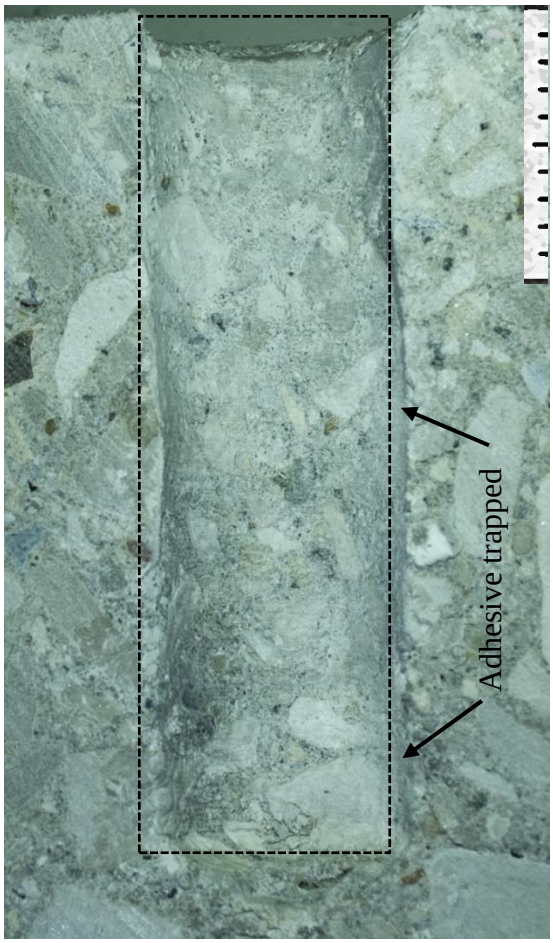

Figure V.3. A drilled hole with curvy wall profile

Figure V.4. A tapped hole and the threads formed in hardened adhesive

Figure V.5. Hole cleaning with a hand pump air blower and a wire brush

Figure V.6. Dust left at bottom of hole after cleaning using compressed air at the top

a) uncleaned holes after drilling in Step 3 (7/8”, 3/4", 5/8”, and 9/16” from left)

b) partially cleaned holes after vacuuming in Step 5a (7/8”, 3/4", 5/8”, and 9/16” from left)

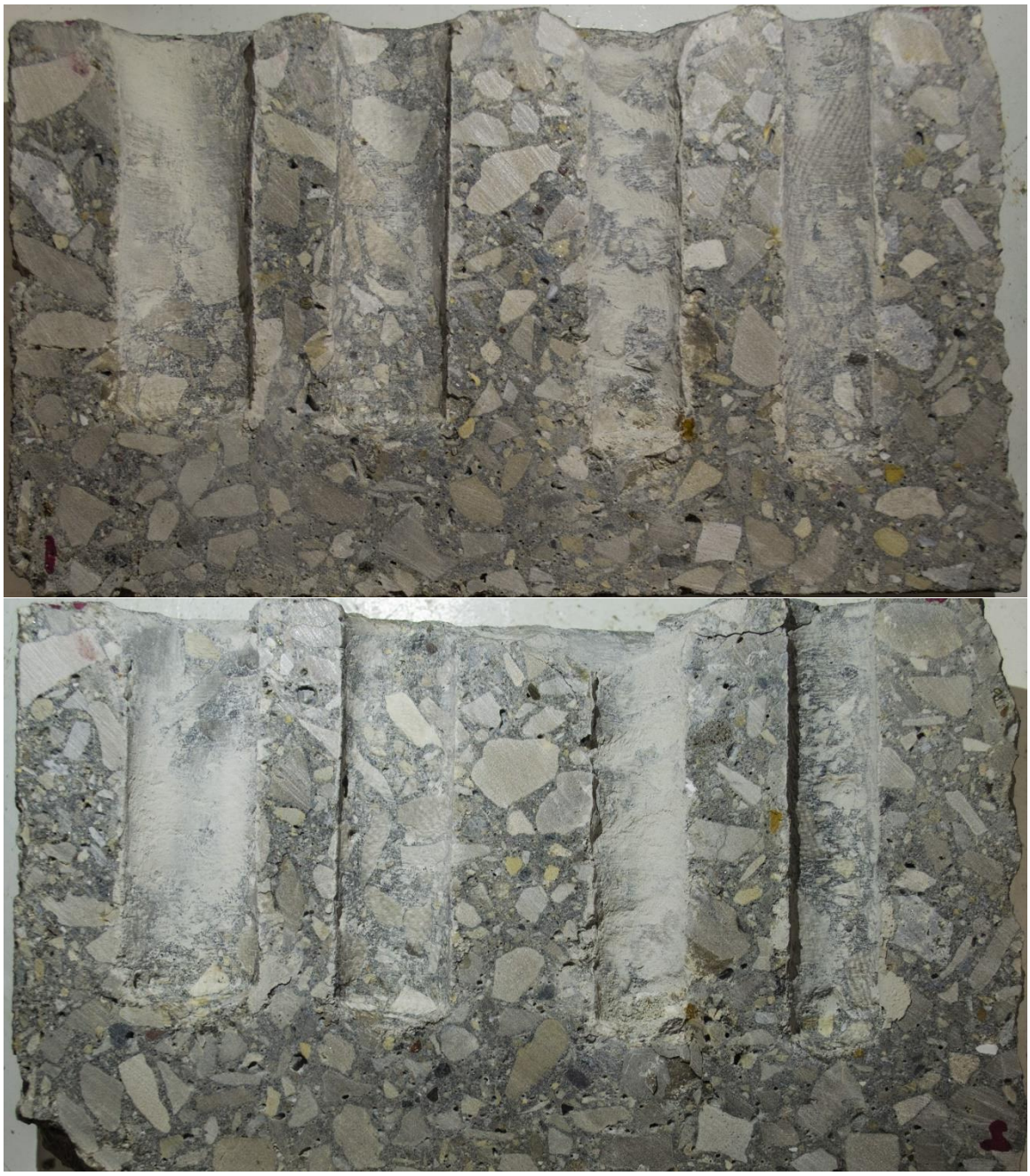

c) fully cleaned holes after cleaning in Step 5c (7/8”, 3/4", 5/8”, and 9/16” from left)

Figure V.7. Drilled holes after various cleaning process shown in two half concrete (Note: the images of the second halves are flipped to align the hole positions)

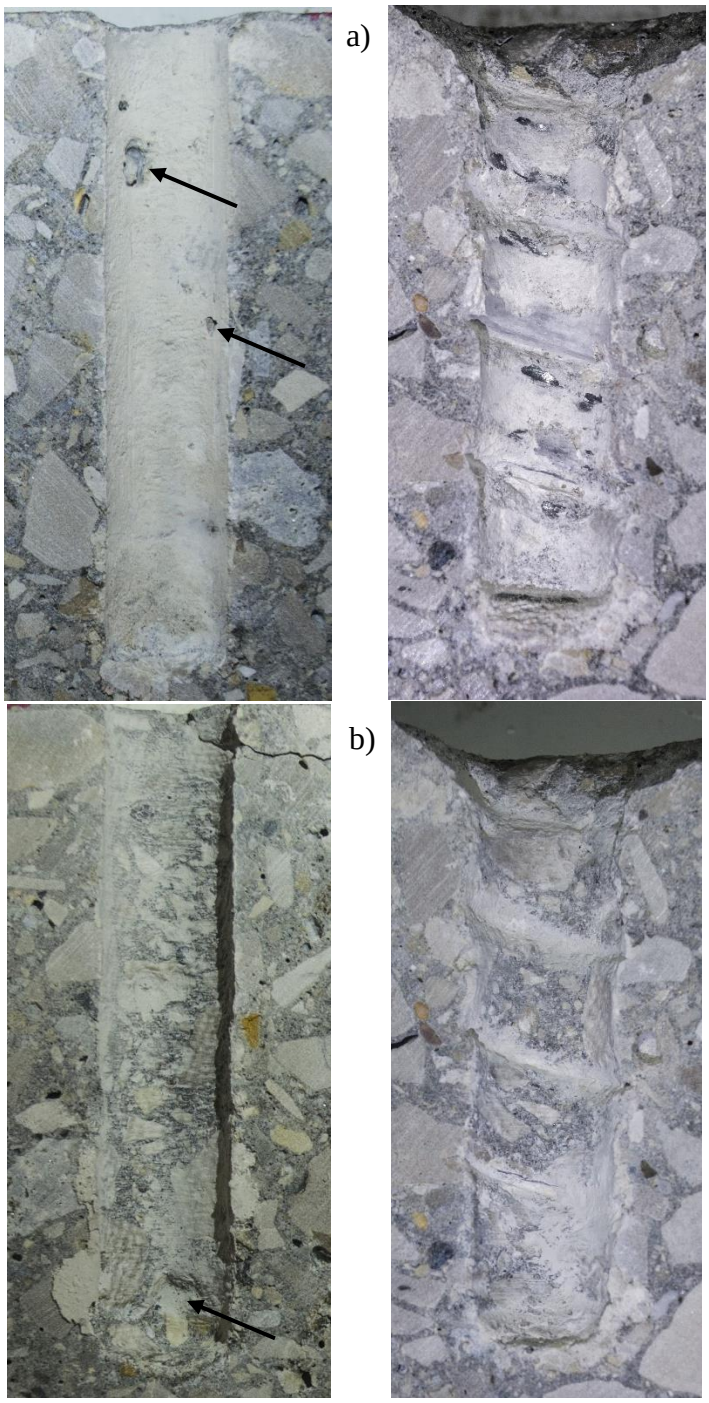

Figure V.8. partially cleaned holes (top) and completely cleaned holes (bottom) (Note the arrows on the left side indicate dents in drilled holes)

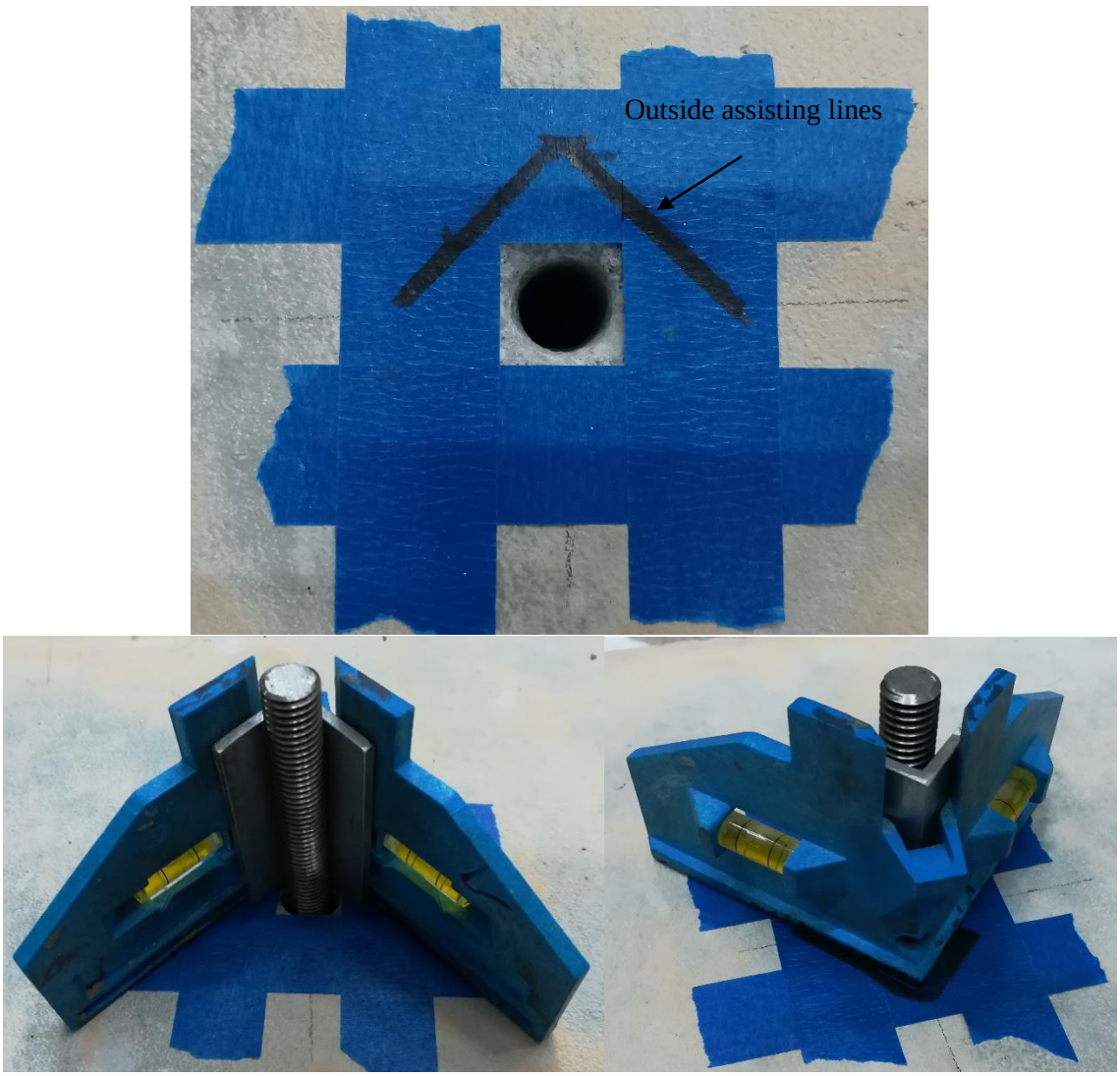

Figure V.9. Assisting lines for anchor placement

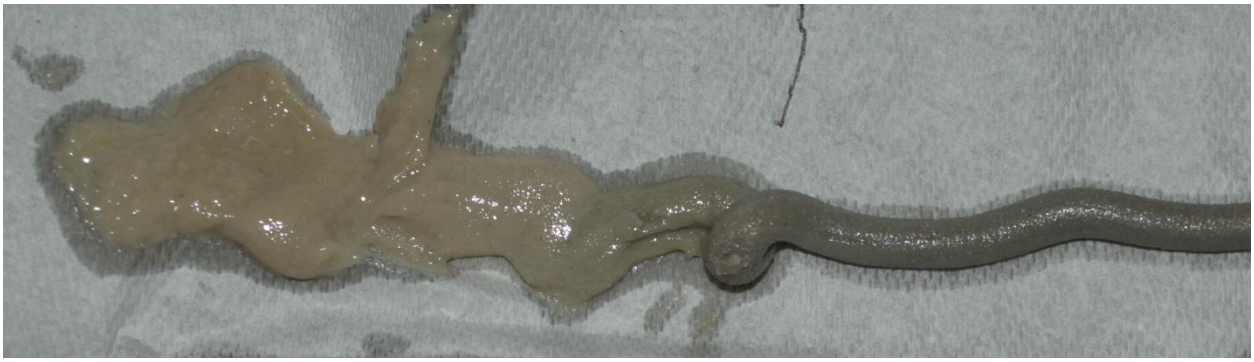

Figure V.10. The color differences of the adhesive

Not yet mixed Partially hardened Fully cured

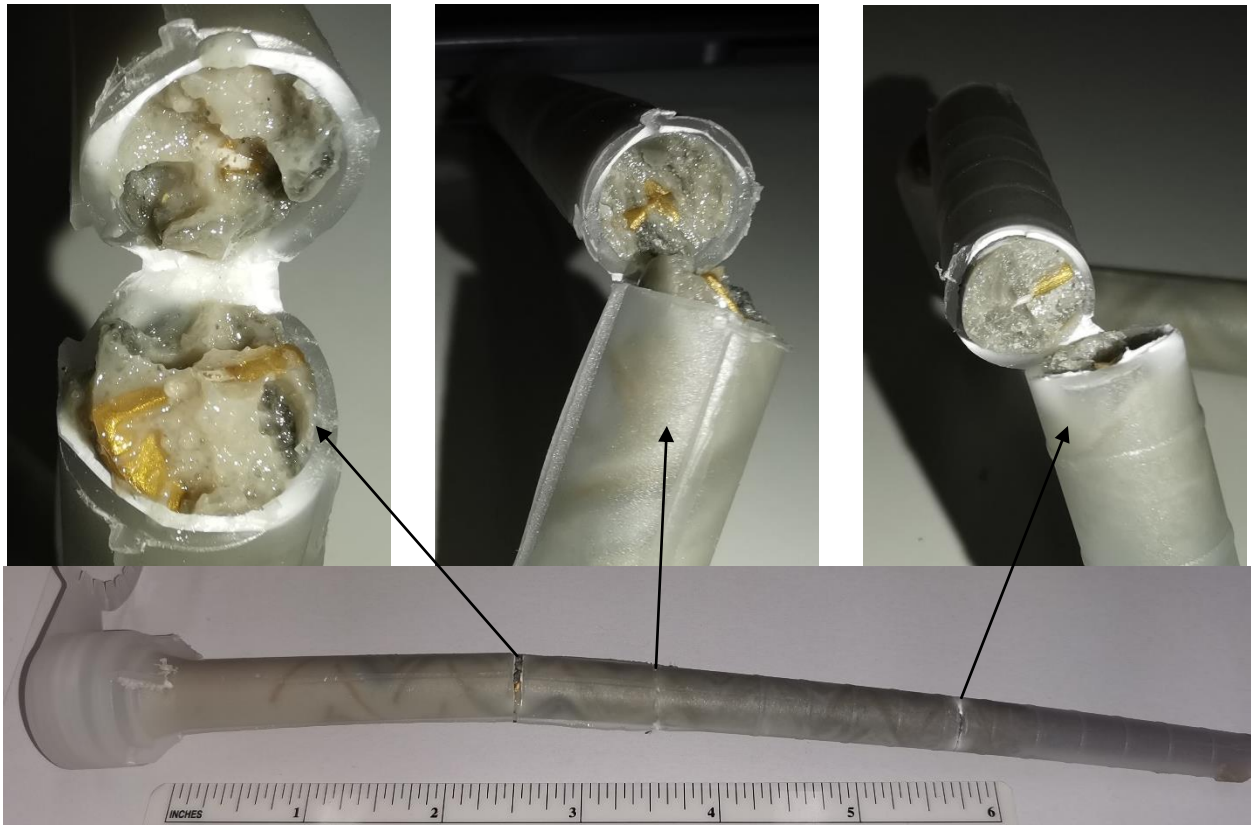

Figure V.11: Curing of adhesive in a mixing tube after 24+ hours

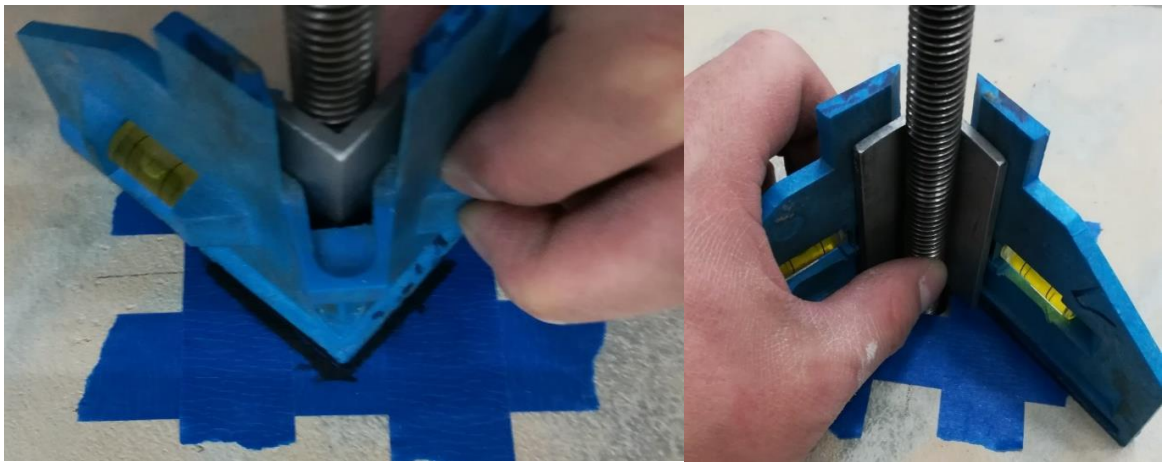

Figure V.12. Anchor installation

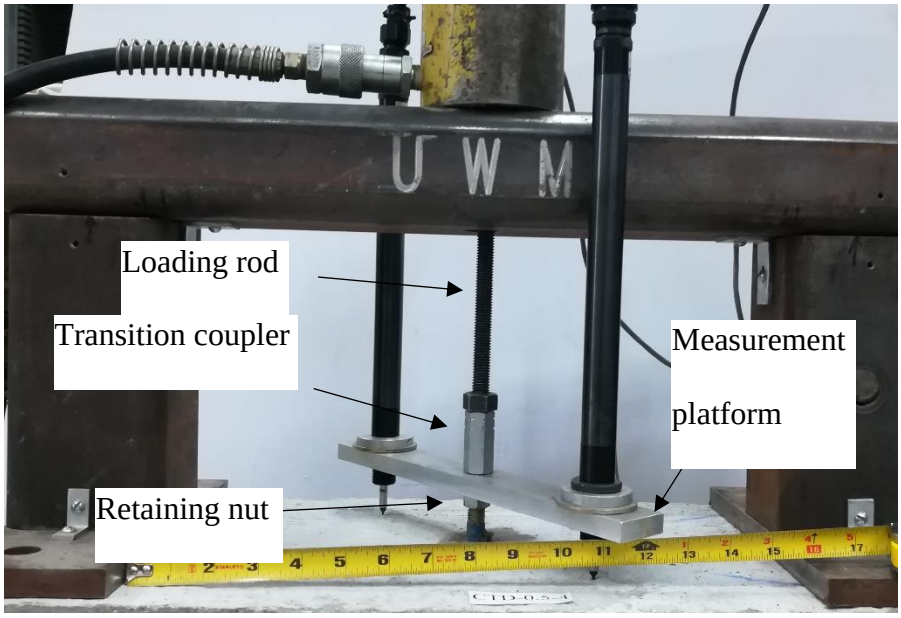

Figure V.13. Typical pullout test setup

Appendix VI: Unconfined Pullout Tests of Adhesive Anchors

A total 56 unconfined pullout tests of adhesive anchors were conducted, including 32 tests with 0.5-in. diameter anchors with a 4-in. embedment depth and 24 tests with 0.625-in. diameter anchors with a 5-in. of embedment depth. The specimen names represent their test variables. For example, Specimen UCT#R50%-0.5-4.0-#1 indicates that

"UC": unconfined pullout tests (C: confined pullout tests)

"T": drilled holes with threads.

"#R": an anchor is installed in a concrete block with anchor reinforcement.

"50%": partially cleaned holes as defined in Appendix V.

"0.5": 0.5-in. diameter anchors.

"4.0": 4.0-in. embedment depth.

"#1": test anchor number (a total of four tests are conducted for each anchor configuration)

The detailed observations are documented below:

1. UC-0.5-4.0-#1

The measured ultimate load is at 10.9 kips [48.5 kN] at a displacement of 0.031 in. [0.79 mm]. Three cracks developed from the anchor at the ultimate load of 10.91 kips [48.5 kN], as shown in Figure VI.1b: two cracks representing splitting in the transverse direction and one in the longitudinal direction. The predicted capacity measuring a 0.44-in. [11.1 mm] deep breakout simultaneously with a 3.5-in. [88.9 mm] deep bond failure (11.54 kips) [51.34 kN]. The anchor was controlled adhesive-concrete interface failure as shown in Figure VI.1c.

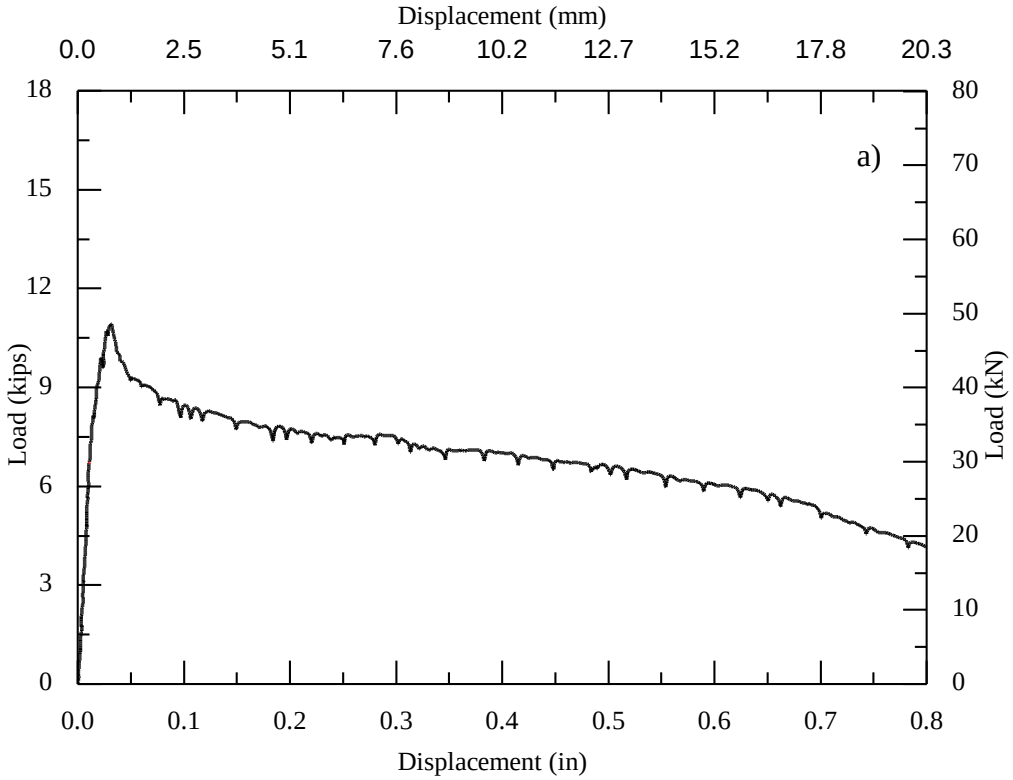

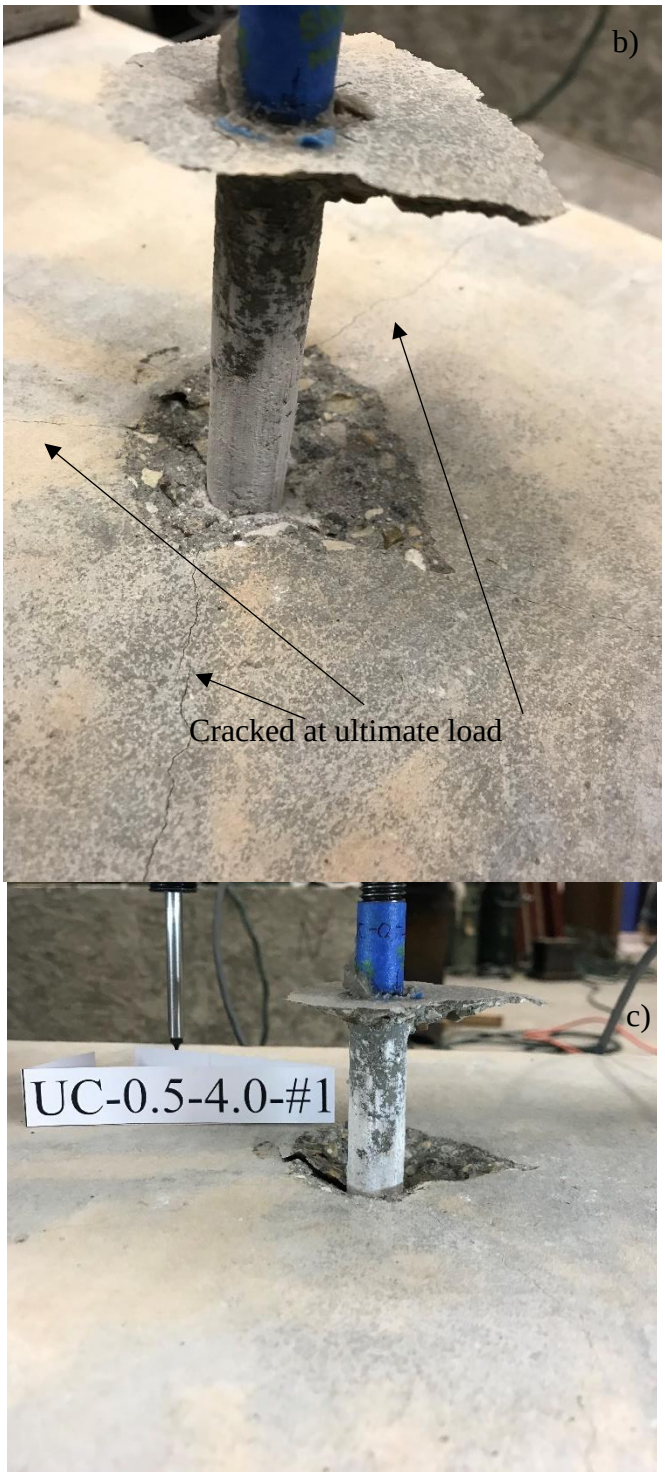

a) load-displacement behavior; b) cracked surface; c) partial cone bond failure

Figure VI.1. Observed behavior of Specimen UC-0.5-4.0-#1

2. UC-0.5-4.0-#2

The measured ultimate load is at 12.69 kips [56.5 kN] at a displacement of 0.023 in. [0.58 mm]. Two cracks developed from the anchor at the load of 12.69 kips [56.5 kN] and crack depth was 2 in. [50.8 mm] as shown in Figure VI.2b. Two cracks representing splitting in the transverse direction. The predicted capacity measuring a 0.73-in. [18.4 mm] deep breakout simultaneously with a 3.25-in. [82.6 mm] deep bond failure (11.37 kips) [50.61 kN]. The anchor was pulled out due to adhesive-concrete interface failure shown in Figure VI.2c.

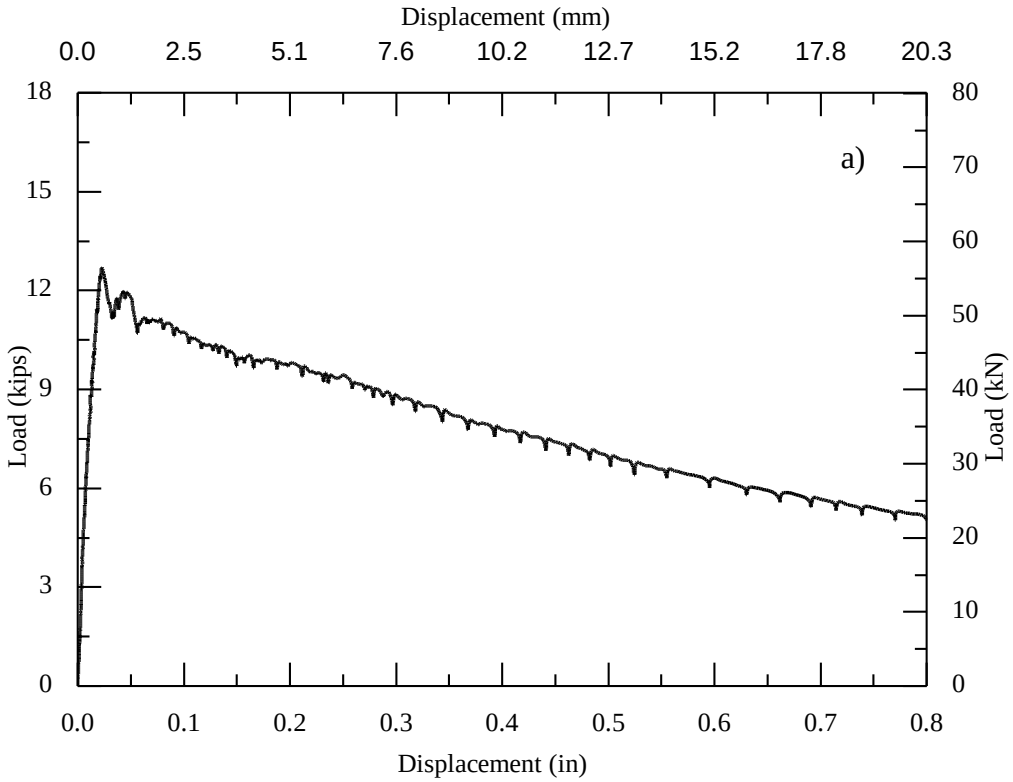

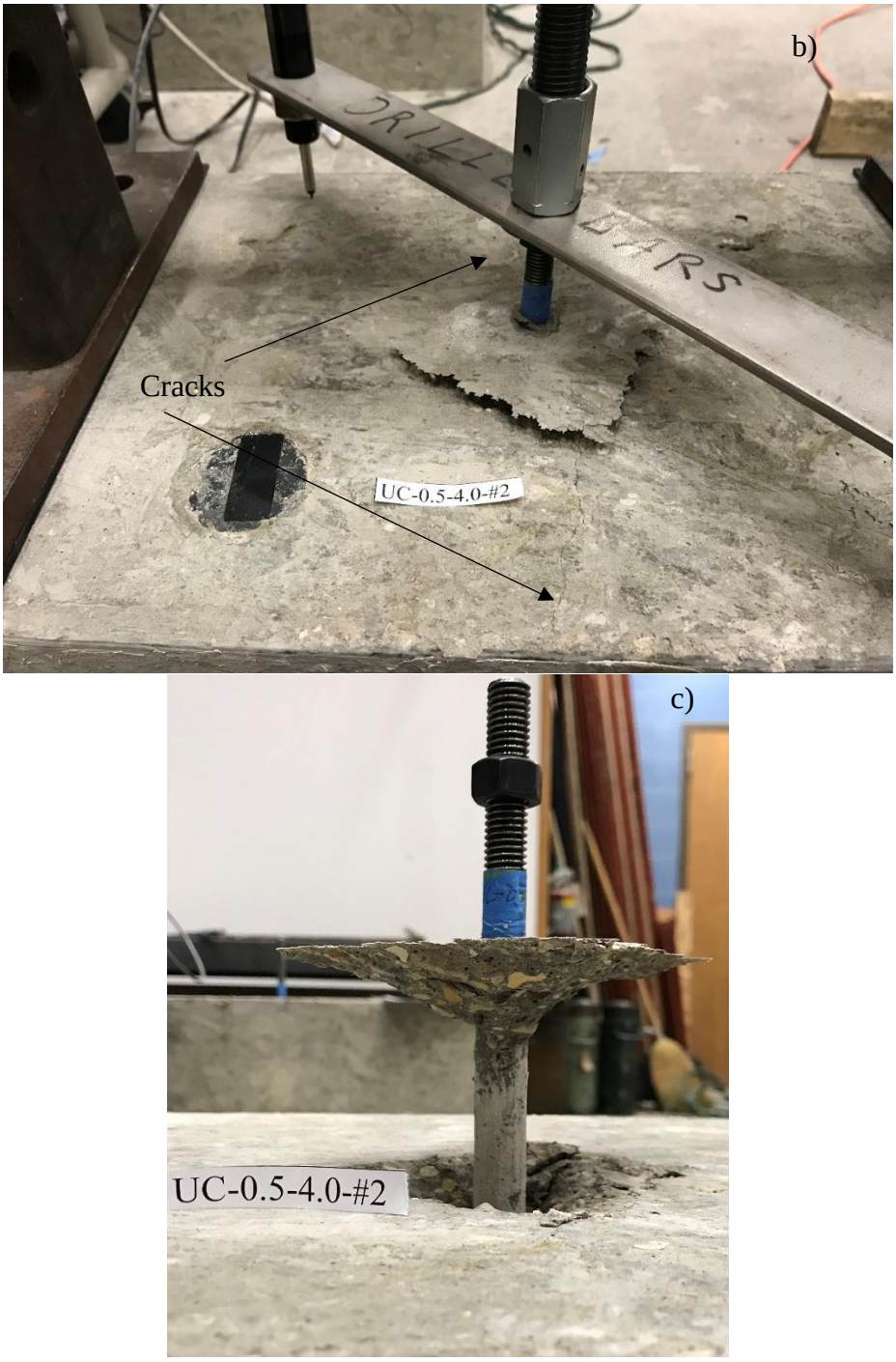

a) load-displacement behavior; b) cracked surface; c) partial cone bond failure

Figure VI.2. Observed behavior of Specimen UC-0.5-4.0-#2

3. UC-0.5-4.0-#3

The measured ultimate load is at 13.4 kips [59.6 kN] at a displacement of 0.041 in. [1mm]. An initial crack caused by the previous test represented splitting in the transverse direction at the bottom edge as shown in Figure VI.3b. One crack represented splitting in the transverse direction at the top edge while the load reached 12.2 kips [54.3 kN] as shown in Figure VI.3c. The predicted capacity in cracked concrete measuring a 1.75-in. [44.5 mm] deep breakout simultaneously with a 2.25-in. [57.2 mm] deep bond failure (10.16 kips) [45.23 kN]. The anchor was pulled out with a concrete cone due to adhesive-concrete interface failure shown in Figure VI.3d.

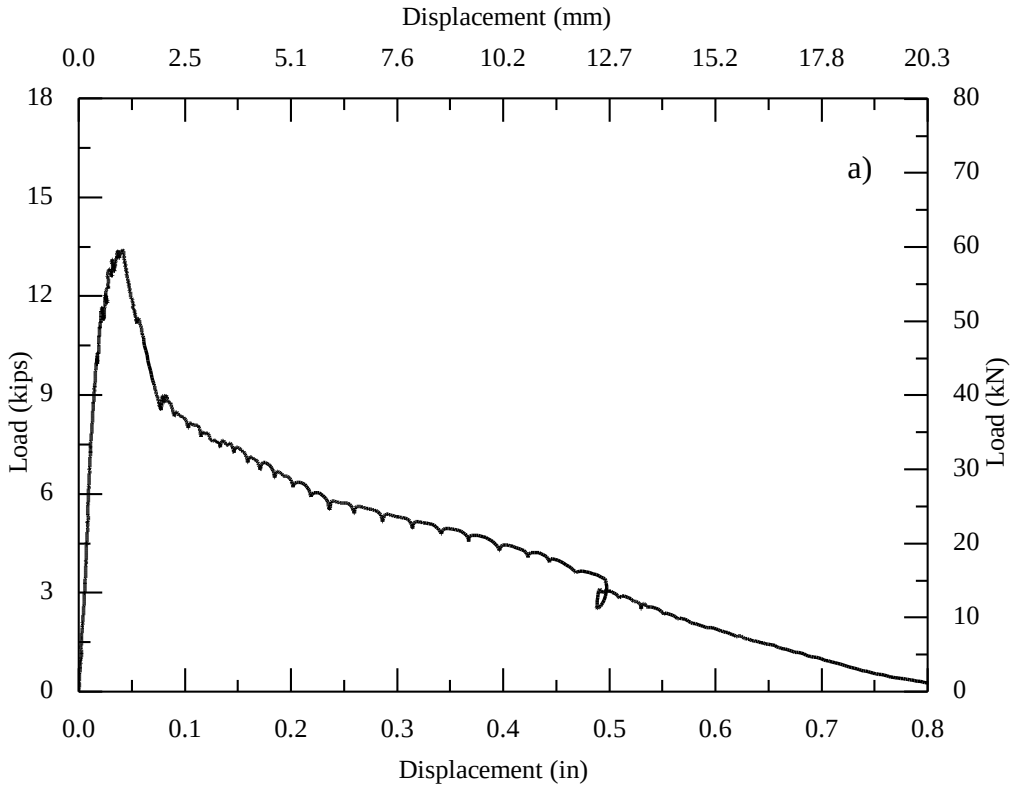

a) load-displacement behavior; b) initial cracked surface; c) cracked surface; d) partial breakout cone

Figure VI.3. Observed behavior of Specimen UC-0.5-4.0-#3

4. UC-0.5-4.0-#4

The measured ultimate load is at 11.27 kips [50.2 kN] at a displacement of 0.045 in. [1.1 mm] Two cavities with approximately 1/8 in. [3.2 mm] diameter were about 1 in. [25.4 mm] from the bottom of the drilled hole. As shown in Figure VI.4b, one crack represented splitting in the transverse direction at the load of 6.6 kips [29.4 kN]; one represented splitting in the longitudinal direction at the load of 11.2 kips [49.8 kN] and one represented splitting in the diagonal direction at the load of 11.2 kips [49.8 kN]. The predicted capacity measuring a 2.67-in. [67.7 mm] deep breakout simultaneously with a 1.25-in. [31.8 mm] deep bond failure (12.15 kips) [54.07 kN]. The anchor was pulled out due to concrete breakout failure shown in Figure VI.4c. Crack lines of the concrete cone bypassed stirrups. As shown in Figure VI.4d, a bump occurred on the anchor surface.

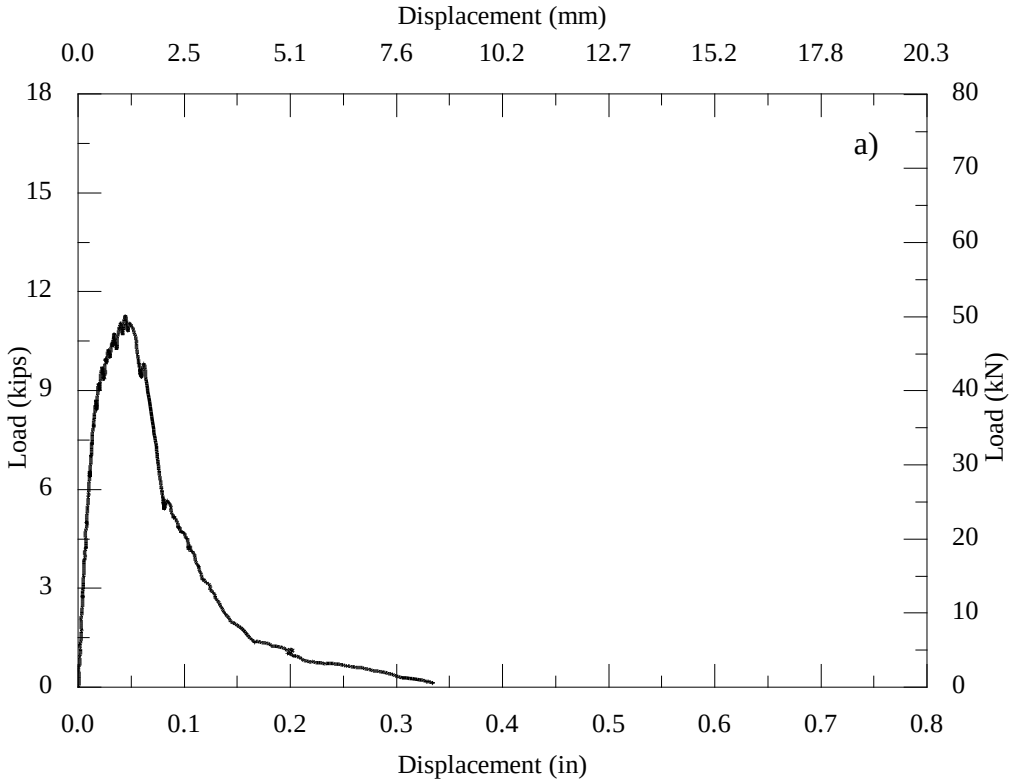

a) load-displacement behavior; b) cracked surface; c) concrete breakout cone in block; d) anchor with adhesive

Figure VI.4. Observed behavior of Specimen UC-0.5-4.0-#4

5. UCT-0.5-4.0-#1

The measured ultimate load is at 12.39 kips [55.14 kN] at a displacement of 0.032 in. [0.81 mm]. As shown in Figure VI.5b, one crack represented splitting and passing the anchor in the transverse direction at the load of 11.23 kips [50 kN] with 1.5 in. [38.1 mm] crack depth; one represented splitting and passing the anchor in the longitudinal direction at the load of 11.23 kips [50 kN]. The displacement did not increase at 0.1 in. [2.54 mm] due to LVDT probes were moved with the damaged concrete. The predicted capacity measuring a 2.87-in. [72.8 mm] deep breakout simultaneously with a 1 -in. [25.4 mm] deep bond failure (12.31 kips) [54.80 kN]. The anchor was pulled out with a concrete cone due to concrete breakout failure shown in Figure VI.5c. Crack lines of the concrete cone bypassed stirrups.

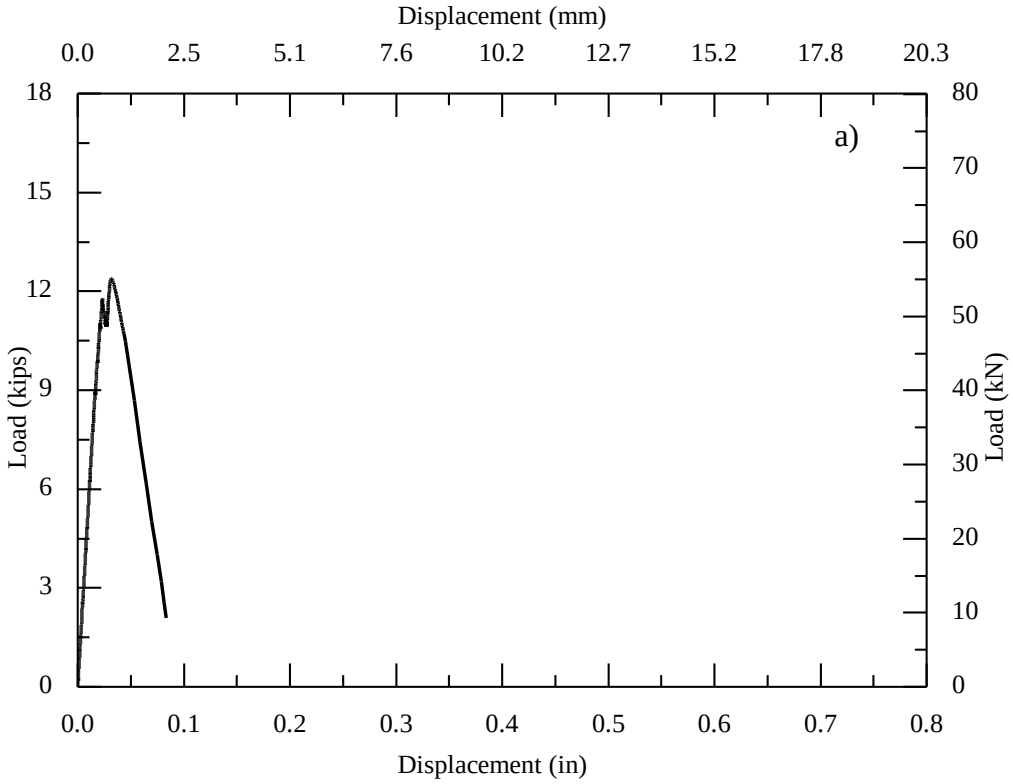

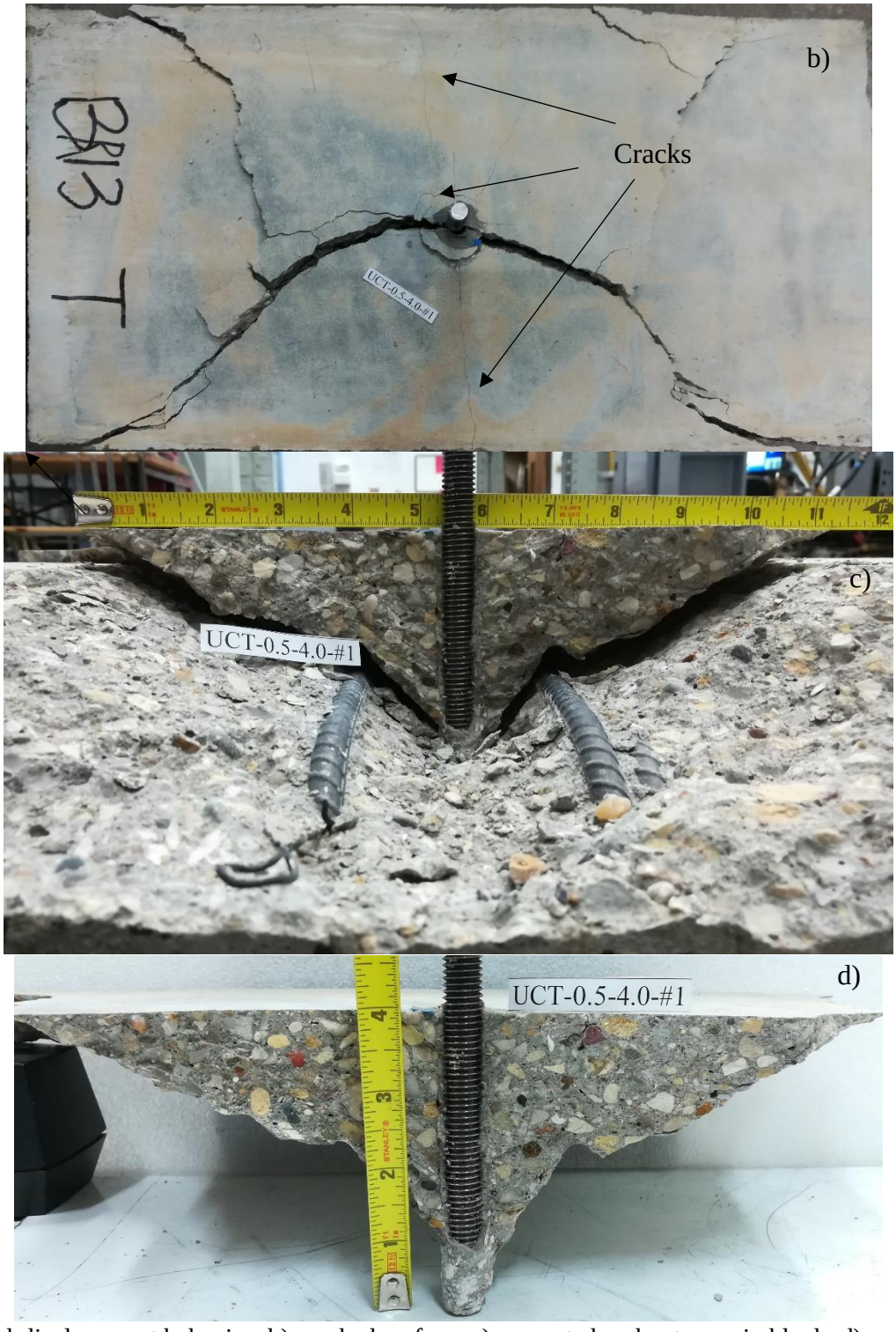

a) load-displacement behavior; b) cracked surface; c) concrete breakout cone in block; d) concrete breakout cone

Figure VI.5. Observed behavior of Specimen UCT-0.5-4.0-#1

6. UCT-0.5-4.0-#2

The measured ultimate load is at 10.98 kips [48.86 kN] at a displacement of 0.052 in. [1.32 mm]. As shown in Figure VI.6b, one crack represented splitting and passing the anchor in the transverse direction at the load of 10.17 kips [45.26 kN]; two cracks represented splitting and passing the anchor in the diagonal direction at the load of 8.77 kips [39.03 kN]. The anchor was 0.5 in. close to one side of stirrups due to the stirrup position was moved during the process of pouring concrete. The predicted capacity measuring a 2.32-in. [59 mm] deep breakout simultaneously with a 1.5 -in. [38.1 mm] deep bond failure (11.39 kips) [50.70 kN]. The anchor was pulled out with a concrete cone due to concrete breakout failure shown in Figure VI.10c. Crack lines of the concrete cone bypassed stirrups.

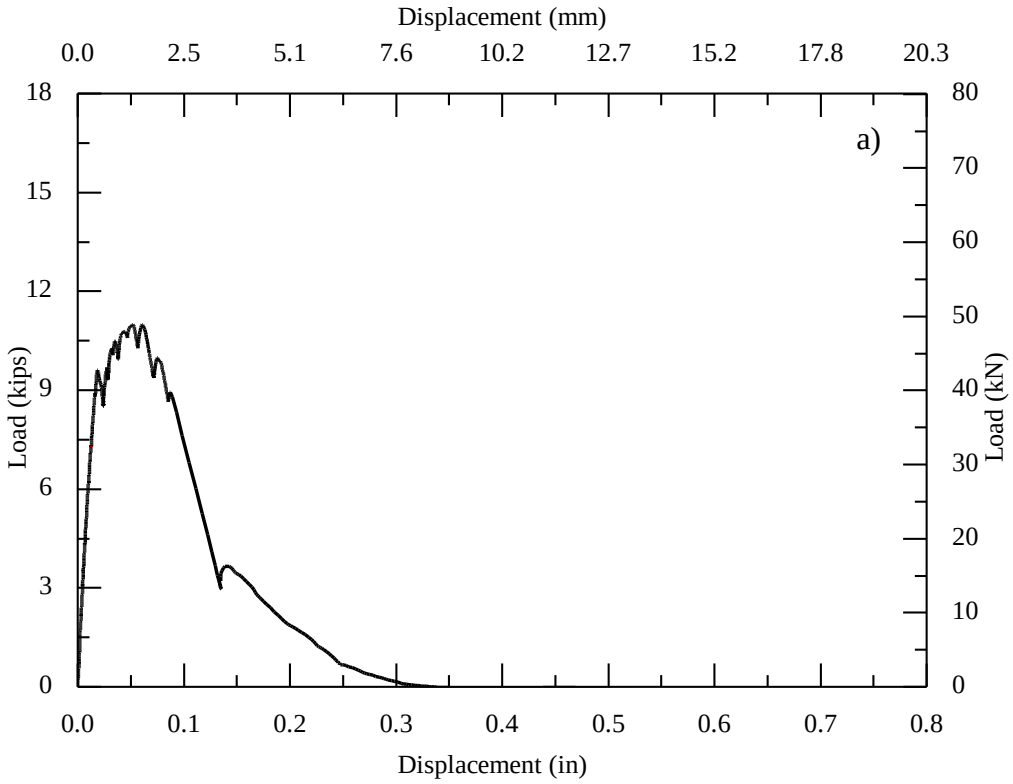

a) load-displacement behavior; b) cracked surface; c) concrete breakout cone in block; d) concrete breakout cone

Figure VI.6. Observed behavior of Specimen UCT-0.5-4.0-#2

7. UCT-0.5-4.0-#3

The measured ultimate load is at 11.74 kips [52.24 kN] at a displacement of 0.039 in. [0.99 mm]. Two initial cracks were generated by previous tests. One was in the transverse direction, which was about 1 in. away from the right side of the anchor. Another was in the transverse direction, which was about 2 in. away from the left side of the anchor. As shown in Figure VI.7b, one crack represented splitting and passing the anchor in the transverse direction at the load of 11.74 kips [52.24 kN]; one cracks represented splitting and passing the anchor in the longitudinal direction at the load of 11.74 kips [52.24 kN]. The predicted capacity in cracked concrete measuring a 3.09-in. [78.5 mm] deep breakout simultaneously with a 0.88-in. [22.2 mm] deep bond failure (10.02 kips) [44.6 kN]. The anchor was pulled out with a concrete cone due to concrete breakout failure shown in Figure VI.7c.

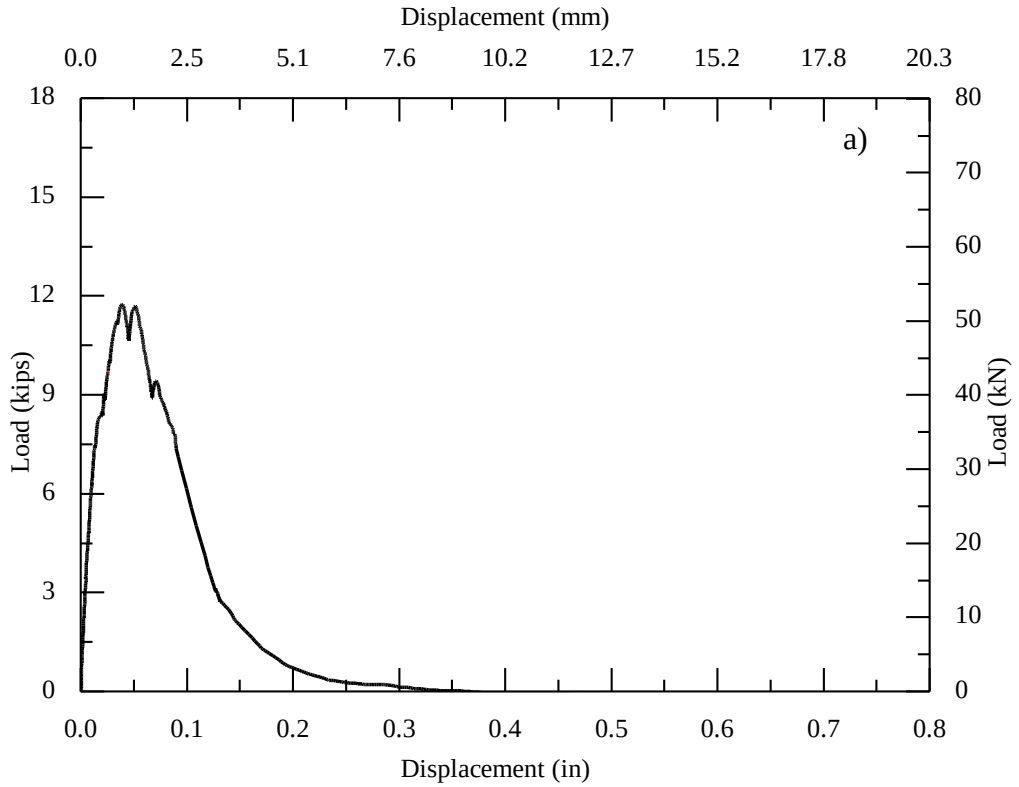

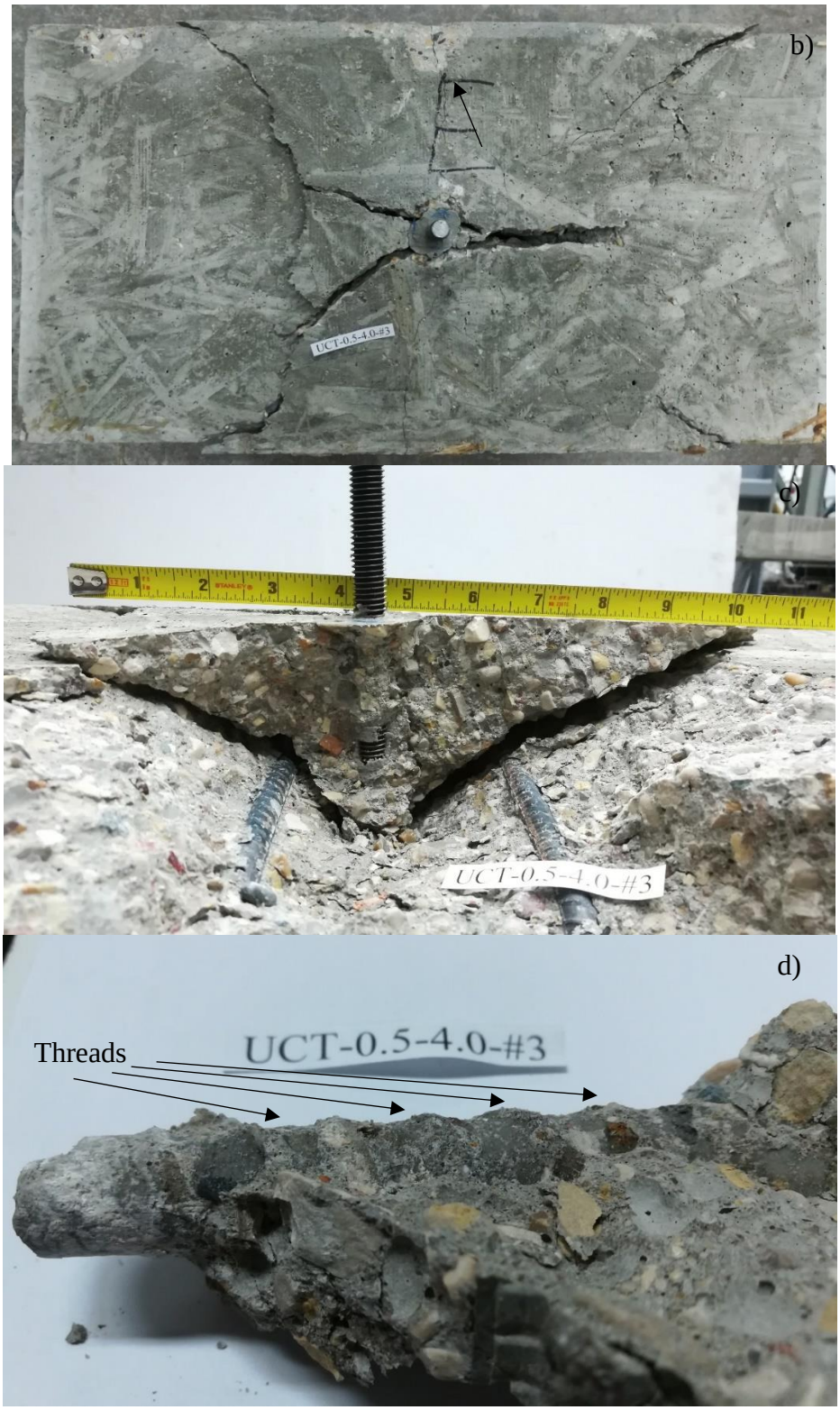

a) load-displacement behavior; b) cracked surface; c) concrete breakout cone in block; d) concrete breakout cone

Figure VI.7. Observed behavior of Specimen UCT-0.5-4.0-#3

8. UCT-0.5-4.0-#4

The measured ultimate load is at 10.97 kips [48.82 kN] at a displacement of 0.036 in. [0.91 mm]. One initial crack was generated by previous tests and the crack was across the transverse section, which was about 1.5 in. away from the right side of the anchor. One crack represented splitting and passing the anchor in the longitudinal direction at the load of 10.7 kips [47.62 kN]. The predicted capacity in cracked concrete measuring a 2.79-in. [70.9 mm] deep breakout simultaneously with a 1.13 -in. [28.6 mm] deep bond failure (9.77 kips) [43.48 kN]. The anchor was pulled out with a concrete cone due to concrete breakout failure shown in Figure VI.8c and 8d. Threads were formed on the anchor surface and crack lines of the concrete cone bypassed stirrups.

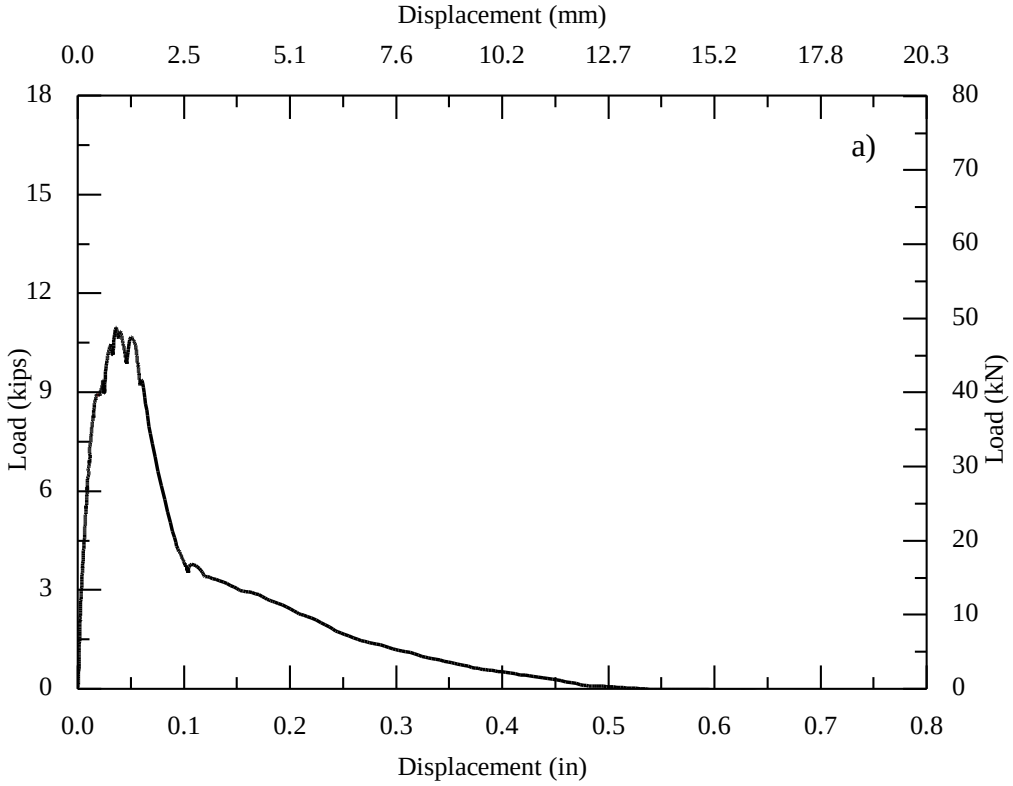

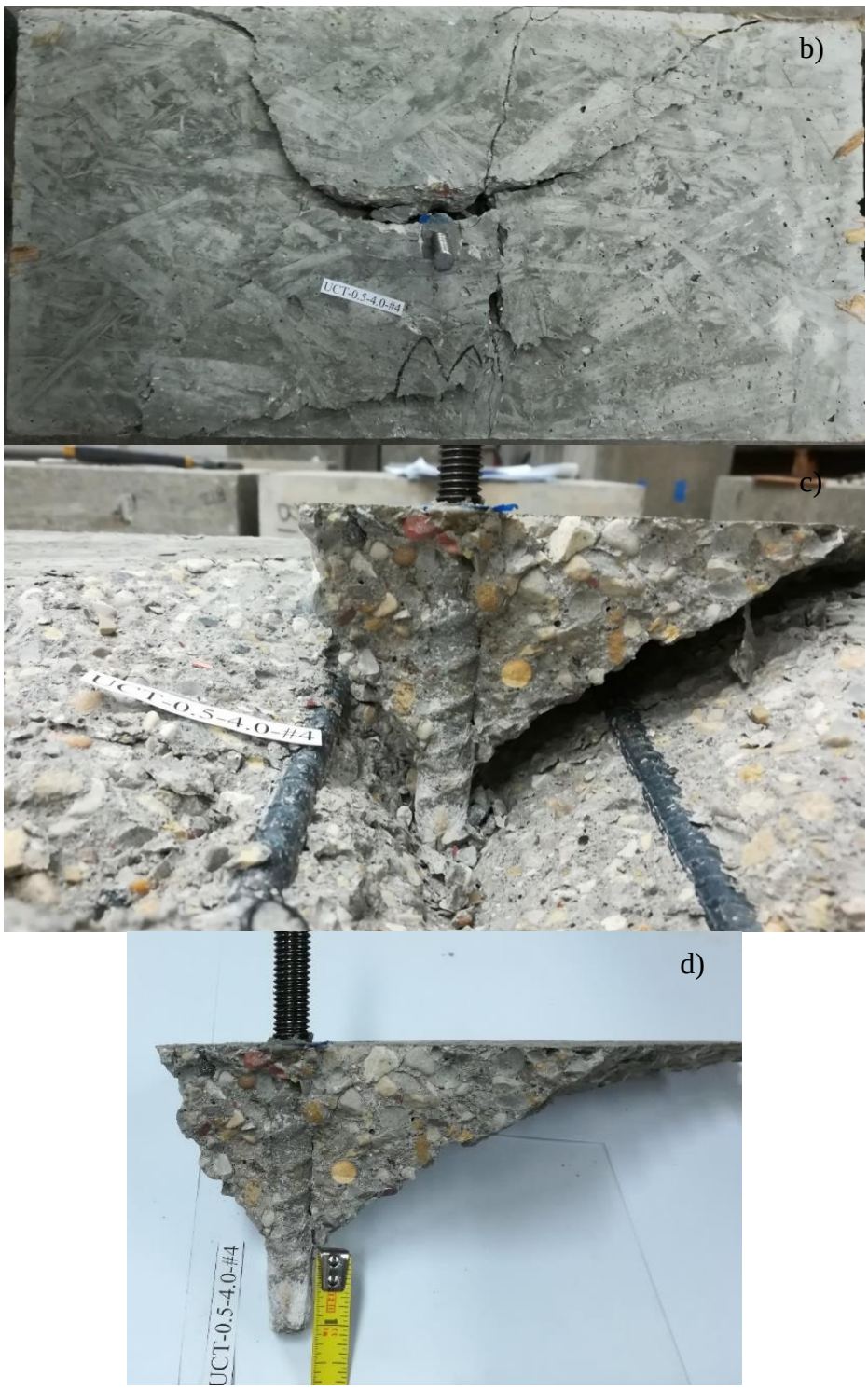

a) load-displacement behavior; b) cracked surface; c) concrete breakout cone in block; d) concrete breakout cone.

Figure VI.8. Observed behavior of Specimen UCT-0.5-4.0-#4

9. UCT#R-0.5-4.0-#1

The measured ultimate load is at 13.76 kips [61.23 kN] at a displacement of 0.037 in. [0.94 mm]. One crack represented splitting and passing the anchor in the transverse direction at the load of 11.77 kips [52.38 kN]. The load sharply declined to approximately 3 kips as the displacement increased slowly due to the concrete breakout. The predicted capacity measuring a 2.59-in. [65.8 mm] deep breakout simultaneously with a 1.25 -in. [31.8 mm] deep bond failure (11.81 kips) [52.56 kN]. The anchor was pulled out with a concrete cone due to concrete breakout failure shown in Figure VI.9c and 9d. Crack lines of the concrete cone bypassed stirrups.

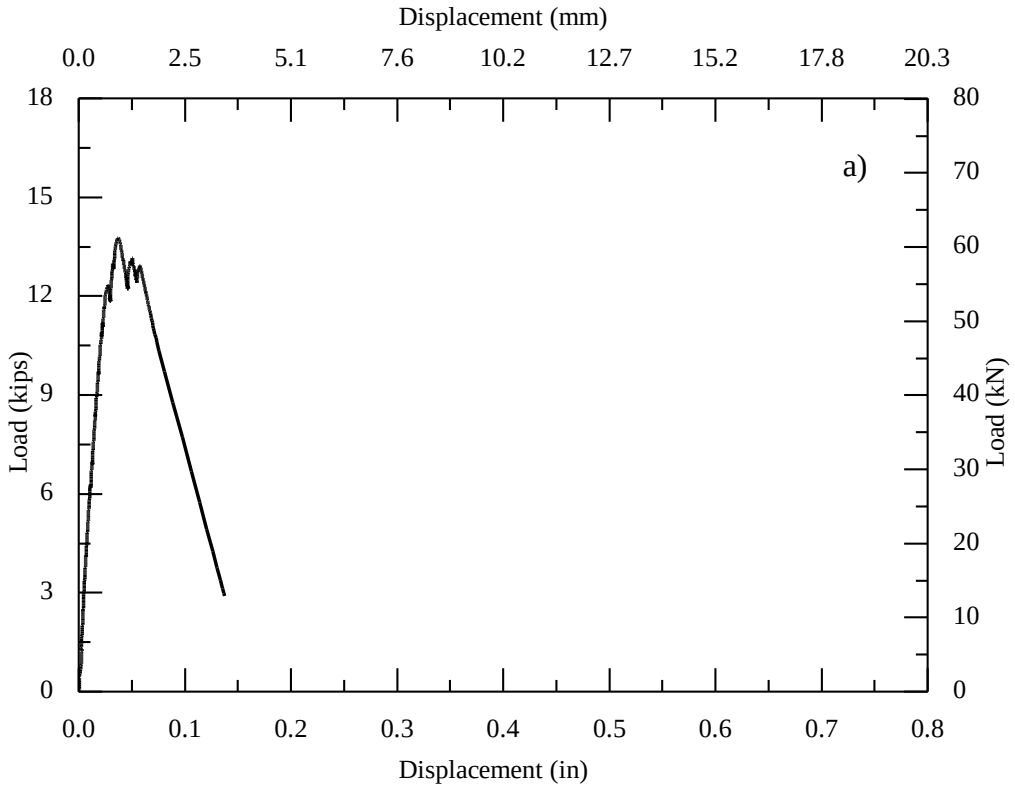

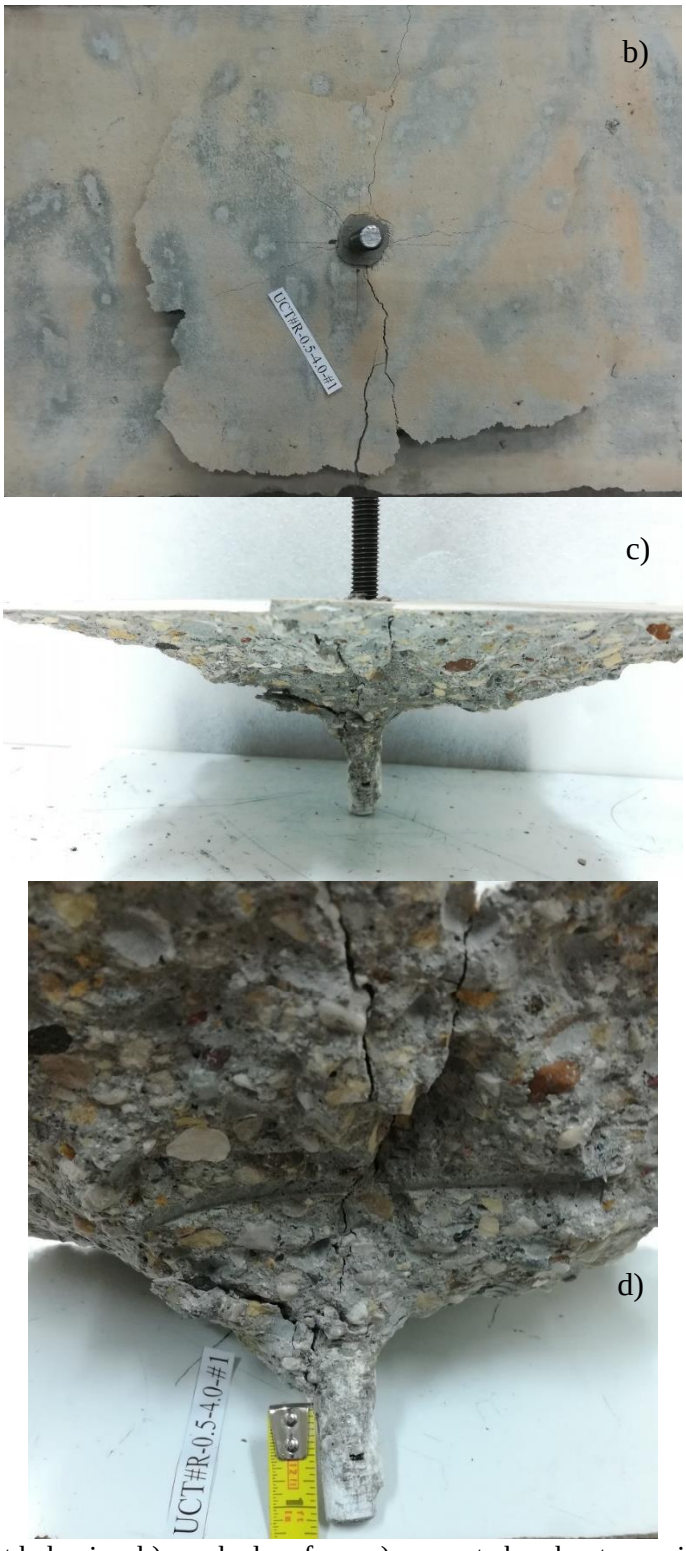

a) load-displacement behavior; b) cracked surface; c) concrete breakout cone in block; d) concrete breakout cone with marks of the reinforcing bar.

Figure VI.9. Observed behavior of Specimen UCT#R-0.5-4.0-#1

10. UCT#R-0.5-4.0-#2

The measured ultimate load is at 16.81 kips [74.8 kN] at a displacement of 0.075 in. [1.91 mm]. As shown in Figure VI.10b, one crack represented splitting and passing the anchor in the transverse direction at the load of 12.31 kips [54.78 kN] with 1 in. [25.4 mm] crack depth. one crack represented splitting and passing the anchor in the diagonal direction at the load of 14.98 kips [66.66 kN]. The load sharply declined to approximately 3 kips [13.35 kN] as the displacement increased slowly due to the concrete breakout. The width of those cracks was enlarged. The anchor was pulled out with a concrete cone due to adhesive-concrete and adhesive-steel failure shown in Figure VI.10c and 10d. Crack lines of the concrete cone bypassed stirrups. As shown in Figure VI.10d and 14e, the anchor reinforcement was 0.5 in. [12.7 mm] away from the concrete surface. The adhesive steel interface failure occurred below 1 3/4 in. of the anchor and this failure mode normally occurred in confined tests. The ultimate load (16.81 kips) [74.8 kN] was 5% lower than the anchor failure load (17.7 kips) [78.77 kN] due to the concrete was damaged before the test. The ultimate load was close to the anchor failure load. The predicted capacity measuring a 1.31-in. [33.3 mm] deep breakout simultaneously with a 2.63 -in. [66.7 mm] deep bond failure (11.08 kips) [49.3 kN].

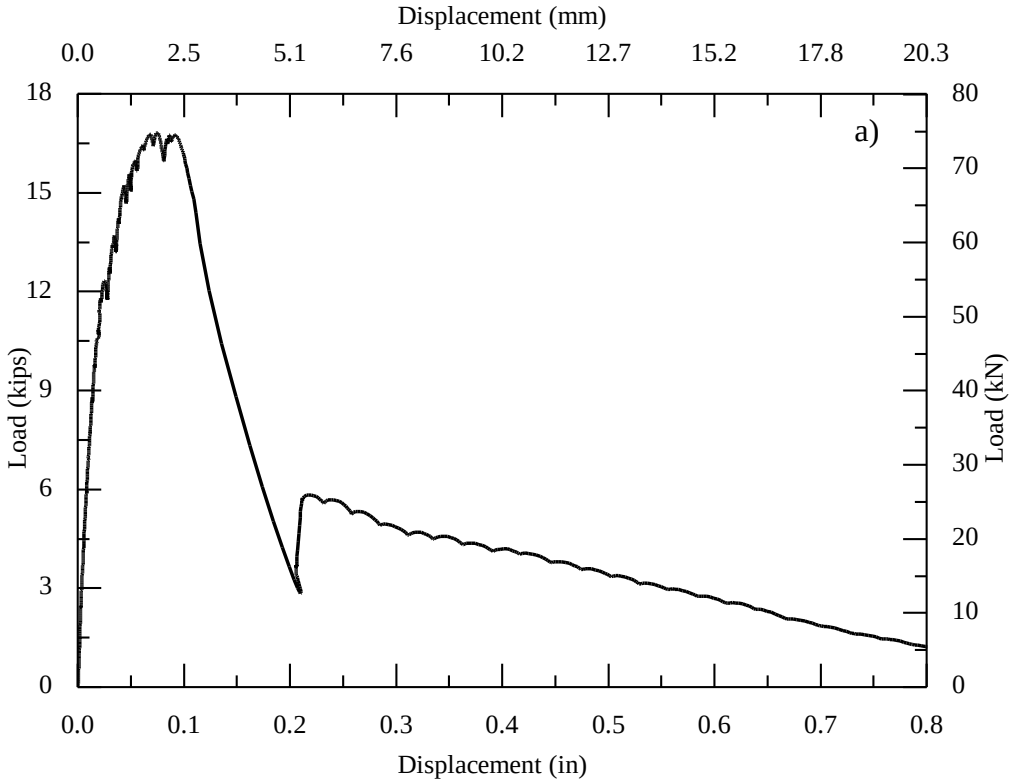
Displacement (mm)
0.0
2.5
5.1
7.6
10.2
12.7
15.2
17.8
20.3
a)
Load (kips)
Load (kN)
0
3
6
9
12
15
18
0
10
20
30
40
50
60
70
80
0.0
0.1
0.2
0.3
0.4
0.5
0.6
0.7
0.8
Displacement (in)


b)
b)
UCT#R-0.5-4.0-#2

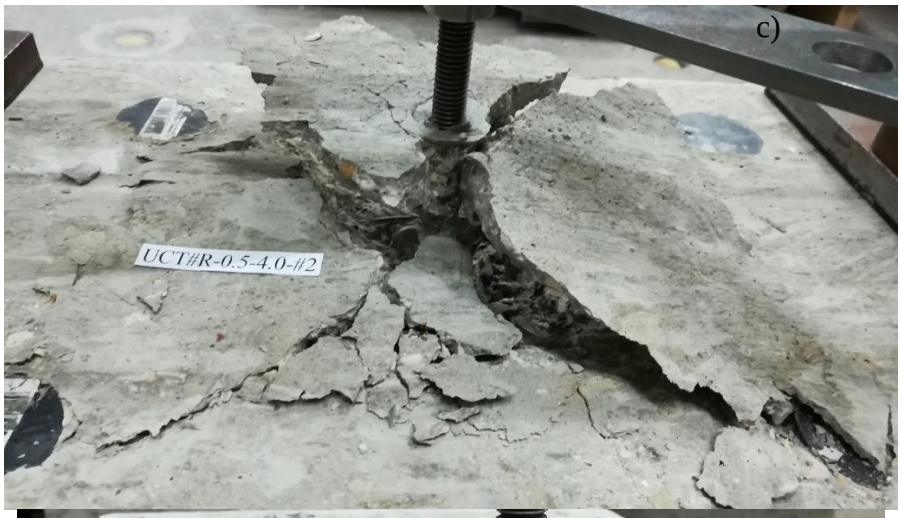
c)
UCT#R-0.5-4.0-#2


d
UCT#R-0.5-4.0-#2


e
UCT#R-0.5-4.0-#2

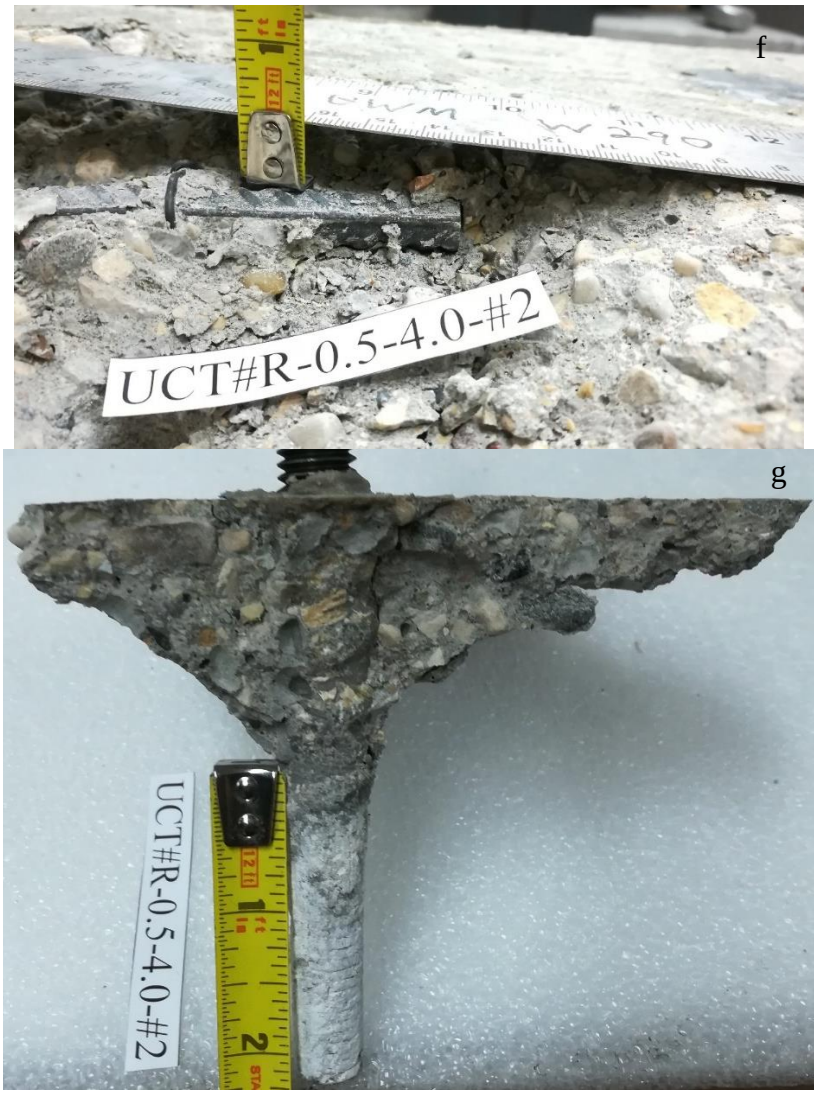

a) load-displacement behavior; b) c) cracked surface; d) e) partial cone bond failure in block; f) location of anchor reinforcement; g) partial cone bond failure.

Figure VI.10. Observed behavior of Specimen UCT#R-0.5-4.0-#2

11. UCT#R-0.5-4.0-#3

The measured ultimate load is at 12.67 kips [56.38 kN] at a displacement of 0.067 in. [1.7 mm]. One initial crack was generated by previous tests and the crack was across the transverse direction, which was about 1.5 in. [38.1 mm] away from the left side of the anchor. As shown in Figure VI.11b, one crack represented splitting and passing the anchor in the diagonal direction at the load of 10.7 kips [47.62 kN]. The load sharply declined to approximately 2.5 kips [11.13 kN] as the displacement increased slowly due to the concrete breakout. The predicted capacity in cracked concrete measuring a 2.18-in. [55.2 mm] deep breakout simultaneously with a 1.75 -in. [44.5 mm] deep bond failure (9.79 kips) [43.56 kN]. The anchor was pulled out with a concrete cone due to concrete breakout failure shown in Figure VI.11c and 11d. Crack lines of the concrete cone bypassed stirrups.

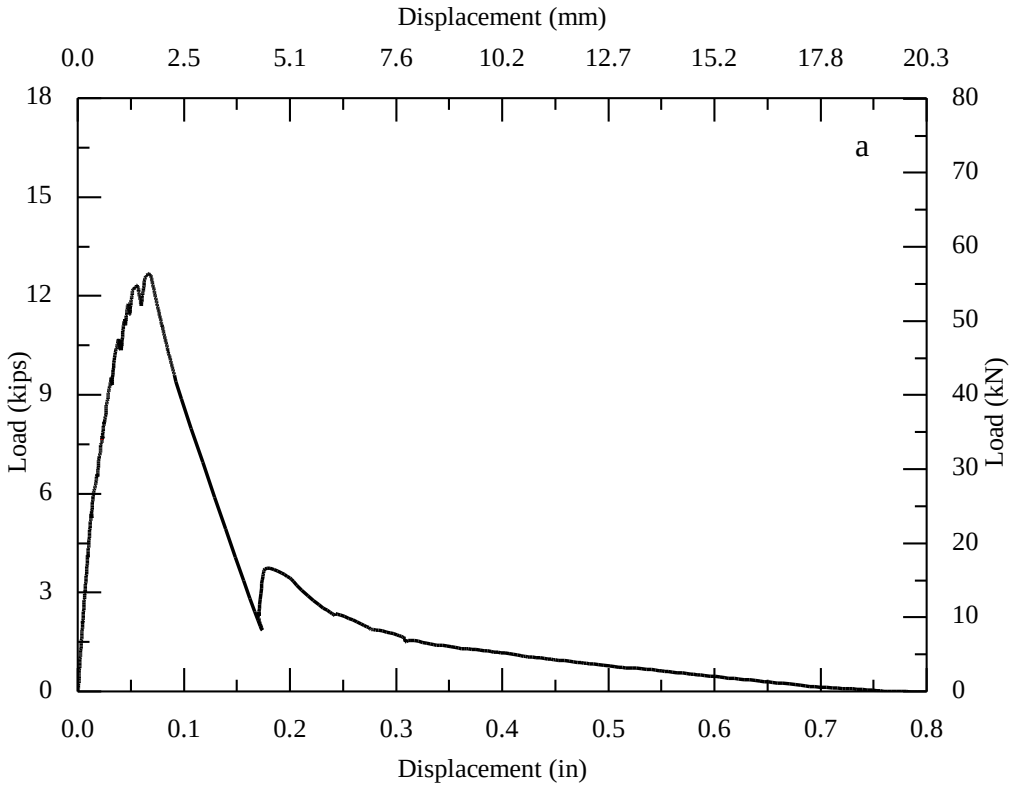

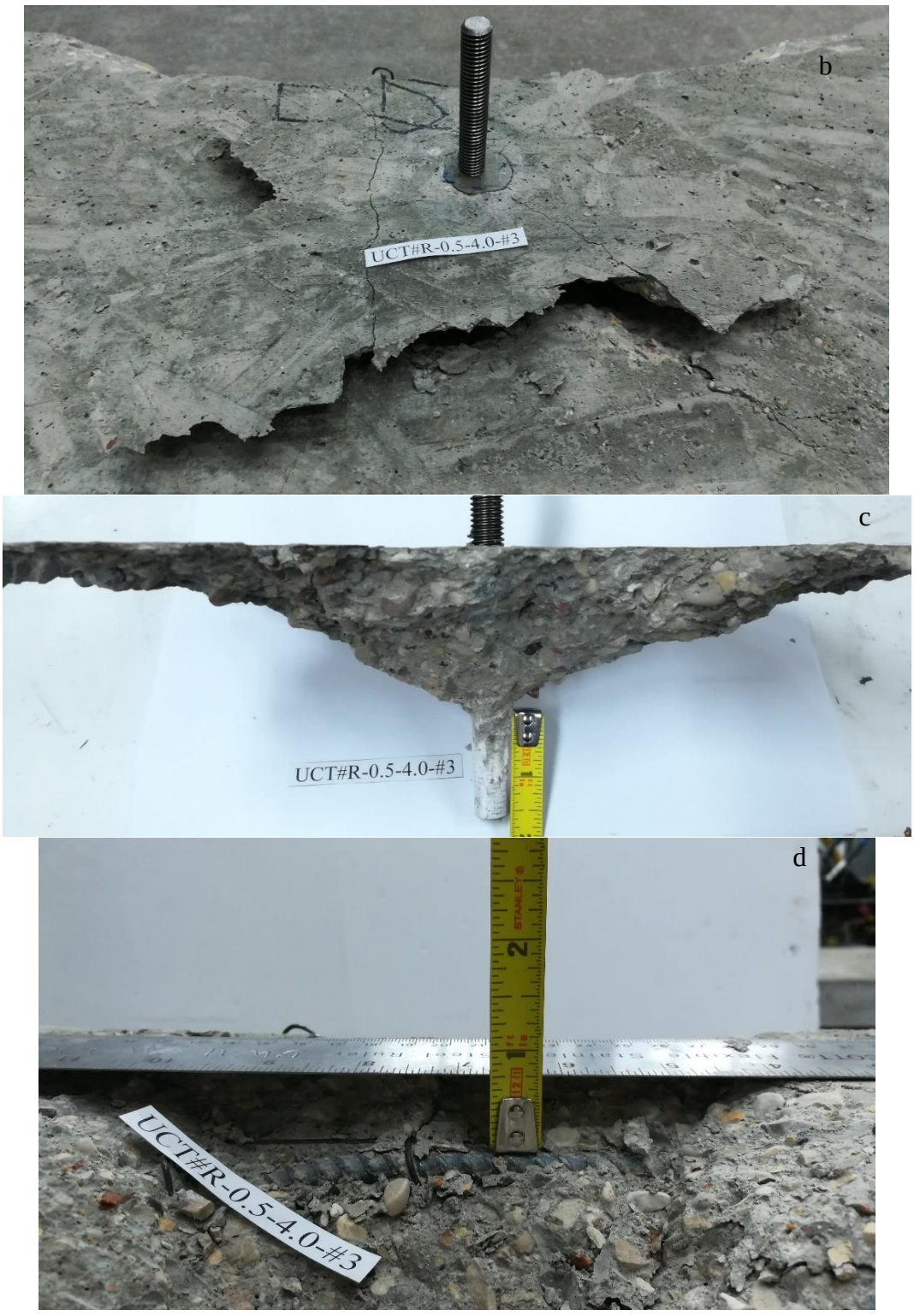

a) load-displacement behavior; b) cracked surface; c) concrete breakout cone; d) location of anchor reinforcement;

Figure VI.11. Observed behavior of Specimen UCT#R-0.5-4.0-#3

12. UCT#R-0.5-4.0-#4

The measured ultimate load is at 11.61 kips [51.66 kN] at a displacement of 0.049 in. [1.24 mm]. One initial crack was generated by previous tests and the crack was across the transverse direction, which was about 1 in. [25.4 mm] away from the left side of the anchor. As shown in Figure VI.12b, one crack represented splitting and passing the anchor in the diagonal direction at the load of 10.7 kips [47.62 kN]. The load sharply declined to approximately 5 kips as the displacement increased slowly due to the concrete breakout. Then, another large fracture sound occurred, and the load dropped to approximately 4 kips. The predicted capacity measuring a 2.04-in. [51.8 mm] deep breakout simultaneously with a 2-in. [50.8 mm] deep bond failure (10.18 kips) [45.29 kN]. The anchor was pulled out with a concrete cone due to adhesive-concrete and adhesive-steel interface failure shown in Figure VI.12c and 12d.

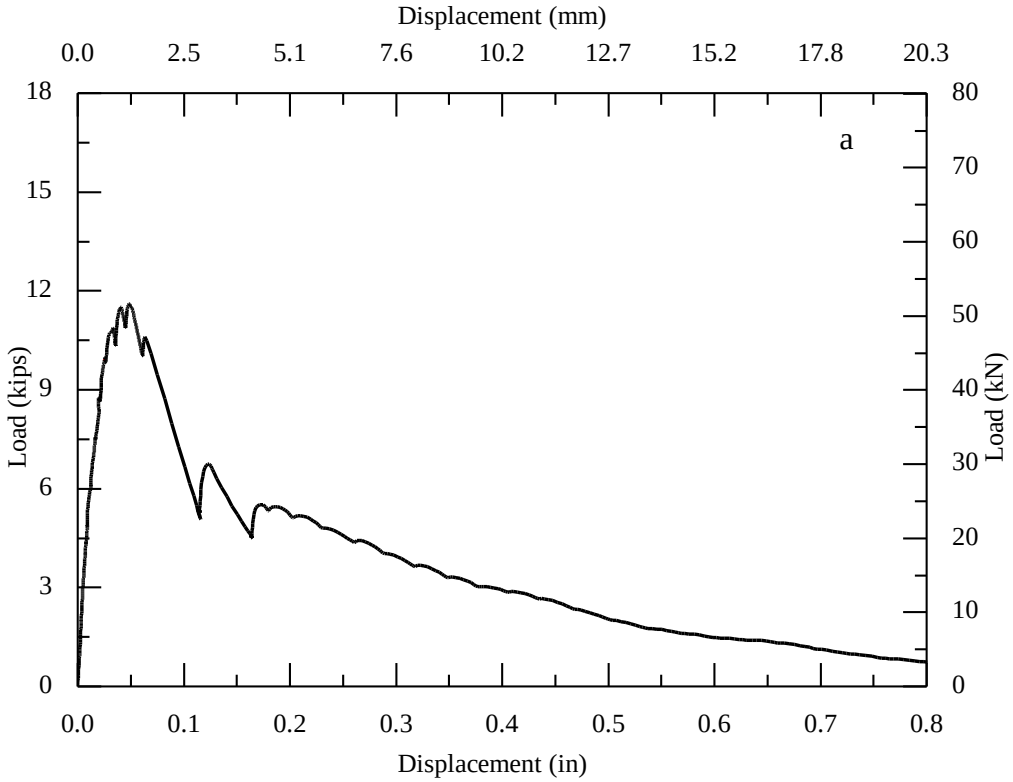

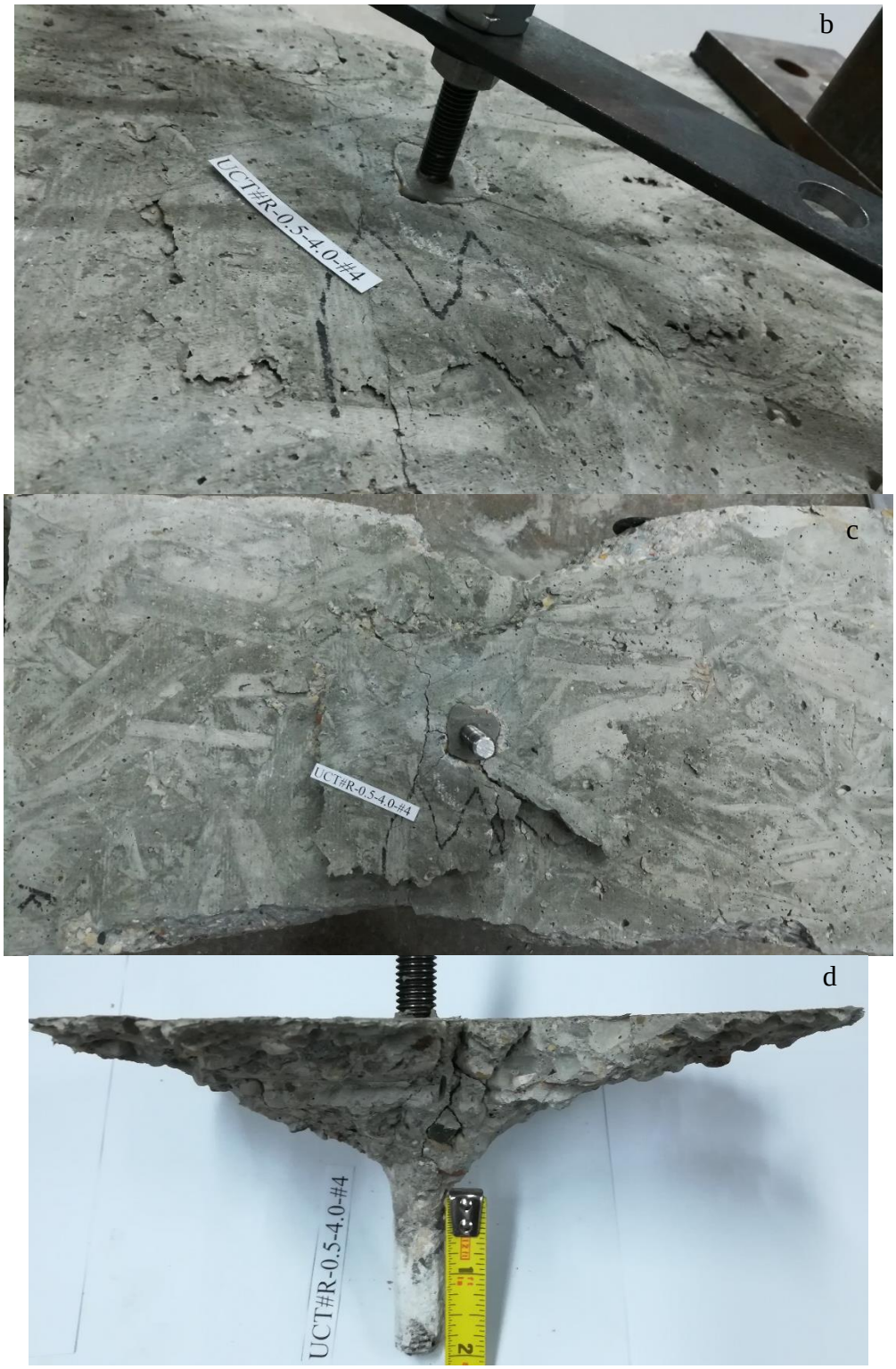

a) load-displacement behavior; b) cracked surface; c) partial cone bond failure in block; d) partial cone bond failure

Figure VI.12. Observed behavior of Specimen UCT#R-0.5-4.0-#4

13. UC0%-0.5-4.0-#1

The measured ultimate load is at 3.79 kips [16.87 kN] at a displacement of 0.643 in. [16.33 mm]. A circular crack appeared along the anchor at the load of 2.46 kips [10.95 kN] as shown in Figure VI.13b. After passing the ultimate load, the load remained constant as the displacement increased due to the frictional resistance was generated by the rough surface of the drilled hole. The anchor was pulled out with a small concrete cone due to adhesive-concrete interface failure shown in Figure VI.13c.

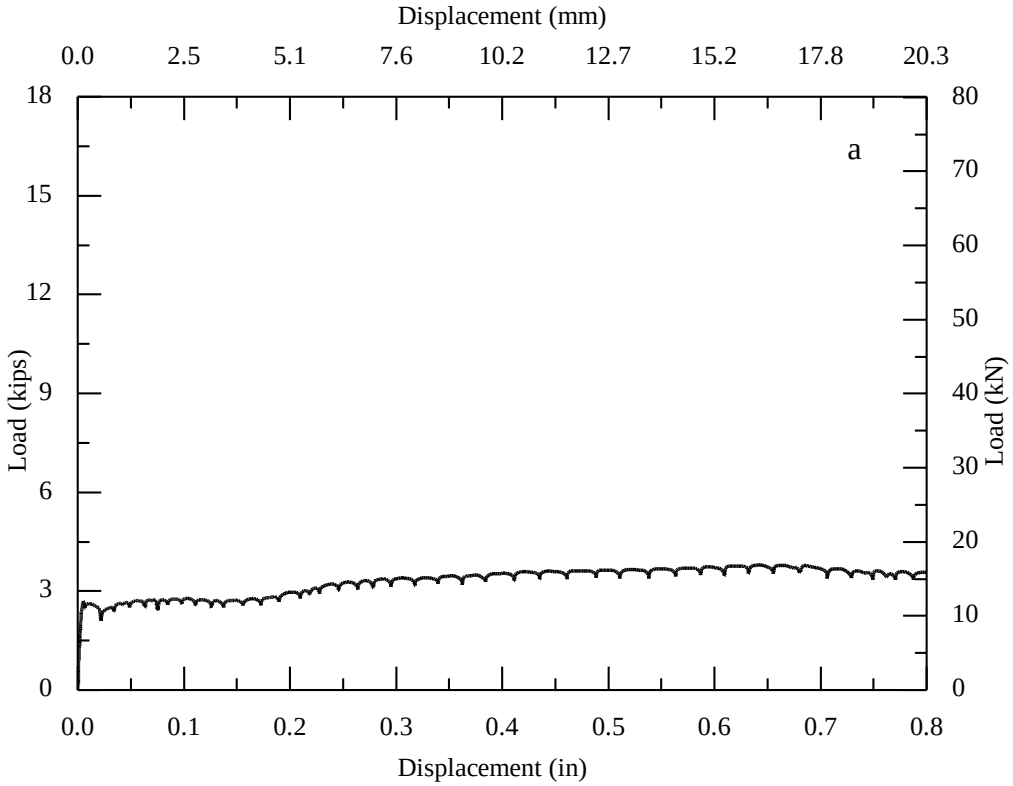

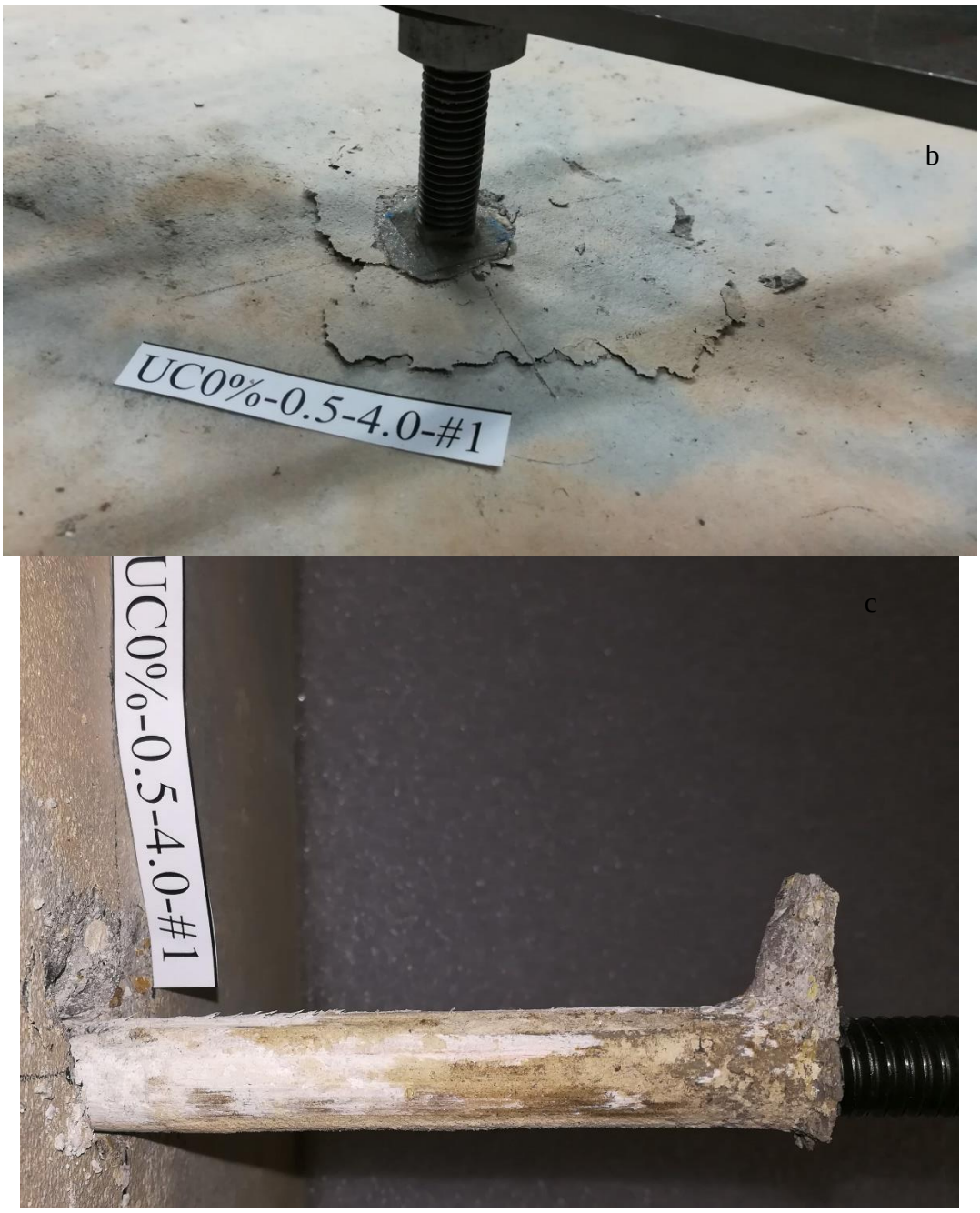

a) load-displacement behavior; b) cracked surface; c) partial cone bond failure

Figure VI.13. Observed behavior of Specimen UC0%-0.5-4.0-#1

14. UC0%-0.5-4.0-#2

The measured ultimate load is at 3.56 kips [15.84 mm] at a displacement of 0.013 in. [0.33 mm]. A circular crack appeared along the anchor at the load of 3.21 kips [14.28 kN] as shown in Figure VI.14b. After passing the ultimate load, the load remained constant as the displacement increased due to the frictional resistance was generated by the rough surface of the drilled hole. The anchor was pulled out with a concrete cone due to adhesive-concrete interface failure shown in Figure VI.14c.

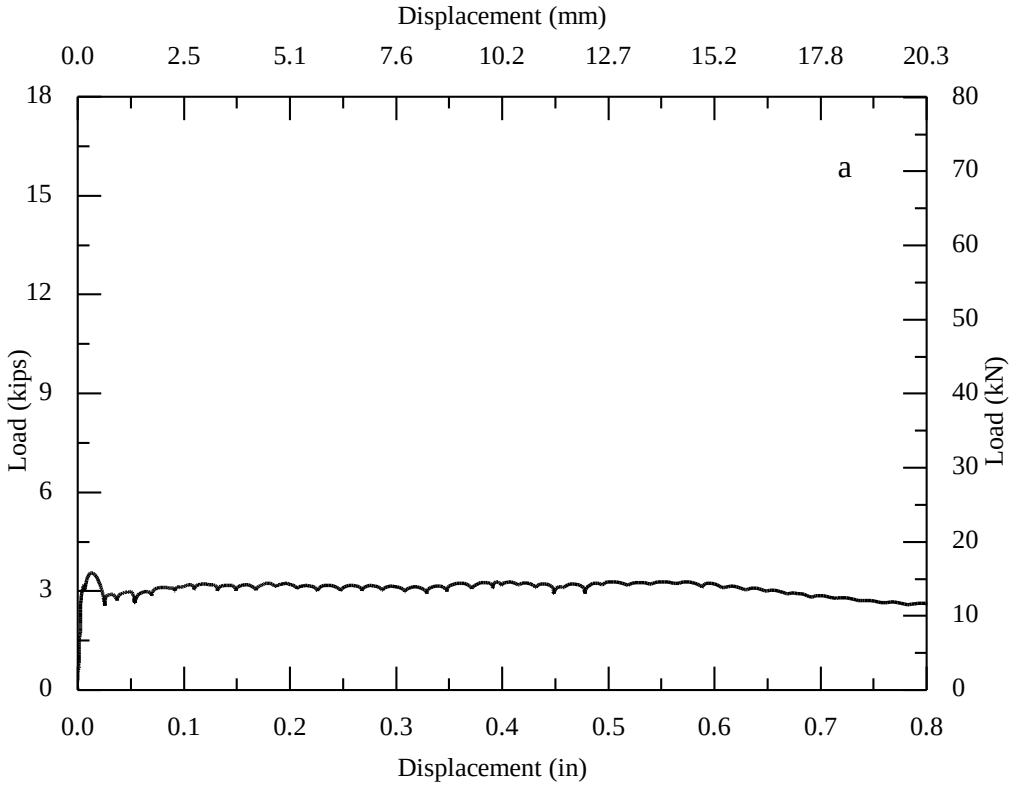

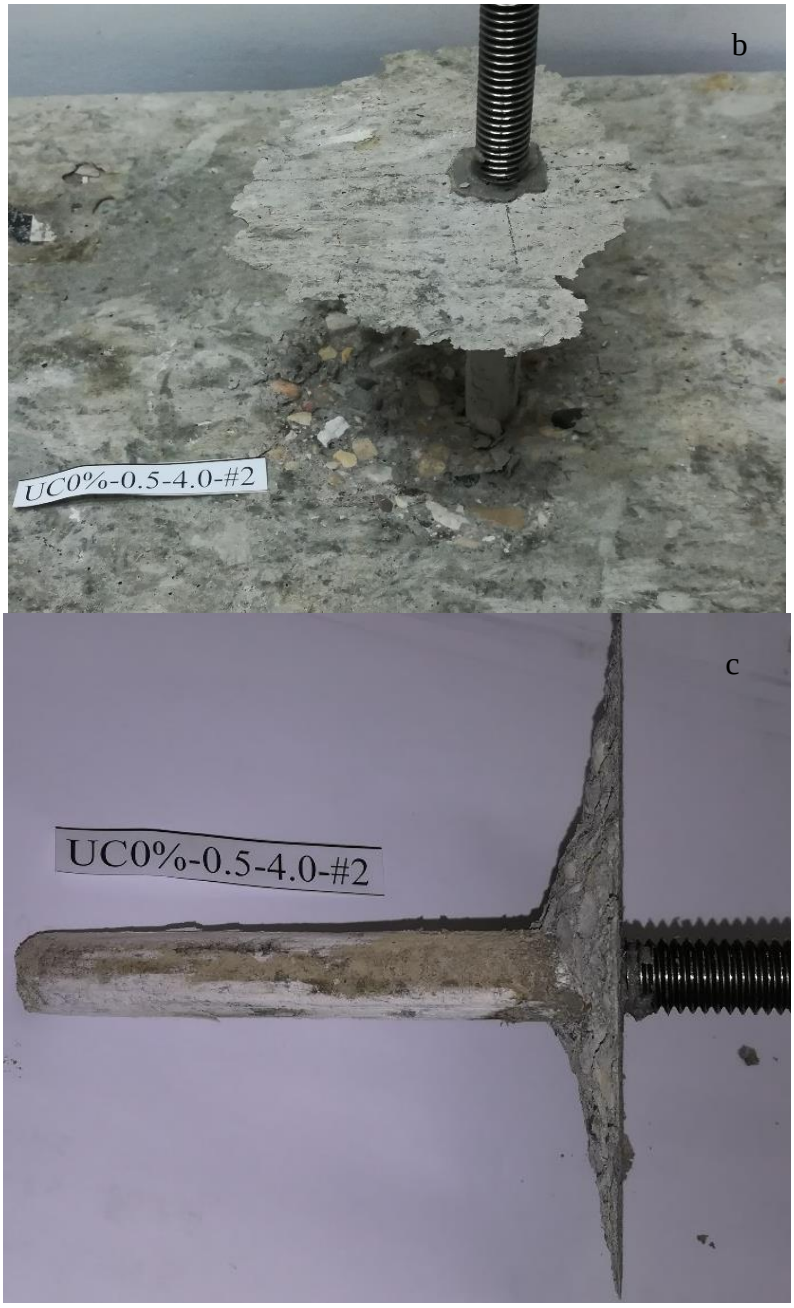

a) load-displacement behavior; b) cracked surface; c) partial cone bond failure

Figure VI.14. Observed behavior of Specimen UC0%-0.5-4.0-#2

15. UC0%-0.5-4.0-#3

The measured ultimate load is at 1.78 kips [7.92 kN] at a displacement of 0.093 in. [2.36 mm]. A circular crack appeared along the anchor at the load of 1.61 kips [7.14 kN] as shown in Figure VI.15b. After passing the ultimate load, the load remained constant as the displacement increased due to the frictional resistance was generated by the rough surface of the drilled hole. The anchor was pulled out with a small concrete cone due to adhesive-concrete interface failure shown in Figure VI.15c.

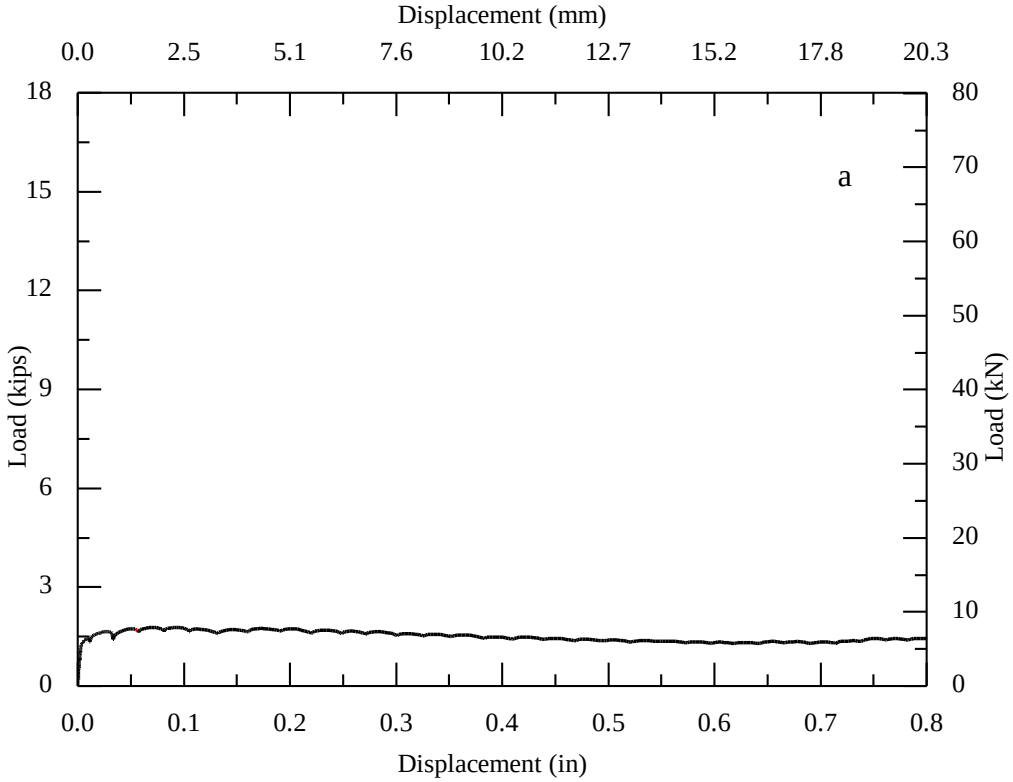

a) load-displacement behavior; b) cracked surface; c) partial cone bond failure

Figure VI.15. Observed behavior of Specimen UC0%-0.5-4.0-#3

16. UC0%-0.5-4.0-#4

The measured ultimate load is at 2.13 kips [9.48 kN] at a displacement of 0.010 in. [0.25 mm]. A circular crack appeared along the anchor at the load of 2.13 kips [9.48 kN] as shown in Figure VI. 16b. After passing the ultimate load, the load remained constant as the displacement increased due to the frictional resistance was generated by the rough surface of the drilled hole. The anchor was pulled out with a small concrete cone due to adhesive-concrete interface failure shown in Figure VI.16c.

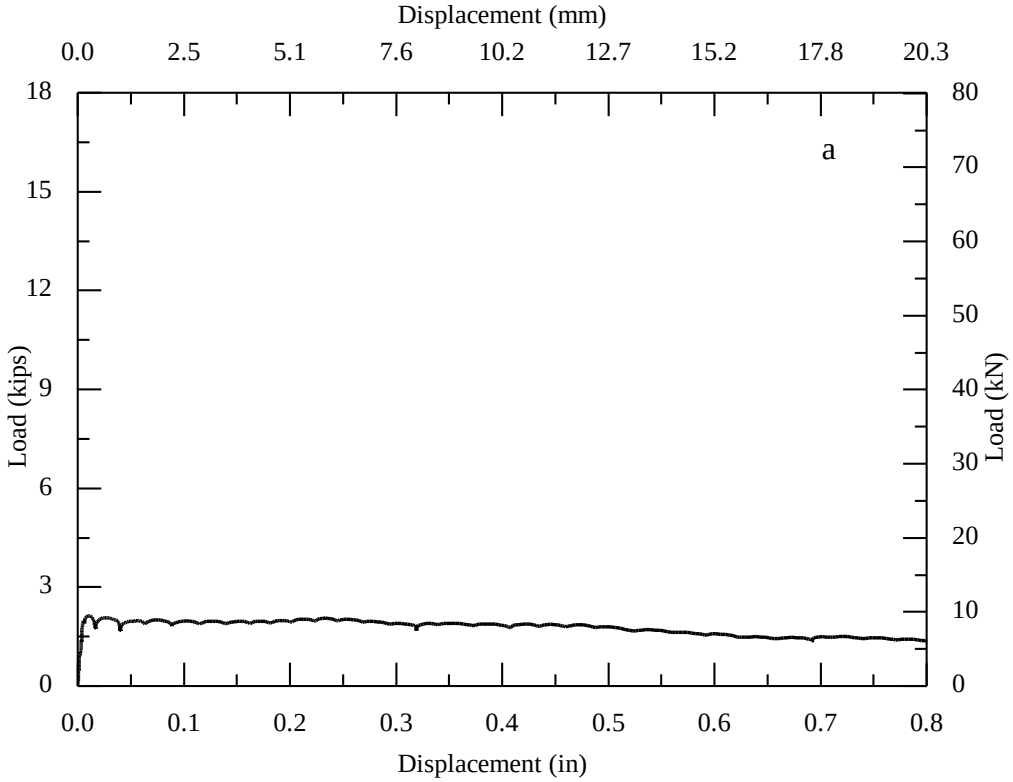

a) load-displacement behavior; b) cracked surface; c) partial cone bond failure

Figure VI.16. Observed behavior of Specimen UC0%-0.5-4.0-#4

17. UC50%-0.5-4.0-#1

The measured ultimate load is at 6.44 kips [28.66 kN] at a displacement of 0.022 in. [0.56 mm]. A circular crack appeared along the anchor at the load of 6.31 kips [28.09 kN] as shown in Figure VI.17b. After passing the ultimate load, the load dropped slowly as the displacement increased due to the frictional resistance was generated by the rough surface of the drilled hole. The anchor was pulled out with a concrete cone due to adhesive-concrete interface failure shown in Figure VI.17c.

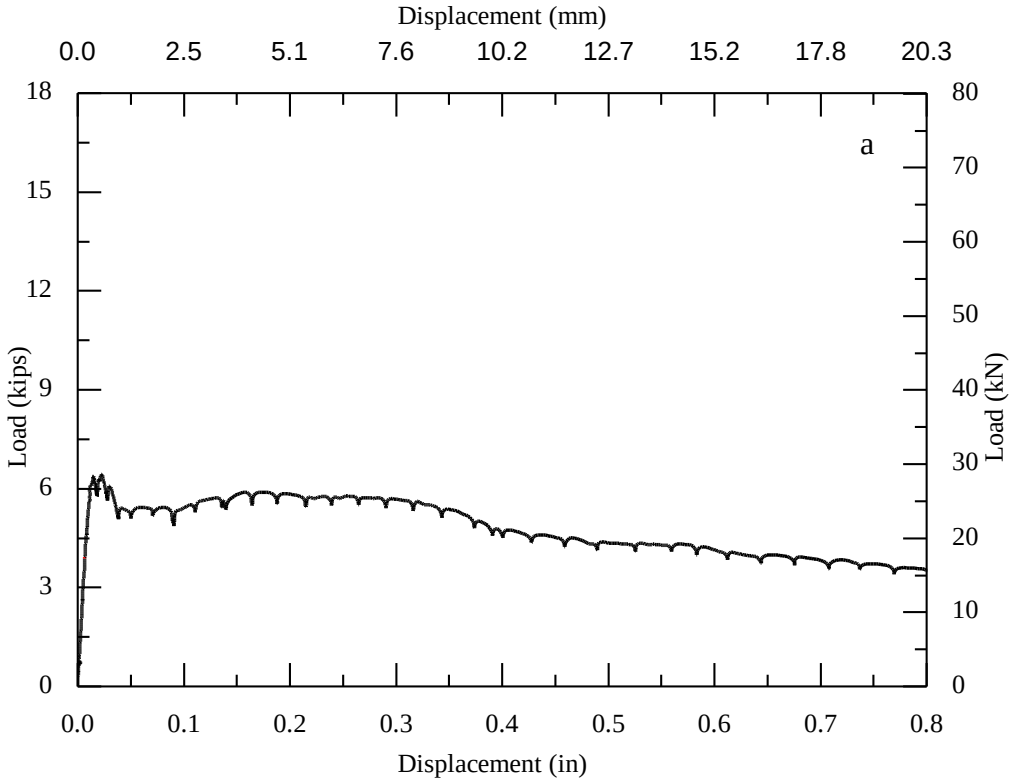

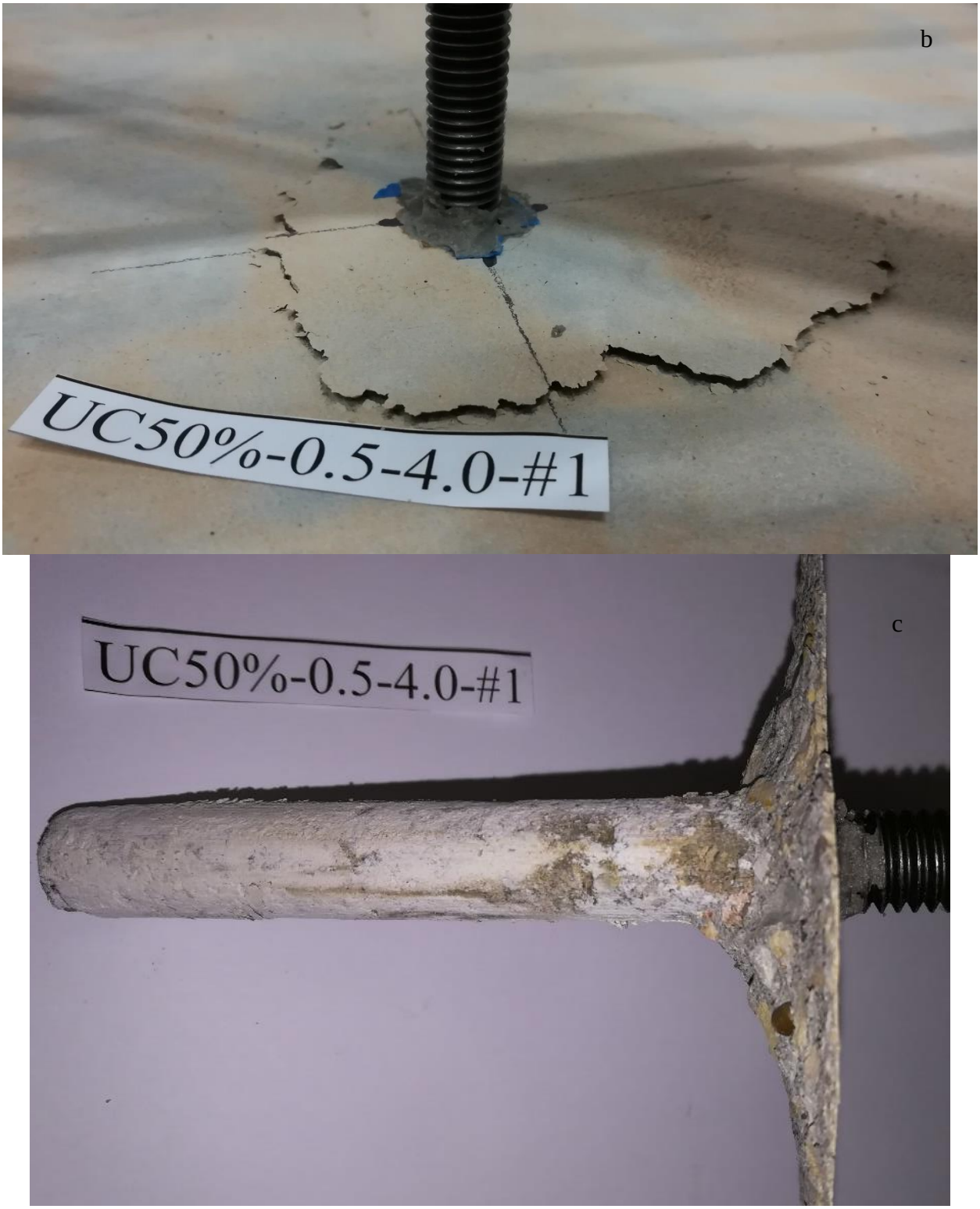

a) load-displacement behavior; b) cracked surface; c) partial cone bond failure

Figure VI.17. Observed behavior of Specimen UC50%-0.5-4.0-#1

18. UC50%-0.5-4.0-#2

The measured ultimate load is at 6.53 kips [29.06 kN] at a displacement of 0.080 in. [2.03 mm]. A circular crack appeared along the anchor at the load of 6.42 kips [28.57 kN] as shown in Figure VI.18b. After passing the ultimate load, the load dropped slowly as the displacement increased due to the frictional resistance was generated by the rough surface of the drilled hole. The anchor was pulled out with a concrete cone due to adhesive-concrete interface failure shown in Figure VI.18c.

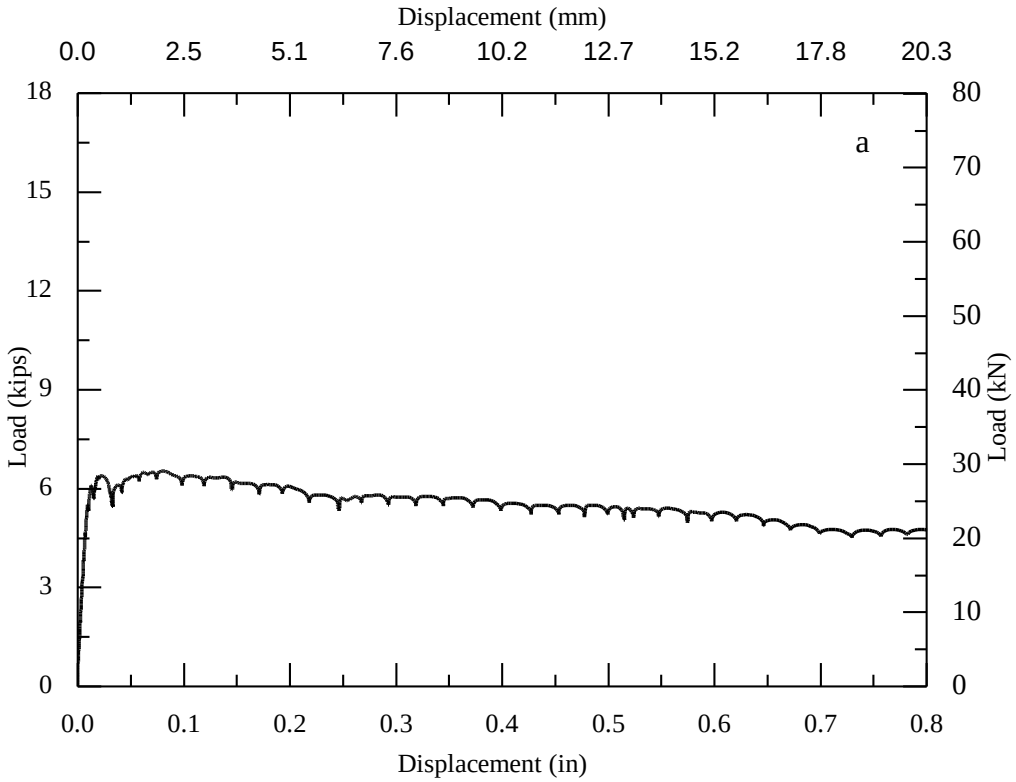

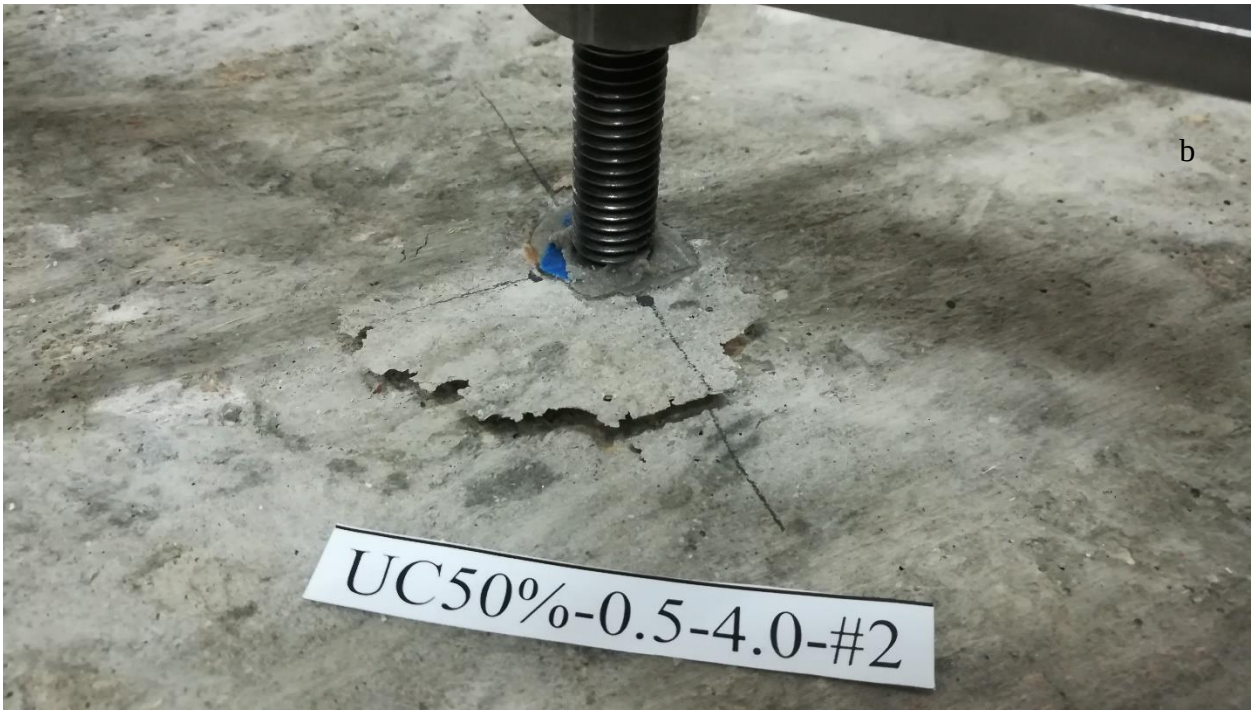

a) load-displacement behavior; b) cracked surface; c) partial cone bond failure

Figure VI.18. Observed behavior of Specimen UC50%-0.5-4.0-#2

19. UC50%-0.5-4.0-#3

The measured ultimate load is at 8.06 kips [35.87 kN] at a displacement of 0.278 in. [0.71 mm]. A circular crack appeared along the anchor at the load of 7.38 kips [32.85 kN] as shown in Figure VI.19b. After passing the ultimate load, the load dropped slowly as the displacement increased due to the frictional resistance was generated by the rough surface of the drilled hole. The anchor was pulled out with a concrete cone due to adhesive-concrete interface failure shown in Figure VI.19c.

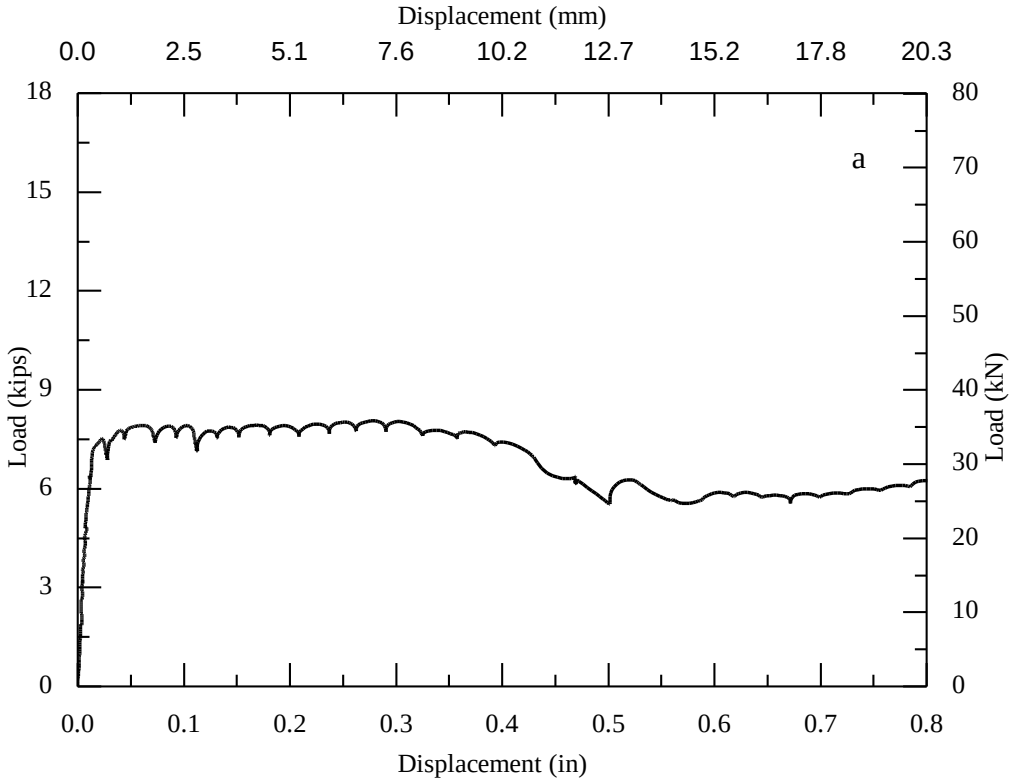

a) load-displacement behavior; b) cracked surface; c) partial cone bond failure

Figure VI.19. Observed behavior of Specimen UC50%-0.5-4.0-#3

20. UC50%-0.5-4.0-#4

The measured ultimate load is at 6.33 kips [28.17 kN] at a displacement of 0.048 in. [1.22 mm]. A circular crack appeared along the anchor at the load of 4.82 kips [21.43 kN] as shown in Figure VI.20b. After passing the ultimate load, the load remained constant as the displacement increased due to the frictional resistance was generated by the rough surface of the drilled hole. The anchor was pulled out with a concrete cone due to adhesive-concrete interface failure shown in Figure VI.20c.

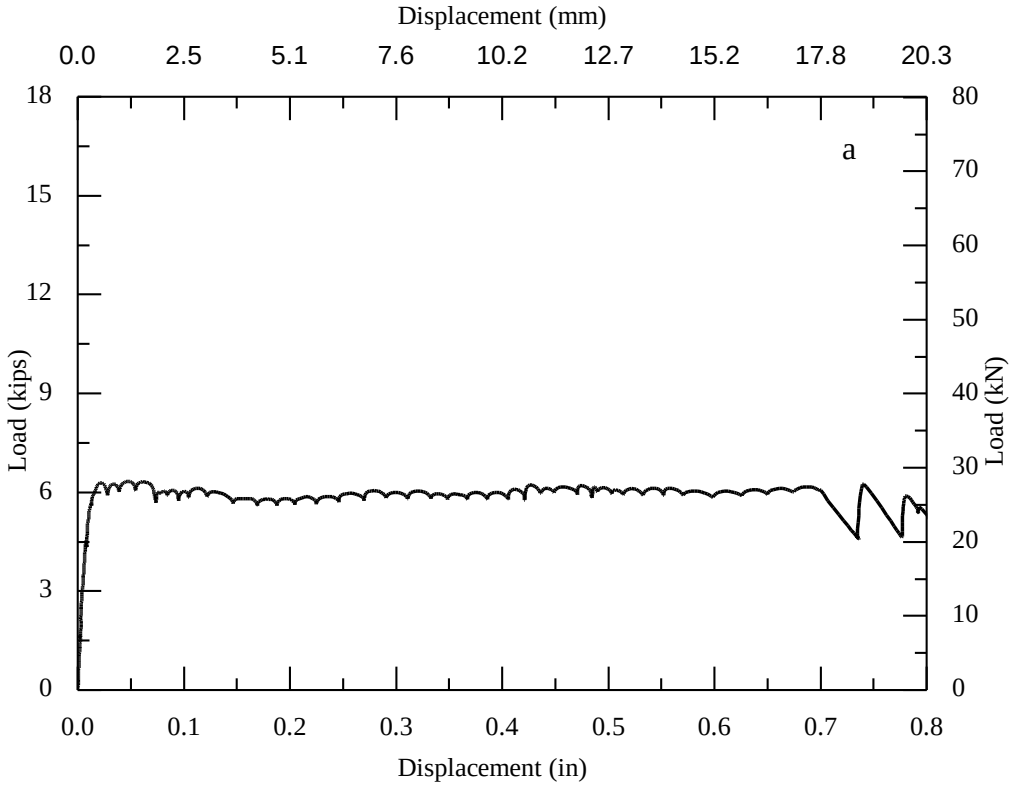

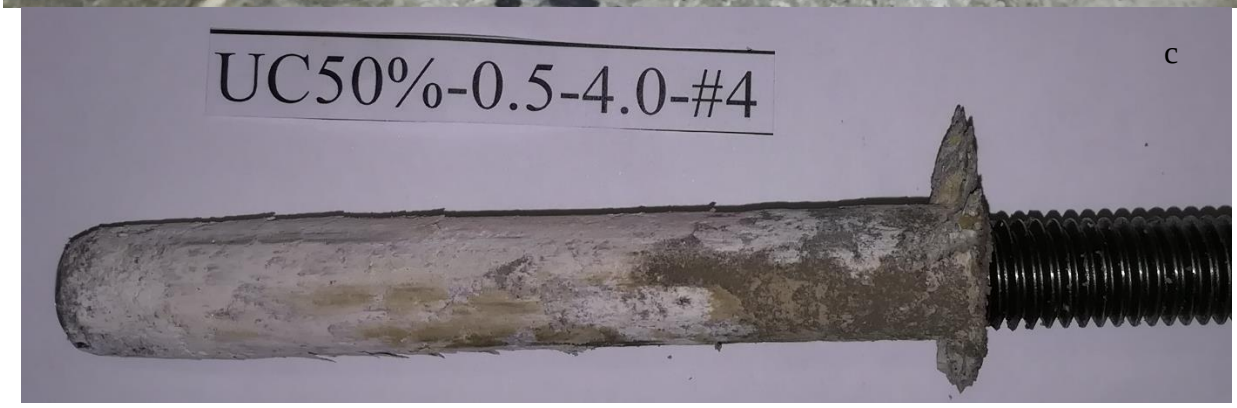

a) load-displacement behavior; b) cracked surface; c) partial cone bond failure

Figure VI.20. Observed behavior of Specimen UC50%-0.5-4.0-#4

21. UCT0%-0.5-4.0-#1

The measured ultimate load is at 7.57 kips [33.69 kN] at a displacement of 0.077 in. [1.96 mm]. A circular crack appeared along the anchor at the load of 4.82 kips [21.43 kN] as shown in Figure VI.21b. After passing the ultimate load, the load was up and down as the displacement increased due to the threads sheared off continually and the frictional resistance generated by the rough surface of the drilled hole. The anchor was pulled out with a concrete cone due to adhesive-concrete interface failure shown in Figure VI.21c.

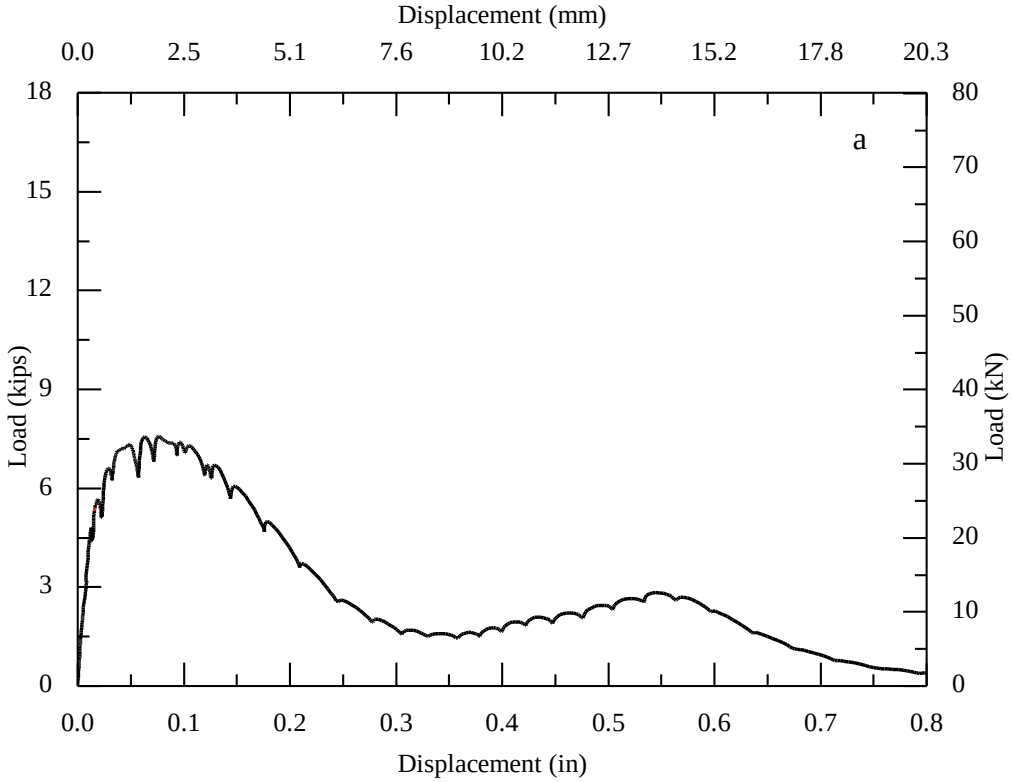

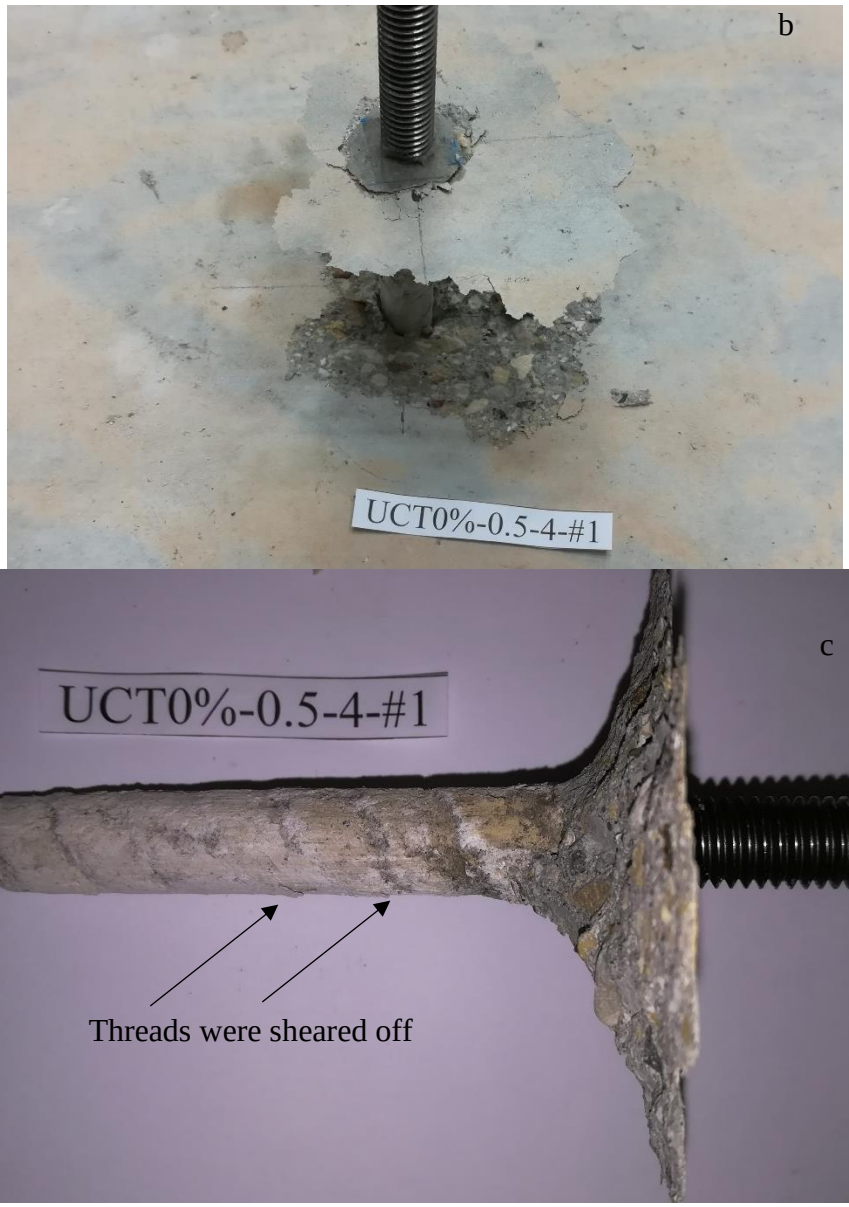

a) load-displacement behavior; b) cracked surface; c) partial cone bond failure

Figure VI.21. Observed behavior of Specimen UCT0%-0.5-4.0-#1

22. UCT0%-0.5-4.0-#2

The measured ultimate load is at 6.07 kips [27.01 kN] at a displacement of 0.057 in. [1.45 mm]. A circular crack appeared along the anchor at the load of 4.6 kips [20.47 kN] as shown in Figure VI.22b. After passing the ultimate load, the load was up and down as the displacement increased due to the threads sheared off continually and the frictional resistance generated by the rough surface of the drilled hole. The anchor was pulled out with a concrete cone due to adhesive-concrete interface failure shown in Figure VI.22c.

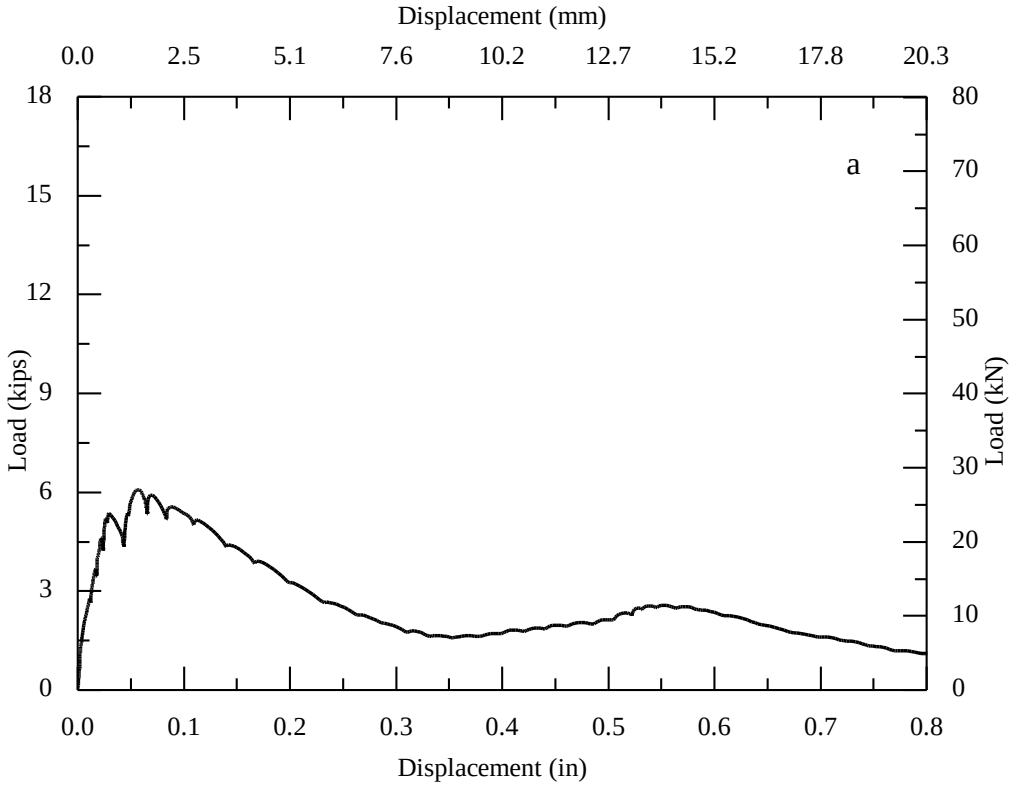

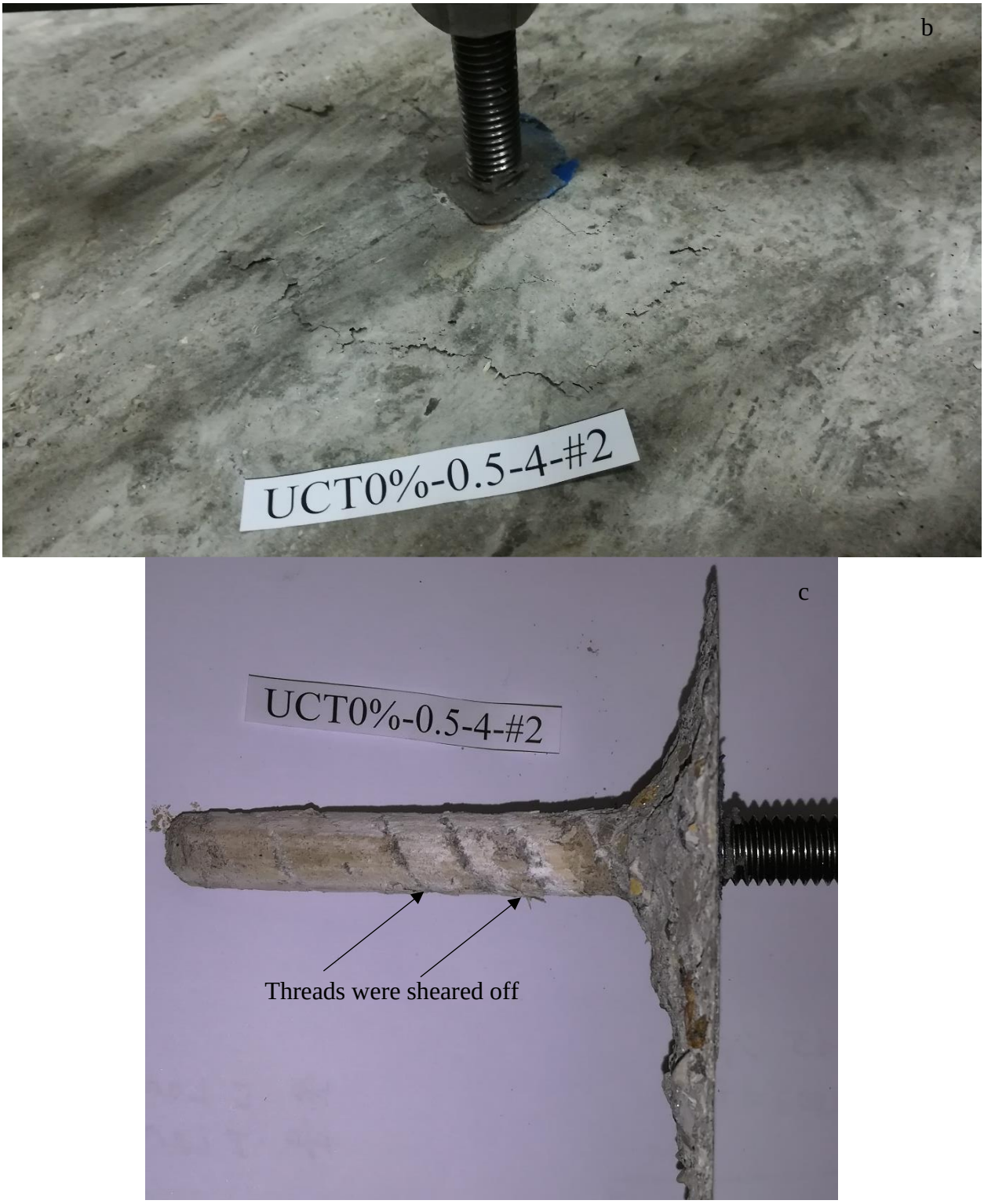

a) load-displacement behavior; b) cracked surface; c) partial cone bond failure

Figure VI.22. Observed behavior of Specimen UCT0%-0.5-4.0-#2

23. UCT0%-0.5-4.0-#3

The measured ultimate load is at 5.71 kips [25.41 kN] at a displacement of 0.123 in. [3.12 mm]. A circular crack appeared along the anchor at the load of 3.75 kips [16.69 kN] as shown in Figure VI.23b. After passing the ultimate load, the load was up and down as the displacement increased due to the threads sheared off continually and the frictional resistance generated by the rough surface of the drilled hole. The anchor was pulled out with a concrete cone due to adhesive-concrete interface failure shown in Figure VI.23c.

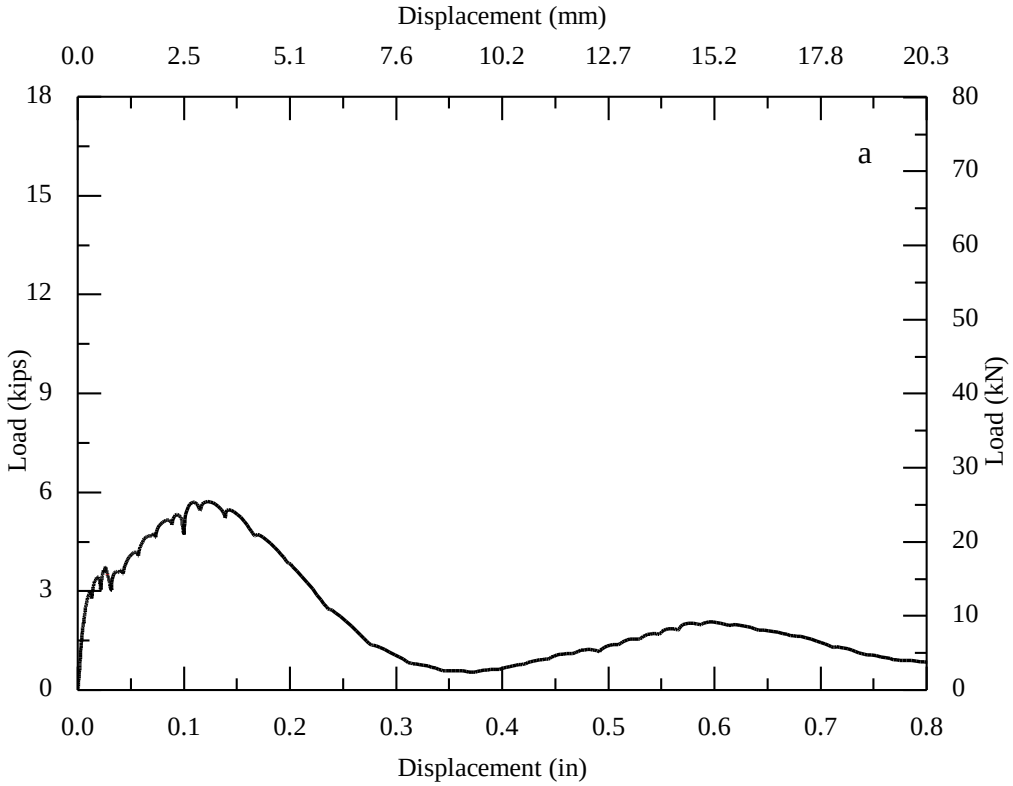

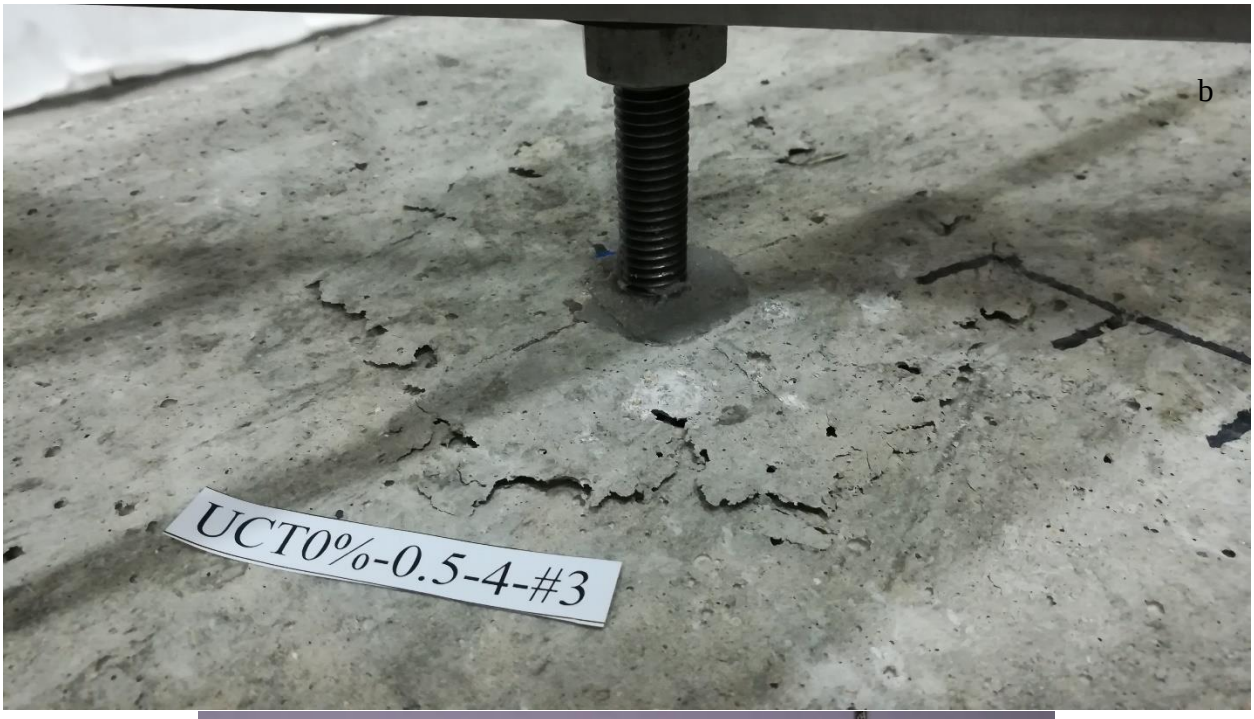

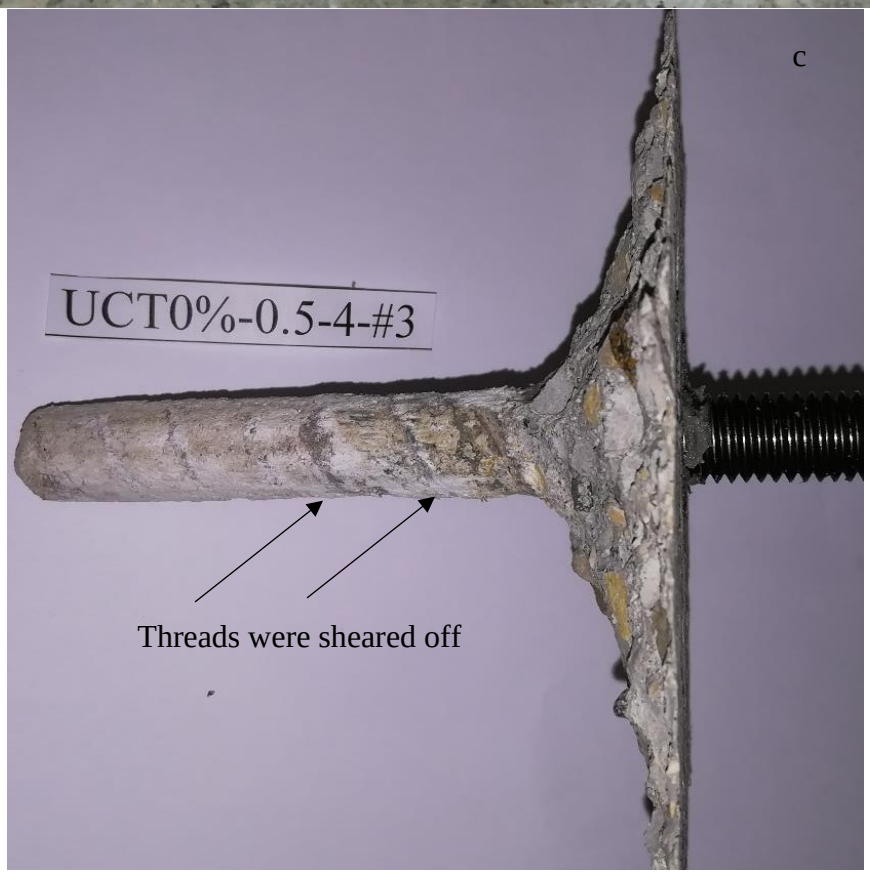

a) load-displacement behavior; b) cracked surface; c) partial cone bond failure

Figure VI.23. Observed behavior of Specimen UCT0%-0.5-4.0-#3

24. UCT0%-0.5-4.0-#4

The measured ultimate load is at 7.05 kips [31.37 kN] at a displacement of 0.093 in. [2.36 mm]. A circular crack appeared along the anchor at the load of 3.75 kips [16.67 kN] as shown in Figure VI.24b. After passing the ultimate load, the load was up and down as the displacement increased due to the threads sheared off continually and the frictional resistance generated by the rough surface of the drilled hole. The anchor was pulled out with a concrete cone due to adhesive-concrete interface failure shown in Figure VI.24c.

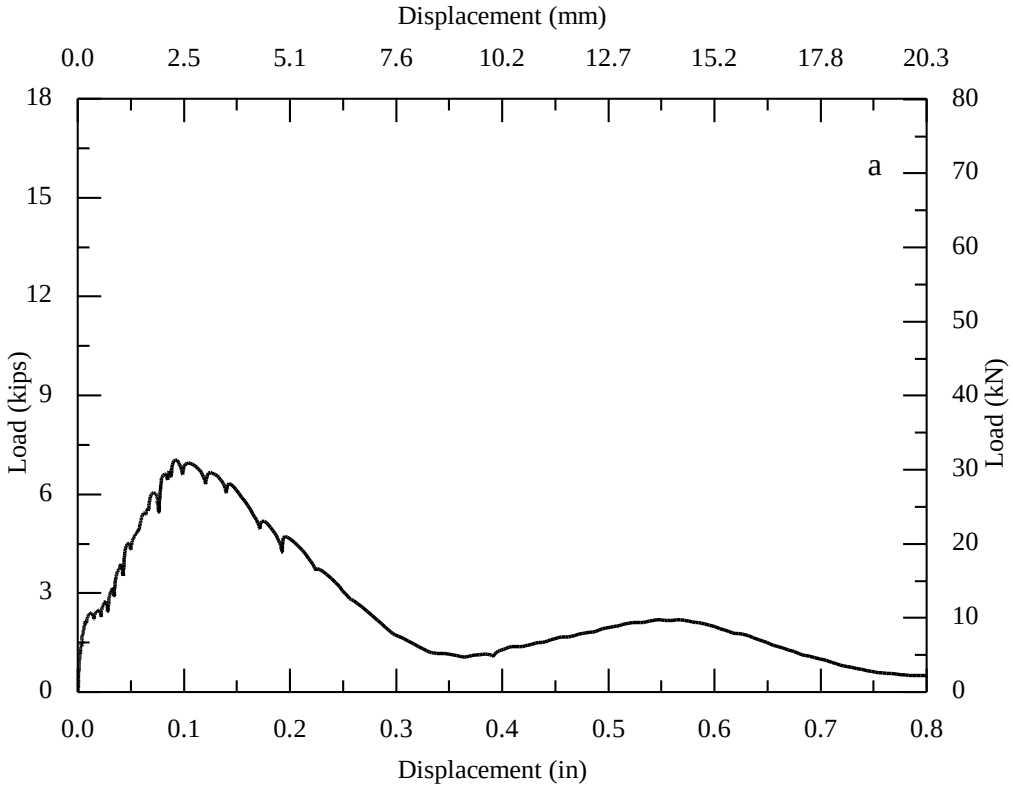

a) load-displacement behavior; b) cracked surface; c) partial cone bond failure

Figure VI.24. Observed behavior of Specimen UCT0%-0.5-4.0-#4

25. UCT50%-0.5-4.0-#1

The measured ultimate load is at 12.83 kips [57.09 kN] at a displacement of 0.038 in. [0.97 mm]. A circular crack appeared along the anchor at the load of 11.77 kips [52.38 kN] as shown in Figure VI.25b. After passing the ultimate load, the load dropped quickly as the displacement increased due to the threads sheared off continually and the frictional resistance generated by the rough surface of the drilled hole. The anchor was pulled out with a concrete cone due to adhesive-concrete and adhesive-steel interface failure shown in Figure VI.25c.

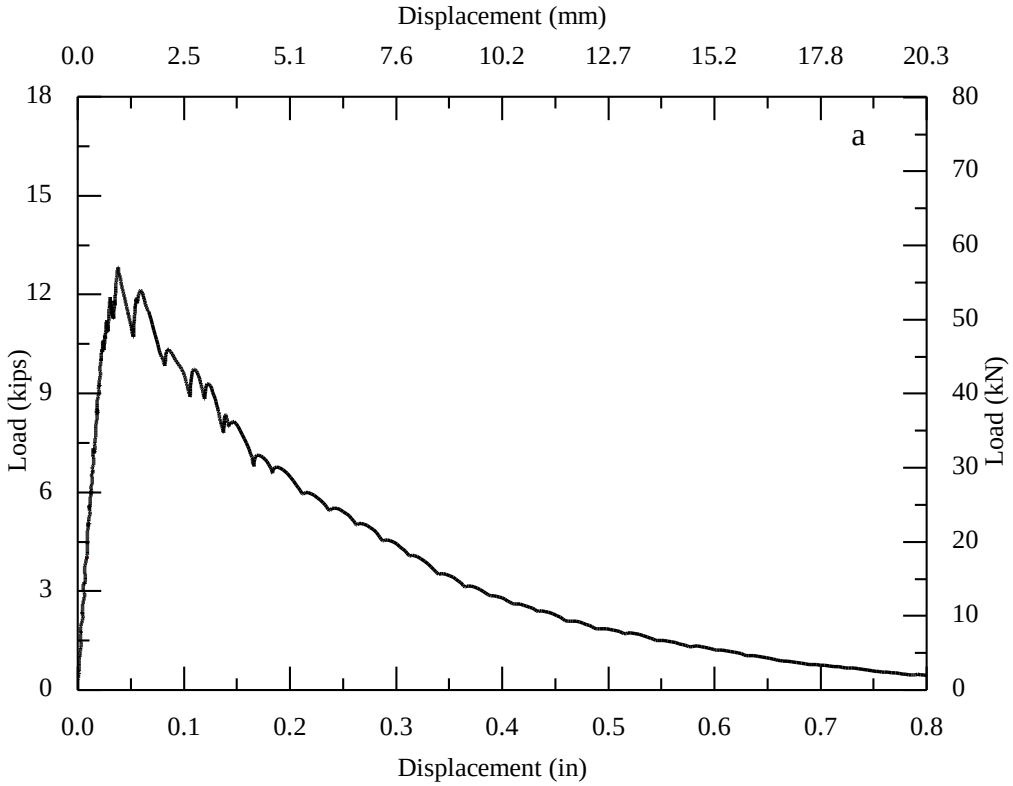

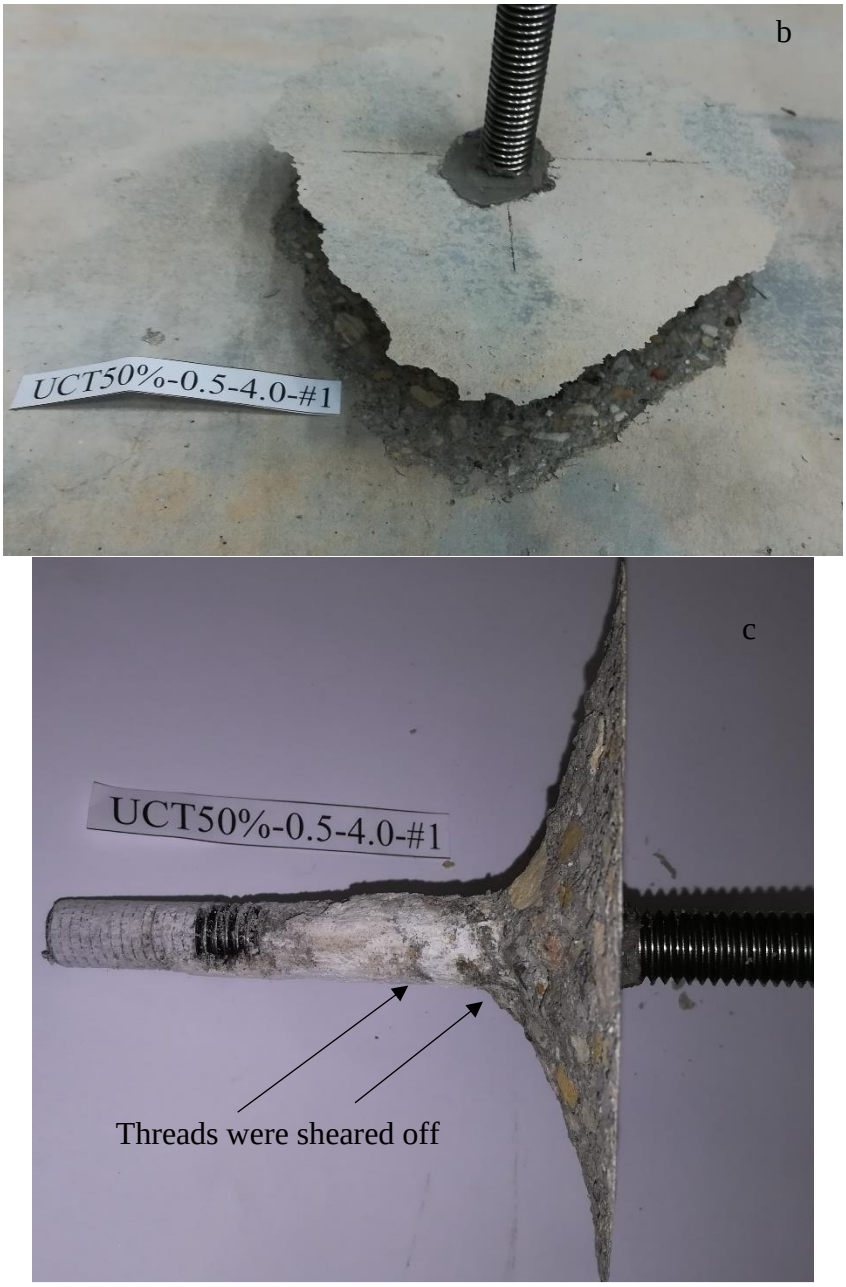

a) load-displacement behavior; b) cracked surface; c) partial cone bond failure

Figure VI.25. Observed behavior of Specimen UCT50%-0.5-4.0-#1

26. UCT50%-0.5-4.0-#2

. The measured ultimate load is at 13.70 kips [60.97 kN] at a displacement of 0.095 in. [2.41 mm]. As shown in Figure VI.26b, a circular crack appeared along the anchor at the load of 10.7 kips [47.62 mm]. One crack represented splitting and passing the anchor in the transverse direction at the load of 13.38 kips [59.52 kN]. After passing the ultimate load, the load was up and down as the displacement increased due to the threads sheared off continually and the frictional resistance generated by the rough surface of the drilled hole. The anchor was pulled out with a concrete cone due to adhesive-concrete interface failure shown in Figure VI.26c.

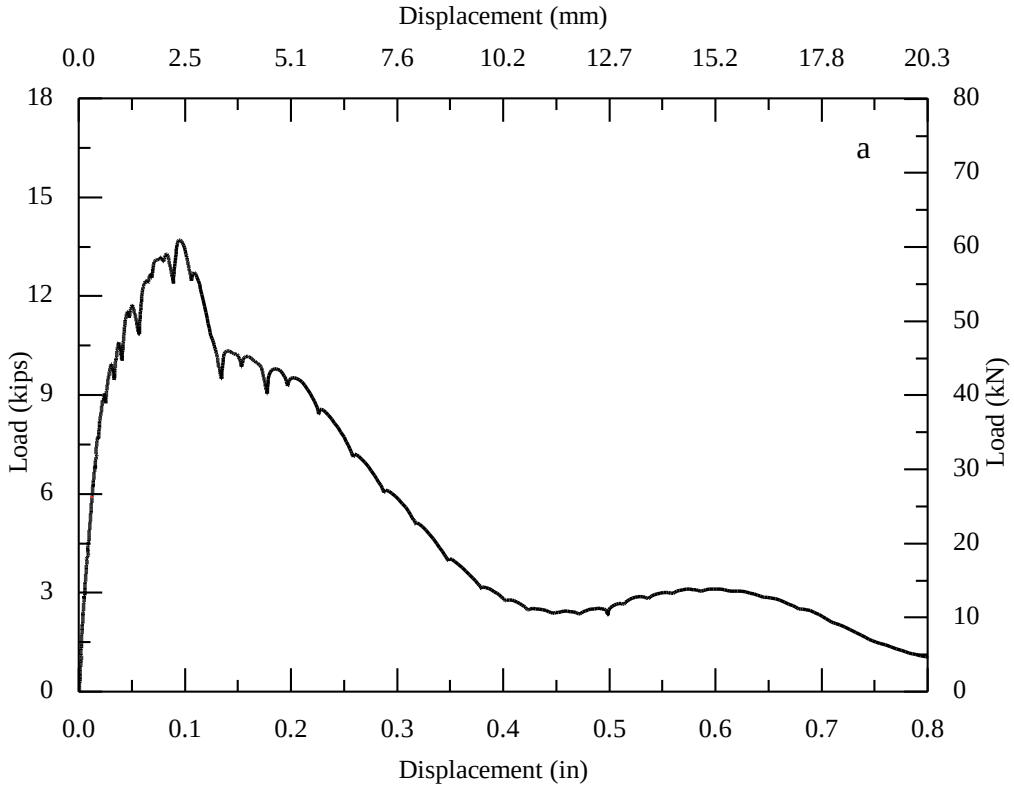

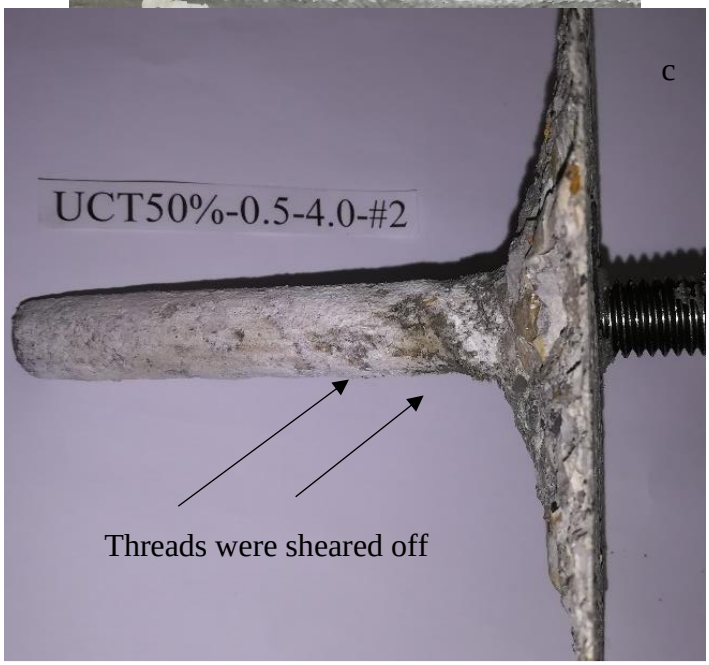

a) load-displacement behavior; b) cracked surface; c) partial cone bond failure

Figure VI.26. Observed behavior of Specimen UCT50%-0.5-4.0-#2

27. UCT50%-0.5-4.0-#3

The measured ultimate load is at 12.11 kips [53.89 kN] at a displacement of 0.041 in. [1.04 mm]. A circular crack appeared along the anchor at the load of 10.7 kips [47.62 kN] as shown in Figure VI.27b. After passing the ultimate load, the load dropped quickly as the displacement increased due to the threads sheared off continually and the frictional resistance generated by the rough surface of the drilled hole. The anchor was pulled out with a concrete cone due to adhesive-concrete interface failure shown in Figure VI.27c.

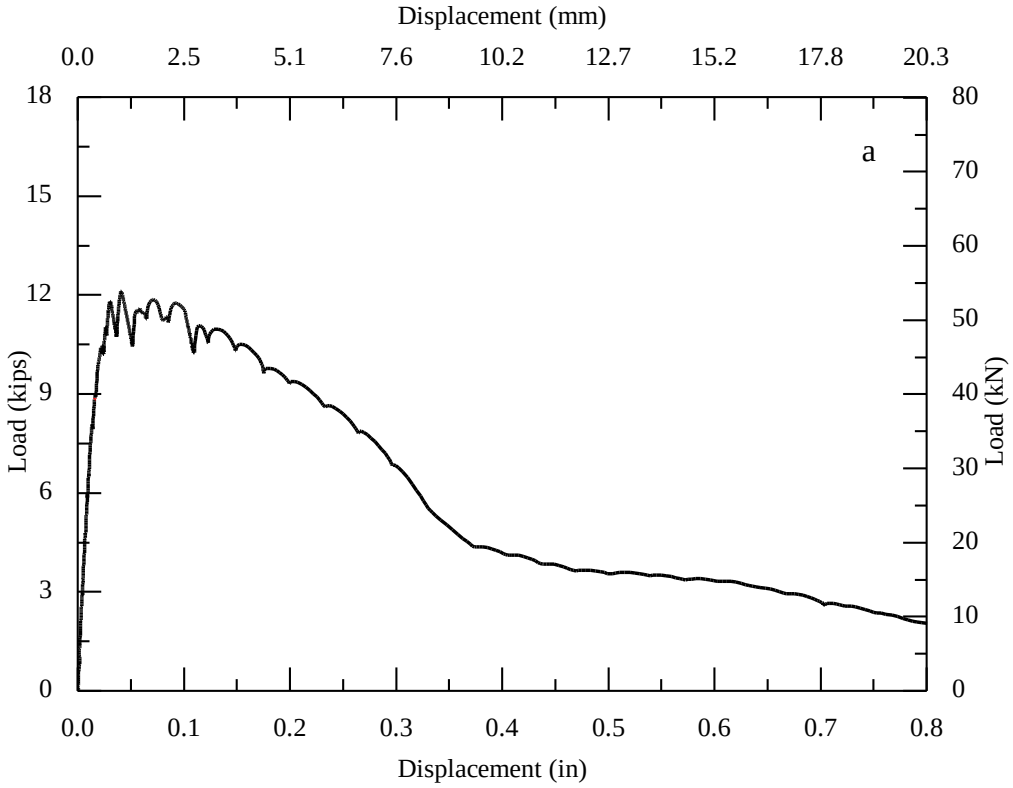

a) load-displacement behavior; b) cracked surface; c) partial cone bond failure

Figure VI.27. Observed behavior of Specimen UCT50%-0.5-4.0-#3

28. UCT50%-0.5-4.0-#4

The measured ultimate load is at 13.61 kips [60.56 kN] at a displacement of 0.030 in. [0.76 mm]. As shown in Figure VI.28b, a circular crack appeared along the anchor at the load of 13.38 kips [59.52 kN]. One crack represented splitting and passing the anchor in the transverse direction at the load of 12.84 kips [57.14 kN]. After passing the ultimate load, the load dropped gradually as the displacement increased due to the threads sheared off continually and the frictional resistance generated by the rough surface of the drilled hole. The anchor was pulled out with a concrete cone due to adhesive-concrete and adhesive-steel interface failure shown in Figure VI.28c.

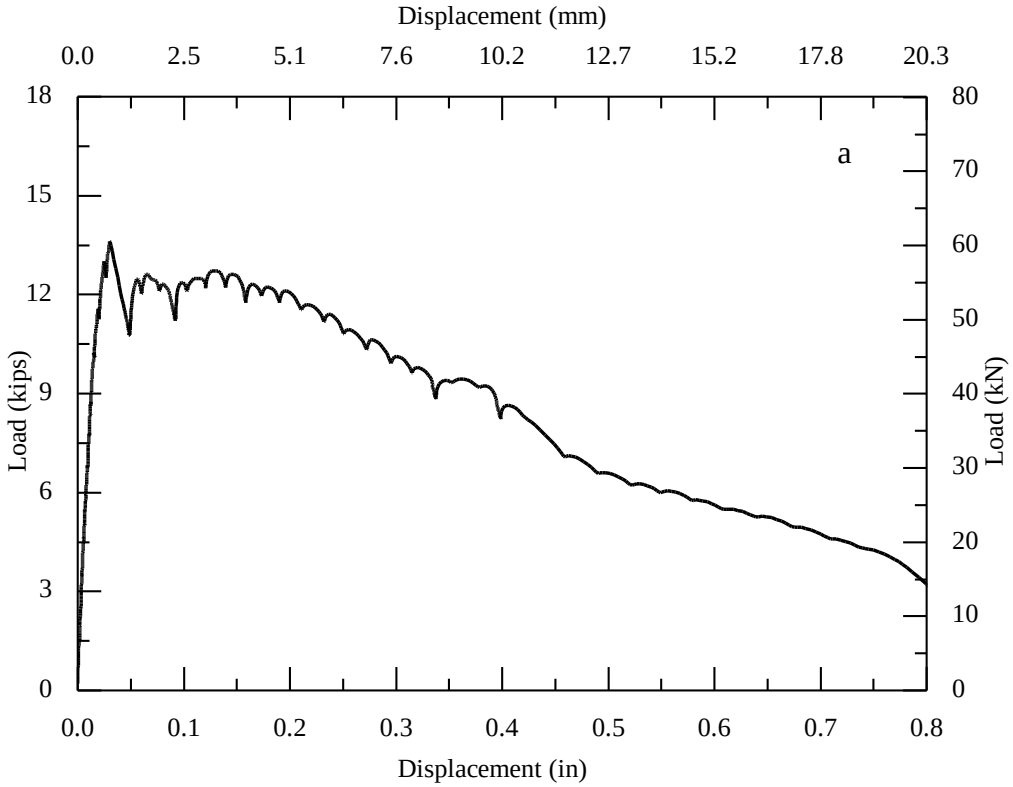

a) load-displacement behavior; b) cracked surface; c) partial cone bond failure

Figure VI.28. Observed behavior of Specimen UCT50%-0.5-4.0-#4

29. UCT#R50%-0.5-4.0-#1

The measured ultimate load is at 12.28 kips [65.7 kN] at a displacement of 0.094 in. [2.39 mm]. A circular crack appeared along the anchor while the load reached 7.49 kips [33.33 kN] as shown in Figure VI.29b. After passing the ultimate load, the load was up and down as the displacement increased due to the threads sheared off continually and the frictional resistance generated by the rough surface of the drilled hole. The anchor was pulled out with a concrete cone due to adhesive-concrete interface failure shown in Figure VI.29c.

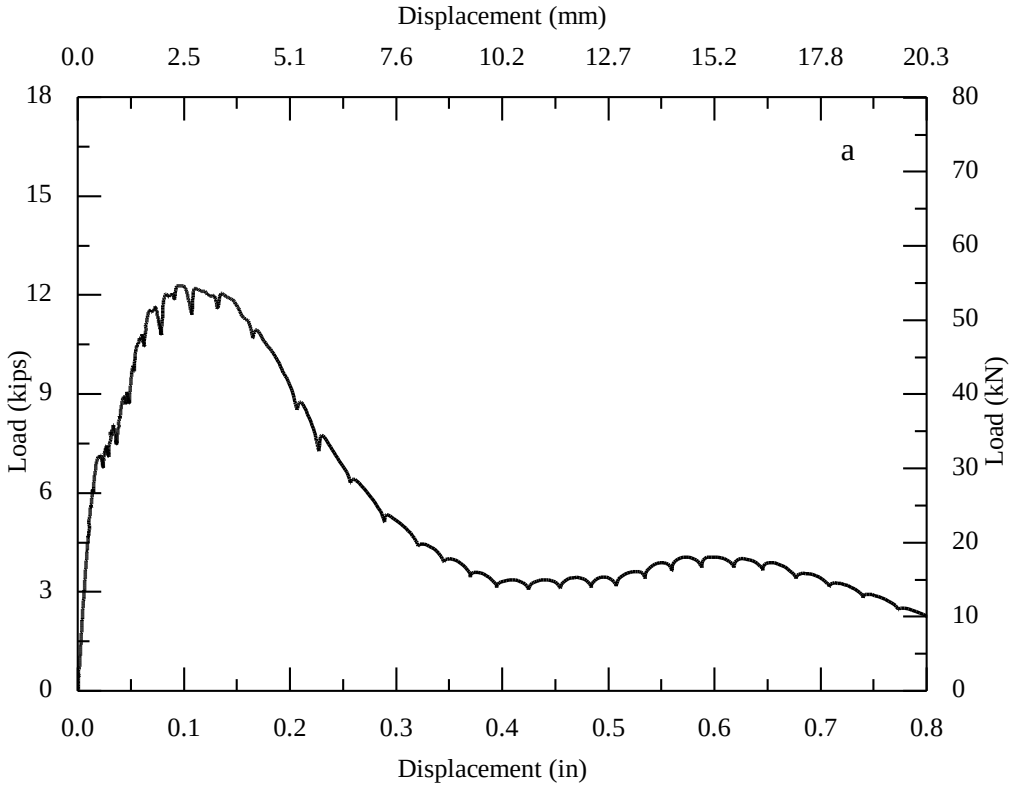

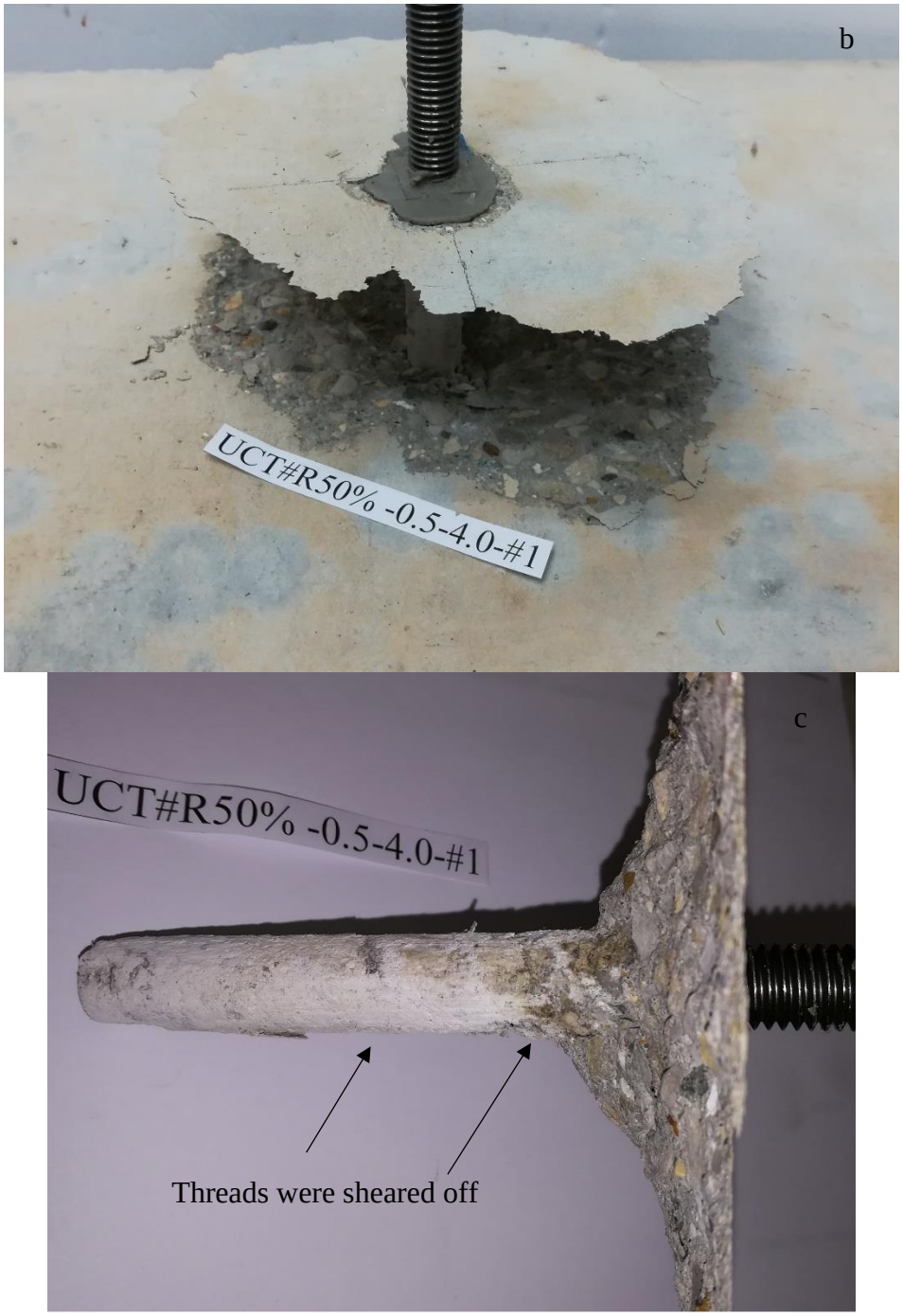

a) load-displacement behavior; b) cracked surface; c) partial cone bond failure

Figure VI.29. Observed behavior of Specimen UCT#R50%-0.5-4.0-#1

30. UCT#R50%-0.5-4.0-#2

The measured ultimate load is at 12.85 kips [57.18 kN] at a displacement of 0.117 in. [2.97 mm]. A circular crack appeared along the anchor at the load of 10.43 kips [46.42 kN] as shown in Figure VI.30b. After passing the ultimate load, the load was up and down as the displacement increased due to the threads sheared off continually and the frictional resistance generated by the rough surface of the drilled hole. The anchor was pulled out with a concrete cone due to adhesive-concrete interface failure shown in Figure VI.30c.

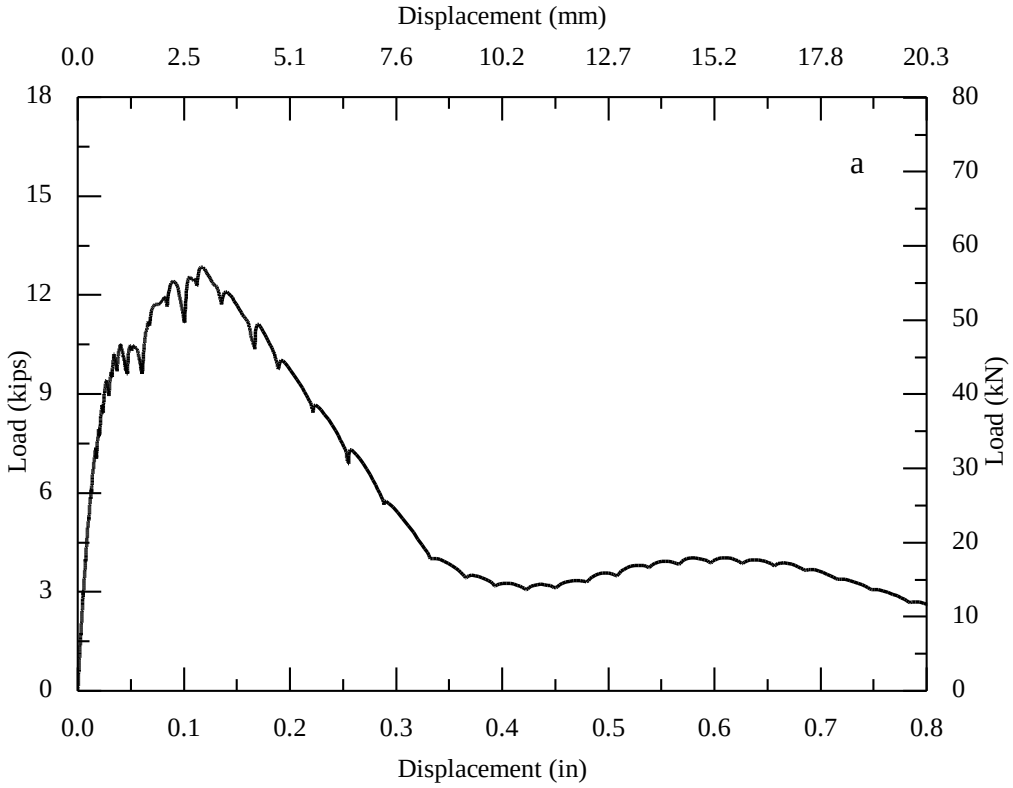

a) load-displacement behavior; b) cracked surface; c) partial cone bond failure

Figure VI.30. Observed behavior of Specimen UCT#R50%-0.5-4.0-#2

31. UCT#R50%-0.5-4.0-#3

The measured ultimate load is at 13.08 kips [58.21 kN] at a displacement of 0.070 in. [1.78 mm]. As shown in Figure VI.31b, a circular crack appeared along the anchor at the load of 13.08 kips [58.21 kN]. One crack represented splitting and passing the anchor in the transverse direction at the load of 10.38 kips [46.19 kN]. After passing the ultimate load, the load dropped quickly as the displacement increased due to the threads sheared off continually and the frictional resistance generated by the rough surface of the drilled hole. The anchor was pulled out with a concrete cone due to adhesive-concrete and adhesive-steel interface failure shown in Figure VI.31c.

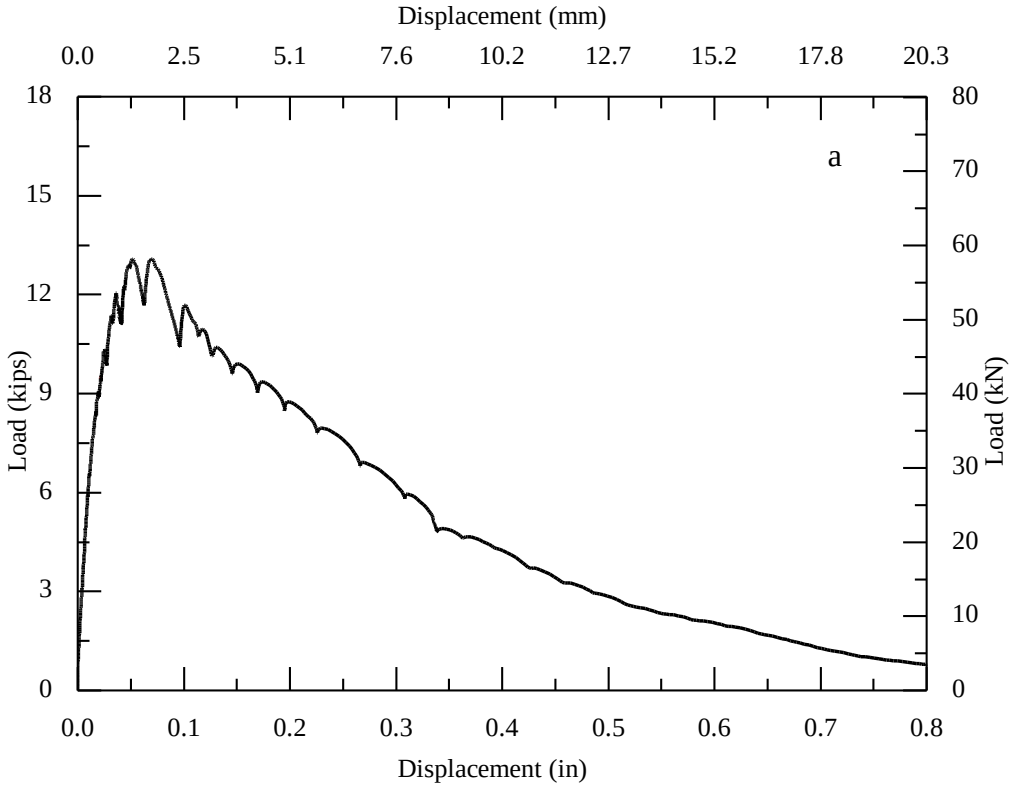

a) load-displacement behavior; b) cracked surface; c) partial cone bond failure

Figure VI.31. Observed behavior of Specimen UCT#R50%-0.5-4.0-#3

32. UCT#R50%-0.5-4.0-#4

The measured ultimate load is at 11.27 kips [50.15 kN] at a displacement of 0.051 in. [1.3 mm]. One initial crack was generated by previous tests and the crack was in transverse direction, which was about 1 in. [25.4 mm] away from on the right side of the anchor. As shown in Figure VI.32b, a circular crack appeared along the anchor at the load of 10.7 kips [47.62 kN]. One crack represented splitting and passing the anchor in the transverse direction at the load of 110.17 kips [45.23 kN]. After passing the ultimate load, the load dropped quickly as the displacement increased due to the threads sheared off continually and the frictional resistance generated by the rough surface of the drilled hole. The anchor was pulled out with a concrete cone due to adhesive-concrete and adhesive-steel interface failure shown in Figure VI.32c.

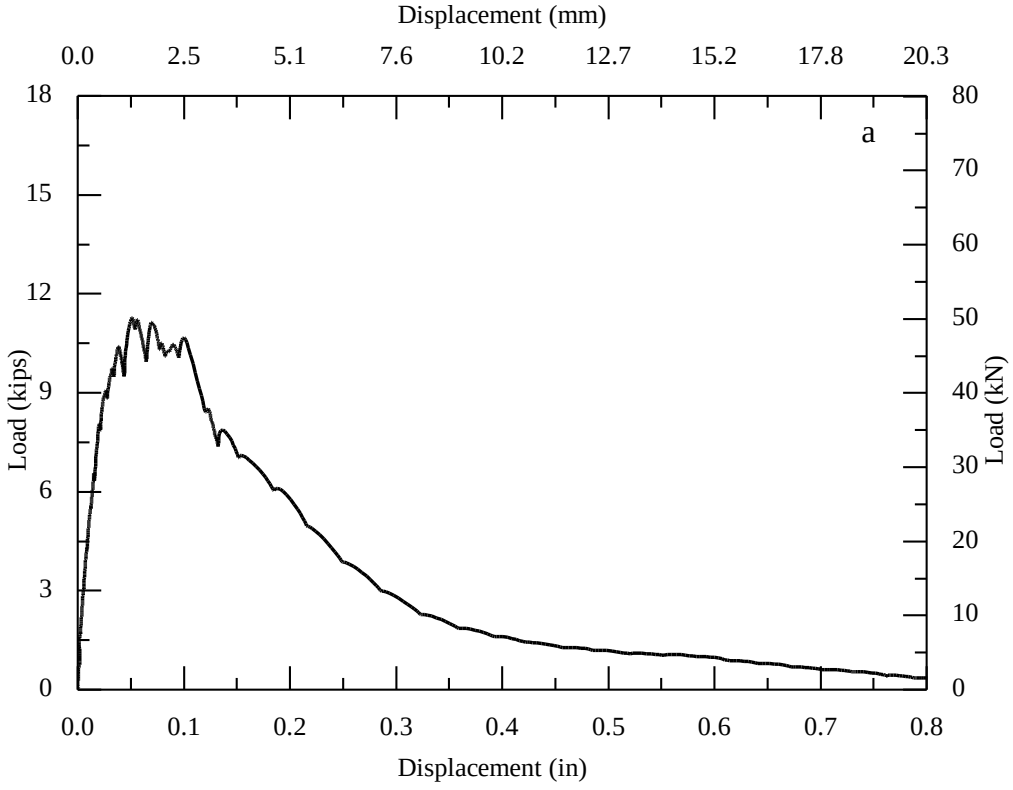

a) load-displacement behavior; b) cracked surface; c) partial cone bond failure

Figure VI.32. Observed behavior of Specimen UCT#R50%-0.5-4.0-#4

33. UC-0.625-5.0-#1

The measured ultimate load is at 16.57 kips [73.74 kN] at a displacement of 0.018 in. [0.46 mm]. As shown in Figure VI.33b, one crack represented splitting and passing the anchor in the transverse direction at the load of 16.57 kips [73.74 kN] with 1.5 in. [38.1 mm] crack depth; one represented splitting in the transverse direction at the load of 16.57 kips [73.74 kN] with 1.5 in. [38.1 mm], which was about 2.5 in. [63.5 mm] away from the left side of the anchor. The predicted capacity measuring a 2.87-in. [72.9 mm] deep breakout simultaneously with a 2 -in. [50.8 mm] deep bond failure (16.25 kips) [72.33 kN]. The anchor was pulled out with a concrete cone due to concrete breakout failure shown in Figure VI.33c.

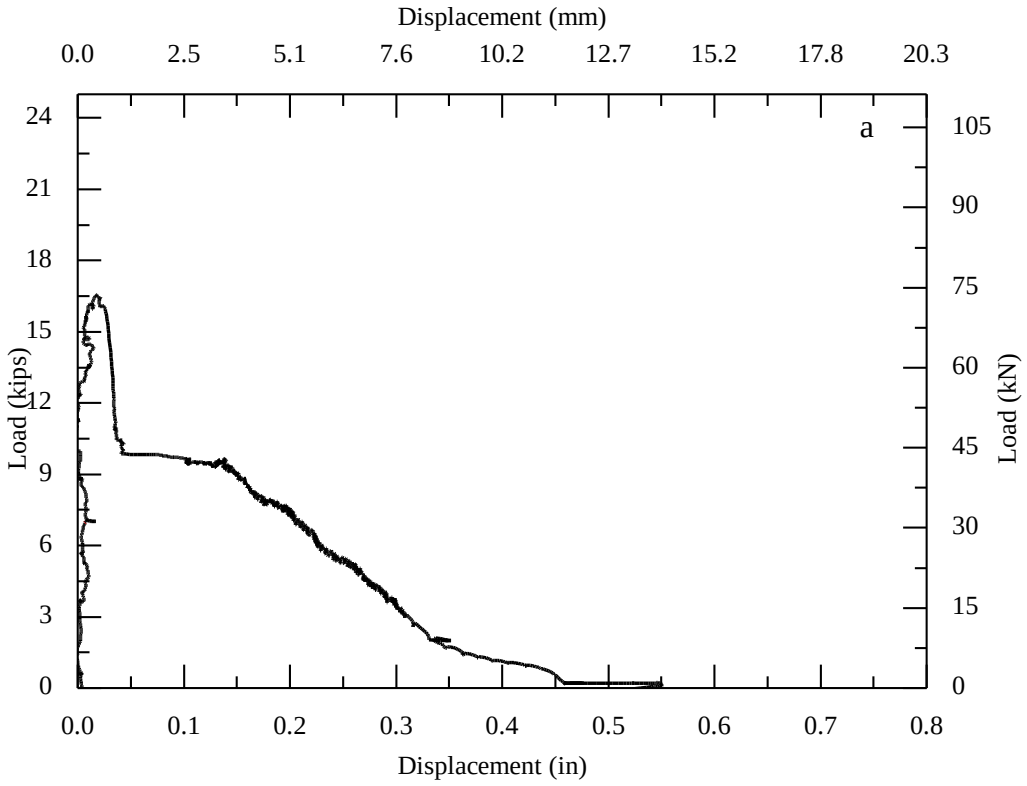

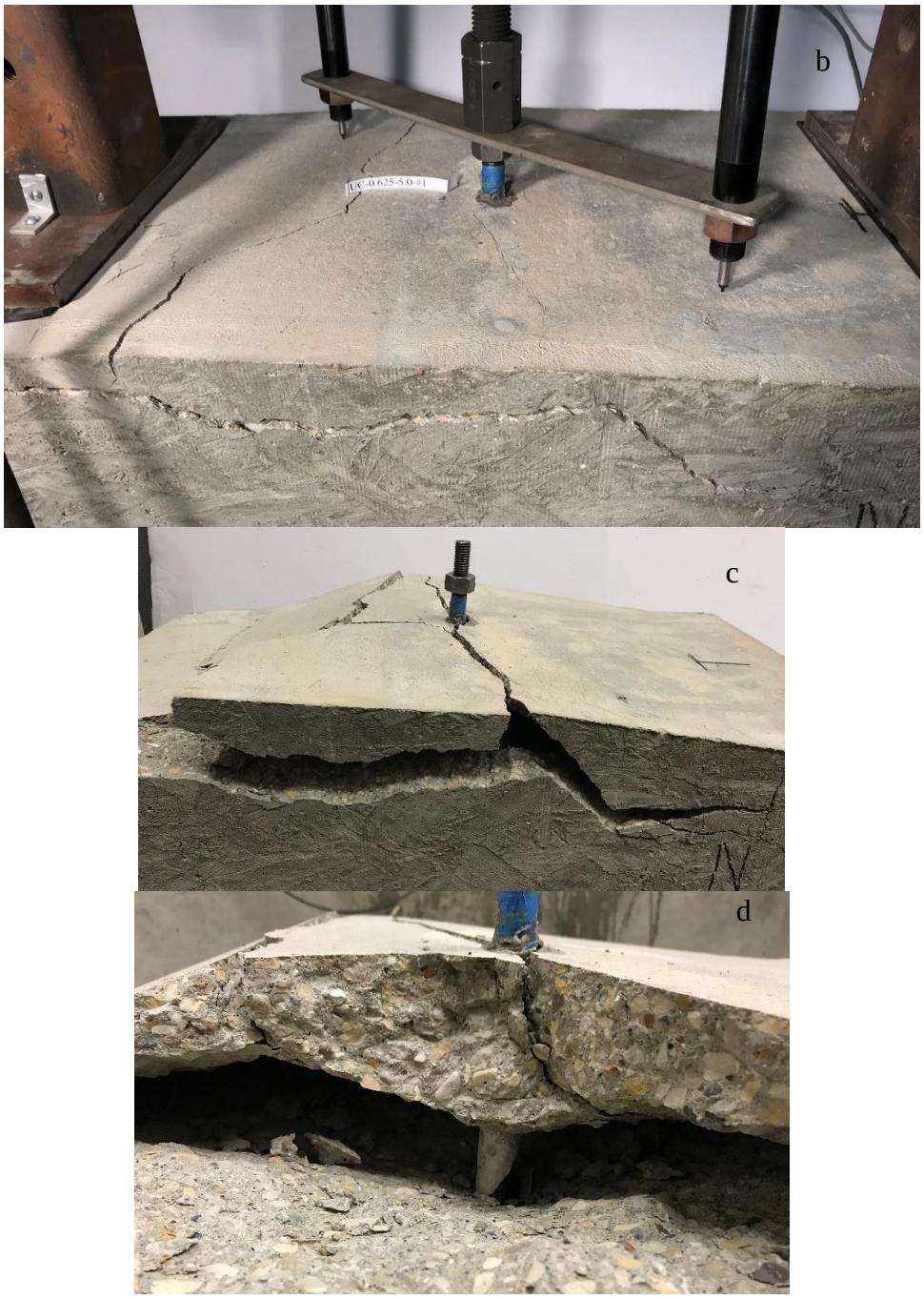

a) load-displacement behavior; b) cracked surface; c) d) concrete breakout failure.

Figure VI.33. Observed behavior of Specimen UC-0.625-5.0-#1

34. UC-0.625-5.0-#2

The measured ultimate load is at 18.46 kips [82.15 kN] at a displacement of 0.021 in. [0.53 mm]. As shown in Figure VI.34b, one crack represented splitting and passing the anchor in the transverse direction at the load of 18.46 kips [82.15 kN] with 2 in. [50.8 mm] crack depth; one cracks represented splitting and passing the anchor in the longitudinal direction at the load of 18.46 kips [82.15 kN]. The predicted capacity measuring a 4.09-in. [103.76 mm] deep breakout simultaneously with a 0.75 -in. [19.05 mm] deep bond failure (18.25 kips) [81.22 kN]. The anchor was pulled out with a concrete cone due to adhesive-concrete interface and concrete breakout failure shown in Figure VI.34c.

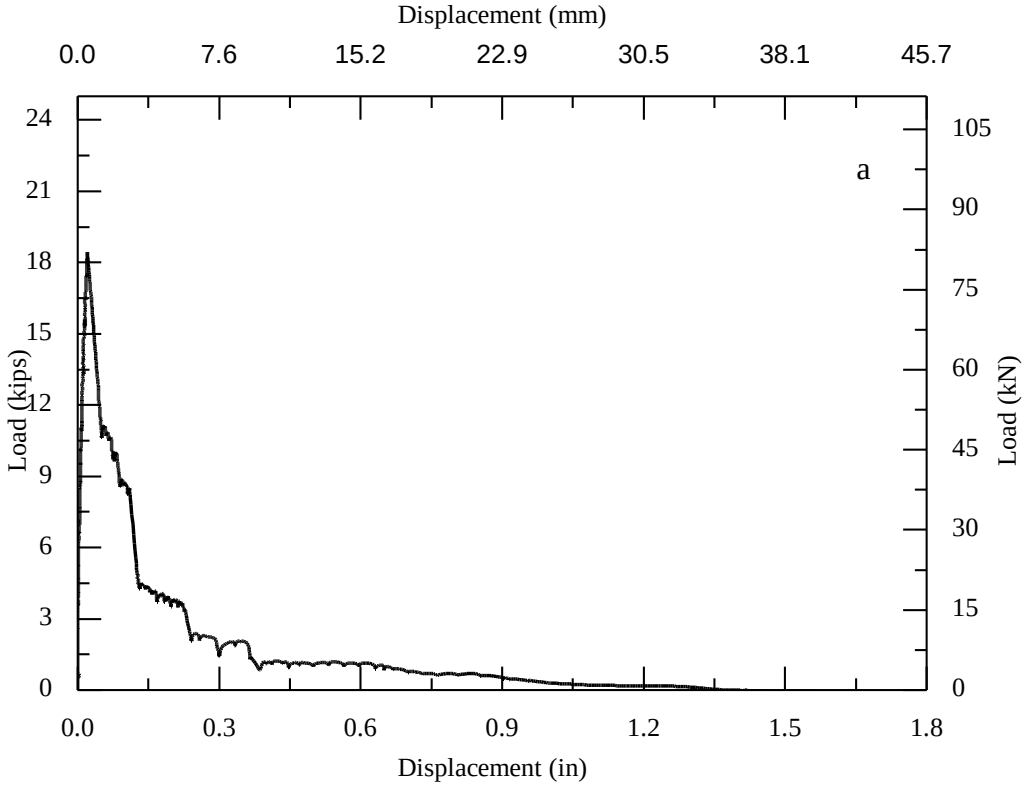

a) load-displacement behavior; b) c) cracked surface; d) concrete breakout failure.

Figure VI.34. Observed behavior of Specimen UC-0.625-5.0-#2

35. UC-0.625-5.0-#3

The measured ultimate load is at 12.76 kips [56.78 kN] at a displacement of 0.034 in. [0.86 mm]. As shown in Figure VI.35b, three initial cracks were generated by previous tests. One crack was across the longitudinal direction and two cracks were in the transverse direction. As shown in Figure VI.35b, one crack represented splitting and passing the anchor in the transverse direction at the load of 12.76 kips [56.78 kN] with 1.5 in. [38.1 mm] crack depth. The predicted capacity in cracked concrete measuring a 1.06-in. [26.87 mm] deep breakout simultaneously with a 3.75 -in. [95.25 mm] deep bond failure (14.7 kips) [65.43 kN]. The anchor was pulled out with a concrete cone due to adhesive-concrete interface failure shown in Figure VI.35c and VI.35d.

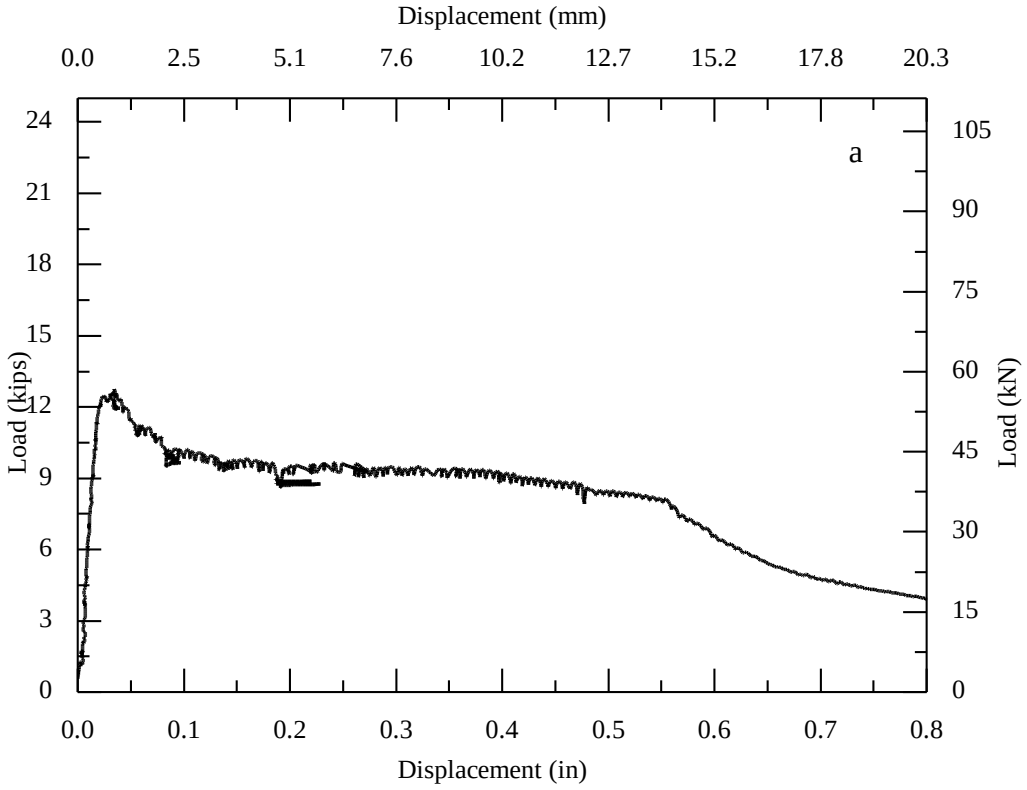

a) load-displacement behavior; b) cracked surface; c) d) partial cone bond failure.

Figure VI.35. Observed behavior of Specimen UC-0.625-5.0-#3

36. UC-0.625-5.0-#4

The measured ultimate load is at 10.63 kips [47.3 kN] at a displacement of 0.746 in. [18.95 mm]. As Figure VI.36b shown, one initial crack was generated by previous tests and the crack was across the longitudinal direction. One crack represented splitting and passing the anchor in the transverse direction at the load of 9.1 kips [40.5 kN]. The predicted capacity in cracked concrete measuring a 0.92-in. [23.37 mm] deep breakout simultaneously with a 4 -in. [101.6 mm] deep bond failure (15.31 kips) [68.13 kN]. The anchor was pulled out with a concrete cone due to adhesive-concrete interface failure shown in Figure VI.36c.

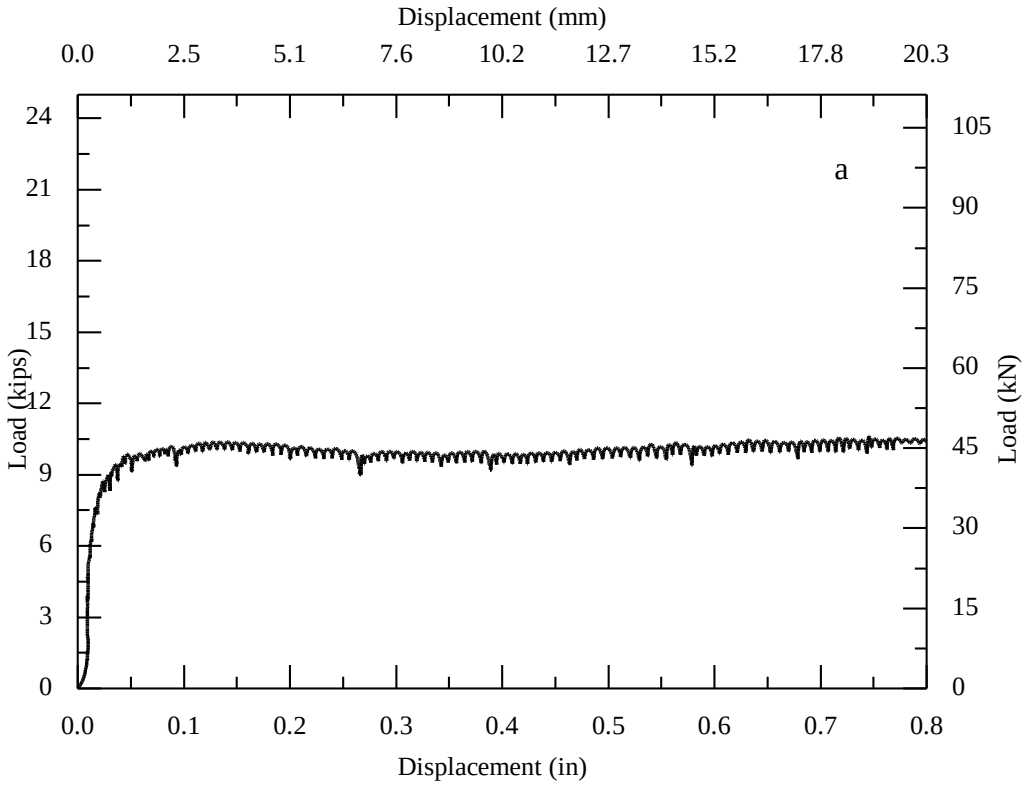

a) load-displacement behavior; b) cracked surface; c) partial cone bond failure.

Figure VI.36. Observed behavior of Specimen UC-0.625-5.0-#4

37. UCT-0.625-5.0-#1

The measured ultimate load is at 21.56 kips [95.94 kN] at a displacement of 0.047 in. [1.19 mm]. As Figure VI.37b shown, a circular crack with appeared along the anchor before the load reached 21.56 kips [95.94 kN]. After passing the ultimate load, the load dropped sharply as the displacement increased due to the concrete was damaged and the threads sheared off. The predicted capacity measuring a 2.88-in. [73.03 mm] deep breakout simultaneously with a 2 -in. [50.8 mm] deep bond failure (16.28 kips) [72.43 kN]. The anchor was pulled out with a concrete cone due to concrete breakout failure shown in Figure VI.37c.

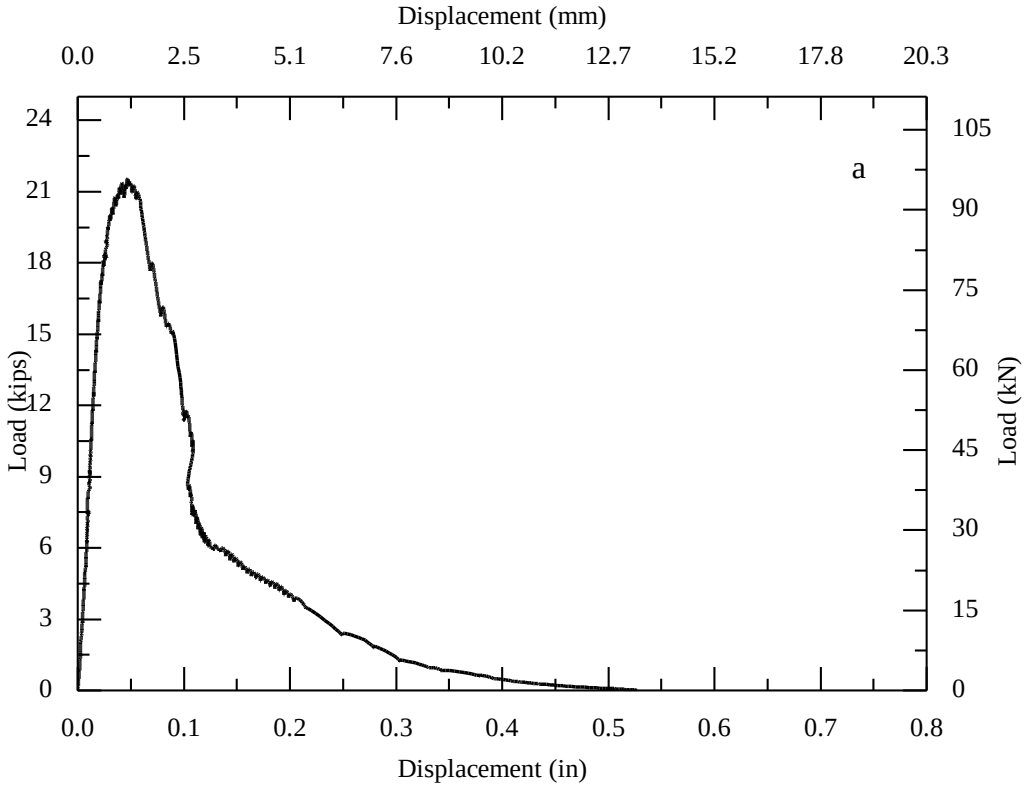

a) load-displacement behavior; b) cracked surface; c) anchor location; d) concrete breakout cone.

Figure VI.37. Observed behavior of Specimen UCT-0.625-5.0-#1

38. UCT-0.625-5.0-#2

The measured ultimate load is at 20.10 kips [89.45 kN] at a displacement of 0.037 in. [0.94 mm]. As shown in Figure VI.38b, a circular crack appeared along the anchor before the load reached 20.10 kips [89.45 kN]. After passing the ultimate load, the load dropped gradually as the displacement increased due to the frictional resistance generated by the rough surface of the drilled hole. The predicted capacity measuring a 2.21-in. [56.1 mm] deep breakout simultaneously with a 2.63 -in. [66.68 mm] deep bond failure (15.48 kips) [68.86 kN]. The anchor was pulled out with a concrete cone due to adhesive-concrete interface failure shown in Figure VI.38c.

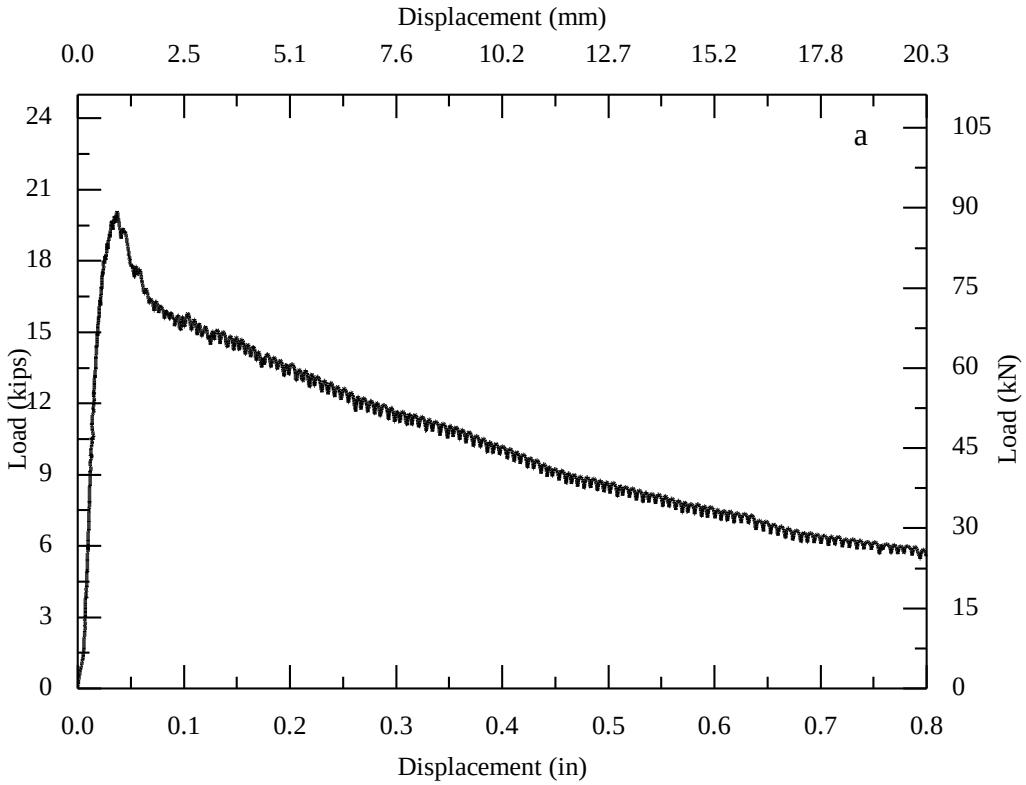

a) load-displacement behavior; b) cracked surface; c) partial cone bond failure.

Figure VI.38. Observed behavior of Specimen UCT-0.625-5.0-#2

39. UCT-0.625-5.0-#3

The measured ultimate load is at 21.36 kips [95.05 kN] at a displacement of 0.040 in. [1.02 mm]. As shown in Figure VI.39b, a circular crack appeared along the anchor before the load reached 21.36 kips [95.05 kN]. One crack represented splitting and passing the anchor in the transverse direction at the load of 15.52 kips [69.04 kN] with 1.5 in. [38.1 mm] crack depth. After passing the ultimate load, the load dropped sharply as the displacement increased due to the concrete was damaged and the threads sheared off. The predicted capacity measuring a 2.38-in. [60.33 mm] deep breakout simultaneously with a 2 -in. [50.8 mm] deep bond failure (13.98 kips) [62.22 kN]. The anchor was pulled out with a concrete cone due to concrete breakout failure shown in Figure VI.39c and VI.39c.

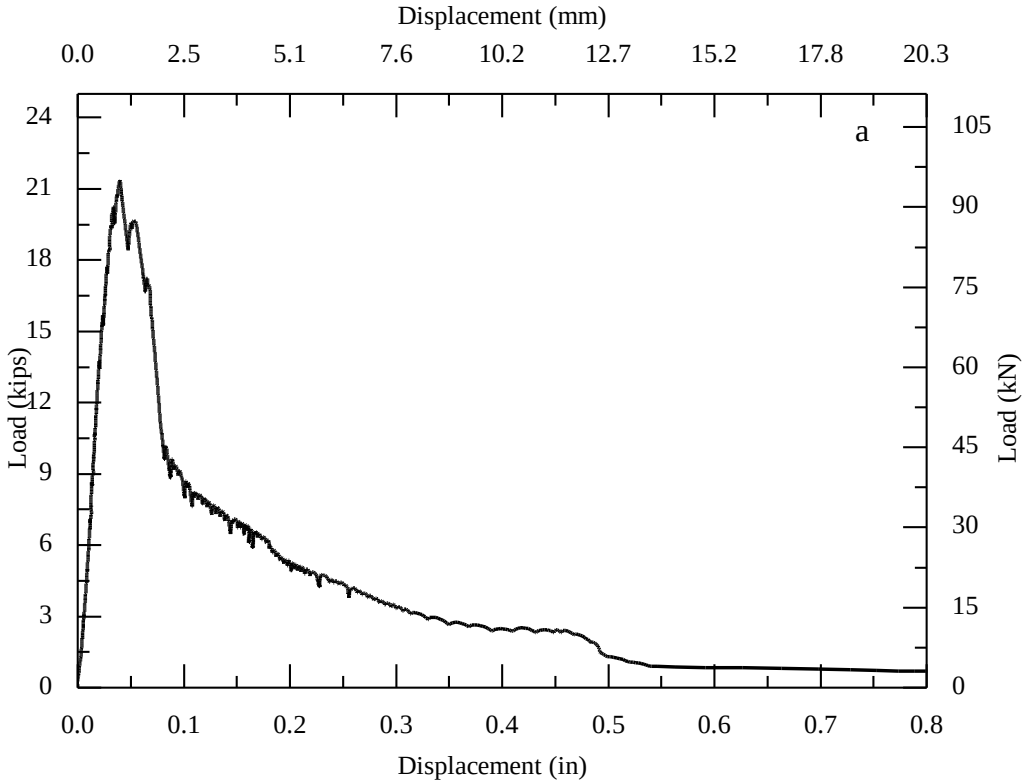

a) load-displacement behavior; b) cracked surface; c) concrete breakout cone in block; d) concrete breakout cone.

Figure VI.39. Observed behavior of Specimen UCT-0.625-5.0-#3

40. UCT-0.625-5.0-#4

The measured ultimate load is at 19.95 kips [88.78 mm] at a displacement of 0.054 in. [1.37 mm]. As shown in Figure VI.40b, a circular crack appeared along the anchor at the load of 13.38 kips [59.54 mm]. One crack represented splitting and passing the anchor in the transverse direction at the load of 19.26 kips [85.71 kN]. After passing the ultimate load, the load dropped sharply as the displacement increased due to the concrete was damaged and the threads sheared off. The predicted capacity measuring a 2.63-in. [66.68 mm] deep breakout simultaneously with a 2.13 -in. [53.98 mm] deep bond failure (15.54 kips) [69.17 kN]. The anchor was pulled out with a concrete cone due to concrete breakout failure shown in Figure VI.40c.

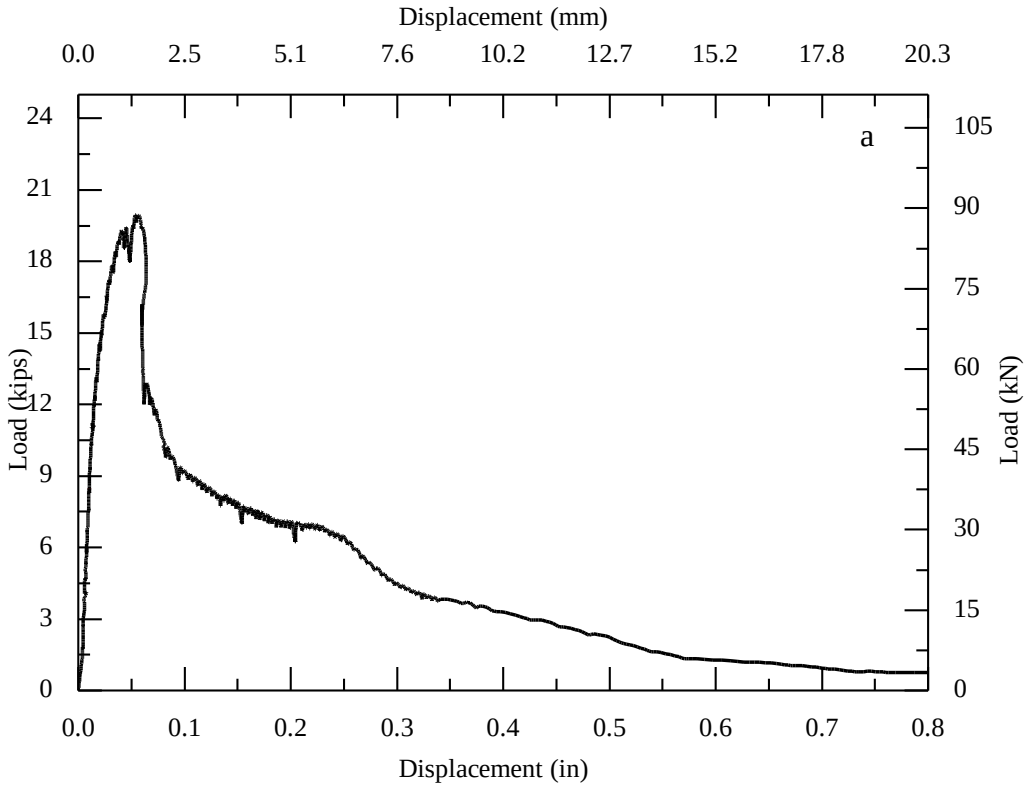

a) load-displacement behavior; b) cracked surface; c) concrete breakout cone in block; d) e) concrete breakout cone.

Figure VI.40. Observed behavior of Specimen UCT-0.625-5.0-#4

41. UCT#R-0.625-5.0-#1

The measured ultimate load is at 22.55 kips [100.35 kN] at a displacement of 0.038 in. [0.97 mm]. As shown in Figure VI.41b, a circular crack appeared along the anchor at the load of 17.44 kips [77.61 kN]. One crack represented splitting and passing the anchor in the transverse direction at the load of 22.47 kips [99.99 kN]. After passing the ultimate load, the load dropped gradually as the displacement increased due to the concrete was damaged and the threads sheared off. The predicted capacity measuring a 2.09-in. [53.14 mm] deep breakout simultaneously with a 2.88 -in. [73.03 mm] deep bond failure (15.87 kips) [70.64 kN]. The anchor was pulled out with a concrete cone due to adhesive-concrete interface failure shown in Figure VI.41c and 41d.

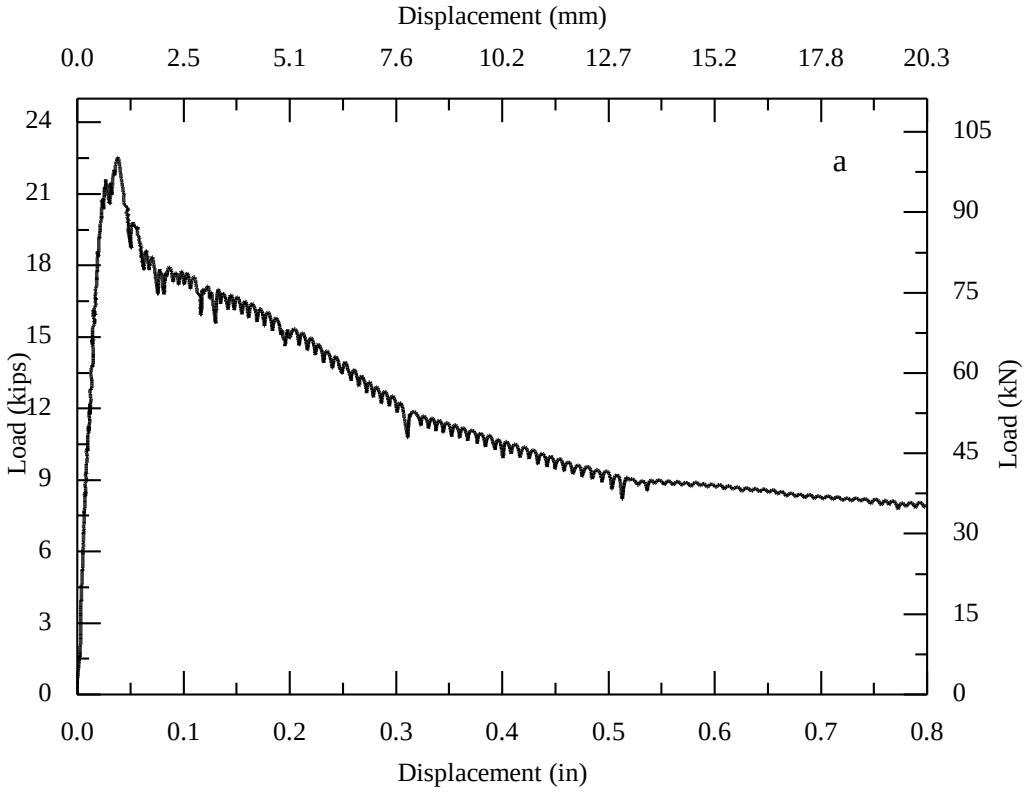

a) load-displacement behavior; b) cracked surface; c) partial cone in block; d) partial cone bond failure.

Figure VI.41. Observed behavior of Specimen UCT#R-0.625-5.0-#1

42. UCT#R-0.625-5.0-#2

The measured ultimate load is at 23.48 kips [104.49 kN] at a displacement of 0.044 in. [1.12 mm]. As shown in Figure VI.42b, a circular crack appeared along the anchor at the load of 21.94 kips [97.61 kN]. After passing the ultimate load, the load dropped gradually as the displacement increased due to the concrete was damaged and the threads sheared off. The predicted capacity measuring a 2.17-in. [55.17 mm] deep breakout simultaneously with a 2.75 -in. [69.85 mm] deep bond failure (15.76 kips) [70.15 kN]. The anchor was pulled out with a concrete cone due to adhesive-concrete interface failure shown in Figure VI.42c.

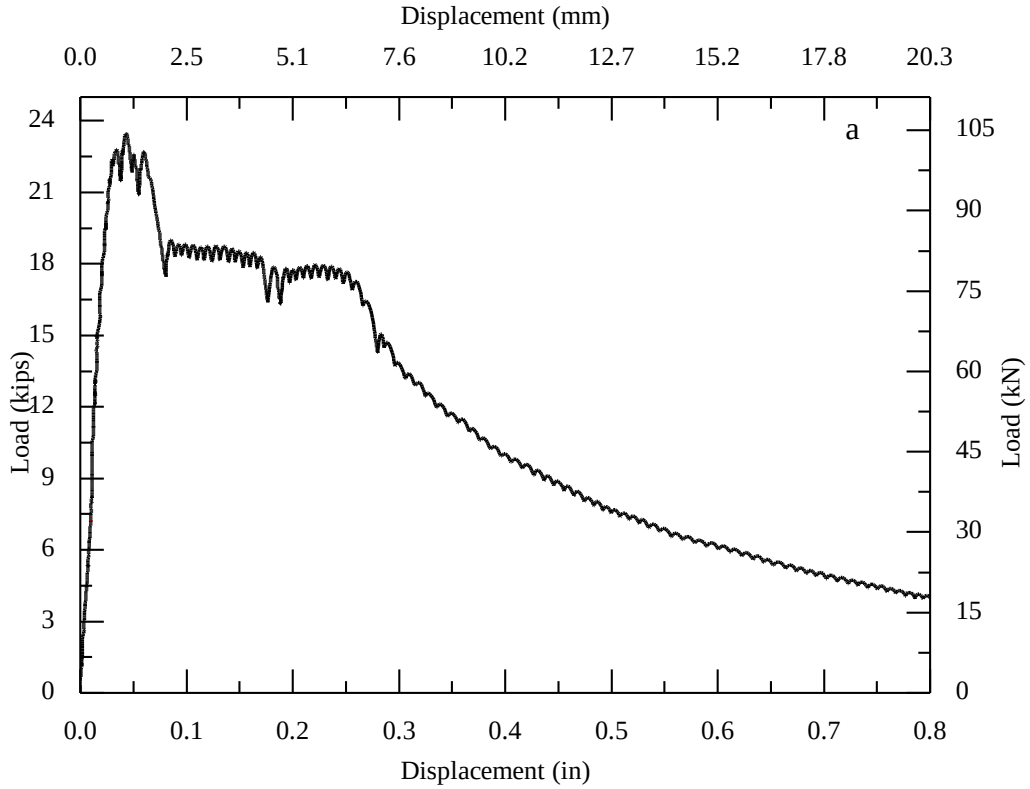

a) load-displacement behavior; b) cracked surface; c) partial cone bond failure.

Figure VI.42. Observed behavior of Specimen UCT#R-0.625-5.0-#2

43. UCT#R-0.625-5.0-#3

The measured ultimate load is at 23.51 kips [104.62 kN] at a displacement of 0.053 in. [1.35 mm]. As shown in Figure VI.43b, a circular crack appeared along the anchor at the load of 23.51 kips [104.62 kN]. One crack represented splitting and passing the anchor in the transverse direction at the load of 20.87 kips [92.85 kN] with 2 in. [50.8 mm] crack depth. After passing the ultimate load, the load dropped sharply as the displacement increased due to the concrete was damaged and the threads sheared off. The predicted capacity measuring a 2.56-in. [65.09 mm] deep breakout simultaneously with a 2.38 -in. [60.33 mm] deep bond failure (16.14 kips) [71.83 kN]. The anchor was pulled out with a concrete cone due to adhesive-concrete interface failure shown in Figure VI.43c.

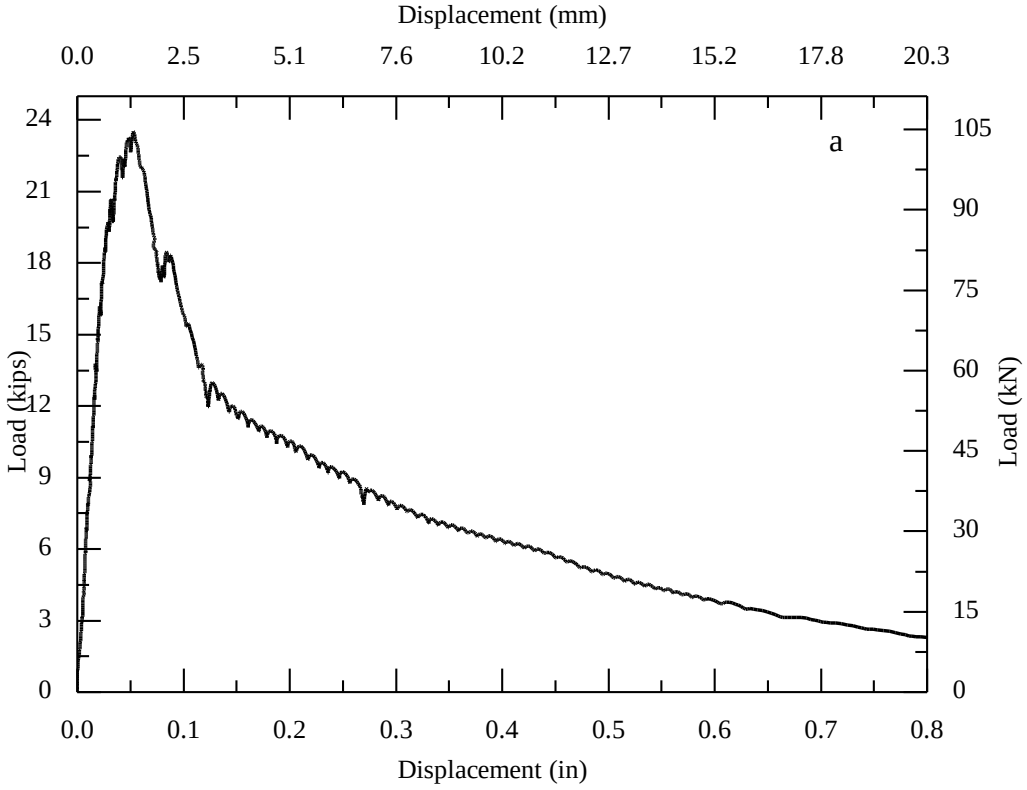

a) load-displacement behavior; b) cracked surface; c) partial cone bond failure.

Figure VI.43. Observed behavior of Specimen UCT#R-0.625-5.0-#3

44. UCT#R-0.625-5.0-#4

The measured ultimate load is at 23.09 kips [102.75 kN] at a displacement of 0.069 in. [1.75 mm]. As shown in Figure VI.44b, a circular crack appeared along the anchor at the load of 21.94 kips [97.61 kN]. One crack represented splitting and passing the anchor in the transverse direction at the load of 21.94 kips [97.61 kN]. After passing the ultimate load, the load dropped sharply as the displacement increased due to the concrete was damaged and the threads sheared off. The predicted capacity measuring a 2.13-in. [53.98 mm] deep breakout simultaneously with a 2.75 -in. [69.85 mm] deep bond failure (15.57 kips) [69.28 kN].The anchor was pulled out with a concrete cone due to adhesive-concrete and adhesive-steel interface failure shown in Figure VI.44c and VI.44d.

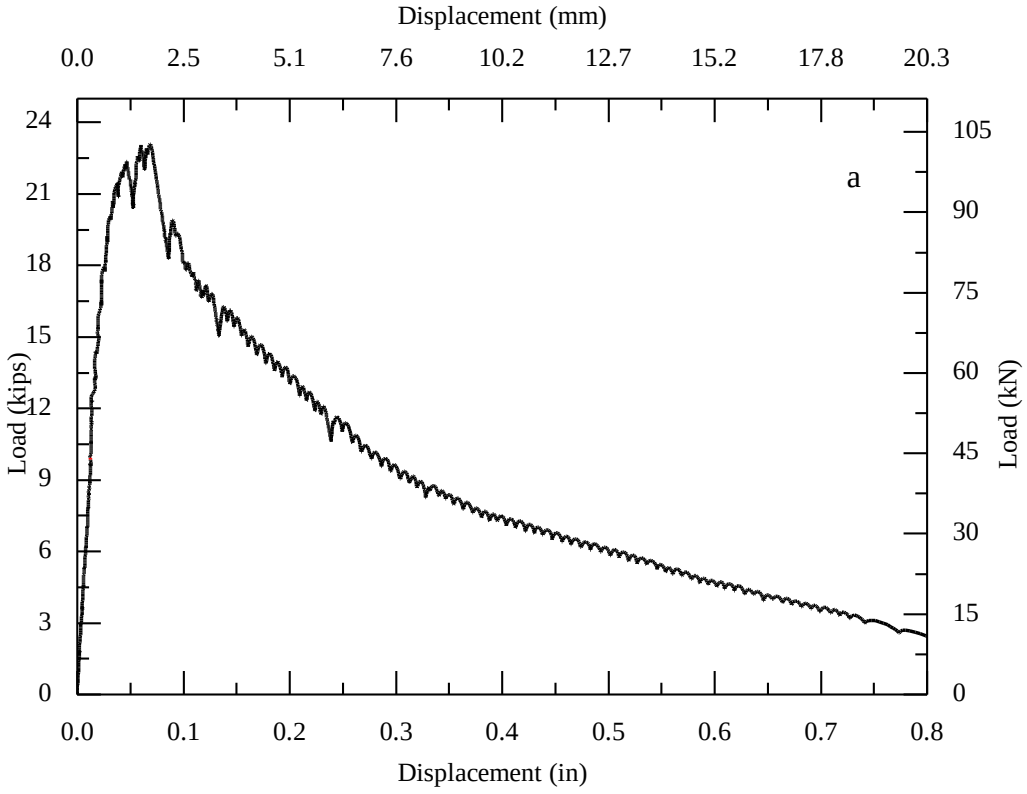

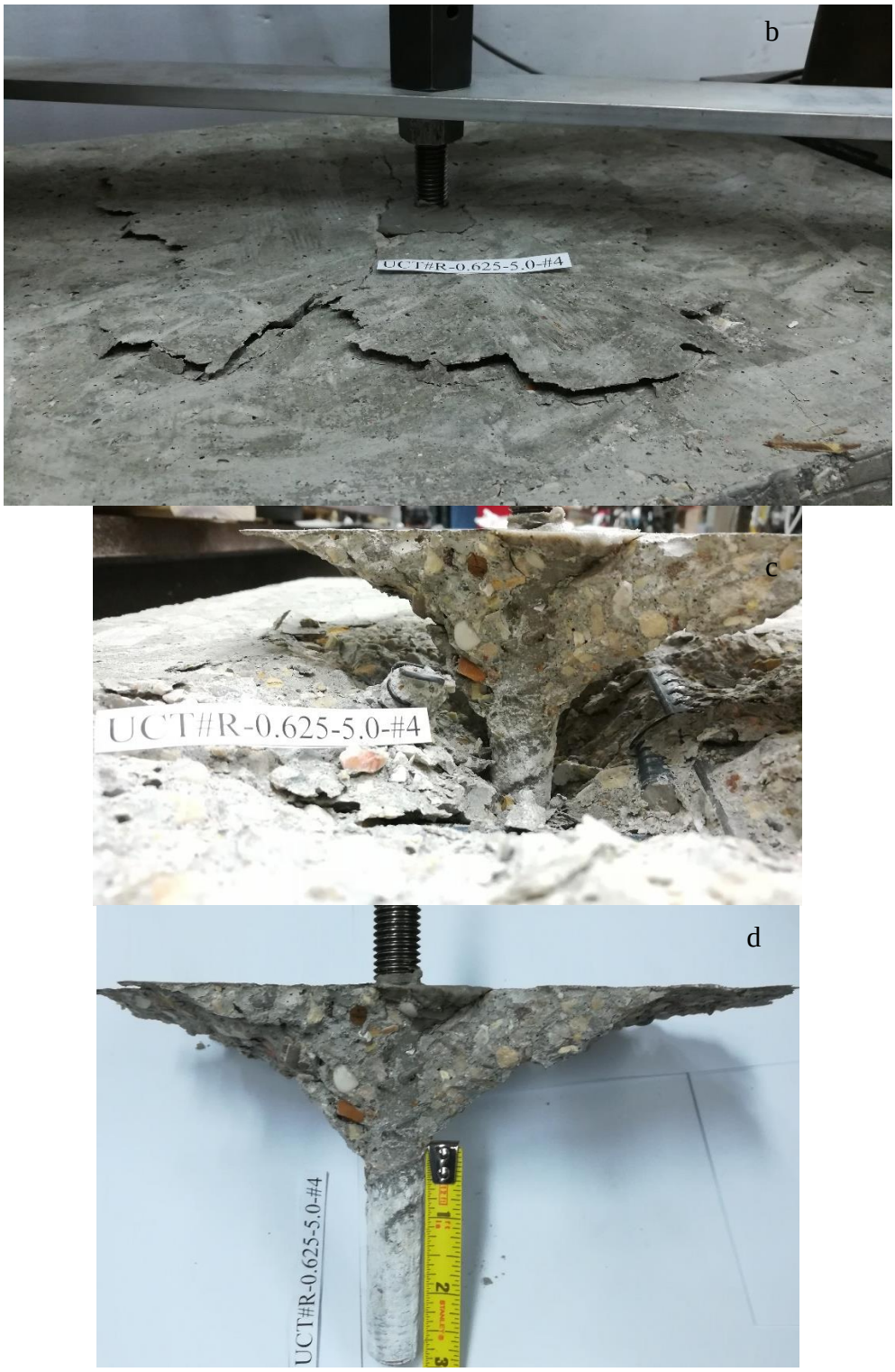

a) load-displacement behavior; b) cracked surface; c) partial cone bond failure.

Figure VI.44. Observed behavior of Specimen UCT#R-0.625-5.0-#4

45. UC0%-0.625-5.0-#1

The measured ultimate load is at 5.12 kips [22.78 kN] at a displacement of 0.281 in. [7.14 mm]. As Figure VI.45b shown, a circular crack appeared along the anchor at the load of 3.75 kips [16.67 kN]. After passing the ultimate load, the load remained constant as the displacement increased due to the frictional resistance was generated by the rough surface of the drilled hole. The anchor was pulled out with a small concrete cone due to adhesive-concrete interface failure shown in Figure VI.45c.

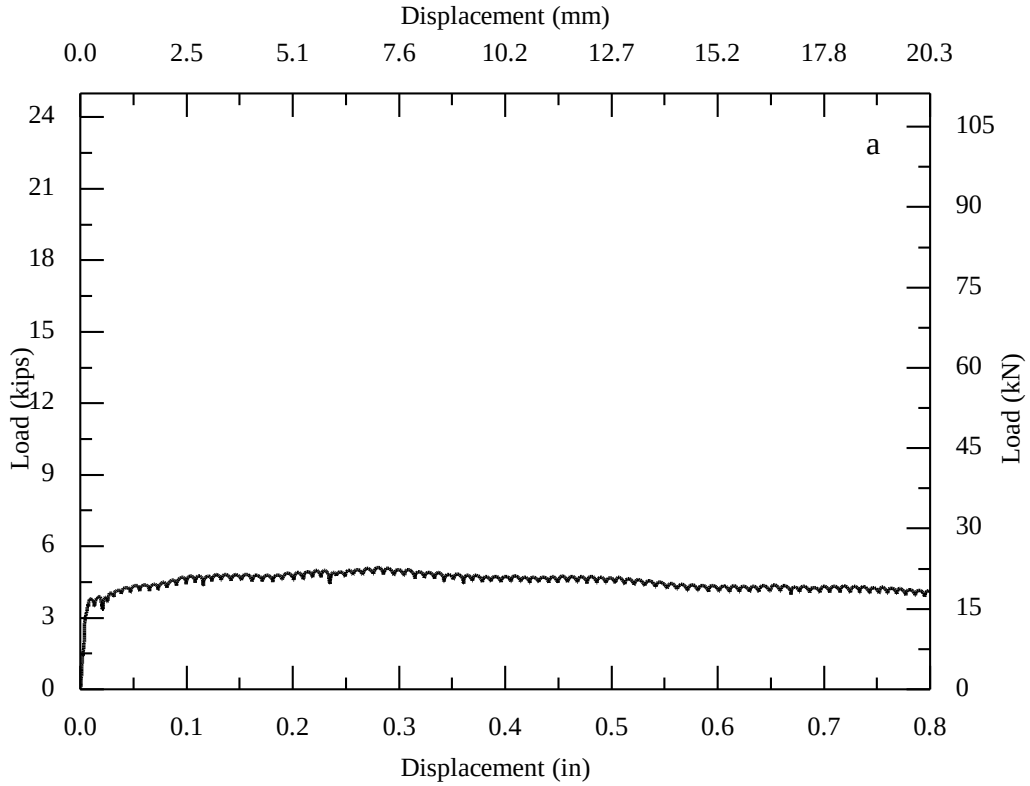

a) load-displacement behavior; b) cracked surface; c) partial cone bond failure.

Figure VI.45. Observed behavior of Specimen UC0%-0.625-5.0-#1

46. UC0%-0.625-5.0-#2

The measured ultimate load is at 5.47 kips [24.34 kN] at a displacement of 1.219 in. [30.96 mm]. As shown in Figure VI.46b, a circular crack appeared along the anchor at the load of 1.61 kips [7.14 kN]. After passing the ultimate load, the load remained constant as the displacement increased due to the frictional resistance was generated by the rough surface of the drilled hole. The anchor was pulled out with a small concrete cone due to adhesive-concrete interface failure shown in Figure VI.46c.

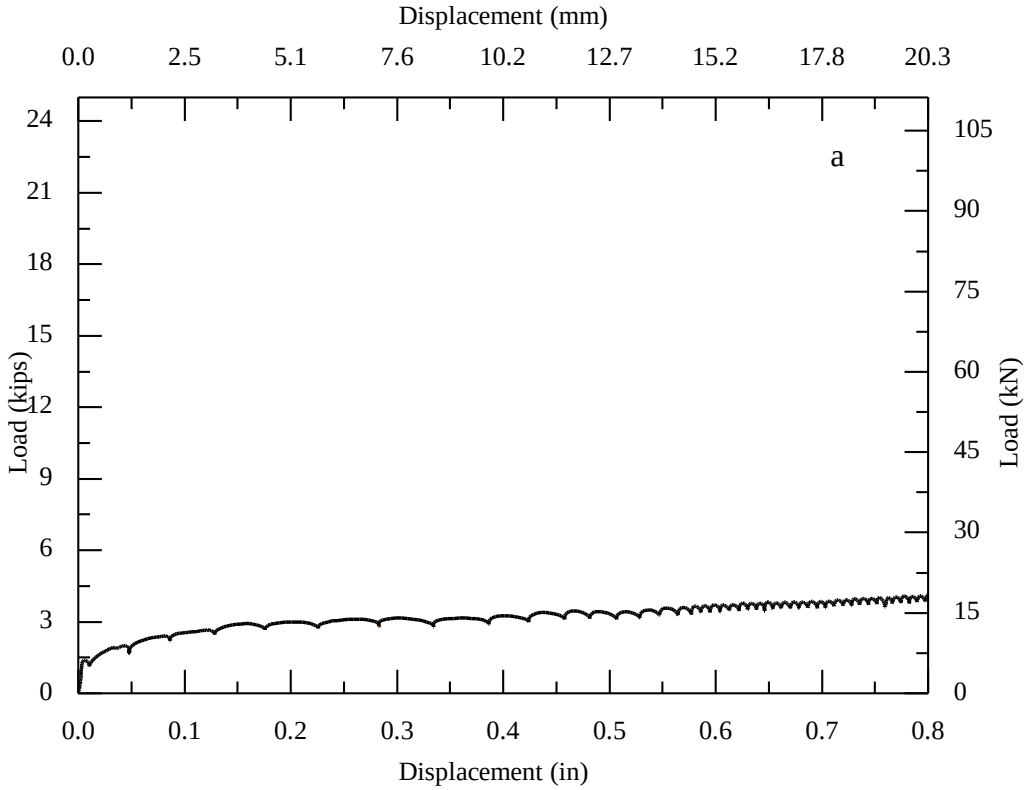

a) load-displacement behavior; b) cracked surface; c) partial cone bond failure.

Figure VI.46. Observed behavior of Specimen UC0%-0.625-5.0-#2

47. UC0%-0.625-5.0-#3

The measured ultimate load is at 4.53 kips [20.16 kN] at a displacement of 0.653 in. [16.59 mm]. As shown in Figure VI.47b, a circular crack appeared along the anchor at the load of 3.75 kips [16.67 kN]. After passing the ultimate load, the load remained constant as the displacement increased due to the frictional resistance was generated by the rough surface of the drilled hole. The anchor was pulled out with a small concrete cone due to adhesive-concrete interface failure shown in Figure VI.47c.

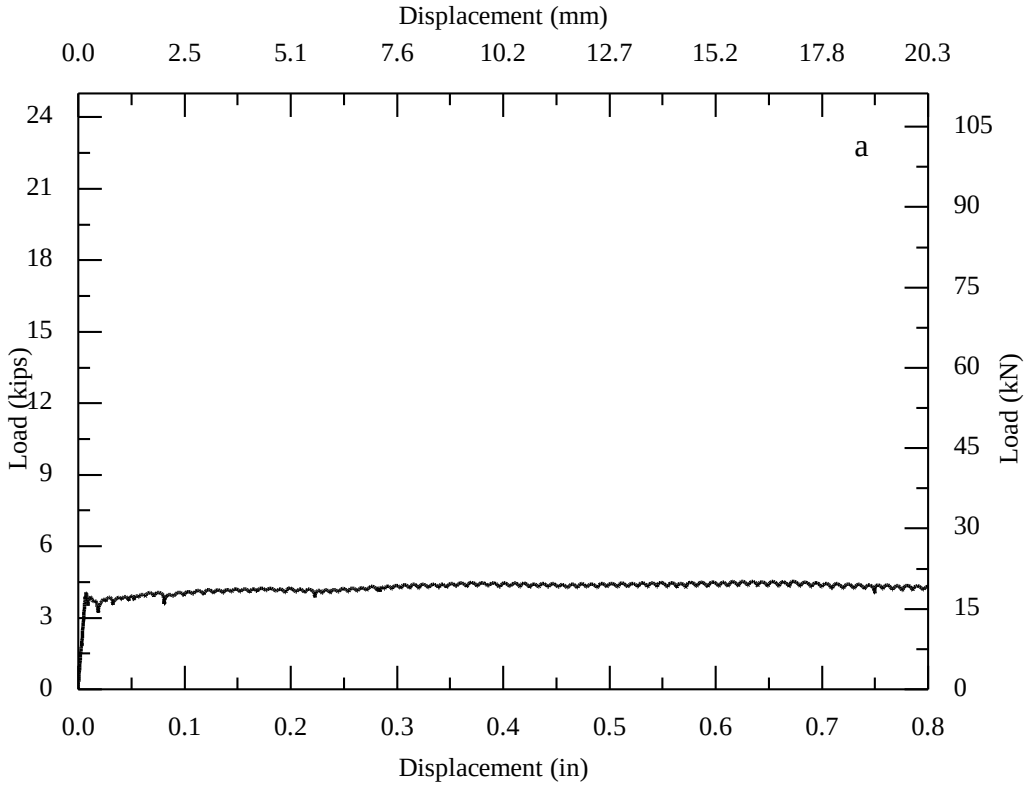

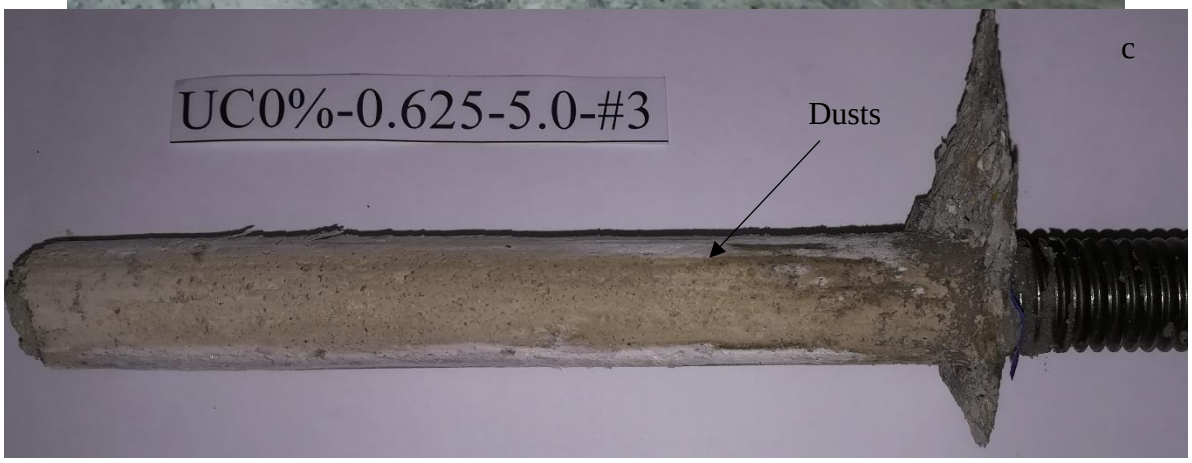

a) load-displacement behavior; b) cracked surface; c) partial cone bond failure.

Figure VI.47. Observed behavior of Specimen UC0%-0.625-5.0-#3

48. UC0%-0.625-5.0-#4

The measured ultimate load is at 4.12 kips [18.33 kN] at a displacement of 0.125 in. [3.18 mm]. As shown in Figure VI.48b, a circular crack appeared along the anchor at the load of 3.32 kips [14.76 kN]. After passing the ultimate load, the load remained constant as the displacement increased due to the frictional resistance was generated by the rough surface of the drilled hole. The anchor was pulled out with a small concrete cone due to adhesive-concrete interface failure shown in Figure VI.48c.

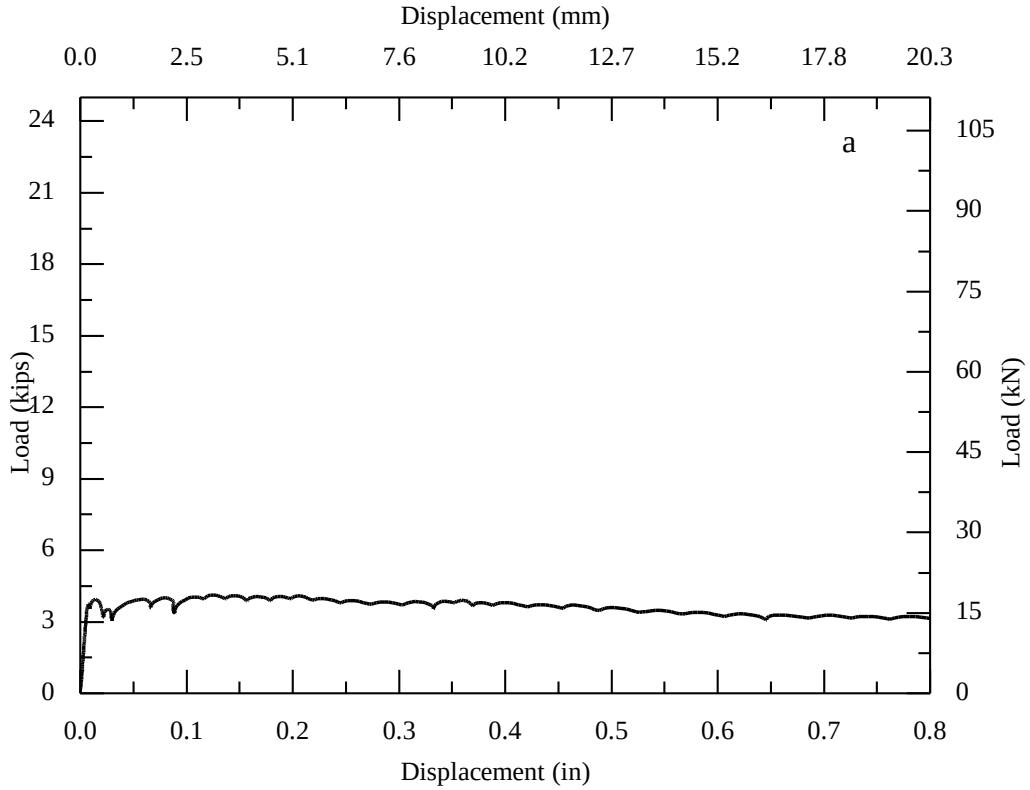

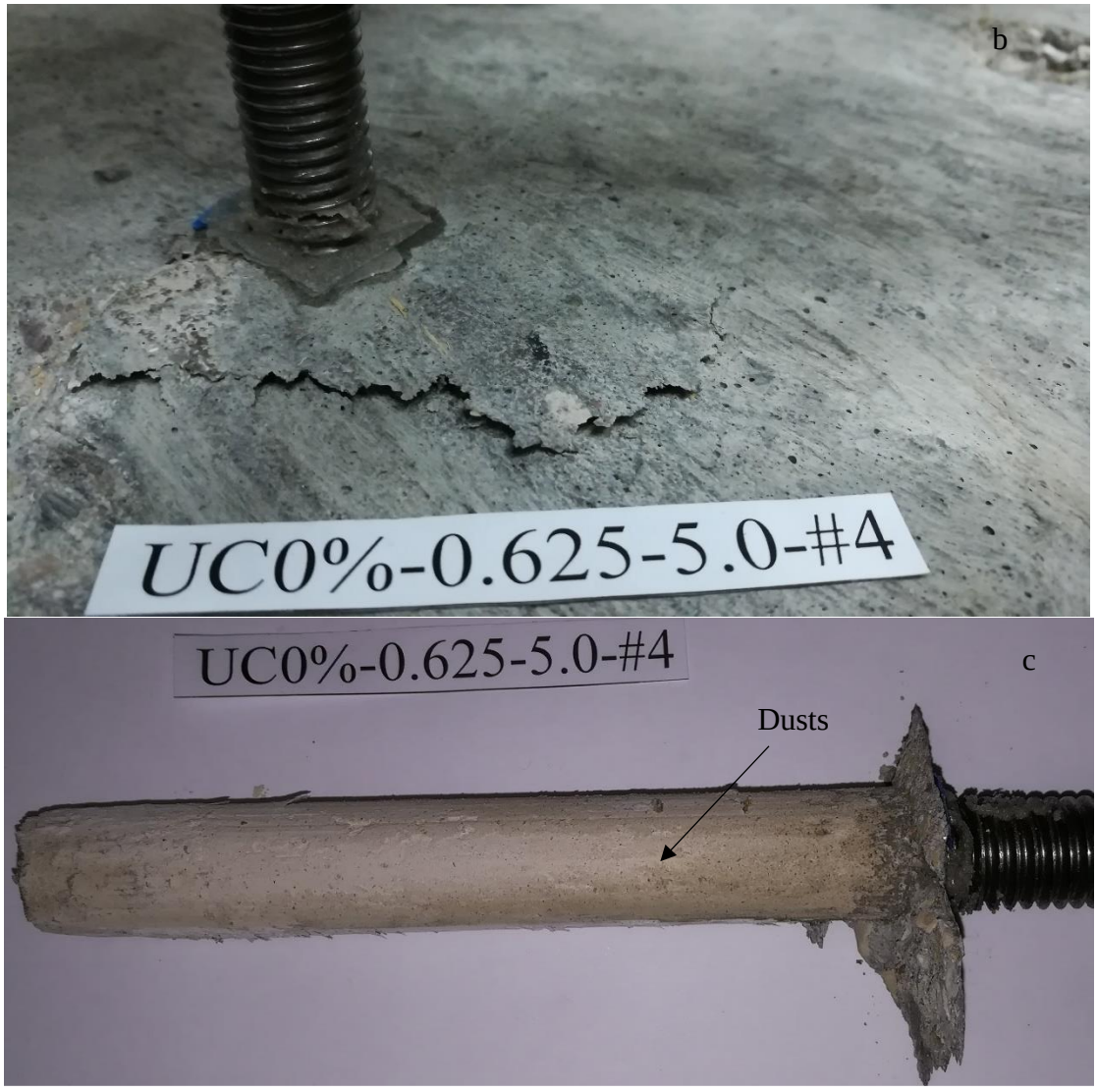

a) load-displacement behavior; b) cracked surface; c) partial cone bond failure.

Figure VI.48. Observed behavior of Specimen UC0%-0.625-5.0-#4

49. UC50%-0.625-5.0-#1

The measured ultimate load is at 10.94 kips [48.68 kN] at a displacement of 0.214 in. [5.44 mm]. As shown in Figure VI.49b, a circular crack appeared along the anchor at the load of 9.63 kips [42.85 kN]. After passing the ultimate load, the load dropped slowly as the displacement increased due to the frictional resistance was generated by the rough surface of the drilled hole. The anchor was pulled out with a concrete cone due to adhesive-concrete interface failure shown in Figure VI.49c.

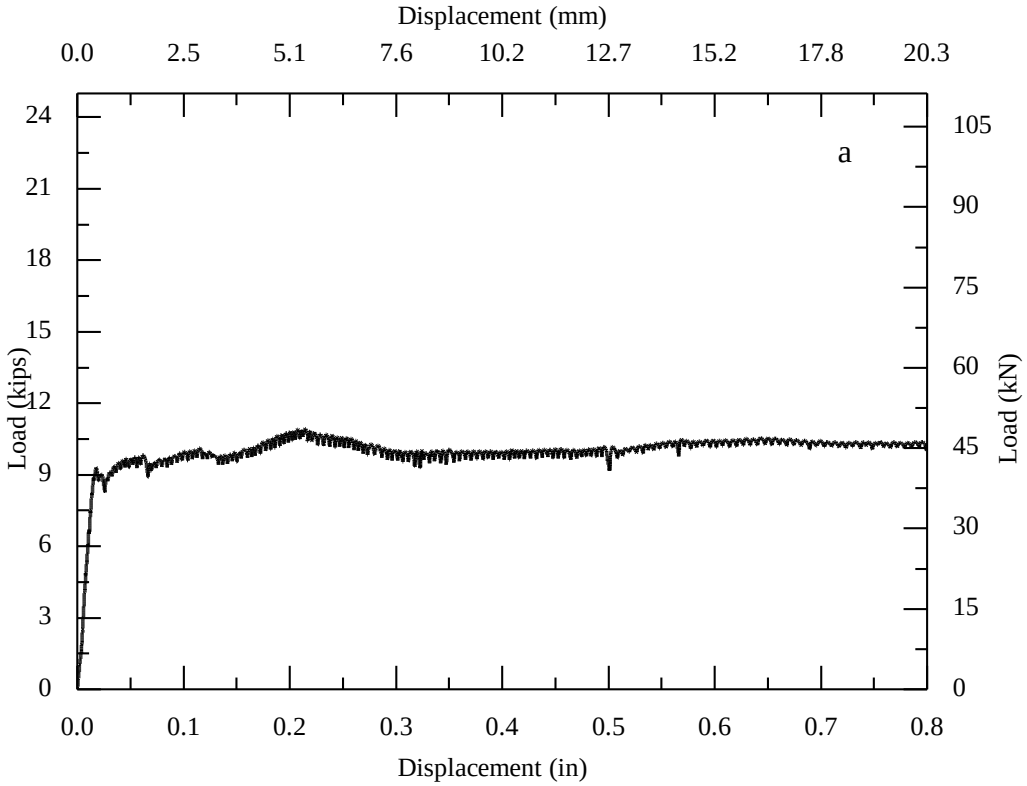

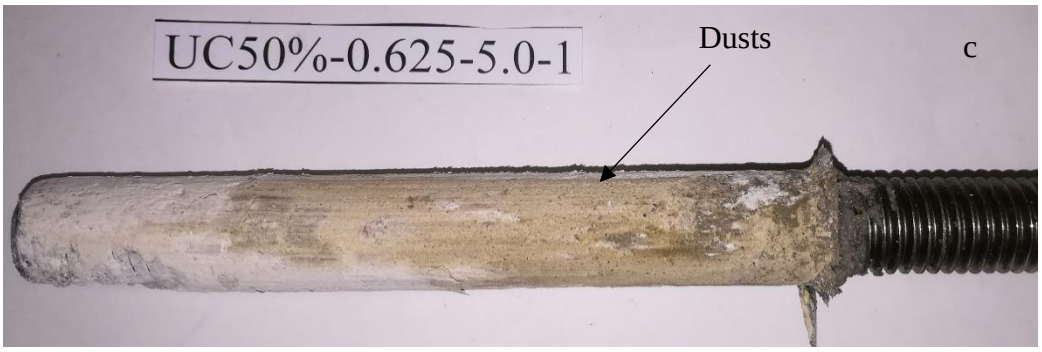

a) load-displacement behavior; b) cracked surface; c) partial cone bond failure.

Figure VI.49. Observed behavior of Specimen UC50%-0.625-5.0-#1

50. UC50%-0.625-5.0-#2

The measured ultimate load is at 9.94 kips [44.23 kN] at a displacement of 0.121 in. [3.07 mm]. As shown in Figure VI.50b, a circular crack appeared along the anchor at the load of 6.42 kips [28.57 kN]. After passing the ultimate load, the load dropped slowly as the displacement increased due to the frictional resistance was generated by the rough surface of the drilled hole. The anchor was pulled out with a concrete cone due to adhesive-concrete interface failure shown in Figure VI.50c.

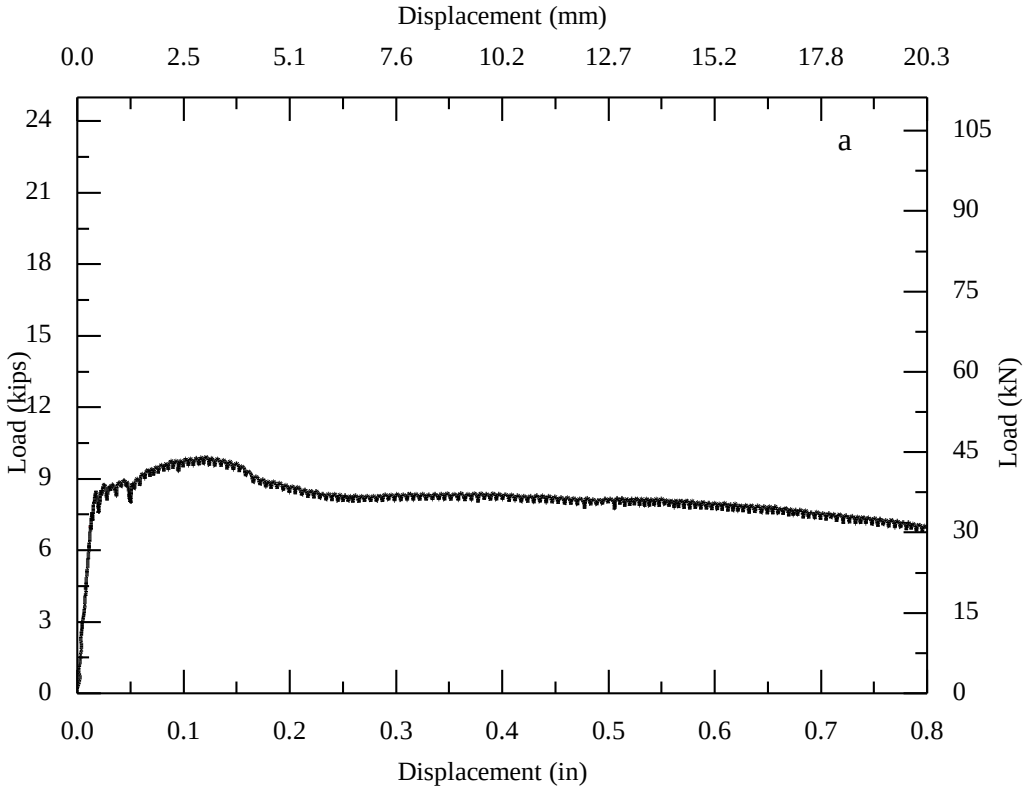

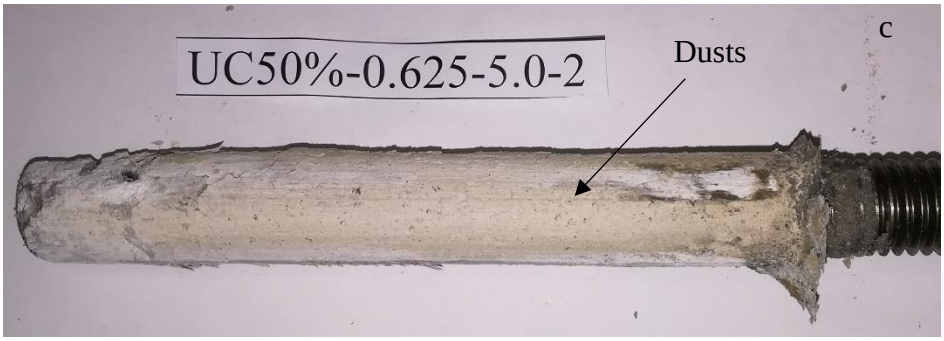

a) load-displacement behavior; b) cracked surface; c) partial cone bond failure.

Figure VI.50. Observed behavior of Specimen UC50%-0.625-5.0-#2

51. UC50%-0.625-5.0-#3

The measured ultimate load is at 11.11 kips [49.44 kN] at a displacement of 0.573 in. [14.55 mm]. As shown in Figure VI.51b, a circular crack appeared along the anchor at the load of 7.49 kips [33.33 kN]. After passing the ultimate load, the load dropped slowly as the displacement increased due to the frictional resistance was generated by the rough surface of the drilled hole. The anchor was pulled out with a concrete cone due to adhesive-concrete interface failure shown in Figure VI.51c.

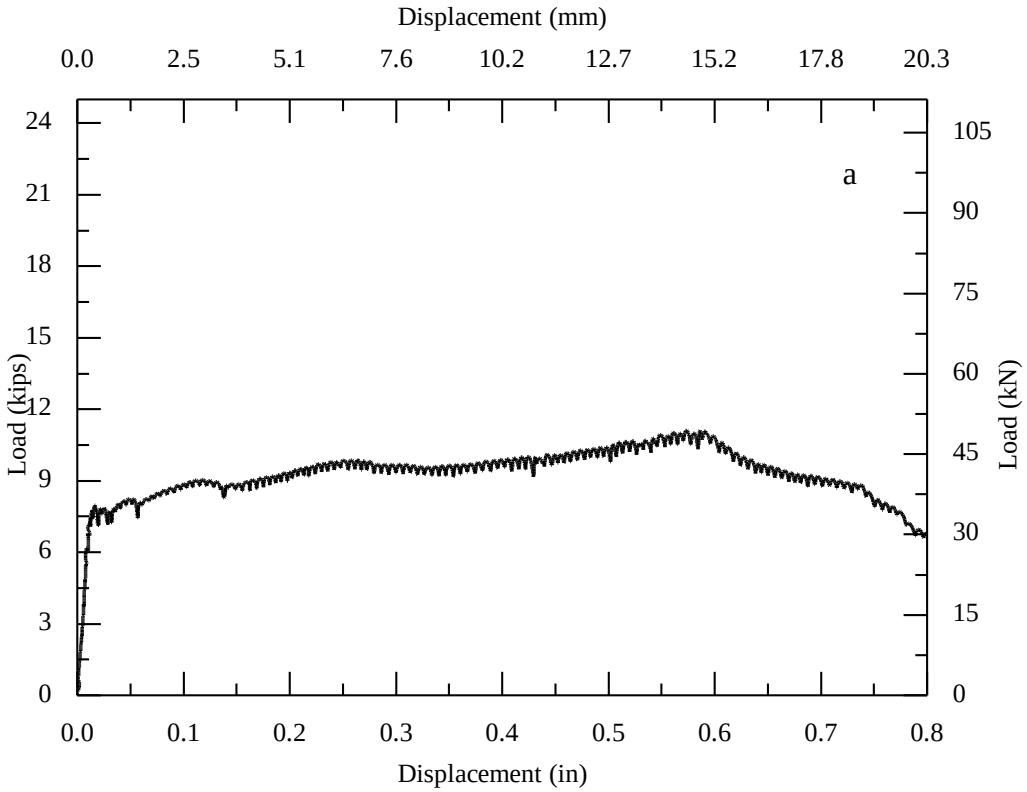

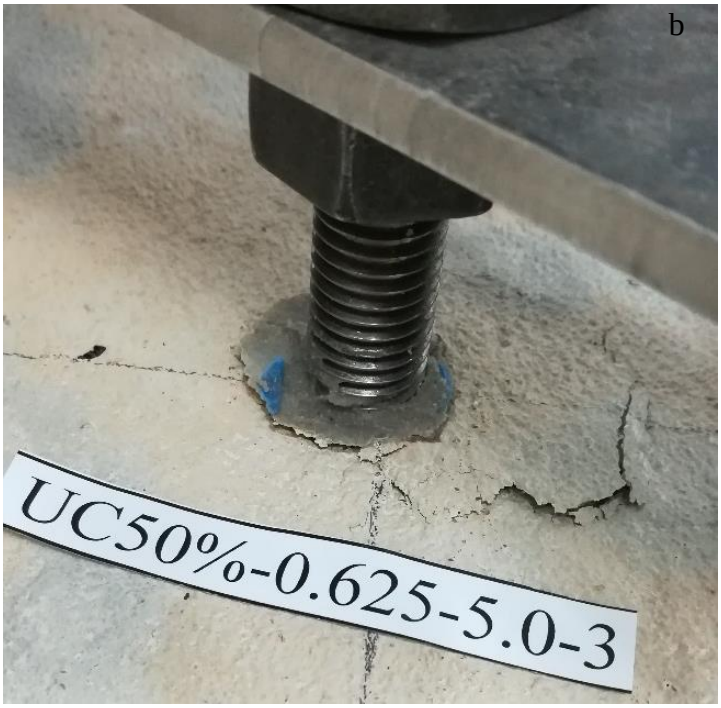

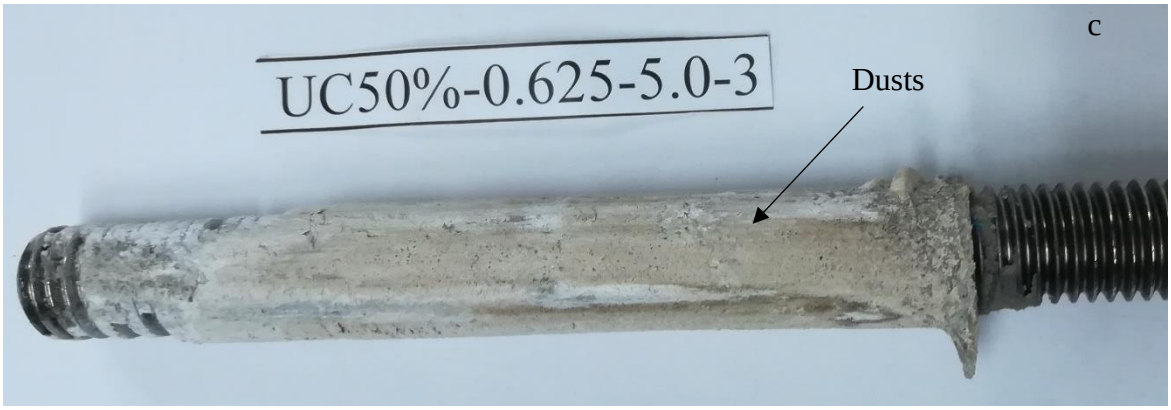

a) load-displacement behavior; b) cracked surface; c) partial cone bond failure.

Figure VI.51. Observed behavior of Specimen UC50%-0.625-5.0-#3

52. UC50%-0.625-5.0-#4

The measured ultimate load is at 8.27 kips [44.24 kN] at a displacement of 0.174 in. [4.42 mm]. As shown in Figure VI.52b, a circular crack appeared along the anchor at the load of 6.74 kips [30 kN]. After passing the ultimate load, the load dropped slowly as the displacement increased due to the frictional resistance was generated by the rough surface of the drilled hole. The anchor was pulled out with a concrete cone due to adhesive-concrete interface failure shown in Figure VI.52c.

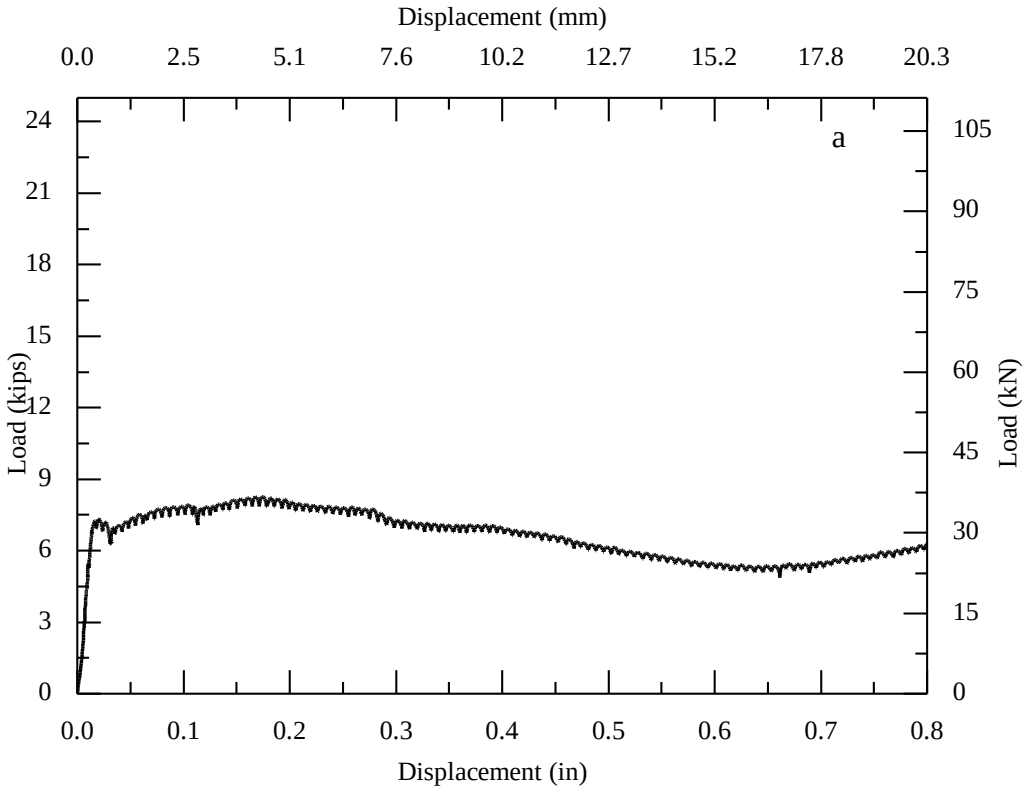

a) load-displacement behavior; b) cracked surface; c) partial cone bond failure.

Figure VI.52. Observed behavior of Specimen UC50%-0.625-5.0-#4

53. UCT50%-0.625-5.0-#1

The measured ultimate load is at 11.61 kips [51.66 kN] at a displacement of 0.061 in. [1.55 mm]. As Figure VI.53b shown, a circular crack appeared along the anchor at the load of 11.61 kips [51.66 kN]. After passing the ultimate load, the load was up and down as the displacement increased due to the threads sheared off continually and the frictional resistance generated by the rough surface of the drilled hole. The anchor was pulled out with a concrete cone due to adhesive-concrete interface failure shown in Figure VI.53c.

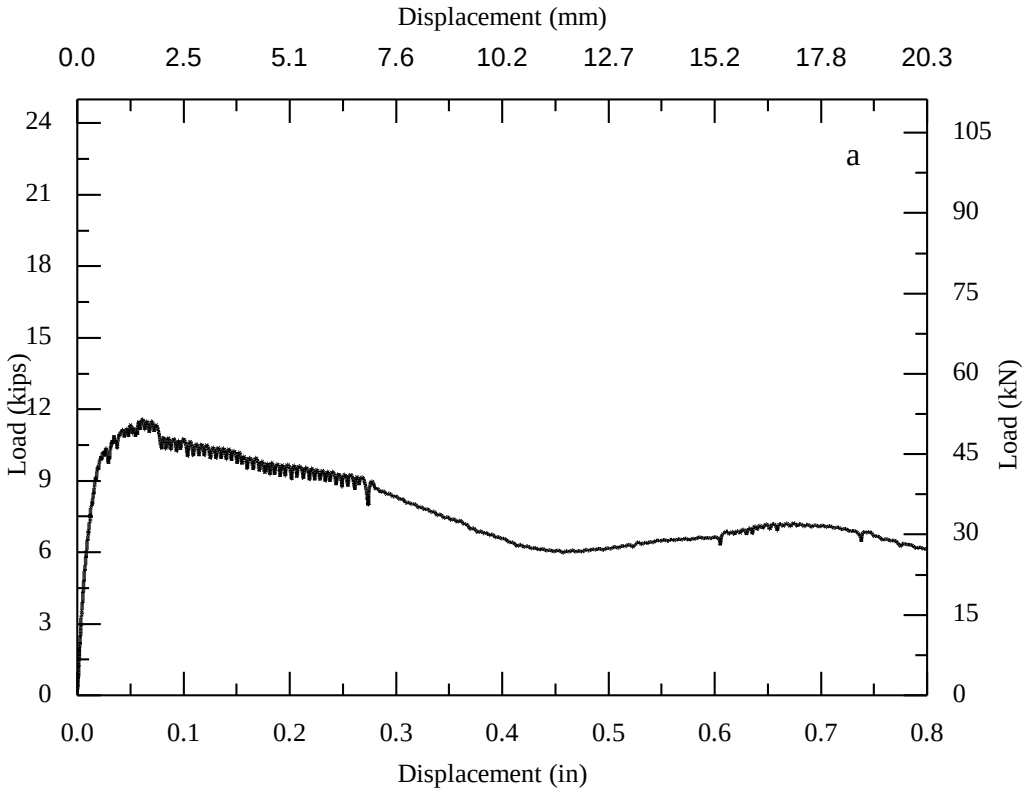

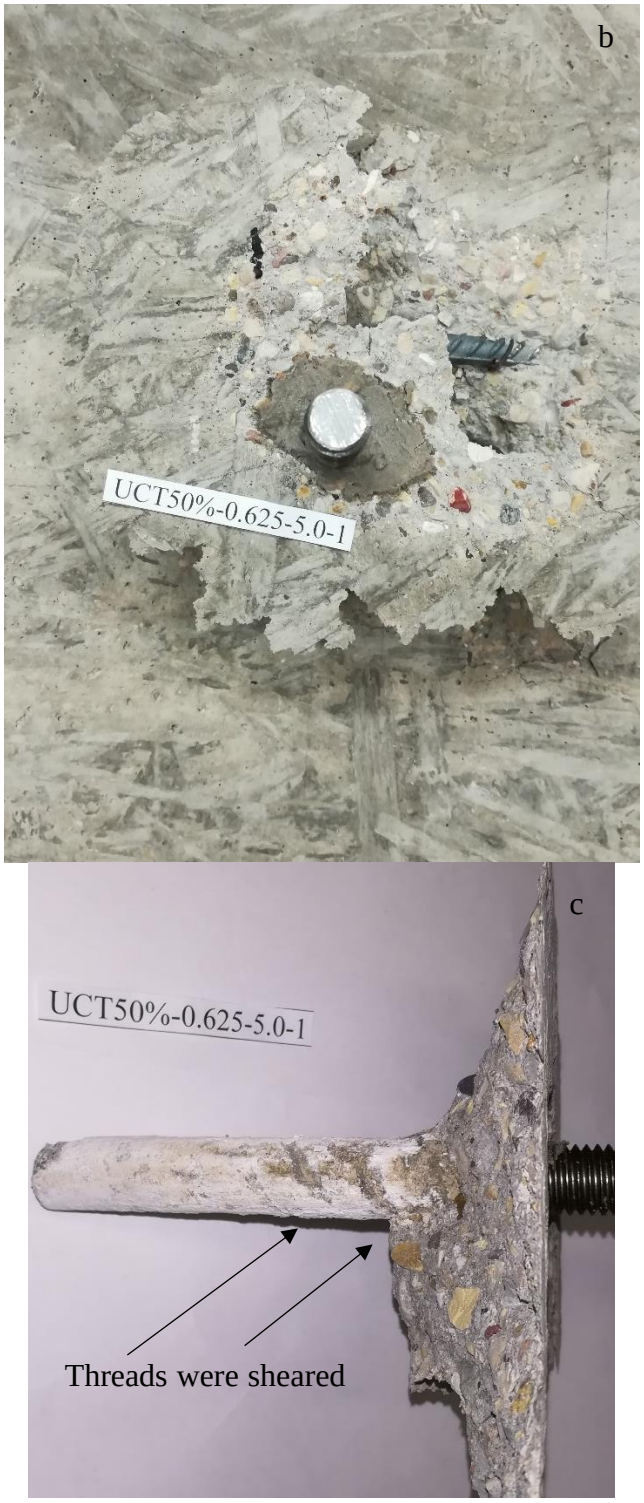

a) load-displacement behavior; b) cracked surface; c) partial cone bond failure.

Figure VI.53. Observed behavior of Specimen UCT50%-0.625-5.0-#1

54. UCT50%-0.625-5.0-#2

The measured ultimate load is at 16.47 kips [73.29 kN] at a displacement of 0.127 in. [3.23 mm]. As shown in Figure VI.54b, a circular crack appeared along the anchor at the load of 16.47 kips [73.29 kN]. After passing the ultimate load, the load was up and down as the displacement increased due to the threads sheared off continually and the frictional resistance generated by the rough surface of the drilled hole. The anchor was pulled out with a concrete cone due to adhesive-concrete interface failure shown in Figure VI.54c.

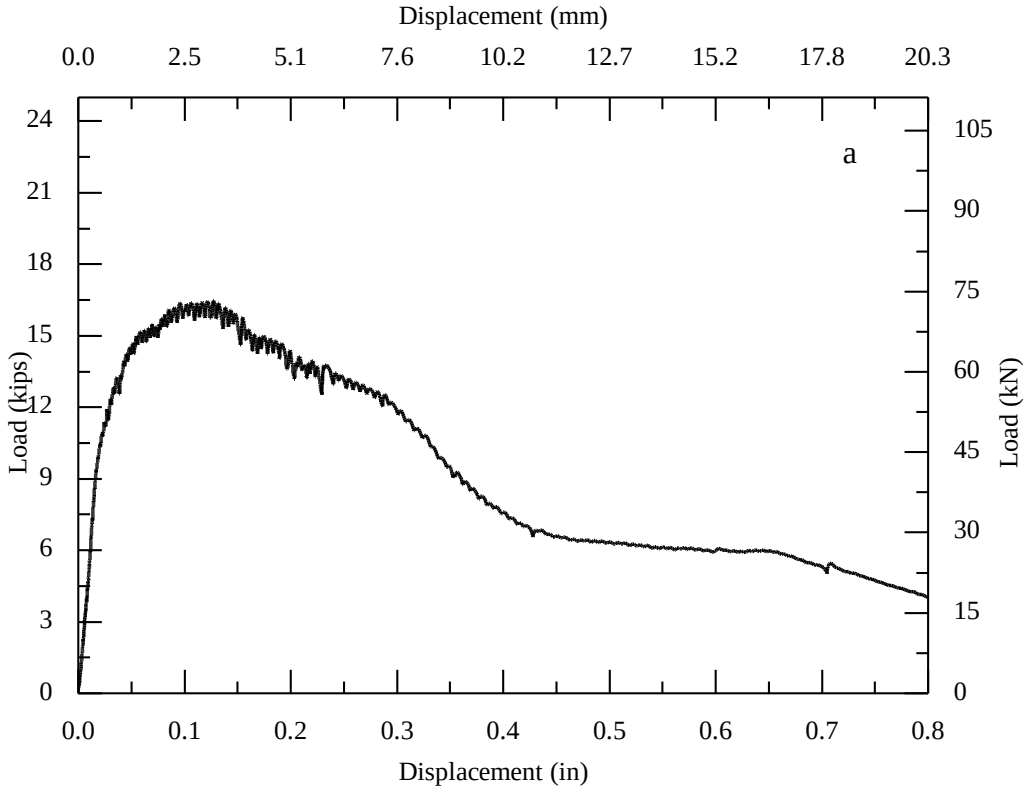

a) load-displacement behavior; b) cracked surface; c) partial cone bond failure.

Figure VI.54. Observed behavior of Specimen UCT50%-0.625-5.0-#2

55. UCT50%-0.625-5.0-#3

The measured ultimate load is at 16.63 kips [74 kN] at a displacement of 0.099 in. [2.51 mm]. As shown Figure VI.55b, a circular crack appeared along the anchor at the load of 11.24 kips [50 kN]. After passing the ultimate load, the load was up and down as the displacement increased due to the threads sheared off continually and the frictional resistance generated by the rough surface of the drilled hole. The anchor was pulled out with a concrete cone due to adhesive-concrete interface failure shown in Figure VI.55c.

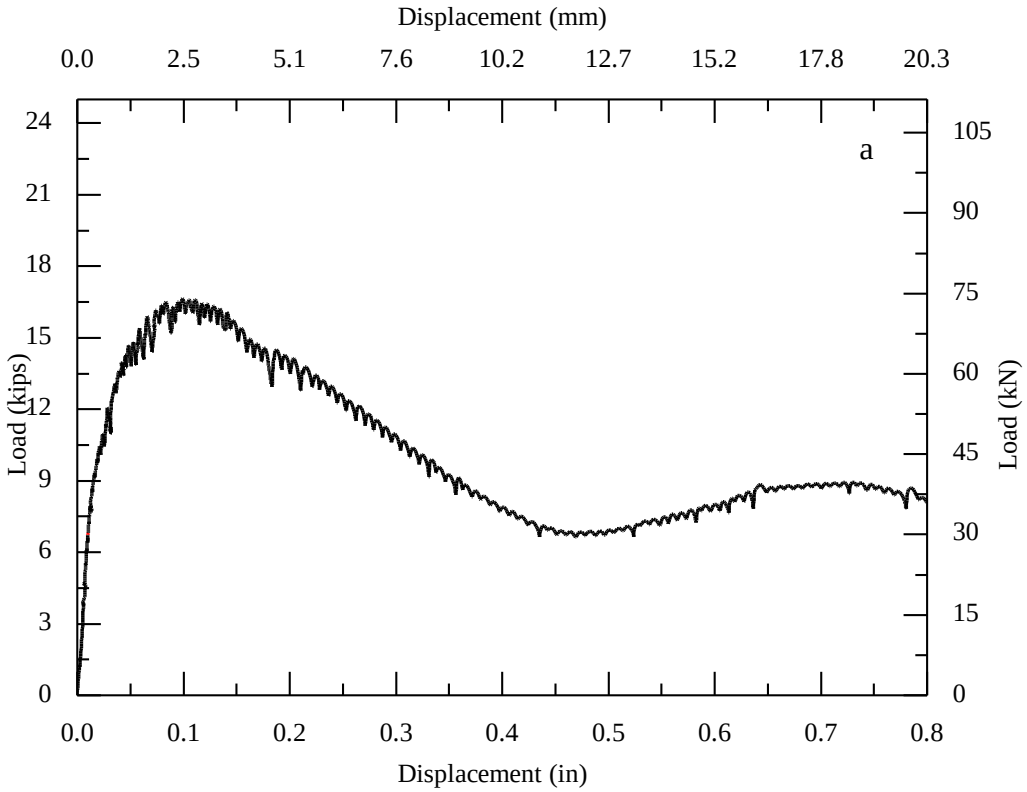

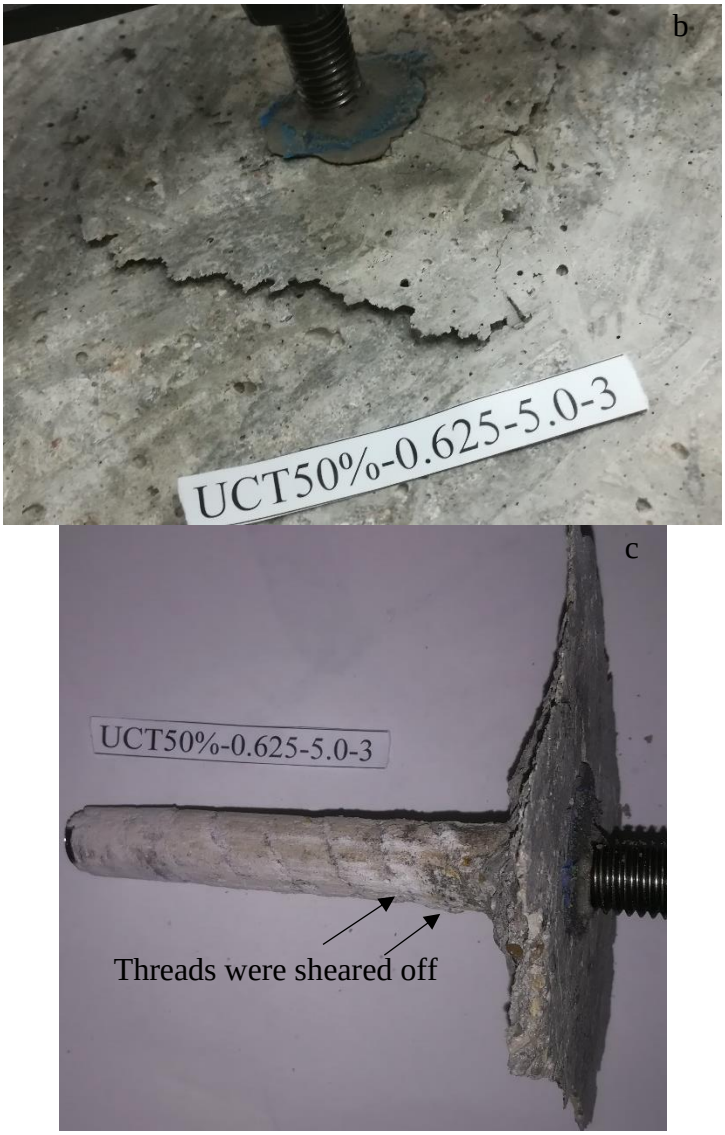

a) load-displacement behavior; b) cracked surface; c) partial cone bond failure.

Figure VI.55. Observed behavior of Specimen UCT50%-0.625-5.0-#3

56. UCT50%-0.625-5.0-#4

The measured ultimate load is at 16.28 kips [87.1 kN] at a displacement of 0.097 in. [2.46 mm]. As shown in Figure VI.56b, a circular crack appeared along the anchor at the load of 12.84 kips [57.14 kN]. After passing the ultimate load, the load was up and down as the displacement increased due to the threads sheared off continually and the frictional resistance generated by the rough surface of the drilled hole. The anchor was pulled out with a concrete cone due to adhesive-concrete interface failure shown in Figure VI.56c.

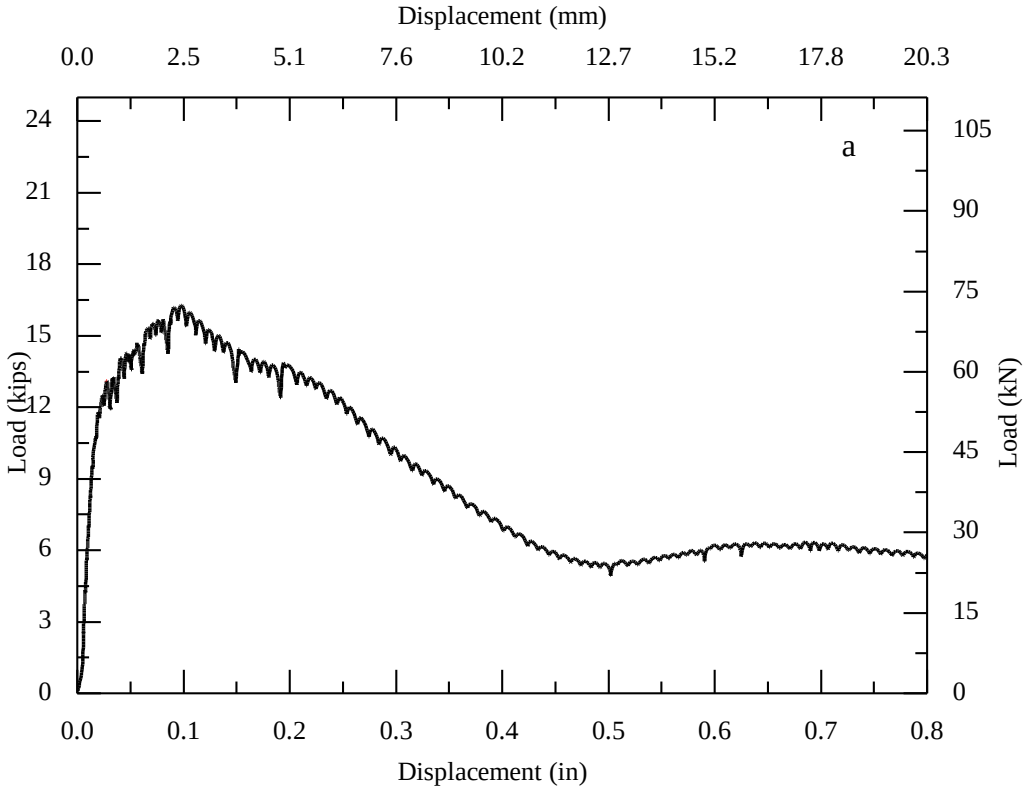

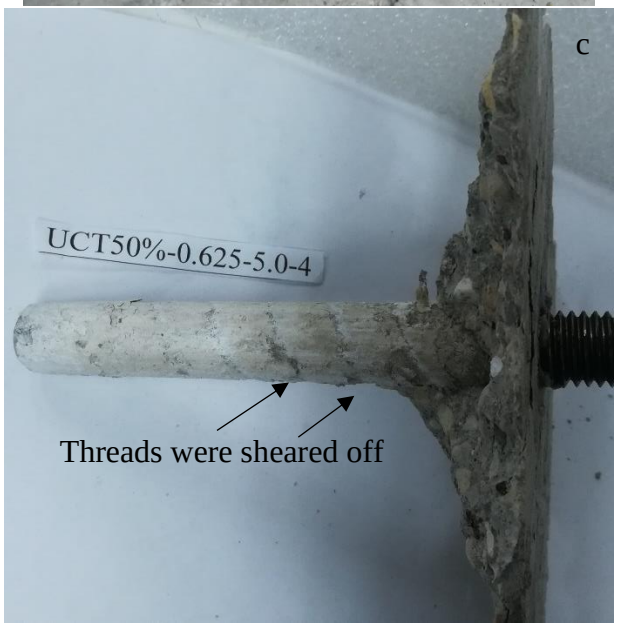

a) load-displacement behavior; b) cracked surface; c) partial cone bond failure.

Figure VI.56. Observed behavior of Specimen UCT50%-0.625-5.0-#4

Appendix VII: Confined Pullout Tests of Adhesive Anchors

A total 16 confined pullout tests of adhesive anchors were conducted, including 8 tests with 0.5-in. diameter anchors with a 3-in. embedment depth and 8 tests with 0.5-in. diameter anchors with a 2-in. of embedment depth. A total of 12 additional tests were performed for partially clean holes. The specimen names represent their test variables. For example, Specimen CT50%-0.5-2.0-#1 indicates that

“C”: confined pullout tests.

“T”: drilled holes with threads.

“50%”: partially cleaned holes as defined in Appendix V.

“0.5”: 0.5-in. diameter anchors.

“2.0”: 2.0-in. embedment depth.

“#1”: test anchor number (a total of four tests are conducted for each anchor configuration)

“AC”: adhesive-concrete interface failure.

“AS”: adhesive-steel interface failure.

The detailed observations are documented below:

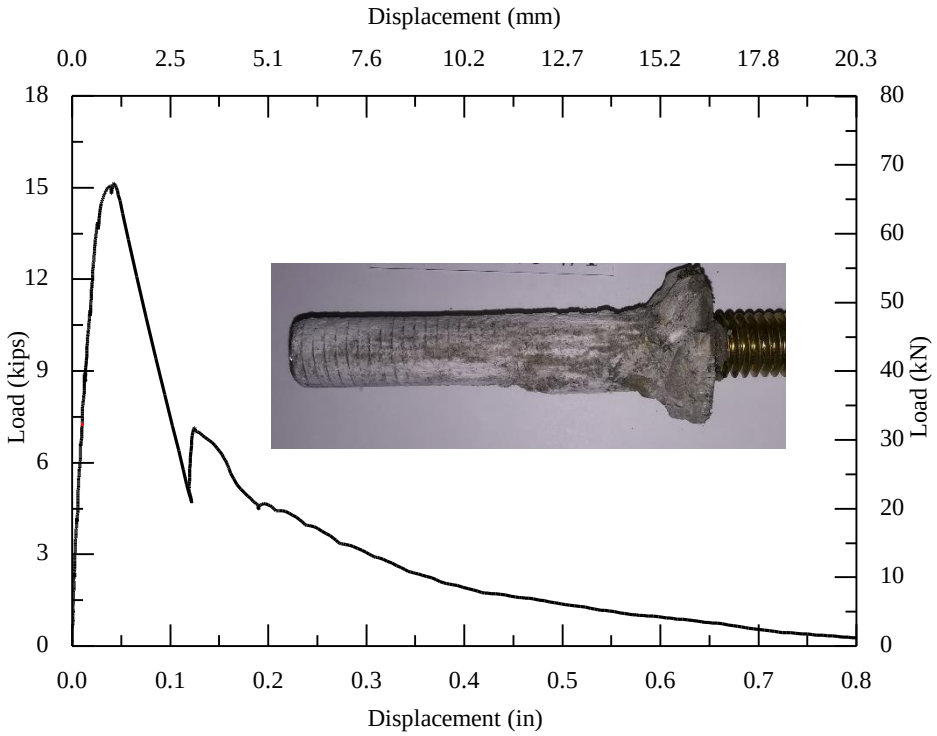

Figure VII.1. Adhesive-steel failure (trial confined test C-3.0-#1)

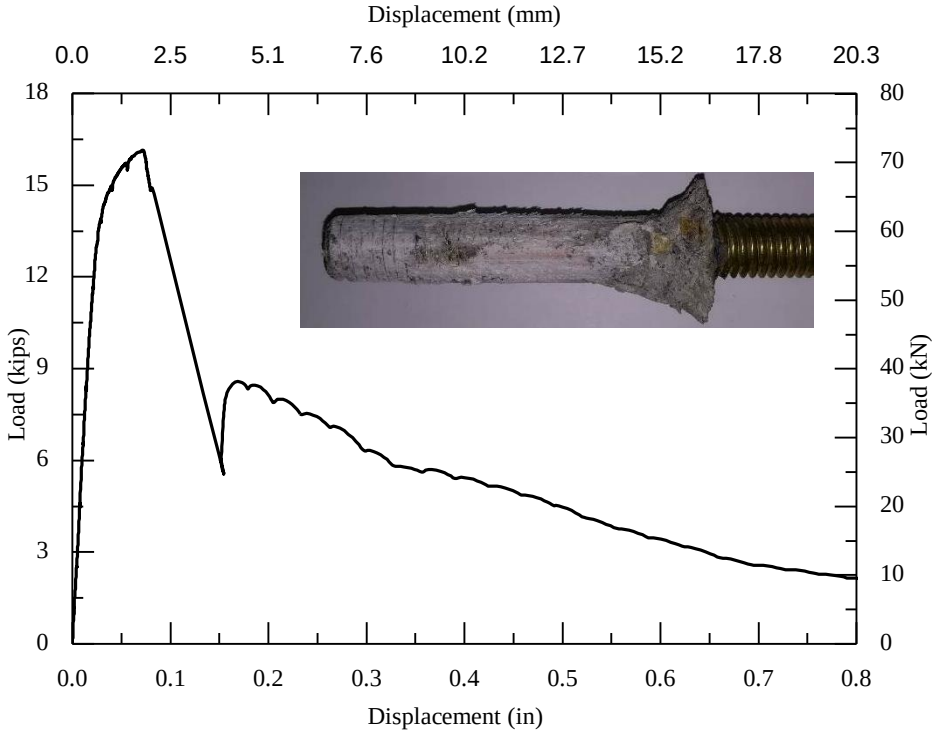

Figure VII.2. Adhesive-steel failure (trial confined test C-3.0-#2)

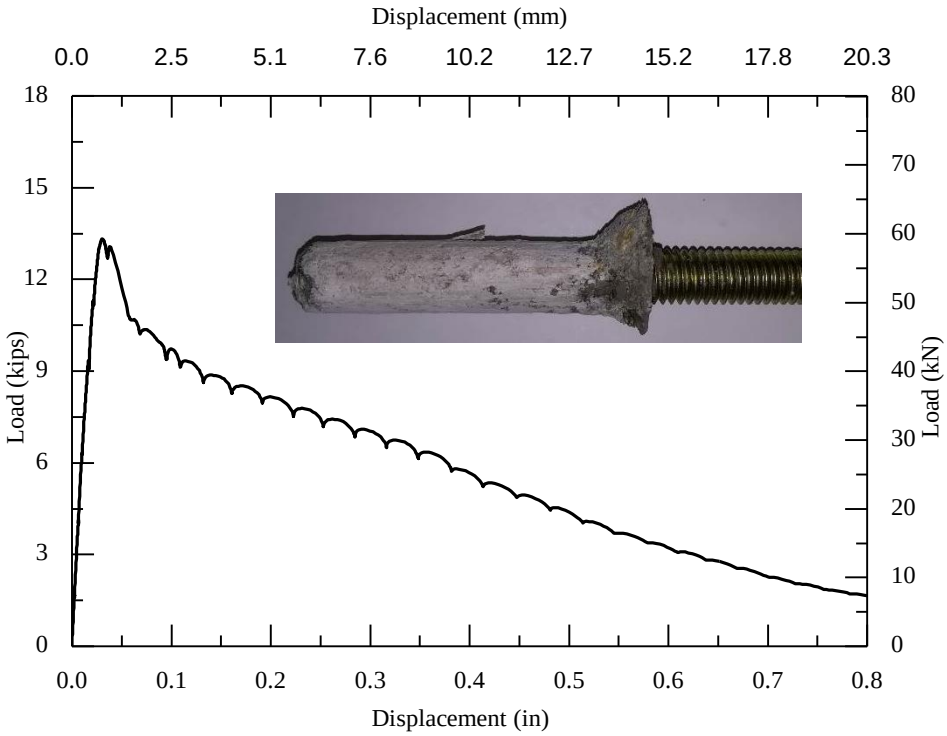

Figure VII.3. Adhesive-concrete failure (trial confined test C-3.0-#3)

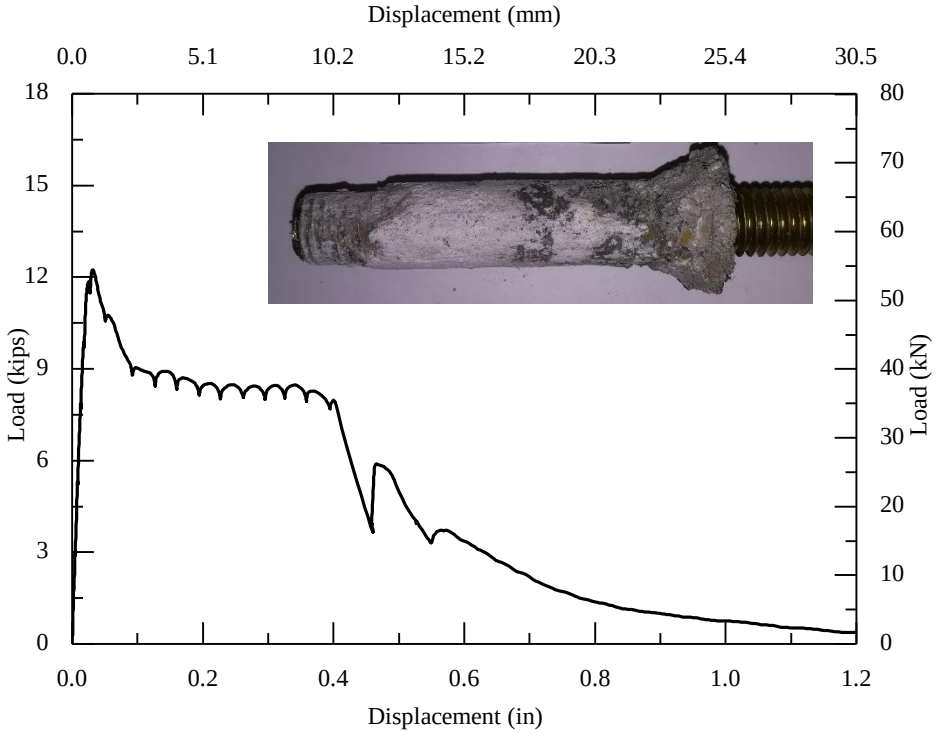

Figure VII.4. Adhesive-concrete failure (trial confined test C-3.0-#4)

Table VII.1. Summaries of confined tests.

NO	Specimens	Anchor diameter (in.)	h_{ef} (in.)	Bond length (in.)	Ultimate load (kips)	Bond stress (psi)	Failure mode
1	C-0.5-2.0-#1	0.5	2	1.919	9.59	3182	AC
2	C-0.5-2.0-#2	0.5	2	1.9615	7.98	2590	AC
3	C-0.5-2.0-#3	0.5	2	1.925	10.44	3453	AC
4	C-0.5-2.0-#4	0.5	2	2.012	11.19	3541	AC
5	C-0.5-3.0-#1	0.5	3	3.015	11.53	2435	AC
6	C-0.5-3.0-#2	0.5	3	2.976	11.36	2430	AC+AS
7	C-0.5-3.0-#3	0.5	3	2.8425	13.33	2987	AC
8	C-0.5-3.0-#4	0.5	3	2.846	12.24	2740	AC
9	CT-0.5-2.0-#1	0.5	2	1.946	10.60	3468	AS
10	CT-0.5-2.0-#2	0.5	2	1.864	12.37	4225	AC+AS
11	CT-0.5-2.0-#3	0.5	2	2	10.77	3430	AC+AS
12	CT-0.5-2.0-#4	0.5	2	1.89	9.45	3186	AS
13	CT-0.5-3.0-#1	0.5	3	2.792	13.49	3078	AS
14	CT-0.5-3.0-#2	0.5	3	2.935	14.05	3049	AS
15	CT-0.5-3.0-#3	0.5	3	2.929	15.20	3306	AS
16	CT-0.5-3.0-#4	0.5	3	2.809	13.00	2948	AC+AS
17	C50%-0.5-2.0-#1	0.5	2	2.049	3.35	1042	AC
18	C50%-0.5-2.0-#2	0.5	2	1.814	4.17	1464	AC
19	C50%-0.5-2.0-#3	0.5	2	2	2.65	843	AC
20	C50%-0.5-3.0-#1	0.5	3	2.946	4.63	1000	AC
21	C50%-0.5-3.0-#2	0.5	3	2.934	7.11	1545	AC
22	C50%-0.5-3.0-#3	0.5	3	2.935	4.91	1065	AC
23	CT50%-0.5-2.0-#1	0.5	2	2.034	8.88	2779	AC+AS
24	CT50%-0.5-2.0-#2	0.5	2	1.891	7.61	2563	AC+AS
25	CT50%-0.5-2.0-#3	0.5	2	1.985	5.20	1668	AC+AS
26	CT50%-0.5-3.0-#1	0.5	3	2.994	11.52	2451	AC+AS
27	CT50%-0.5-3.0-#2	0.5	3	2.987	15.30	3262	AC+AS
28	CT50%-0.5-3.0-#3	0.5	3	2.925	11.19	2437	AC+AS

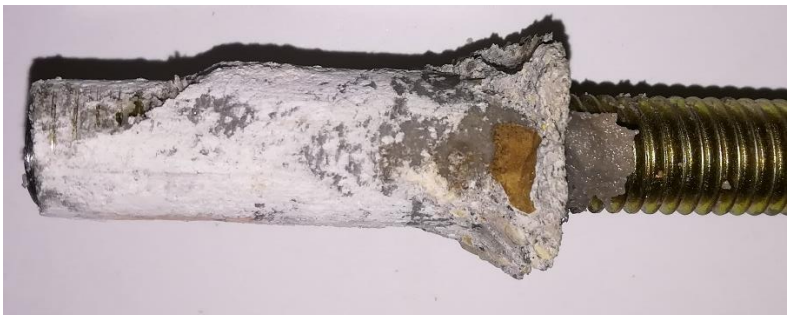

Figure VII.5. C-0.5-2.0-#1

Figure VII.6. C-0.5-2.0-#2

Figure VII.7. C-0.5-2.0-#3

Figure VII.8. C-0.5-2.0-#4

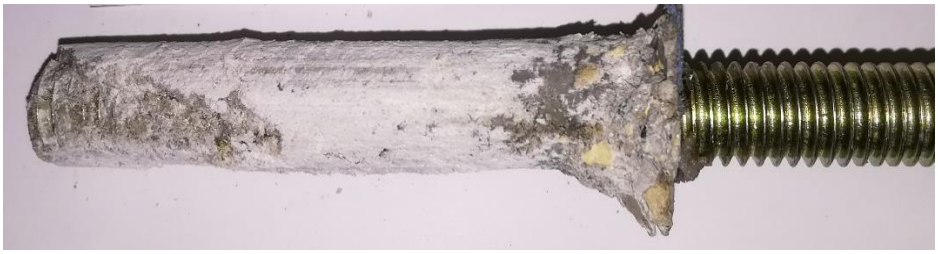

Figure VII.9. C-0.5-3.0-#1

Figure VII.10. C-0.5-3.0-#2

Figure VII.11. C-0.5-3.0-#3

Figure VII.12. C-0.5-3.0-#4

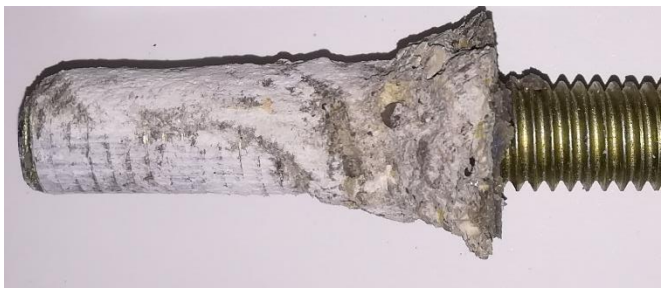

Figure VII.13. CT-0.5-2.0-#1

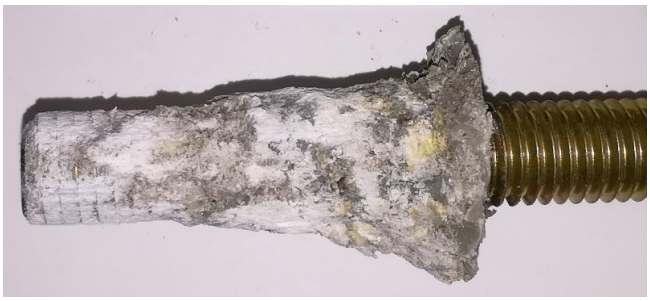

Figure VII.14. CT-0.5-2.0-#2

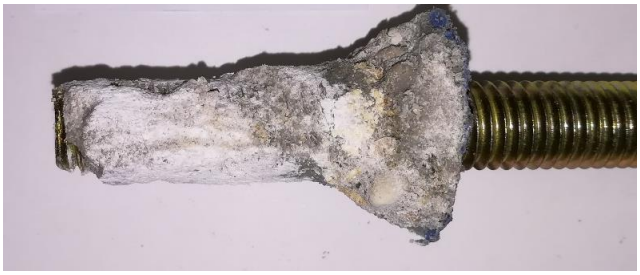

Figure VII.15. CT-0.5-2.0-#3

Figure VII.16. CT-0.5-2.0-#4

Figure VII.17. CT-0.5-3.0-#1

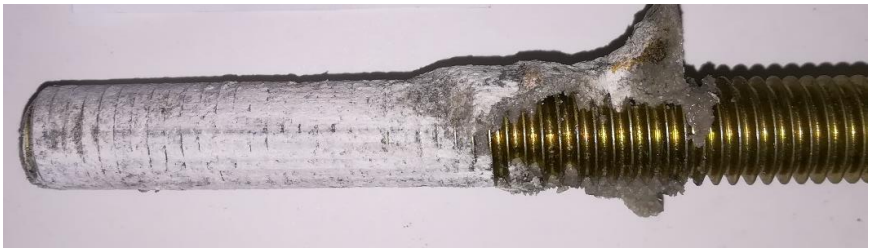

Figure VII.18. CT-0.5-3.0-#2

Figure VII.19. CT-0.5-3.0-#3

Figure VII.20. CT-0.5-3.0-#4

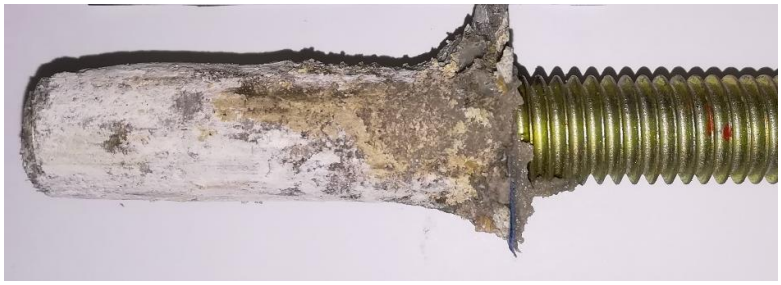

Figure VII.21. C50%-0.5-2.0-#1

Figure VII.22. C50%-0.5-2.0-#2

Figure VII.23. C50%-0.5-2.0-#3

Figure VII.24. C50%-0.5-3.0-#1

Figure VII.25. C50%-0.5-3.0-#2

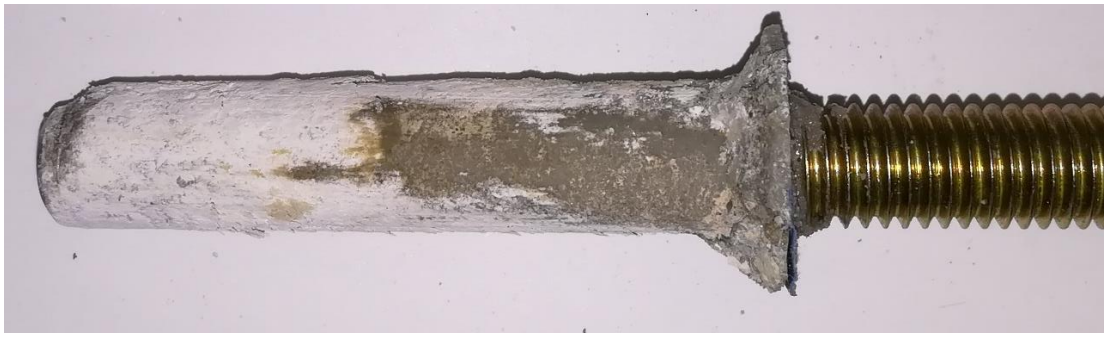

Figure VII.26. C50%-0.5-3.0-#3

Figure VII.27. CT50%-0.5-2.0-#1

Figure VII.28. CT50%-0.5-2.0-#2

Figure VII.29. CT50%-0.5-2.0-#3

Figure VII.30. CT50%-0.5-3.0-#1

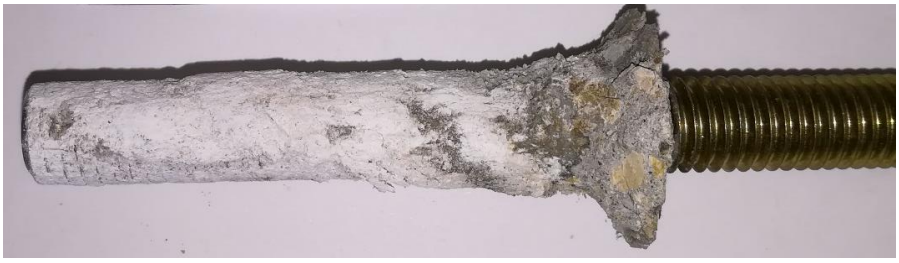

Figure VII.31. CT50%-0.5-3.0-#2

Figure VII.32. CT50%-0.5-3.0-#3

Appendix VIII: Formwork and Reinforcement Cages

VIII.1 Formwork

As shown Figure VIII.1, the plywood was cut into desired pieces that ensure the inside dimensions of block formwork were met the requirement (12×12×24 in. [305×305×610 mm] and 15×15×28 in. [381×381×711 mm]. Two L shape wood sticks were screwed on each corner shown in Figure VIII.2. The pilot holes should be preparing before putting any screws on the wood sticks to avoid the crack on the stick during screwing. The wood sticks at the bottom of the block were screwed on the floorboard to prevent the block movement during pouring concrete. Use one screw at each wood stick to fix the block 12×12×24 in. [305×305×610 mm] on the floorboard; Used more than two screws at each wood stick to fix the block 15×15×28 in. [381×381×711 mm]. The triangle plywood 10 × 10 in. [254 × 254 mm] shown in Figure VIII.3 was used to enforce the block stiffness to prevent side pressure produced by concrete for deep concrete blocks. As shown Figure VIII.3, embedded parts for lifting were installed in the middle of each transverse board. For The inner gap of the formwork was sealed by using the caulk to avoid leaking. Then, the inner surfaces of the formwork were applied by using the oil before concreting acted as mold release agent.

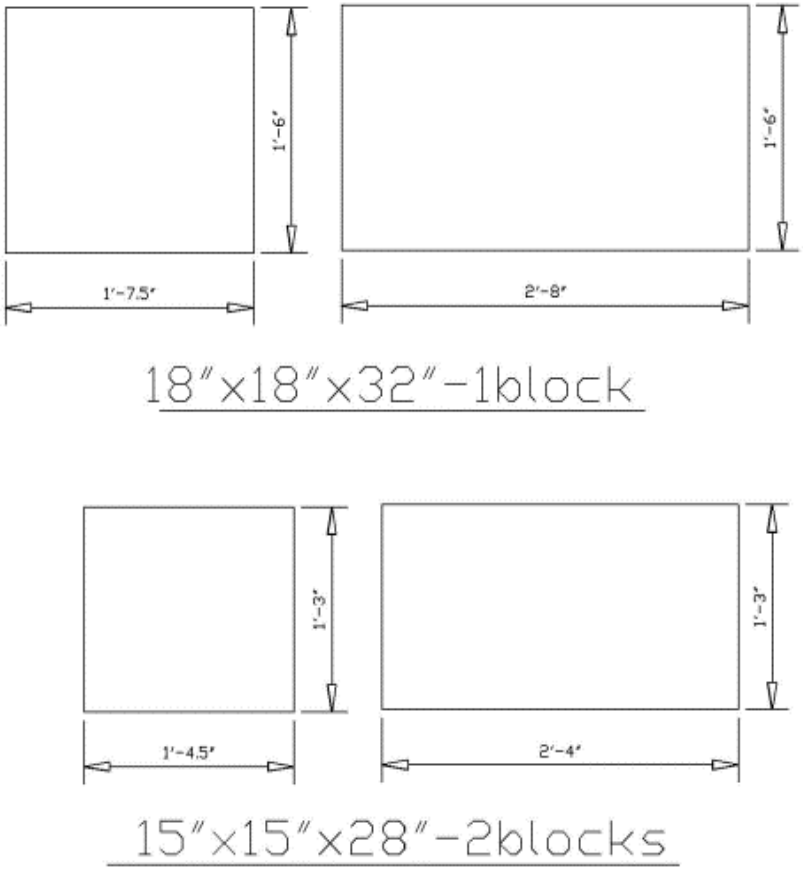

Figure VIII.1. The formwork of a block.

Figure VIII. 2. L shape wood sticks screwed on the block.

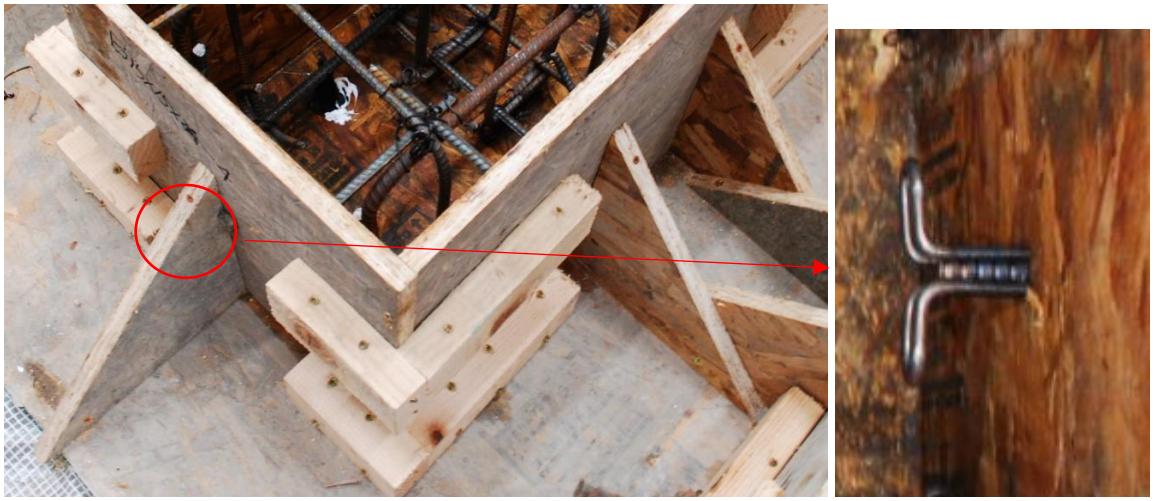

Figure VIII.3. Triangle plywood enforced stiffness of block formwork (15”x15”x28”) and embedded Parts for Lifting

VIII.2 Reinforcement cages

The ASTM A165 rebars (#3 and #4) for the tests in this study were purchased from Menards. The rebars were kept to the same indoor environment (roughly with a consistent temperature of 70 degrees Fahrenheit). The amount of rebars (Figure VIII.4) is calculated by the equations (HCCLRS 2017) shown as follows:

Perimeter of rectangle A= the outside perimeter of cross-section – 8 concrete covers

The length of longitudinal rebar B= the outside of long length – 2 concrete covers

The length of C- hook C = the outside length of cross-section – 2 concrete covers + $2d_b$

90-degree hook length D= $d_b + \frac{D_1}{2} + 12\ d_b$.

135-degree hook length E = $6d_b$ or 3in. min.

90-degree bend length F = $\frac{1}{4}\pi(D_1 + d_b)$.

135-degree bend length G = $\frac{135}{360}(D_1 + d_b)$.

Total cutting length of rectangular stirrup = A + 2 E -3 F – 2 G.

Total cutting length of longitudinal rebar = B + 2 D -2 F.

Total cutting length of C- hook (#3 & #4) = C + 8.5 d_b + 5 $d_b \times 2$

Where the concrete cover is 1.5 in. [38 mm] based on not exposed to weather or in contact with ground (ACI 318.14, Table 20.6.1.3.1); D_1 is finished inside bend diameter (#3 = 2 ¼ in. [57 mm] and #4 = 3 in. [76 mm]); d_b is rebar diameter;

All rebars were bent by the rebar plant except the C - hook. As shown in Figure VIII.5, we used MBC -16B Bender /Cutter to bend the C- hooks. First, use the equation of C- hook to calculate the total cutting length of C-hook. Second, mark the 5 d_b on the rebar from each end. Third, adjust the bending roller shown in Figure VIII.6. The numbers on bender cam are 16, 13, 10 meaning 16 mm

or #5 (5/8 in.) rebars, 13 mm or #4 (1/2 in.) rebars and 10 mm or #3 (3/8 in.) rebars. Fourth, put one end of the rebar shown in Figure VIII.7 to produce a 90-degree bend with one pull down of the handle. The c hooks were shown in Figure VIII.8

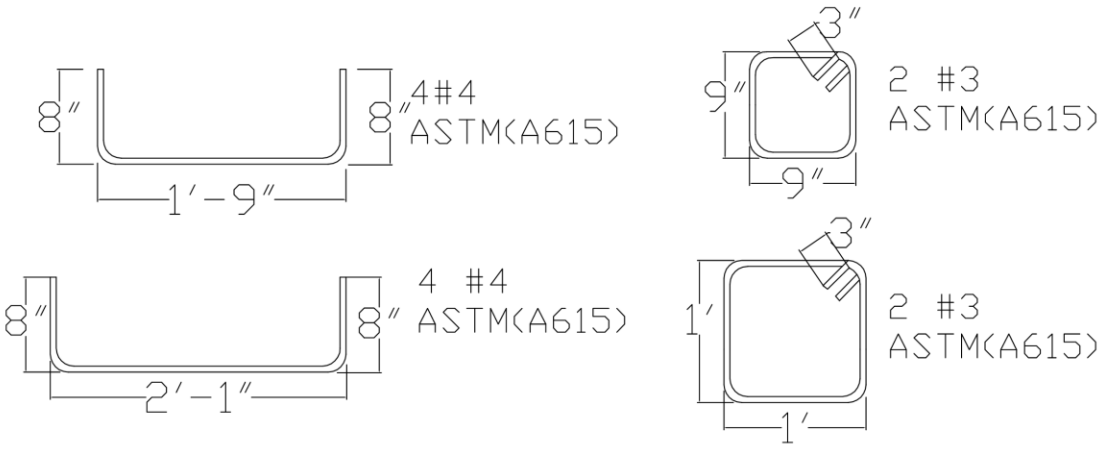

Figure VIII.4. Reinforcement for each block

Figure VIII. 5. MBC -16B Bender /Cutter (BNP. (2020, 3 31))

Figure VIII. 6. Adjust the bending roller (BNP. (2020, 3 31)

Figure VIII.7. Bending point

Figure VIII.8. C hooks

Appendix IX: Preliminary Unconfined Tests

Unconfined pullout tests are performed to evaluate the new adhesive anchors in drilled holes with concrete dusts or moisture. Note that confined tension tests are usually conducted to measure the tension resistance of the adhesive anchor dominated by bond strength. It is envisioned that the adhesive anchors will have greatly improved tensile capacity with threads such that the failure mode may change from bond failure to concrete breakout failure; hence, unconfined pullout tests are used in this group if tests.

The tests consider the condition of drilled holes with concrete dusts and moisture. Two groups of anchors are installed in a concrete block: three traditional adhesive anchors and three new adhesive anchors. Within each group, one anchor is installed in cleaned hole, one in dusty hole, and the last in moisture hole. The embedment depth is chosen as 4 in. to obtain the uniform bond stress model for adhesive anchors according to Cook et al. (1998). Specifically, the embedment depth (4 inch) [102 mm] to the anchor diameter (1/2 inch) [13 mm] ratio does not exceed 20 and the hole diameter (5/8 inch) [16 mm]to the anchor diameter (1/2 inch) [13 mm] ratio does not exceed 1.5. Anchors are installed with edge distance of 1.5 times the embedment depth. Six concrete blocks with dimensions of 12×12×24 in. [305×305×610 mm] were cast. The average compressive strength was 8570 psi [59 MPa] at 28 days from the tests of standard 4 inch by 8-inch [101.6 × 203.2 mm] cylinders cast at the same time at the test members according to ASTMC39. The concrete mix design from a commercial batching plant is shown in Table IX.1.

The procedure was based on ACI 355.4-11 Section 7.5 with full cleaning effort (manufacturer's printed installation instructions, MPII) in dry concrete conditions. The adhesive was allowed to cure for the time specified in the MPII plus an additional 24 hours (ACI 355.4-11 Section 8.7).

IX.1 Installation procedure of adhesive anchors

1. **Installation procedure in unclean holes**. The drilled holes did not apply the hand pump and a wire brush to remove the debris. This test evaluates the sensitivity of an anchor system installed in uncleaned holes.
2. **Installation procedure in threaded holes**. The holes were drilled with a 5/8 drill [16 mm] bit first. Then, the screw anchor was driven into the hole using an impact wrench to create threads in the hole. This test evaluates the sensitivity of an anchor system installed in the threaded holes.
3. **Installation procedure of water-filled holes**. The procedure was based on ACI 355.4-11 Section 7.7. After cleaning the hole, the water was directly into the hole to simulate the moisture condition (Figure IX.1). Then, the nozzle was inserted into the bottom of the hole and as the adhesive was injected the water pushed out of the hole. This test evaluates the sensitivity of an anchor system installed in water-filled holes. To investigation water penetration, we used plumber putty to build a little dam along the anchor and filled water in the dam, as shown in Figure IX.1

Based on the above installation procedure, 36 anchors are installed in a: unclean smooth dry hole (USD), unclean threaded dry hole (UTD), clean smooth dry hole (CSD), clean threaded dry hole (CTD), clean smooth wet hole (CSW) and clean threaded wet hole (CTW).

The unconfined testing setup is shown in Figure IX.2. A self-balanced loading frame was used and tension loads were applied to a test anchor by a coupling rod. The pullout displacement of the anchor was measured using two LVDT's and the applied load was measured by a load cell placed at top of the hydraulic jack. Two linear variable differential transformers (LVDTs) were fixed at

each end of an aluminum flat bar locked between a hex nut and a coupling nut to directly measure axial displacement of an anchor. An IO Tech DaqBook 2000 was used to collect data from the LVDT's and the load cell.

IX.2 Test results

A total 36 unconfined pullout tests of adhesive anchors were conducted. The pullout test results, in terms of the ultimate tensile capacity, are listed in Table IX.2. The meaning of labels for all figures are shown below.

"025E": ¼ in. adhesive was filled in the drilled hole

"05E": ½ in. adhesive was filled in the drilled hole.

"325": the embedment depth was 3.25 inches.

"F": the drilled hole was filled full water.

"P": ponding that a little dam was built along an anchor and filled with water in the dam.

"SC": saturated concrete that the hole remains flood for minimum of 8 days (ACI 355.4.11_7.6)

IX.2.1 Series 0: exploratory tests.

The first series of tests was the exploratory tests, before which, the mechanism of the new adhesive anchors was not clear to us. The anchors were installed in an old concrete slab from a previous study conducted in the lab. The test focused on embedded connections on the side faces of the slabs. Figure IX.3 shows the results of the 6 tests of series 0. Note that in this group of tests, hole cleaning in Specimen CTD and CSD did not follow the MPII; instead, the dusts were simply removed using compressed air. The capacity of anchor in "clean" smooth hole (CSD) is about 8 kips [35.6 kN], partially higher than the code specified capacity. This is expected because the code specified capacity corresponds to 5% fractile of all tests in a study (ACI 318, 2014). The capacity

of the anchor in clean threaded hole (CTD) was only slightly higher than that of CSD. The images of the specimens after the tests, shown in Figure IX.4, indicates the threads in CTD was not clearly formed, which may have been due to improper installation.

The anchor in the unclean hole (USD) had a very low capacity (2 kips) [8.9 kN] as expected because dusts left in the hole significantly impact the bond between adhesive and concrete. Meanwhile, the anchor in the unclean threaded hole (UTD) had a greatly improved capacity (5.6 kips) [24.9 kN] compared with USD. The ultimate is lower than that in the cleaned holes though it is still higher than the code stipulated capacity. The relatively lower capacity may be explained by a shorter embedment: dusts occupied the bottom of the hole hence; the embedded length was reduced to 3.25 in. [83 mm] s shown in Figure IX.5.

The anchors in wet holes was again installed differently from ACI 355.4 procedures. A wet brush was used to introduce moisture on the wall of the drilled holes. This process also cleaned holes; therefore, the anchor in the wet smooth hole (CSW) had a slightly higher capacity (9.0 kips) [40 kN] compared with CSD. When the threads were introduced in wet holes, the measured capacity was not improved because the test was terminated before the full anchor capacity could be reached. In this case, the slab split in half. The test of slab connections took out some concrete, which may have weakened the slab along the broken line as shown in Figure IX.6. The split slab provided, however, provided a clear view of the threads engaging the surrounding concrete, which is the expected behavior.

IX.2.2 Series 1: Tests of anchors with 4-inch embedment

The anchors were installed in concrete blocks with reinforcement in the lab. Figure IX.7 shows the results of the 4 tests of series 1. There were no CSW and CTW records because operators made a mistake that they did not record the data while pulling out these anchors. Note that in this group of tests, mixing epoxy in Specimen CSD did not follow the MPII; instead, the first three full strokes of adhesive through the mixing nozzle were placed into the drilled hole. This is responsible for the observation that the epoxy did not reach full strength. As a result, the capacity of anchor in CSD was only about 4.7 kips [20.9 kN], 25 percent lower than the code specified capacity. The capacity of the anchor in clean threaded hole (CTD) was 155 percent greatly higher than the code specified capacity. The images of the specimens after the tests, shown in Figure IX., indicates the threads in CTD was fully formed along the embedment depth. The failure mode was concrete breakout.

The anchor in the unclean hole (USD) had a capacity (7.3 kips) [32.5 kN], which was slightly higher than the code specified capacity because dusts left in the hole impact the bond between adhesive and concrete. Meanwhile, the anchor in the unclean threaded hole (UTD) had a greatly improved capacity (11.7 kips) [52.1 kN] compared with USD. The ultimate is 86 percent higher than the code stipulated capacity. The relatively higher capacity may be explained by a depth embedment and the embedded length was increased to 4 in. [102 mm].

IX.2.3 Series 2: Tests of anchors with 4-inch embedment

The anchors were installed in concrete blocks with reinforcement in the lab. Figure IX.9 shows the results of the 6 tests of series 2. Note that in this group of tests, placing epoxy in Specimen USD was different from the previous two groups: the mixing nozzle was kept at the bottom of the drilled hole, and excessive amount of epoxy was dispensed. This may cause that raising epoxy

level cleaned dusts on inside surfaces in the drilled hole. The capacity of anchor in USD is about 13.3 kips [59.2 kN], 112 percent higher than the code specified capacity. The image (USD) in Figure IX.10 shows that there was steel-adhesive interface failure on the part of the anchor due to high adhesion on interface between the concrete and the epoxy. This may contribute to high bond strength of the USD. The capacity of the anchor in unclean threaded hole (UTD) was 117% greatly higher than the code specified capacity. The images of the specimens after the tests, shown in Figure IX.10, shows the steel-adhesive failure was along the embedment depth and indicates the threads in UTD was slightly impacted by dusts in the drilled hole.

The capacity of anchor in CSD is about 13.9 kips [61.9 kN], 145 percent higher than the code specified capacity. The images of the specimens after the tests, shown in Figure IX.10, shows the steel-adhesive failure was on the part of bottom of the anchor. This may cause the high bond strength. The capacity of the anchor in clean threaded hole (CTD) was 15.4 kips [68.5 kN] and was 145 percent greatly higher than the code specified capacity. The images of the specimens after the tests, shown in Figure IX.10, indicates the threads in CTD was fully formed along the embedment depth. The failure mode was concrete breakout.

For the clean smooth wet holes, after cleaning the hole, the water was directly into the hole to simulate the moisture condition. This process might clean holes; therefore, the anchor in the wet smooth hole (CSW) had a slightly lower capacity (9.8 kips) compared with CSD. The image (CSW) in Figure 11 shows that the surfaces of the epoxy are white compared with regular dark color and indicates that the epoxy may interact with the water. This may reduce the bond strength. When the threads were introduced in wet holes, the measured capacity was greatly improved because the steel-adhesive interface failure occurred on the tested anchor although there were interactions between the epoxy and the water. Figure IX.11 shows that CSW occurred concrete-adhesive

interface failure and CTW had concrete-adhesive and steel-adhesive interface failure with formed threads.

IX.2.4 Series 3: Tests of anchors with 4-inch embedment

Figure IX.12 shows the results of the 8 tests of series 3. The anchors in the unclean hole (USD) had low capacities (5.1 kips, 4.1 kips, 6.3 kips) [22.7 kN, 18.2 kN, 28 kN] as expected because dusts left in the hole significantly impact the bond between adhesive and concrete. Figure IX.13 shows that the dusts covered most of parts of the embedment depth to be a bond breaker on the interface between the concrete and adhesive. One USD with half epoxy was very low capacity (2.9 kips) [12.9 kN] because dusts left in the hole and lack of the epoxy greatly impact the bond between adhesive and concrete. These USDs shows unexpected results depended on how dusts covered on the interface between adhesive and concrete. However, lack of the epoxy can greatly impact the bond strength.

Figure IX.14 shows anchors in the clean smooth holes (CSW+P) with ponding condition had higher capacities (13.2 kips and 13.4 kips) [58.7 kN and 59.6 kN] than the code stipulated capacity. Figure IX.14 shows that the steel-adhesive interface failure occurred on the part of the anchors and the surfaces of the epoxy were regular dark color due to very little water penetrated concrete to impact the epoxy under ponding condition in short term. They had the concrete-adhesive and the steel-adhesive interface failure. However, the anchor in the wet smooth hole (CSW+P+F) with full water condition had a greatly lower capacity (6 kips) [26.7 kN] compared with CSW+P. Figure IX.14 shows that the surfaces of the epoxy were white compared with regular dark color and indicates that the epoxy may interact with the water. This may reduce the bond strength. The anchor in the wet smooth hole (CSW+05E +F) with full water condition had a slightly lower capacity (5.1 kips) [22.7 kN] compared with CSW+P+F. From the image of a tested anchor

(CSW+05E+F), the anchor threads were exposed without enough epoxy to cover. The lack of the epoxy also can impact the bond strength under moisture condition.

IX.2.5 Series 4: Tests of anchors with 4-inch embedment

Figure IX.15 shows the results of the 7 tests of series 4. The anchors in the unclean hole (USD+05E) had low capacity (3.9 kips) [17.4 kN] as expected because dusts left in the hole and lack of the epoxy significantly impact the bond between adhesive and concrete. As shown in Figure IX.16, after removing dusts on the surface, many areas were not covered by the epoxy. Meanwhile, the anchor in the unclean threaded hole (UTD+05E) had an improved capacity (5.8 kips) [25.8 kN] compared with USD+05E. In the Figure IX.16, there no enough epoxy to form the threads in on the anchor surfaces. The same things occurred on USD+025E and UTD+025E. The anchors in the unclean hole (USD+0.25E) and the unclean threaded hole (UTD+0.25E) had greatly lower capacities (0.4 kips and 0.8 kips) [1.8 kN and 3.6 kN] due to lack of the adhesive compared with USD+05E and UTD+05E. However, the ultimate load in the unclean threaded hole is still higher than that in the unclean holes under lack of the epoxy. These relatively lower capacity can indicate that lack of the epoxy is an adverse effect to weaken bond strength. The anchors in the unclean hole (USD) had very low capacity (1.7 kips) [7.6 kN]. As shown in Figure IX.16, after removing dusts on the surfaces, the most of interfaces between the concrete and the epoxy were not covered by the epoxy due to heavy dusts. This indicated that the bond strength in the unclean hole depends on how dusts covered on the interface between adhesive and concrete.

Figure IX.17 shows the anchor in the clean threaded wet holes (CTW+F) with refilling full water condition had higher capacities (9.2 kips) [40.9 kN] than the code stipulated capacity. Figure IX.17 shows that the steel-adhesive interface failure occurred along the embedment depth and the surfaces of the epoxy were regular dark color. Those harden epoxies on the anchor threads were

easy to remove by hands due to the water interacted with the epoxy. This may cause the low bond strength in the threaded wet hole. The anchor in the clean smooth wet holes (CSW+F) with refilling full water condition had higher capacities (9.3 kips) [41.4 kN] than the code stipulated capacity. Figure IX.17 shows that the surfaces of the epoxy were white color and those epoxies on the anchor threads were easy to remove due to the water interacted with the epoxy. Both cases indicated that the full water in the drilled holes can significantly impact epoxy strength.

IX.2.6 Series 5: Tests of anchors with 4-inch embedment

Figure IX.18 shows the results of the 5 tests of series 5. The anchors in the unclean threaded hole (UTD) had high capacities (8.1 kips) [36 kN] compared with USD and it is still higher than the code stipulated capacity. The capacity of anchor in CTD is about 16.3 kips [72.5 kN], 160 percent higher than the code specified capacity. The images of the specimens after the tests, shown in Figure IX.19, shows the steel-adhesive failure was along embedment depth. The threads in the drilled holes improved the adhesion on interface between the concrete and the epoxy. This adhesive was larger than the mechanical interlock between the steel and the epoxy. This may cause the high bond strength. The capacity of the anchor in clean threaded hole (CSD) was 14 kips [62.3 kN] and was 123 percent greatly higher than the code specified capacity. As shown in Figure 19, the anchors (CSW+SC) installed in the saturated concrete with refilling full water may improve the bond strength, which was 139 percent of the code required capacity.

IX.3 Summary

- The standard installation of adhesive anchors is critical to conduct steady results.
- The tensile capacities of adhesive anchors may impact by the amount of the epoxy in the drilled holes.
- The tensile capacities may impact by the epoxy without mixing completely in the drilled holes.
- The tensile capacities may not impact by the water condition because the water cannot penetrate concrete to influence interfacial epoxy in the short term.
- The tensile capacities can be improved by adding threads in the drilled holes under dusty and moisture conditions.
- Adding threads in drilled hole under clean condition may change the failure mode from bond failure to concrete breakout failure.

Figure IX.1. Water-filled the hole and ponding water

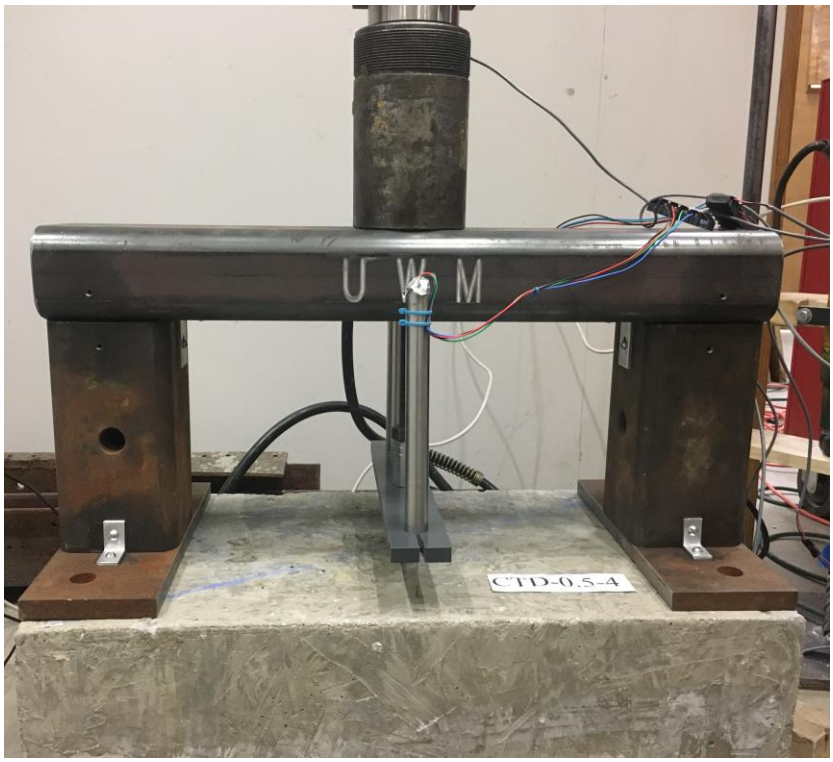

Figure IX.2. Unconfined testing apparatus

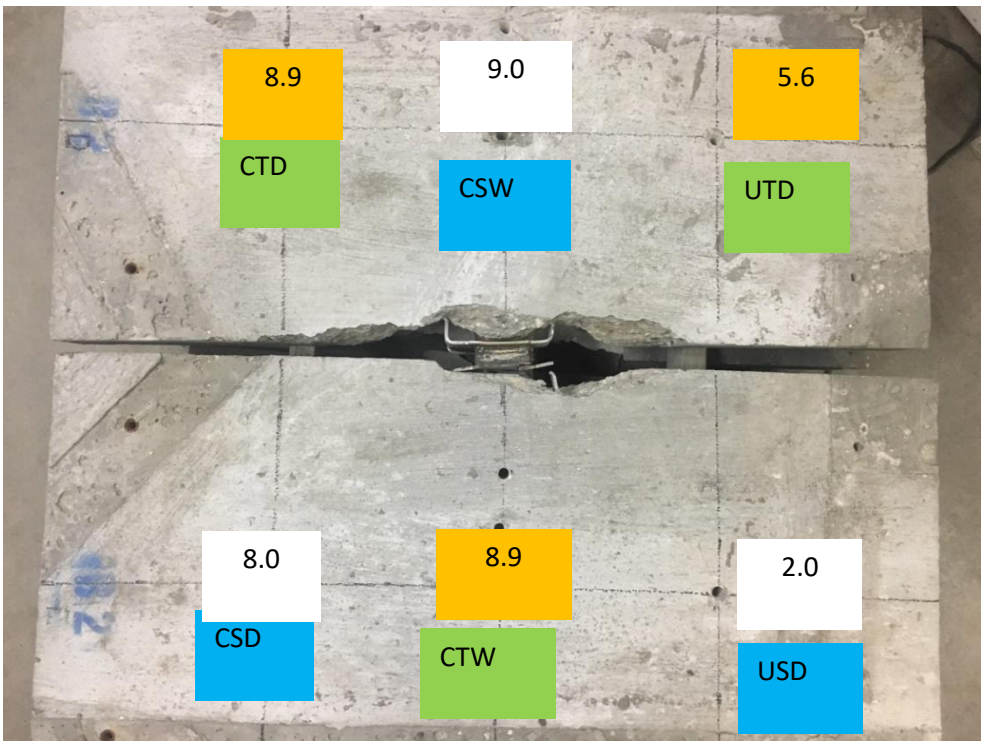

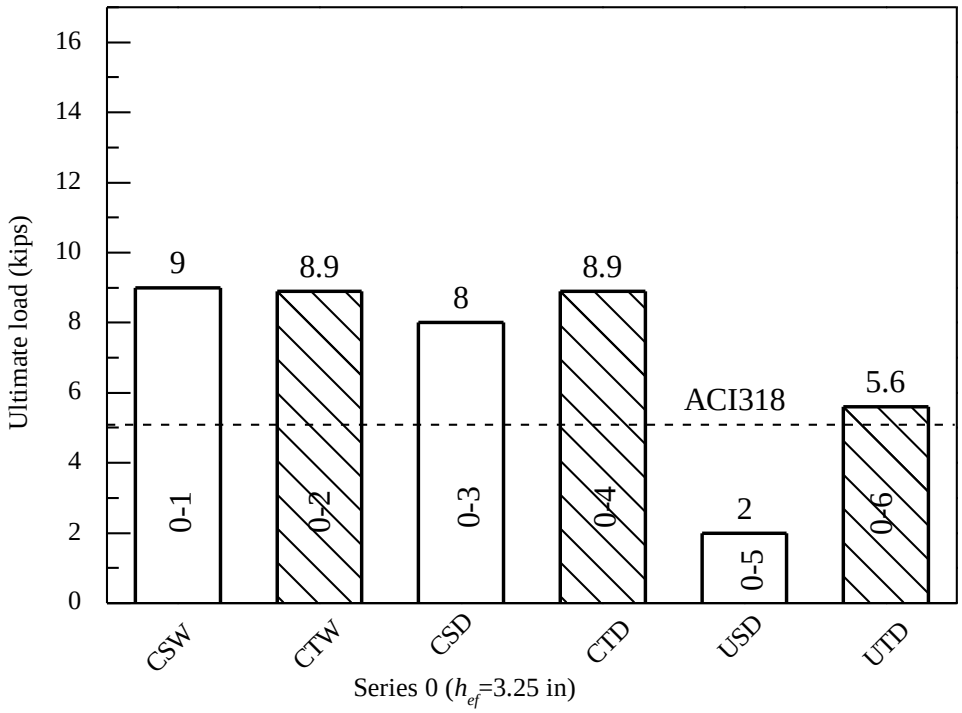

Figure IX.3. The results of the 6 tests of series 0

Figure IX.4. Tested anchors CSD vs CTD

Figure IX.5. Tested anchors UTD vs CTD (12292017)

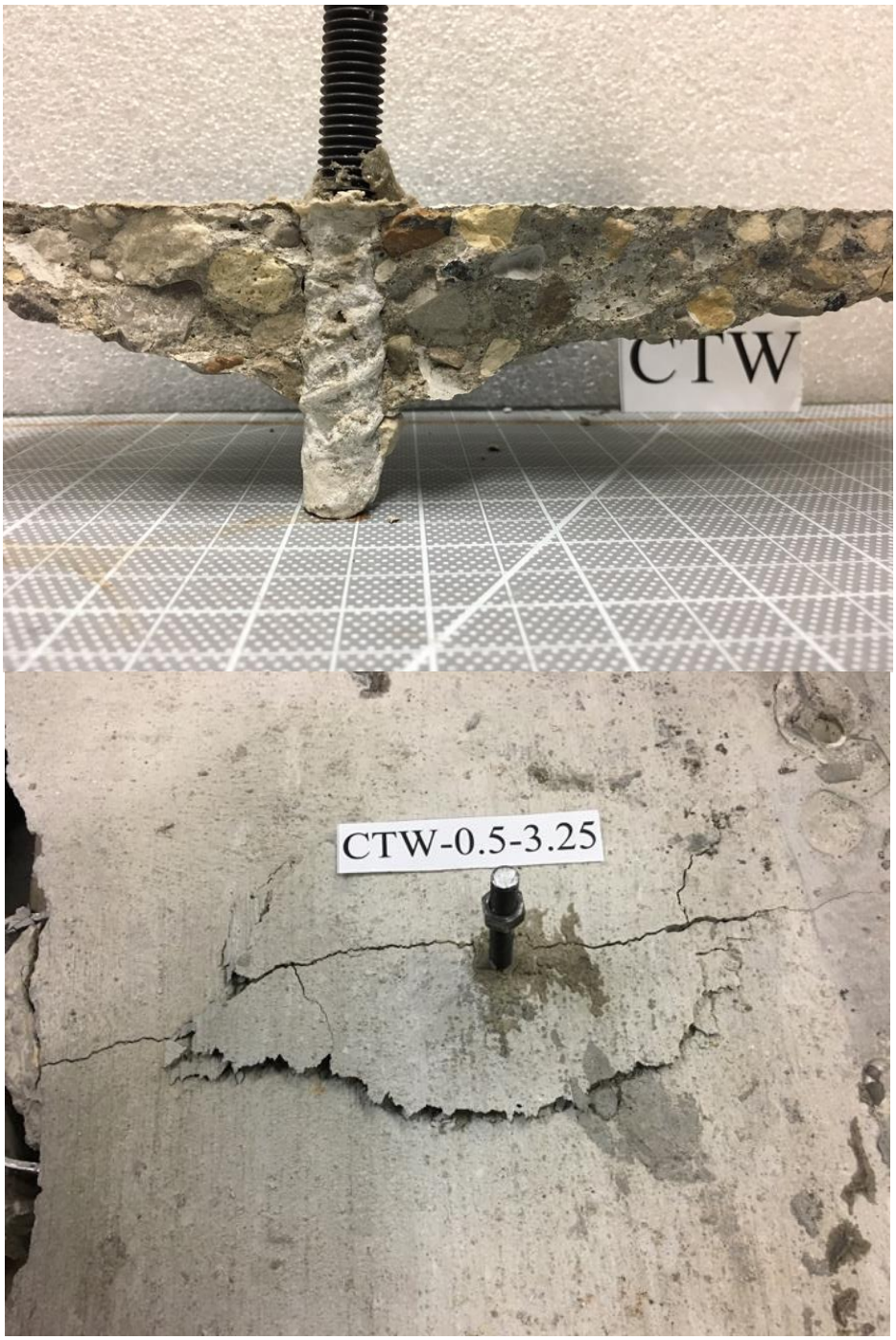

Figure IX.6. Failure of CTW specimen before ultimate load was achieve (12292017)

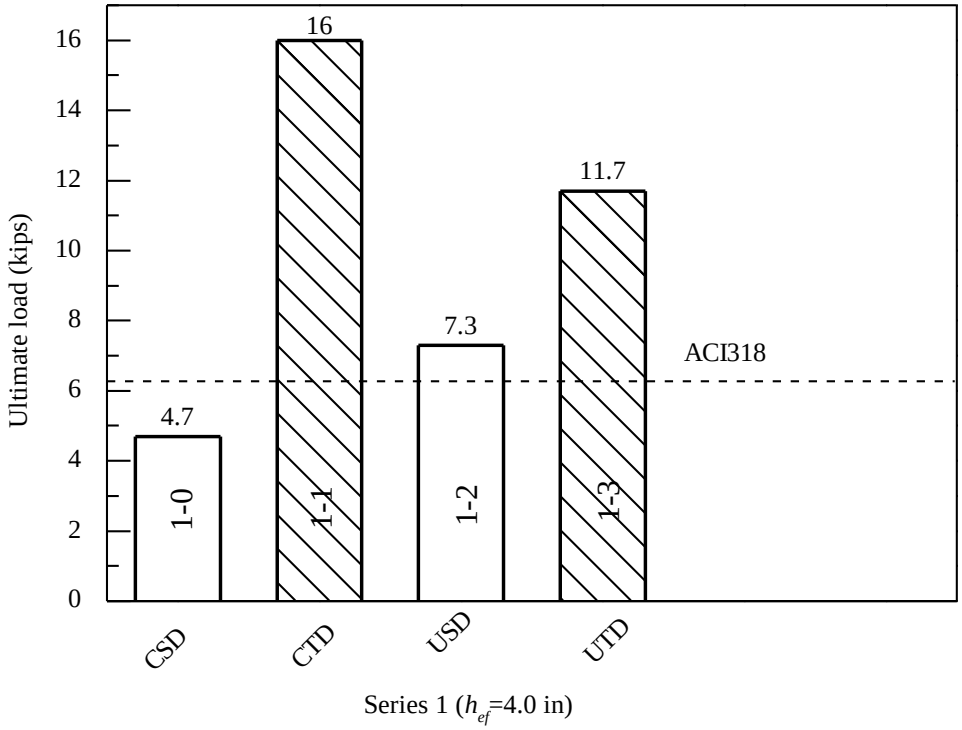

Figure IX.7. The results of the 4 tests of series 1

Figure IX.8. Concrete breakout failure of CTD (3032018)

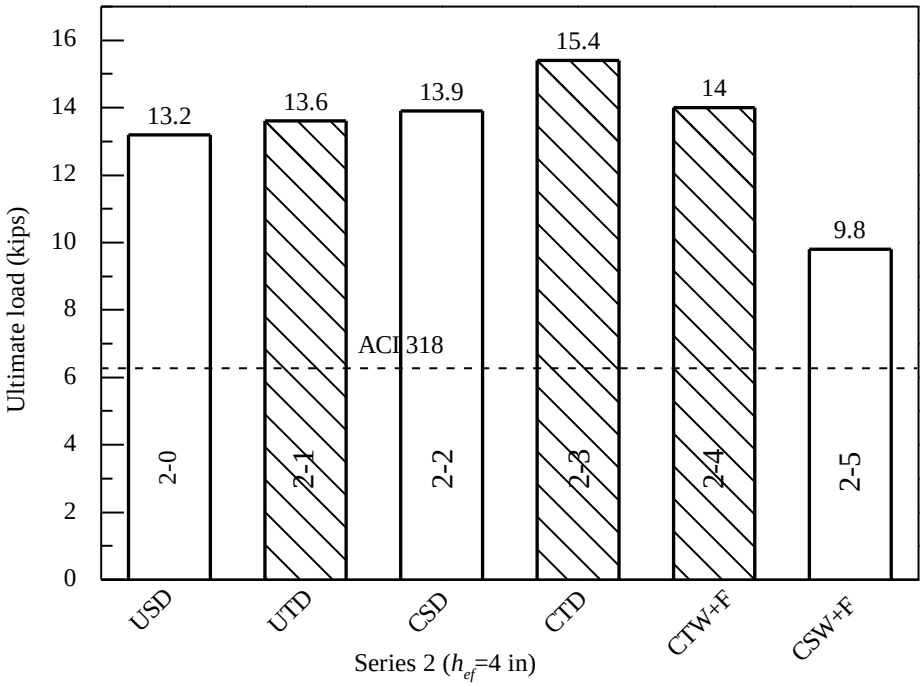

Figure IX.9. The results of the 6 tests of series 2

Figure IX.10. Tested anchors USD, UTD, CSD and CTD (03082018 and 3132018)

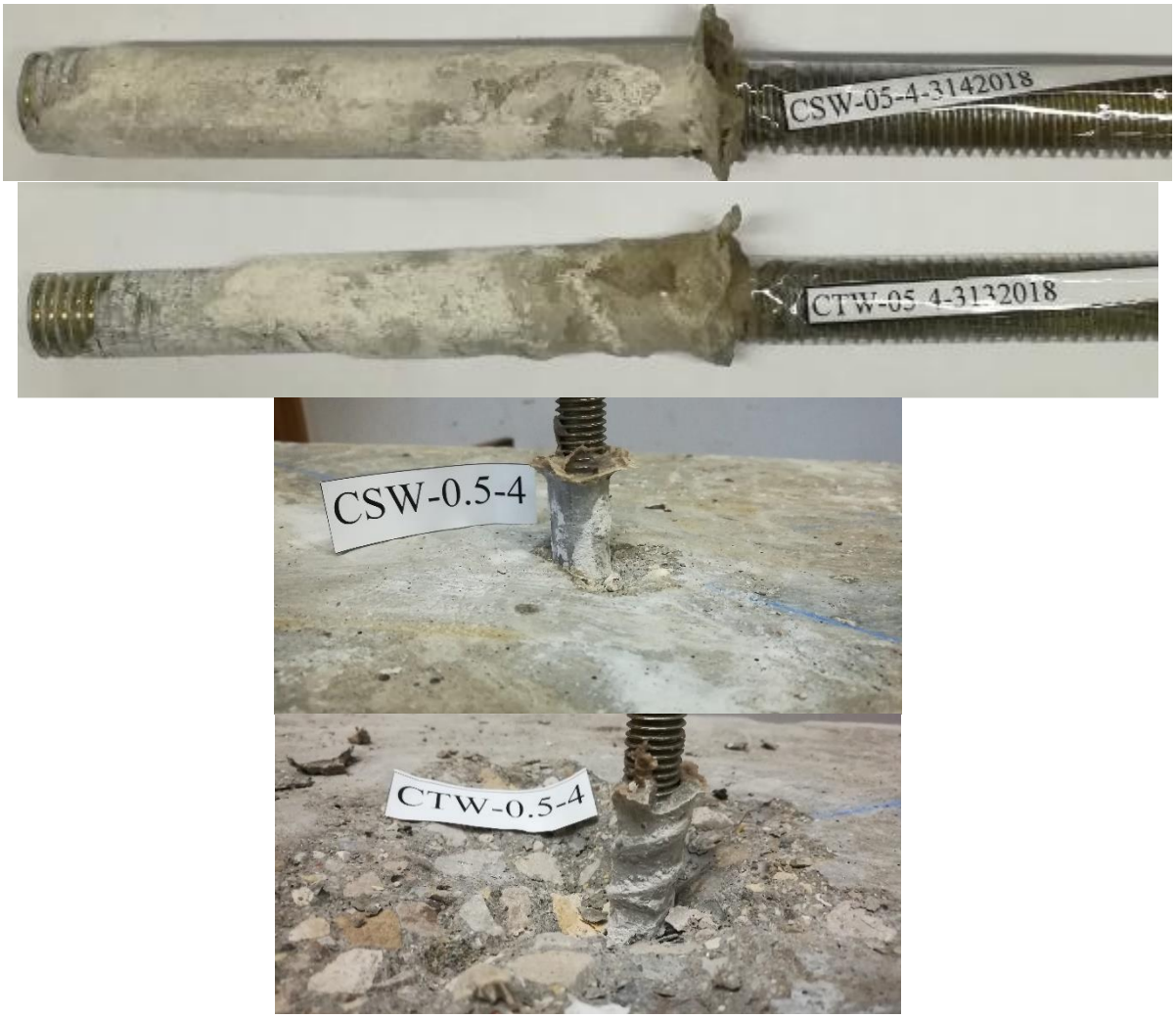

Figure IX.11. Tested anchors CSW vs CTW (3132018 and 3142018)

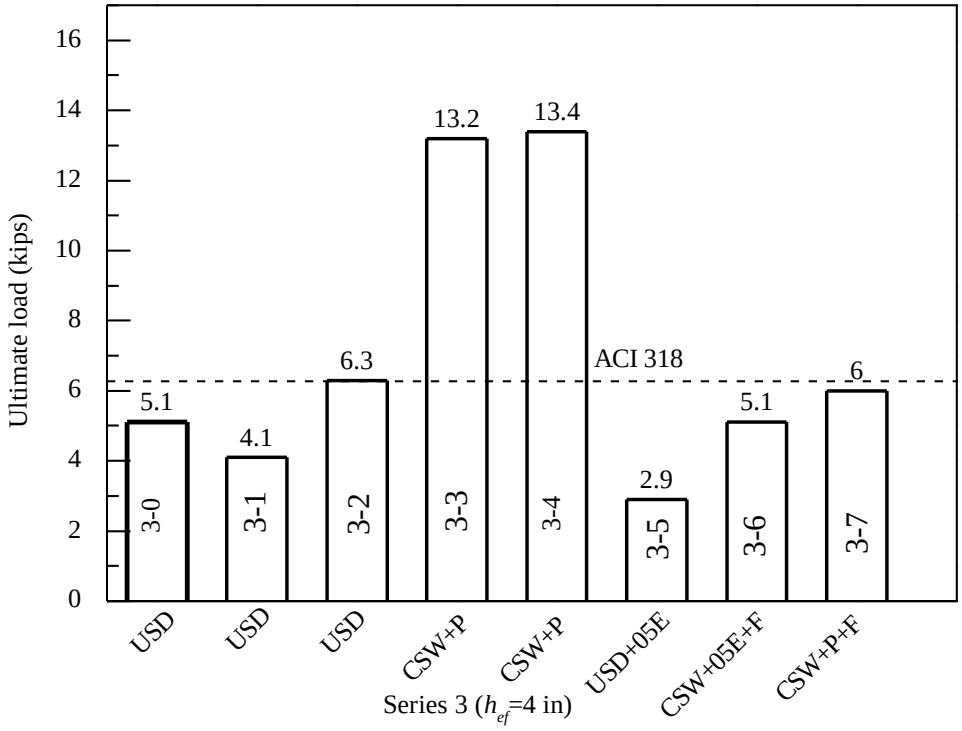

Figure IX.12 The results of the 8 tests of series 3

Figure IX.13. Tested anchors USD (3212018 and 3222018)

Figure IX.14. Tested anchors CSW (3212018 and 3222018)

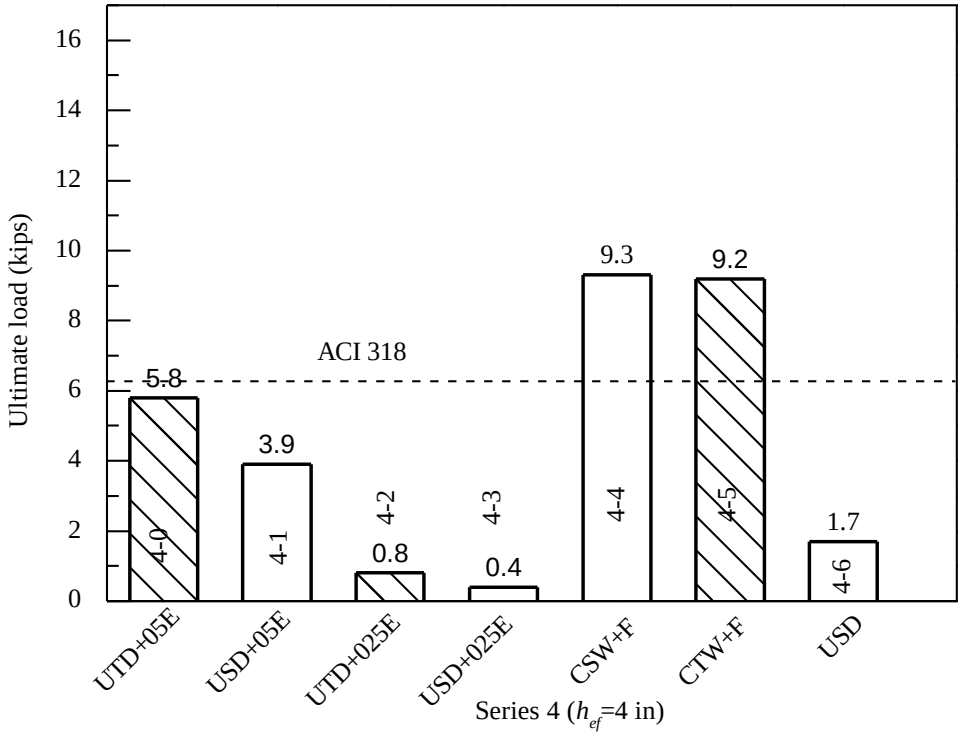

Figure IX.15 The results of the 7 tests of series 4

Figure IX.16. Tested anchors (USD vs UTD) after removing dusts (4162018 and 4182018)

Figure IX.17. Tested anchors (CSW+F vs CTW+F) (4182018)

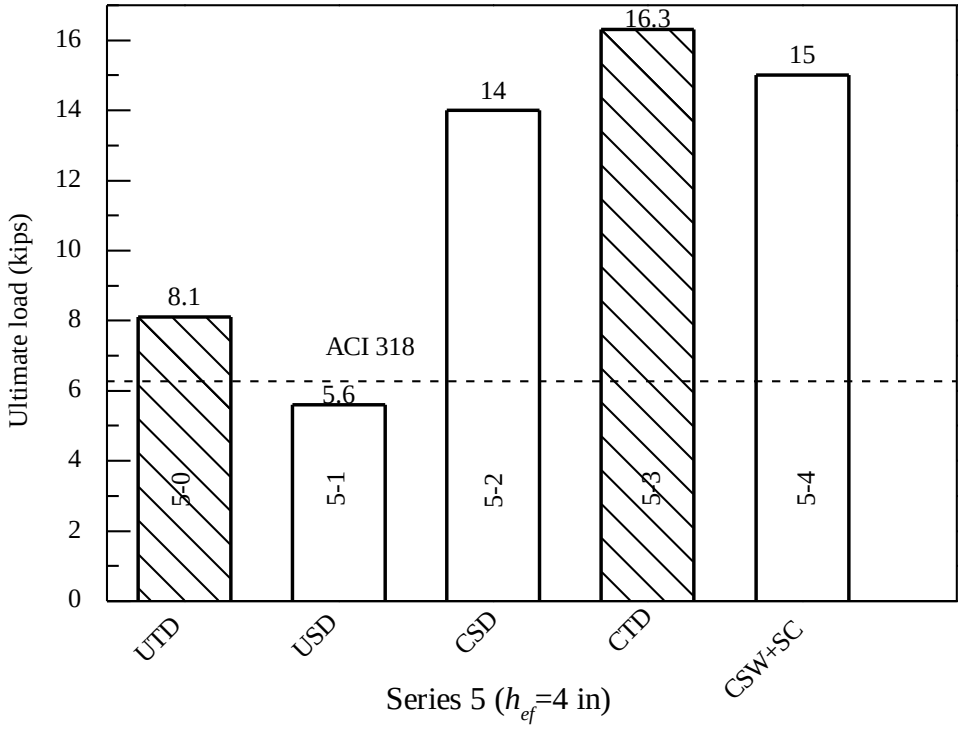

Figure IX.18. The results of the 5 tests of series 5

Figure IX.19. Tests anchors USD, UTD, CSD, CTD and CSW (9242018)

Table IX.1 Concrete mix design

Formula	511	
Load Size	5.5	yards
#1 AE/FA	7.5	bag
Torp Sand	6920	lbs
#1 Stone	9340	lbs
Cem 2 (St Mar	3090	lbs
Cem 4 (Fly As	780	lbs
AE 260	5	fluid ozs
Water Reducer	78	fluid ozs
V 1000	312	fluid ozs
Cold Water	28	gallons
Water	70	gallons

Table IX.2 Results of unconfined pullout tests

Series	Day	Specimen	Maximum load (kips)	Reasons
1-0	3032018	CSD-05-4-3032018	4.7	The epoxy did not mix well.
1-1	3032018	CTD-05-4-3032018	16.0	
1-2	3032018	USD-05-4-3032018	7.3	Dust
1-3	3032018	UTD-05-4-3032018	11.7	Dust impacted a little
2-0	3082018	USD-05-4-03082018	13.2	The hole was cleaned by the epoxy.
2-1	3082018	UTD-05-4-03082018	13.6	Dust did not impact.
2-2	3082018	CSD-05-4-03082018	13.9	
2-3	3132018	CTD-05-4-3132018	15.4	
2-4	3132018	CTW (F)-05-4-3132018	14.0	Full water did not impact
2-5	3142018	CSW (F)-05-4-3142018	9.8	Full water mixed epoxy
3-0	3212018	USD-05-4-1-3212018	5.1	Dust
3-1	3212018	USD-05-4-2-3212018	4.1	Dust
3-2	3212018	USD-05-4-3-3212018	6.3	Dust
3-3	3212018	CSW(P)-05-4-1-3212018	13.2	Water did not penetrate the concrete in short time.

3-4	3212018	CSW(P)-05-4-2-3212018	13.4	Water did not penetrate the concrete in short time.
3-5	3222018	USD(05E)-05-4-3222018	2.9	Half epoxy
3-6	3222018	CSW(05E+F)-05-4-3222018	5.1	Half epoxy+ water impacted
3-7	3222018	CSW(P+F)-05-4-3-3222018	6.0	Water impacted
4-0	4162018	UTD(05E)-05-4-4162018	5.8	
4-1	4162018	USD(05E)-05-4-4162018	3.9	
4-2	4182018	UTD(025E)-05-4-4182018	0.8	
4-3	4182018	USD(025E)-05-4-4182018	0.4	
4-4	4182018	CSW(F1)-05-4-4182018	9.3	
4-5	4182018	CTW(F1)-05-4-4182018	9.2	
4-6	4182018	USD-05-4-4182018	1.7	
5-0	9242018	UTD-05-4-9242018	8.1	
5-1	9212018	USD-05-4-9212018	5.6	
5-2	9242018	CSD-05-4-9242018	14.0	
5-3	9242018	CTD-05-4-9242018	16.3	
5-4	9242018	CSW(SC)-05-4-9242018	15.0	Saturate concrete
0-1	12292017	CSW-05-325	9.0	
0-2	12292017	CTW-05-325	8.9	
0-3	12292017	CSD-05-325	8	
0-4	12292017	CTD-05-325	8.9	
0-5	12292017	USD-05-325	2	
0-6	12292017	UTD-05-325	5.6	

Appendix X: ABAQUS input file example

```
*Heading
** Job name: 3DAAnchor4in_6200psi Model name: Model-1
** Generated by: Abaqus/CAE 2018
*Preprint, echo=NO, model=NO, history=NO, contact=NO
**
** PARTS
**
*Part, name=AAnchor
*Node
      1,           0.,           0.,          12.
...
    199, -0.0666349903, 0.0667491034,          10.5
*Element, type=C3D8R
 1,  85,  86, 171, 170,  15,  14,  80,  79
...
112,  64,  21,   3,  12, 167, 130,  58,  71
** Section: AnchorSteel
*Solid Section, elset=_PickedSet3, material=Steel
,
** Section: Adhesive
*Solid Section, elset=_PickedSet2, material=Adhesive
,
*End Part
**
*Part, name=Bars#5
*Node
      1,         -10.,           4.,           0.
...
      6,           0.,           4.,           0.
*Element, type=T3D2
1, 1, 2
```

```
...
5, 5, 6
** Section: Bars#5
*Solid Section, elset=_PickedSet2, material=SteelBar
0.31,
*End Part
**
*Part, name=BlockBase
*Node
      1,           0.,           6.,           8.
...
    140,         -12.,           0.,           0.
*Element, type=C3D8R
 1,  21,  22,  26,  25,   1,   2,   6,   5
...
72, 135, 136, 140, 139, 115, 116, 120, 119
** Section: ConcBlock
*Solid Section, elset=_PickedSet2, material=Concrete
,
*End Part
**
*Part, name=BlockTop
*Node
      1, -0.220970869,  0.220970869,          12.
...
    981,  -1.50091314,   1.80249095,           8.
*Element, type=C3D8R
  1,  41,  42,  52,  51, 150, 151, 161, 160
...
704, 869, 867, 850, 845, 978, 976, 959, 954
** Section: ConcBlock
*Solid Section, elset=_PickedSet2, material=Concrete
,
```

```
*End Part
**
*Part, name=Plastic
*Node
      1,           0.,           6.,         0.25
...
     40,          -4.,           0.,           0.
*Element, type=C3D8R
 1, 11, 12, 17, 16,  1,  2,  7,  6
...
12, 34, 35, 40, 39, 24, 25, 30, 29
** Section: Plastic
*Solid Section, elset=_PickedSet2, material=Plastic
,
*End Part
**
** ASSEMBLY
**
*Assembly, name=Assembly
**
*Instance, name=AAnchor-1, part=AAnchor
*End Instance
**
*Instance, name=BlockBase-1, part=BlockBase
*End Instance
**
*Instance, name=Bars#5-1, part=Bars#5
          0.,           0.,         10.5
*End Instance
**
*Instance, name=BlockTop-1, part=BlockTop
*End Instance
**
```

*Instance, name=Plastic-1, part=Plastic

-8., 0., 12.

*End Instance

**

** Constraint: CP-3-BlockBase-1-BlockTop-1

*Tie, name=CP-3-BlockBase-1-BlockTop-1, adjust=yes, type=SURFACE TO SURFACE

CP-6-BlockTop-1, CP-4-BlockBase-1

** Constraint: CP-4-Plastic-1-BlockTop-1

*Tie, name=CP-4-Plastic-1-BlockTop-1, adjust=yes, type=SURFACE TO SURFACE

CP-6-Plastic-1, CP-7-BlockTop-1

** Constraint: LongBar

*Embedded Element, host elset=_PickedSet33

** Nonlinear Springs in Z-direction

*Element, type=Spring2, elset=Springs-z *Springs added in ASSEMBLY*

1, AAnchor-1.12, BlockTop-1.2 *Nodes read from CAE at coincident locations*

2, AAnchor-1.71, BlockTop-1.111

3, AAnchor-1.70, BlockTop-1.220

4, AAnchor-1.69, BlockTop-1.329

5, AAnchor-1.68, BlockTop-1.438

6, AAnchor-1.67, BlockTop-1.547

7, AAnchor-1.66, BlockTop-1.656

8, AAnchor-1.65, BlockTop-1.765

9, AAnchor-1.13, BlockTop-1.3

10, AAnchor-1.72, BlockTop-1.112

11, AAnchor-1.73, BlockTop-1.221

12, AAnchor-1.74, BlockTop-1.330

13, AAnchor-1.75, BlockTop-1.439

14, AAnchor-1.76, BlockTop-1.548

15, AAnchor-1.77, BlockTop-1.657

16, AAnchor-1.78, BlockTop-1.766

17, AAnchor-1.148, BlockTop-1.764

18, AAnchor-1.151, BlockTop-1.655

19, AAnchor-1.154, BlockTop-1.546
20, AAnchor-1.157, BlockTop-1.437
21, AAnchor-1.160, BlockTop-1.328
22, AAnchor-1.163, BlockTop-1.219
23, AAnchor-1.166, BlockTop-1.110
24, AAnchor-1.63, BlockTop-1.1
*Spring, NONLINEAR, elset=Springs-z *Define nonlinear spring element*
3, 3 *Displacements at DOF 3 (Z-direction)*
used
-0.08, -0.7 *Symmetric behavior, can be different*
-0.08, -0.5 *Format: loads, displacements*
-0.16, -0.08
-0.16, -0.02
0, 0
0.16, 0.02
0.16, 0.08
0.08, 0.5
0.08, 0.7
*End Assembly
**
** MATERIALS
**
** Elastic adhesive material
*Material, name=Adhesive
*Elastic
3150., 0.38
** Elastic concrete
*Material, name=ConcElastic
*Elastic
4488.2, 0.17
** Concrete material using damage plasticity model
*Material, name=Concrete
*Elastic

4488.2, 0.17
*Concrete Damaged Plasticity
38., 0.1, 1.16, 0.67, 5e-05
*Concrete Compression Hardening
2.76606, 0.
3.13545, 1.39813e-06
3.48836, 2.27679e-05
3.82417, 4.79478e-05
4.1419, 7.71548e-05
4.44038, 0.000110651
4.71834, 0.000148719
4.97454, 0.000191637
5.2078, 0.000239664
5.41716, 0.000293019
5.60183, 0.000351873
5.76132, 0.000416337
5.89543, 0.000486456
6.00427, 0.000562206
6.08825, 0.000643493
6.1481, 0.000730158
6.1848, 0.000821982
6.19956, 0.000918694
6.19379, 0.00101998
6.16906, 0.00112549
6.12703, 0.00123485
6.06943, 0.00134769
5.99798, 0.00146361
5.91442, 0.00158222
5.82043, 0.00170317
5.71759, 0.00182608
5.60743, 0.00195062
5.49135, 0.00207649
5.37064, 0.00220338

5.24646, 0.00233105
5.11987, 0.00245926
4.9918, 0.00258779
4.86308, 0.00271647
4.73442, 0.00284514
4.60643, 0.00297365
4.47965, 0.0031019
4.35451, 0.00322978
4.23138, 0.00335722
4.11056, 0.00348414
3.9923, 0.00361049
3.87677, 0.00373623
3.76412, 0.00386133
3.65446, 0.00398576
3.54786, 0.00410951
3.44435, 0.00423257
3.34395, 0.00435494
*Concrete Tension Stiffening
0.62,0.
** Elastic material for plastic sheets below reaction
*Material, name=Plastic
*Elastic
29000., 0.3
** Steel anchor material
*Material, name=Steel
*Elastic
29000., 0.25
*Plastic
111.803, 0.
111.917, 0.00643601
112.03, 0.00646269
112.185, 0.00660848
112.363, 0.00670861

112.443, 0.00679439
112.554, 0.00681177
112.734, 0.00689539
112.819, 0.00700683
112.916, 0.00707238
113.021, 0.00708634
113.177, 0.00717069
113.264, 0.00724713
113.375, 0.00737247
113.462, 0.00746703
113.544, 0.0075093
113.67, 0.00757902
113.772, 0.00766415
113.857, 0.00778469
113.954, 0.00780752
114.214, 0.00792302
114.448, 0.00815518
114.618, 0.0082717
114.756, 0.00846291
114.931, 0.00853707
115.055, 0.00861584
115.188, 0.00876666
115.287, 0.00901502
115.765, 0.00947202
116.679, 0.0106616
116.784, 0.0107832
116.842, 0.0109311
116.978, 0.0110383
117.073, 0.0111766
117.74, 0.012312
117.846, 0.0124692
117.91, 0.0126064
118.406, 0.013412

118.511, 0.0135161
118.576, 0.0136677
118.681, 0.013838
119.001, 0.0144775
119.103, 0.0146068
119.183, 0.0148114
119.278, 0.0150057
119.355, 0.01516
119.45, 0.0152714
119.546, 0.0154156
120.444, 0.0160299
121.499, 0.0170406
122.185, 0.0190065
123.02, 0.0211149
123.918, 0.0232471
124.738, 0.0254396
125.563, 0.0278826
126.34, 0.0306345
127.007, 0.033173
127.605, 0.0357906
128.104, 0.0385834
128.447, 0.041487
128.739, 0.0442037
128.912, 0.046934
128.886, 0.0497068
128.919, 0.0518356
128.952, 0.0539651
128.886, 0.056053
128.746, 0.0583727
128.543, 0.0604094
128.225, 0.0626368
127.815, 0.0648256
127.32, 0.0670169

126.732, 0.0693716
126.09, 0.0714917
125.362, 0.073713
124.563, 0.0763106
123.706, 0.0784985
122.781, 0.0808946
121.807, 0.0832921
120.787, 0.0856609
119.677, 0.0880719
118.51, 0.0904586
117.3, 0.0929438
115.969, 0.0953967
114.557, 0.0979902
113.081, 0.100551
111.484, 0.103139
109.78, 0.10563
107.991, 0.108188
106.061, 0.110834
104.039, 0.113547
101.826, 0.11628
99.449, 0.118986
0.01, 0.121614
** Material for steel bars
*Material, name=SteelBar
*Elastic
29000., 0.25
**
** INTERACTION PROPERTIES
**
*Surface Interaction, name=An2Conc
1.,
*Friction
0.,

*Surface Behavior, no separation, pressure-overclosure=HARD
*Surface Smoothing, name=CP-2-BlockTop-1-AAnchor-1
, _CP-2-BlockTop-1-AAnchor-1_msm_1, CIRCUMFERENTIAL, 0., 0., 8., 0., 0., 9.
_CP-2-BlockTop-1-AAnchor-1_ssm_1, , CIRCUMFERENTIAL, 0., 0., 8., 0., 0., 9.
**
** BOUNDARY CONDITIONS
**
** Name: Reaction Type: Displacement/Rotation
*Boundary
_PickedSet42, 1, 1
_PickedSet42, 2, 2
_PickedSet42, 3, 3
** Name: Xsym Type: Symmetry/Antisymmetry/Encastre
*Boundary
_PickedSet40, XSYMM
** Name: Ysym Type: Symmetry/Antisymmetry/Encastre
*Boundary
_PickedSet44, YSYMM
**
** INTERACTIONS
**
** Interaction: CP-2-BlockTop-1-AAnchor-1
*Contact Pair, interaction=An2Conc, small sliding, type=SURFACE TO SURFACE, geometric correction=CP-2-BlockTop-1-AAnchor-1
CP-3-AAnchor-1, CP-2-BlockTop-1
** --
**
** STEP: Step-1
**
*Step, name=Step-1, nlgeom=NO, inc=2000
Anhcor pullout 0.5 in.
*Static, stabilize=0.001, allsdtol=0.05, continue=NO
1e-08, 0.5, 1e-25, 0.0005

```
**
** BOUNDARY CONDITIONS
**
** Name: Loading Type: Displacement/Rotation
*Boundary
_PickedSet43, 3, 3, 0.5
**
** CONTROLS
**
*Controls, reset
*Controls, parameters=time incrementation
 , , , , , , , 25, , ,
**
** OUTPUT REQUESTS
**
*Restart, write, frequency=0
**
** FIELD OUTPUT: F-Output-1
**
*Output, field, variable=PRESELECT
**
** HISTORY OUTPUT: H-Output-1
**
*Output, history, variable=PRESELECT
*End Step
```

Curriculum Vitae

Hua Liu

Education

August 2020 **University of Milwaukee, Milwaukee, Wisconsin**
PhD of Engineering 3.7/4.0
Civil and Structural Engineering
Thesis Title: Novel Adhesive Anchoring System Through Engineered Interface

May 2013 **East Carolina University, Greenville, North Carolina**
Master of Science, 3.3/4.0
Construction Management

September 2004 **Fuzhou University, Fuzhou, China**
Bachelor of Engineering, 3.0/4.0
Civil Engineering

July 2002 **Liming Vocational University, Quanzhou, China**
Certificate of Construction Technology
Construction Technology

Relevant Work Experience

University of Wisconsin-Milwaukee **Milwaukee, Wisconsin**
Teaching Assistantship **September 2016 to May 2019**

- Assist and support faculty members to grade homework and exams
- Teach course sessions and help students to understand key knowledge on courses
- Encourage and help students to achieve their learning goals
- Course Title: Engineering Surveying, Strength of Material and Design of Steel Structures

University of Wisconsin-Milwaukee **Milwaukee, Wisconsin**
Graduate Research Assistant **January 2018 to August 2020**
Research project funded by the UWM Research Foundation

- Adhesive anchor background research
- Develop experimental methods and setups
- Execute experimental tests (confined and unconfined pullout tests)
- Develop theoretical analysis based on experimental results
- Compilation of research reports

East Carolina University **Greenville, North Carolina**
Graduate Research Assistantship **May 2012 to April 2013**

- Provided transcription research interviews and educational information analysis for qualitative research projects
- Assisted college professor with literature review on using wordless picture books to support bilingual children's language and literacy development.

Tianjin Huaxia Architectural Design Co., Ltd **Fuzhou, China**
Engineer-in-Training and Structural Engineer **September 2007 to August 2010**

- Conducted structural analyses and design of reinforced concrete beams and columns of multistoried and high-rise commercial, residential and industry buildings.
- Assisted Site Engineers on multiple projects and solved design and construction quality problems.

Hui'an Luocheng Construction Development Co., Ltd **Quanzhou, China**
Engineer-in-Training **October 2004 to September 2007**

- Assisted civil engineers and project managers in construction quality and structural design aspects in construction activities, including quality control, schedule and cost control, and design related issues.
- Reviewed and verified structural drawings to determine the margin of error.
- Communicated with site engineer and structural engineer to develop solutions to ensure quality assurance, improve on structural drawings, and minimize risks.
- Checked superintendents' submittals and conducted quality and final inspections.

Chinese Construction Corporation **Fuzhou, China**
Technician **June 2004 to October 2004**

- Performed the duty of a construction supervisor and supervised constructors in various constructions projects/sites
- Applied civil and construction technology.

Chinese Construction Corporation **Fuzhou, China**
Technician Internship **April 2002 to July 2004**

- Assisted civil engineers in quality control and structural design related activities, including quality control, schedule, and design related issues.

Projects Involved

- **January 2016 to July 2017 Graduate Research Assistant**

  - January 2018 to May 2020, New adhesive anchor, verified the concept of a new adhesive anchoring system in harden concrete. Conducted experimental tests and finite element analysis, Milwaukee, Wisconsin, US.
  - September 2019 to January 2020, helped Da Lu (Visiting Scholar) to provide independent tests for the alpha setup of adhesive anchors, Milwaukee, Wisconsin, US.
  - June 2018 to August 2018, Spancrete Hollow Cord bending and shear tests, helped Rahim Reshadi (Lab manager) to set up tests and collected and analyzed the data.
  - January 2016, Big beam competition, designed a 17-feet beam of prestressed concrete by using finite element analysis, Milwaukee, Wisconsin, US.
  - April 2016, Poster competition, designed a poster of predicting the behavior of concrete bridge girders using finite element method, Milwaukee, Wisconsin, US.

- **September 2007 to August 2010 Structural Engineer**

  - January 2010, Gongyuan Dao NO 1, frame-shear structure of 18-storey residence (21,000 m^2), Shangrao City, Jiangxi Province, China.
  - December 2009, Gaoshan middle school, frame structure of school building (22,000 m^2), GaoshanTown, FuQing City, Fujian Province, China.
  - November 2009, WujianZhogDui, frame structure of military building (2200 m^2), Fuzhou City, Fujian Province, China.
  - September 2008, MinchengShijia, frame-shear structure of 11-storey residence (7000 m^2), Fengyang City, Anhui Province, China.
  - June 2008, Shaxian Yu le City, frame-shear structure of 3-storey entertainment center (15,000 m^2), Shangmin City, Fujian Province, China.
  - March 2008, LongyanHuitong, frame-shear structure of 18-storey residence (15,000 m^2), LongyanCity, Fujian Province, China.
  - October 2007, ShishiXinyi development district, frame structure of 2-storey industry factory (8000 m^2), ShishiCity, Fujian Province, China.

- **September 2004 to August2007 Technician**

October 2004 to January 2006, Fujian Medical University, frame-shear structure of 18-storey hospital building, Fuzhou City, Fujian Province, China.

Computer Skills:

Complete project documentations: SAP, AutoCAD, SketchUp, Origin, Microsoft Office products. Familiar with MATLAB and ABAQUS.

Awards and Achievements

• Spring 2020	CEAS Chancellor's Graduate Student Award
• Spring 2018	Asia Faculty and Staff Association Student Award (2rd place)
• Fall 2016	CEAS Chancellor's Graduate Student Award
• Spring 2016	CEAS Chancellor's Graduate Student Award
• November 2014	Building License of General Contractor NC (Limited)
• December 2009	Engineer in Training (EIT) Certification(Intermediate)
• July 2005	Engineer in Training (EIT) Certification(Primary)
• December 2003	National Computer Ranking Examination
• 2001-2002	Second Prize Scholarship, Liming Vocational University
• 2000-2001	First Prize Scholarship, Liming Vocational University
• 1999-2000	First Prize Scholarship, Liming Vocational University

Research Interests:

- Anchor design and analyses
- Structural Engineering
- Material feature analysis
- Numerical Methods such as Finite Element Methods (FEM)